Fracture mechanics studies of non-yielding materials like concrete : modelling of tensile fracture and applied strength analyses

Gustafsson, Per-Johan

1985

CODEN: LUTVDG/(TVBM-1007)/1-422/(1985)

FRACTURE MECHANICS STUDIES OF NON-YIELDING MATERIALS LIKE CONCRETE:

Modelling of Tensile Fracture and Applied Strength Analyses

Per Johan Gustafsson

ISSN-0348-7911

0.1 Preface and acknowledgements

The work presented in this thesis has been carried out at the Division of Building Materials, Department of Civil Engineering, Lund Institute of Technology, Sweden and has been made financially possible by means of grants from The Foundation for Swedish Concrete Research (Stiftelsen Svensk Betongforskning) and The Swedish Board for Technical Development (STU).

Essential bases for the work are due to professor Arne Hillerborg, head of the Division of Building Materials. He initiated fracture mechanics research at the Division of Building Materials and proposed an admirably simple macroscopical description of the "simple" fracture of a specimen in uniform tension. This description seems to be particularly useful during tensile fracture analysis of non-yielding materials such as concrete and seems also to be theoretically consistent. The description has formed the base for fracture mechanics research carried out at the Division of Building Materials by professor Hillerborg and by the former staff members tekn. dr. Matz Modeer and tekn. dr. Per-Erik Petersson and, where the present work is concerned, by the author.

I wish to thank professor Arne Hillerborg not only for general bases for the work but also for invaluable guidance, support and encouragement during the course of the work and for reading the manuscript and proposing corrections. I wish also to thank my other teachers and friends at the Division of Building Materials, the above mentioned former staff members included, for support and for practical help (see below) during the production of this report.

I wish also to thank professor Hans Petersson, head of the Division of Structural Mechanics, and my other teachers and friends at the Division of Structural Mechanics for their help, in particular where the access to computer programs is concerned, and for their encouragement and interest.

The work has to a certain extent involved correspondence and informal contacts with researchers and engineers at institutions and building companies in Sweden and abroad. I wish to take this opportunity to express my appreciation to these researchers and engineers and thank for inspiration and help as well as kindness and interest.

During the production of this report [illegible] has carried

through a comprehensive work by typing the manuscript into a somewhat disobedient and tired computer and also typing the tables and formulas. Mrs Marita Karlsson has given significant indirect support by taking care of parts of Mrs Nilssons more regular tasks. Mrs Britt Andersson has carried through a comprehensive work by preparing the figures and also giving assistance during the final preparation of the report. Mrs Margaret Malmström and Miss Monica Hedin have corrected linguistic errors. I wish to thank for the important practical help.

In order to be neutral, in following parts of this thesis the author is reffered to as the writer. The thesis, - in the following called a report-, shall be presented to the University of Lund.

Of course, efforts have been made to avoid errors. In spite of this, it is likely that errors can be found. Therefore, it is advisable not to take correctness of all numbers and formulas and so on for granted and to make checks before possible use of any of the contents.

The writer hopes that a reader of this report shall find results or discussions that may be of interest to the reader.

Lund, General Elections Day, September 15, 1985
Per Johan Gustafsson

0.2 Contents

0.3 Summary

In this report, fracture mechanics studies of tensile stress induced fracture of non-yielding materials such as concrete are presented. The greatest part of the report deals with applied strength and fracture analyses of specimens and structural members: fracture mechanics specimens, beams loaded in tension, bending or shear, pipes and longitudinally reinforced concrete beams failing in diagonal tension. Although different theoretical models of tensile failure and crack development are utilized and studied, almost all parts of this report are based on, concerned with, or related to the model for tensile fracture and strain localization called "the fictitious crack model". Numerical calculations are carried out with help of a computer and most of them by means of the finite element method. Fracture models are compared with respect to basic characteristics and numerical results. Comparisons to test results reported in literature are presented. The applied calculations are preceded by, and accompanied with, some more general and more or less theoretical descriptions, studies and discussions regarding strength, fracture and fracture models.

In Chapter 1 introductory remarks are made, and in particular general limitations of the present work are listed. Among these limitations: (1) the materials are studied on such a macroscopical scale that they may be assumed to have identical, or stochastically identical properties in all infinitesimal points, (2) the material outside a fracture zone is assumed to behave in a linear elastic manner, (3) only a single discrete fracture zone or crack is considered.

Chapter 2 is also of a rather general introductory nature. Basic reasons for structural failure and methods for failure load prediction are separated into three groups each. It is argued that the most important reason for failure of structures made of non-yielding materials may be fracture, i.e. decrease of stress in the material at increased deformation. It is also argued that it is beneficial from the point of view of generality to establish methods for failure load prediction on the basis of assumptions regarding the mechanical properties of the material, i.e. primarely on assumptions regarding the stress vs. deformation properties.

Chapter 3 concerns descriptions and theoretical and numerical studies of tensile fracture models and methods of strength analyses subsequently

applied in Chapters 4 and 5.

In Section 3.2 basic characteristics of the fictitious cack model are described and discussed. Analogy between tensile stress strain localization and bending moment curvature localization is noticed. The magnitude of relevant material property parameters for different materials is surveyed. An analytical and numerical study of the stress and displacement field close to the tip of a fracture zone may also be found in this Section.

In Section 3.3, strain distribution, instability and localization in a specimen in uniform uniaxial tension is studied.

In Section 3.4 material models for analysis of fracture and strength are surveyed with respect to applicability and assumed extension of fracture process region. The linear elastic fracture mechanics and the Weibull theory are dealt with in an somewhat more detailed manner. The strength of corners in large specimens made of brittle materials and with arbitrary opening angle is discussed.

In Section 3.5 hypotheses regarding structural strength as suggested by fictitious crack analysis are discussed. These concern common properties of the strength functions $\sigma_u/f_t = f(d/\ell_{ch})$, where σ_u/f_t is the normalized structural strength and d/ℓ_{ch} is the ratio between the absolute size of the structure and a characteristic length of the material. The strength function is justified. Upper and lower bounds of the strength, and upper and lower bounds of the slope of the strength function are formulated. Expressions for the asymptotical shape of the strength function at large d/ℓ_{ch} are discussed and compared to numerical results.

In Section 3.6 possible finite element methods for fictitious crack analysis and for linear elastic fracture mechanics analysis are briefly surveyed. The methods used during the present calculations are described in a more detailed manner. Where fictitious crack analysis is concerned, convergency in calculated load carrying capacity during mesh refinement is studied.

In Chapter 4, applied strength and fracture analyses of a few unreinforced specimens and structural members are found. This Chapter is rather extensive and for a survey of the specimens, the fracture models and the

types of results, Fig 4.1 (1) (Chapter 4, page 2) may be helpful. The specimens dealt with have been chosen so that different aspects of strength analysis and fracture are dealt with in the different Sections. Comparisons are made to experimental results from literature. In conjunction to the applied analyses a few theoretical discussions may be found.

It may be appropriate to supplement the information given in Fig 4.1 (1) with some additional information. In Section 4.2 bending moment vs. fracture hinge rotation relations may be found and in this Section is also a few other matters regarding bending failure and flexural strength discussed, i.a. a combination of the fictitious crack model and the Weibull model. The specimen studied in Section 4.3 was used in an experimental study which has often been refered to and also, on some points, questioned in literature. In Section 4.4 the effect of a groove along a crack propagation path and the effect of pre-stressing is studied. In Section 4.5 the effect on experimentally determined material properties of an undesired non-uniform stress distribution within test specimens is studied and the possiblity to determine tensile stress vs. deformation properties by means of indirect methods is discussed. The statically indeterminate ring-failure dealt with in Section 4.6 involves unloading of fracture sections and the strength of statically indeterminate beams is discussed. Section 4.7 concerns crack growth from the corner in an orthotropic material and the modes of ultimate failure of the actual type of beam is discussed. From the point of view of design, parts of Sections 4.2, 4.6 and 4.7 may be of special practical interest. The results of Chapter 4 indicate that it is meaningful to take into account fracture softening and strain localization during strength analysis of non-yielding materials such as concrete, mortar and wood.

Chapter 5 concerns shear strength analysis of longitudinally reinforced concrete beams by means of the fictitious crack model. Rather crude approximations are adopted during these finite element calculations. The steel-concrete interaction is modelled in a conventional manner by means of bond stress-slip elements, the fracture zone development is modelled according to the fictious crack model and a special purpose method is used during check of compressive failure in the upper edge of the beam. For each beam, different assumptions regarding the location of the single discrete fracture zone are considered. For the different fracture zone locations, the load at unstable crack growth and the load at final

failure is calculated. The shear strength is then obtained with the help of a diagram which, for beams sensitive to shear, shows a load carrying capacity valley in the shear span.

Shear strength is calculated for a rather large number of beams. The calculations indicate a strong influence of ratio d/ℓ_{ch} on the shear strength. d represents the absolute size of the beam and ℓ_{ch} the characteristic length of the concrete. Comparisons are made to experimental results, empirical and semi-empirical expressions and to theoretical upper and lower bounds of the shear strength. The strong influence of absolute size is in agreement with experimental results. Agreement is also found with respect to the relative influence of the ratio between bending moment and shear force, the percentage of longitudinal reinforcement and magnitude of prestress in the reinforcement. The absolute values of shear strength are underestimated by the theoretical calculations. This is believed to be due primarely to the crude and conservative modelling of the fracture zone and to the disregardment of dowel action.

Empirical, semi-empirical and theoretical size effect relations are surveyed. It is found that the empirical relations are in fair agreement with each other and with the numerical results in the intermediate range of size, but, if taking into account all sizes, only the numerical results are consistent with the basic theoretical hypotheses of Section 3.5. On the basis of the present numerical results and on shear strength studies reported in literature, a few special and general remarks on shear strength analysis are made, e.g. with regard to building code design expressions and model-testing with the help of micro-concretes. Essential conclusions in Chapter 5 are that theoretical calculations based on mechanical properties of materials are able to indicate size effect in shear strength, that the size effect may be explained by strain localization and instability during fracture softening and that the characteristic length, ℓ_{ch}, of concrete is theoretically identified as a parameter of great significance for shear strength.

0.4 Notations

Notations and symbols are explained in the text where they first occur. Below, symbols used in more than one Section are listed. Other symbols are explained in the actual Sections where they are used. Symbols and notations in the different studies in this report have been chosen in comformity with the corresponding main literature references and with common practice, and in some cases a symbol has different meanings in different Sections.

Latin capital letters:

A 1) area
2) abbreviation of lengthy expressions

B thickness (Section 4.3)

C constants

E modulus of elasticity

G 1) energy release rate
2) shear rigidity

G_c critical energy release rate

G_F fracture energy, eq (3.2:2)

K stress intensity factor

K_c critical stress intensity factor

M bending moment

M_u ultimate bending moment

P load, force

P_u ultimate load

S 1) accumulated probability
2) slip steel-concrete

U potential energy

V 1) shear force
2) volume

V_f shear force at instability

V_u ultimate shear force

W 1) work
2) width (Section 4.3)

Latin lower-case letters:

a depth (of crack or fracture zone)

a_i coefficient

b breadth, width

c 1) compliance
2) constant in exponent position

d measure of absolute size (often depth of beam)

f_f flexural strength

f_t tensile strength

i integer number

j integer number

k stiffness

ℓ length

ℓ_{ch} $=EG_F/f_t^2$, characteristic length of material

m measure of scatter (Weibull)

r 1) coordinate in r-θ system
2) radius of circle

s 1) length of fracture zone
2) coefficient of variation

t thickness

u displacement in x-direction

v displacement in y-direction
w widening of fracture zone
$w_\perp$ widening of fracture zone ($\perp$ to fracture plane)
$w_{//}$ shear deformation of fracture zone
x coordinate
y coordinate
z coordinate

Greek capital letters:

$\Delta\cdot$ increment/addition in $\cdot$
Δx side length of finite element
Θ 1) coordinate in r-Θ system
2) relative rotation in fracture hinge
$O(\cdot)$ term with first order $\cdot$
Π multiplication
Σ summation
Φ rotation

Greek lower-case letters:

α 1) opening anle of corner, Fig 3.4 (9)
2) coefficient
β 1) angle
2) coefficient
γ 1) angle (inclinatio)
2) coefficients, eq (3.4:10) and eq (4.2:6)
3) shear strain
δ deflection
ε strain
λ coefficient, Fig 3.4 (9)
μ mikro, 10^{-6}
ν Poissons ratio
π 3.14159...
σ stress
$\sigma(\bar{x})$ σ_1 in point $\bar{x}$
σ_i internal initial stress
$\sigma_i(\bar{x})$ σ_1 in point $\bar{x}$ at time i
σ_u $\sim P_u/d^2$, normalized ultimate load
σ_x stress in x-direction
σ_y stress in y-direction
σ_1 first principal stress
σ_2 second principal stress
σ_3 third principal stress
τ shear stress

---

1. INTRODUCTION

1.1 General introduction and aim of report

The study presented in this report may be considered as part of the research work carried out at the Division of Building Materials on the tensile fracture of concrete and other materials with similar fracture mechanics characteristics: its modelling, experimental determination of fracture mechanics properties and applied theoretical fracture analyses of specimens and structural members. Major parts of this research previously reported in English may be found in (Hillerborg, Modeer and Petersson, 1976), (Modeer, 1979) and (Petersson, 1981).

A major part of this report deals with some applied computational analyses of tensile stress induced fracture of some specimens and structural elements with and without initial cracks. Different methods of strength and fracture analysis, all based on assumptions regarding the mechanical properties of materials, are dealt with during the actual applied calculations and also, to some extent, during more general studies and discussions. The modelling and the influence of the post peak tensile stress behaviour of materials are elucidated while the pre-peak stress behaviour and the behaviour at high compressive stresses are treated in a very brief and simple manner.

The pre-peak stress behaviour of materials and its influence on the overall behaviour of structures have been investigated theoretically and experimentally in extensive research works during the last century and have become a comparatively well established and developed part of the science of strength of materials. This development has been strongly supported by the assumptions of continuity and homogeneity of materials, making it possible to utilize the concepts of continuum mechanics of homogeneous media and associated mathematical tools. No real material is a continuous and homogeneous medium, but at any reasonable ratio between the size of the studied body and the size of the heterogenities of the material, these assumptions appear to be appropiate and well adapted to their purpose when analysing the pre-fracture behaviour. On the other hand, during analyses of fracture and calculation of ultimate load carrying capacity of specimens and structural elements, the concepts of continuum mechanics of homogeneous media are in general not sufficient as the continuum behaviour at the

start of fracture of the material: strain instability and strain localization. At fracture the local properties of the small scale non-continuous micro structure of the material becomes decisively important. Thus, one difficulty in the analysis of fracture is to find a macroscopical description of the mechanical properties of the fracture process region, i.e. a description of the small scale fracture behaviour of the material, which may be combined with a description of the mean macroscopical pre-fracture mechanical properties of the material.

Among researchers, teachers and engineers of building materials and building structures, the post-peak stress behaviour, i.e. fracture mechanics, appears to have attracted much less interest than the pre-peak stress behaviour. This is rather remarkable as theoretical calculations of the ultimate load carrying capacity of almost any specimen, structural detail, structural element or entire structure require, in one way or another, some tacit or explicit assumption regarding the post-peak stress behaviour of the material. With few exceptions one of two extreme assumptions regarding the behaviour after the peak stress or the limit strain have been adopted: an immediate drop in the stress to zero or an unlimited strain capacity at peak stress. One reason for the delay of incorporation of fracture mechanics into the analyses of building structures may be that many non-metallic materials are apparently brittle, but in spite of this they often don't seem to behave in accordance with the predictions of linear elastic fracture mechanics. Another reason for the delay may be that traditional fracture mechanics models only apply to specimens with pre-existing cracks or sharp notches. Furthermore, suitable numerical methods of calculation have not become available until the last decades and, due to the lack of continuity at fracture, the traditional fracture mechanics models, often adapted to analytical methods of calculation, might have been associated with theoretical and advanced mathematics. From these points of view it is understandable that many building engineers and teachers of civil engineering might previously have regarded fracture mechanics as useless and theoretical.

Specifically where concrete is concerned, tensile fracture and cracking are, i.a. according to Argyris, Faust and William (1979), the primary ingredients of the non-linear behaviour of concrete structures, and, as i.a. suggested by the results presented in in this report, the tensile fracture properties often have a major influence on the ultimate load carrying capac[illegible] In spite of this, it is only some 20 years ago,

(Kaplan,1961), since the first experimental study of cracking in concrete was carried out in view of the traditional linear elastic fracture mechanics *); some years later, (Hughes and Chapman,1966), the descending branch of a stress-deformation curve of concrete in tension was recorded and published; in 1967, (Ngo and Scordelis,1967), cracks were, for the first time, taken into account in a finite element analysis of a concrete beam **); some ten years later, (Hillerborg, Modeer and Petersson, 1976), a description of the tensile fracture was presented, which enabled consideration of the changing properties of a growing and moving process region and a unified method for the analyses of specimens with and without pre-existing cracks; and in recent years advanced finite element programs have been developed for the analyses of concrete structures taking into account, in different manners, the discrete cracking in concrete, (Grootenboer,1979), (Saouma and Ingraffea, 1981). Please note that the above mentioned references only cover a few of the contributions to the development.

Thus, in recent decades interest in the post peak tensile stress behaviour (fracture mechanics, strain softening and strain localization, material damage and damage localization) of concrete and similar materials has grown and is now being dealt with at a number of institutions in different countries. This report deals essentially with some studies of applications of fracture mechanics during the strength analyses of concrete and similar materials, and, in general terms, the aim of the report is to contribute to the knowledge within this area of research.

The ultimate goal of the kind of research presented in this report may be to achieve improvements in design. In practice, the design of most building structures is governed by codes, but the work on development of new codes is in turn influenced by practical experiences and experimental and theoretical research. Where the Swedish concrete building codes are concerned, it is interesting to know that different basic assumptions regarding the stress-deformation behaviour of the material seem to have

*) A historical review of experimental applications of fracture mechanics to concrete has been presented by Mindess (1983).

**) A brief history of finite element analysis of reinforced concrete has been presented by Scordelis, Nilson and Gerstle (1982).

influenced the work on the development of the codes, see Fig 1.1(1). This figure is simplified and shows only a schematic illustration. It seems, however, that the code in 1945 was primarily only influenced by the assumption of linear elasticity. In the code from 1957 some rules based on the theory of plasticity were included, and the code from 1979, BBK-79, was not only influenced by the assumption of linear elasticity but was also strongly influenced by the assumption of plasticity. The development of BBK-79 was probably only to a small extent influenced by considerations of fracture mechanics, but it might be logical to guess that work on the development of future codes will be increasingly influenced by considerations of the complete stress-deformation curve of the material, including the descending fracture mechanics part of the curve.

It is also interesting that the logical development illustrated in Fig 1.1 (1) appears to be analogous to the historical development regarding pioneering studies within new areas of research of the mechanical behavoiur of materials: elasticity, Hook, 1676; plasicity, Tresca, 1864; fracture mechanics, Griffith, 1921. As in this report some studies of the influence of the scatter in strength are included, it may also be mentioned that a pioneering study within this area of research was presented by Weibull in 1939.

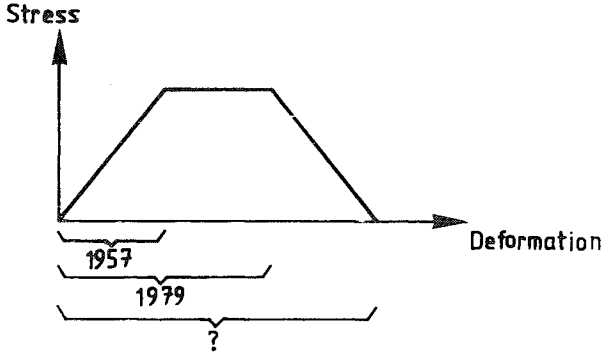

Fig 1.1(1) An illustration, - schematical and simplified -, of the development of the Swedish concrete building codes.

1.2 Method of investigation

The studies on which this report are based, have essentially been performed by means of efforts to carry out applied computational fracture analyses of some specimens and structural elements. The material model called the fictitious crack model, FCM, giving a description of the behaviour of materials when fracturing in tension, has formed the basis for the work. The model of unlimited plasticity and the two models of linear elastic fracture, i.e. linear elastic fracture mechanics and the strength concept of linear elastic brittle materials, have also been utilized and studied. Where studies of the influence of scatter in strength are concerned, the density function of Weibull has been utilized. Most of the numerical calculations have been performed with the help of the finite element method, and for this purpose public finite element programs have been utilized and smaller special-purpose programs have been developed. Experimental test data, reported in literature, have been very helpful during studies of the computational results.

1.3 Limitations

The major limitations of the analyses are as listed below. The listed limitations concern the applied computational analyses, while some discussions to a certain extent are extended beyond the limitations.

* The fracture of materials is studied on such a scale of size, in this case called a macroscale, at which composite materials such as cement paste, wood, mortar, concrete and fibre reinforced concrete may be assumed to have identical, or stocastically identical, properties in all infinitesimal parts while the composite material reinforced concrete, on the contrary, is dealt with as a two-phase material at the current scale of size.

* The analyses concern tensile stress induced tensile fracture and the growth of a single discrete tensile crack.

* The path of crack growth is known or assumed in advance and, apart from a study of the crushing strength of pipes, structural interaction between two or more cracks has not been taken into account.

* Before start of fracture. the material is assumed to behave in a linear

elastic manner.

* The specimens and the structural elements studied are assumed to be in a state of plane stress, and the theory of small strains and small global displacements is adopted.

* Time dependency on the properties of materials is not taken into account, and quasistatic structural behaviour is assumed.

---

2. THE PREDICTION OF FAILURE LOADS

2.1 Introduction

In this report fracture load calculations are carried out by means of descriptions of the tensile stress-deformation properties of non-yielding materials like concrete. Fracture is one of the phenomena that may cause failure of structures, and descriptions of stress-deformation properties of materials form the base for one of the methods of failure load prediction. In this chapter, a brief survey and discussion of the causes of failure and the methods of failure load prediction can be found. The chapter is of a rather general introductory nature and it is not necessary to read this chapter in order to understand the contents in subsequent chapters.

2.2 Causes of failure

The ultimate load carrying capacity, the failure load, of building structures and elements is governed by instability. This instability may be due to large displacements, great strains, fracture of the material or combinations of these three causes of instability. The decisive cause of instability and the magnitude of the load at instability are dependent on the geometry and the size of the structure, the distribution of the loads acting on and within the structure, and the mechanical properties of the material. Indirectly, failure of a structure may be due to a great number of causes. One example is deterioration of the material, but this is reflected as a variation of the mechanical properties of the material during the lifetime of the structure. No indirect causes of failure will be further discussed, only the direct causes of failure from the point of view of theoretical structural analysis will be surveyed.

Buckling of a slender column made of ordinary mild steel represents an example of the instability caused by large displacements. This type of instability is a result of significant alterations to the conditions of equilibrium due to the changes in the geometry of the structure. In most cases, the instability due to large displacements is of interest during the analysis of structures which have a significant capacity of deformation before ultimate failure, in particular if the action-lines of the loads are rotated or moved during the deformation.

When a reinforcement bar, or some other bar made of mild steel, becomes unstable during tensile loading it is normally due to great strains. During the development of great strains, the size of the load carrying cross section decreases significantly and consequently the load carrying capacity may decrease even if the stresses within the material increase. The development of great strains is usually localized to a very small part of the structure and, if an engineering small strain approach is used during the structural analysis, the instability due to large strains resembles instability due to fracture of the material. This reflects two different measures of stress: true stress (increasing) and nominal stress (decreasing). However, the development of large strains involves significant changes in the local geometry and thereby significant changes in the three dimensional state of stress and these changes, as well as the extent to which the large strains are localized, are dependent on the geometry of the specimen. Consequently, if the engineering small strain approach is used and the instability due to large strains is dealt with as a fracture of the material, one may not expect the apparent fracture mechanics properties of the material to be independent of the geometry of the specimen. For example, it is well known that the apparent critical stress intensity factor of steel, as evaluated during assumption of plane strain, is not only dependent on the properties of the material but is also dependent on the thickness of the specimen. The structural instability due to large strains is of interest when analysing mild steel and similar materials which have a significant capacity of deformation before such a state of stress and deformation is reached at which the material becomes unstable, i.e. starts to fracture. During analysis of instability involving large strains, consideration of the three dimensional state of stress may be of great importance.

Probably the most common prime cause of failure and instability of building structures is fracture: the decreasing ability of materials to transfer stress during increased deformation. A number of examples may be found. The failure of most structural elements made of cement composites (paste, mortar, unreinforced concrete and fibre reinforced concrete), rock, wood, ceramics, cast iron and glass is likely to be due to fracture. When snow or soil start to slide down a hill it is basically due to fracture of the materials. A number of large steel structures, such as ships, pressure vessels and bridges, have collapsed due to rapid progressive fracture of the material. Where metal alloys are concerned,

the risk of fracture precipitated by structural stress concentrators, initial cracks, fatigue and weld discontinuities is well known. Fracture in structural connectors built up of dowels, friction joints, welds, glue or nails may serve as additional examples.

Where unreinforced concrete specimens and structural elements are concerned, it seems rather obvious that the instability is, with few or no exceptions, governed by fracture of the material. Not only the ultimate strength, but also the post peak stress fracture mechanics properties of the unreinforced concrete are decisive for the use of this material, in which the ultimate tensile stress may be reached due merely to rather small variations in the temperature or moisture conditions of the environment.

As to reinforced concrete structures, they comprise a number of entirely different types and they are, on the macroscopical level, built up of two materials with entirely different mechanical properties: concrete and steel. Consequently it is impossible to make any general prediction with regard to the type of instability at the final collapse of reinforced concrete. In addition, the instability may often be governed by a combination of causes, for instance fracture and large global displacements. However, the frequent requirement of limited allowed displacements is usually more restrictive than the requirement of avoiding instability and total collapse caused by large global displacements or large strains (in the steel). Consequently, in the cases where the requirement of avoiding instability and total collapse are decisive for the design, it is probable that the risk of fracture is of the prime importance. Normally, this fracture takes place as a development and growth of cracks in the concrete. In macroscopical regions of structural tensile stress, cracks may develop and start to propagate; close to the reinforcement bars, a few splitting cracks or a large number of smaller cracks may develop with anchorage failure as the result; in regions of high compressive stress, a small or large number of cracks may develop parallel to the direction of the compressive stress with splitting or crushing and a loss of ability to sustain the compressive stress as a result. If concrete did not start to fracture at as low tensile stress or strain as it does, then the instability load (as well as the displacements and the general non-linear behaviour and possibly also the tightness and durability) of reinforced concrete structures would have been entirely different. The low tensile strength of concrete does not mean that this

strength is neglible or unimportant: on the contrary, if the tensile strength had been zero, or if the tensile fracture toughness had been zero, then, most probably, it simply would have been impossible to use reinforced concrete as a structural material. It may thus be argued that the tensile strength and the tensile fracture toughness of the concrete are decisive properties for the use of reinforced concrete as a structural material.

The applied analyses in this report only concern fracture and single discrete cracking in macroscopical regions of high tensile stress. Where the analysis of cracking close to reinforcement bars is concerned, recent research has been presented by Ingraffea, Gerstle, Gergely and Saouma (1983). A study of the crack propagation under high compressive states of stress was presented as early as in 1928. A more recent study has been presented by Lusche (1972), and Carino, Nilson and Slate (1974) have presented unanimous results for bi-axial states of stress. The theoretical modelling of the pre-fracture stress-strain behaviour of concrete under high compressive states of stress has been the subject for the development of advanced three-dimensional non-linear models adapted to finite element analyses: see (Chen,1981), (Nilsson, 1979), (Glemberg, 1984) and also other references given in these references. Where the modelling of post compressive fracture behaviour is concerned, it may be difficult to take into account the strain instability and the possible strain localization in a theoretically correct manner in such a way that also the physical behaviour is reproduced in a sufficiently realistic manner. However, a shear-band model for the strain localization and the fracture softening within a band of localized shear deformations during compressive fracture has been presented by Pietruszczak and Mroz (1981).

2.3 Methods of failure load prediction

The methods of failure load prediction may be separated into different kinds of groups, and in practice different methods of failure load prediction are often combined. Below the methods are separated into three large groups.

The straight forward method is to make experimental ultimate load carrying capacity tests on the actual type of structure. An obvious disadvantage of this method is that the structure gets destroyed during the test. However,

this direct experimental method may be a useful aid for the design of structural elements which are planned to be manufactured in series. In addition, this direct method is of very great value during studies of the accuracy of more general empirical or theoretical methods of failure load prediction, which have been developed independently of the actual tests results.

The second and often more convenient method of failure load prediction is the interpolation or, in more general cases, the statistical regression analysis. In this method, data obtained from tests on structural elements of similar geometry, material and load are used together with some more or less arbitrarily chosen interpolation formula. If the amount of test data is sufficient, such predictions of the strength of common types of structural elements may be the simplest way to achieve a safe design, and many rules in building codes concerning the load carrying capacity of common types of structural elements have probably arisen from this type of analysis. Although this method may be very useful in many cases, it has some disadvantages which may be noted as the apparent simplicity of the method and the close connection to actual test results may result in an overestimation of the value and the applicability of the method.

The method requires no knowledge or understanding about the causes and mechanisms of failure. This convenient feature may turn out to be a disadvantage where the desired safety is concerned. The failure of wooden beams with different slenderness ratio and with jags by the supports, discussed in section 4.7, might serve as an illustrative example of this matter. For such beams, simple considerations of the probable failure mechanisms show that the load carrying capacity varies with the slenderness ratio in such an irregular manner that the application of any normal smooth interpolation formula is likely to give misleading results.

Where assembled statically indeterminate structures are concerned, the discussed method of failure load prediction is usually combined with some assumption regarding the distribution of the forces within the structure, chosen in such a way that the different structural members are in equilibrium with each other, but without consideration of the actual stiffness and fracture properties of the members and the structural connectors. This common engineering approach basically rests on the lower bound theorem of plasticity, and it is consequently tacitly assumed that the fracture ductility of the structural members is infinite and,

furthermore, that instability due to large global displacements of the structure does not occur. This may yield an overestimation of the load carrying capacity, particularly if the structure is of a great physical size. At increased physical size, the requirements on the toughness properties of the material for fair applicability of the theory of plasticity increases and, furthermore, if the structure is assembled from large number of structural elements into a large slender structure the risk for instability due to large global displacements becomes significant.

A more obvious disadvantage of empirical interpolation formulas for the strength of structural elements is their limited range of validity. Thus, they may not be used if the design concerns uncommon qualities of materials, types of geometries or types of loads. Often the range of validity is not clearly defined, which can lead to mis-interpretation. In this case the influence of the absolute size of a structural element on its strength may serve as one example. Other examples may be some of the many relations between the compressive strength of concretes and other properties of concretes or its relation to the strength of structural elements: it may be that such relations are valid only as long as some other variable (in some cases perhaps the tensile strength) happens to be changed in accordance with some unique function of the compressive strength.

Other risks for miss-interpretation of empirical formulas concern their accuracy and estimations of the scatter in strength between nominally equal structural elements. To determine the accuracy of of an empirical formula, test data entirely independent of the test data used during the development of the formula and arbitrarily chosen within the claimed range of validity should be used. The mean deviation between the predictions of a formula obtained by means of regression analysis and the test data on which the formula is based, may not produce any valid information about the reliability and the accuracy of the formula and may not produce any valid information about the scatter in strength between nominally equal structural elements either. When developing empirical formulas intended for the use in building codes or elsewhere, it might be a good idea to separate the available test data into two independent parts: one part for use when developing of the formula, and the other part for use during the determination of the accuracy of the formula.

The third method of failure load prediction is based on experimental studies of the mechanical properties of the parts of structures or the parts of structural elements. The mechanical properties of the parts primarily concern their stress-deformation behaviour, but may also concern interaction between the state of stress and deformation and the temperature, transfer of mass and time dependent chemical or physical changes of the parts. In the case of concrete, the influence on the deformation of stress, temperature, content of moisture (shrinkage), continued hydration and lasting loads (creep) may serve as exemplifications. Although the method is primarily based on experimental studies of the stress-deformation behaviour of the parts, i.e. their stiffness properties, the method is usually called the theoretical method. Knowing the stiffness properties of the parts, it is in principle possible to calculate the load-displacement behaviour of any structure or structural element built up of such parts. The basic relations, i.e. equilibrium and geometrical compatibility between the parts, that enable these calculations form the basis for structural mechanics, see (Petersson and Thelandersson, 1982) or text-books on structural mechanics. Direct applications of this structural mechanics method seem to be rare. Instead the method is generalized:

The description of the properties of the parts may consern small or large parts of structures. From the point of view of generality it is thereby preferable to determine the properties of small parts, as, i.a., if the parts are small enough, i.e. infinitesimal volumes of the material, any structure may be regarded as being built up of such small parts and, furthermore, the state of stress and deformation of an infinitesimal volume can be defined with the help of a limited number of variables. Basically when using this wellknown generalized structural mechanics method, three tasks have to be faced: experimental investigations of the mechanical properties of specimens made of the studied material; development of a description of the mechanical properties of an infinitesimal volume of the material; and finally calculation of the mechanical properties of the assembled structures to be studied. These three tasks are usually not very easy to solve in practice and during applied analyses a number of simplifying assumptions normally have to be made. One advantage of the method is its generality: once the mechancial properties of the material have been defined it is in principle possible to obtain the properties of any structure made of this material by means

of theoretical calculations. Another advantage is the possibility to comparatively clearly define the bases and the simplifying assumptions that are adopted during an analysis.

Some of the difficulties involved in applied analyses by means of the actual generalized structural mechanics method may be mentioned. Ideally, the experimental investigations should regard the surface tractions (the stresses) acting on the specimen (of finite size) in all of the infinite number of possible kinematical boundary conditions, and, if not only the first part of the stress-deformation response is to be obtained, requirements regarding the stiffness and the stability of the testing-system must be met. The development of a description of the mechanical properties of a characteristic infinitesimal volume of material is bound to involve, sometimes tacitly, generalizations and assumptions: knowing the load-deformation behaviour of the parts of a structure, the behaviour of the structure can in principle be calculated, but if the behaviour of a structure or a specimen is known , the behaviour of the parts cannot be determined without the use of additional assumptions which may, or may not, reflect the true properties of the parts. Finally, the theoretical analysis of a structure assembled from infinitesimal parts involves an infinite number of degrees of freedom. Normally this makes it necessary to introduce artificial restrictions for the allowable distributions of stress or deformation within the structure. Such restrictions are characterized by, for instance, beam theory, plane stress, plane strain or, where finite element analyses are concerned, some certain choice of shape functions for the allowable distributions of the deformations within the finite elements.

The generalizations, assumptions and test results utilized during the development of descriptions of the mechanical properties of materials are summarized in material models. For a limited number of loading conditions, the validity and accuracy of such models can be tested indirectly by means of comparisons between theoretical results predicted by the model and experimental test results. In this way some models may be shown to be invalid or inaccurate, but, on the other hand, it is difficult, and probably impossible, to prove that a model is generally valid and accurate.

Most material models are formulated as a description of the characteristics of an infinitesimal volume of material. Taking into

account that the major part of a piece of material consists, on the atomic scale of size, of empty space, it is obvious that these material models don't give a valid description of the actual properties of an infinitesimal volume of the material. However, the applicability of material models seems to rest on a basic assumption: if the material model is capable of correctly predicting the behaviour of macroscopical finite pieces of the material, then the model is also capable of predicting the behaviour of larger specimens or structures built up of these finite pieces of the material, no matter whether the model gives a correct or erroneous description of the behaviour of the smaller parts of the macroscopical finite pieces of the material. As a result of this, an apparently trivial test of the possibilty for validity of material models may be formulated: the model must be such that it, together with the associated computational method for the analyses of assembled structures, can reproduce the very test results on which the description of the material properties is based. From this point of view, two methods for the description of the uniaxial tensile stress-deformation properties shall be studied in section 3.3.

When making the choice of simplification necessary for the applied analyses by means of the "theoretical" method, it may be of importance to take into account the goal of the analysis. Thus some differences between analyses of the pre-fracture behaviour of structures at normal service loads and the analyses of fracture and ultimate load carrying capacity may be noted. At the analyses of fracture and ultimate load carrying capacity: it is neccessary to know or make some assumption of the post peak stress behaviour of the material (provided that a peak stress is assumed to exist at some certain deformation); the material properties in a very small part of the structure may be decisive to the failure load of the entire structure; the deformations within the structure may become very irregular and localized; as more than one incremental change in the state of stress and deformation may satisfy the equations of equilibrium, material properties and geometrical compatibility, these basic equations of structural analysis may sometimes have to be supplemented with an equation for stability analysis of states of equilibrium. These features deviate from those of the analyses of the pre-fracture stiffness properties of structures. During such analyses the post peak stress behaviour of the material is of no consern; the simplifications adopted when describing the mean characteristic properties of the material might preferably be chosen differently; stresses and deformations within the structure are usually

smoothly distributed; and an incremental change in the load acting on the structure corresponds normally to only one possible state of stress and deformation within the structure that satisfies the equations of equilibrium, material properties and geometrical compatibilty.

In addition to the methods for failure load prediction discussed above, other more special methods are available. These methods are normally developed only for special applications and may be useful in such applications but are normally not intended to give a contribution to the development of general methods with a wide range of potential applicability, not restricted to some certain type of structural elements. Within the analysis of the propagation of sharp pre-existing cracks, the resistance curve method of different kinds may serve as an example of a special purpose method with a comparatively wide theoretically possible applicability. This method may be regarded as a kind of theoretical method, but is not based on a description of the stress vs deformation properties of the material. When the load carrying capacity is estimated very approximately by means of intuition, perpaps by someone not trained in engineering, the normal procedure may be to first estimate a probable kinematical failure mechanism and then estimate the magnitude of load corresponding to this mechanism. This method, sometimes very convenient and useful, may be regarded as a special method but may also be regarded as an application of the upper bound theorem of plasticity at the tacit assumption of ideal plastic stress vs deformation properties of the material.

It may also be appropiate to include some remarks with regard to failure load predictions by means of linear elastic fracture mechanics. On the one hand, this theory comprises and is to great extent based on an assumption of stress vs deformation properties of the material and might therefore be referred to the group above called the theoretical method of failure load prediction. On the other hand, the properties of materials assumed within this theory are obviously unrealistic (infinite tensile strength) to such an extent that this theory perhaps should be referred to the group of special methods, in particular as the theoretically possible applicability is limited to specimens with sharp pre-existing cracks. However, in spite of the unrealistic basic assumption the actual theory can sometimes be successfully applied during failure load predictions (but not during realistic studies of the fracture process in the material). Broberg (1982) has emphasized the importance and the central role of the Barenblatt

consept of atonomy or self-similarity in usually practiced conventional fracture mechanics and it seems that success during application of the linear elastic fracture mechanics basically rests on this autonomy. The autonomy means that the mechanical events within the fracture process region are only dependent of the properties of the material and are consequently, within each class of specimens, independent of the geometrical size and shape of the specimen. Autonomy is at hand if all relevant geometrical dimensions of the specimen are very large in comparison to some merely material property dependent characteristic length of the material. In such cases the mechanical events within a fracture region can be modelled in an unrealistic manner, provided that the same unrealistic approach is used both during interpretation of test results and during subsequent theoretical failure load predictions. This also means that the parameter that relates crack growth to external load can be chosen in different and rather arbitrary manners, e.g. theoretical stress or strain intensity, theoretical stress or strain at some point in the vicinity of the process region, theoretical crack opening angle, theoretical crack opening displacement, theoretical energy density or theoretical energy release rate.

It may be noticed that "brittleness" of a material is not (alone) decisive for successful application of linear elastic fracture mechanics, but instead the ratio between the "brittleness" and a relevant geometrical dimension of the specimen, e.g. the depth of the initial crack. The "brittleness" is primarily governed by a characteristic, or intrinsic, length of the material, but is also influenced by the shapes of the normalized stress vs deformation curves of the material. The importance of (large) dimensions for applicability of linear elastic fracture mechanics is well-known among fracture mechanics researchers, but, according to subsequent chapters, it also seems that the importance of (small) dimensions for applicability of the theory of (unlimited) plasticity may be equally great.

Most probably, for potential general applicability, methods of failure load prediction must, in one way or another, be based on a defined description and assumption of the stress-deformation properties of the material. The description of the stress-deformation properties might not necessarily refer to an imagined infinitesimal characteristic volume of the material, but this common approach seems convenient from a number of points of view. This approach is applicable to the macro level of size and

at this level the material may be described as being looked upon as quasi homogeneous. However, during the development of the material models it may be helpful to numerically model or to think of the material as a structure put together of elements or pieces of finite size. In some cases it might also be helpful to, in turn, consider these small finite parts as being built up of smaller finite pieces, reflecting the hierarchic structural nature of most materials. Modelling of the mechanical behaviour of the microstructure of materials may lead to a possibility to study the influence of the non-unifrom properties, the scatter in strength, the non-uniform fracture and the non-uniform forces within the microstructure at zero and non-zero external load. Such a modelling might provide a starting point for development of models of the macroscopical quasi homogeneous properties, and may facilitate the understanding of some of those properties of materials like concrete which are difficult to understand by intuition if the material is thought of as a continuous homogeneous medium. It may be of particular interest that consideration of non-uniform forces within the microstructure at zero external load should lead to a possibility to model permanent "plastic" deformations in materials built up of elastic and brittle pieces which accordingly, one by one, don't exhibit any plastic deformations. A numerical study of the tensile fracture and fracture localization in an idealized material built up at random of brittle bars with finite length has been presented by Burt and Dougill (1977).

A development towards more modulated models of the behaviour of materials and more efficient finite element methods for the numerical calculations, should reduce the need for extensive experimental investigations and purely statistical-empirical formulas for the strength of structural elements. However, also the so called theoretical methods of failure load prediction require experimental studies and experimental data: during the development of the material model; during the determination of required material property parameters; and finally during the verification of the validity and the accuracy of the theoretical method. In many cases, application of the theoretical methods of failure load prediction involve significant difficulties and drastic simplifications may have to be made. However, general relations, estimations and understanding obtained by means of theoretical studies are often very useful, also where the structural elements which can not be theoretically analysed in a modulated manner are concerned. As a matter of fact, some convenient general relations obtained with the help of theoretical studies are utilized and

generally accepted to such an extent that it may be easy to forget that the relations may be based on idealizing assumptions regarding the properties of the material.

---

3. MATERIAL MODELS FOR THE ANALYSIS OF FRACTURE INDUCED BY TENSILE STRESS

3.1 Introduction

This chapter deals with material models of tensile fracture and cracking, which are primarily intended for the analysis of concrete and similar non-yielding apparently brittle materials. The type of models dealt with are based on assumptions regarding the macroscopical mechanical properties of materials expressed with reference to a characteristic infinitesimal volume of the material, and the models dealt with are intended for use in quantitative strength analysis of structures, structural members and specimens.

Most of the sections in this chapter directly or indirectly concern the fictitious crack model. In Section 3.2 the model is described and discussed, material property parameters are surveyed and the stress field close to tip of the fracture zone is studied. In Section 3.3 strain instability and strain localization in uniaxial tension are studied. In Section 3.4 material models of tensile stress induced fracture, other than the fictitious crack model, are dealt with. Section 3.5 concerns some hypotheses regarding ultimate strength, and in Section 3.6 methods of applied numerical calculations by means of the finite element method are dealt with.

3.2 The fictitious crack model (FCM)

3.2.1 Introduction

Sections 3.2.2, 3.2.3 and 3.2.4 concern a description and discussion of the model in question, order of magnitude of material property parameters and the stress field close to the tip of the fracture zone, respectively.

Before describing the model, it may be appropriate to refer to some previous presentations of the actual model. Its name, "fictitious crack model", and its abbreviation, "FCM", was first used in a thesis by Modeer (1979), the first report in English that gave a description of the model was presented by Hillerborg (1978), and, before that, Hillerborg, Modeer and Petersson (1976) presented a numerical analysis of the flexural

strength of unreinforced concrete by means of the model which was later on called the fictious crack model. The comprehensive work by Petersson (1981) has also attracted attention to the model. The model was first used by Hillerborg (1973) in a Swedish compendium for a course about building materials and was intended to provide students with an interpretation of experimental results obtained by Evans and Marathe (1968). These experimental results regarded the load vs. deformation behaviour of a concrete specimen during direct stable uniaxial tensile loading.

Models more or less similar to the fictitious crack model were proposed before the fictitious crack model was proposed. Two such models are the Dugdale model and the Barenblatt model. It may be that the original features of the fictitious crack model are the rational macroscopical description of the fracture of the un-notched uniaxial tensile specimen and the assumption of analogy between this type of fracture and the behaviour of the fracture process region in front of a growing crack. Numerical analysis of a fracture process region by means of a stress vs. widening relation has been carried out previously: Andersson and Bergkvist (1970), and the model studied in this paper was suggested by prof B Broberg in 1968. In recent years the fictitious crack model and other similar models have been dealt with in a number of experimental and theoretical studies, and a large number of reports and papers have been prepared by a number of researchers. However, it is not the intention of this study to try to compile a list of these reports and papers.

3.2.2 Description and discussion

In this report the bases of the fictitious crack model are described in essentially the same manner as in the previous presentations of the model, see Section 3.2.1. The model is based on a description of the macroscopical behaviour of materials in uniaxial tension. Before peak load, see Fig 3.2 (1), the deformations along the specimen are assumed to be uniformly distributed, and the total elongation, $\Delta\ell$, of the specimen may be written as the total length of the specimen times the constant strain:

$$\Delta\ell = \ell\varepsilon \qquad (3.2{:}1)\ a)$$

At the moment of peak load, i.e. when $dP/d\Delta\ell=0$, a localized fracture zone

is assumed to start to develop. This fracture zone is not assumed to start to grow from any of the edges of the actual specimen in uniform tension, but is assumed to develop simultaneously across an entire cross-section. During further total elongation the stress along the specimen decreases and the parts of the specimen outside the localized fracture zone start to unload, i.e. both the stress and the uniform strain decrease according to the unloading branch in the stress vs. strain diagram of the actual material. Also in the localized fracture zone the stress decreases, but this zone is softening, not unloading, i.e. the stress decreases during increased deformation. After peak load, the total elongation of the specimen is the sum of the uniform deformation along the specimen, which is assumed to be proportional to the length of the specimen, plus the additional localized deformation within the fracture zone, w, which is assumed to be independent of the length of the specimen:

$$\Delta \ell = \ell \varepsilon + w \qquad (3.2{:}1)\ b)$$

During numerical calculations the fracture zone is assumed to be localized to a section with initially zero width. In reality the fracture zone is not a straight plane and in reality the fracture zone is also likely to have some extension along the specimen. However, as long as the total length of the uniform tensile specimen is greater than the extension of the fracture region, the assumed value of this extension is of no importance regarding the analysis of the global behaviour of the specimen.

For materials which are isotropic at the moment of peak stress, it is assumed that the fracture plane orientates itself perpendicular to the first principal strain in the actual infinitesimal volume of the material at the moment of peak stress. This orientation of the fracture plane is the only orientation that can be uniquely defined for an isotropic material in 1D state of stress. For materials which are orthotropic and for materials which become orthotropic before the fracture zone develops, no general assumption has been stated with regard to the orientation of the fracture zone.

Where the present numerical applications are concerned, the question of the orientation is rather theoretical as the orientation is assumed in advance. However, during the analysis of concrete and similar initially isotropic materials, the orientation has been chosen in accordance with estimations of the direction of the first principal strain. During a study

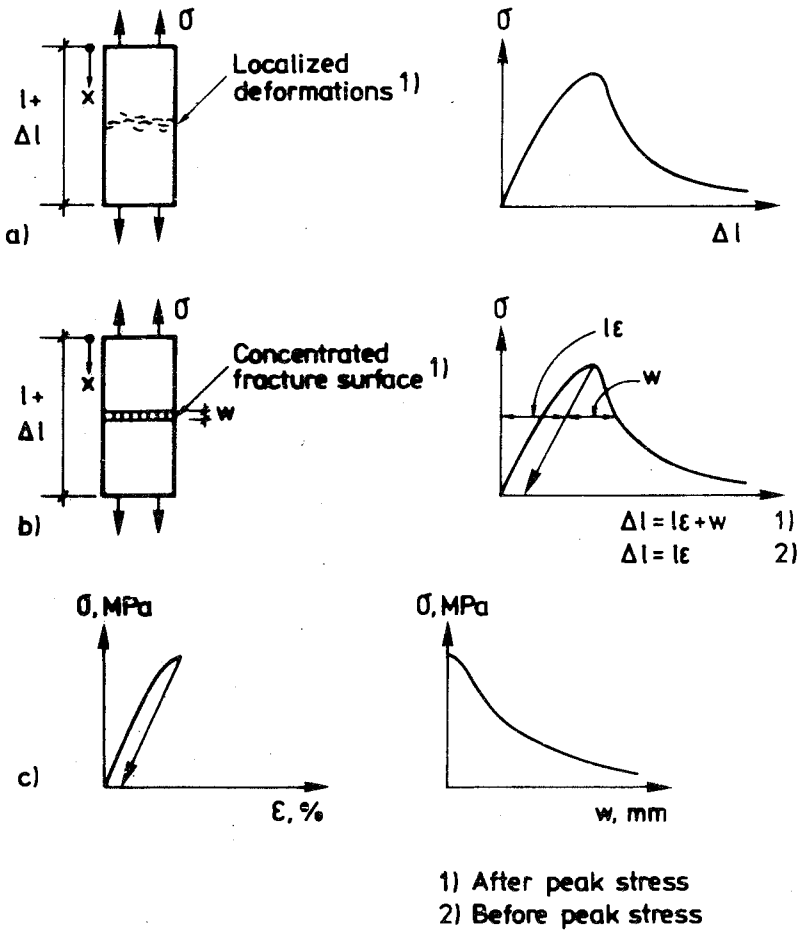

Fig 3.2 (1) Main characteristics of the fictitious crack model description of tensile fracture.
a) Possible realistic structural behaviour (concrete)
b) Model of structural behaviour
c) Model for description of the properties of the material

of wood, see Section 4.7, the orientation was chosen in accordance with the direction of the grain.

Eq:s (3.2:1) a) and b) are kinematical relations. In order to define the

mechanical properties of the material two relations are used: one stress vs. strain relation valid for the material outside the fracture zone and one stress vs. elongation relation valid for the fracture zone. Thus the σ vs. ε and the σ vs. w diagrams of the type shown in Fig 3.2 (1) c) are assumed to define the uniaxial tensile mechanical properties of the material. Both these diagrams may include unloading branches and the curves may be dependent on the loading speed, the loading history and the temperature, but are assumed to be independent of the shape and size of the specimen and are accordingly assumed to represent the mechanical properties of the material in the sense that they give a description of the local mechanical action of each infinitesimal volume of the material.

The description of the properties with reference to an infinitesimal volume, the assumption of local action and the consistent assumption of zero, or infinitesimal, initial width of the fracture zone are consistent with basic assumptions utilized in conventional continuum mechanics. However, the assumptions impose some restrictions with regard to the possibility of analysing all (hypothetical) types of uniaxial P vs. $\Delta\ell$ curves. Thus the assumptions suggest that the P vs. $\Delta\ell$ curves shown in Fig 3.2 (2) a) and b) cannot be interpreted by means of the fictitious crack model. In terms of the actual model, at point A in Fig 3.2 (2) a) a fracture zone develops in which the deformations are finite and at point B an infinite number of infinitely closely located fracture zones are predicted to develop. The sum of the deformations in these zones is infinite, which is in disagreement with the (hypothetical) uniaxial P vs. $\Delta\ell$ curve. It is not known whether any real material with essentially time and loading path independent properties can clearly behave as indicated in Fig 3.2 (2) a) or b) during a direct uniaxial tensile test of a uniform specimen. It might be that some fibre reinforced composites can behave in this manner, and during the transition from the elastic range to the plastic range mild steel seems to have some tendency towards such a behaviour. The types of P vs. $\Delta\ell$ curves indicated in Fig 3.4 (2) c) and d) can be interpretated by means of the fictitious crack model without any extension or modification of the model. Fig:s c) and d) are examples of curves where the first local maximum is also the global maximum, and Fig:s a) and b) are examples of curves where the first local maximum is not the global maximum.

During all numerical applications presented in this report, the σ vs. ε curve has been simplified to a straight line, i.e. before fracture a linear

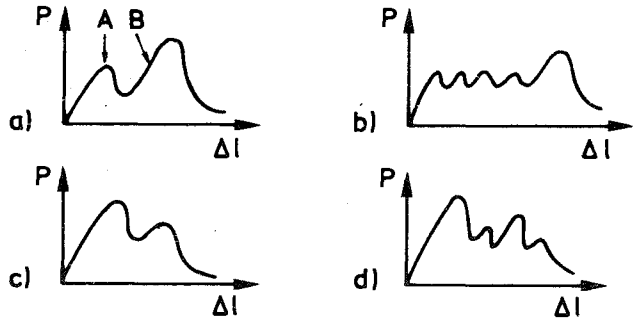

Fig 3.2 (2) Hypothetical P vs. $\Delta\ell$ curves with multiple maxima for materials in direct uniaxial tension.
a) and b) contradict the fictitious crack model
c) and d) do not contradict the fictitious crack model

elastic behaviour of the material is assumed, Fig 3.2 (3) a). Where the σ vs. w curve is concerned, several different shapes have been applied. However, in most of the calculations either the simple straight line shape, Fig 3.2 (3) b), or the bi-linear shape, Fig 3.2 (3) c), has been used. The bi-linear shape has been developed by Petersson (1981) on the bases of experimental tests of different qualities of concrete and seems to be a reasonable approximation for this type of material: see Fig 8.15 in Petersson (1981). All the σ vs. w curves applied in this report are linear, bi-linear or multi-linear. The division of the curve into linear pieces have been adopted in order to facilitate the numerical calculations. Non-linear σ vs. w curves with a continuous variation in $d\sigma/dw$ for $w>0$ have been applied by Nilsson and Oldenburg (1982) and Glemberg (1984) ($\sigma/f_t = e^{-cw}$), and by Catalano and Ingraffea (1982), Ingraffea, Gerstle, Gergely and Saouma (1984) and Ingraffea and Gerstle (1984) ($\sigma/f_t = C_1/(C_2+w)+C_3+C_4 w$), and by Reinhardt (1984) ($\sigma/f_t = 1-(w/c_1)^c$).

The non-linear curves mentioned above have a $d\sigma/dw<0$ for $w=0$. However, it may be more realistic to assume a non-linear curve so that $d\sigma/dw=0$ for $w=0$, and recently Gopalaratnam and Shah (1984) have proposed a such non-linear curve ($\sigma/f_t = e^{-cw^{1.01}}$). One of the piece-wise linear curves presently applied has $d\sigma/dw=0$ for $w=0$.

A $d\sigma/dw>0$ for $w=0$ seems to contradict the basic assumptions of the

fictitious crack model. However, if a material such as concrete, within which the strength is most likely scattered, is modelled on the assumption of deterministic properties of the material, it may be argued that a σ vs. w curve with $d\sigma/dw>0$ for w=0 may provide a better description of the true behaviour of the uniform uniaxial tensile specimen. If one considers the influence of scatter, one may also arrive at the conclusion that the σ vs. ε and the σ vs. w curves are size dependent, i.e. dependent of the length of the specimen. One may imagine that a number of specimens with reasonably scattered P vs. $\Delta\ell$ curves are assembled into a chain and then the assembled long specimen pulled and the recorded P vs. $\Delta\ell$ curve used for evaluation of the σ vs. ε curve and the σ vs. w curve. For a resonable scatter, such an imagined test may suggest that the recorded σ vs. ε curve becomes more and more linear at increased length of the specimen, that great strains become concentrated to the subsequent fracture region before peak stress (for experimental verification of this suggestion, test results presented by Heilman, Hilsdorf and Finsterwalder (1969) might be relevant), and, of course, that the mean tensile strength decreases at increased length.

The simplified σ vs. w curves shown in Fig 3.2 (3) are normalized into dimensionless stress vs. elongation curves: σ/f_t vs. $w/(G_F/f_t)$. f_t is the tensile strength of the material and G_F is the fracture energy of the material. By definition, G_F is equal to the area under the σ-w curve:

$$G_F = \int_0^\infty \sigma(w)\, dw \qquad (3.2:2)$$

G_F may be expected to be equal to the total work carried out by the external force, P, divided by the area of the fracture section only if (1) the material outside the single tensile fracture zone behaves in a linear or non-linear elastic manner, if (2) no energy is lost in the loading arrangement in between the points where force and elongation is measured, if (3) no initial stresses within the specimen, e.g. shrinkage stresses, are released during the test, if (4) the test is stable and if (5) P is the only force that carries out work (in particular, work carried out by dead-weight may not always be negligible).

It might be questioned why w is normalized to G_F/f_t instead of to, for example, the value of w that corresponds to σ=0, w_c. It seems, however, that G_F is often a suitable and convenient parameter: (1) while it is rather difficult, and for some materials probably even impossible, to

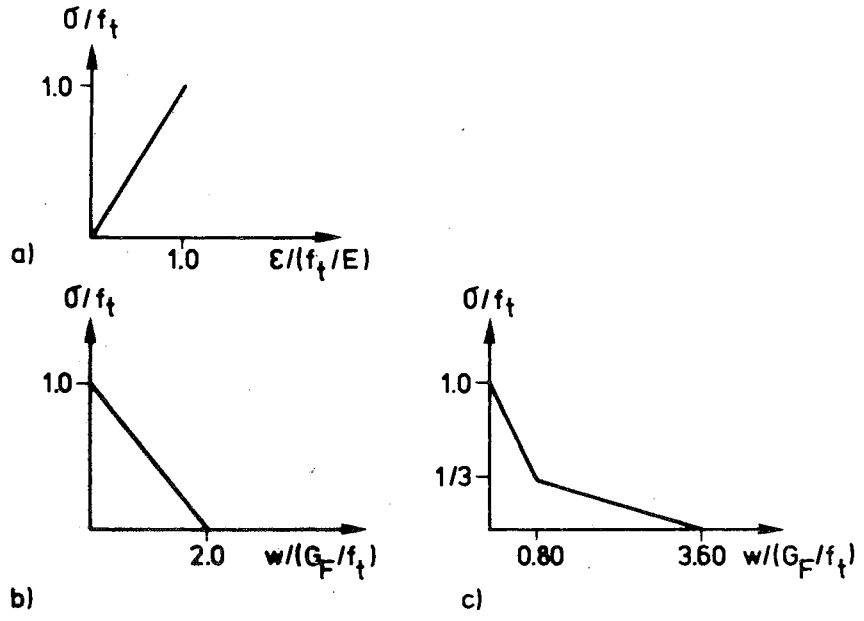

Fig 3.2 (3) Simplified material property curves.
a) σ vs. ε , linear elastic
b) σ vs. w, straight line (SL)
c) σ vs. w, bi-linear, concrete (C)

carry out stable direct tensile tests, the value of G_F can often be determined rather easily by means of ordinary testing equipment; (2) it is difficult to obtain and define any accurate value of w_c as, at least in the case of concrete, it seems that $d\sigma/dw$ is close to zero when σ approaches zero: (3) for very large specimens with deep pre-existing cracks, G_F corresponds to the parameter G_c of linear elastic fracture mechanics, and for such specimens the ultimate load is proportional to the square root of G_F, but is independent of the shape of the σ vs. w curve and also independent of the (small) value of w_c.

Eq (3.2:1) b) indicates that $\Delta\ell$ is not proportional to ℓ after peak stress. This suggests that it is not very useful to present experimental or theoretical data regarding the softening behaviour of materials in terms of σ vs. $\Delta\ell/\ell$, unless the gauge length, ℓ, is indicated. This also means that it is difficult to compare theoretical results to experimental data

regarding the "total mean strain" across a propagating fracture zone if the gauge length is unknown.

The two basically most essential requirements for validity of the fictitious crack description of the tensile fracture are that a descending branch in the P vs. $\Delta\ell$ behaviour exists and that the fracture takes place within a localized fracture zone. The existence of a descending branch in the tensile P vs. $\Delta\ell$ behaviour of materials, in particular an apparently brittle material like concrete, might contradict intuition, but has been verified in a number of direct experimental tests on concrete: Hughes and Chapman (1966), Evans and Marathe (1968), Petersson (1981), Gylltoft (1983), Reinhardt (1984), Gopalaratnam and Shah (1984), and maybe also by others. A complete P vs. $\Delta\ell$ curve for rock (sandstone) in uniaxial tension may be found in Krech and Chamberlain (1974). The requirement that the fracture is localized and accordingly that the deformation behaviour inside and outside the fracture region, respectively, are entirely different after peak stress, is supported by experimental results presented by Heilman, Hilsdorf and Finsterwalder (1969) and is also supported by theoretical arguments of the type dealt with in Section 3.3. In addition this matter may be supported by intuition: it is easy to imagine that a specimen in tension will fracture into exactly two pieces, separated by a single localized fracture section which finally attains zero strength without any simultaneous decrease in the strength of the two pieces.

During application of the model in question to the analysis of other specimens than the uniform tensile specimen, it is simply assumed that each infinitesimal volume of the material behaves and fractures as in uniaxial tension. This means that the maximum principal stress criterium is used for start of fracture, and that the σ vs. ε and σ vs. w relations are not influenced by the 2D or 3D state of stress. For concrete and similar materials, these assumptions should be reasonable as long as the absolute value of the smallest principal stress is less than about 3 or 4 times the uniaxial tensile strength of the material. The treatment of each infinitesimal volume of the material as being in the state of uniaxial tension, also means that the effect of possible rotations of the principle direction of the deformation within the fracture zone are not taken into account. If the specimen, the load or the fracture zone propagation path is such that this direction rotates, then shear stresses are very likely to develop across the fracture zone and the normal tensile stress is also

very likely to be affected. However, no assumption has been made with regard to the description of this effect. Rather obvious extensions of the model would be to take into account the influence of the 2D or 3D state of stress on the σ vs.ε performance, the fracture criterion and the σ vs. w performance, and to take into account the influence of possible rotation in the direction of deformation by means of relations which in the simplest case are of the type $\sigma = \sigma(w_\perp , w_{||})$ and $\tau = \tau(w_\perp , w_{||})$, where $w_\perp$ and $w_{||}$ are the deformations of the fracture zone perpendicular and along the fracture plane, respectively, and where σ and τ are the normal and shear stresses across the fracture plane. These extensions might perhaps not involve any difficulties in principle, but may involve significant difficulties when it comes to the experimental determination of the actual material properties and to applied numerical calculations.

The fictitious crack model has been described and discussed above in a rather engineering-like manner. An other fairly similar model has been described in a more mathematical manner by Bazant and Oh (1981) and Bazants and Oh (1983).

From the analogy between a tensile specimen and a beam in bending, it is rather obvious that the structural behaviour of a beam and the moment vs. deformation properties of a section of a beam may be described by means of one moment vs. curvature curve and one moment vs. rotation curve in the manner indicated in Fig 4.2 (18). This type of description is linked to beam-theory (and slab-theory) and is accordingly not estimated to be very suitable for analysis of in-plane interaction between closely located fracture zones. A quantitative difference between a concrete specimen in uniaxial tension and a beam in uniform bending is that the behaviour of the tensile specimen is probably not very much affected by constraints (plane stress or plane strain) perpendicular to the specimen, while the behaviour of the beam is probably significantly dependent on whether the normal force is zero or the elongation is zero. This may make a difference of importance between the analysis of in-plane loaded plates (by means of plane stress or plane strain theory) according to the principles of Fig 3.2 (1) and possible analysis of perpendicular to plane loaded plates (by means of slab-theory) according to the principles of Fig 4.2 (18).

3.2.3 Order of magnitude of material property parameters

Within the fictitious crack model, the properties of the material are defined by means of one stress vs. strain relation and one stress vs. widening relation. If the shapes of these two curves are known, then the curves can be described by means of three parameters. During all the present analyses, the material is assumed to behave in a linear elastic manner before fracture (ν=0.2 and plane stress) and the maximum principal stress fracture criterium is adopted. This makes it natural to choose the three following parameters: (1) tensile strength, f_t, (2) modulus of elasticity, E, and (3) fracture energy, G_F.

These material parameters govern the strength, fracture and deflection properties of structures built up from the actual material. If only the strength of the structure or specimen is to be studied, then the absolute values of the stiffness properties of the material are of no importance, only the strength, f_t, and a measure of the ratio between the slope of the σ vs. ε curve and the slope of the σ vs. w curve. The slope of the σ vs. ε curve is E and a general measure of the slope of the linear or non-linear σ vs. w curve is $f_t/(G_F/f_t)$. Thus a measure of the ratio between the slopes of the two curves is EG_F/f_t^2. This ratio has the dimension length, and is called the characteristic length of the material and is denoted ℓ_{ch}.

ℓ_{ch} is an intrinsic material length parameter and may be looked upon as a measure of the brittleness of the material during fracture. ℓ_{ch} governs the size of the fracture process zone and, together with f_t, it governs the strength of specimens with and without initial cracks. The value of ℓ_{ch} is of significance regarding the choice of suitable method of strength analysis (please see Sections 3.4 and 3.5 and other parts of this report), and a low value of ℓ_{ch} suggests that the load carrying capacity of the specimen or structure is sensitive to notches and initial cracks.

In Fig 3.2 (4) approximate values of ℓ_{ch} ($\equiv EG_F/f_t^2$), f_t, E, G_F, $\sqrt{EG_F}$ and G_F/f_t for some different types of building materials have been compiled. For large specimens with deep initial cracks, $\sqrt{EG_F}$ corresponds to the linear elastic fracture mechanics strength parameter K_c. G_F/f_t is a measure of the width, or opening, of the fracture zone: for the linear and bi-linear shapes of the σ-w curve (Fig 3.2 (3)), the opening that corresponds to zero stress is $2G_F/f_t$ and $3.6\ G_F/f_t$, respectively. It should be noted that the values indicated in Fig 3.2 (4) are approximate and that

they are only intended to provide a survey of the order of magnitude. The values of the parameters may also be significantly different for different qualities of the same type of material. In addition, the shapes of the σ vs. ε and σ vs. w curves are not the same for the different types of materials. Thus, for instance, the shape of the σ vs. w curve of steel fibre reinforced concrete is normally quite different from that of plain concrete. Similarly, the shape of the σ vs. ε curve of steel is often quite different from that of concrete. Steel may have a very strongly non-linear σ vs. ε curve and the indicated value of E corresponds to the stiffness during unloading. For estimation of the size of the fracture zone, this value of E is probably more appropiate than the secant modulus.

Material	ℓ_{ch} mm	f_t MPa	E MPa	G_F N/m	$\sqrt{EG_F}$ MPa$\sqrt{m}$	G_F/f_t mm
Steel fibre concrete	30000.	4.	30000.	15000.	20.	4.
Glass fibre mortar, new	4000.	8.	25000.	10000.	15.	1.3
Glass fibre mortar, aged	1000.	5.	25000.	1000.	5.	.2
Concrete	400.	3.5	35000.	140.	2.	.04
Mortar	120.	3.5	25000.	60.	1.	.02
Wood fibre board	120.	7.	4000.	1500.	2.	.2
Sandstone	100.	.7	5000.	10.	.2	.014
Gypsum	20.	1.	4000.	5.	.14	.005
Steel	20.	1000.	200000.	100000.	150.	.1
Glass fibre/polyester	15.	140.	12000.	25000.	20.	.2
Marble	15.	20.	80000.	75.	2.	.004
Wood, perpend. to grain	10.	4.	500.	400.	.5	.1
Cement paste	10.	4.	10000.	15.	.5	.004
Aerated concrete, 300 kg/m^3	10.	.5	800.	3.	.05	.006
Aerated concrete, 600 kg/m^3	10.	1.2	1700.	10.	.15	.008
Carbon fibre/epoxy laminate	8.	600.	70000.	40000.	50.	.07
MDF cement paste	.6	100.	40000.	140.	2.	.0014
Plexiglas	.5	70.	7000.	400.	2.	.006
Glass	.5	30.	75000.	5.	.6	.0002

Fig 3.2 (4) Order of magnitude of fracture mechanics material property parameters. The values of the parameters may be significantly different for different qualities of the same type of material.

Fig 3.2 (4) has been compiled from estimations which are based essentially on data presented in the following references: Gustafsson (1977) (steel fibre concrete, glass fibre concrete and lightweight concrete), Helmersson (1978) (wood fibre board, wood, gypsum and plexiglass), Petersson (1981) and Hillerborg (1983) (concrete), Petersson (1982) and Alford, Groves and Double (1982) (MDF Cement paste, i.e. macro defect free cement paste, i.e. extremely high strength cement paste), Modeer (1979) (mortar and paste), Hillerborg (1980) (paste, glass), Aronsson (1984) (glass fibre polyester and carbon fibre/epoxy laminate), Krech and Champerlain (1974) (sandstone) and Ouchterlony (1981) (marble).

3.2.4 Stress and displacement close to tip of fracture zone

According to the fictitious crack model a drastic change in the mechanical behaviour of the material takes place at the tip of the fracture zone, particularly if the stress-strain curve is assumed to be linear. At the tip of the fracture zone the deformation changes from relative strain to absolute deformation and in addition the tangential stiffness of the material changes from positive to negative. This invokes the suspicion that the distribution of stress and displacement may not be very smooth close to the tip of the fracture zone and it has also been put into question whether or not it is theoretically possible for a finite non-zero stress to exist exactly at the tip of the fracture zone. Consequently it may be difficult to study the detailed performance very close to, and within, the tip of the fracture zone by means of numerical methods.

The question whether or not it is possible to define and calculate a state of stress exactly at the tip of the fracture zone is, of course, of great importance on grounds of principle and is also of an apparently somewhat confusing nature. In the Barenblatt description of a self-similar fracture zone, a non-zero finite stress at the tip is proposed, but subsequent authors have refered to this finite stress in the Barenblatt description as being a postulate and consequently not as necessarily being a consistent result of assumptions regarding the mechanical properties of materials.

The stresses (the tractions) acting across the fracture zone may formally be regarded as a load acting on the specimen, and the stresses within the specimen may then be calculated as a linear combination of the stresses

produced by the tractions across the fracture zone and the stresses produced by the external load. However, at zero tractions the external load produces an infinite stress at the tip of the fracture zone, and at zero external load the tractions produce an infinite (negative) stress at the tip of the fracture zone. A reason for misleading confusion may then be that the actual external load at equilibrium may be regarded as being calculated by means of an equation where these two infinite stresses are added and put equal to a certain finite value, i.e. the tensile strength of the material. During applied finite element calculations, the two stresses do not become infinite, but - which also may be a reason for misleading confusion - the two stresses become greater and greater without any limit during refinement of the finite element mesh. (Where convergency during mesh refinement is concerned, please see Section 3.6.4)

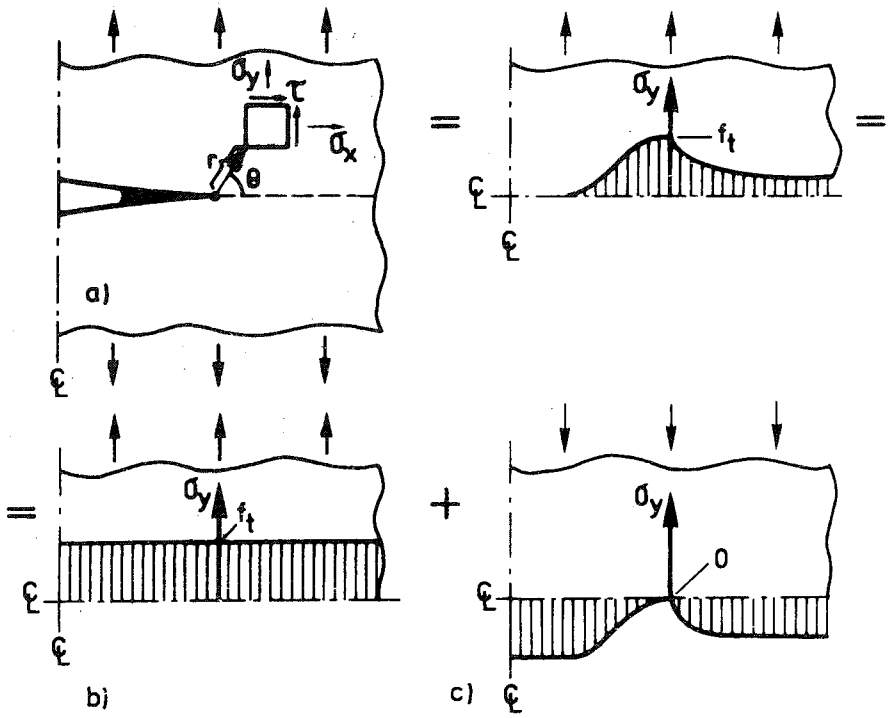

Fig 3.2 (5) A fracture zone in a plate and the dividing up of stresses.

In order to understand the performance close to the tip of the fracture zone, the fundamental case of an infinite centre cracked plate, Fig 3.2 (5) a), is studied. It [illegible] results of such a

study for other cases of loading. The stress acting across the fracture zone is regarded as an external load, and the loading case shown in Fig 3.2 (5) a) is separated into the two cases of loading shown in Fig 3.2 (5) b) and c). Case b) corresponds to a uniform tensile stress distribution: $\sigma_y \equiv f_t$ and $\sigma_x \equiv \tau \equiv 0$. In case c) the σ_y component of stress is zero at the tip of the fracture zone.

The separation into two cases of loading is possible because the material outside the fracture zone is linear elastic. However, validity of the separation requires that the total opening of the fracture zone and the crack proves to be greater than, or equal to, zero. Validity of this trivial assumption is evident from the subsequent results regarding the distribution of displacements.

In addition, in the actual figure the stress in the tip is put equal to f_t. According to the material property description, the stress in the tip may have any value less than, or equal to, f_t. Presently the common and interesting case when the stress in the tip is equal to f_t will be dealt with, but an analogous discussion should be possible to carry out also for any smaller positive stress in the tip. Such smaller stresses may develop during cyclic loading. The actual assumption regarding the stress in the tip requires that the principal stress in no point in the vicinity of the tip proves to be greater than f_t. Validity of this assumption is evident from the subsequent results regarding stress distribution.

For case c), it is now, as a temporary guess, assumed that $\sigma_y = 0$ not only exactly in the tip but also along a non-zero distance behind the tip. For case c), this means that the general linear elastic results regarding the stress and displacement close to a tip of a crack, eq (3.4:1) and eq (3.4.2), are applicable in a small vicinity of the tip. In these relations $a_1 = 0$ as $\sigma_y = 0$ in the tip. Taking into account only the dominating terms in the actual relations and then adding case b) to case c), the following result is obtained:

$$\begin{cases} \sigma_x = \sigma_{xo} - \sqrt{r}\,\dfrac{3a_3}{4}\{5\cos(\theta/2)-\cos(-3\theta/2)\} + \ldots \\ \sigma_y = f_t - \sqrt{r}\,\dfrac{3a_3}{4}\{3\cos(\theta/2)+\cos(-3\theta/2)\} + \ldots \\ \tau = r\,4a_4\sin\theta + \ldots \end{cases} \qquad (3.2{:}3)$$

σ_{xo} is identical to $-4a_2$. Where the components of displacement in the x- and y-directions, u and v, are concerned the following result is obtained in the case of plane stress. The actual coordinate system is fixed by u=v=0 in the point r=0 and by v=0 along the line $\theta=0^0$.

$$\begin{cases} u = \frac{1}{E}\{r(\sigma_{xo}-\nu f_t)\cos\theta - \\ \qquad r^{3/2}a_3\{(7/2-\nu/2)\cos(3\theta/2) - (3/2+3\nu/2)\cos(-\theta/2)\} + \ldots \\ v = \frac{1}{E}\{r(f_t-\nu\sigma_{xo})\sin\theta - \\ \qquad r^{3/2}a_3\{(5/2-3\nu/2)\sin(3\theta/2)+(3/2+3\nu/2)\sin(-\theta/2)\} + \ldots \end{cases} \qquad (3.2{:}4)\ a)$$

In the case of plane strain:

$$\begin{cases} u = \frac{1+\nu}{E}\{r(\sigma_{xo}(1-\nu)-\nu f_t)\cos\theta - \\ \qquad r^{3/2}a_3\{(7/2-4\nu)\cos(3\theta/2)-3/2\cos(-\theta/2)\} + \ldots \\ v = \frac{1+\nu}{E}\{r(f_t(1-\nu)-\nu\sigma_{xo})\sin\theta - \\ \qquad r^{3/2}a_3\{(5/2-4\nu)\sin(3\theta/2)+3/2\sin(-\theta/2)\} + \ldots \end{cases} \qquad (3.2{:}4)\ b)$$

The fracture zone widening, w, is equal to 2v ($\theta=180^0$). Thus, according to eq (3.2:4) the fracture zone widening in the close vicinity of the tip of the fracture zone is:

$$w = \frac{1}{E} 8a_3 r^{3/2} \qquad \text{at plane stress} \qquad (3.2{:}5)\ a)$$

$$w = \frac{(1-\nu^2)}{E} 8a_3 r^{3/2} \qquad \text{at plane strain} \qquad (3.2{:}5)\ b)$$

To investigate whether the above temporary guess for the loading case of Fig 3.2 (5) c) is valid, it may now be checked if both eq (3.2:3) and eq (3.2:4) (or eq (3.2:5)) together with the constitutive equation of the fracture zone give $\sigma_y = f_t$ and $\partial\sigma_y/\partial r=0$ when $r\to 0$ at $\theta=180^0$. (3.2:3) gives $\sigma_y \equiv f_t$ at $\theta=180^0$ and consequently that $\partial\sigma_y/\partial r=0$ at $\theta=180^0$. If the constitutive equation is $\sigma_y=f(w)$ then, for $\theta=180^0$, (3.2:5) gives (at plane stress):

$$\sigma_y = f(w(r)) \tag{3.2:6}$$

$$\frac{\partial \sigma_y}{\partial r} = \frac{\partial (f(w(r)))}{\partial r} = w^{1/3} \; \frac{3}{2}\left(\frac{8a_3}{E}\right)^{2/3} \frac{df(w)}{dw} \tag{3.2:7}$$

Consequently it is required that the σ-w curve is as follows:

$$f(w) \to f_t \qquad \text{when } w \to 0 \tag{3.2:8}$$

$$w^{1/3} \frac{df(w)}{dw} \to 0 \qquad \text{when } w \to 0 \tag{3.2:9}$$

These conditions for validity of eq:s (3.2:3) to (3.2.5) close to the tip of a fracture zone do not impose any very strong limitations on the shape of the σ-w curve: sufficient conditions are that the peak stress in the σ-w curve coincides with the peak stress in the σ-ε curve and that the slope of the σ-w curve (at small w) is finite.

The phrases "close to the tip" and "in the vicinity of the tip" are used above to describe the currently studied region, but no exact definition of the size of this region can be given. However, the important thing is not the size of the region but the knowledge of the existence of such a region in the vicinity of the tip, including the tip, in which eq:s (3.2:3) and (3.2:4) are valid. If the region is made extremely small, then these relations should be exact, and if relations are applied during calculation of stress or displacement at an increasing distance from the tip, then the result will become more and more approximate.

As an iterative calculation, eq (3.2:3) gives the first order result regarding the stress across the fracture zone, i.e. $\sigma_y = f_t$ at $\theta = 180^o$, while the second order result can be obtained by means of eq (3.2:5) together with the constitutive equation for the behaviour of the fracture zone. For the stress across the crack propagation path this gives:

$$\sigma_y = f_t + \frac{8a_3 r^{3/2}}{E} \frac{df(w)}{dw} \qquad \text{for } \Theta = 180^o \tag{3.2:10 a)}$$

$$\sigma_y = f_t - 3a_3\sqrt{r} \qquad \text{for } \Theta = 0^o \tag{3.2:10 b)}$$

$df(w)/dw$ is the slope of the σ-w curve for small w and the result for $\theta = 0^o$ is taken from eq (3.2:3). The above eq (3.2:10) a) is valid for plane stress.

The discussion a[illegible] an infinite

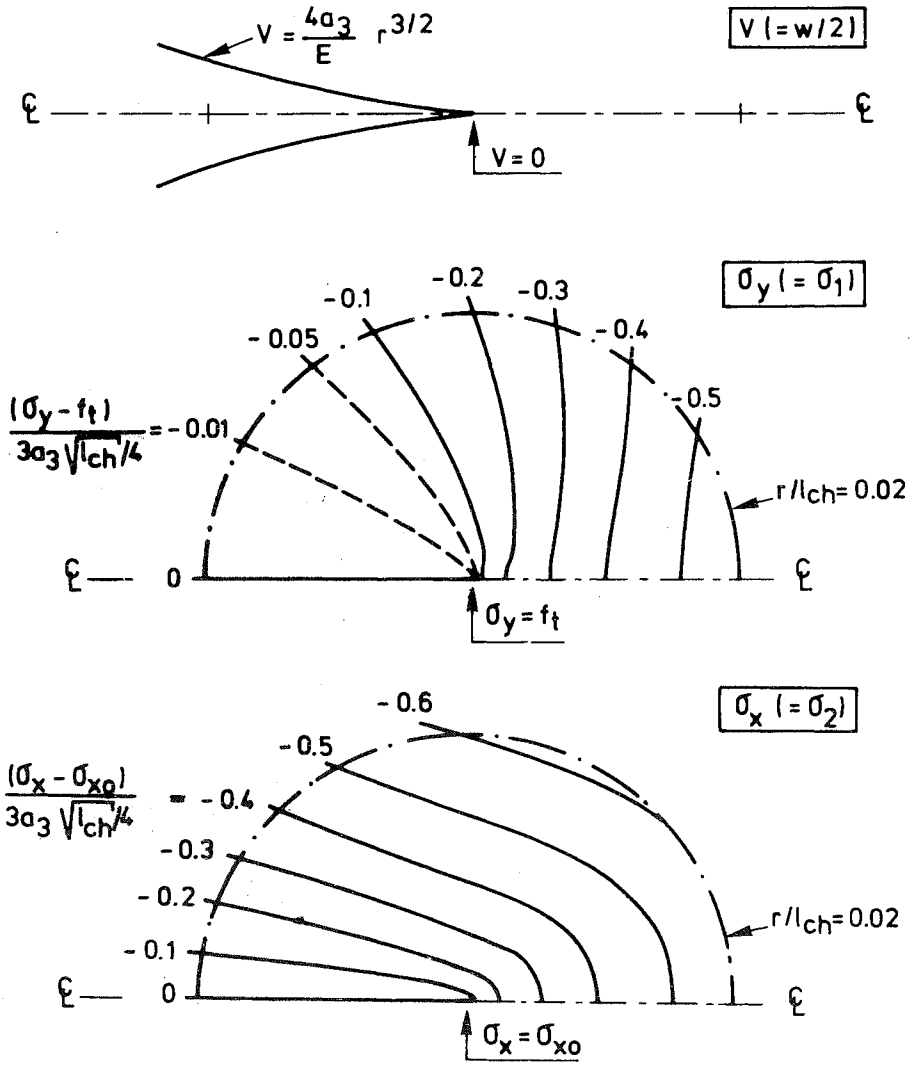

Fig 3.2 (6) Theoretical fracture zone opening displacement (plane stress) and stress distribution in the close vicinity of the tip of fracture zones (acc to dominating term in series expansion).

centre-cracked plate in tension, but it is probable that the above relations regarding the shape of the distribution of stress and displacement close t [illegible] ode 1 fracture.

The above discussion can be repeated for all cases where a dividing up of the stresses can be made in a similar manner as shown in Fig 3.2 (5). For other types of external loading it is probable that the actual shapes of the stress and displacement distribution are still valid as one may expect a self-similarity of the behaviour of the material in the close vicinity of the tip as long as this close vicinity is small in comparison to the length of the fracture zone and also small in comparison to the distance to boundaries of the specimen and the points where load is applied.

The distribution of stress, eq (3.2:3), and the displacement in the y-direction at $\theta = 180^{o}$, i.e. the fracture zone opening displacement, eq (3.2:5), are illustrated in Fig 3.2 (6). In eq (3.2.3) it can be noticed that σ_x and σ_y dominate over the shear stress, τ. Even if $\sigma_{xo} = f_t = 0$, σ_x and σ_y are dominating over τ at small r as $\sigma_x - \sigma_{xo}$ and $\sigma_y - f_t$ are both proportional to $\sqrt{r}$, while τ is proportional to r. This means, if $\sigma_y \geq \sigma_x$, that the first principal stress, σ_1, is equal to σ_y and that the second principal stress, σ_2 is equal to σ_x. The shape of the fracture zone opening illustrated in Fig 3.2 (6), i.e. $w \sim r^{3/2}$, is consistent with the rather well-known result presented by Barenblatt (1963). In particular, Barenblatt demonstrated that the faces of a crack must close smoothly.

Eq (3.2.3) (and eq (3.2:10)) produce interesting information about the stress field and some particular features may be noticed. At the tip of the fracture zone σ_x and σ_y are finite and the shear stress is zero. For $\theta \neq 180^{o}$, the gradient in σ_x and σ_y approaches infinity very close to the tip, and in the tip the stress distribution breaks. When $r \to 0$, the same limit values for the components of stress are obtained for all θ. The directions of the principal stresses, σ_1 and σ_2, are the same for all θ, and these directions coincide with the orientation of the actual mode-1 fracture zone. At any constant (small) distance from the tip, σ_y has its smallest, not greatest, magnitude in front of the fracture tip, i.e. at $\theta = 0^{o}$. The ratio between σ_y and σ_x in the tip of the crack is not restricted to having some certain value, but is dependent on the global geometry of the specimen and the type of the loading. In most cases one may expect $\sigma_y > \sigma_x$, but in some case one may expect $\sigma_x \geq \sigma_y$. $\sigma_x > \sigma_y$ means that the mode-1 fracture zone will start to try to grow perpendicular to the previous direction. This will activate shear stresses in the fracture zone and the subsequent crack propagation path may become curved. An example of a specimen where σ_x may become greater than σ_y is the double cantilever beam. It is poss

; during mode-1

fracture mechanics tests by means of the double cantilever beam. In order to attain the desired crack propagation along the symmetry line of this specimen, one may have to pre-stress the specimen in the x-direction: an example may be found in Fig 4.4 (1).

The above mentioned features of the stress field produced by the fictitious crack model may be compared to the corresponding features of the stress field produced by the linear elastic fracture mechanics, eq (3.4:1). This theory predicts an infinite stress in the tip and instead a finite measure of the stress is obtained from the limit value of the stress times $\sqrt{r}$, when $r \to 0$. Furthermore, this measure has no limit value in its truer sense as it approaches different values for different θ, and is therefore defined as the limit along a certain line, i.e. along $\theta = 0^{o}$. The shear stress is not predicted to be zero in the region $r \to 0$, and the direction of the first principal stress is different for different θ. These matters may give rise to confusion during theoretical analyses by means of the linear elastic fracture mechanics, particularly if the stress field is utilized during the prediction of the crack propagation path. Approaches for the prediction of the propagation path based on some direction of the first principal stress, based on the point of the maximum first principal stress in the vicinity of the tip or based on energy density in the vicinity of the tip have been proposed. It is, however, probable that such approaches may be successfully applied in a majority of cases only if they simply predict that the mode-1 crack will continue to grow straight ahead. But then it is difficult to explain possible deviations from this path. With regard to the prediction of the subsequent propagation path of a mode-1 crack, the basic difference between eq (3.2:3) and linear elastic fracture mechanics is that the stress in the tip is described by two variables σ_y and σ_x, and only one variable (the stress intensity factor), respectively.

Eq (3.2:3) and eq (3.2:4) are difficult to verify or demonstrate by means of the results of numerical calculations. This is due to the break in the stress field at r=0 and the infinite gradient in stress when $r \to 0$ (at $\theta \mp 180^{o}$). However, in order to attain some verification and also in order to illustrate the analytical and numerical fields of displacement and principal stress, the three point bend beam shown in Fig 3.2 (7) is analysed by means of the finite element method. The beam is initially unnotched and at the studied moment of fracture zone propagation, the tip of the fracture [illegible] beam, i.e. the node

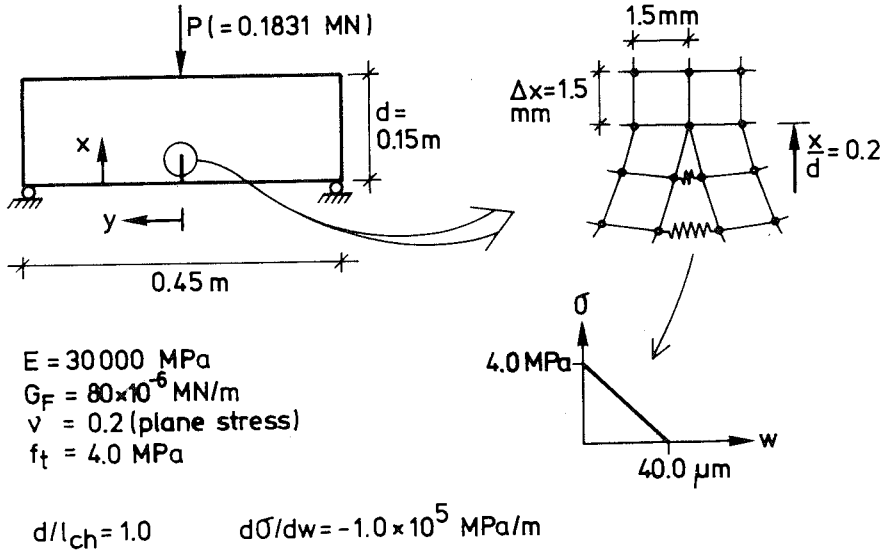

Fig 3.2 (7) Characteristics of the specimen (short un-notched beam with the width, b, =1.0 m) used during a finite element verification of the performance close to the tip of a fracture zone. A fine finite element mesh is applied close to the tip. Total number of elements in x-direction = 50, and in y-direction 28 (symmetrical half).

along the centre line of the beam located at x/d=0.2000 is the first node which is not opened and in which a fracture zone modelling spring is not inserted. In this node, the nodal force divided by $b\Delta x$ is equal to f_t. The calculation is carried out with the help of an easy-to-use finite element program developed by Petersson and Bäcklund (1973) for linear elastic analysis of plates. The parts of the beam outside the fracture zone are modelled by the rectangular 4-node plane stress element of Turner, Clough et al., presented in 1956. This element has, in particular, the ability to represent exactly pure bending, free of shear strain.

Eq:s (3.2:3), (3.2:4) and (3.2:10) give information about the shape of the distribution of stress, displacement and stress across the symmetry line of the beam in the vicinity of tip, but give no information about the location of the tip and the numerical values of $\sigma_{...}$ and a_2. These unknown

factors can be obtained by substitution of stress, displacement and/or nodal forces in the analytical relations. Presently eq (3.2:10) and the calculated nodal forces are utilized to obtain the location of the tip (indicated by Δr) and the numerical value of a_3, valid for the actual example. The sum of the nodal forces in the vicinity of the tip should equal the corresponding area under the $\sigma_y(r)$ curve at $\theta=0^o$ and $\theta=180^o$. With the notation shown in Fig 3.2 (8) this gives:

$$\int_{-(j+1/2)\Delta x-\Delta r}^{(j+1/2)\Delta x-\Delta r} \sigma_y(r)dr = \sum_{i=-j}^{j} P_i$$

$$\int_{-(j-1/2)\Delta x-\Delta r}^{(j-1/2)\Delta x-\Delta r} \sigma_y(r)dr = \sum_{i=-(j-1)}^{j-1} P_i \qquad i = -j....0....j,\ j \geq 2 \qquad (3.2:11)$$

In this system of two equations Δr and a_3 are the two unknown facors, while it is assumed that $\sigma_y(o)=P_o/b\Delta x(=f_t)$. Eq (3.2:11) is non-linear, but can be solved with the help of iterations. The results for j=2,3,4 and 5 are shown in Fig 3.2 (9). For j=1, the equation has no solution. About the same result is obtained for the different lengths of integration, and the values $a_3=4.80$ MPa/$\sqrt{m}$ and $\Delta r/\Delta x=0.36$ are used in the subsequent comparisons. Eq (3.2:11) represents only one of many possibilities to determine a_3 and Δr, but it is believed to be better to carry the fitting to the sum of stress (nodal forces) than to the stress in certain points. Here it has been assumed that $\sigma_y(o)=P_o/b\Delta x$. This assumption is not necessary if eq (3.2:11) is supplemented with an additional equation. Such an equation, close at hand, is equilibrium in moment between the nodal forces and the theoretical stress distribution. In Fig 3.2 (8) the numerically obtained stress across the symmetry line of the beam is represented by a histogram, while an alternative would be to represent this stress distribution in accordance with the stress at the edge of the plate elements along the symmetry line.

In other parts of this report knowledge of eq (3.2:10) is not utilized and during the analyses of the fracture zone length the tip of the fracture zone is assumed to be located exactly in the node where $P_o/b\Delta x=f_t$. This assumption is in accordance with previous analyses by means of the fictitious crack model. In general, one may expect $\Delta r/\Delta x$ to be influenced by the shape

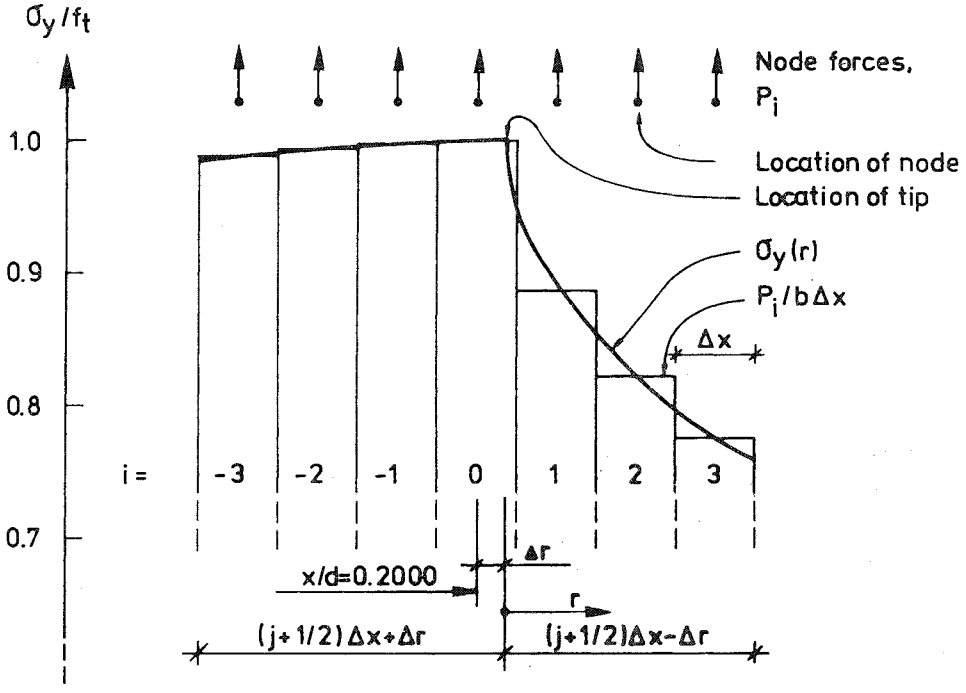

Fig 3.2 (8) Notation used in eq (3.2:11). The Figure also shows the actual stress across the symmetry line of the specimen shown in Fig 3.2 (7): the curve shows the analytical result for a_3=4.80 MPa/ $\sqrt{m}$ and $\Delta r/\Delta x$=0.36, and the histogram shows the FEM-results.

j	$\Delta r/\Delta x$	a_3, MPa/ $\sqrt{m}$
1	-	-
2	.37	4.82
3	.35	4.77
4	.36	4.79
5	.37	4.79
Present choice	.36	4.80

Fig 3.2 (9) $\Delta r/\Delta x$ and a_3 for the numerical example of Fig 3.2 (7) as obtained from eq (3.2:11) at different j. Notation acc to Fig 3.2 (8).

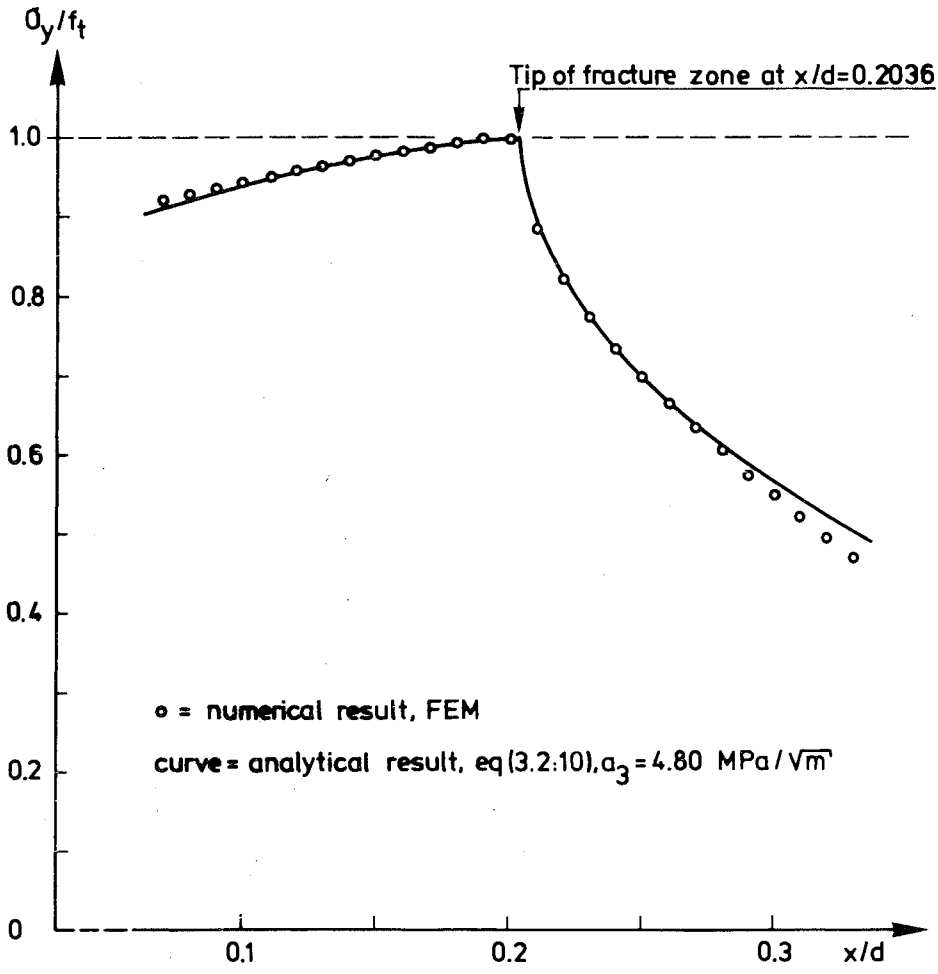

Fig 3.2 (10) Stress across the symmetry line of the specimen shown in Fig 3.2 (7).

In Fig 3.2 (10) the theoretical and numerical results are compared, and in Fig 3.2 (8) an enlargement may be found. It seems that the theoretical and numerical results are in agreement in the vicinity of the tip. Extension of the theoretical curve all the way to the edge of the beam, i.e. to x/d= 0, gives σ_y/f_t=0.83, while the finite element results give σ_y/f_t=0.87.

Substitution of σ_x in the centre of the elements close to the tip in eq (3.2:3) gives $\sigma_x = 1.3$ MPa, i.e. $\sigma_{xo}/f_t = 0.32$. Thus, in the actual example $\sigma_2/\sigma_1 = 0.32$ in the tip of the fracture zone. Knowing a_3 and σ_{xo}, the displacements and principal stresses can be calculated. In Fig 3.2 (11) the theoretical displacements are compared with the corresponding numerical result and in Fig 3.2 (12) the principal stresses are shown in the same manner. During the analytical calculation of σ_1 and σ_2, only the dominating terms in eq (3.2:3) have been taken into account. Consequently, shear stress has not been included in the analytical calculation of σ_1 and σ_2. Where the displacements in the x-direction are concerned, a slight deviation between the analytical and theoretical results can be observed. This deviation is due to different reference points: the numerical result is shown for u=0 at x/d=0.2000, while the analytical result is shown for u=0 at x/d=0.2036. The actual figures show agreement between the analytical and numerical results. The figures also illustrate that the deformations are smooth and that the direction of the principal stresses is uniform.

Where the shear stresses are concerned, the numerical result suggests that τ is very small in the vicinity of the tip and that τ seems to be approaching zero when $r \to 0$. These features are in agreemewnt with eq (3.2:3). However, with the exception of these features, agreement with respect to the distribution of the (very small) shear stresses is not found. One explanation for this might be that a_4 is zero, or close to zero, and that the shear stress is consequently dominated by a subsequent term in the series expansion of $\tau(r, \theta)$. Another explanation might be that the present particular finite element analysis is not suitable where a study of the distribution of the very small shear stresses close to the tip is concerned. Such a study may require a very fine finite elelement mesh and a very high nummerical accuracy.

In order to reduce the numerical work, during many numerical fictitious crack analyses substructure technique is utilized and only the nodal quantities along the fracture propagation path are calculated. Thus it may be noticed that the above relations should make it possible to calculate not only the location of the tip and a_3, but also σ_{xo}, from the nodal quantities along the propagation path, i.e. from the nodal forces and displacements. If, - in contradiction to the fictitious crack model -, the fracture zone is assumed to be a band of initially non-zero width, then it is probably diff[illegible] regarding the

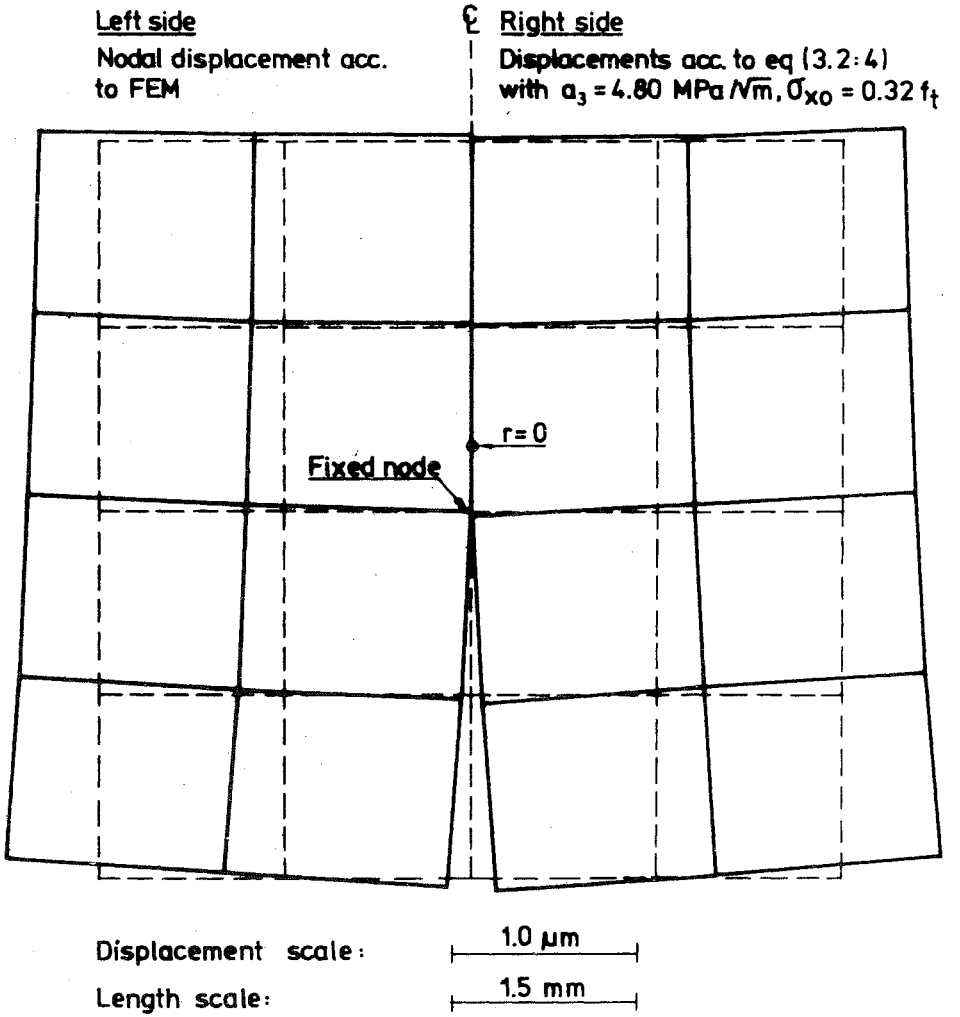

Fig 3.2 (11) Displacements in the vicinity of the tip of the fracture zone in the specimen shown in Fig 3.2 (7) acc to FEM and theoretical formula, respectively.

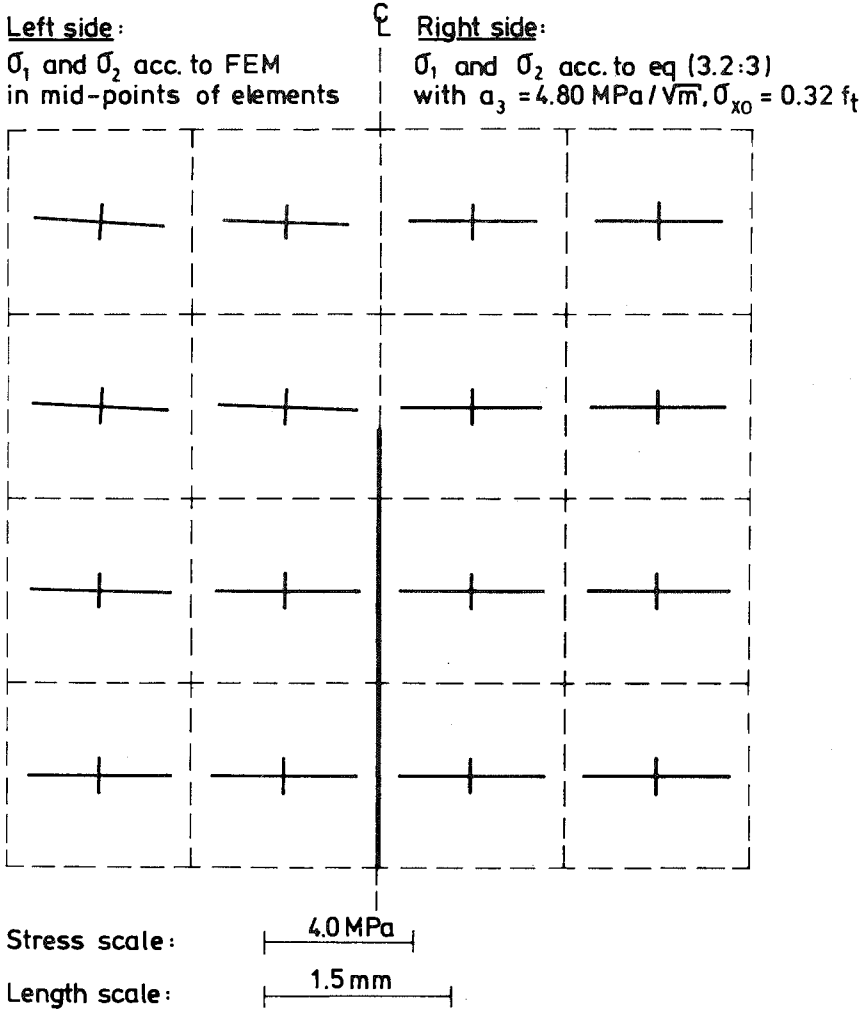

Fig 3.2 (12) Principal stresses (magnitude and direction) in the vicinity of the tip of the fracture zone in the specimen shown in Fig 3.2 (7) acc to FEM and theoretical formula, respectively.

performance close to the tip.

During some earlier studies of fracture zones, a stress distribution across the fracture zone is assumed and then the corresponding σ-w curve (or some corresponding relation) is calculated. According to eq:s (3.2:9) and (3.2:10), if this assumed stress distribution, i.e. $\sigma_y(r)$ at $\theta = 180°$, has a non-zero gradient when $r \to 0$ then the corresponding σ-w curve must have an infinite slope for $w \to 0$ (and/or eq (3.2:8) must be violated). Ståhle (1983) assumed a linear variation in $\sigma_y(r)$ (at $\theta = 180°$) and, according to a graphical display of the numerical results, it seems that the slope in the corresponding σ-w curve is great, and perhaps infinite, for $w \to 0$. Ståhle also carried out the reverse calculation, i.e. calculated $\sigma_y(r)$ at the assumption of a linear linear σ-w curve. In this case, according to a graphical display of the results (obtained by means of a special numerical method), it seems that the gradient of the stress distribution, $\sigma_y(r)$ at $\theta = 180^o$, is small, and perhaps zero, when $r \to 0$. Also this result is consistent with eq:s (3.2:9) and (3.2:10). Some other numerical results presented in literature seem to suggest that the stress distribution has no breaking at r=0 or no infinite stress gradient in front of the tip. Such results are not consistent with the present study and may merely be due to a general smooth interpolation in between the points where the stress is calculated.

It may be concluded that the fictitious crack model does not seem to produce any inconsistencies regarding the performance in the actual region, i.e. in the tip of the fracture zone and its close surroundings. The state of stress exactly in the tip of a fracture zone seems to be possible to define and calculate. The numerical comparison seems to support validity of the actual relations, or, vice versa, it seems to be possible to analyse the vicinity of the tip by means of the finite element method. Mixed mode loading has not been dealt with above. A natural extension of the above discussion may be to try to apply the same type of approach to that type of loading.

3.3 Ability to reproduce uniaxial tensile behaviour

3.3.1 Introduction

A prime requirement of a material model, a method for the description of the properties of materials, should be that the description of a material becomes such that, together with accepted laws of nature, it does not produce results that contradicts those experimental results on which the actual description is based. From this simple and fundamental point of view two methods for the description of the mechanical properties of materials in uniaxial tension will be discussed. Section 3.3.2 deals with the stress vs. strain description, and Section 3.3.3 deals with the fictitious crack description.

For this discussion we imagine that the σ vs. $\Delta\ell$ curve in Fig 3.2 (1) a) has been obtained during a direct tensile test of a uniform specimen, a bar with the inital length, ℓ. The loading speed is imagined to have been slow, so that inertia forces can be ignored, the force of gravitation is assumed to be zero, and stress and deformation perpendicular to the bar are assumed to be zero. This means that the phenomenon of necking is not dealt with. The cross sections of the bar are assumed to remain plane during elongation of the bar and the sections are denoted by their distance, x, to one of the ends of the bar in its initial state. This end is assumed to be fixed, and the movement of the section x is denoted u(x). Thus $u(0)=0$ and $u(\ell)=\Delta\ell$.

By means of the test results, the mechanical properties are described in the two different ways and these descriptions are then imagined to be handed over to a person who is asked to predict a σ vs.$\Delta\ell$ behaviour of a bar with an inital length of ℓ. The prediction is carried out by means of the following law: taking into account all kinematically admissable variations, mechanical systems will incrementally behave in such a way that the incremental work supplied to the system is minimized. The studied system consists of the bar, while the external forces acting on the bar are assumed to be outside the system. Thus the interaction between the system and its surroundings is defined by the kinematical relations $u(0)=0$ and $u(\ell)=\Delta\ell$.

The discussions in Sections 3.3.2 and 3.3.3 concern an incremental analysis startin [illegible] iese

discussions are carried out on the assumption that the incremental stiffness of any given section of material at any given time (this stiffness may be positive or negative) is equal during a positive and negative increment in its deformation. In Section 3.3.4 the conditions of stability are surveyed for the different cases of different sign of the incremental stiffness depending on the sign of the increment. These cases are studied on the assumption that the states of the bar have been reached by aid of some external constraint along the bar which is subsequently removed.

Theoretically, the present discussion is equally valid for uniaxial compression and uniaxial tension, but during compression it may be that stresses and deformations perpendicular to the bar may be of great importance. A beam in uniform bending is analogous to a specimen in uniform tension and the present discussion and the present results are accordingly applicable to the analysis of beams by changing force into moment, strain into curvature and fracture zone widening into fracture hinge rotation. The analogy between a beam in bending and the tensile specimen requires that neighbouring sections of the beam interact only through a single variable, i.e. the bending moment, and accordingly not through non-plane deformations of the sections. This means that the analogy is not suitable for studies of in-plane interaction between closely located fracture zones in a beam.

3.3.2 Stress vs. strain model

It might be that a better name for the intended model would be the smeared model, the strain softening model or perhaps the conventional model. In this model the experimental results are transferred into a description of

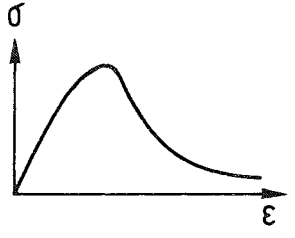

Fig 3.3 (1) ıranch.

the properties of the material on the assumption that the strain, ($\varepsilon = du/dx$), is constant along the bar (or along the gauge length), i.e. on the assumption $\varepsilon = \Delta\ell/\ell$. The description is shown in Fig 3.3 (1).

The descending branch in the σ vs.ε curve in Fig 3.3 (1) clearly contradicts the Druckers postulate of "stability in small" ($\Delta\sigma\Delta\varepsilon > 0$, (Chen and Saleeb, 1982)). On the other hand, postulates form be base for theories, but say nothing about their own validity. Thus, the violation of the actaul postulate does not necessarily mean that the stress vs. strain approach is invalid. If softening exists, then theoretical results derived from the assumption of stability in the sense of Druckers demand may not be valid. Key-words for such theoretical results are uniqueness, normality and convexity.

Consider the studied bar again. The incremental work, ΔW, necessary to attain a small strain increment, $\Delta\varepsilon(x)$, along the bar is:

$$\Delta W = \int_0^\ell \left(\sigma(x) + \frac{\Delta\varepsilon(x)}{2} \left.\frac{d\sigma}{d\varepsilon}\right|_x\right) \Delta\varepsilon(x)\, dx \qquad (3.3{:}1)$$

The kinematically admissible strain increment distributions are restricted by:

$$\int_0^\ell \Delta\varepsilon(x)dx = \Delta u(\ell) \qquad (3.3{:}2)$$

where a $\Delta u(\ell) \geq 0$ is prescribed. Integration by parts indicates that a necessary requirement for equilibrium, i.e. a necessary requirement for $d\sigma/dx = 0$ for all x, is the equality

$$\int_0^\ell \sigma(x)\Delta\varepsilon(x) = \sigma(\ell)\Delta u(\ell) \qquad (3.3{:}3)$$

Eq:s (3.3:1) and (3.3:3) give:

$$\Delta W = \sigma(\ell)\Delta u(\ell) + \int_0^\ell \frac{(\Delta\varepsilon(x))^2}{2} \left.\frac{d\sigma}{d\varepsilon}\right|_x dx \qquad (3.3{:}4)$$

When ΔW is minimized, $\Delta u(\ell)$ may not be subjected to variation as its value is prescribed.

With the first increment in $u(\ell)$ at hand, $\varepsilon(x) \equiv \sigma(x) \equiv 0$ and accordingly $\left.d\sigma/d\varepsilon\right|_x \equiv$ constant > 0. In this case, taking into account that $\Delta\varepsilon(x)$ is taken in square in increment

$\Delta\varepsilon(x) \equiv$ constant. With the next and subsequent increments at hand, $\dot{\varepsilon}(x) \neq 0$ and $\dot{\sigma}(x) \neq 0$ but as long as $\Delta\varepsilon(x)$ is constant then $d\sigma/d\varepsilon\big|_x$ is constant and as long as this constant value of $d\sigma/d\varepsilon\big|_x$ is greater than zero, eq (3.3:4) shows that $\Delta\varepsilon(x) \equiv$ constant. This means that the imagined experimental test results are correctly reproduced, and accordingly the stress vs. strain model may be valid in the range $d\sigma/d\varepsilon > 0$.

When the value of $\varepsilon(x)$ corresponding to $d\sigma/d\varepsilon\big|_x \equiv 0$ is reached, ΔW is minimized by arbitrary $\Delta\varepsilon(x)$ and a zero-energy disturbance is sufficient to produce a $\Delta\varepsilon(x)$ not identical to zero. These zero-energy disturbances are bound to produce a $d\sigma/d\varepsilon < 0$ in at least some part of the bar. (The σ vs. ε curve has $d\sigma/d\varepsilon = 0$ in only one point.) And if $d\sigma/d\varepsilon < 0$ in at least some part of the bar, eq (3.3.4) shows that ΔW can attain an arbitrary small value if, for instance, $\Delta\varepsilon(x)$ is assigned a large value in some point where $d\sigma/d\varepsilon < 0$ and a constant negative value along the rest of the bar. The lack of a minimum of ΔW means that the subsequent behaviour cannot be determined and the possibility $\Delta W < 0$ means that the bar will immediately fracture in an unstable manner. This result contradicts the imagined experimental results on which the actual description of the properties of the material is based. Thus it may be concluded that the stress vs. strain model is not valid in the range $d\sigma/d\varepsilon < 0$.

In the theoretical case when the σ vs. ε curve is such that $d\sigma/d\varepsilon = 0$ in a finite interval of ε, the prediction of the σ vs. $\Delta\ell$ behaviour becomes arbitrary as the prediction becomes governed by the arbitrary zero-energy disturbance when $\varepsilon(x)$ has reached the values corresponding to $d\sigma/d\varepsilon = 0$. Thus the experimental results may be contradicted and accordingly the stress vs. strain model is not valid in the range $d\sigma/d\varepsilon = 0$ if $d\sigma/d\varepsilon = 0$ in a finite interval of ε.

The conclusion that the stress vs. strain model is not valid when $d\sigma/d\varepsilon < 0$ is not believed to be any new finding and has most probably been derived from earlier studies, which may have been presented a very long time ago. The conclusion regarding stress vs. strain curves with a descending branch is not only a theoretical matter, but is also of great practical importance. Test results regarding tensile softening of materials should not be described in terms of stress vs. strain, and such a description of softening should not be used during numerical calculations. In this case only the uniaxial state of stress has been studied, but it is reasonable to suspect t stress vs. strain

does not become valid because of a more general state of stress.

The stress vs. strain model dealt with above gives a description of the properties of materials with reference to an infinitesimal volume, which interacts only with the neighbouring infinitesimal volumes (local action). This is consistent with conventional continuum mechanics and, unless nothing else is explicitly stated, reference to a localy acting infinitesimal volume is tacitly always assumed. However, if the description is made by means of a stress vs. strain curve plus a defined finite length of material for which the curve is stated to be valid, then the discussion above is not applicable. In this non-conventional stress vs. strain approach, strain is not calculated as du/dx, but as $\Delta\ell_{def}/\ell_{def}$, ℓ_{def} being the length which is given in the material property description. In this case, when predicting the behaviour of the studied bar, the bar should be considered as, if possible, being built up of a finite integer number of pieces with the length ℓ_{def}. Another non-conventional stress vs. strain approach is to refer the ascending branch to an infinitesimal volume and the descending branch to a defined finite length. Perhaps this approach might seem somewhat inconsistent, but the discussion above has not dealt with this approach and accordingly the results above do not suggest that this approach is not valid. This latter non-conventional stress vs. strain description has been used by Gylltoft (1983), Bazant and Oh (1983) and others.

3.3.3 Fictitious crack model

The fictitious crack description of the material properties is shown in Fig 3.2 (1) c). As long as $d\sigma/d\varepsilon>0$, the actual model coincides with the model dealt with in Section 3.3.2, which correctly reproduced the test results in this range. Then the more difficult point where $d\sigma/d\varepsilon|_x \equiv d\sigma/dw|_x \equiv 0$ is reached. In this case the system is in neutral equilibrium and may be altered by a zero-energy disturbance. The new state of equilibrium for a system in neutral equilibrium after a zero-energy disturbance is a state of stable equilibrium if a state of stable equilibrium exists in the kinematically admissable immediate vicinity of the neutral state. In the case of the stress vs. strain model, no such kinematically admissable stable state existed in the immediate vicinity of the neutral state. After the disturbance, $w>0$ (and thus $d\sigma/dw<0$) in at least some parts of the bar, ℓ_+, while $d\sigma/d\varepsilon$:

If a stable state exists, the minimum of ΔW will be greater than zero, taking into account all admissable variations not indentical to zero during zero energy transfer to the system ($\Delta u(\ell)=0$):

$$0 < \Delta W = \int_{\ell_-} \frac{(\Delta\varepsilon(x))^2}{2} \frac{d\sigma}{d\varepsilon}\Big|_x dx + \int_{\ell_o} 0\, dx + \sum_n \frac{(\Delta w(x))^2}{2} \frac{d\sigma}{dw}\Big|_x \qquad (3.3:5)$$

n is the number of sections along the part ℓ_+ of the bar. So far this number may be finite or infinite, but not zero. ℓ_o is the length of the bar where $d\sigma/d\varepsilon=d\sigma/dw=0$. If equilibrium, this length must be zero as different values of $d\sigma/d\varepsilon$ or $d\sigma/dw$ in different points along the bar would mean that the stress is varying.

The admissable variations are restricted by:

$$0 = \int_{\ell_-} \Delta\varepsilon(x)dx + \sum_n \Delta w(x) \qquad (3.3:6)$$

For any constant non-zero value of the integral in eq (3.3:6), the integral in eq (3.3:5) attains its smallest value if $\Delta\varepsilon(x)$ is uniform and this value is positive and finite. For any constant non-zero value of the sum in eq (3.3:6), the sum in eq (3.3:5) attains a negative value and this value can be made infinite if $n\geq 2$. Thus a stable state can exists only if n=1. This result indicates that the model for description of the structural behaviour, Fig 3.2 (1) b) is consistent with the model for description of the properties of the material, Fig 3.2 (1) c).

The requirement n=1 and the result that a uniform distribution of $\Delta\varepsilon(x)$ corresponds to minimum of ΔW makes it possible to obtain a simple sufficient requirement for the existence of a stable state of equilibrium. Eq:s (3.3:5) and (3.3:6) give:

$$0 < \frac{d\sigma}{d\varepsilon} + \ell \frac{d\sigma}{dw} \qquad (3.3:7)$$

But, with the notation $\Delta u \equiv \Delta u(\ell)$,:

$$\frac{\Delta\sigma}{\Delta u} = \frac{\Delta\sigma}{\ell\Delta\varepsilon + \Delta w} = \frac{(\Delta\sigma/\Delta w)(\Delta\sigma/\Delta\varepsilon)}{\Delta\sigma/\Delta\varepsilon + \ell(\Delta\sigma/\Delta w)} \qquad (3.3:8)$$

and a comparison between these two relations, taking into account that $(\Delta\sigma/\Delta w)(\Delta\sigma/\Delta\varepsilon)<0$, indicates that if $\Delta\sigma/\Delta u$ is finite and negative then eq (3.3:7) is valid. Thus the restriction (3.3.7) regarding the ability of the fictitio branch of the test

results is that the test results actually did expose a stable descending branch, i.e. not a sudden drop where $\Delta\sigma/\Delta u \to -\infty$.

The subsequent incremental behaviour of the bar may be dealt with in essentially the same manner. However, the subsequent behaviour is more simple to analyse as, according to the description of the properties of the material, no new section where w>0 can develop after peak stress. Eq (3.3:7) is also applicable during the subsequent increments, and where $\Delta\varepsilon$ and Δw are concerned, the following results are obtained:

$$\Delta\varepsilon = \frac{\Delta u(\ell)}{\ell}\left(1 - \frac{d\sigma/d\varepsilon}{d\sigma/d\varepsilon + \ell\, d\sigma/dw}\right) \qquad (3.3{:}9)\ a)$$

$$\Delta w = \Delta u(\ell)\left(\frac{d\sigma/d\varepsilon}{d\sigma/d\varepsilon + \ell\, d\sigma/dw}\right) \qquad (3.3{:}9)\ b)$$

In the theoretical case when the σ vs. ε curve or the σ vs. w curve is such that $d\sigma/d\varepsilon=0$ or $d\sigma/dw=0$ in a finite interval of ε or w, the prediction of the σ vs. $\Delta\ell$ curve becomes governed by the arbitrary zero-energy disturbances when the peak stress is reached. Thus the experimental results may be contradicted and accordingly the fictitious crack model, just as in the case of the stress vs. strain model, is not valid if the incremental stiffness is zero in a finite interval of ε or w.

If, in addition to the two material property curves, it is explicitly stated within the material property description that w>0 in exactly one section, then the experimental results can be reproduced correctly also if $d\sigma/dw=0$ in a finite interval of w. (But not if $d\sigma/d\varepsilon=0$ in a finite interval of ε.) However, an explicit statement already in the material property description that w>0 in exactly one section would mean that the material in each section, in some way, is assumed to know and take into account what is happening in the other sections, even if the stress acting on the section is not altered.

Eq (3.3:7) is of practical interest regarding to the possibilities of carring out experimental stable tensile tests. If this eq is contradicted, then it is not possible to obtain a stable σ vs. $\Delta\ell$ curve during slow and monotonous loading, no matter how stiff the testing machine is. As mentioned in section 3.2.2, the characteristic length of materials, ℓ_{ch}, may be regarded as a measure of the ratio $(d\sigma/d\varepsilon)/(d\sigma/dw)$. In the case of a linear σ vs. ε curve and a bilinear σ vs. w curve according to Fig 3.2 (3) c), $(d\sigma/d\varepsilon)/(d\sigma/dw)=-(6/5)\ell_{ch}$ in the steepest part of σ vs. w curve. In this case eq (3.

$$\ell < (6/5)\ell_{ch} \qquad (3.3:10)$$

This is a theoretical upper limit for the length of the specimen in the case of a linear σ vs. ε curve and the bi-linear σ vs. w curve. If the testing machine is not infinitely stiff, then a shorter specimen must be used in order to obtain a stable σ vs. $\Delta\ell$ curve. If fast closed loop tensile testing equipment is used, then it might be possible to successfully use longer specimens than those according to the theoretical upper limit for slow and monotonous loading. Approximate values of ℓ_{ch} for some different materials may be found in Fig 3.2 (4).

3.3.4 Stability, uniqueness and strain distribution in uniaxial tension

Refer once more to the bar studied in Sections 3.3.1-3.3.3. As in Section 3.3.2, the mechanical properties of the material are assumed to be described by a stress vs. strain curve with a descending branch, but the incremental stiffness is not assumed to be independent of the sign of the increment. The incremental stiffness during a positive increment in strain is denoted $(d\sigma/d\varepsilon)_+$, and the incremental stiffness during a negative increment in strain is denoted $(d\sigma/d\varepsilon)_-$. Both these stiffnesses are allowed to be greater than, equal to or less than zero, which means that nine combinations can be found. With the help of some external constraint along the bar, the bar is brought to a state of equilibrium, i.e. $\sigma(x) \equiv$ constant, and then the constraint is removed and the state of the equilibrium is studied by means of calculating the minimum of the incremental work ΔW, taking into account all kinematically admissable variations. During the study of the state of the current equilibrium, these variations are restricted by the boundary condition $\Delta u(\ell)=0$.

The calculation of ΔW_{min} does not involve any essential difficulties and the result is shown in Fig 3.3 (2) a). In Fig 3.3 (2) b) the corresponding different combinations of the sign of the incremental stiffness are illustrated. The numerical values of the two stiffnesses are of no importance, and the total strain in the different points along the bar does not have to be equal.

It may be questioned whether all the nine combinations illustrated in Fig 3.3 (2) b) a ording to the

stress vs. strain description, materials with properties corresponding to "U" (unstable) in Fig 3.3 (2) a) can not exist in reality. Where decrease in stress at increased deformation is concerned, according to experimental test results such materials exist in reality. Where increase in stress at decreased deformation is concerned, it is not known if any common building material is able to expose such a behaviour. However, in nature it is not unusual that force between bodies increase during decrease in the distance between the bodies. Thus, for example, a material with the ability of exposing increased stress during decreased deformation may be obtained if a number of small magnets are assembled into a chain. After an initial elongation of this chain, the stress in the chain increases during decrease in deformation of the chain.

In order to study whether the behaviour within a bar is unique, it may be investigated whether only one incremental strain distribution, $\Delta\varepsilon(x)$, corresponds to ΔW_{min}. In this case, the behaviour of the bar is unique. The existence of a unique minimum is not only dependent on the properties of the bar, but is also dependent on $\Delta u(\ell)$: being greater than, equal to or less than zero, or arbitrary. The result is shown in Fig 3.3 (3).

In all the cases where a unique incremental strain distribution can be found, the distribution is uniform. In the cases of neutral and unstable equilibrium, no unique incremental strain distribution can be found. However, if introducing the artificial subsidiary condition $\left|\Delta\varepsilon(x)\right|_{max} \leq$ constant, then minimum points can be obtained for the cases of unstable equilibrium. Such strain distributions valid for $\Delta u(\ell)=0$ are indicated in Fig 3.3 (4). Due to the artificial subsidiary condition these results may

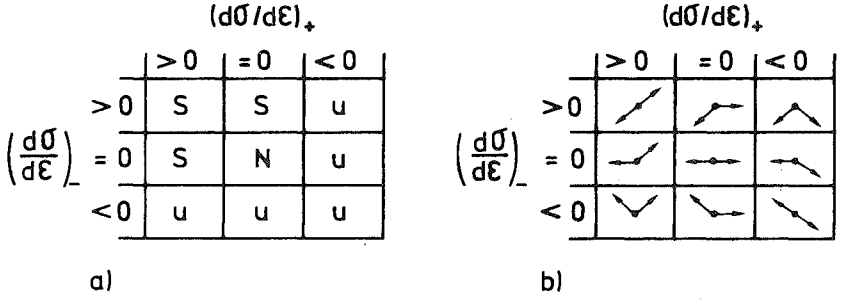

Fig 3.3 (2) a) States of equilibrium: S=stable, N=neutral and U=unstable.
b) [illegible] $(d\sigma/d\varepsilon)_-$.

be of limited interest. However, it might be of some interest to notice that the combination $(d\sigma/d\varepsilon)_- = \text{constant} > 0$ and $(d\sigma/d\varepsilon)_+ \to 0_-$ gives $\alpha \to 1$, i.e. strain localization. This combination and behaviour are reminders of the fictitious crack model and the structural behaviour at peak stress as obtained from of this model.

$(d\sigma/d\varepsilon)_+$

$\left(\frac{d\sigma}{d\varepsilon}\right)_-$	>0	$=0$	<0
>0	Y	Y	N
$=0$	Y	N	N
<0	N	N	N

$\Delta u(l) = \text{const} = 0$

$(d\sigma/d\varepsilon)_+$

$\left(\frac{d\sigma}{d\varepsilon}\right)_-$	>0	$=0$	<0
>0	Y	N	N
$=0$	Y	N	N
<0	N	N	N

$\Delta u(l) = \text{const} > 0$

$(d\sigma/d\varepsilon)_+$

$\left(\frac{d\sigma}{d\varepsilon}\right)_-$	>0	$=0$	<0
>0	Y	Y	N
$=0$	N	N	N
<0	N	N	N

$\Delta u(l) = \text{const} < 0$

$(d\sigma/d\varepsilon)_+$

$\left(\frac{d\sigma}{d\varepsilon}\right)_-$	>0	$=0$	<0
>0	Y	N	N
$=0$	N	N	N
<0	N	N	N

$\Delta u(l) = \text{arbitrary const}$

Fig 3.3 (3) Possibility of finding a unique strain increment. Y=yes, N=no.

$(d\sigma/d\varepsilon)_+$

$\left(\frac{d\sigma}{d\varepsilon}\right)_-$	>0	$=0$	<0
>0	0	0	$\alpha = *)$
$=0$	0	N	$\alpha = 1/2$
<0	$\alpha = **)$	$\alpha = 1/2$	$\alpha = 1/2$

$$*) = \max \text{ of } \left\{ \frac{1}{2}, \sqrt{\frac{(d\sigma/d\varepsilon)_-}{(d\sigma/d\varepsilon)_- - (d\sigma/d\varepsilon)_+}} \right\}$$

$$**) = \min \text{ of } \left\{ \frac{1}{2}, 1 - \sqrt{\frac{-(d\sigma/d\varepsilon)_+}{(d\sigma/d\varepsilon)_- - (d\sigma/d\varepsilon)_+}} \right\}$$

Fig 3.3 (4) Incremental strain distributions $\Delta\varepsilon(x)$ that minimizes ΔW in the condition $\Delta u(\ell)=0$ and the artificial subsidiary condition $\Delta\varepsilon(x) \leq \text{constant}$. $\alpha\ell$ is the length of the part of the bar where $\Delta\varepsilon(x)$ constant<0, and $(1-\alpha)\ell$ is the length where $\Delta\varepsilon(x)$ constant>0. N means no unique

3.4 Material models for analysis of fracture and strength

3.4.1 Introduction

In Section 3.4.2 restrictions regarding the applicability of material models are dealt with, and in this section also approaches for the modelling of the process region in front of a crack are put together. In this report two conventional non-trivial methods of fracture analysis are applied. Basic relations and assumptions of these two methods, i.e. linear elastic fracture mechanics and Weibull-theory, are summarized in Sections 3.4.3 and 3.4.4 together with a few remarks. The other methods of fracture analysis applied in this report are either described elsewhere in this report or may be considered as being trivial where the present applications are concerned. In Section 3.4.5 strength analysis of brittle specimens with inwards corners with arbitrary opening angles is dealt with, and it is noticed that the detailed properties of a fracture zone may be of significance for load carrying capacity, also where large specimens made of brittle materials are concerned.

3.4.2 Limitations of applicability and extension of process region

The methods used during the theoretical analysis of strength and fracture by means of material models may first be divided into one "material strength concept" group and one "structural strength concept" group, see Fig 3.4 (1). The characteristic of the "structural strength concept" is the inconsistent assumption that the entire structure will fail as soon as the adopted fracture criterion is reached in one point of the material. When using the "material strength concept" fracture is only assumed to develop at the point, or points, where the adopted fracture criterion is reached. In Fig 3.4 (1) only two material models are indicated for the structural concept, but all models that can be used within the material concept can also be used within the structural concept. The reverse is not always possible: It may be questioned whether the original Weibull-model can be used within the material concept.

During proportional loading and linear elastic behaviour of the material, the structural concept is very convenient to use as only a single linear calculation is required. This may be the reason why the structural concept and the assumptions of proportional loading and linear elasticity are very

frequently used during engineering work.

The structural concept may produce very inaccurate predictions of the failure load, but from the safety point of view the concept is justifiable. Regardless of the properties of the material, the structural concept always produces a prediction of a failure load less than or equal to the prediction produced by the material concept, and if the properties of the material are correctly described, the material concept produces the correct prediction. The use of linear elasticity within the structural concept may also be justified: the failure load obtained is a lower bound solution within the theory of plasticity, which is also a lower bound of the true failure load if the material behaves in accordance with the theory of plasticity.

Due to the basic assumptions of the Weibull-model (Section 3.4.4), the model is restricted to the analysis of materials with zero fracture energy and accordingly the softening must be abrupt. The Weibull-model cannot, due to the singularity in stress, be used during the analysis of specimens with inwards corners or sharp cracks. Dependent on the value of the Weibull material property parameter, such a specimen is either predicted to have zero load carrying capacity or else fracture is not predicted to occur at the tip of the corner or at the tip of the crack. In order to obtain some more realistic results for specimens with cracks or inwards corners, one would have to make the material property parameter dependent on the shape of the specimen.

The stress vs. strain type of models within the "material strength concept" represents a large group of models, both simple and very advanced. The characteristics of the intended models are that the stress vs. deformation properties of the materials are described in terms of only stress vs. strain with reference to an infinitesimal volume and that fracture, or softening, is assumed to develop when some finite stress or strain is reached. In some cases, the models contain a stress vs. strain relation with a softening branch. The models don't produce any meaningful result if the specimen has a crack or an inwards corner. The fracture energy of the material, i.e. the energy/unit fracture surface required to bring the material from peak stress to complete fracture, is restricted to being zero and the softening is accordingly abrupt. For specimens without cracks or internal corners, meaningful results regarding the load carrying capacity can often be obtained, but it is disturbing to know that once the

Type of material models	Restrictions regarding: [1] Geometry of specimen,	[2] Softening behaviour	Fracture energy	Influence of scatter commonly considered
Group "structural strength" models:				
Eng. stress vs. strain	180	∞	0	No
Weibull	180	∞	0	Yes
Group "material strength" models:				
Stress vs. strain	180	∞	0	No
LEFM	0	∞	$0 - \infty$	No
Unlimited plasticity	0 - 180	0	∞	No
Section 3.4.5	0 - 180	∞	$0 - \infty$	No
FCM	0 - 180	$0 - \infty$	$0 - \infty$	No

1) $\alpha = 0^{o}$: sharp crack, $\alpha = 180^{o}$: no crack or internal corner

2) $d/\ell_{ch} = 0$: no softening, $d/\ell_{ch} = \infty$: abrupt softening

Fig 3.4 (1) Restrictions regarding applicability of material models.

adopted fracture criterium has been reached, and a crack has started to develop, then there is zero resistance to growth of the crack. This reminds one about the structural strength concept. However, if the structure is statically indeterminate or if the crack tip during its spontaneous growth reaches a point where the stress is zero, then it may also be meaningful to apply the material strength concept during strength analysis by means of the stress vs strain models. An example of this is strength analysis of reinforced concrete beams in bending.

The conventional linear elastic fracture mechanics is restricted to the analysis of sharp cracks, the fracture energy of the material can be arbitrary, but the softening must be abrupt. The theory of plasticity can be applied during strength analysis of specimens with arbitrary shape, but the material must not soften. The opposite to the theory of plasticity in

the other extreme of softening behaviour is discussed in Section 3.4.5. In Fig 3.4 (1) this method is referred to the material strength concept, but, as discussed in more detail in Section 3.4.5, it may be the case that the method should be referred to the structural strength concept. Finally, the fictitious crack model can be applied during the analysis of specimens with and without cracks and corners, the fracture energy, as well as the softening behaviour, may be arbitrary.

As suggested in Fig 3.4 (1), the influence of scatter is not very often taken into account in material models. This is a drawback of the models, but does not represent any basic limitation of the models as, in principle, it may be possible to extend the models and take the influence of scatter into consideration. In Section 4.2.5 efforts are made to extend material models taking the scatter into consideration during applied analysis of flexural strength, Fig 4.2 (15).

In order to carry out a meaningful fracture analysis of a specimen with a crack, it is nessecary to take into account a finite non-zero fracture energy of the material. This means that the existance of a fracture process region must be considered and that two of the models indicated in Fig 3.4 (1) are applicable during such fracture analyses. (The model indicated by "Section 3.4.5" coincides with LEFM in the case of analysis of a sharp crack.) The actual two models. i.e. LEFM and FCM, represent two out of three basic approaches, each such approach being characterized by an assumption regarding the extension of the fracture process region: please see Fig 3.4 (2). According to the two first approaches, the extension of the process region is represented by a point and by a line, respectively (2D specimen). During possible application of the third approach, the heterogenous structure of the materials is considered explicitly and the process region may become a surface (if the specimen is modelled 2D). Any model according to the third approach does not seem to have been established and it is not known whether this approach has been applied during any study of crack growth. In addition to the actual three basic approaches, modifications are also available. A few such modifications are shown in Fig 3.4 (2).

The choice of suitable approach for some certain fracture analysis is essentially dependent on: (1) intended accuracy and purpose of calculation, (2) specific knowledge about the mechanical properties of the material, (3) available computer capacity and (4) the size of a "relevant"

Process region		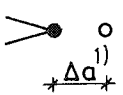	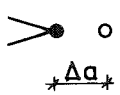		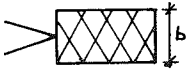	
Type of approach	Basic approach, large specimens	Modified	Modified	Basic approach, homogen. spec.	Modified	Basic approach, heteroge. spec.
Size of region: x-direction y-direction	 0 0	 const ≠ 0 0	 Not defined 0	 Not prescribed 0	 Not prescribed const = b ≠ 0	 Not prescribed Not prescribed
Description of fracture properties	1 parameter, e.g. K_c	2 parameters, e.g. $K_c + \Delta a$	1 curve, e.g. $K_R(\Delta a)$	1 curve, $\sigma(w)$	1 curve+1 para., $\sigma(\varepsilon) + b$	Several curves
Required (size of relevant specimen dimension)/(size of relevant process region dimension)	≳ very large	≳ large	≳ large	≳ small	≳ small	≳ very small
Example of model	LEFM	Equiv. crack length approaches	Resistance curve approaches	FCM	Blunt crack model with gradual softening	No established model known

1) Δa = distance between location of initial crack tip and its assumed location during strength calculations

Fig 3.4 (2) Approaches for modelling of the process region in front of a mode-1 crack.

dimension of the specimen and the magnitude of a "relevant" measure of the extension of the process region. These aspects are contradictory in the sense thar they do not suggest that any certain approach always is more suitable and convenient than other approaches. Provided that the computer capacity and the material knowlegde are sufficient, the range of applicability of the approaches to the right in Fig 3.4 (2) is great while the range of applicability of the approaches to the left is much more limited. No general rule has been found possible to formulate, but, for most cases, one may expect that approaches to the left in the figure are suitable during analysis of "large" specimens and that approaches to the right are suitable during analysis of smaller specimens and during verification of the approaches to the left in the figure.

3.4.3 Linear elastic fracture mechanics

In linear elastic fracture mechanics, the material is assumed to be linear elastic without any limit, i.e. the stresses and strains are allowed to become infinite. In spite of the possibility of extremely great strains, the concept of small strains is adopted within the actual theory. The linear elastic fracture mechanics concerns analysis of pre-existing cracks, and of the three modes of fracture, illustrated in most hand-books in fracture mechanics, only mode 1, the opening mode, will be dealt with here. Relations given below are taken from (Owen and Fawkes, 1982), (Bäcklund, 1977) and (Hedner et al., 1976).

The stresses in a plate with a mode 1 crack, Fig 3.4 (3), are (in the static case):

$$\begin{cases} \sigma_x = \sum_{n=1}^{\infty} r^{(n/2-1)} \frac{n}{2} a_n \left\{ \left[2 + \frac{n}{2} + (-1)^n\right] \cos\left[\theta\left(\frac{n}{2} - 1\right)\right] - \left[\frac{n}{2} - 1\right] \cos\left[\theta\left(\frac{n}{2} - 3\right)\right] \right\} \\ \sigma_y = \sum_{n=1}^{\infty} r^{(n/2-1)} \frac{n}{2} a_n \left\{ \left[2 - \frac{n}{2} - (-1)^n\right] \cos\left[\theta\left(\frac{n}{2} - 1\right)\right] + \left[\frac{n}{2} - 1\right] \cos\left[\theta\left(\frac{n}{2} - 3\right)\right] \right\} \\ \tau = \sum_{n=1}^{\infty} r^{(n/2-1)} \frac{n}{2} a_n \left\{ \left[\frac{n}{2} - 1\right] \sin\left[\theta\left(\frac{n}{2} - 1\right)\right] - \left[\frac{n}{2} + (-1)^n\right] \sin\left[\theta\left(\frac{n}{2} - 1\right)\right] \right\} \end{cases}$$

(3.4:1)

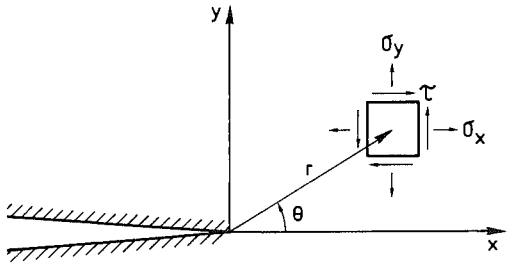

Fig 3.4 (3) A crack and coordinate axes.

a_n are constants and their values depend on the boundary conditions. If $a_1 \neq 0$ then σ_y in the tip of the crack is infinite, and if $a_1=0$ then σ_y in the tip of the crack is zero. (This remarkable result, i.e. that the stress must be either zero or infinite, is interesting to compare to the corresponding result produced by the fictitious crack model: as indicated in Section 3.2.4, in this case $a_1=0$ but nevertheless σ_y may have a non-zero finite value at the tip.)

The displacements, u and v, in the x and y directions are:

$$\begin{cases} u = \dfrac{(1+\nu)}{E} \sum_{n=1}^{\infty} r^{n/2} a_n \left\{ \left[\kappa + \dfrac{n}{2} + (-1)^n \right] \cos\left[\theta \dfrac{n}{2}\right] - \dfrac{n}{2} \cos\left[\theta\left(\dfrac{n}{2} - 2\right)\right] \right\} \\ v = \dfrac{(1+\nu)}{E} \sum_{n=1}^{\infty} r^{n/2} a_n \left\{ \left[\kappa - \dfrac{n}{2} - (-1)^n \right] \sin\left[\theta \dfrac{n}{2}\right] + \dfrac{n}{2} \sin\left[\theta\left(\dfrac{n}{2} - 2\right)\right] \right\} \end{cases} \qquad (3.4:2)$$

If ν, Poisson's ratio, is zero, then $\kappa = 3$. If $\nu \neq 0$, then $\kappa = (3-\nu)/(1+\nu)$ in the case of plane stress and $(3-4\nu)$ in the case of plane strain.

For mode 1, the definition of the stress intensity factor, K, is:

$$K = \lim_{\substack{r \to 0 \\ \theta = 0}} \sigma_y \sqrt{2\pi r} \qquad (3.4:3)$$

Thus the stress intensity factor is proportional to the first constant in the series expression of the stresses: $K = a_1/\sqrt{2\pi}$. a_1, and accordingly K, has the dimension stress $\sqrt{\text{length}}$, e.g. MPa $\sqrt{\text{m}}$. For specimens of equal shape, K is proportional to the load, normalized regarding the size of the specimen in square, P/d^2, and to the square root of the size of the specimen, $\sqrt{d}$.

The energy release rate during crack extension, G, is:

$$G = \frac{-1}{b} \frac{\partial U}{\partial a} \qquad (3.4:4)$$

b is the thickness of the specimen, a is the length of the crack and U is the potential energy of the studied system. The system consists of the specimen, or a part of the specimen, and the forces acting on the specimen, or on part of the specimen. For the linear elastic material in the quasi-static condition, eq:s (3.4:1), (3.4:2) and (3.4:4) give:

$$\begin{aligned} G &= K^2/E && \text{for plane stress} && \text{a)} \\ G &= K^2 (1-\nu^2)/E && \text{for plane strain} && \text{b)} \end{aligned} \qquad (3.4:5)$$

Keeping the load (i.e. the external forces and stresses, but not possible prescribed displacements) and the shape and the size of specimen equal, K is equal in plane stress and in plane strain, while G is less in plane strain than in plane stress.

So far no strength parameter has been introduced. To define the strength of materials within the linear elastic fracture mechanics two different approaches are used: the critical stress intensity approach and the critical energy release rate approach. In the critical stress intensity approach, the value of K at the instant when the crack starts to extend is assumed to be a material property parameter. This parameter, the critical stress intensity factor, is denoted K_c. In the critical energy release rate approach, the value of G at the instant when the crack starts to extend is assumed to be a material property parameter. This parameter, the critical energy release rate, is denoted G_c. If the K_c approach is valid, then G_c is somewhat different in plane stress and plane strain, and if the G_c approach is valid then K_c is somewhat different in plane strain and plane stress. All applied linear elastic fracture mechanics analysis in this report are carried out on the assumption of plane stress and eq (3.4:5) a) is used to relate both K to G and K_c to G_c. As ν is about 0.2 for concrete and as the load at crack growth is proportional to K_c, or $\sqrt{G_c}$, the difference between eq:s (3.4:5) a) and b) is small and accordingly of minor practical importance during the analysis of concrete and similar materials.

When $K=K_c$, or $G=G_c$, the crack is predicted to start to grow. Dependent on

the type of load and dependent on the geometry of the specimen, the crack growth can be stable, neutral or unstable. The crack growth in most of the common specimens loaded by a force becomes unstable when $K=K_c$, but this is not always the case: for example please see the specimen in Fig 4.3 (1) and the corresponding K(a) relations in Fig 4.3 (2). Naturally, a crack may grow in a stable manner also if the specimen is loaded through a prescribed deflection or through a development of internal stresses within the specimen, caused by a development of temperature or moisture gradients within the specimen. The crack growth is stable if $\partial K/\partial a<0$, neutral if $\partial K/\partial a=0$ and unstable if $\partial K/\partial a>0$.

Finally it can be noted that the distribution of stress in the vicinity of the crack tip produced by the linear elastic theory is unrealistic for all materials, specimens and structures. In spite of this, under certain conditions the linear elastic fracture mechanics can be successfully applied during the analysis of the global behaviour of specimens and structures. This apparent contradiction may be explained by the principle of autonomy together with the principle of Saint-Venant.

3.4.4 Weibull model

Basic relations of the Weibull model may be found in (Weibull, 1939 (151)). (Weibull, 1939(153)), (Hult, 1966) and (Dyrbye, 1979) have also been used during interpretation of the model. Weibull has dealt with different statistical theories for the strength of materials, but when the Weibull model is referred to, usually the weakest link model for continuous statistically homogenous materials is intended. Also in this report this model is intended when the Weibull model is referred to.

In the actual model the material is assumed to be linear elastic before fracture. At the instant of fracture the stress is assumed to suddenly drop to zero, and the fracture in a point of the material is assumed to occur when the state of stress in that point reaches the fracture state of stress of that point. The fracture state of stress is not equal in different points, but is distributed according to some probability density function. The strength of neighbouring points is not correlated and, during applications of the model, the family of density functions of Weibull are used. These functions are subsequently referred to as one function in whic[illegible] ent values.

When the fracture state of stress is reached in one point, it is asumed that the entire specimen fails. During applications of the model it seems also tacitly assumed that the external loading system is proportional. Unless otherwise stated, this is also assumed in the subsequent discussion. Unless otherwise stated, it is also assumed that the strength of a point of material is independent of the direction of the stress, i.e. a complete correlation between strength in different directions is assumed.

It may be that the Weibull model should not be interpretated as one model, but as a group of different analogous alternative models: fracture can be assumed possible to initiate only on the surface of the specimen or also within the volume of the specimen, the two or three parameter density functions can be used, and different 2D or 3D fracture criteria can be adopted. As the different alternatives are analogous, only one alternative will be dealt with more closely: fracture is assumed possible within the volume of the specimen, the two parameter density function is used and the first principal stress criterion is adopted. This alternative is the alternative used during applied calculations, presented in Sections 4.2.5 and 4.6.4.

Consider a unit volume of material, V_o, exposed to a uniform uniaxial tensile stress. The probability of failure of this specimen before the stress σ is reached is according to the actual theory:

$$S = 1 - e^{-(\sigma/\sigma_o)^m} \qquad (3.4:6)$$

σ_o and m are material property parameters. The dimensionless parameter m is a measure of the scatter in strength between different unit volumes and σ_o is a type of measure of the mean strength. To be more exact, σ_o is the load that gives a 63.2 % probability of fracture of the unit volume, V_o. The reference unit volume, V_o, for σ_o can be chosen arbitrarily, but in order to enable use of mathematics for continuous functions it is convenient to chose V_o as an infinitesimal volume.

For m=5, the distribution function (3.4:6) is shown in Fig 3.4 (4) together with the corresponding density function. When m is greater than about 3.5 the density function is warped to the right and for m less than about 3.5, warped to the left. When m is greater than about 2.5 the general shap[illegible]ly similar to the

density function of Gauss with only one exception of importance in principle: the density is equal to zero for σ/σ_o equal to or less than zero.

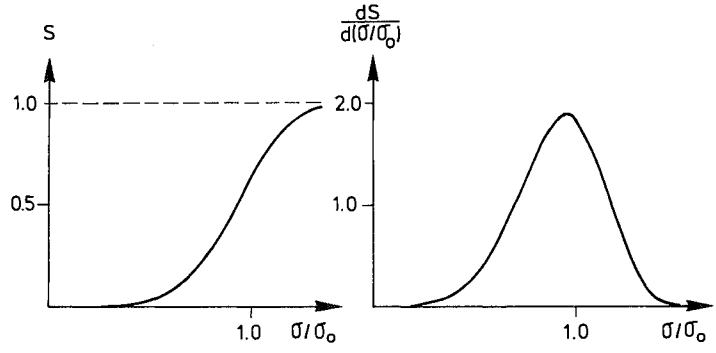

Fig 3.4 (4) Distribution, S, of Weibull for m=5 (s=23 %) and corresponding density function, $dS/d(\sigma/\sigma_o)$.

Now consider a specimen put together of infinitesimal unit volumes. The probability of failure of this specimen is equal to the probability of fracture occurring in one of the unit volumes. In turn this probability is equal to one, minus the probability that failure does not occur in unit volume number one, times the probability that failure does not occur in unit number two, times ... Thus (3.4:6) gives

$$S = 1 - e^{-\int_V (\sigma(\bar{x})/\sigma_o)^m \, dV/V_o} \qquad (3.4:7)$$

In this case S is the probability of failure of the specimen, $\sigma(\bar{x})$ is the field of the first principal tensile stresses within the specimen and V is the volume of the specimen. In points where the first principal stress is less than zero, $\sigma(\bar{x})=0$.

In cases of proportional loading the magnitude of the stresses $\sigma(\bar{x})$ can be indicated by the magnitude of the stress at some characteristic point. Denoting the stress at this characteristic point σ_{cp}, then $\sigma(\bar{x})=\sigma_{cp}(\sigma(\bar{x})/\sigma_{cp})$. Putting this into (3.4:7), it can be seen that constants c can be found so that $S(c(\sigma_{cp}/\sigma_o))$ becomes equal for all specimens. This means that the shape of the failure distribution function is the same for [illegible] there is a

certain coefficient of variation, s, and a certain ratio between the arithmetic mean of the failure load and the median mean of the failure load, $\bar{\sigma}_{cp}/\tilde{\sigma}_{cp}$. The coefficient of variation, s, is the standard deviation of the failure load divided by the arithmetic mean of the failure load. The possibility of definitely determining s and $\bar{\sigma}_{cp}/\tilde{\sigma}_{cp}$ from m is another convenient feature of the two-parameter Weibull distribution. Numerical results regarding s vs. m are given in Figs 3.4 (5) and 3.4 (6), and results regarding $\bar{\sigma}_{cp}/\tilde{\sigma}_{cp}$ vs. m are given in Figs 3.4 (6) and 3.4 (7).

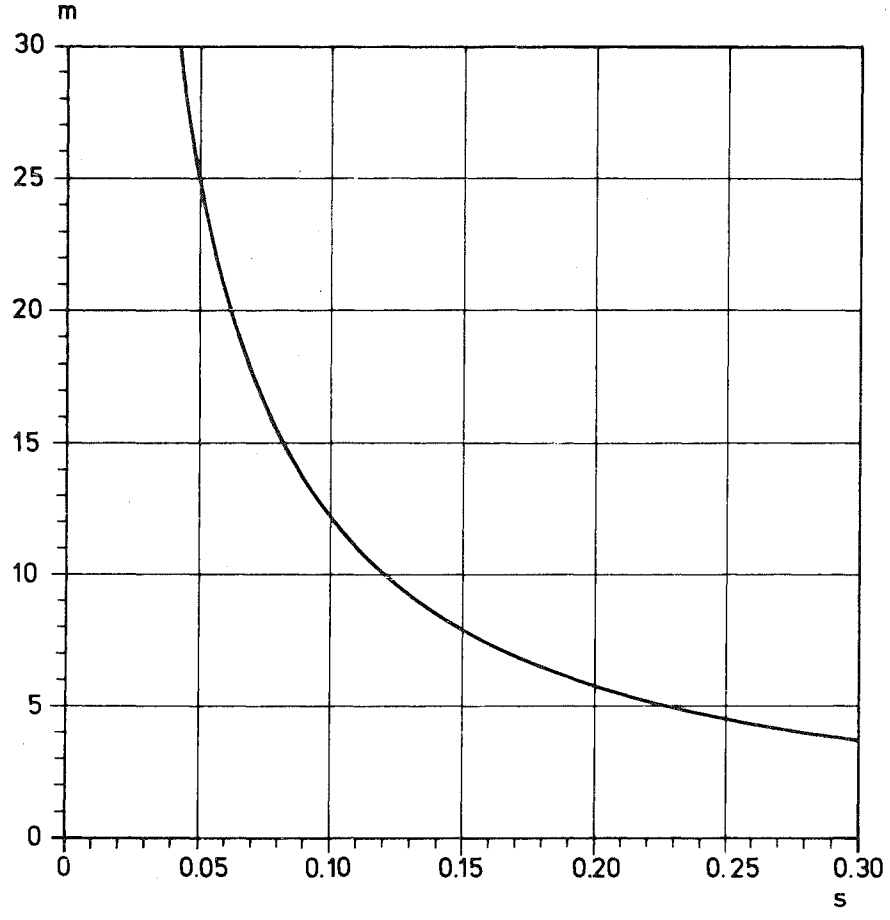

Fig 3.4 (5) Weibull parameter, m, versus coefficient of variation, s, in t[illegible]

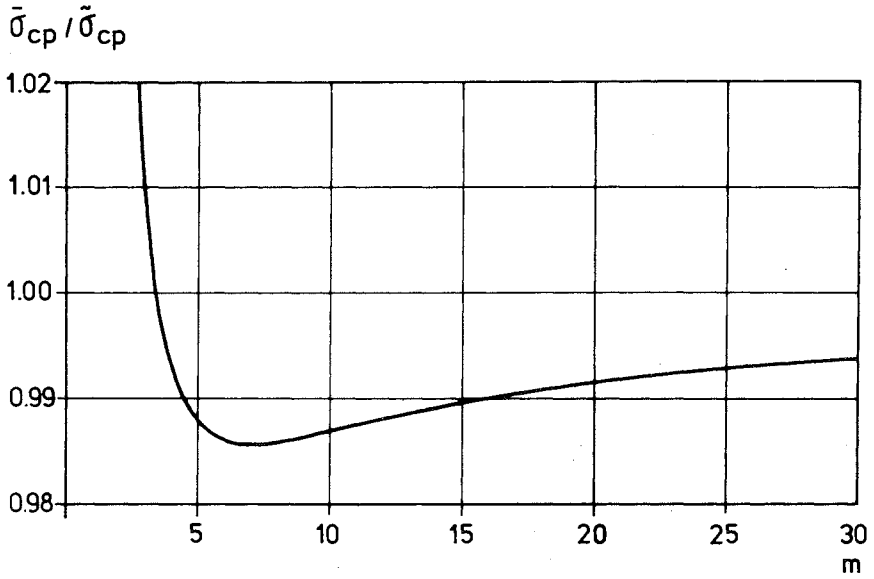

Fig 3.4 (6) Ratio between arithmetic mean failure load and median mean failure load, $\bar{\sigma}_{cp}/\tilde{\sigma}_{cp}$, versus the Weibull parameter, m.

m	s	$\bar{\sigma}_{cp}/\tilde{\sigma}_{cp}$
.2	15.84	750.0
.3	5.408	31.42
.4	3.141	8.308
.5	2.236	4.163
.7	1.462	2.137
1.0	1.0000	1.443
1.4	.7238	1.184
2.0	.5227	1.065
3.0	.3635	1.009
4.0	.2805	.9934

m	s	$\bar{\sigma}_{cp}/\tilde{\sigma}_{cp}$
5.0	.2291	.9880
7.0	.1680	.9857
10.0	.1203	.9869
14.0	.0874	.9891
20.0	.0620	.9915
30.0	.0418	.9939
40.0	.0315	.9952
50.0	.0253	.9961
100.0	.0127	.9980
200.0	.0064	.9990

Fig 3.4 (7) Coefficient of variation, s, and ratio mean strength/median strength, $\bar{\sigma}_{cp}/\tilde{\sigma}_{cp}$, for different m in the interval .2 to 200.

These numerical relations were obtained by means of numerical integration with the help of a computer. If it is utilized that $\bar{\sigma}_{cp}/\tilde{\sigma}_{cp}$ is independent of the geometry of the specimen, the calculation of $\bar{\sigma}_{cp}/\tilde{\sigma}_{cp}$ vs. m may not be of great practical interest. However, during applications of the Weibull theory reference is often made to the median mean instead of the arithmetic mean, and in such cases the $\bar{\sigma}_{cp}/\breve{\sigma}_{cp}$ vs. m relation may be helpful. The s vs. m relation may be of interest since s is a more well-known measure of scatter than m and as s is also easier to estimate from experimental results. If making interpolations in the s vs. m relation of Fig 3.4 (7), the interpolations should be carried out in $\ell n(s)$ vs. $\ell n(m)$, rather than directly in s vs. m.

By means of (3.4:7) the probability of failure before the external load corresponding to σ_{cp} has been reached can be calculated. But it may be more interesting to calculate a mean value of the failure load. S=1/2 gives the median mean of the failure load expressed in σ_o, m and V_o:

$$\tilde{\sigma}_{cp} = \{\int_V (\frac{\sigma(\bar{x})}{\sigma_{cp}\sigma_o})^m \frac{dV}{V_o \ell n 2}\}^{-1/m} \qquad (3.4:8)$$

For a specimen in uniform tension one obtains $\tilde{\sigma}_{cp} \equiv \tilde{f}_t = (\ell n 2\ V_o/V)^{1/m}\ \sigma_o$. For more complex specimens, the value of $\tilde{\sigma}_{cp}$, or the corresponding aritmethric mean, $\bar{\sigma}_{cp}$, can preferably be related to $\tilde{f}_t$, or $\bar{f}_t$. This gives a general relation:

$$\frac{\bar{\sigma}_{cp}}{\bar{f}_t} = \{\frac{V_t}{V}\}^{1/m}\ \gamma^{1/m} \qquad (3.4:9)$$

where V_t is the volume of the tensile specimen corresponding to the tensile strength $\bar{f}_t$, V is the volume of the actual specimen, and γ is a dimensionless parameter. γ is independent of the volume of the specimen and the magnitude of the load, but depends on m and the geometrical shape of the specimen:

$$\gamma = \frac{V \cdot \sigma_{cp}^m}{\int_V \sigma(\bar{x})^m\, dV} \qquad (3.4:10)$$

Fig 3.4 (5) and eq.s (3.4:9) and (3.4:10) indicate the relations used

during the applications of the conventional Weibull model in this report. In some cases $\aleph$ is calculated analytically, and in some cases numerically.

If the three parameter Weibull model is used instead of the presently discussed two parameter model, then σ/σ_o in (3.4:6) is replaced by $(\sigma-\sigma_{limit})/\sigma_o$, where σ_{limit} is the third material property parameter. σ_{limit} indicates the stress below which the probability of failure is zero. For the three parameter model one may not expect s vs. m to be independent of the geometry of the specimen.

If failure is assumed possible to initiate only on the surfaces of the specimen, then volume in the above relations is replaced by area.

If a 2D or 3D fracture criterion is used eq.s (3.4:9) and (3.4:10) should still be valid if the first principal stresses, $\sigma(\bar{x})$, are replaced by the equivalent uniaxial tensile stress as calculated in accordance with the adopted fracture criterion.

The first principal stress criterion used at present, is applied in such a manner that only the first principal stresses are integrated over the volume in (3.4:10). Tacitly this means that the strength in any certain point of the material is equal in different directions of stress, i.e. complete correlation. An alternative would be to assume that the strength in the different principal directions of stress are not correlated. In this case the integral in (3.4:10) should be replaced by the sum of three integrals: one for the first principal tensile stresses, one for the second principal tensile and one for the third principal tensile stresses. If the strength in the different directions is not correlated then, as a result of the corresponding version of (3.4:10), the fracture load of a three-axially uniformly loaded cube of unit volume becomes governed by:

$$\left(\frac{\bar{\sigma}_1}{f_t}\right)^m + \left(\frac{\bar{\sigma}_2}{f_t}\right)^m + \left(\frac{\bar{\sigma}_3}{f_t}\right)^m - 1 = 0 \qquad (3.4:11)$$

σ_1, σ_2 and σ_3 are the principal tensile stresses. In the case of plane stress, this fracture criterion is shown in Fig 3.4 (8) for some different values of m. This Figure shows the tension-tension space and (3.4:11) does not allow compressive fracture. However, the effect of compressive stresses might be taken into account by changing f_t to f_c in those terms

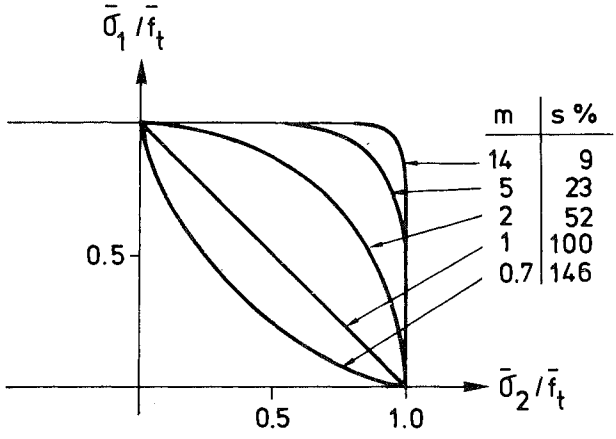

Fig 3.4 (8) Failure criterion for biaxially loaded unit cube in tension-tension region = apparent biaxial fracture criterion of material.

of (3.4:11) where the principal stress is less than zero. Fig 3.4 (8) shows that the effect of biaxial stress in the tension-tension region is rather small if s is less than about 25 %. This is in agreement with the behaviour of concrete. By principle, (3.4:11) is interesting from a few different points of view: (1) an apparent biaxial failure surface can be obtained during tests even if the material is such that the strength in one direction is quite independent of the stress in an other direction; (2) the biaxial state of stress produces an apparent decrease in strength in contrast to the yield criterion of von Mises, valid for many metals; (3) in cases of extreme scatter in strength ($m<1$, $s>100$ %) an apparent concave fracture surface is obtained. In (Weibull, 1939 (151)) polydimensional tensile stresses are dealt with in another manner.

In Section 4.6.6 a reference to this section is made regarding to the possibility of applying the Weibull model in cases of non-proportional loading, e.g. if shrinkage stresses develop within a specimen before the external load is applied or if two, or several, external non-proportional loads are applied to the specimen. In cases of non-proportional loading, the probability of failure before a certain state of load is reached, is in general dependent on the loading path even if the material is linear elastic. To analyse the probability of failure, the load may be applied in small increments and the corresponding total first principal tensile stresses at the times i $\sigma(\bar{x})_i$ calculated. Due to the linear elastic

behaviour of the material the components of stress (in the case of plane stress, $\sigma_{xi}(\bar{x})$, $\sigma_{yi}(\bar{x})$ and $\tau_i(\bar{x})$) can be calculated as the time dependent linear combination of the components of stress corresponding to each of the two, or several, non-proportional loads acting on the specimen. This means that the effort to calculate $\sigma_i(\bar{x})$ is not very dependent on the number of increments, in particular not if the loading system is such that the direction of the first principal stresses does not rotate. To obtain the development of the probability of failure, the following approach might then be used:

$$\Delta S_i = \exp\{-\int_{V_i}(\sigma_{max}(\bar{x})/\sigma_o)^m \frac{dV}{V_o}\} - \exp\{-\int_{V_i}(\sigma_i(\bar{x})/\sigma_o)^m \frac{dV}{V_o}\}$$

$$S_i = S_{i-1} + \Delta S_i \quad S_0 = 0 \quad \sigma_0(\bar{x}) \equiv 0 \quad i = 1, 2, 3 \ldots,$$

$$\sigma_{max}(\bar{x}) = \text{max of } \sigma_j(\bar{x}) \text{ in point } \bar{x} \text{ for } j = 0, 1, 2, \ldots, (i-1)$$

$$V_i = \text{volume where } \sigma_i(\bar{x}) \geq \sigma_{max}(\bar{x}) \qquad (3.4:12)$$

This gives the probability of failure as a function of time. In turn this leads to the possibility of calculating different types of mean values of the failure load. For instance in the case of shrinkage followed by external loading, the mean failure load can be calculated with account to all specimens or with account only to those specimens which have not failed before the external load is applied. Inspection of (3.4:12) shows, as may be expected, that ΔS_i is always greater or equal to zero. Inspection of (3.4:12) also shows that the probability of failure before $\sigma_i(\bar{x})$ is reached, is equal for all loading paths when V_i is constant. An example of such a case is the bending of a beam followed by simultaneous bending and tension. In such special cases of non-proportional loading, it should be possible to use (3.4:7) instead of (3.4:12). Eq (3.4:12) has not been numerically tested.

In section 3.4.2 and 4.7.1 it is said that the Weibull model, i.e. the weakest link model for continuous statistically homogenous materials of Weibull, is not applicable during the analysis of pre-existing cracks. This can be seen in eq:s (3.4:1) and (3.4:7). When $m > 4$ the probability of fracture in the tip of the crack is predicted to be 100 % regardless of how small the load is, and when $m < 4$ the probability of fracture in the tip of the crack is predicted to be 0 % regardless of how large the load is. The singularity in the tip of corners. Section 3.4.5 gives the same type of strange results.

3.4.5 Strength of brittle corners

Firstly some matters regarding the stresses close to the tip of an inwards corner in a linear elastic plate, Fig 3.4 (9), are summarized in this section. This forms the basis for a subsequent discussion of the strength of corners in brittle materials. In the last part of the section attention is attracted to an analogy between strength analysis of corners in the in-plane loaded plates and strength analysis of corners in slabs exposed to bending. Analysis of specimens with inwards corners with an arbitrary opening angle, α, is general in the sense that the analysis of specimens with a sharp crack only is a special case, $\alpha=0$, and that specimens without any corner in its conventional sense, only is another special case, $\alpha = 180^{o}$. Where strength analysis of brittle specimens is concerned, these two special cases correspond to the linear elastic fracture mechanics and to the ordinary linear elastic strength theory, respectively.

Recently the stress field close to the tip of a corner has been studied by Carpenter (1984). In this paper of Carpenter, references to previous studies may also be found. It appears that the major contribution to the solution of the general corner problem of a linear elastic plate was presented by Williams in 1952 and 1957 in two papers referred to as classical. Eq (3.4:13) below, utilized in the present study, is taken from (Hellan, 1979) and may also be found in (Carpenter, 1984).

The components of stress in a linear elastic isotropic plate may be written as $r^{\lambda-1} f_1 + r^{\lambda-1} f_2 + ...$, where $0 < \lambda_1 < \lambda_2 <....$ and f_i are functons of θ. The stresses very close to the tip of the corner are totally dominated by the first term in the sum, and if $\lambda_1 < 1$ then the stresses approach infinity as $r \to 0$. λ_1 is dependent on the opening angle of the corner and can be obtained as the smallest $\lambda > 0$ that satisfies either of the two equations:

$$\pm \lambda \sin 2(\pi-\alpha/2) + \sin 2\lambda(\pi-\alpha/2) = 0 \qquad (3.4:13)$$

By means of this equation also λ_2, λ_3 ... can be obtained, but in this case only λ_1 will be dealt with. Eq (3.4:13) can be solved numerically by a suitable standard computer library routine for search of zero points of analytic complex functions. In Fig 3.4 (9) the result of such a search for λ_1 for different α may be found. For all α, the imaginary part of λ_1 proved to be zero. In the actual figure, and subsequently, λ_1 is simply denoted as λ, or $\lambda(\alpha)$.

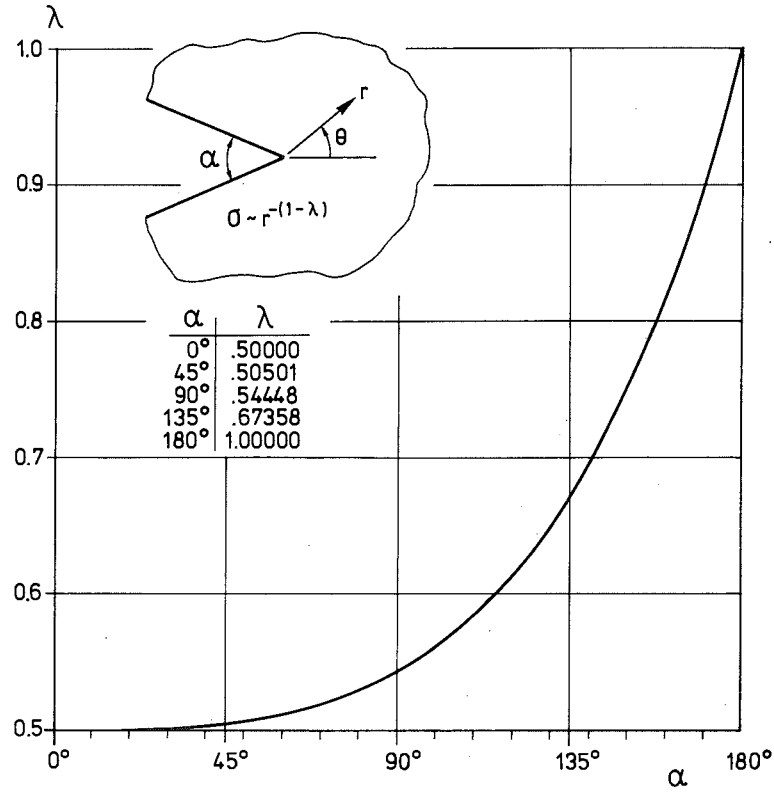

Fig 3.4 (9) Stress, σ, close ($r \to 0$) to the tip of a corner in an isotropic linear elastic plate loaded in modes 1 and 2.

One approach to strength analysis of corners in brittle specimens, at rather close hand, would be to define generalized stress intensity factors: $K_\alpha \sim \sigma(r) r^{1-\lambda}$, where $r \to 0$, and by experimental tests on the actual material determine critical values, $K_{\alpha c}$, of these generalized stress intensity factors. This means that a strength parameter must be experimentally determined for each α. For $\alpha=0$ one would obtain $K_{\alpha c} = K_c$, for $\alpha = 180^0$ one would obtain $K_{\alpha c} = f_t$, and for each other α one would have to make an experimental tests in order to determine the relevant strength parameter. This approach does not seem very rational.

Another rather analogous, but more rational and informative, approach might be the following. According to the dimensional analysis in Section

3.5.1, if the properties of the material can be described by means of the fictitious crack model, then the ultimate fracture load, σ_u/f_t, is a function of d/ℓ_{ch}. The problem at hand is to find this function, $f(d/\ell_{ch})$, for different α. For the validity of the above discussed stresses close to a corner in a linear elastic material, Fig 3.4 (9), the fracture region must be concentrated on the point of singular stresses. This means that it is necessary that $f_t \to \infty$ or, alternatively, that $d/\ell_{ch} \to \infty$. This is equivalent to the assumed brittleness of the specimens in the currently adopted sense of brittleness of specimens. Starting from r=0, the fracture zone, or the fracture point, is assumed to have the extension Δr, where, in the extreme limit, $\Delta r \to 0$. In accordance with the concept of autonomy it is also assumed that the size of the fracture zone, and also the stresses and the mechanical events within the fracture zone, are independent of the absolute global size of the specimen. This means that Δr, although close to zero without any limit, is equal in specimens of different sizes.

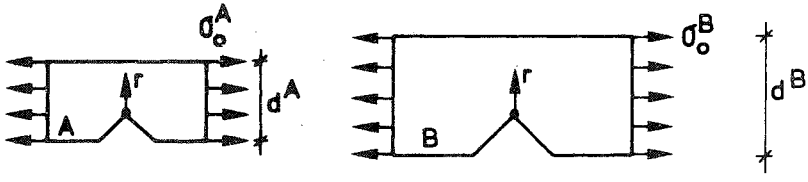

Fig 3.4 (10) Two specimens of different size.

To determine the function $f(d/\ell_{ch})$ (for $d/\ell_{ch} \to \infty$) two specimens, A and B of different size, d^A and d^B, but equal shape, load and material properties are studied, Fig 3.4 (10). As the loads and the geometrical shapes are equal, the distribution of the stresses may be assumed to be equal and the magnitude of these stresses are proportional to the external loads, σ_o^A and σ_o^B. For small r the first term in the series expression for stress dominates, and accordingly for small r:

$$\sigma^A(r) = C_1 \sigma_o^A \left(\frac{r}{d^A}\right)^{-(1-\lambda)}$$

$$\sigma^B(r) = C_1 \sigma_o^B \left(\frac{r}{d^B}\right)^{-(1-\lambda)} \qquad (3.4:14)$$

C_1 is a constant of proportionality. According to the assumptions above, the properties of the fracture process zones (or the fracture process points) in A and B are equal and at the instant of instability of the zones (points) the forces transferred by the zones (points) are assumed

to be equal:

$$\int_0^{\Delta r} \sigma^A(r)dr = \int_0^{\Delta r} \sigma^B(r)dr, \quad \Delta r \to 0 \qquad (3.4:15)$$

(3.4:14) together with (3.4:15) give $\sigma^A_{o,u}/\sigma^B_{o,u} = (d^A/d^B)^{-(1-\lambda)}$, i.e. $\sigma_{o,u} \sim d^{-(1-\lambda)}$. For the function $f(d/\ell_{ch})$ this gives:

$$\frac{\sigma_u}{f_t} = C\left(\frac{d}{\ell_{ch}}\right)^{-(1-\lambda)} \qquad (3.4:16)$$

σ_u is an abbreviation of $\sigma_{o,u}$, the external load at the instant of fracture normalized with respect to the size of the specimen. The constant C is independent of E, G_F, f_t and d (if d/ℓ_{ch} has large values). Of course the value of C is dependent on the geometrical shape of the specimen, and, even if d/ℓ_{ch} is large, for $0<\alpha<180^o$ one may also expect that C is dependent on the shape of the normalized σ vs. w curve, i.e. the shape of the σ/f_t vs. $w/(G_F/f_t)$ curve. For $\alpha=0^o$ and $\alpha=180^o$ one may not expect C to be dependent of the shape of the normalized σ vs. w curve (if d/ℓ_{ch} has large values).

The above suggestions regarding dependence of the shape of the normalized σ vs. w curve are according to numerical results and theoretical arguments. For $\alpha=180^o$, eq (3.4:16) (and also numerical results presented in Chapter 4. and also the theoretical discussion in Section 3.5) indicates that the fracture energy has no influence on the strength if d/ℓ_{ch} has large values. Consequently, the σ vs. w curve and its shape is of no matter.

For $\alpha=0^o$ informative numerical results may be found in Sections 4.3 and 4.4. For the very large d/ℓ_{ch}, these results seem to suggest that the fracture zone is fully developed at the instant of instability, and, consistently, also that the instability load as obtained during calculations with due account to the non-zero size of the fracture zone equals the instability load as obtained at the assumption of a single fracture point (LEFM) in which the energy consumption equals the energy consumption during movement (without change of its shape) of a fully developed fracture zone. From a theoretical point of view this may be briefly explained as follows: if a local vicinity-region to the fracture zone (the fracture point) is fixed to the tip of the fracture zone, then, if $\alpha=0^o$, the geometrical shape of this vicinity, its boundary conditions and its properties do not change during movement of tip

For $0<\alpha<180^{o}$, a few numerical results may found in Section 4.7. But, where the actual discussion is concerned, these numerical results may not be very relevant and informative. However, for the actual region of α, local vicinity-regions to the fracture zone change their boundary conditions during movement and there is accordingly no reason to expect that the fracture zone growth may become unstable first when the fracture zone is fully developed. Instead one may expect that only a first part of the fracture zone is developed at the instant of instability. This means that the remainig last part of the σ vs. w curve is of no matter for the load at instability, and of no matter for the size of the fracture zone at instability either. The first part of the curve, on the other hand, is of matter in both these respects.

It is interesting to notice that the shape of the σ vs. w curve might be of great significance for the global strength of specimens with inwards corners also when d/ℓ_{ch} is large. This contradicts the opinion that the shape of the actual curve is of no matter during strength analysis of large specimens made of brittle materials, i.e. during strength analysis of specimens in which the fracture zone is very small in comparison to the size of the specimen. Accordingly, it may be of interest to try to, in some way, determine the shape of the actual curve also for brittle materials such as glass, cement paste and wood. (Of course, the shape of this curve for these brittle materials is also of interest during analyses of notched specimens, if having a notch tip radius with is not very small, and not very great either, as compared to the characteristic length of the material. If the tip radius is very small, then the LEFM may be applied, and if very great, then the conventional limit stress criterium may be applied.)

The numerical value of the constant C corresponding to a geometrical shape of the specimen and a shape of the normalized σ vs. w curve, may be calculated by means of the finite element method, taking into account the development of the fracture zone. Provided that d/ℓ_{ch} is large enough, the calculated ultimate load gives directly the numerical value of C. As d/ℓ_{ch} should be large, a fine finite element mesh may be required in the vicinity of the tip of the corner. However, in this regard it might be a good idea to calculate the ultimate load for two fairly large d/ℓ_{ch} and then utilize eq (3.5:6). This should make it possible to choose smaller d/ℓ_{ch} and accordingly a coarser element mesh.

(3.4:16) should be valid for the extreme limit $d/\ell_{ch} \to \infty$, but is also believed to be a useful approximation for large enough finite values of d/ℓ_{ch}. To estimate how accurate (3.4:16) is for some particular value of d/ℓ_{ch}, in general a numerical calculation may have to be carried out. If the accuracy is known for some particular d/ℓ_{ch}, the accuracy for larger d/ℓ_{ch} may be expected to be better. During increase in d (or d/ℓ_{ch}) first the size of the fracture zone at failure, Δr, (or $\Delta r/\ell_{ch}$) reaches an almost constant value (numerical results may be found in Section 4.7) and then, during a further increase in d (or d/ℓ_{ch}) $\Delta r/d$ approaches zero. To produce exact results, (3.4:16) requires not only that Δr (or $\Delta r/\ell_{ch}$) is constant, but also that $\Delta r/d \to 0$

Regarding the relative influence of size and material property parameters, it is informative to write (3.4:16) in the following way:

$$\sigma_u = C \cdot \left(\frac{EG_F}{d}\right)^{1-\lambda} f_t^{2\lambda-1} \qquad (3.4:17)$$

Although being exact only if $d/\ell_{ch} \to \infty$, this relation, also illustrated in Fig 3.4 (11), should be of practical interest. When $\alpha=0^o$, see Fig 3.4 (11), a doubling of E or G_F or a halving of d produce a 41 % increase in σ_u, while a change in f_t has no influence on σ_u. When $\alpha=180^o$, σ_u is proportional to f_t and independent of E, G_F and d. When $\alpha=90^o$, a 100 % increase in f_t produces only a 6 % increase in σ_u, while a 100 % increase in E or G_F or a 50 % decrease in d produces a 37 % increase in σ_u.

In Section 3.4.1, the method of failure load calculation in Fig 3.4 (1) called "Section 3.4.5", i.e. the method represented by (3.4:16), was with some hesitation included in the "material strength concept" group of theoretical methods of failure load prediction. This means that not only the load at fracture in the tip of the corner (or, if $\alpha=180^o$, at the surface of the specimen) should be possible to calculate, but also, which is the reason for the hesitation, the load carrying capacity after start of crack growth. The method represented by eq (3.4:16) enables analysis of the load at fracture of the corner and analysis of the load when a very deep crack has developed from the corner, but does not allow for analysis of the load carrying capacity in the interval of time in between. In this interval, the requirement $d/\ell_{ch} \to \infty$, or that d/ℓ_{ch} is large, is not met: when comparing the size d of specimens with a different geometrical

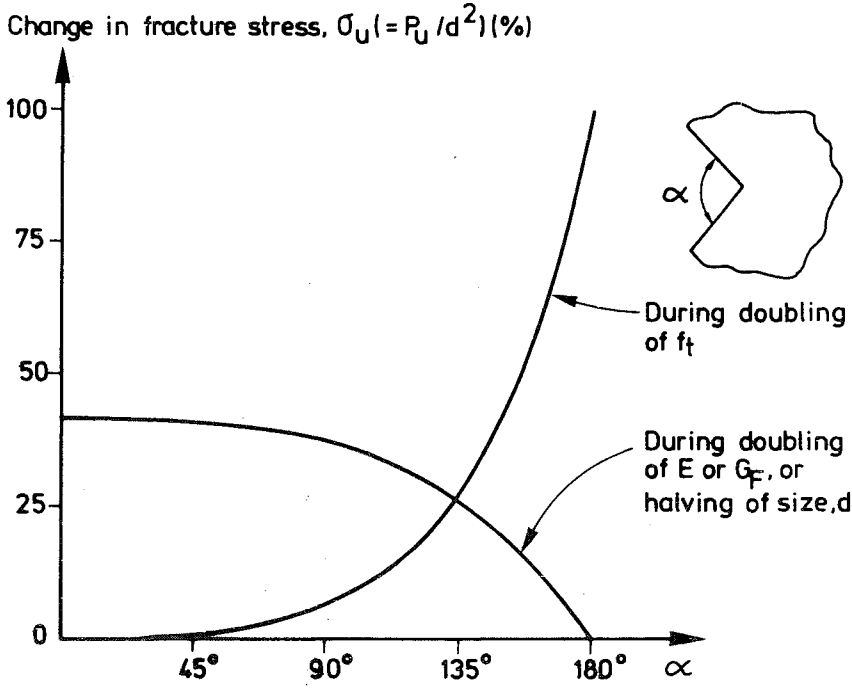

Fig 3.4 (11) Influence of different parameters, (E, G_F, d, and f_t) on the strength (σ_u) of a corner in a brittle specimen ($d/\ell_{ch} \to \infty$) vs. the opening angle, α, of the corner.

shape regarding this requirement, d should be taken as being the distance from the fracture process region to the closest disturbance. By disturbances are thereby meant all loads or boundaries, except the two straight boundaries that meet in the fracture process region. However, from the practical point of view, in many cases the load at fracture of the corner is of prime practical interest even if this load may not always represent the ultimate failure load of the specimen. It is interesting to note that if failure occurs first when a deep crack has developed, then $\lambda = 0.5$ in (3.4:16) and (3.4:17), regardless of the initial value of the corner opening, α. As will be discussed in Section 3.5.4, this also means that the function $\sigma_u / f_t = f(d/\ell_{ch})$ may not always be smooth, but may, in some cases, have a breaking (a knee-point) even for large d/ℓ_{ch}.

Eq (3.4:13) and the corresponding variation in stress close to the tip of corners indic[illegible] mode loading, i.e.

mode 1 plus mode 2. Eq (3.4:16), on the other hand, is only valid for mode 1 as f_t and G_F refer to mode 1. However, this equation should also be valid for mixed mode loading if the strength and fracture energy of the material in the actual mixed mode are proportional to f_t and G_F, respectively.

Eq (3.4:13) is valid for isotropic linear elastic materials. For ortotropic materials, no correspondance to this equation is known to the writer. Accordingly it is not known whether Fig 3.4 (9) and eq (3.4:16) are valid for ortotropic materials, such as wood. The mixed mode fictitious crack analysis presented in Section 4.7 of a 90^o-corner in wood does not exclude the possibility that (3.4:16) is also valid for ortotropic materials.

Since the basic equation for a linear elastic slab in bending (without loads acting on the studied part of the slab) is the same as the basic equation for the above studied linear elastic in-plane loaded plate (without body-forces acting on the studied part of the plate), the above relations should be applicable also where the strength of inwards corners in brittle slabs in bending are concerned. The actual basic equation is the biharmonic equation. For the case of a slab in bending: σ corresponds to bending moment/length; σ_u corresponds to ultimate load carrying capacity, expressed as ultimate bending moment/length in some point away from the fracture region; f_t corresponds to ultimate bending moment/length of a section of the slab; E corresponds to the slope of the bending moment vs. curvature relation of a section of the slab (dimension: bending moment); G_F corresponds to the area under the fracture hinge vs. curvature relation of the slab (dimension: force); and d corresponds to the in-plane size of the slab, i.e. not the thickness of the slab. This gives the possibility to calculate a characteristic length, $(\ell_{ch})_{slab}$, for sections of beams and slabs. Application of the above relations regarding the strength of inwards corners to slabs in bending requires that the slab is brittle, i. e. that $(d/\ell_{ch})_{slab} \to \infty$ or, if approximate results are accepted, that $(d/\ell_{ch})_{slab}$ is large.

A limitation of the ordinary theory for slabs in bending is that perpendicular-to-plane deflection is the only variable in the basic equation. During the (tensile) fracture of a brittle slab in bending, in-plane forces and deformations may develop as a result of, and have influence on, the de ges in the slab.

A slab exposed to such a loading system that perpendicular-to-plane shear stresses develop in the tip of a sharp crack, or in the tip of a corner, is loaded in mode 3. The basic equation for this perpendicular-to-plane shear problem (or torsion problem) is the Laplace equation, $\nabla^2 u=0$, where u is the displacement perpendicular to the plane. According to Aking (1980), Lehman (1959) showed that the solution to this equation has an $O(r^{\pi/(2\pi-\alpha)})$ singularity in the tip of a corner. This should mean that the perpendicular-to-plane shear stresses close to the corner are proportiondal to $r^{-(1-\lambda)}$, where $\lambda=\pi/(2\pi-\alpha)$. A comparison between this convenient explicit relation, valid for mode 3, and the corresponding relation for mode 1 and 2, indicated in Fig 3.4 (9), shows that λ is the same for $\alpha = 0$ and $\alpha = 180^0$, but not in the interval $0<\alpha<180^0$.

3.5 General hypotheses regarding strength suggested by fictitious crack analyses

3.5.1 Introduction. The strength function $\sigma_u/f_t = f(d/\ell_{ch})$.

This section deals with properties of the strength functions $\sigma_u/f_t = f(d/\ell_{ch})$. Many earlier and present results regarding ultimate load carrying capacity obtained during applications of the fictitious crack model have been presented by means of graphical illustrations of such functions. Thus the components in these functions might be fairly well-known and they are also described in this introduction. In this introduction, a justification of the possibility of describing ultimate load carrying capacity by means of the actual strength functions may also be found.

In Section 3.5.2 four general hypotheses are proposed. Theses hypotheses concern the upper bound of strength and the lower bound of strength, and upper and lower bounds for the magnitude of influence of d/ℓ_{ch} on σ_u/f_t.

In Section 3.5.3 restrictions are made and then less general "zero order", "first order" and "second order" approximations of $f(d/\ell_{ch})$ at large d/ℓ_{ch} are discussed. The need for such approximate relations originates primarily from the limited computational capacity of computers: if the fictitious crack model is to be applied during numerical finite element analysis of specimens with very large d/ℓ_{ch}, then the finite element meshes may have to be very fine.

In Section 3.5.4 the approximate relations are compared to a few numerical results. In Section 3.5.5 the hypotheses of Section 3.5.2 are compiled.

Throughout Section 3.5 it is assumed that the ultimate failure of the actual specimens and structures is caused by fracture and not by, nor influenced by, "large" displacements (e.g. buckling) or "large" strains (e.g. necking). In addition, quasistatic equilibrium is assumed to be present at each instant of time.

Throughout Section 3.5 it is also assumed that the mechanical properties of the material can be described in accordance with a generalization of the fictious crack model: Before the adopted fracture criterion of the material is reached, the properties are assumed to be described by means of a stress vs. ! fracture

criterion (2) is reached, a localized fracture surface is assumed to develop in the actual point, and the properties of this section are described by a stress vs. relative displacement relation (3), where in the general case the relative displacement, or deformation, consists of three components. The above three material relations are not allowed to be entirely independent, instead the stress-variable in these three relations must be connected according to eq (3.2:8). This connection simply means that the peak stress in a stress vs. strain relation must equal the corresponding state of stress in the fracture criterion, which in turn must equal the stress at zero relative displacement in the corresponding stress vs. relative displacement relation. A special limitation of the applicability of the actual model is illustated in Fig 3.2 (2) and a restriction regarding the shape of the stress vs. relative displacement relation is indicated by eq (3.2:9). If several loads are applied to the specimen or structure, these loads are assumed be proportional. In particular, the development of shrinkage stresses within a specimen before the external load is applied gives non-proportional loading. In order not to make it necessary to discuss tensile and compressive states of stress seperately, it is also assumed in this section that the fracture criterion surface can be represented by some closed surface without any hole or opening. When true or exact strength properties of a specimen or structure are referred to in Section 3.5, it is tacitly assumed that the above mentioned assumptions are valid.

The components of the strength function may be interpreted as follows: d as a measure of the absolute size of the specimen, ℓ_{ch} as a measure of the ratio between the slope of the stress vs. strain relation and the stress vs. fracture zone deformation relation, f_t as a measure of the "size" of the fracture criterion and σ_u, finally, as a measure of the ultimate load carrying capacity of the specimen or structure as expressed in the dimension stress. Thus, for instance, if the specimen is loaded by a point load, P, then $\sigma_u \sim P_u/d^2$. In the case of a linear elastic stress vs. strain relation, ℓ_{ch} is defined as EG_F/f_t^2, where E is the measure of the slope of the stress vs. strain relation and f_t^2/G_F the measure of the slope of the stress vs. fracture zone deformation relation.

Each strength function is valid for a "group" of specimens. By a group of specimens it is then meant specimens of equal geometrical shape (and with equal arrangement of the loading) made of materials with equal shape of the stress vs. strain relations, the fracture criterion surfaces and the

stress vs. relative displacement relations. Consequently, within each group of specimens, each specimen is defined by 6 (not independent) parameters. One parameter defines the absolute size of the specimen, two parameters define the stress vs. strain relation (one parameter for the "size" of the stress space and one parameter for the "size" of the corresponding strain space), one parameter defines the "size" of the fracture criterion, and two parameters defines the stress vs. relative displacement relation (one parameter for the "size" of the stress space and one parameter for the "size" of the corresponding deformation space). According to the above, the "sizes" of the stress spaces in the three material relations must be connected. Consequently, within each group of specimens, each specimen is defined by 4 independent parameters. This means that the ultimate load carrying capacity, σ_u, may be influenced by 4 independent parameters. The choice of these parameters can be made in different manners. Here the parameters d, f_t, E and ℓ_{ch} are chosen.

Within each group of specimens, σ_u may change only if any of the above 4 parameters is changed. However, if comparing two specimens with different E but with equal d, f_t and ℓ_{ch} and subjected to equal load (force), the magnitude of strains and deformations is different but the distribution of the strains and deformations is equal and the stresses in the two specimens are identical. (This is explained in a more detailed manner below, and if the load does not only include forces but also imposed displacements, then these imposed displacements must be proportional to 1/E.) As the stresses in these two specimens are identical at each instant, also the ultimate strengths, σ_u, are equal. Thus σ_u is independent of E at constant d, f_t and ℓ_{ch}. This means that only four parameters are involved during strength analysis: σ_u and the three parameters which may have influence on σ_u, i.e. d, f_t and ℓ_{ch}.

The possibility of describing ultimate strength by means of the strength function might now be simplest explained and justified by means of dimensional analysis. Relations between physical quantities are independent of the units used during quantifying of the quantities and the fictitious crack model does not require that some special units are used when quantities are quantified. Thus any coupling between the four parameters, which altogether have two dimensions (stress and length), must be possible to describe by means of a dimensionless relation. Such a dimensionless relation can be written as $\sigma_u/f_t = f(d/\ell_{ch})$. This is not the only possibility of formally writing a dimensionless relation between the

four parameters, but it is a suitable and convenient possibility. Alternatively, a coupling between the four parameters can be expressed as, for instance, $\sigma_u/(\sqrt{EG_F/d}) = g(f_t/(\sqrt{EG_F/d}))$, where G_F is given by the identity $\ell_{ch} = EG_F/f_t^2$. In the case of initial stresses within the specimen (caused by non-proportinal loading, e.g. shrinkage) an additional parameter enters into the analysis and in this case the strength function may be written $\sigma_u/f_t = f(d/\ell_{ch}, \sigma_i/f_t)$, where σ_i is a measure of the magnitude of the initial stresses. A recent general investigation of fundamental principles of dimensional analysis has been presented by Barr (1984).

According to one of the steps in the above justification, if comparing two specimens with different E but with equal d, f_t and ℓ_{ch} and subjected to equal load (force), the distribution (not the magnitude) of strains and deformations is equal in the two specimens and the stresses are identical in the two specimens. This step may require a more detailed explanation: Assume that the stresses in two specimens, A and B, are, in fact, identical and that the strains in specimen A can, in fact, be expressed as a constant C times the strains in specimen B and that the deformations in specimen A can, in fact, be expressed as the constant C times the deformations in specimen B. Is this consistent with different E and equal d, f_t, ℓ_{ch} and load? Equal magnitude of stress is consistent with equal load (equilibrium). Equal constant of propornality, C, for both strain and deformation is consistent with equal size, d (geometrical condition). The assumptions of identical stress and proportional strain and proportional deformation means that the stress vs. strain curves and the stress vs. deformation curves for the materials in the two specimens must be identical with the exception of only a proportional difference in the magnitude of strain and deformation. This is consistent with different E at constant ℓ_{ch} and f_t: ℓ_{ch} is the ratio between the slope of the stress vs. strain curve and the slope of the stress vs. deformation curve, and a change in E at constant ℓ_{ch} and constant f_t means that the stress vs. strain and the stress vs. deformation curves are unchanged with the exception of only a proportional change in strain and deformation.

The above explanation of a step in the justification of the strength function is carried out "backwards" and for validity of the explanation it must be noticed that the explanation can be repeted for each instant during the course of loading. If the explanation was applied only at some certain instant during the course of loading, there is a theoretical possibility that identical stresses and proportional strain and

deformation distributions may have been produced by different stress vs. strain and/or stress vs. deformation curves.

Often the sensitivity in σ_u to changes of the parameters involved in a strength analysis is of interest. By the sensitivity is meant $(\Delta\sigma_u/\sigma_u)/(\Delta X/X)$, where X may represent d, f_t, E, or G_F and where ΔX represents a small change in the actual parameter and $\Delta\sigma_u$ the corresponding change in ultimate strength. In order to facilitate sensitivity calculations, the strength function, $\sigma_u/f_t=f(d/\ell_{ch})$, may be written in the following manner by means of derivation:

$$\begin{aligned}\Delta\sigma_u/\sigma_u = {} & (\Delta f_t/f_t)\{1+2(d/\ell_{ch})(f'/f)\} + \\ & (\Delta d/d)(d/\ell_{ch})(f'/f) - \\ & (\Delta E/E)(d/\ell_{ch})(f'/f) - \\ & (\Delta G_F/G_F)(d/\ell_{ch})(f'/f)\end{aligned}$$

where f is an abbreviation of $f(d/\ell_{ch})$ and where f' is an abbreviation of $d(f(d/\ell_{ch}))/d(d/\ell_{ch})$, i.e. the slope of the curve. If knowing f and f' from, for example, finite element calculations, the sensitivity to different parameters may be calculated by means of the above relation. The sensitivity to f_t plus two times the sensitivity to E (or G_F or 1/d) is equal to 1.0. The above relation is not valid only for the fictious crack model, but for all models where the ultimate strength may be expressed by means of the strength function. According to many conventional models σ_u/f_t=constant, which means that f'/f=0. According to the linear elastic fracture mechanics, $(d/\ell_{ch})(f'/f)=-0.5$. According to Section 3.5.2, if the loading is proportional, application of the fictitious crack model gives $-0.5\leq(d/\ell_{ch})(f'/f)\leq 0$. For specimens without initial cracks or inwards corners, numerical calculations (Chapters 4. and 5.) suggest that the absolute value of the actual sensitivity ratio is especially large in the case of shear failure of longitudinally reinforced concrete beams. In cases of non-proportional loading, the absolute (apparent) value of the actual sensitivity ratio may become very large and greater than 0.5.

3.5.2 Upper and lower bounds of strength and general influence of d/ℓ_{ch}

In this section four hypotheses are given: I, II, III and IV. Hypotheses are statements which may be true, but have not been proved to be true. The only verification is that at present the writer knows of no accurate numerical or theoretical result which contradicts the hypotheses. Although being hypotheses, they do of course not represent an arbitrary set of statements.

Regarding the influence of d/ℓ_{ch} on σ_u/f_t:

I. Within each group of specimens or structures, an increase in d/ℓ_{ch} can never produce an increase in σ_u/f_t.

Two of the results of I are that the maximum of σ_u/f_t is approached when $d/\ell_{ch} \to 0$ and that the minimum of σ_u/f_t is approached when $d/\ell_{ch} \to \infty$. These limits are:

II. When $d/\ell_{ch} \to 0$, σ_u/f_t will without any limit approach a finite upper bound, and this upper bound is equal to the ultimate load given by the (exact) theory of plasticity.

III. When $d/\ell_{ch} \to \infty$, σ_u/f_t will without any limit approach a lower bound, and this lower bound is equal to the ultimate load given by the ("material strength concept" of the) finite maximum stress or strain theory of brittle materials.

A result of II is that the (exact) theory of plasticity always produces a limit load which is greater than, or equal to, the "true" limit load. This means that the "effectiveness parameter", often used during applied limit load analyses by means of the theory of plasticity, must be less than, or equal to, unity. This is not very surprising and seems to be a generally accepted fact. The word in parenthesis, (exact), is used to indicate that the upper and lower bound solutions within the theory of plasticity are not intended. These upper and lower bounds give upper and lower bounds to the limit load produced by the (exact) theory of plasticity, not upper and lower bounds to the true limit load.

A result of III is that the ("material strength consept" of the) theory of brittle materials always gives a limit load which is less than, or equal

to, the true limit load. This is a rather convenient result, especially if it is utilized that the "structural strength consept" of the theory of brittle materials always gives a limit load less than, or equal to, the limit load given by the "material strength concept". It is, however, required that the actaul, perhaps non-linear, stress vs. strain relation of the material is taken into account when the lower bound of the limit load is calculated. For specimens with a sharp initial crack or a sharp inwards corner, the "structural strength concept" gives $\sigma_u = 0$.

If a linear stress vs. strain relation is used during calculation of the limit load in accordance with either of the two concepts of the theory of brittle materials, then a lower bound to the limit load given by the (exact) theory of plasticity is obtained and/or a lower bound to the true limit load is obtained. A lower bound to the (exact) plasticity solution is obtained if the stresses in all points in the specimen or structure are allowed to be anywhere within the fracture criterion surface of the material. A lower bound to the true limit load is obtained if the stresses in all points in the specimen or structure are allowed only to be anywhere within the start-of non-linear-behaviour criterion surface of the material.

The strength function is in general different for the different groups of specimens. However, the upper and lower bounds given by hypotheses II and III are equal for groups of specimens. The upper bound is equal for all groups of specimens that differ only in the shape of stress vs. strain relation and the stress vs. deformation relation. In addition, according to a theorem of the theory of plasticity, the upper bound is not influenced by internal initial stresses within the specimen. Thus, for example, for the flexural strength of a rectangular cross section one obtains $f_f/f_t = 3(f_c/f_t)/((f_c/f_t)+1)$ when $d/\ell_{ch} \to 0$, regardless of the shape of the stress vs. strain relation, the shape of the stress vs. deformation relation and initial stresses. f_c is the compressive strength of the material and $f_f \equiv \sigma_u \equiv M_u/(bd^2/6)$. The lower bound is the same for all groups of specimens that differ only in the shape of the stress vs. deformation relation.

Hypothesis I is formulated in the negative manner. In reality, however, there seem to be very few exceptions to the rule that an increase in d/ℓ_{ch} will produce a decrease in σ_u/f_t, i.e. not an unchanged constant value. Thus, from the practical point of view, the question is not whether σ_u/f_t

is influenced or not, but whether the influence is of an insignificant or significant magnitude. A first estimation of the answer to this question can be obtained by means of a comparison between the upper bound, II, and the lower bound, III.

Obviously d/ℓ_{ch} can generally be expected to be of great importance if the specimen contains a sharp initial crack or a sharp inwards corner. For other specimens, the magnitude of the influence of d/ℓ_{ch} is greatly dependent on the shape of stress vs. strain relation of the material. An example of this is given in Fig 3.5 (1). This figure shows the upper and lower bounds for the ultimate bending moment capacity of two beams with a rectangular cross section, made of different materials with stress vs. strain relations that approximately reflect the behaviour of mild steel and unreinforced concrete, respectively. The stress vs. strain relation "A" gives $1.37 \leq f_f/f_t \leq 1.50$ during variation in d/ℓ_{ch}, while the stress vs. strain relation "B" gives $1.00 \leq f_f/f_t \leq 2.73$ during variation in d/ℓ_{ch}. The actual example of how the significance of d/ℓ_{ch} can be estimated in a simple manner accordingly suggests that d/ℓ_{ch} may not be expected to have any great influence on the bending capacity of a beam (without any notch) made of mild steel. Where the beam made of unreinforced concrete is concerned, the actual example suggests that fictitious crack analysis may be of great pratical interest.

While hypothesis I gives the lower bound regarding the magnitude of the influence of d/ℓ_{ch} on σ_u/f_t, hypothesis IV gives the upper bound:

IV. If E, G_F and d are kept constant, then an increase in f_t will never produce a decrease in the ultimate load, σ_u.

This means that $\partial\sigma_u/\partial f_t \geq 0$ if E, G_F and d are kept constant. Thus, with the help of the rules of derivation, hypothesis IV can be formulated in the alternative manner:

$$\frac{-d(\sigma_u/f_t)}{d(d/\ell_{ch})} \leq \frac{\sigma_u}{f_t} \frac{1}{2d/\ell_{ch}}$$

The solution to the differential equation obtained in the limiting case of equality is $\sigma_u/f_t \sim 1/\sqrt{d/\ell_{ch}}$. This means that hypothesis IV can also be formulated in

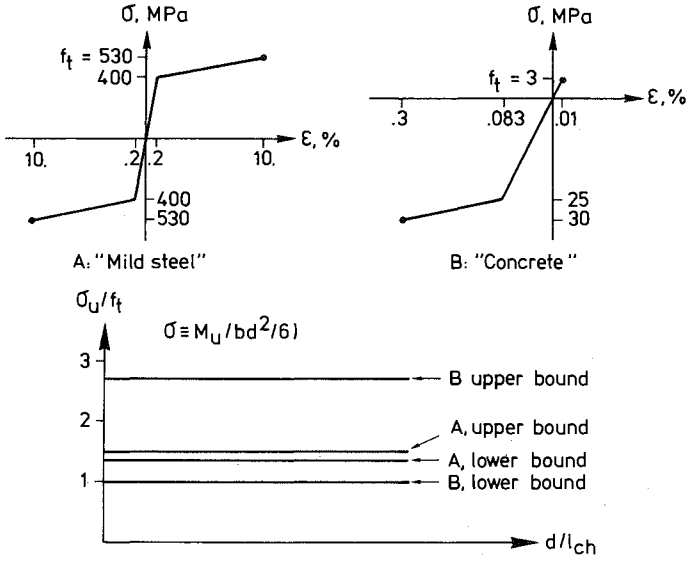

Fig 3.5 (1) Two materials with different stress vs. strain curves, and corresponding upper and lower bounds of bending moment capacity of beams with rectangular cross section during variation in d/ℓ_{ch}.

If $f((d/\ell_{ch})_o) = (\sigma_u/f_t)_o$ then

$$\sigma_u/f_t = \begin{cases} \leq \dfrac{A}{\sqrt{d/\ell_{ch}}} & \text{when } d/\ell_{ch} \leq (d/\ell_{ch})_o \\ \geq \dfrac{A}{\sqrt{d/\ell_{ch}}} & \text{when } d/\ell_{ch} \geq (d/\ell_{ch})_o \end{cases}$$

where $A \equiv (\sigma_u/f_t)_o\sqrt{(d/\ell_{ch})_o}$

This alternative formulation shows a conclusion regarding the linear elastic fracture mechanics: For 2D specimens with a sharp initial crack made of a material with a linear elastic stress vs. strain relation, the linear elastic fracture mechanics gives an upper bound to σ_u/f_t for finite d/ℓ_{ch} if the linear elastic fracture mechanics (with $G_f = G_c$) gives the

correct σ_u/f_t when $d/\ell_{ch} \to \infty$.

The requirements for (possible) validity of the above hypotheses are presently made generous. However, the limitations made in Section 3.5.1 should not be forgotten. Where hypotheses II and III are concerned, the requirement of proportional loading is not estimated to be necessary. However, where hypothesis IV is concerned, numerical results presented in Chapter 4. shows that the requirement of proportional loading is necessary: if internal initial stresses, e.g. caused by non-uniform shrinkage, are present before the external load is applied, then, if d, E, G_F and σ_i/f_t are constant, an increase in f_t may produce a decrease in the ultimate value of the external load, σ_u.

3.5.3 Zero, first and second approximations of $f(d/\ell_{ch})$ at large d/ℓ_{ch}

This section deals with approximate analytical expressions of the strength function for in-plane proportionally loaded "statically determinate" 2D specimens with large d/ℓ_{ch}, made of materials with an isotropic linear elastic stress vs. strain performance outside the fracture process zone. By "statically determinate" it is in this case meant that the failure is governed by the growth of only one tensile fracture zone. The actual expressions of the strength function, - zero, first and second order approximations -, are believed to approach the exact result when $d/\ell_{ch} \to \infty$ and are approximations with different degrees of accuracy when d/ℓ_{ch} is finite. It is intended that the approximations should be such that, for each group of specimens, a finite d/ℓ_{ch} exists beyond which the accuracy of the approximations increase in a continuous manner during a further increase in d/ℓ_{ch}. Thus the approximations should facilitate strength analysis of specimens with large d/ℓ_{ch}. For such specimens analytical relations may be needed due to the fine element meshes normally required during finite element analysis of such large and brittle specimens by means of the fictious crack model. Occasionally the actual relations may also be found to be useful during strength analyses of certain specimens with fairly small d/ℓ_{ch}.

Before going on to the actual approximations, the possibility for abrupt breakings in $f(d/\ell_{ch})$ should be noticed and a corresponding restriction regarding the interpretation in Section 3.5.3 of σ_u should be made. In general σ_u is - measure of the ultimate load-carrying capacity during the

course of complete collapse, while in the following, σ_u may be interpretated as the load at the first instability of the initial crack, corner or edge at which the fracture zone is assumed to start to develop. In some cases this load only represents a local maximum in the carrying capacity during the course of collapse. Thereby it is of special interest to notice that the type of maximum, i.e. local or global, may not only depend on "group" of specimens ("group" is defined in Section 3.5.1), but may also depend on the absolute size of the specimen, i.e. depend on the value of ratio d/ℓ_{ch}. This is the case even if only specimens with very large d/ℓ_{ch} are considered.

An example of this is illustrated in Fig 3.5 (2). For the interpretation of this illustration, please see Fig:s 4.3 (1) and 4.3 (2) where in particular the occurrence of a descending part in the upper curve in Fig 4.3 (2) is of importance for the actual example. For the sake of simplicity, the exemplification in Fig 3.5 (2) concerns a specimen with such a relative size of the hole, that the break-point occurs at such a large d/ℓ_{ch} that σ_{u1}=constant and $\sigma_{u2} \sim 1/\sqrt{d/\ell_{ch}}$ in the vicinity of the break-point. If the break-point occurs at a smaller d/ℓ_{ch}, these relations are not valid, but the crossing between the two curves may still be expected to produce an abrupt breaking in the strength function.

In the example in Fig 3.5 (2) the breaking is such that the rate of decrease in σ_u/f_t decreases, while examples of specimens with the opposite property may also be found. Such a specimen may be obtained if two plates, one with a centre crack and one with a centre hole, are put together into a structure so that the structure collapses if any of the two plates collapses.

The zero order approximation (below called the zero approximation) should be accurate if the absolute size of the fracture zone is not greater than zero exactly. The load carrying capacity given by the actual approximation is such that an additional increment in load will produce start of the development of a fracture zone. Consequently, the zero approximation is:

$$\sigma_u/f_t = 0 \quad \text{when } \alpha < 180^o \tag{3.5:1}$$

$$\sigma_u/f_t = C_o \quad \text{when } \alpha = 180^o \tag{3.5:2}$$

The angle α is defined in Fig 3.4 (9). The value of the constant C_o can be

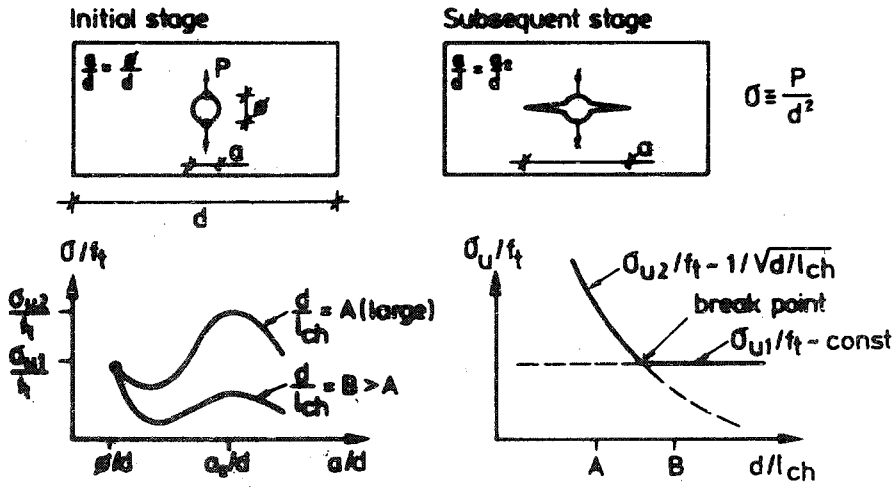

Fig 3.5 (2) Examplification to possibility of abrupt break-points in a σ_u/f_t vs. d/ℓ_{ch} curve.

obtained during an ordinary linear elastic analysis of the actual specimen. Normally σ_u is defined with reference to the stress in such a point in the specimen that C_o becomes equal to 1.0.

The first order approximation (below called the first approximation) should be accurate if the size of the fracture zone is infinitesimal in comparison to the size of the specimen:

$$\sigma_u/f_t = C_{1\alpha}(d/\ell_{ch})^{-(1-\lambda(\alpha)} \qquad \text{when } \alpha < 180^o \qquad (3.5:3)$$

$$\sigma_u/f_t = C_o(1+\frac{(C_1C_2/2)}{d/\ell_{ch}}) \qquad \text{when } \alpha = 180^o \qquad (3.5:4)$$

For $\alpha=0^o$, (3.5:3) is known from linear elastic fracture mechanics and for $0^o<\alpha<180^o$, a justification may be found in Section 3.4.5. The funtion $\lambda(\alpha)$ is given in Fig 3.4 (9). $C_{1\alpha}$ is a constant for each group of specimens and for $\alpha=0^o$, $C_{1\alpha}$ may also be expected to be independent of the shape of the σ vs. w curve. For $\alpha=0^o$, computational methods for calculation of $C_{1\alpha}$ are known from linear elastic fracture mechanics and for $0^o<\alpha<180^o$, the calculation of $C_{1\alpha}$ is very briefly discussed in Section 3.4.5. The actual

approximation for $\alpha=180^{o}$ may require an explanation.

Please see Fig 3.5 (3) where stress distributions close to the edge of a specimen are shown. For $\alpha=180^{o}$, the linear elastic stress distribution close to the edge of a specimen may be written $a_1+a_2(r/d)+a_3(r/d)^2+...$ and currently only the first two terms in this series shall be taken into account. Thus, if the stress at the edge is f_t then the linear elastic stress distribution close to the edge is $\sigma(r)=f_t(1-C_2(r/d))$, where C_2 is a constant. It is now assumed that the load carrying capacity is goverened by the true stresses along a length which is proportional to $\ell_{ch} : C_1\ell_{ch}$. According to the principle of Saint-Venant the stress acting across the length $C_1\ell_{ch}$ can be replaced by an statically equivalent stress distribution without any influence on the far-away stresses and consequently without any influence on the load carrying capacity. An approximately statically equivalent stress distribution can be obtained if the linear elastic stresses, $\sigma(r)$, are increased by Δf_t. The condition that the resultant of the stresses should be equal gives:

$$f_t C_1\ell_{ch} - f_t \frac{C_2}{2}\frac{(C_1\ell_{ch})^2}{d} + \Delta f_t C_1\ell_{ch} = C f_t \ell_{ch} \qquad (3.5:5)$$

The right hand part of this equation represents the resultant of the true stresses and the constant of proportionality, C, is dependent on the choice of C_1. When $\ell_{ch}\to 0$, Δf_t should approach zero and in order to fulfil this condition C_1 is chosen so that $C_1=C$. For finite d/ℓ_{ch} this choice represents an approximation. Having made the above approximations, eq (3.5:4) is obtained by replacing f_t in eq (3.5:2) with $f_t+\Delta f_t$, where Δf_t is obtained from eq (3.5:5) with $C=C_1$.

The choice $C=C_1$ means that the mean stress across the region $C_1\ell_{ch}$ is equal to f_t. This can be compared to the theoretical stress distribution close to the tip of a fracture zone, eq (3.2:3), and suggests that $C_1\ell_{ch}$ is the length of the fracture zone in large specimens at the instant of instability and that the stress across a fracture zone is constant ($=f_t$) at the instant of instability of the large specimens. These two suggestions, applicable to the specimens with $\alpha=180^{o}$, may be useful during verifiction of the actual approximation by means of finite element calculations with account taken to the development of a fracture zone of finite size.

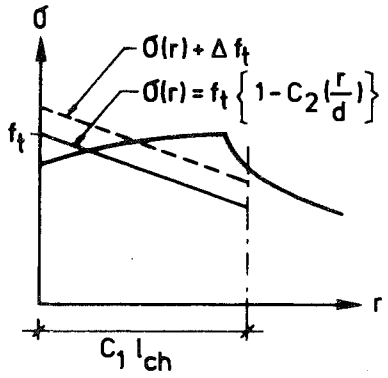

Fig 3.5 (3) Stress distributions close to the edge of a specimen.

The second order approximation (below called the second approximation) should be accurate if d/ℓ_{ch} is such that the size of the fracture zone at the instant of instability has approached close to the constant size reached when the size of the specimen, d, is increased towards infinity. Thus the size of the fracture zone may be non-zero and also finite in comparison to d, but should be close to its asymptotical absolute size. The assumption of existance of an asymptotical size at the instant of instability is supported by results of numerical calculations and may also be supported by the principle of autonomy for the behaviour of fracture regions in large specimens. For $\alpha > 0^o$, in general this size may not be expected to equal to the size of the fully developed fracture zone. Although the fracture region is allowed to have a size, the region is not allowed to fill up so much of the specimen that the shape of the linear elastic stress distribution in the far-away stress field is altered during the development of the fracture zone. This condition is propably not very important as it is beleived to be less restrictive than that of an almost constant size of the fracture zone. The choice of approximation is:

$$\sigma_u/f_t = C_{1\alpha}(d/\ell_{ch} + C_{2\alpha})^{-(1-\lambda(\alpha))} \quad \text{when } \alpha < 180^o \qquad (3.5{:}6)$$

$$\sigma_u/f_t = C_o\left(1 + \frac{(C_1C_2/2)}{d/\ell_{ch}+(C_1C_2/2)}\right) \quad \text{when } \alpha = 180^o \qquad (3.5{:}7)$$

To obtain eq (3.5:6) the true stresses acting across the fracture zone and

its vicinity are replaced by an approximately statically equivalent stress distribution. Such a stress distribution, see Fig 3.5 (4), is assumed to be possible to obtain with a sufficient accuracy if the linear elastic stresses are moved $a_1 \ell_{ch}$, where a_1 is a constant. This may be temporarily regarded as an increase in the depth of the crack or corner from a to $a+a_1 \ell_{ch}$. However, this would mean that the geometrical shape of the specimen would be changed. In order to avoid this and in order to obtain the influence of size, the total size of the specimen is changed proportionally, i.e. d is changed into $d(a+a_1 \ell_{ch})/a=d+C_{2\alpha} \ell_{ch}$. By making this change in eq (3.5:3), eq (3.5:6) is obtained. The constant $C_{2\alpha}$ may be obtained by means of a numerical calculation of σ_u/f_t for some such large d/ℓ_{ch} that the size of the fracture zone at instability has closely reached its asymptotical value. While $C_{1\alpha}$ may be expected to be independent of the shape of the σ vs. w curve when $\alpha=0^o$, $C_{2\alpha}$ may be expected to be dependent on the shape of this curve for all α.

For $\alpha=0^o$, $\lambda(\alpha)$ is equal to 1/2, and in this case, where the relative influence of absolute size, d, on σ_u/f_t is concerned, eq (3.5:6) is in agreement with a size effect law presented by Bazant (1984). This size effect law has been deduced by means of dimensional analysis and consideration of energy release rate. According to the present study, the actual law is valid only for large brittle specimens with an initial crack, but has been applied also to specimens without initial cracks and to specimens with such small d/ℓ_{ch} that one may hardly expect the size of the fracture zone at instability to have reached close to its asymptotical size. An interesting application of the size effect law during a statistical study of test results regarding the size effect in shear failure of longitudinally reinforced concrete beams has been presented by Bazant and Kim (1984) and the law has also been applied during a study of the strength of unreinforced concrete pipes. From a general point of view, if $C_{1\alpha}$ and $C_{2\alpha}$ are determined from experimental test results and used as general curve fitting parameters, provided that the variation in d/ℓ_{ch} is limited, it is probable that eq (3.5:6) with $\lambda(\alpha)=1/2$ may be applied also to specimens without initial cracks and to specimens with small d/ℓ_{ch}. This is because the general properties of eq (3.5:6) are consistent with hypotheses I and IV, discussed in Section 3.5.2. Recently, Bazant (1985) has generalized the size effect law by means of series expansion. In this generalized law an arbitrary large number of empirical constants may be included. However, as compared to the present study, the asymptotical relation obtained for d=0 shows that also this generalized law is valid

only if $\alpha=0^0$, i.e. for specimens with an initial crack, the length of this initial crack being proportional to the size of the specimen.

For $\alpha=0^0$, eq (3.5:6) is qualitatively similar also to the corresponding relation produced by an inherent flaw model recently studied by Aronsson (1984) during applications of fracture mechanics models during tensile strength analyses of laminates with cracks. By the justification of eq (3.5:6), for $\alpha=0^0$ this relation may also seem similar to the rather well-known effective crack length approach, sometimes used during linear elastic fracture mechanics analysis in order to improve the results of this theory. However, the constant $C_{2\alpha}$ may have different values for different materials (dependent of the shape of the σ vs. w curve) and may have different values also for specimens with different geometrical shapes. Where the shape of the specimen is concerned, if a suitable choice of effective crack length is made, then the effective crack length approach and eq (3.5:6) should give the same result for all specimens which are such that the linear elastic stress intensity factor is proportional to the square root of the length of the crack, the size of the specimen kept constant.

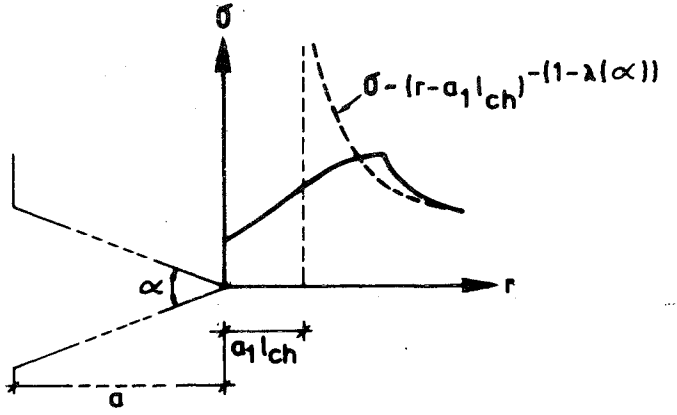

Fig 3.5 (4) Stress distributions at the tip of a corner or a crack.

The second approximation for $\alpha=180^0$ is a modification of the first approximation. In the first approximation no attention is paid to the increase in gradients in the far-away stresses due to the increase in load during the development of the fracture zone. To compensate for this, first the global size of the specimen is increased from d to d+Δd and then the first approxi[illegible]uld be such that

the gradients in the far-away stresses at the global size d+Δd equals the linear elastic gradients at size d. The simplest way to obtain such a modification in an approximate manner may be by means of:

$$(d + \Delta d)/d = (f_t + \Delta f_t)/f_t \qquad (3.5:8)$$

where Δf_t is calculated by means of eq (5.3:5). Application of eq (3.5:4) then gives eq (3.5:7).

A convenient feature of the second approximation for $\alpha=180^o$ is that no new constant is introduced. $(C_1C_2/2)$ may be regarded as one constant, but is written as $C_1C_2/2$ in order to facilitate a physical interpretation. C_2 is governed by the geometrical shape of the specimen. Thus, for example, for a slender beam with depth d and loaded in bending $C_2=2$. C_1 is an approximate measure of the size of the fracture zone in large specimens at the instant of instability and this size may be expected to be governed by the properties of the material. According to finite element results presented in Section 4.2 and shown in Fig 4.2 (21), for the bi-linear shape of the σ vs. w curve shown in Fig 3.2 (3) c) the depth of the fracture zone at instability seems to be about $0.25\,\ell_{ch}$ for large specimens. Thus, for this shape of the σ vs. w curve, a rough estimation of C_1 would be 0.25 while an adjustement between eq (3.5:7) (or eq (3.5:4)) and the finite element results regarding σ_u/f_t for large d/ℓ_{ch} gives $(C_1C_2/2)=0.27$, i.e. $C_1=0.27$. Taking into account the general approximations involved in finite element analysis, the actual deviation in C_1 is very small and, at those values of d/ℓ_{ch} for which there is theoretical justification for believing that eq (3.5:7) is accurate, the corresponding deviation in σ_u/f_t is neglible.

Finally, different approximations of the strength function may be developed for the large d/ℓ_{ch}. The approximations presented above may be regarded as a result of weighings between striving after reasonable justifications and simple relations which may be useful in order to avoid extensive finite element calculations. For application of the second approximation, two finite element calculations have to be carried out: for $\alpha=0^o$ and 180^o, one linear elastic calculation and one fictitious crack calculation, and for $0^o<\alpha<180^o$ two fictitious crack calculations. If the strength at several large d/ℓ_{ch} is to be studied without the use of approximate analytical relations, the computational work may become very large, partly be[illegible]ired during

fictitious crack analysis of specimens with large d/ℓ_{ch}. Of course, it is also often more convenient to deal with an analytical expression than to deal with numerical results. On the other hand, as the relations are approximate for finite d/ℓ_{ch}, care must be taken so that applications with too small d/ℓ_{ch} are avoided.

3.5.4 Comparisons to numerical results

The hypotheses in Section 3.5.2 are such that it is of no advantage to carry out numerical comparisons. The hypotheses are either true or false, and so far they have not been found to contradict numerical results obtained during fictitious crack analyses.

In Fig 3.5 (5) the approximate relations from Section 3.5.3 are compared to finite element results. The finite element result shown in Fig 3.5 (5) a) is valid for the bi-linear shape of the σ-w curve shown in Fig 3.2 (3) c) and is taken from Section 4.2, Fig 4.2 (1). The finite element result shown in Fig 3.5 (5) b) is valid for the straight line shape of the σ-w curve shown in Fig 3.2 (3) b) and is taken from Section 4.3, Fig 4.3 (5). The constant C_1 =0.352 is obtained from the linear elastic stress intensity factor, shown in Fig 4.3 (2). The approximate relations are such that they should be more accurate the greater d/ℓ_{ch} and W/ℓ_{ch} are. Because of this, constants $(C_1C_2/2)$=0.27 and $C_{2\alpha}$=2.2, used in the second approximation, are determined from the values of σ_u/f_t for the largest available d/ℓ_{ch} and W/ℓ_{ch}: 6.4 and 19.5, respectively. For these values of d/ℓ_{ch} and W/ℓ_{ch}, the numerical results regarding the size of the fracture zone at failure, Fig 4.2 (21) and Fig 5.3 (5) e), suggest that this size has approached an almost constant value. However, due to coarse element meshes in comparison to ℓ_{ch} for these large values of d/ℓ_{ch} and W/ℓ_{ch}, the actual values of constants $(C_1C_2/2)$ and $C_{2\alpha}$ may not be very accurate. In addition, if the constants are determined from a known value of σ_u/f_t for large d/ℓ_{ch} or W/ℓ_{ch}, even a small error in σ_u/f_t will result in a great change in the value of the constants. On the other hand, this sensitivity also means that σ_u/f_t, as obtained by means of the second approximation, is correspondingly insensitive to an error in the constants.

It is unfortunate that finite element results are not available for such intervals of d/ℓ_{ch} and W/ℓ_{ch}, where the size of the fracture zone at failure is constant during variation of d and W. However, if the second

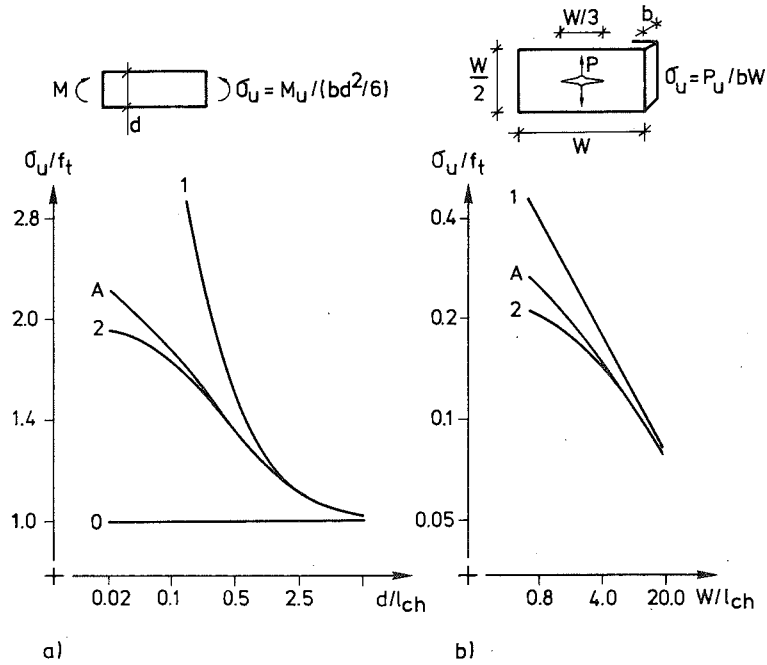

Fig 3.5 (5) Comparisons between approximate relations and numerical results. "A" = fictitious crack analysis by means of the finite element method. "0", "1" and "2" = zero, first and second approximate relations, respectively.

order approximation constants are determined from the finite element results of σ_u/f_t at $d/\ell_{ch}=3.2$ and $W/\ell_{ch}=9.8$ respectively, then, for $d/\ell_{ch}=6.4$ and $W/\ell_{ch}=19.5$, the second approximation gives load carrying capacities that deviate 0.1% and 0.2% respectively from the finite element results. If the second order approximation constants are determined from σ_u/f_t at $d/\ell_{ch}=1.6$ and $W/\ell_{ch}=4.9$, then, for $d/\ell_{ch}=6.4$ and $W/\ell_{ch}=19.5$, the second approximation gives load carrying capacities that deviate 0.2% and 1.0% respectively from the finite element results. This deviations are so small that they might just as well be caused by the general approximations involved in finite element analysis as by the non-constant size of the fracture zone.

For $0^o<\alpha<180^o$, an application ($\alpha=90^o$) of the second approximation may be found in Section 4.7 together with a comparison to corresponding results

obtained by means finite element calculations. However, this application concerns an orthotropic material and is therefore not treated in this Section.

For smaller values of d/ℓ_{ch} and W/ℓ_{ch} than those presently used during the determination of $(C_1C_2/2)$ and $C_{2\alpha}$, the size of the fracture zone is no longer constant but starts to decrease more and more. In this case one may, in general, not expect the second approximation nor the zero and first approximations, to be accurate. In spite of this, the second approximation may occasionally also be found to be useful and accurate for fairly small d/ℓ_{ch}. This is because the general properties of the actual expressions are in agreement with hypotheses I, III and IV and partly in agreement with hypothesis II. By the partly agreement with hypothesis II it is meant that the actual expressions produce a finite strength for $d/\ell_{ch}=0$, but the numerical value of this finite strength may not be in agreement with hypothesis II.

In Section 4.2, Fig 4.2 (2), numerical results regarding f_f are also shown for a case of development of internal stresses within the beam before the external load is applied. In such cases the present approximations are not applicable due to the non-proportional type of loading. In Fig 3.5 (5) b) it can be noticed that the first approximation, i.e. linear elastic fracture mechanics, does not under-estimate σ_u/f_t. This is in accordance with hypothesis IV.

As indicated by Fig 5.3 (5) a), in this case of loading the deviation between the second approximation and the numerical result is also small for those small d/ℓ_{ch} at which the size of the fracture zone is not constant: at $d/\ell_{ch}=0.05$ the deviation is 7.0%, at $d/\ell_{ch}=0.1$ 3.6%, at $d/\ell_{ch}=0.2$ 1.7% and for larger d/ℓ_{ch} continuously smaller. Thus, for this case, - a beam in bending analysed on the assumption of the bi-linear shape of the σ-w curve -, the fictitious crack result obtained during finite element calculations can within engineering accuracy be summarized by eq (3.5:7) if $d/\ell_{ch} \geq 0.1$. In this case, $\sigma_u \equiv f_f \equiv M_u/(bd^2/6)$, $C_o=1$ and $(C_1C_2/2)=0.27$. $C_2=0.27$ corresponds to the bi-linear shape of the σ-w curve and $C_1=2$ corresponds to bending. For a typical concrete $\ell_{ch}=400$ mm and for such a concrete $d/\ell_{ch}=0.1$ corresponds to d=40 mm.

For a beam proportionally loaded by a bending moment, M, and a tensile force, N, $C_o = 1/(1+Nd/(6M))$ and $C_2 = 2/(1+Nd/(6M))$.

Numerical calculations have not been carried out for this type of loading and accordingly the accuracy of eq (3.5:7) for this type of loading is not known. Experimental results may be found in literature. However, if agreement between the experimental results and eq (3.5:7) is found, this does not necessarily mean that eq (3.5:7) accurately reproduces the results that may be obtained during applied numerical calculations.

3.5.5 Survey of the hypotheses regarding σ_u/f_t vs. d/ℓ_{ch}

For the general case, the hypotheses I-IV in Section 3.5.2 may be summarized by:

$$0 \geq \frac{d(\sigma_u/f_t)}{d(d/\ell_{ch})} \geq \frac{-\sigma_u/f_t}{2d/\ell_{ch}} \qquad \text{(3.5:10) a)}$$

$$\lim_{d/\ell_{ch} \to 0} (\sigma_u/f_t) = (\sigma_u/f_t)_{plasticity} \qquad b)$$

$$\lim_{d/\ell_{ch} \to \infty} (\sigma_u/f_t) = (\sigma_u/f_t)_{brittle} \qquad c)$$

For the restricted cases dealt with in Section 3.5.3, the results of the hypotheses are compiled in Fig 3.3 (6). The function $\lambda(\alpha)$ may be found in Fig 3.4 (9).

A general result proposed by eq (3.5:10) and also illustated in Fig 3.5 (6) is that the strength function forms a transition between the theory of brittle materials and the theory of plasticity and that this transition is governed by the fracture mechanics properties of the material and the size of the specimen or structure.

Fig 3.5 (6) also shows an illustration of the extended possibility that the fictitious crack model, and similar models, brings about. While, in principle, it is possible to treat all combinations of d/ℓ_{ch} and α by means of this type of model, the applicability of the conventional models becomes more limited.

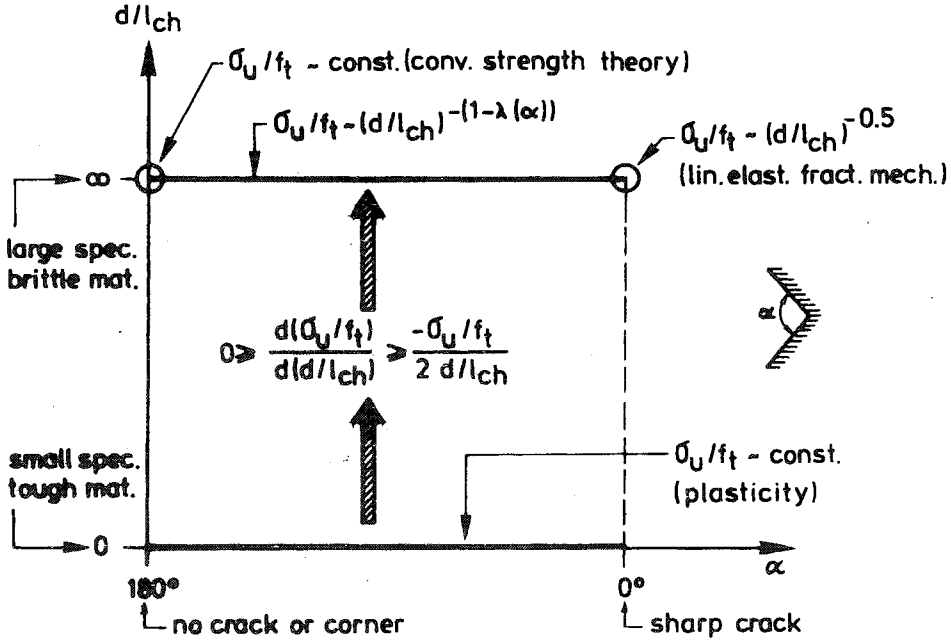

Fig 3.5 (6) Properties of the strength function $\sigma_u/f_t = f(d/\ell_{ch})$ at different d/ℓ_{ch} and α.

3.6 Method of finite element calculations (FCM and LEFM)

3.6.1 Introduction. Computer programs. LEFM.

The major part of Section 3.6 concerns the currently used method of finite element calculation during fictitious crack analyses. Alternative methods are only touched upon. A few experiences regarding methods of linear elastic fracture mechanics analyses by means of the finite element method are discussed in the last part of this introduction.

The finite element method and the access to computers have been decisive for the development and application of the fictitious crack model. Furthermore, where this particular report is concerned, a great part of the work has involved computer aided finite element analysis. However, as the currently used methods are rather trivial and as the purpose of the analyses has not been evaluation or development of finite element methods, the discussion of the actual methods of calculation will be made comparatively brief. General description of the finite element method may be found in, e.g.,(Zienkiewicz, 1977) and (Cook, 1974).

It is appropiate to mention that different kinds of methods might be utilized during numerical fictitious crack analyses: the finite element method, the boundary element method, the finite difference method and, if only special problems are to be studied, other less general methods. However, it seems that the finite element method is the most flexible and well-known method, and in addition the major part of available computer programs is based on this method. These matters have made it natural to use the finite element method.

Most of the present calculations have been carried out with the help of a small non-commercial special-purpose program. An important part (please see Section 3.6.3) of the input data for this program is obtained by means of a general-purpose program for linear elastic analyses, called GENFEM-3 (Wennerström, Glemberg and Petersson, H, 1979). An easy-to-use program developed for linear elastic analysis of plates, called SERFEM (Bäcklund and Petersson, H, 1979), has been used during some of the analyses presented and has also been used during verification analyses.

In the first part of the present work, fictitious crack analyses were carried out with the help of a general-purpose program for linear elastic

analyses, called EUFEMI (Hernelind and Pärletun, 1976). Those analyses are not included in this report. This is not due to some weakness in that particular program, but due to an unsuitable approach to the modelling of the fracture zone (please see Section 3.6.2) applied during those analyses. During some numerical tests, a program for computer aided learning of the finite element method, called CALFEM (Peterson, A and Petersson, H, 1981) was helpful. During some verification analyses, a special-purpose program developed by Petersson, P E (1981) was helpful. This program is developed for fictitious crack analyses of notched three point bend beams and is essentially based on the finite element method.

Some of the figures in this report have been drawn with the help of computer and a program called CAMFEM (Dahlblom and Peterson, A, 1982).

In addition to the numerical results obtained by means of the finite element method, some other numerical results can be found in this report. Most of those calculations have been carried out with the help of computer and small special-purpose programs. The methods of those different small calculations will not be dealt with in this section, but are briefly described in the sections where the relevant results are presented.

During linear elastic fracture mechanics analyses, the calculation of the stress intensity factor may be carried out be means of substitution of stress, strain or displacement into the analytical expression for the performance close to the tip of the crack, or by means of calculation of the J-integral, or by means of calculation of the energy release rate during crack extension. Furthermore, the region close to the tip may be modelled by means of special crack tip elements, distorted iso-parametric elements or conventional plate elements without a singular stress field. During application of the energy release rate technique, either the nodes along the crack propagation path may be opened or the geometry of the elements close to the tip may be altered. During application of the substitution technique, the stress or displacement in different points in the vicinity of the tip may be utilized. In addition to the above mentioned rather well-known approaches, it should be possible to apply the substitution technique by means of calculation of the strain energy in the elements close to the tip. Thus, a large number of possibilities are available for calculation of the linear elastic stress intensity factor.

In order to find a suitable method for the actual applied analyses and in

order to obtain some experience, some of the above mentioned possibilities were numerically tested by means of calculation of the stress intensity factor in the square-shaped centre cracked plate in tension. The test analyses were not very comprehensive, but from the tested possibilities the energy release rate technique with the opening of nodes was the most accurate. The substitution based on strain energy was the next most accurate. The substitutions based on displacement or stress gave scattered results and the accuracy seems to be significantly dependent on the choice of finite element, the choice of component of displacement or stress and the choice of reference point where the displacement or stress is calculated. The displacement substitution technique gave a better impression than the stress substitution technique. Some different elements were also tested, and where the energy release rate technique with node opening is concerned, the best result was obtained by means of the element of Turner, Clough et al. (please see Section 3.6.2). The other elements tested were the 8-node iso-parametric element, the conventional 4-node plane stress element, the quadrilaterial 4-node element (please see Section3.6.2) and the quarter-point distorted 8-node iso-parametric element. The elements are, in a decreasing scale, listed according to the accuracy they gave in the actual test example during application of the energy release rate technique. However, the difference in accuracy of the different elements does not seem to be drastic if, as in the actual test example, rather coarse element meshes with an equal total number of degrees of freedom are compared. In addition, a ranking of element types can probably not be made unique due to different orders of convergence rate of different elements.

However, the choice of a suitable method for calculation of the stress intensity factor is not only a question of accuracy. The energy release technique with node opening requires at least two finite element calculations, or, if the computer time is to be reduced, finite element analyses of at least two loading cases. Furthermore, during analyses of mixed-mode fracture, it is difficult to separate the energy release into K_I and K_{II}. However, if the analyses, as in the actual cases, concern mode-1 fracture along a known path and if the stress intensity is to be obtained versus crack depth and not only for one crack depth, then the mentioned draw-backs are of no importance.

As a result of the above experiences, the choice made was to apply the energy release rate technique with opening of nodes and use the element of Turner, Clough et al.. In addition, this choice makes it possible to

utilize the same special-purpose program and the same substructure elements (please see Section 3.6.3) as used during the fictitious crack analyses. As another result of the actual small study, the question was raised why the possibility of energy substitution does not seem to have gained any interest during studies and discussions of stress intensity calculation. By means of integration, the strain energy in regions in the close vicinity of the crack tip may be obtained from eq (3.4:1). A possibility to improve the results of the substitution techniques, may be by determining a correction factor corresponding to the actual finite element and the actual substitution technique.

Where the application of the energy release rate technique with node opening is concerned, a particular question regards the exact location of the crack tip. The natural choice, used in all present analyses, is to assume that the change in potential energy during a node opening corresponds to the rate when the tip of the crack is located in the midpoint in between the two nodes. An alternative, if the potential energy is calculated for several positions of the first closed node, is to establish an interpolation formula, e.g. based on cubic splines, for the potential energy. Values of the stress intensity may then be calculated for arbitrary positions of the tip by means of derivation. During application of the energy release rate technique, it is essential for the finite element mesh along the crack propagation path to be uniform. The actual technique may alternatively be described as the technique based on calculation of the change in compliance during crack extension. During application of the energy release rate technique with node opening, if 6 or 8 node elements are used, then two nodes are opened at each incremental crack extension.

3.6.2 Modelling of the material inside and outside the fracture region

The material outside the fracture zone is assumed to be linear elastic and has been modelled by means of 4-node plane stress elements of rectangular and quadrilateral shape. The rectangular element used is the element presented by Turner, Clough et al. in 1956. The shape function of this element may be found in, e.g., (Cook, 1974). The element has an internal fifth node and has incompatible deformation modes. From numerical tests it is known that this element usually gives more accurate results than the common 4-node rectangular plane stress element with compatible deformation modes. It may be of particular interest that the utilized rectangular

element has the ability to exactly reproduce pure bending without shear: please see Section 3.2.4 and eq (3.2:3). The utilized quadrilateral element consists of four constant strain triangular elements. In this element, and also in the rectangular element, the internal fifth node is eliminated by means of static condensation.

High order elements have not been utilized. This has partly to do with the presently adopted simple approach to the modelling of the fracture zone and has partly to do with the possibility of an irregular displacement distribution close to the fracture zone, which may not fit the smooth displacement distribution of the high order polynomid shape functions. Where the modelling of cracks and fracture zones in concrete and similar materials are concerned, two possibilities have been debated for more than a decade: the discrete method and the smeared method. With regard to this debate, it may be of importance to distinguish between the material model and the method of numerical calculation. The ficitious crack model is a material model and this material model clearly belongs to the discrete models. Currently the discrete modelling is also applied during numerical calculations. However, it is not known whether a smeared numerical modelling of the discrete fracture zone may make the numerical calculations more effective and flexible.

The smeared method in the sense of a material model with a descending branch in the stress vs. strain curve without attention being paid to the strain localization during fracture, does not seem to have been applied in recent years. This is probably due to the increasing awareness of the phenomena of strain instability and strain localization and the knowledge of the unfortunate influence of the size of the finite elements if that approach is used. It has also become increasingly well-known that the stress in the tip of a crack becomes infinite if the softening of the material is not taken into account, and consequently that it is not meaningful to apply a tensile strength criterion for crack growth if the fracture softening properties of the material is not considered in some way. A recent intentional numerical illustration of the inobjectivety of results obtained from a strength criterion without paying attention to localized softening has been presented by Rots, Nauta, Kusters and Blaauwendraad (1985).

In Fig 3.6 (1) different possibilities for the finite element modelling of a fracture zone with a known propagation path are shown. The approach

denoted I a) is used during the present analyses and has also been applied during previous fictitious crack analyses carried out at the Division of Building Materials. This approach with internodal springs makes the incremental calculations simple (please see Section 3.6.3). A rather similar, but more modulated, modelling is denoted I b). This type of approach, although additionally modulated, has been used by (Ingraffea and Gerstle, 1984) and (Ingraffea, Gerstle, Gergely and Saouma, 1984). The interface element used in these references has three nodes on each side of the fracture zone and the analyses have also concerned cases where the fracture path is not known in advance. In order to avoid updating of the topology, the alternative I c) may be used. This type of approach has been used by Gylltoft (1983) during a study of cyclic loading. The discrete fracture zone may also be numerically modelled as a smeared fracture within a finite element: alternative II. This alternative has been used by Nilsson and Oldenburg (1982), Jiang (1983), Bazant and Oh (1983), Glemberg (1984), Rots, Nauta, Kusters and Blaauwendraad (1985) and others (please see last reference). During application of this alternative, the absolute size of the finite element is taken into account in the imagined descending part of the stress vs. strain curve of the material within the finite element. This is carried out in different ways in the above mentioned references. In alternative III a stress vs. strain curve with a descending branch is not calculated. Instead the existance of a discrete crack within the element is taken directly into account: see Grootenboer (1979). Grootenboer did not apply the fictitious crack model but, from the point of view of numerical calculation, applied fairly similar models. The applied analyses in the above mentioned references corresponding to alternatives II and III have not been restricted to the cases where the crack path is known in advance, but have concerned more general cases where the path is unknown.

While Fig 3.6 (1) shows the possibilities for analyses of cracks with a known path, Fig 3.6 (2) shows the corresponding possibilities for analyses of cracks with an unknown path. Regardless of whether alternative I, II or III is used, such analyses may be carried out with or without updating of the geometry of the finite element mesh. A test calculation during application of alternative I without updating of the mesh may be found in (Modeer, 1979) and has also been discussed by Hillerborg (1982). Applications of alternative I with updating of the mesh may be found in previously mentioned references, presented by Ingraffea et al.. Alternatives II and III have been applied without updating, please see the

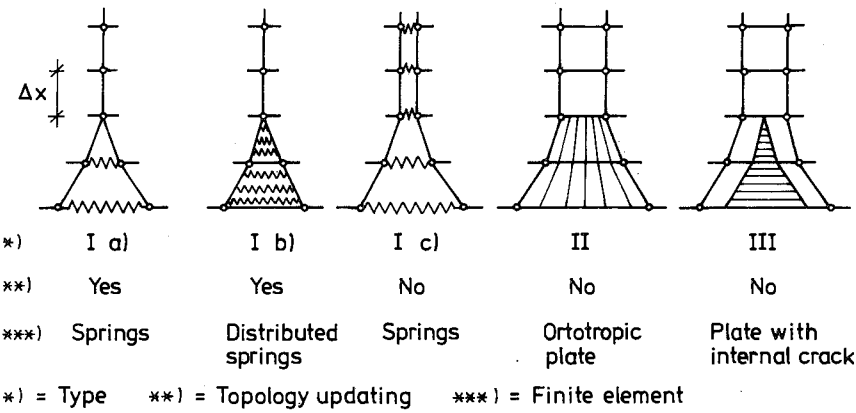

Fig 3.6 (1) Finite element models of fracture zone with known crack path.

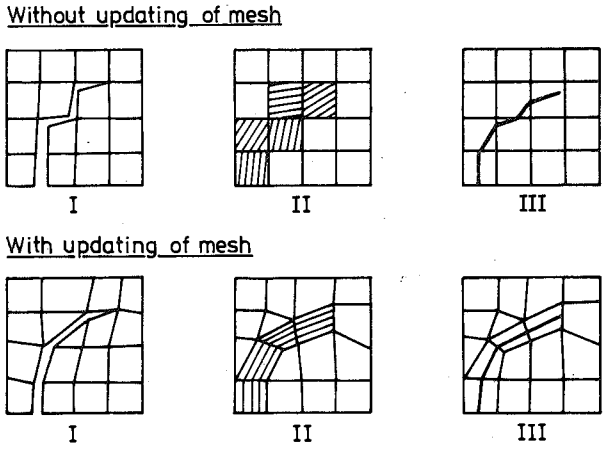

Fig 3.6 (2) Alternatives for finite element modelling of fracture with unknown crack path.

references above. In principle it should also be possible to apply these two alternatives with updating, but no such applications are known. Due to the lack of numerical experience, the writer cannot compare the advantages and disadvantages of the different alternatives.

Where alternative II without updating of the mesh (Fig 3.6 (2)) is

concerned, recent interesting results have been presented by Rots et al. (1985). On the whole these authors seem to have a positive opinion regarding the possibility of modelling discrete cracks with the smeared approach. However, on the basis of numerical results, it is stated that no objectivity is found regarding to the orientation of the finite element mesh: both crack path and load carrying capacity seem to be dependent on the mesh orientation. The crack is found to prefer to follow a straight path parallel to the element boundaries and it seems that the orientation of the fracture zone within the elements may prove to contradict the crack path direction. An explanation for the inobjectivity, proposed by the authors, is that the diagonal distance between the Gauss-points is greater than the straight distance. The actual results suggest that it might be meaningful to test alternative II with updating of the mesh, Fig 3.6 (2). It might also be that it would be meaningful to utilize analytical relations regarding the stresses in the vicinity of a fracture zone tip. For discrete crack representation and mode-1 loading, such a relation may be found in Section 3.2.4. A matter of importance on principle is that during applications of alternative II it seems to be (tacitly) assumed that the fracture zone propagates to the most strained point in the vicinity of the tip and consequently not always according to the direction of the principle stresses in the tip and its vicinity.

Fig 3.6 (1) and 3.6 (2) are only intended for showing basic alternatives. Thus, for instance, in the above mentioned references not only are 4-node elments used but also 3, 6 and 8-node elements. Grootenboer (1979) used the mixed displacement-stress finite element formulation instead of the conventional displacement formulation.

Going back to Fig 3.6 (1) and the method used during the present calculations, i.e. I a), the stiffness of the springs are set equal to $b(\Delta x/2+\Delta x/2)d\sigma/dw$, where b is the width of the specimen and $d\sigma/dw$ the slope of the σ-w curve. The adopted criterion for node opening is: $P_o/(b(\Delta x/2+\Delta x/2))=f_t$. P_o is the nodal force. An alternative to this criterion is: $\sigma_{mean}=f_t$, where σ_{mean} is obtained from the mean value of the stresses in the corner of the elements that meet in the actual node. This alternative has been used by Modeer (1979) and was also used in the first part of this present study. However, this alternative did not always give good results and has not been used during any of the analyses presented in this report. The drawbacks of the criterion based on σ_{mean} are that the stress in the corner of an element is, in general, not very reliable and

that the force $\sigma_{mean} b(\Delta x/2+\Delta x/2)$ is, in general, not in equilibrium with the nodal force, P_o. In spite of this, the criterium based on σ_{mean} may be successfully used during some analyses. One reason for this is that σ_{mean} is a mean value, and the accuracy of a mean value is in general better than the accuracy of the individual terms.

During the shear failure analyses, Section 4.7 and Chapter 5, it has been necessary to make a few modifications of the above described method. These modifications are described in Section 4.7 and Chapter 5. A method used during an analyses of a stactically indeterminate beam, i.e. the cross section of a pipe, by means of fracture hinge bending moment vs. rotation relations is described in Section 4.6.

3.6.3 Non-linear structural behaviour

The global response of a specimen in which softening takes place is non-linear. During finite element analyses, non-linear behaviour is linearized in one way or another. A frequently used approach is to apply the load or the imposed displacement in small increments and update the properties of the material after each increment. Another frequently used approach is to apply the load in larger increments, but carry out equilibrium iterations after each increment. If softening is involved, these incremental approaches means that the (tangential) stiffness of the material will become negative. If this is to be avoided, one possiblity may be to carry out "total" or "direct" iterations based on the segmential stiffness of the material.

Within these three approaches, the linearization of the non-linear response is carried out during the numerical calculation. An alternative to this is to linearize the properties of the material into linear pieces before the finite element calculation is started. This is feasible if the material is expected to behave in a non-linear manner only in a rather small number of points within the specimen and/or if the non-linear properties of the material may be linearized into a rather small number of linear pieces. During the present analyses and also during previous fictitious crack analyses carried out at the Divisions of Building Materials, this approach with a linearization of the properties of the material has been used. The approach has the advantage of being simple and seems to be numerically stable. If fracture takes place along a path with

n nodes and the σ-w curve is linearized into m pieces, then the total number of linear calculations becomes n(m+1).

Within the actual approach the choice of approximations, i.e. the choice of finite element mesh and the choice of linearizations, is made before the start of the finite element calculation. The subsequent step-wise linear finite element calculation is "exact", provided that the numbers have a sufficient number of digits. The possibility of carrying out simple and "exact" calculations is convenient for the analysis of the rather complicated structural behaviour during fracture, typically involving global softening, simultaneous decreases in external load and displacement (quasi-static structural behaviour is assumed), and during short periods of the collapse and very small increments in the external deflection drastic changes in the load carrying capacity and the development of the fracture zone.

If n(m+1) is not very great, then the calculations can be carried out with the help of a linear elastic finite element program together with calculations by hand. The procedure is then to carry out the first linear finite element calculation, evaluate and accumulate the results, prepare the input data for the next linear finite element calculation, and so on. This procedure only requires access to a standard linear elastic finite element program. However, the program must allow a negative stiffness in the fracture zone modelling springs and the algorithm for solution of the system of equations must be capable of treating a stiffness matrix with a negative determinant. The often used direct Gaussian elimation is capable of solving such equations.

The above computer aided hand-calculation procedure was applied during the first part of the present study, but it was discovered that this approach is not very convenient if several calculations are to be carried out. Therefore a simple non-commercial special-purpose program was developed. This program essentially only represents an automatization of the hand-calculation procedure. Thus the program consists of three parts: one part for the (step-wise) linear elastic calculations, one part for the evaluation and accumulation, and one part for the preparation of input data to the next linear increment. Such an automatization reduces calculations by hand, but the computer time and/or the required computer storage may still become significant. However, if the crack path is known or assumed in advance, then the degrees of freedom outside the path may be

eliminated by means of static condensation before the step-wise linear calculation is started. This is because the topology and the material properties only change along the path. During the present analyses the possibility of static condensation is utilized and consequently the crack path is assumed in advance (although a few different alternative paths have been considered in some cases). The static condensation is carried out by means of the previously mentioned program GENFEM-3, and in Fig 3.6 (3) the different steps of the calculations are shown. As shown in this figure, the reduced system of equations may be filed, forming a kind of substructure library. Due to limited core memory it is usually not possible to carrry out the condensation in one step, but instead the final substructure elements are put together from sub-substructure elements.

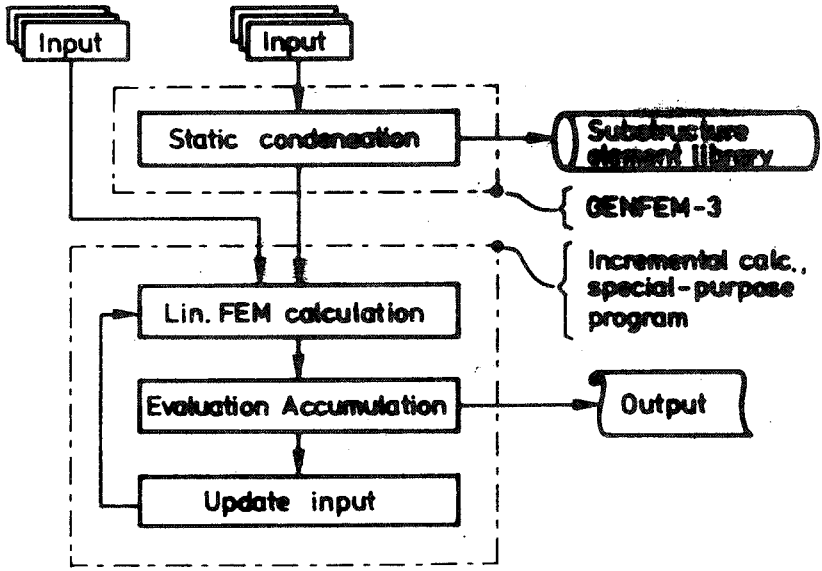

Fig 3.6 (3) Flowchart showing the method used for finite element calculation during fictitious crack analysis.

The method used for treatment of the non-linear structural behaviour is rather trivial and involves few difficulties that may be of interest in principle. One thing that might be expected to cause difficulties is that the value of the determinant of the global stiffness matrix changes from

positive to negative and consequently passes zero. However, as the stiffness is changed incrementally, the probability of the determinant becoming exactly zero is very small. Although not exactly zero, a value close to zero may give a poor solution to the system of equations, in particular if the numerical precision is small. All applied calculations presented in Chapters 4 and 5, have been carried out in "double precision" (about 17 digits of accuracy) and any difficulties caused by a value of the determinant close the zero have not been observed so far. To check whether the solution to the system of equations is correct, the incremental work within the finite elements is calculated and compared to the incremental work carried out by the external load.

Another matter that may be of some interest in principle, is the method for the choice of sign of the incremental external load. During each of the linear finite element calculations, the incremental deflection that corresponds to unit external load is calculated and then the actual sign of the increment is determined. Knowing the sign, the size is calculated as the smallest increment which produce opening of a new node or change in the stiffness of a spring. If the calculations are carried out more or less by hand, then it is usually easy to determine the sign by intuition. But during computerized calculations it is necessary to have some clearly defined criterion. This is, in particular, necessary if the finite element mesh is coarse or unsuitable in some other way. In such cases, the structural behaviour may become jumpy and complicated. The used criterion is that the sign, in a generalized sense, of the change of the global tangential stiffness must equal the sign of the change of the stiffness of the material. The phrase "in a generalized sense" is just to indicate that the sign of the second derivate cannot be used. This is due to the possibility of simultaneous decrease in both load and deflection during quasi-static crack growth. The actual criterion may be more clearly defined by means of the sign of vector rotations:

$$\mathrm{sgn}(S_i)\,\mathrm{sgn}(\bar{e}_z \cdot (\bar{S}_{i-1}\bar{E}_{i-1} \times \bar{E}_i)) = \mathrm{sgn}(\bar{e}_z \cdot (\bar{M}_{i-1} \times \bar{M}_i)) \qquad (3.6{:}1)$$

The vectors are illustrated in Fig 3.6 (4). $\mathrm{sgn}(S_i)$ is the sign of the actual increment and is to be determined. $\bar{e}_z = (0, 0, 1)$ and $\bar{E}_i = (\Delta\delta_i, 1, 0)$ where $\Delta\delta_i$ is the response of the structure when a unit load is applied after the change in the stiffness properties of a spring from $\bar{M}_{i-1}$ to $\bar{M}_i$. $\bar{E}_{i-1}$ is the unit load response of the previous step and S_{i-1} represents the sign of the previous increment. The

criterion represented by eq (3.6:1) is easily programmed and has proved to be useful.

During some of the applied analyses, the influence of internal initial stresses within the structure, caused by shrinkage or pre-stressing of reinforcement, has been studied. From the computational point of view, this is similar to a case of non-proportional loading. Thus the accumulated stresses across the fracture path are not zero when the first external load is applied, but are according to the actual initial stresses.

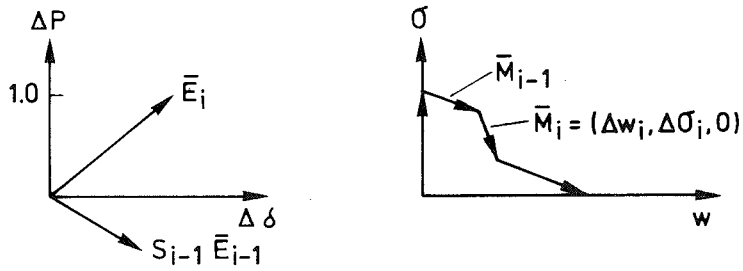

Fig 3.6 (4) Vectors in eq (3.6:1).

3.6.4 Convergence

To illustrate the order of convergence rate, the load acting on the specimen shown in Fig 3.2 (7) is calculated during different refinements of the finite element mesh. In Section 3.2.4 this specimen was numerically studied in order to verify theoretical relations regarding the performance close to the tip of the fracture zone. The specimen is un-notched and at the actual instant the tip is located at $x/d=0.2$, i.e. the nodal force in this point is equal to $f_t b\Delta x$.

In general, if the stress within a finite element is represented by a polynomical expansion of order p, one may expect the error in the calculated stress to be of the order $O(\Delta x^{p+1})$, where Δx is a measure of the size of the element. In the presently used method of calculation, the stress across the fracture zone path is represented by parts in which the stress is assumed to be constant: please see Fig 3.2 (8) and Fig 3.6 (1) I a). Consequently stress to be

of the order $O(\Delta x)$. The accuracy during calculation of the stress in the tip of the crack is the primarily determining factor for the accuracy in the calculated external load. Accordingly the error in the load may be expected to be of the order $O(\Delta x)$, i.e. the convergence rate should be of the order one. Thus, if P is the calculated load and P_e is the exact load, then

$$\frac{P - P_e}{P_e} = C\Delta x + \ldots \qquad (3.6:2)$$

C is a constant of proportionality and $C\Delta x$ is the dominating term in the series expansion. Subsequently only this dominating term is taken into account. (3.6:2) means that the error in P should be reduced to 1/2 for a halving of the mesh spacing.

In order to verify (3.6:2), P is calculated by means of five different element meshes: $d/\Delta x=5$, 10, 20, 40 and 80 and accordingly with 1, 2, 4, 8 and 16 springs in the fracture zone. The same type of plane stress element and the same computer program as used in Section 3.2.4 is used. The above values of $d/\Delta x$ represent the size of the elements in the region around the fracture zone while, for $d/\Delta x$ greater than 10, the mesh is coarser in the other parts of the beam. The computational results are shown in Fig 3.6 (5). These results suggest an almost exact linear relation between the load and the mesh spacing, and are accordingly in very good agreement with (3.6:2).

This agreement enables an estimation of the exact load, P_e, by extension of the straight line to $\Delta x=0$. Such an extension gives $P_e \approx 0.1825$ MN. The results also suggest that modelling of the fracture zone with only one spring gives a result within engineering accuracy. It can also be noticed that any finite size of the elements give an overestimation of the load. An overestimation is to be expected since the peak stress at the tip of the fracture zone is smeared out when, as in the present case, the stress across the fracture path is represented by parts in which the stress is constant. A very important result is, of course, that the load converges towards a certain value when Δx is decreased. However, in view of the discussions in Sections 3.2.4 and 3.3, the existance of a limit value may not be very surprising.

Knowledge of the order of convergence gives the possiblity of obtaining an accurate estimation of P_e from the values of P obtained during two finite

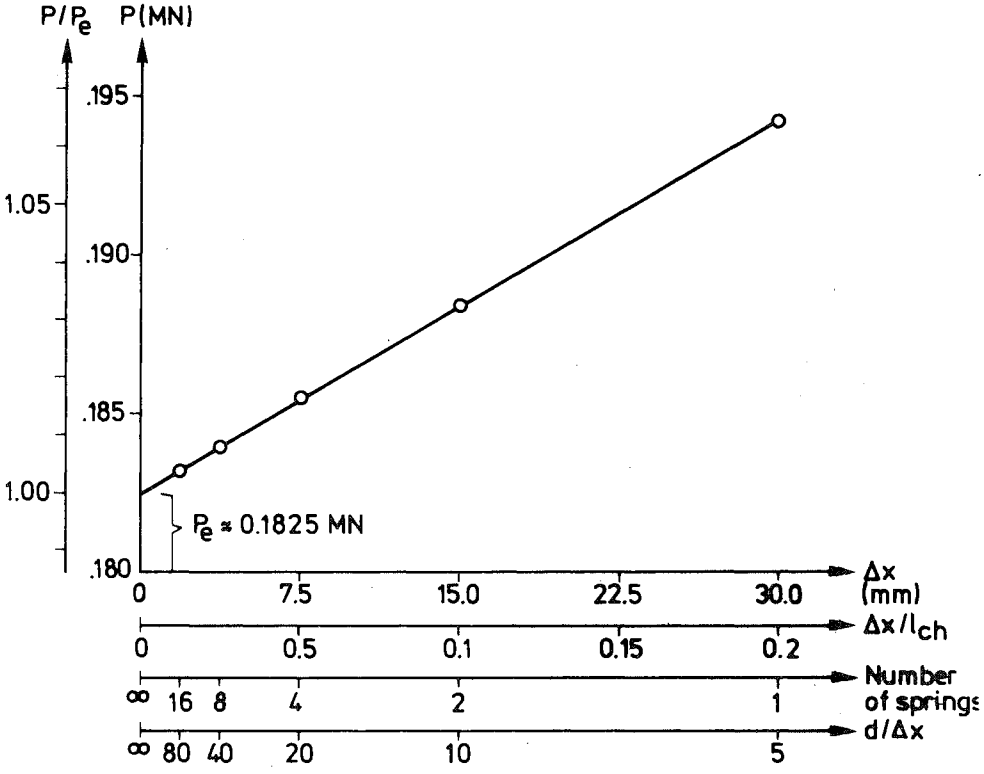

Fig 3.6 (5) Influence of mesh refinement on accuracy: calculated load, P, vs. size of finite elements, Δx. Specimen according to Fig 3.2 (7).

element analyses with different mesh spacing. If P_A is the value of P corresponding to any certain mesh spacing and P_B is the value of P obtained after halving the mesh spacing, then, according to (3.6:2):

$$P_e \approx 2P_B - P_A \qquad (3.6:3)$$

Of course this relation does not eliminate, or reduce, the round-off errors, only the discretization errors. On the other hand, the round-off errors would normally be very small in comparison to the discretization errors.

Application of (3.6:3) to the results of Fig 3.6 (5) give a notable accuracy: a finite element calculation with only one element in the

fracture zone together with a finite element calculation with only two elements in the fracture zone gives a more accurate result than a single calculation with 16 elements in the fracture zone. The corresponding deviations from the estimated exact P_e are about 0.1 % and 0.4 %, respectively.

Although the numerical results in Fig 3.6 (5) are in agreement with eq (3.6:2), it is rather remarkable that the relation between the error and the mesh spacing seems to be not only approximately linear but almost exactly linear. Therefore, in order to verify that the interesting features of the convergence suggested by Fig 3.6 (5) are not by pure chance, three additional convergence analyses have been carried out. The results of the above and the three additional analyses are shown in Fig 3.6 (6). The analysis denoted a/d=0 and $d/\ell_{ch}=1$ is according to the above, i.e. according to Fig 3.6 (5) and Fig 3.2 (7). The analysis denoted a/d=0 and $d/\ell_{ch}=0.25$ is according to Fig 3.2 (7), but $G_F=320\ 10^{-6}$ MN/m. The analysis denoted a/d=0.1 and $d/\ell_{ch}=1$ is according to Fig 3.2 (7), but the beam is assumed to have a sharp notch of depth 0.1d. The analysis denoted a/d=0.1 and $d/\ell_{ch}=0.25$ is according to Fig 3.2 (7), but $G_F=320\ 10^{-6}$ MN/m and the beam is assumed to have a notch depth of 0.1d. The main features of convergence suggested by the additional analyses are in agreement with the result of the first analysis. However, when the fracture zone is modelled with only one spring, then deviations from exactly linear relations can be observed. The straight lines shown in Fig 3.6 (6) are drawn through the two points that correspond to the two finest meshes. These two points are also used during the calculation of P_e, carried out by means of eq (3.6:3).

Above, the load at a given location of the crack tip has been dealt with. The convergence of the ultimate load carrying capacity may not be expected to follow (3.6:2) as well as the load at a given location of the tip. This is because the load is calculated only for the certain locations of the tip that corresponds to the locations of the nodes. If the ultimate load carrying capacity corresponds to a location of the tip in between two nodes, then the ultimate load carrying capacity will be underestimated as compared to the finite element result obtained if a node happens to be located exactly on the location where the exact load reaches its maximum value. On the other hand, according to the results in Fig 3.6 (6), the finite element calculations overestimates the load at the points where the load is calculated.

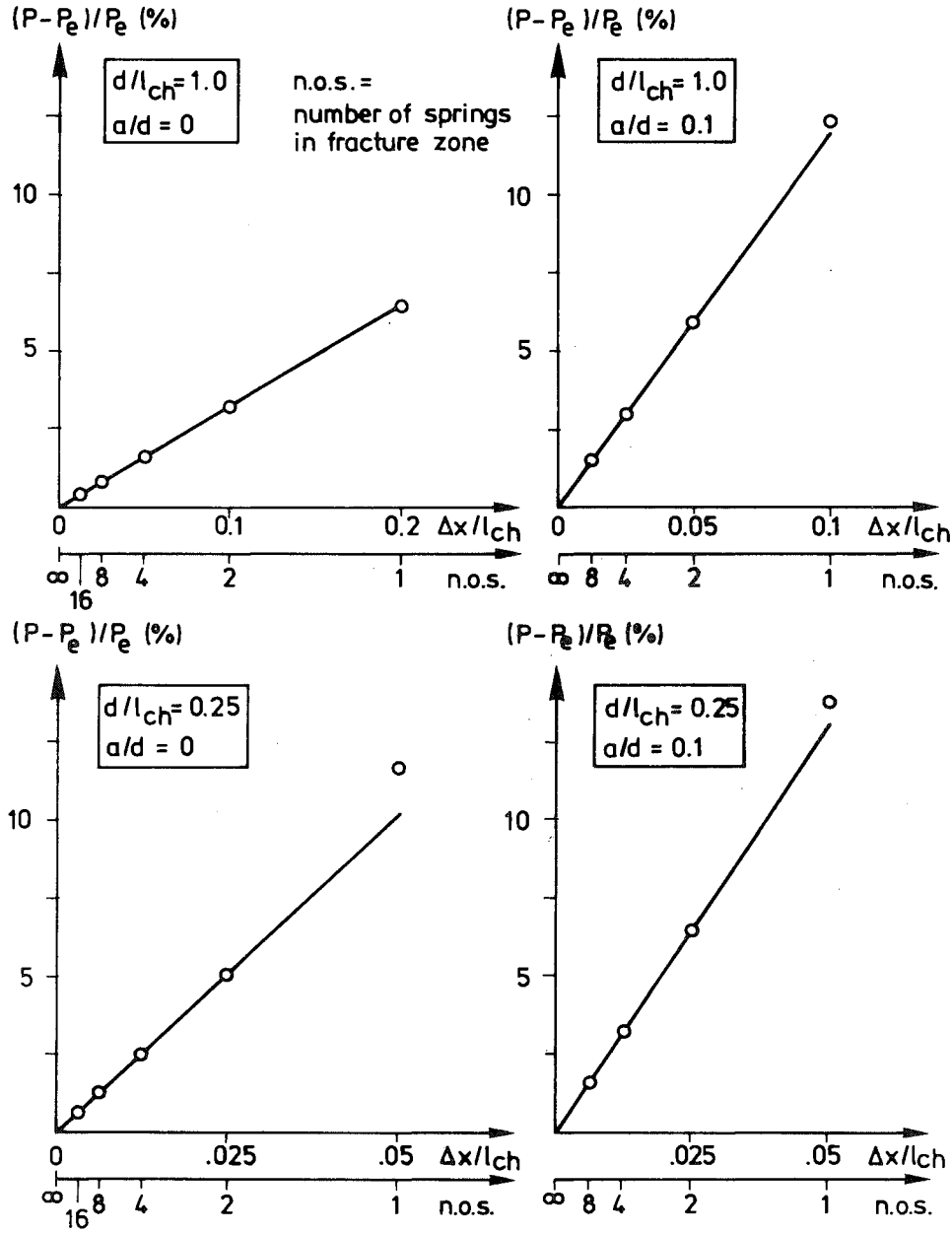

Fig 3.6 (6) Accuracy versus finite element spacing. Comparisons to the theoretically linear relation

It would be good to have a simple general rule of thumb regarding the required mesh spacing for a certain accuracy. However, as a number of things generally influence the accuracy in the actual quantity to be calculated, it is not very easy to formulate such a general rule. The best way to obtain knowledge and experience is probably by means of test calculations. Modeer (1979) suggested that the required mesh spacing should be measured in $\Delta x/\ell_{ch}$ and proposed $\Delta x/\ell_{ch} < 0.2$. This proposal probably concerned the calculation of ultimate load carrying capacity and is probably based on the assumption that the number of springs in the fracture zone should not be too few. This would mean that the length of the fracture zone at failure is assumed to be proportional to ℓ_{ch}. The measure $\Delta x/\ell_{ch}$ has the advantage of making it possible to choose a mesh without any test calculation and may give a reasonable first estimation of required mesh spacing, but is not believed to give a very modulated estimation. One may expect the greatest suitable allowed value of $\Delta x/\ell_{ch}$ to be dependent on the shape of the σ-w curve and maybe also to some extent be dependent on the geometry of the specimen. If the shape of the σ-w curve and the geometry of the specimen are kept constant and if the analyses concern ultimate load carrying capacity, one may still expect the accuracy at constant $\Delta x/\ell_{ch}$ to vary with the only variable left: d/ℓ_{ch}. With small d/ℓ_{ch} the length of the fracture zone at failure as normalized with respect to ℓ_{ch} is smaller than with a large d/ℓ_{ch}: please see, e.g., Fig 5.2 (21) and 5.3 (5) e). Furthermore, where the unnotched specimens are concerned, the fracture zone development has a greater influence on the load carrying capacity of specimens with small d/ℓ_{ch} than on the load carrying capacity of specimen with large d/ℓ_{ch}. Also, of course, if $\Delta x/\ell_{ch}$ is constant, then $d/\Delta x$ may become unrealistically small if d/ℓ_{ch} is very small. For these reasons it is believed that larger $\Delta x/\ell_{ch}$ can be used for large d/ℓ_{ch} than for small d/ℓ_{ch}.

During variation of only d/ℓ_{ch}, for the large and very large d/ℓ_{ch} a constant value of $\Delta x/\ell_{ch}$ should be a good measure of the required mesh spacing. This means that extremely "small" elements may have to be used if the fracture of a very large specimen or the fracture of a very brittle material is to be analysed. However, during strength analysis of these specimens with very large d/ℓ_{ch}, the relations dealt with in Section 3.5 should be of assistance.

4. STRENGTH AND FRACTURE ANALYSES OF SOME UNREINFORCED SPECIMENS AND STRUCTURAL MEMBERS

4.1 Introduction. Survey of specimens studied

The basic aim of models regarding the mechanical behaviour of materials and numerical methods of structural analysis may be to facilitate applied calculations of ultimate load carrying capacity. In this Chapter such strength analyses of different unreinforced specimens and structural members are presented. Although a common theme of the results concerns the ultimate load carrying capacity, the purpose of most of the studies is, from a few different points of view, more comprehensive. Consequently the analyses presented are intended to contribute to the knowledge about fracture, models of fracture and methods of analyses, rather than to form a handbook regarding the strength of a few different specimens.

In order to facilitate reading, a survey of the specimens dealt with in the different Sections is shown in Fig 4.1 (1), which also indicates the models of fracture dealt with and the type of results obtained. The studies presented have been chosen in order to elucidate a few different aspects of strength analyses and in many cases comparisons are made to experimental data from literature. Fig 4.1 (1) shows that different types of models of fracture are dealt with, but it should be made clear that greater parts of the contents, in one way or another, concern the fictitious crack model. This model is emphasized because most of the other models dealt with may be considered as different special cases of the fictitious crack model. To obtain more detailed information about the contents, the reader is referred to the table of contents and to the introduction of each Section.

Section	Specimen	Internal initial stress	Model of fracture					Combinations	Type*) of result
			Brittle	FCM	Plastic	LEFM	Weibull		
4.2		X	X	X	X	X	X	X	M T D
4.3				X		X			M T
4.4		X		X		X			M T
4.5		X	X	X	X				T D
	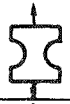		X	X	X				T
4.6		X	X	X	X		X		M D
		X	X	X	X		X		M D
4.7				X		(X)			M D

*) M = of interest in studies of models of fracture and methods of analysis
T = of interest in testing of material properties
D = of interest in design

Fig 4.1 (1) Survey of specimens, models of fracture and type of results, dealt with in Chapter 4.

4.2 Bending of rectangular cross section

4.2.1 Introduction. Previous fictitious crack analyses. Purpose of present study.

Concrete structural members exposed to bending are usually reinforced. But in spite of this, analyses of unreinforced concrete beams loaded in bending have been the subject of a number of experimental and theoretical investigations. One reason for this is that the bend test, being simple to carry out, conveniently provides some information about a very important property of concrete, namely its tensile strength. Another reason, perhaps less important, is that the bend specimen is often suitable for experimental and theoretical research concerning mechanical properties of concrete and that the difficulties regarding studies of the geometrically simple bend-specimen have become something of a challenge to researchers. The flexural strength of unreinforced concrete is of direct practical importance to some mass-produced concrete products, such as paving slabs, sewage pipes and roofing tiles, and some of in-situ cast structures, such as road slabs and airfield runways as well as structural members and structural details which are unreinforced or only slightly reinforced although loaded in bending. Where normally reinforced concrete beams are concerned, the flexural strength of the concrete is used when calculating the cracking load and deflection.

The flexural test is one of the two standard tension tests, but it is a well-known fact that the flexural strength in general does not equal the true uniaxial tensile strength, and experimental results also suggest that the flexural strength is not a constant but is dependent on the geometry of the specimen. Experimental results concerning flexural strength have been collected by Neville (1981) and by Bellander, Peterson and Samuelsson (1980) and these references also provide general discussions of the flexural test as well as additional references on the subject of flexural strength.

The first analyses of the fictitious crack model published in English concerned the flexural strength of unreinforced concrete (Hillerborg, Modeer and Petersson, 1976). Computational results regarding the effect of the beam depth on flexural strength were presented and these theoretical results indicated that the flexural strength decreases with increased depth of the bea[illegible]/e a greater

effect on the strength of deep beams than on the strength of small beams. A comparison between the theoretical predictions and a large number of experimental results showed good agreement. Similar analyses are presented by Modeer (1979), which in particular indicated that the shape of the σ-w curve, at constant values of f_t, E and G_F, significantly influences the ratio between flexural strength and tensile strength. At the moment of ultimate load, the fracture zone is only partly developed and accordingly it was found that the slope of the first part of the σ-w curve is essential to the ultimate strength, while the shape of the last part of the σ-w curve, corresponding to comparatively large values of w and post ultimate load states of fracture of the beam, is often of no importance regarding the ultimate flexural strength. In (Petersson and Gutafsson, 1980) some computational results concerning the influence of the choice of the finite element mesh were presented. These results indicated that the computational method seems to be objective in the sense that the computational results are independent of the size of the finite elements apart, of course, from the effect of normal discretization errors at finite size of the elements. A model rather similar to the fictitious crack model was used by Bazant and Oh (1983). Computational results concerning the effect of beam depth on flexural strength were presented and according to theoretical discussions and by comparison to previous results obained by fictitious crack analysis, it was indicated that it does not make much difference whether the fracture softening is assumed to take place along a line of zero initial width or if it is assumed to take place along a band with an initially non-zero constant width, provided that the assumed strain softening properties of the material within the band are related to the assumed absolute width of the band. The present fictitious crack study of the flexural strength of an unreinforced three-point bend beam without notch and with a rectangular cross-section may be considered as one amplification to the previous analyses.

One main purpose of the present study was to calculate flexural strengths assuming the shape of the σ-w curve in accordance with a proposal by Petersson (1981) based on experimental results obtained during stable tensile tests (Section 4.2.2). Another purpose was to calculate the global load-deflection responses of three-point bend beams and then transform these responses into fracture hinge bending moment vs. fracture hinge rotation relations (Section 4.2.3). Such relations may become useful during structural analyses at a higher structural level than the current "micro-level" in which the fracture zone growth is dealt with in a rather

detailed manner by means of a two dimensional plane stress analysis, taking into account a rather high number of degrees of freedom.

The present calculations were carried out with, and without consideration of initial stresses, which stresses may reflect the effect of a non-uniform distribution of shrinkage strains. In Section 4.2.4 two special characteristics of the fracture hinge moment vs. rotation relations are dealt with: the transfer of energy during the entire course of fracture and collapse, and the shape of the moment vs. rotation relation during advanced stages of collapse. In Section 4.2.5 comparisons to other methods of analysis and to test results can be found together with remarks and discussions: firstly with regard to flexural strength and then with regard to bending moments vs. hinge rotation relations. With regard to flexural strength, this last Section in particular includes a study of the effect of scatter in strength. With regard to hinge rotations it is, more briefly, dealt with a comparison to result obtained by linear elastic fracture mechanics, and it is also briefly dealt with a method for description of the stiffness and fracture properties of beams, and a method for simple calculation of the upper and lower bounds of fictitious crack predictions of the strength of statically indeterminate beams is exemplified.

4.2.2 Ultimate bending moment capacity

A three-point bend beam with a length to depth ratio of 4 was studied. Plane stress, $\nu = 0.2$, was assumed and the bi-linear shape of the σ-w curve, Fig 3.2 (3) c), was adopted. The numerical approach is described in Section 3.6. The symmetrical half of the beam was divided into 6 super-elements, Fig 4.2 (1), each super-element being an assembly of 5 times 40 4-node rectangular non-conformal plane stress elements of the Turner and Clough type and of equal size and shape. Statical condensation was utilized and consequently only the degrees of freedom along the considered fracture zone propagation path along the centre line of the beam were involved in the incremental calculations. In accordance with the principle of Saint-Venant, the current rather fine element mesh close to the supports is not justified if only the ultimate strength and fracture hinge moment vs. rotation relations are to be calculated, but it is desirable when calculating of global stiffness and particularly if the point of instability at d[illegible]ermined. (The

same element mesh was used in a study of a notched beam.)

In some of the calculations initial stresses corresponding to a non-uniform distribution of shrinkage strains were taken into account. In the mid-section of the the beam, these initial stresses were assumed to be parabolically distributed along the depth of the beam and the magnitude of the initial stresses was assumed to be such that the stress in the upper and lower edges of the beam was equal to the tensile strength of the concrete, f_t. This assumption of magnitude and distribution is valid for the fracture section, located at the centre of the beam, while the initial stresses are smaller closer to the ends of the beam.

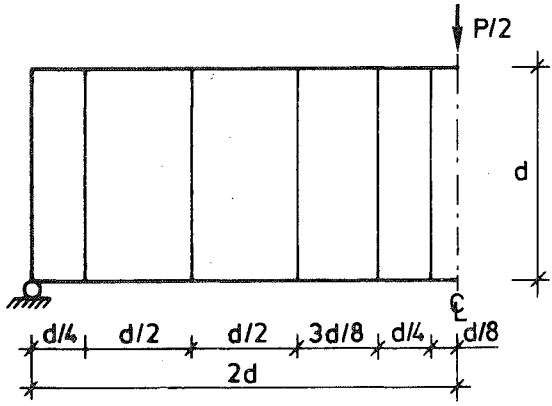

Fig 4.2 (1) Geometry and finite element mesh of the beam studied. Each of the six "super"-elements consists of 5 (horizontal direction) times 40 (vertical direction) 4 node rectangular elements of equal size and shape.

The flexural strengths were calculated at values of the ratio d/ℓ_{ch} ranging from 0.025 to 6.4, and the computational results are shown numerically in Fig 4.2 (2) and graphically in 4.2 (3). The number of finite elements required to model the grovth of the fracture zone accurately, increases at increased size of the beam, i.e. at increased value of the ratio d/ℓ_{ch}, and the computed flexural strength at $d/\ell_{ch}=6.4$ is probably not very accurate as the depth of the fracture zone at ultimate load at $d/\ell_{ch}=6.4$ corresponded to the depth of only one finite element, both where zero initial stress and initial stress were concerned. The current si[illegible]e zone

propagation path, $d/\ell_{ch}=6.4$ corresponds to $\Delta x=0.16\,\ell_{ch}$, where Δx is the distance between the nodes along the fracture path. This value of the ratio $\Delta x/\ell_{ch}$ may be compared to the proposal made by Modeer (1979) with respect to the required maximum distance between the nodes, namely $\Delta x<0.2\,\ell_{ch}$, which may however be somewhat overgenerous. When $d/\ell_{ch}\rightarrow\infty$ respectively $d/\ell_{ch}\rightarrow 0$ the fictitious crack predictions of flexural strength coincide with those of the linear elastic brittle theory and the ideal plastic theory respectively, regardless of whether initial stresses are present or not.

The values of flexural strength are indicated in Fig 4.2 (2) and 4.2 (3) as the ratio between the currently predicted ultimate load and the ultimate load as predicted by the linear elastic brittle theory when the initial stress is zero. The ultimate load according to the latter theory coincides with the load at the instant when the stress in the lower edge of the beam equals f_t. For a slender beam in three-point bending this load is equal to $(4/\ell)f_t(bd^2/6)$. For a short beam this expression is only approximate. A more accurate expression for the ultimate load of a beam in three-point bending, as predicted by the linear elastic brittle theory, is provided by Timoshenko and Goodier (1951): $(4/\ell)f_t(bd^2/6)/(1.0-0.1773d/\ell)$. The currently presented values of flexural strength, obtained at $\ell/d=4$, are normalized to this more accurate linear elastic brittle value of flexural strength. In the case of three-point bending of a short beam, this means that f_f/f_t should be interpreted as $(P_u\ell/4)(1.0-0.1773d/\ell)/(f_t bd^2/6)$ where P_u is the ultimate load. Normally in the case of the bending of a slender beam, f_f/f_t should preferably be interpretated as $M_u/(f_t bd^2/6)$ where M_u is the ultimate bending moment. Accordingly f_f/f_t should approach 1.0 when $d/\ell_{ch}\rightarrow\infty$.

At $d/\ell_{ch}\rightarrow\infty$, i.e. in the case of a linear elastic brittle behaviour of the material, the formula of Timoshenko and Goodier yields $P_u=1.046\,(4/\ell)f_t(bd^2/6)$ at $d/\ell=1/4$, while the finite element results yielded $P_u=1.053\,(4/\ell)f_t(bd^2/6)$. This finite element value of P_u is obtained by means of linear extrapolation: the bending stress is assumed to be zero at the depth d/2 of the beam and the interelement nodal force in the lower edge of the beam is assumed to represent the mean stress along the half of the depth of one element, i.e. the nodal force in the lower edge of the beam divided by d/80 is assumed to represent the stress at the depth d/160 of the beam. The 0.7 % difference in flexural strength at $d/\ell_{ch}\rightarrow\infty$ acc[illegible]ier

respectively according to the finite element results may be explained by the approximations involved in finite element analysis and may approximately be considered to be of negligible magnitude.

The main features of the currently obtained values of flexural strength are in agreement with the results of previous fictitious crack analyses.

d/ℓ_{ch}	$\frac{M_u}{f_t(bd^2/6)/(1-0.1773d/\ell)}$	
	No init. stress, $\sigma_i/f_t = 0$	Init. stress, $\sigma_i/f_t = 1.0$
$\to 0$	2.867	2.867
0.025	2.157	2.087
0.050	1.982	1.858
0.10	1.794	1.585
0.20	1.601	1.271
0.40	1.419	0.935
0.80	1.263	0.666
1.60	1.148	0.409
3.20	1.079	0.181
6.40	1.040	0.074
$\to \infty$	1.000	0.000

Fig 4.2 (2) Ultimate bending moment, M_u, at different values of d/ℓ_{ch} and with and without consideration of initial stress according to Fig 4.2 (3). M_u as obtained in the present finite element fictitious crack analyses of a three point bend beam: $d/\ell = 1/4$ and σ-w curve according to Fig 3.2 (3) c). Values at $d/\ell_{ch} \to 0$ resp $\to \infty$ are obtained analytically.

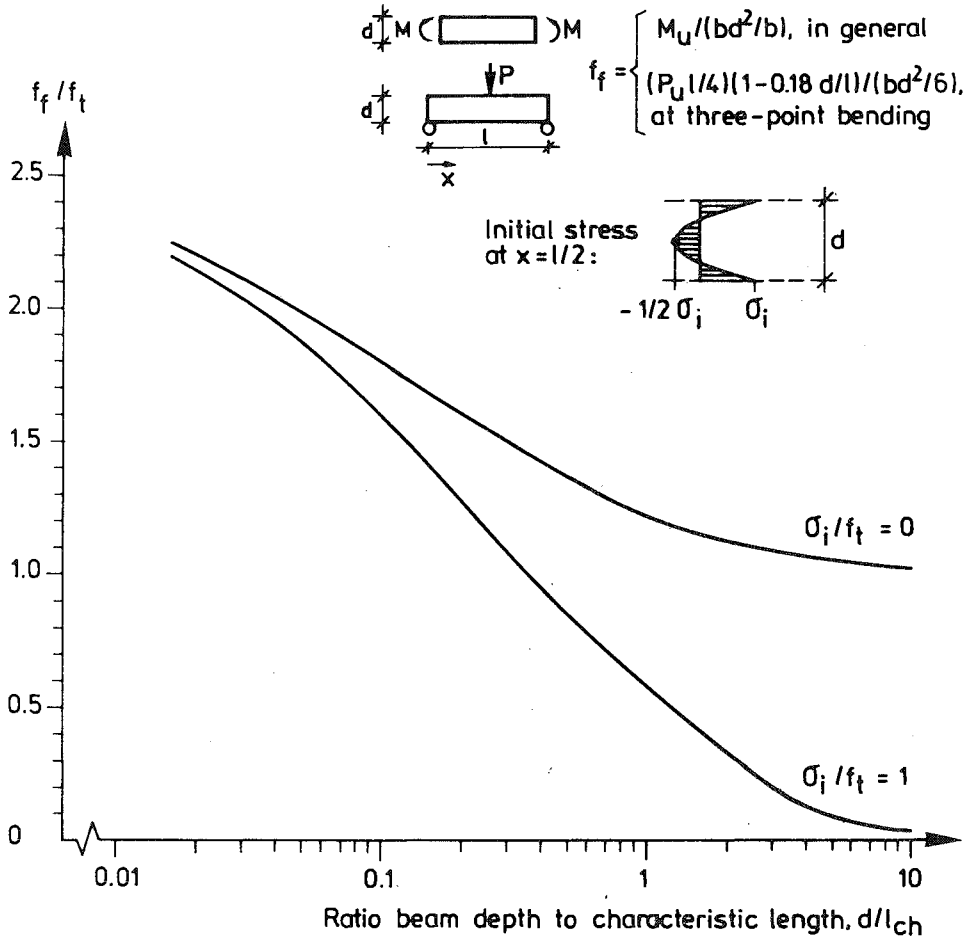

Fig 4.2 (3) Ratio flexural strength and tensile strength, f_f/f_t, vs. ratio between beam depth and characteristic length of material, d/ℓ_{ch}. Theoretical result of fictitious crack analysis. Shape of the σ-w curve in accordance with Fig 3.2 (3) c).

4.2.3 Fracture hinge moment vs. rotation relations

During strength analyses of statically indeterminate beams as well as during some other analyses, calculations are made easier if it is possible to replace the two-dimensional plane stress analysis by the more simple ordinary beam-theory type of analysis. In order to include consideration of the fracture properties of the beam in such an analysis, one may model the behaviour of the fracture section by a one degree of freedom moment spring element. The non-linear properties of this spring should then be determined in such a way that the external bending stiffness of the beam is equal when analysed according to Fig 4.2 (4) a) respectively according to Fig 4.2 (4) b). The spring in Fig 4.2 (4) b) should consequently reproduce then bending capacity of the fracture section vs. the additional rotation that arises due to fracture of the material. In the case of the uniform bending moment along the beam, it is obvious that several fracture zones will start to develop from the lower edge of the beam before the ultimate bending moment is reached. First after peak moment, one of the fracture zones will dominate the fracture of the beam. In the current study, however, only one fracture zone is considered and the present fracture hinge moment vs. rotation relations are valid for the additional deformations in a beam due to the development of one fracture zone. If the growth of several fracture zones were considered, the ascending part of the moment vs. deformation response of a section of a beam should normally be descrided in the moment-curvature diagram. General separation of deformation into curvature and rotation is illustated in Section 4.2.5.

The properties of the moment springs have not been obtained by analysis of a beam in uniform bending, Fig 4.2 (4) a), but by load-deflection analysis of a beam in three-point bending, Fig 4.2 (4) c). The load-deflection responses, P vs. δ, that formed the basis for the calculation of the stiffness properties of the springs, M vs.θ , were obtained during the plane stress finite element fictitious crack analysis described in Section 4.2.2. Knowing P vs. δ, M vs.θ were obtained by the relations:

$$M = \frac{P\ell}{4}$$

$$\theta = \frac{4}{\ell}(\delta - \delta_o) = \frac{4}{\ell}(\delta - \frac{P}{k}) \qquad (4.2:1)$$

where k is the stiffnes of the specimen before the start of fracture zone growth and th[illegible].2 (4) c). It may

be noted that the rotation θ only models, and should only model, the additional deflection due to the fracture zone propagation. Thus additional deflections, i.e. deflections obtained during plane stress analysis byt not during ordinary beam-theory analysis, due to local deformations close to the supports, local deformations close to the point of load application and shear deformations along the beam are not included in the rotation θ.

The computational results are shown in Fig 4.2 (5) to Fig 4.2 (10). The complete curves in these figures show in a dimensionless manner bending moment vs. rotation, i.e. M/M_o vs. $\theta/(f_t/E)$, at different values of the ratio d/ℓ_{ch}. The dashed curves show the depth of the fracture zone: a denotes the distance from the lower edge of the beam to the point were the stress is equal to f_t and d is the total depth of the beam. M_o is the bending moment at the start of fracture zone grovth: $M_o = 1.046\, f_t (bd^2/6)$ in the case of three-point bending of a beam with a length to depth ratio of 4. Fig 4.2 (5), 4.2 (7) and 4.2 (9) refer to the case of zero initial stress and correspond to the ranges 0-0.8, 0-8.0 respectively 0-80 of the rotation $\theta/(f_t/E)$. Fig 4.2 (6), 4.2 (8) and 4.2 (10) refer similarly to the case of non-zero initial stress. The M/M_o vs. $\theta/(f_t/E)$ curves shown are as obtained from the numerical calculations and consequently they are not ideally smooth non-linear curves but consist of a large number (70) of linear pieces, reflecting the piece-wise linear incremental finite element calculation of the load-deflection response of the respective beam. In spite of the piece-wise linear type of calculation the M vs. θ curves exhibit a very smooth over-all non-linear shape, with the exception of the curves corresponding to high values of d/ℓ_{ch}. The calculations were stopped after 70 increments but the M vs. θ curves may be extended by extrapolation. This will be discussed in Section 4.2.4.

Fig 4.2 (5) to 4.2 (10) indicates that a decrease in d/ℓ_{ch} does not only produce an increase in the ultimate bending capacity but also a drastic increase in the rotation capacity. The computational results also indicate that initial stress has much more effect on the M vs. θ curves at high values of d/ℓ_{ch} than at low values of d/ℓ_{ch}. These two features of the M vs. θ curves may also be realized by considering the transfer of energy during the course of fracture and collapse, see Section 4.2.4. It is interesting to notice that a stable fracture requires that the applied bending moment has to be temporarily negative in the case where $d/\ell_{ch}=6.4$ and inititial st [illegible] teresting,

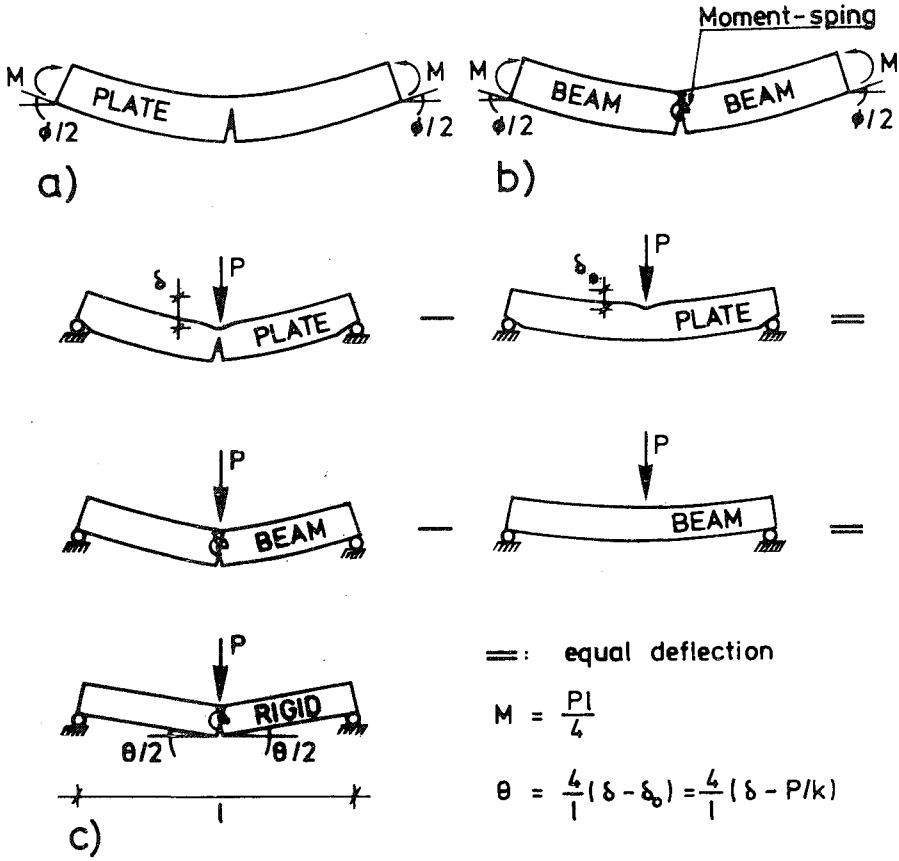

Fig 4.2 (4) a) and b): Slender beam in pure bending and with a single fracture zone modelled by, a), plane stress and by, b) beam theory. Definition of M vs.θ : the properties of the moment spring, M vs.θ , is such that M vs. ϕ is equal in a) and b).

c): Illustration of the method currently used to obtain M vs.θ by means of plane stress load-deflection analysis.

although not surprising, that the relative depth of the fracture zone, a/d, at ultimate load is greater at low values of d/ℓ_{ch} than at high values of d/ℓ_{ch}. Results regarding the depth of the fracture zone may also be found by Fig 4.2 (21). This latter figure shows the length, s, of the zone at different o

The computational results indicate that $\Delta\theta/\Delta(a/d)$ is very small at the beginning of the fracture and great during the advanced stages of the collapse, and with respect to discussions of simultaneous growth of several cracks it is of particular interest to note that the computational results seem to suggest that $d\theta/d(a/d) \rightarrow 0$ when $a/d \rightarrow 0$. This condition suggests that the change of the slope of the bending moment vs. curvature curve of, for instance, a beam in uniform bending is finite even if the fracture zones in the lower edge of the beam are very closely located at the start of fracture of the material. The condition also suggests that the fracture zones in the lower edge of the beam have to be infinitely closely located in order to attain a non-zero change in the slope of the bending moment vs. curvature curve at the start of fracture of the material. During very advanced stages of the collapse of the beam, i.e. when a/d approaches 1.0, $d\theta/d(a/d)$ must approach infinity as a/d cannot extend beyond 1.0.

In fig 4.2 (5) to 4.2 (10) the properties of the fracture hinge are shown as M/M_o vs. $\theta/(f_t/E)$ at different d/ℓ_{ch}. In order to save space one may prefer to relate M/M_o to $\theta/(f_t/E)d/\ell_{ch}$ at the different values of d/ℓ_{ch}. It may, however, be somewhat confusing to use the same variable, d/ℓ_{ch}, in two places and the latter alternative does not illustrate the different rotation capacity at different d/ℓ_{ch} quite as clearly. It may be noted that the size of the area under complete curves M/M_o vs. $\theta/(f_t/E)d/\ell_{ch}$ at different values of d/ℓ_{ch} is constant, provided that the initial stress is zero, see Section 4.2.4.

4.2.4 Two characteristics of the fracture hinge M vs. θ curves

In order to reduce the computational work, the incremental calculations of the M vs. θ relations presented in 4.2.3 were stopped before the bending capacity of the fracture section reached zero and the beam as competely broken into two pieces. The M vs. θ curves may however be extrapolated and in this Section two features of the M vs. θ relations, which ought to facilitate such extrapolations, will be dealt with. These two features concern the area under the complete M vs. θ curves and an estimation of the shape of the curves during advanced stages of the collapse, respectively.

The beam being studied as a body in plane stress, an energy balance for the beam during an infinitesimal increment of time, dt, yields:

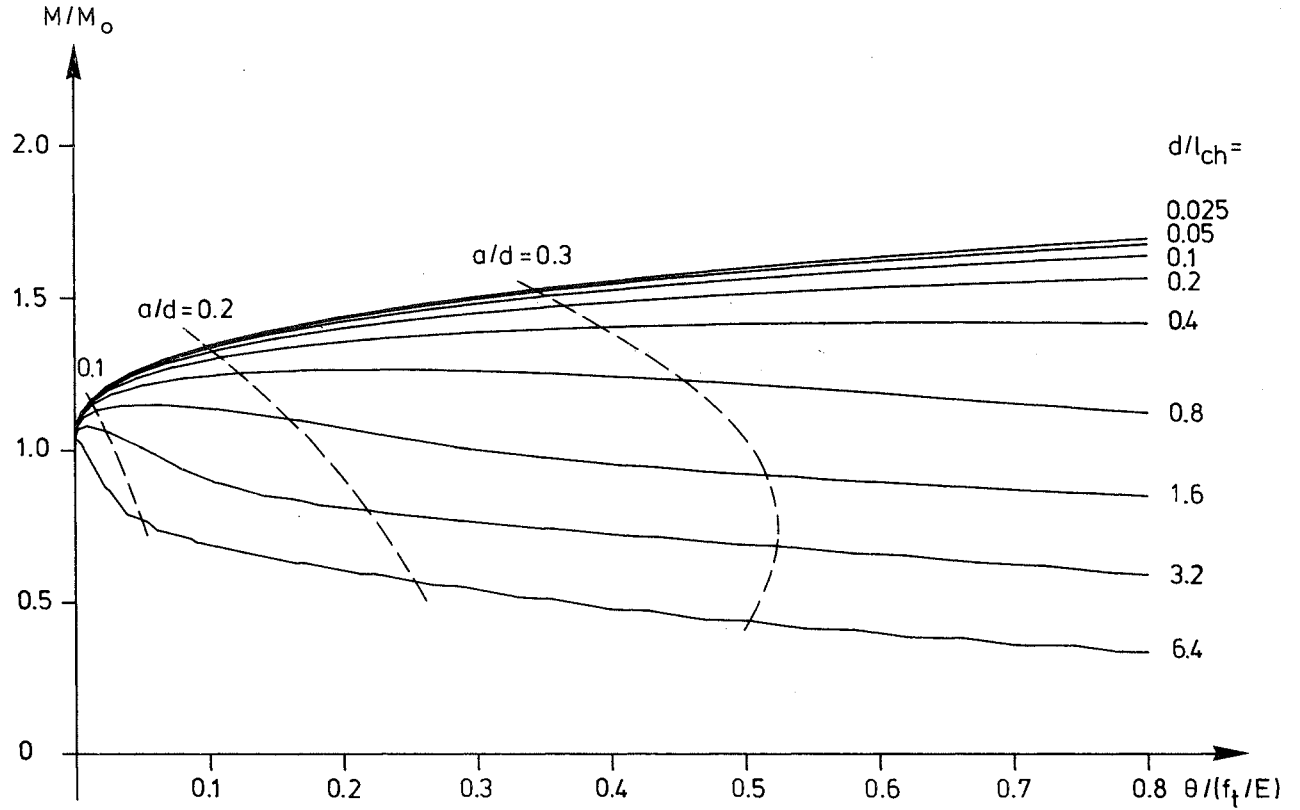

Fig 4.2 (5) Bending moment vs fracture hinge rotation in the range $0 \leq \theta/(f_t(E) \leq 0.8$ at different d/ℓ_{ch}. a/d indicates relative depth of the fracture zone. No initial stress. Shape of σ-w-curve acc. to Fig 3.2 (3) c

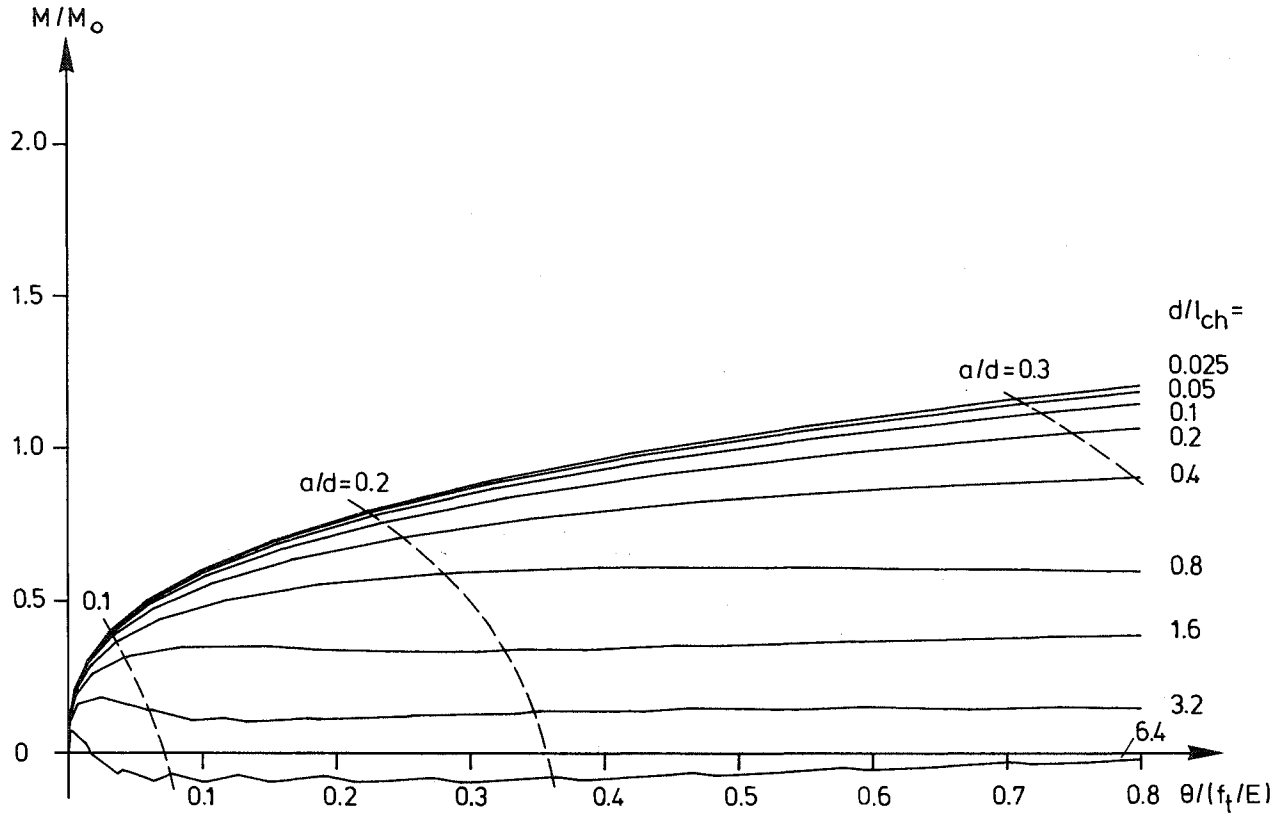

Fig 4.2 (6). Bending moment us fracture hinge rotation in the range $0 \leq \theta/(f_t/E) \leq 0.8$ at different d/ℓ_{ch}. a/d indicates relative depth of the fracture zone. Initial stress, $\sigma_i/f_t=1.0$, acc. to Fig 4.2 (3). Shape of σ-w-curve acc. to Fig 3.2 (3) c).

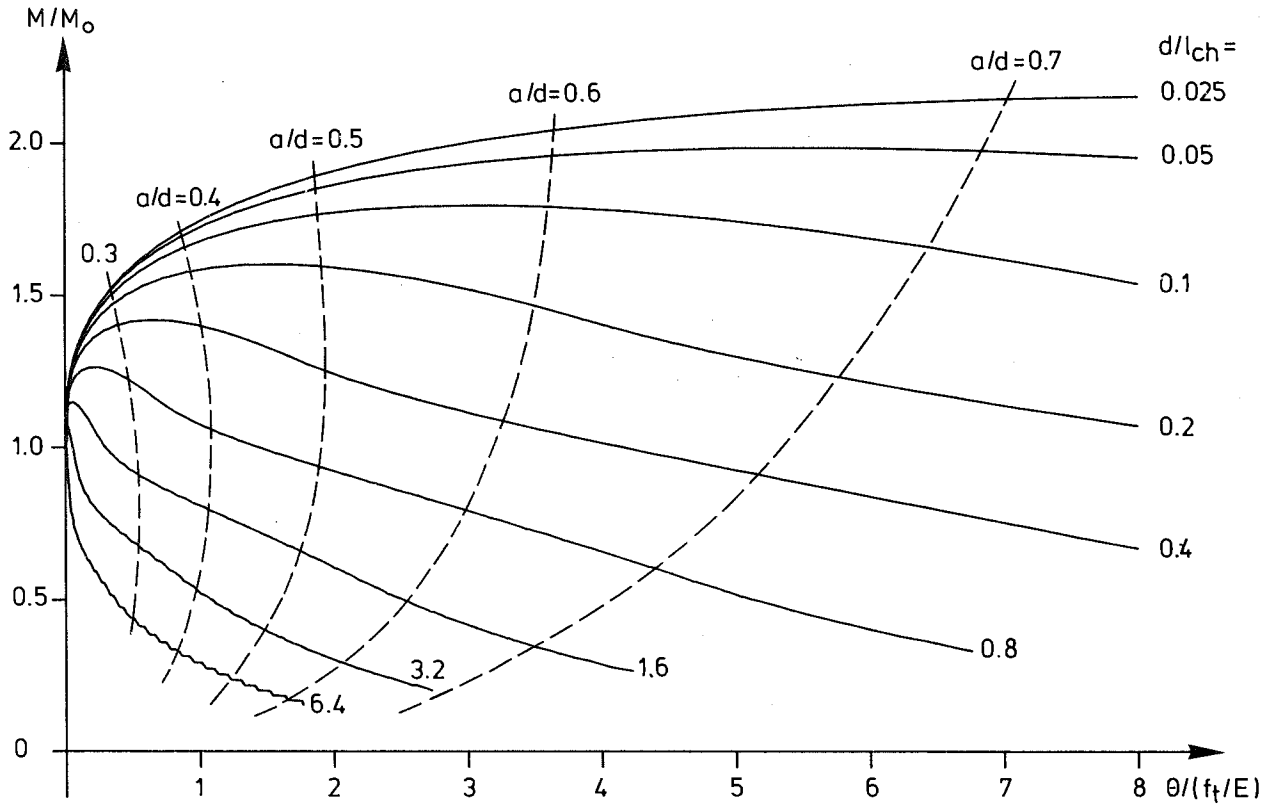

Fig 4.2 (7) Bending moment vs fracture hinge rotation in the range $0 \leq \theta/(f_t/E) \leq 8.0$ at different d/ℓ_{ch}. a/d indicates relative depth of the fracture zone. No initial stress. Shape of σ-w-curve acc. to Fig 3.2 (3) c).

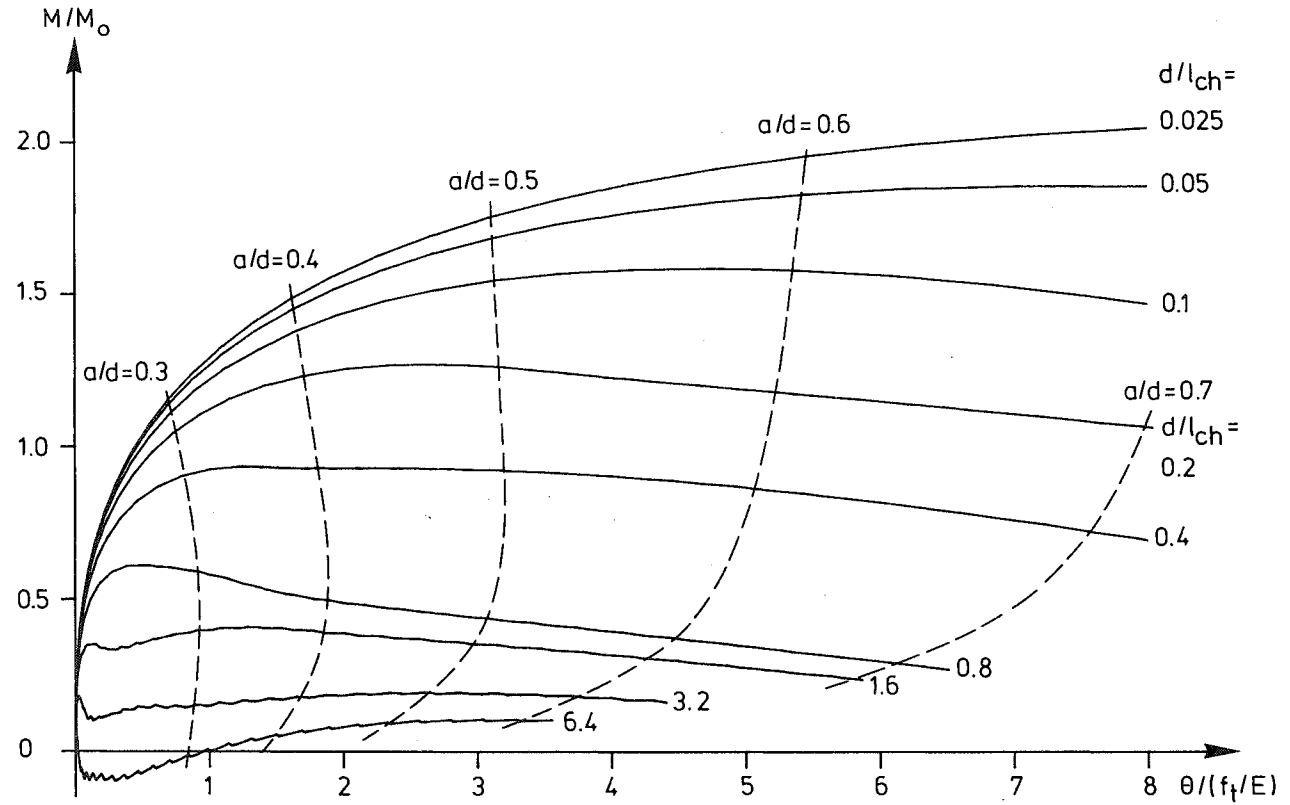

Fig 4.2 (8) Bending moment vs fracture hinge rotation in the range $0 \leq \theta/(f_t/E \leq 8.0$ at different d/ℓ_{ch}. a/d indicates relative depth of fracture zone. Initial stress, $\sigma_i/f_t = 1.0$, acc. to Fig 4.2 (3). Shape of σ-w-curve acc. to Fig 3.2 (3) c).

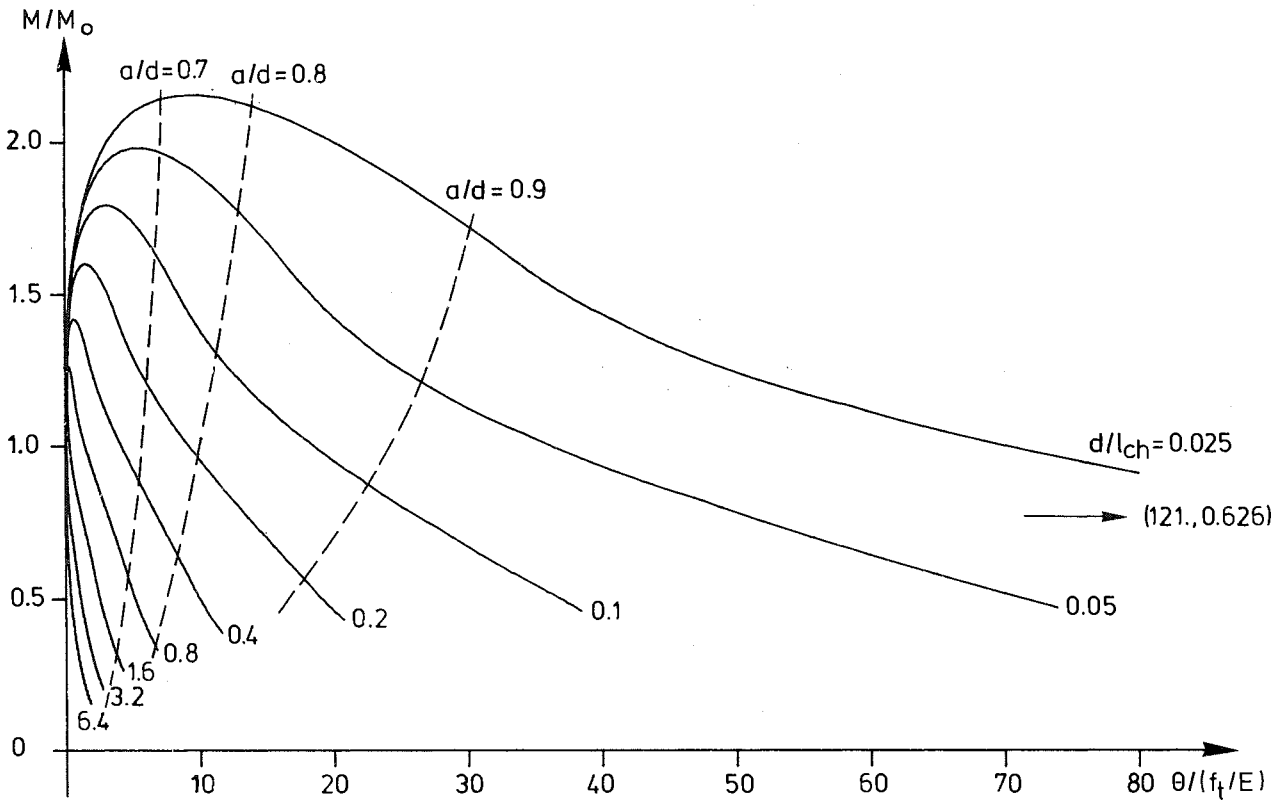

Fig 4.2 (9) Bending moment vs fracture hinge rotation in the range $0 \leq \theta/(f_t/E) \leq 80.0$ at different d/ℓ_{ch}. a/d indicates relative depth of the fracture zone. No initial stress. Shape of σ-w-curve acc. to Fig 3.2 (3) c

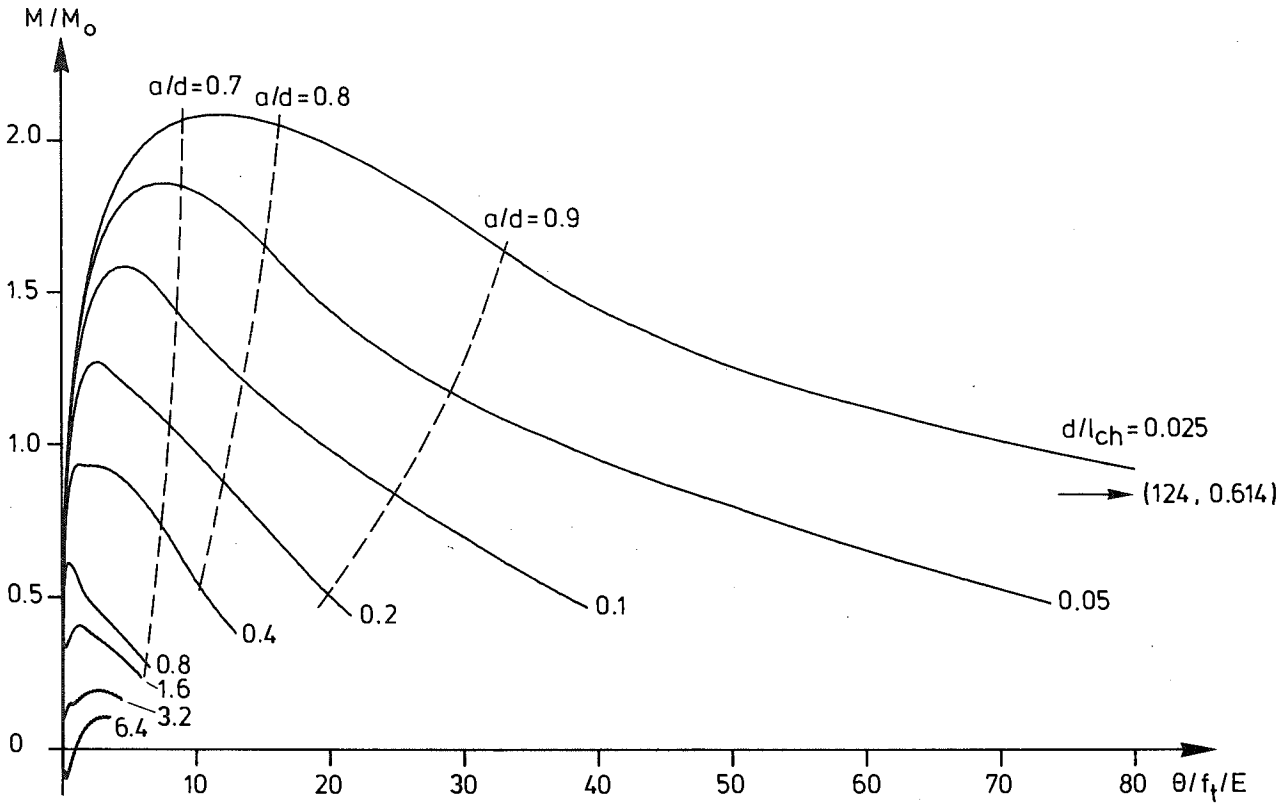

Fig 4.2 (10) Bending moment vs fracture hinge rotation in the range $0 \leq \theta/(f_t/E) \leq 80.0$ at different d/ℓ_{ch}. a/d indicates relative depth of the fracture zone. Initial stress, $\sigma_i/f_t = 1.0$, acc. to Fig 4.2 (3). Shape of σ-w-curve acc. to Fig 3.2 (3) c).

$$P\dot{\delta}\,dt = \int_A \{t\}^t\{\dot{w}\}dA\,dt + \int_V \{\sigma\}^t\{\dot{\varepsilon}\}dV\,dt + \int_V \rho\{\dot{u}\}\{\ddot{u}\}\,dV\,dt \qquad (4.2:2)$$

where P is the load acting on the beam, $\dot{\delta}$ is the rate of deflection, $\{t\}^t=(\sigma_\perp, \sigma_{II})$ is the stress (or traction) acting across the fracture zone, $\{\dot{w}\}^t=(\dot{w}_\perp, \dot{w}_{II})$ is the rate of deformation within the fracture zone (in the present case $\sigma_{II}=\dot{\sigma}_{II}=w_{II}=\dot{w}_{II}=0$ and $w_\perp$ is usually denoted simply by w), $\{\sigma\}^t=(\sigma_x, \sigma_y, \tau_{xy})$, $\{\dot{\varepsilon}\}^t=(\dot{\varepsilon}_x, \dot{\varepsilon}_y, \dot{\gamma}_{xy})$ and ρ is the density of the material. A represents the area of the fracture zone (in the present case A=bd. In those parts of bd which are not fractured at the studied instance of time, $\dot{w}_\perp=0$ and consequently those parts do not contribute to the integral.) and V represents the volume of the specimen (in the present case $V = bd\ell$).

Integration of the left side of eq (4.2:2) with respect to time from start of loading, t=0, to complete fracture, $t=t_\infty$, yields:

$$\int_0^{t_\infty} P\dot{\delta}dt = \int_0^{t_\infty} M\dot{\theta}dt + \int_0^{t_\infty} \frac{P\dot{P}}{K}dt = \int_0^{t_\infty} M\dot{\theta}dt + \frac{1}{2}\left[\frac{P^2}{K}\right]_0^{t_\infty} = \int_0^{\infty} Md\theta \qquad (4.2:3)$$

When $t=t_\infty$, P (and M) has reached zero and apart from one point (with zero area) in the upper edge of the beam, the beam is completely broken into two pieces. In eq (4.2:3) the first equality is obtained by derivation and by using the definitions of M and θ, eq (4.2:1). The second equality is obtained by integration by parts, and finally it is utilized that P=0 at t=0 and at $t=t_\infty$. The last term represents a summation of $M(\theta)d\theta$ and this sum is equal to the sum of $M(t)\theta(t)dt$ if the function $M(\theta)$ exists, i.e. if only one M corresponds to each θ.

Mathematically, the sum of $M(\theta)d\theta$ is not defined if the function $M(\theta)$ does not exist, but for conveniency the last integral in (4.2:3) may also be used if more than one M corresponds to each θ as long as it is evident that the integral in such cases will be calculated as the sum of $M(t)\theta(t)dt$.

Integration of the three terms of the right side of eq (4.2:2) from t=0 to $t=t_\infty$ is dealt with individually. In the present case $\dot{w}_{II}=0$, which by the definition of G_F yields the first term:

$$\int_0^{t_\infty}\int_A \{t\}^t\{\dot{w}\}dA\,dt = G_F\,bd \qquad (4.2:4)$$

For the second term, the assumed elasticity of the material gives:

$$\int_0^{t_\infty} \int_V \{\sigma\}^t \{\dot{\varepsilon}\} dV \, dt = \frac{1}{2} \int_V \{\sigma\}^t \{\varepsilon\} dV \Big|_{t=t_\infty} - \frac{1}{2} \int_V \{\sigma\}^t \{\varepsilon\} dV \Big|_{t=0} \qquad (4.2:5)$$

In the case of no initial stress, the sum of $\{\sigma\}^t \{\varepsilon\}\, dV$ is of course zero at t=0. As no external forces act on either of the two halves of the beam, considered individually, either at t=0 or at $t=t_\infty$ and as further on no plastic deformations are assumed to occur outside the fracture-surface, each half of the beam will resume its original undeformed shape after complete collapse. Thus, in the case of no initial stress, the sum of $\{\sigma\}^t \{\varepsilon\}\, dV$ is zero also at $t=t_\infty$.

When calculating the integral (4.2:5) in the case of initial stress, it is convenient to utilize that the change in the strain energy within the two elastic halves of the beam from t=0 to $t=t_\infty$ is equal to minus the work required to resume the original state of stress and strain within the two elastic halves of the beam. Furthermore, the original state of stress and strain is resumed if the stresses acting on the boundaries of each of the two halves of the beam at t=0 are applied to the two halves at $t=t_\infty$. Additionally, inspection of the integral (4.2:5) shows that the value may be written as $\gamma_1 bd\ell\sigma_i/E$, where σ_i is a measure of the magnitude of the initial stress (at presently σ_i is defined as the value of the initial stress in the lower edge of the mid-section of the beam) and γ_1 is a dimensionless number that depends on the geometrical shape of the beam and the distribution of the initial stresses within the beam. As to variations in the geometrical shape of the beam, γ_1 is independent of b and in variations of ℓ and d the principle of Saint-Venant may be utilized if the beam has a reasonable slenderness. The stresses applied to the boundaries of the halve of the beam at t=t are statically equivalent to zero force and zero moment and thus only the vicinity of the fracture section is affected. Consequently the value of the integral (4.2:5) is independent of ℓ (if large) and as the volume of the material in the vicinity of the fracture section is proportional to d^2, $\gamma_1 \sim d/\ell$ at variations of the geometrical shape of the beam. This means that (4.2:5) may be writen as $\gamma bd^2\sigma_i^2/E$, where γ is a dimensionless number which depends on the shape of the distribution of the internal initial stresses within the beam.

The value of γ a[illegible] tial stress

acting across the fracture section was obtained by a single conventional linear elastic analysis of the symmetrical quarter-part of the beam, loaded as indicated in Fig 4.2 (11). In accordance with the discussion above, the value of γ was obtained from the finite element result by means of the relation:

$$\gamma \frac{bd^2\sigma_i^2}{E} = -4b \int_0^{d/2} \frac{1}{2} \sigma_x(y) u_x(y) dy \qquad (4.2:6)$$

The calculation yielded $\gamma = -0.075$. With the help of a standard finite element program, values of γ corresponding to other types of distribution of initial stress may be obtained by means of the same simple method.

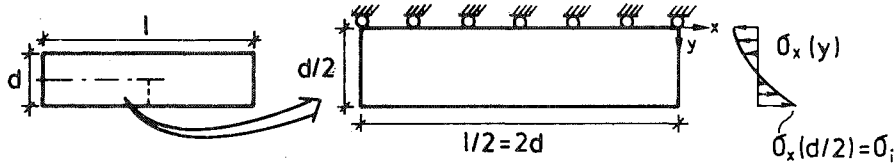

Fig 4.2.(11) External load, $\sigma_x(y) = \sigma_i(6(y/d)^2 - 1/2)$, applied to a quarter-part of the beam in order to calculate total release of strain energy during fracture.

The last term in eq (4.2:3) represents the change in kinetic energy. In the present type of incremental quasi-static analysis which is carried out in such a way that the equilibrium is always maintained, this term is equal to zero. This means that $\dot{\delta}$ has to be small and may additionally require, particularly if a slender beam is analysed or if d/ℓ_{ch} is high, that $\dot{\delta}$ is temporarily assigned negative values in order to avoid development of inertia forces and thus maintain the static equilibrium during the entire course of collapse of the beam.

For a slender beam $M_o = f_t\, bd^2/6$ and for this case eq (4.2.2) to eq (4.2:6) finally yields:

$$\int_0^{\infty} \frac{M}{M_o}\, d\left(\frac{\theta}{f_t/E}\right) = \frac{6}{d/\ell_{ch}} + 6\gamma\left(\frac{\sigma_i}{f_t}\right)^2 \qquad (4.2:7)$$

where $\gamma = -0.075$ in the case of parabolic distribution of the initial stress.

The present st and $\ell/d=4$, in

which case $M_o = f_t bd^2/(6(1-0.1773/4))$ and at this value of M_o eq (4.2:2) to eq (4.2:6) yields:

$$\int_0^\infty \frac{M}{M_o} d\left(\frac{\theta}{f_t/E}\right) = \frac{5.73}{d/\ell_{ch}} + 5.73\ \gamma\left(\frac{\sigma_i}{f_t}\right)^2 \qquad (4.2:8)$$

where γ has the same value as in (4.2:7). (4.2:8) may become useful if one wants to control possible extrapolations of the curves in Fig 4.2 (5) to 4.2 (10). If the M vs. θ curves of these figures are to be used for analyses of slender beams, in which case $M_o = f_t bd^2/6$, one may possibly consider multiplying the values of $\theta/(f_t/E)$ indicated in the figures by 1.046 in order to assure that eq (4.2:7) is fulfilled. This means that the rotation capacity becomes somewhat better for a slender beam, coresponding to the somewhat smaller bending moment capacity of the slender beam.

At zero initial stress, eq (4.2:8) indicates that the area under the normalized M vs. θ curve is reciprocally proportional to d/ℓ_{ch}. Regarding the influence of initial stress, (4.2:8) indicates that the M vs θ curve is much more affected at high values of d/ℓ_{ch} than at low values of d/ℓ_{ch}. This agrees with the numerical results of Section 4.2.3 and is basically due to the fact that the release of initial strain energy is proportional to the volume of the beam, i.e. proportional to d^3 at equal geometrical shape of the beams, while the total energy required to atain total collapse is proportional to the area of the fracture surface, i.e. proportional to d^2. At $\sigma_i/f_t=1.0$ and $d/\ell_{ch}=0.025$ the release of initial strain energy only represents 0.2 % of the total work of fracture, while at $\sigma_i/f_t=1.0$ and $d/\ell_{ch}=6.4$ the release of initial strain-energy represents 48 % of the total work of fracture: see Fig 4.2 (12). At $\sigma_i/f_t=1.0$ and $d/\ell_{ch}=13.3$ the area under the M vs. θ curve becomes zero and at higher values of d/ℓ_{ch} the total external work required to attain complete collapse becomes negative. In such cases either the external action, P, has to be such that energy is extracted from the beam during collapse or alternatively the beam will behave in an unstable manner in which case a part of the initial strain energy will be transformed into kinetic energy. If d/ℓ_{ch} is increased indefinitely, the area under the normalized M vs.θ curve approaches the finite value $-0.43(\sigma_i/f_t)^2$. If d/ℓ_{ch} is decreased towards zero, which at constant d corresponds to an ideal plastic fracture behaviour of the material, eq (4.2:8) indicates that initial stress does not affect the area under the M vs. θ curve.

It is of some in[illegible] and (4.2:8) are

independent of the shape of the σ-w curve. And it is also of interest to note that the ratio σ_i/f_t is in square in these relations. This means that the total area under M vs. θ curves are indpendent of the sign of the initial stress, although the shape of the M vs. θ curves may be expected to be significantly affected. As to the intermediate range $0 < \sigma_i/f_t < 1$ the computational results obtained by (Hillerborg, Modeer and Petersson, 1976) for $\sigma_i/f_t = 0$, 0.5 and 1.0 suggest that the influence of σ_i/f_t on the ultimate bending moment capacity may be approximately proportional to σ_i/f_t. This possible approximate relation together with the observation that the area under the M vs. θ curve is affected in proportion to σ_i/f_t in square may enable rough estimations of M vs. θ curves in the intermediate range $0 < \sigma_i/f_t < 1$.

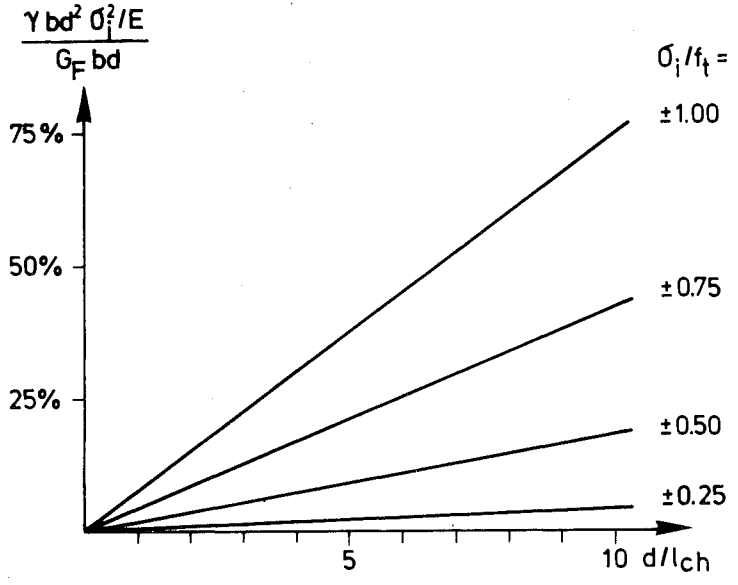

Fig 4.2 (12) Contribution from the release of strain-energy, $\gamma bd^2\sigma_i^2/E$, to the total required work of fracture, $G_F bd$, vs. ratio d/ℓ_{ch} at different magnitudes of the parabolically distributed initial internal stress.

We now turn to an estimation of the stiffness properties of the fracture hinge at advanced stages of collapse. During advanced stages of collapse an open crack developes in the lower edge of the beam, and if the remaining stress-transferring part of the fracture is small in comparison to the depth of the beam one may assume that the distribution of stress, strain and absolute deformation in the vicinity of the fracture zone is governed only by the properties of the material and is thus independent of the absolute length and depth of the beam and also independent of the type of beam and the type of load acting on the beam, provided that the different possible loads are statically equivalent and act on the beam at locations far away from the fracture zone. Thus the bending moment, M, is governed only by the properties of the material at each (large) value of the rotation, θ. But as M_o is proprotional to d^2, this leads to a proportionality between M/M_o and $1/d^2$ at equal material properties and at equal (large) rotation, θ. Furtermore, M/M_o has a specific value in every combination of d/ℓ_{ch} and $\theta/(f_t/E)$ which means that a change in d is equivalent to a change in $1/\ell_{ch}$. Accordingly, at advanced stages of collapse:

$$\frac{M}{M_o} = \frac{1}{(d/\ell_{ch})^2} f(\theta/(f_t/E)) \qquad (4.2:9)$$

where f, at a defined shape of the σ-w curve, is only a function of $\theta/(f_t/E)$. The function, f, may be of a different type at a different shape of the σ-w curve. (4.2:9) is believed to be increasingly accurate at increasing θ, and at the limit an exact relation, provided that the loads acting on the beam are located far away from the fracture zone. In the case of three-point bending, the local action of the point-load introduces a disturbance in the stresses in the vicinity of the fracture zone. Such local disturbance means that the function f may become somewhat dependent of the type of load that causes the bending of the beam. The influence of the stresses caused by the local action of the point-load are, however, probably negligible in comparison to the stresses caused by the bending, especially if the beam is slender. Similarly, the release of possible initial stresses in the vicinity of the fracture zone may have some effect on stresses and deformations even in the very last stage of the collapse. Consequently, in the cases of three-point bending and initial stress, the function $f(\theta/(f_t/E))$ may not be exactly the same as when the loads are located far away from the fracture section. However, the effect of the local disturbance is probably small, which means that the M/M_o vs. $\theta/(f_t/E)$ curves would coincide

at large values of $\theta/(f_t/E)$.

Good accuracy in (4.2:9) requires that a open crack has developed in the lower edge of the beam and secondly that the remaining stress-transferring part of the fracture section is small in comparison to the depth of the beam. At the ends of the M/M_o vs. $\theta/(f_t/E)$ curves in Fig 4.2 (9) and Fig 4.2 (10), with the exception of the curves corresponding to $d/\ell_{ch}=0.025$, the first requirement is fulfilled while the second requirement is poorly fulfilled: at $\sigma_i/f_t=0$ and $d/\ell_{ch}=0.05$ the ratio between the remaining stress-transferring part of the fracture section and the depth of the beam is 1.0; at $\sigma_i/f_t=0$ and $d/\ell_{ch}=6.4$ the ratio is 0.55; at $\sigma_i/f_t=1.0$ and $d/\ell_{ch}=0.05$ the ratio is 1.0; at $\sigma_i/f_t=1.0$ and $d/\ell_{ch}=6.4$ the ratio is 0.53. But if we temporarily assume that the requirements are fulfilled to such an extent that the accuracy in (4.2:9) is satisfactory, then this relation enables significant extensions of the M/M_o vs. $\theta/(f_t/E)$ curves in Fig 4.2 (9) and Fig 4.2 (10) even if eq (4.2:9) does not provide any information about the function $f(\theta/(f_t/E))$. Taking Fig 4.2 (9) as an example: at $d/\ell_{ch}=0.025$ $M/M_o=0.626$ at $\theta/(f_t/E)=121$ which for $d/\ell_{ch}=0.05$ and $\theta/(f_t/E)=121$ means that $M/M_o=0.626/4=0.157$; at $d/\ell_{ch}=0.05$ $M/M_o=0.469$ at $\theta/(f_t/E)=73.9$ which for $d/\ell_{ch}=0.1$ and $\theta/(f_t/E)=73.9$ means that $M/M_o=0.469/4=0.117$; and so on. The procedure may then be repeated until the curves are all extended to $\theta/(f_t/E)=121$. The same approach may be applied to Fig 4.2 (10). The simple and convenient type of extrapolation is believed to be of sufficient accuracy where many types of practical utilization of the M/M_o vs. $\theta/(f_t/E)$ curves are concerned.

(4.2:9) is a simple and, if θ is large enough, probably an exact relation. An equally attractive relation with respect to the type of function $f(\theta/(f_t/E))$ has not been found. Approximate estimations may, however, be obtained by considering the change in the distribution of stresses and deformations in the vicinity of the fracture zone at an increased fracture hinge rotation, θ. By means of the ordinary beam theory and considering energy release rate (Gustafsson, 1977) indicated that the bending moment, M, decreases at increased θ but never reaches zero exactly, no matter how large the rotation, θ, is. This suggests that $f(\theta/(f_t/E))$ should be such that the value zero is approached asymptotically. (Petersson, 1981) studied load vs. deflection, P vs. δ, of a three-point bend beam at advanced stages of collapse, assuming that the unfractured parts of the beam are entirely stiff and that the collapse takes place as a rotation around a hinge and that the

boundaries of the fracture zone are kept straight. This assumption led to the relation $P \sim 1/\delta^2$, which should be improved if one obtains a relations between M and θ at the same assumption ($M \sim 1/\theta^2$) and in addition takes into account the additional deflection due to elastic deformations of the unfractured part of the beam: $P \sim 1/(\delta - P/K)^2$. (Petersson, 1981) and (Petersson, 1982) studied the relevance of the relation $P \sim 1/\delta^2$ by means of experimental investigations and found that the relation seemed to be a good approximation. However, due to the method used during the interpretation of the experimental results, the relevance of the relation $M \sim 1/\theta^2$ was tested, not the relevance of the relation $P \sim 1/\delta^2$. These experimental results therefore suggest that the relation $M \sim 1/\theta^2$ may be a good approximation. During a theoretically study of the double torsion specimen, (Hillerborg, 1983) obtained approximate M vs. θ relations by means of simplifying assumptions concerning stresses and deformations in the vicinity of the fracture section: At a constant distance, $\ell_o/2$, from the centre-line of the beam plane cross sections were assumed to remain plane, while within the region of the length ℓ_o the shear rigidity of the material was assumed to be zero and accordingly this part of the beam acts as if it consisted of a number of horizontal independent parallel bars. Regardless of the choice of the value of the length ℓ_o, these assumptions suggest that the shape of the distribution of the deformations and stresses at the fracture section remains unchanged from the moment when an open crack developes in the lower edge of the beam and only becomes more and more concentrated towards the upper edge of the beam when the rotation θ increases. This means that $M \sim 1/\theta^2$. If the length ℓ_o is equal to zero (and in addition the parts of the beam outside the fracture section are assumed to be ideally stiff) then the assumptions of Hillerborg coincide with those of Petersson. The assumptions of Hillerborg may be improved if the length ℓ_o is not assigned a constant value, but is being related to the depth of the remaining stress-transferring part of the fracture section: preferably ℓ_o should be assumed to decrease when the depth of the stress-transferring part decreases during the increase in rotation, θ. This later assumption suggests that the shape of stress distribution does not remain constant and in particular that the compressive stress in the upper edge of the beam does not remain contant at advanced stages of collapse but becomes larger and larger as the rotation is increased. An exact relation between M and θ corresponding to some assumed relation between ℓ_o and the depth of the remaining part of the fracture section has not been developed, but the findings referred to above together w[illegible]t that a

relation of the type $M \sim 1/\theta^n$ may be a reasonable conjecture. If adopting this type of relation, eq (4.2:9) yields:

$$\frac{M}{M_o} = \frac{1}{(d/\ell_{ch})^2} \frac{C}{(\theta/(f_t/E))^n} \qquad (4.2:10)$$

In the constant shape of the σ-w curve C and n should be constants, and the value of these two constants may be determined with the help of eq (4.2:6) and a known value of M/M_o, $(M/M_o)_o$, at some (large) value, $(\theta/(f_t/E))_o$, of the rotation $\theta/(f_t/E)$. (4.2:6) and (4.2:10) yields:

$$n = 1 + \frac{(M/M_o)_o \, (\theta/(f_t/E))_o}{\frac{5.73}{d/\ell_{ch}} + 5.73\gamma(\frac{\sigma_i}{f_t})^2 - \int_o^{(\theta/(f_t/E))_o} \frac{M}{M_o} \, d(\frac{\theta}{f_t/E})} \qquad (4.2.11)$$

$$C = (d/\ell_{ch})^2 (M/M_o)_o (\theta/(f_t/E))_o^n \qquad (4.2.12)$$

With the help of these expressions and the numerical results of 4.2.3, n and C can be calculated. Ideally n and C should be independent of d/ℓ_{ch} and σ_i/f_t, but as indicated in Fig 4.2 (13) a) n and C do not remain constant. This may have a different explanation. One possible explanation is that the current values of $(\theta/f_t/E))_o$, (which values were put equal to the value of the rotation at the end of each respective curve in Fig 4.2 (9) and 4.2 (10)), are too small to ensure an accuracy of eq (4.2:9). An other possible explanation is that the proportionality between M and $1/\theta^n$ does not apply. It is interesting to note that n, although not being exactly constant, is almost constant and close to 2.0. The variation in C must be compared to the very large variation in $(d/\ell_{ch})^2$.

The results in Fig 4.2 (13) a) indicate that a good accuracy of the proportionality $M/M_o \sim 1/(d/\ell_{ch})^2$ requires larger values of $(\theta/(f_t/E))_o$ than the current ones, and that a proportionality between M and $1/\theta^n$, $2.0 \lesssim n \lesssim 2.1$, may be a good approximation at large values of θ. A few other relations between M and θ have been tried, but these have not been found as accurate as $M\ 1/\theta^n$. Eq (4.2:10) together with the values of n and C shown in Fig 4.2 (13) a) may of course be used in order to attain approximate extensions of the M/M_o vs. $\theta/(f_t/E)$ curves in Section 4.2.3.

	$\sigma_i/f_t=0.0$		$\sigma_i/f_t=1.0$	
d/ℓ_{ch}	n	c	n	c
0.025	1.98	5.3	2.00	6.0
0.050	2.04	7.7	2.05	8.0
0.10	2.06	8.5	2.06	8.9
0.20	2.06	8.8	2.07	10.0
0.40	2.09	10.5	2.11	13.5
0.80	2.08	11.3	2.13	17.7
1.6	2.11	14.2	2.18	28.8
3.2	2.10	17.1	2.18	42.1
6.4	2.08	20.7	2.21	71.8

Fig 4.2 (13) a) Coefficient n and C in eq (4.2:10) corresponding to the curves shown in Fig 4.2 (9) and (Fig 4.2 (10) and calculated by means of eq (4.2.11) and eq (4.2:12).

Where the numerical results in Fig 4.2 (13) a) and eq:s (4.2:9) and (4.2:10) are concerned, it may be of interest to make a comparison to an anlytical relation between M/M_o and $\theta/(f_t/E)$ valid at the extreme limit $d/\ell_{ch} \to 0$ and $\theta/(f_t/E) \to \infty$. If, 1), d, G_F and f_t are assigned fixed values and, 2), $E \to \infty$, then the fracture develops as a rotation around a hinge in the upper edge of the fracture section and the boundaries of fracture zone remain plane during the fracture. If further on, 3) $w_c < \theta\, d$, where w_c is the width of the fracture zone corresponding to zero stress, then an open crack has developed at the edge of the fracture section. In these conditions and if the shape of the σ-w curve is known, the bending moment, M, may be calculated for any value of θ. Expressed in the dimensionless variables M/M_o, d/ℓ_{ch} and $\theta/(f_t/E)$ one obtains:

If 1) $d/\ell_{ch} \to 0$
2) $\Theta/(f_t/E) \to \infty$
3) $\Theta/(f_t/E)(d/\ell_{ch}) \geq \alpha$

then

$$\frac{M}{M_o} = \frac{1}{(d/\ell_{ch})^2} \quad \frac{C}{(\Theta/(f_t/E))^n} \qquad (4.2:13)$$

where $\alpha = 3.60$
$n = 2.00$
$C = (74/75)/(1/(6(1-.1773/4))) = 5.7$

The numerical values of α and C are dependent on the shape of the σ-w curve, and the present values are valid for the bi-linear shape shown in Fig 3.2 (3) c). In the case of a non-zero constant value of d/ℓ_{ch} and $\theta/(f_t/E)) \to \infty$, it is very probable that the ratio between the size of the fracture zone and the size of the ligament grows without limit and that the function $f(\theta/(f_t/E))$ approaches a proportionality to $1/(\theta/(f_t/E))^2$, but never quite reaches it. In theory, when $d/\ell_{ch} \to \infty$ and $\theta/(f_t/E) \to \infty$ it is quite possible that a limit for the function $f(\theta/(f_t/E))$ does not exist. However, in the last two cases, i.e. d/ℓ_{ch} = non-zero constant and $d/\ell_{ch} \to \infty$, there is no definite proof.

Standing at the end of a M vs. θ curve of Fig 4.2 (9) or Fig 4.2 (10), we have now armed ourselve with some different possibilities, i.e. eq (4.2:8) and eq (4.2:9) and eq (4.2:10) together with Fig 4.2 (13) a), which hopefully enables us to calculate M for the very large θ. But the most suitable method of extrapolation is partly dependenet on its purpose, which is why the extension of the curves in Fig 4.2 (9) and Fig 4.2 (19) is left to the interested reader. In most practical applications the values of M at very larges values of θ are not believed to be very important. However, some of the relations dealt with in this Section are

	$\sigma_i/f_t=0$				$\sigma_i/f_t=1.0$			
d/ℓ_{ch}	A	B	C	D	A	B	C	D
.025	121.	.626	152.	229.	124.	.614	153.	229.
.050	73.9	.469	81.8	115.	73.7	.480	80.2	114.
.10	38.4	.459	40.7	57.3	39.2	.467	39.6	56.9
.20	20.7	.430	20.3	28.7	21.6	.439	19.3	28.2
.40	11.6	.387	10.2	14.3	13.0	.381	9.42	13.9
.80	6.76	.332	5.08	7.16	8.50	.290	4.55	6.73
1.6	4.23	.265	2.57	3.58	5.87	.236	1.98	3.15
3.2	2.73	.202	1.29	1.79	4.41	.162	.754	1.36
6.4	1.77	.154	.642	.895	3.56	.106	.154	.466

$A \equiv (\theta/(f_t/E))_o \quad B \equiv (M/M_o)_o \quad C \equiv \int_o^{(\theta/(f_t/E))_o} (M/M_o) d(\theta/(f_t/E))$

$D \equiv \int_o^{\infty} (M/M_o) d(\theta/(f_t/E))$

Fig 4.2 (13) b) Values of rotation, $(\theta/(f_t/E))_o$, and moment, $(M/M_o)_o$, at the ends of the curves in Fig 4.2 (9) and Fig 4.2 (10), and the area under the curves from zero to $(\theta/(f_t/E))_o$ and from zero to infinity.

of some interest in principle, not only where extrapolations are concerned. Accurate estimations of M for large θ are of particular interest for evaluation of experimental results concerning determination of the fracture energy, G_F, by means of bending tests of notched beams. The purpose of the present study has not been to investigate this matter, i.e. the influence of the dead-weight on evaluation of G_F, but for the convenience of anyone who is interested in this problem and in the development of a function $f(\theta/(f_t/E))$ for large $\theta/(f_t/E)$, Fig 4.2 (13) b) shows the present values of $(\theta/(f_t/E))_o$, $(M/M_o)_o$ and the area under the curves from zero to $(\theta/(f_t/E))_o$ and from zero to infinity.

4.2.5 Remarks and comparisons

Firstly in this Section remarks and comparisons are made with regard to the ultimate flexural strength, compare with Section 4.2.2. After that, a few remarks and comparisons are made with regard to the study of fracture hinges, compare with Sections 4.2.3 and 4.2.4.

A number of experimental investigations regarding the flexural strength of unreinforced concrete beams are reported in literatsure: please see the references in Section 4.2.1 and also (Bonzel, 1965) and (Ivanyi, 1976). Bonsel and Ivanyi summarize experimental knowledge in a rather thorough manner by discussing a number of experimental results and provide a number of references on the subject of flexural strength. A recent, though essentially theoretical, study has beeen presented by (König and Jahn, 1983). Interesting results regarding the flexural strength of model concrete mixes (mortar) has been presented by (Saabnis and Mirza, 1979).

In the quantitative sense the test results obtained during different experimental investigations can hardly be expected to be entirely unanimous. In spite of this there seems to be an almost complete experimental agreement with respect to some more or less unexpected general features of the flexural strength:

1) the flexural strength does not equal the tensile strength;
2) the flexural strength increases at decreased depth of the beam;
3) the flexural strength is less at four-point bending than at three-point bending;
4) the flexural strength decreases at increased length of the beam.

These features are all in disagreement with the commonly adopted theory of deterministic linear elastic brittle behaviour of concrete in tension. In order to explain these more or less unexpected features a number of explanations have been put forward. But with reference to eight different experimental investigations carried out from 1922 to 1955. Ivanyi stated in 1976 "....feststellen, dass in Balken-versuchen erzielte Zugfestigkeiten sowohl von der Art der Belastung - eine oder zwei Einzallasten - als auch von den Abmessungen dess Prufkörpes abhängig sind; inbesondnere fiel eine starke Abhängigkeit von der Balkenhöhe auf. Eine schlussige Erläuterung dieses Phänomens is aus der Litterature bis heute nicht bekannt."

The disagreement between the traditional theory and test results might to some extent be explained by such things as different maturity of the concrete in different parts of the specimen due to water separation and the unavoidable temperature gradients at hardening, non-uniform shrinkage during possible drying of the specimen, lack of large aggregate particles close to the edges of the specimen and so on. But if we assume that the concrete may be considered as an isotropic stochastically homogenous material and that no macroscopically non-uniform initial stresses are present within the specimen, then the deviation between the traditional theory and the test results may be caused by:

1) non-linear stress-strain response of the material;
2) the existence of a non-brittle tensile fracture softening;
3) scatter in the strength properties;
4) different rates of deformation of the material in different geometry of the specimen and different types of loading.

A non-linear stress-strain response can explain a difference between f_f and f_t, but cannot explain any influence on f_f of beam depth or type of loading. The existence of non-brittle tensile softening, as taken into account in the present fictitious crack calculations, provides an explanation to differences between f_f and f_t and the influence of beam depth on f_f. Scatter in strength can, in a qualitative sense, theoretically explain both the difference between f_f and f_t, the influence of beam depth and the influence of the type of loading. Different rates of deformation of the material may to some extent influence recorded ratios between f_f and f_t.

In the calculations in Section 4.2.2 only the non-brittle softening

behaviour of the material was considered. Here the effect of the other three possible reasons for deviations from the conventional theory shall also be discussed. Before this, however, one should be reminded that the softening of the material was only taken into account in the cross section that was exposed to the greatest bending moment. Consideration of simultaneous growth of several fracture zones may have some effect on predicted flexural strength, but this effect on the predicted ultimate strength is believed to be small.

Consideration of a non-linear σ-ε curve most likely influences the predicted values of f_f, but it is difficult to estimate as to how and to which extent. If non-linearities were to be taken into account, but not scatter, then it is very probable that the calculated values of f_f/f_t would increase at high values of d/ℓ_{ch}, while f_f/f_t at low values of d/ℓ_{ch} would be less infuenced. This may be realized by considerating the limiting cases $d/\ell_{ch} \rightarrow \infty$, corresponding to the lower limit of f_f/f_t, and $d/\ell_{ch} \rightarrow 0$, corresponding to the upper limit of f_f/f_t. In this second case non-linearities of the σ-ε curve do not influence f_f/f_t, whereas in the first case f_f/f_t is easy to calculate at any assumption with respect to the shape of the σ-ε curve. Fair assumptions with respect to the shape of the σ-ε curve indicate that the predicted values of f_f/f_t may be increased by about 10-50 % at $d/\ell_{ch} \rightarrow \infty$. However, this does not appear to be in agreement with experimental results. In the theoretical study by (König and Jahn, 1983) it is, with reference to tests by Heilmann in 1976, stated that the limit value for the flexural strength of very deep beams is only 7-9 % higher than the tensile strength. This disagreement for the very large beams might be explained by scatter in the strength of the material and by scatter in the stiffness properties of the material. As a scatter in strength means that the weakest desicive part is weaker in large beams than in small beams, the non-linear part of the σ-ε curve close to peak stress is activated in a smaller number of points in the large beam than in the small beam. Consequently it may be reasonable to expect that the representative mean σ-ε curve is less non-linear in large beams than in small beams. Where intermediate values of d/ℓ_{ch} are concerned, a non-linear shape of the σ-ε curve should have a beneficial effect on the stress distribution above the fracture zone, but probably a bad effect on the ability of the fracture zone to transfer stresses. Qualitatively, a decreased value of the tangential stiffness of the unfractured material in the vicinity of the fracture zone might be looked upon as a decrease in ℓ_{ch} (a decrease in E) at least if the tangential stiffness during loading

can be assumed to be equal to the tangential stiffnes during unloading. This would mean that the contribution from the fracture zone to the total bending moment capacity would become less if a non-linear σ-ε curve is taken into account. This matter suggests a decrease in predicted values of f_f in non-linear σ-ε relations. It may thus be concluded that the shape of the σ-ε curve most probably influences predicted values of f_f, but it is not known whether the magnitude of this influence is significant or negligible and it is nor yet known whether a non-linear modelling of the σ-ε response would yield an increase or decrease in predicted values of f_f.

In order to estimate how scatter in strength may influence predictions of f_f/f_t one may first consider a single fracture section and then different locations of the fracture section. We assume that the strength of different small parts of the fracture section is according to some probability density function with a certain mean value. Furthermore, it is assumed that the strength of adjoining small parts of the fracture section are independent of each other. On an assumption of ideal brittle fracture behaviour of the material, the strength of the fracture section is governed by the weakest small part of the fracture section. This is not the case if the tensile fracture softening properties of the material are taken into account. Instead, in this case a large number of the small parts of the fracture zone - weak parts and strong parts, and more or less fractured parts - all influence the bending moment capacity and each contributes to resisting the external bending moment. If the breadth to depth ratio of the beam is not exceptionally great, it may thus be reasonable to assume that the different parts of the section co-operate in the same manner as a number of parallel bars. This would mean that the flexural strength of the studied fracture section is governed by a summation, or integration, of the strength of the different small parts. In mean, a sum is not influenced by scatter. Thus if we test a number of specified fracture sections the mean flexural strength obtained would be independent of the magnitude of the scatter in strength between different individual small parts of the fracture section.

During bending or pulling of a specimen, fracture is not bound to take place at some certain pre-specified section, but instead the fracture section will be located where the resistance is least in comparison to the external action. In contradiction to the study of the strength of a certain section, the strength of a specimen is consequently not governed

by a sum of the strength of different possible fracture sections but by the weakest link. This means that the mean strength of specimens is not only dependent on the mean strength of the different sections, but also clearly dependent on the scatter in strength between different sections.

To sum up the theoretical and somewhat simplified discussion above: the strength of each section is governed by some kind of mean value of the strength properties of the material and mean values are independent of scatter; the strength of the total specimen is governed by an extreme value of the strength of the different sections and extreme values are dependent on scatter. In order to enable numerical calculations on the basis of this qualitative discussion to be carried out the following assumptions are made: the ratio f_f/f_t of each particular section is in accordance with the fictitious crack prediction; the scatter in strength between different sections is described by the Weibull density function; the magnitude of the scatter in strength (the coefficient of variation) between different sections is independent of the size and shape of the sections. The Weibull density function is chosen because it makes calculations simple and because this function appears to describe scatter in strength of most engineering materials in rather a realistic manner. The assumption of constant coefficient of variation independent of the depth and width of the cross section can be discussed, but makes calculations more simple and clear. Similarly, the initial assumption of zero correlation in strength between adjoining small parts of the fracture section can be discussed, but also this assumption makes the calculations more simple and clear. The concept of the "weakest link" and the Weibull density function have been dealt with previously (Section 3.4.4), and integration yields the following relations:

During constant bending moment along the bend specimen

$$\frac{\bar{f}_f}{\bar{f}_t} = \left(\frac{f_f}{f_t}\right)_{section}\left(\frac{\ell_t}{\ell_f}\right)^{1/m} \qquad (4.2{:}14)\ a)$$

During three-point bending

$$\frac{\bar{f}_f}{\bar{f}_t} = \left(\frac{f_f}{f_t}\right)_{section}\left(\frac{\ell_t}{\ell_f}\right)^{1/m}\ (m+1)^{1/m} \qquad (4.2{:}14)\ b)$$

During four-point, third-point bending

$$\frac{\bar{f}_f}{\bar{f}_t} = \left(\frac{f_f}{f_t}\right)_{section} \left(\frac{\ell_t}{\ell_f}\right)^{1/m} \left(\frac{3(m+1)}{m+3}\right)^{1/m} \qquad (4.2.14)\ c)$$

$\bar{f}_f$ is the predicted mean flexural strength of a specimen of length ℓ_f, $\bar{f}_t$ is the mean uniaxial tensile strength of a specimen of length ℓ_t. $(f_f/f_t)_{section}$ is the ratio between the flexural strength and tensile strength as predicted by fictitious crack calculations in which scatter is not taken into account, see Section 4.2.2. m is the parameter in the Weibull density function that defines the magnitude of the scatter. As the Weibull density function is adopted, the scatter in strength between different sections is equal to the recorded scatter in strength between different specimens provided that the scatter is expressed as the corresponding coefficient of variation. Values of m corresponding to different values of the coefficient of variation may be found in Fig 3.4 (5).

At zero scatter $m \to \infty$ and then eq (4.2:14) indicates that $\bar{f}_f/\bar{f}_t$ is equal to $(f_f/f_t)_{section}$, i.e. equal to the fictious crack predictions of Section 4.2.2. It is, however, believed that more realistic predictions ought to be obtained if non-zero scatter is assumed - some comparisons will be dealt with subsequently. The sensitivity to the magnitude of the scatter is illustrated in Fig 4.2 (14), but in the subsequent comparisons we shall throughout assume that the coefficient of variation in strength is either 0 %, corresponding to $m \to \infty$, or 8.7 %, corresponding to m=14. In eq (4.2:14), the relation corresponding to uniformly distributed load along the beam has not be included since this relation proved to be lengthy. The relation may be found by comparison to eq (4.6:11). See also Fig 4.6 (5), where numerical values may be found. Eq (4.2:14) requires that the bend and tensile specimens respectively have cross sections of constant depth and width along the specimen, but it is probably not very complicated to derive similar relations in the case of varying width and depth of the cross section along the specimen.

The rate of deformation during flexural and tensile testing is likely to have som influence on the recorded values of strength. Thus, for instance, at a constant rate of deflection of a beam in bending the rate of deformation within the material is increased at an increased depth of the beam, provided that the length of the beam is kept constant. This would theoretically [illegible] the flexural strength of deep

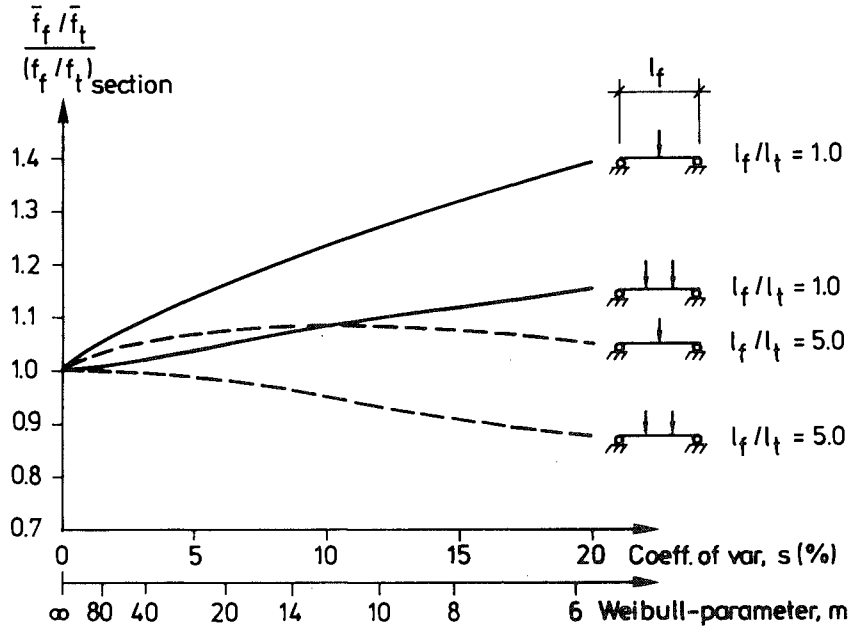

Fig 4.2 (14) Theoretical prediction, eq (4.2:14), regarding influence of scatter in strength on the ratio between mean flexural strength, $\bar{f}_f$, of a specimen of length l_f and mean unaxial tensile strength, $\bar{f}_t$, of a specimen of length l_t. $(f_f/f_t)_{section}$ = ratio between flexural strength and tensile strength of individual cross sections = fictitious crack prediction of $\bar{f}_f/\bar{f}_t$ at zero scatter in strength.

beams. The frequently referred to results of McNeely and Lash in 1963 do not, however, suggest any clear influence of the rate of loading on flexural strenth if the stress rate is within the approximate range 1 MPa/min to 10 MPa/min, which range probably cover most short time static tests of strength. As to very substantial variations in the rate, the experimental results seem to suggest that a ten times increase in the rate gives in mean an approximate 10 % increase in the flexural strength. (Other investigators have found both smaller and greater influence of the rate of loading.) But as static short time flexural and tensile tests are normally carried out in such a way that failure takes place after approximately the same time independent of the geometry of the specimen and the type of load, it appears to be a fair approximation to neglect the possible influence of different rates of deformation on recorded relations

between flexural and tensile strength and on relations between flexural strengths of different types of specimens.

To sum up this discussion on how properties of concrete, not taken into account in the fictitious crack calculation in Section 4.2.2, may influence the predictions of flexural strength: modelling of the simultaneous growth of several cracks is not believed to have any major influence on the prediction of ultimate strength; consideration of a non-linear σ-ε curve (and also a more modulated non-linear shape of the σ-w curve) is likely to influence the predictions, but it is not known in which way nor whether the influence is significant or negligible, the influence of scatter is taken into account by means of eq (4.2:14); the influence of rate of loading is estimated to be negligible regarding normal short time static tests.

So far we have concentrated on theoretical predictions by using the fictitious crack model, but in order to make comparisons, different theoretical models are put together in Fig 4.2 (15). The models in this figure might be looked upon as different special cases of the type of model represented by eq (4.2:14), and the six different models represent the six possible combinations with regard to the type of assumption concerning fracture toughness (the value of ℓ_{ch} : zero, infinite or more realistic) and scatter (the value of m: infinite or more realistic). With the exception of the "plastic stochastic" model, the models of the figure are all well-known or have been discussed above or in previous Sections. The plastic stochastic model is analogous to eq (4.2:14), but each cross-section of the specimen is assumed to be able to behave in an ideal plastic manner.

The models in Fig 4.2 (15) basically represent different assumptions with regard to the stress-deformation behaviour of concrete in tension, and judging by the basic assumptions it appears quite clear that the fictitious crack model, taking scatter into account, ought to produce better and more realistic predictions than any of the other models.

Judging from comparisons between predictions and tests, one may immediately conclude that the traditionl deterministic linear elastic brittle model and the two plastic models are clearly inaccurate in both the qualitative and quantitative sense.

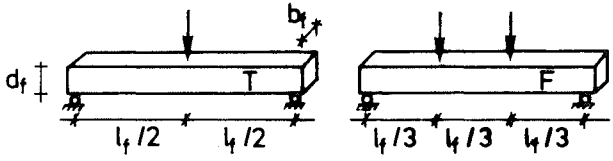

$$f_f = \frac{M_u}{b_f d_f^2/6}$$

Model	a) l_{ch}	a) m	Type of basic tensile stress-deformation assumption	Predicted infl. on $\bar{f}_f$: b_f	d_f	l_f	T,F	Predicted infl. on $\bar{f}_t$: b_t	d_t	l_t
Lin.elast. brittle	0	∞		No	No	No	No	No	No	No
Lin.elast.brittle stochastic (Weibull)	0	–		Yes	Yes	Yes	Yes	Yes	Yes	Yes
Fict.crack	–	∞		No	Yes	No	No	No	No	No
Fict. crack stochastic	–	–		No	Yes	Yes	Yes	No	No	Yes
Plastic	∞	∞		No	No	No	No	No	No	No
Plastic stochastic	∞	–		No	No	Yes	Yes	No	No	Yes
Reality			b)	No b)	Yes b)	Yes b)	Yes b)	?	?	Yes b)

a) Values of mat. prop. parameters if the models are regarded as different special cases of the stoc. fict. crack model.

b) Guess, essentially based on test results reported in litterature.

Fig 4.2 (15) (Part 1 of 2) Summing up of theoretical models, which predict ratio between mean flexural strength, $\bar{f}_f$, and mean uniaxial tensile strength, $\bar{f}_t$, of concrete and similar materials.

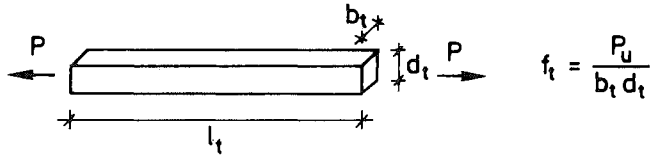

Prediction of $\bar{f}_f / \bar{f}_t$	Type of load
1.0	T, F
$((b_t d_t l_t)/(b_f d_f f_f))^{1/m} (2(m+1)^2)^{1/m}$	T
$((b_t d_t l_t)/(b_f d_f f_f))^{1/m} (6(m+2)^2/(m+3))^{1/m}$	F
acc. to Fig 5.2 (3)	T, F
$(f_f/f_t)_{section} (l_t/l_f)^{1/m} (m+1)^{1/m}$ c)	T
$(f_f/f_t)_{section} (l_t/l_f)^{1/m} (3(m+1)/(m+3))^{1/m}$	F
3.0	T, F
$3.0 (l_t/l_f)^{1/m} (m+1)^{1/m}$	T
$3.0 (l_t/l_f)^{1/m} (3(m+1)/(m+3))^{1/m}$	F

c) $(f_f/f_t)_{section}$ acc. to Fig 5.2 (3)

Fig 4.2 (15) (Part 2 of 2) Summing up of theoretical models, which predict ratio between mean flexural strength, $\bar{f}_f$, and mean uniaxial tensile strength, $\bar{f}_t$, of concrete and similar materials

The Weibull-model and the fictitious crack model, scatter taken into account, expose similarities regarding the prediction of flexural strength: the predicted relative influence of the type of load and the length of the beam are quite the same and both models predict a decrease in strenght at increased depth of the beam. One basic difference between the models concerns the predicted influence of the width of the beam: according to the Weibull-model an increase in the width of the beam has quite the same effect as an increase in the depth, while according to the present fictitious crack prediction the width of the beam is of no importance. Any experimental numerical values regarding possible influence of the width of the beam, other variables kept constant, is not known to the writer. However, after a discussion about a number of tests carried out in different laboratories (Bonzel, 1965) concludes: "Zusammenfassend kann aus den besherigen Versuchen gefolgt werden, dass im Bereich ublicher Abmessungen grössere Balken geringere Biegezugfestigkeiten ergeben als kleinere. Jedoch beeinflusst die Balkenbreite die Biegezugfestigkeiten nahezu nicht."

Also (Ivanyi 1976) went through test results available in literature and stated at a discussion of the Weibull-model that this model is "offensichtlich falsch" as the model predicts the same influence of the width, length and depth of the beam. During flexural tests of beams with rectangular cross section and made of china it was found that the strength became significantly greater if the cross section was placed lying (width>depth) instead of standing. This is in disagreement with the Weibull-model, which predicts equal strength for each case, but in agreement with the fictitious crack prediction. The difference in strength may however also be caused by possible anisotropy of the china. Another qualitative difference between the models concerns the strength of extremely deep beams: According to the Weibull-model the flexural strength approaches zero, while according to the ficitious crack model the strength approaches a non-zero value which at approximately equal length of the flexural and tensile specimens respectively is of about the same magnitude as the uniaxial tensile strength. Also with regard to this qualitative difference between the models it is found that the Weibull-model is in disagreement with test results, while the fictitious crack prediction may be correct: With reference to the test carried out by Heilmann in 1976, König and Jahn (1983) state that the limit flexural strength for very large beams is from 1.07 to 1.09 times the uniaxial tensile strength, and not zero. We may therefore da ıs, that the

Weibull-model does not predict flexural strength correctly. Numerical, quantitative comparisons between tests and predictions support this conclusion, see Fig 4.2 (16).

In some Weibull-type analyses weak parts of the material are not assumed to be distributed over the volume of the specimen, but only over the surfaces. But by the same type of discussion as described above, one may conclude that this alternative type of Weibull-analysis does not predict flexural strength correctly either.

It is unfortunately often difficult to carry out accurate numerical comparisons to tests reported in literature as the required information about basic material properties and about the manner in which the tests were carried out is often not available in detail. In spite of this, some comparisons will be made. (Petersson, 1981) determined flexural strength, uniaxial tensile strength, fracture energy, G_f, and modulus of elasticity, E, for different qualities of concrete. During the flexural tests three-point bending was applied and the specimens had the dimensions $\ell_f b_f d_f$ = 200 x 50 x 50 mm^3, where ℓ_f was the free distance between the supports. The tensile specimens had a cross section of $b_t d_t$ = 50 x 50 mm^2 and the loaded part of the specimens had a nominal length of 80 mm. During the tensile tests a certain type of grip with wedge-shaped rubber inserts was used and it was reported that these inserts were deformed during loading in such a manner that the loaded part of the specimen might in reality have had a length of 120 mm. As to the current theoretical predictions it is assumed that the loaded part of the tensile specimen had a length of 100 mm. In Fig 4.2 (16) the experimental results of Petersson are indicated by dots and the current theoretical results by curves. As to the theoretical results in which scatter is taken into account, the parameter m is put equal to 14. In none of the theoretical results is any influence of the limited length to depth ratio of the specimens taken into account: As to the Weibull-prediction influence of shear stresses are not taken into account and the bending stresses are assumed to vary linearly along the depth of the beam, and where to fictitious crack predictions are concerned it is assumed that the results in Fig 4.2 (3) may be interpretated as $M_u/(f_t bd^2/6)$ in spite of the limited length to depth ratio of the three-point bend specimen. In the deterministic fictitious crack prediction one may easily take into account the influence of the limited length to depth ratio with the help of Fig 4.2 (3). This is, however, not d ;tent approach at

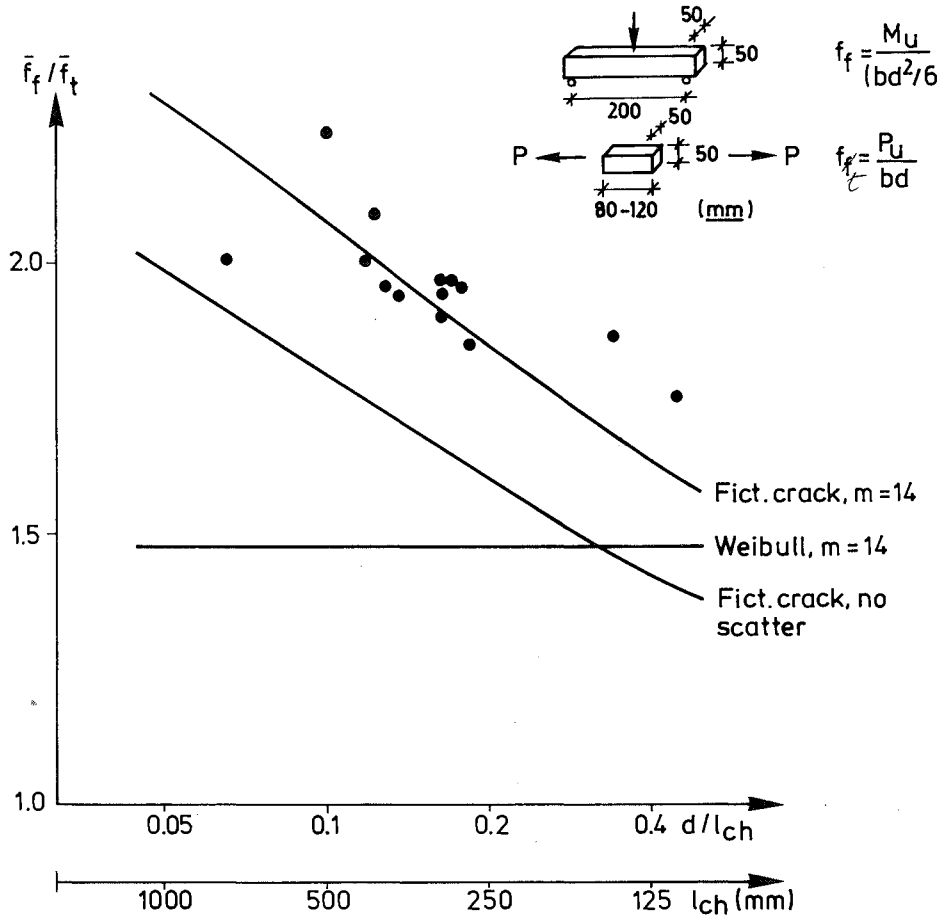

Fig 4.2 (16) Ratio flexural strength to uniaxial tensile strength, f_f/f_t, vs. ratio d/ℓ_{ch}. d=constant=50 mm. Experimental results according to (Petersson, 1981) and predictions according to three theoretical models of fracture. The dots represent mean values.

the different theoretical predictions. Fig 4.2 (16) indicates that the influence of the material property ℓ_{ch} seems to be satisfactorily described by the fictitious crack model and that the absolute values of the ratio between flexural strength and tensile strength are accurately predicted when a reasonable magnitude of scater in strength is taken into account. Of cours[illegible] influence of ℓ_{ch}

and the prediction of the ratio between flexural strength and tensile strength is in disagreement with the experimental results. The theoretical predictions of the ordinary deterministic linear elastic brittle model and the plastic models are not indicated in Fig 4.2 (16), but are very much in disagreement with the experimental results.

The influence of ℓ_{ch} on the ratio f_f/f_t indicated in Fig 4.2 (16) may be of practical importance, in particular in comparisons between low, normal and high strength types of concrete. In high strength types of concrete one may expect that the crack will pass through the aggregate particles instead of around them. This may cause a decrease in G_F which together with an increase in f_t will probably result in a more brittle behaviour (a decreased $\ell_{ch}=EG_F/f_t^2$) of the high strength types of concrete and thereby a decrease in the ratio between flexural and tensile strength. The experimental results obtained by (Petersson, 1981) indicate that an improvement in the strength of the concrete (the water-cement-ratio varied from 0.7 to 0.3) from f_t=2.4 MPa to f_t=4.5 MPa gave a decrease in ℓ_{ch} from 510 mm to 280 mm and a decrease in f_f/f_t from about 2.24 to about 1.94. Decrease in ratio f_f/f_t during improvement of the quality of the concrete is also reported by Neville (1981). A diagram by Neville showing f_f vs. f_t yields: f_f/f_t=2.00 at f_t=1.0 MPa; f_f/f_t=1.77 at f_t=2.0 MPa; and f_f/f_t=1.65 at f_t=4.0 MPa. More careful work during mixing and casting of high strength concrete may also influence f_f by decreased scatter in strength: if the flexural and tensile specimens are of equal length, according to Fig 4.2 (14) a decreased scatter produces a decrease in f_f/f_t.

In addition to the comparison in Fig 4.2 (16), in Fig 4.2 (17) (three pages) different test results from literature are compared to the theoretical results obtained by means of the fictitious crack model, taking the influence of scatter into account by means of eq (4.2:14), assuming a 8.7 % scatter in strength corresponding to m=14. The latter figure concerns the relative influence of depth of the beam, length of the beam and type of loading. While information required to enable comparisons with regard to absolute values of flexural stength is not available to the writer, the current theoretical curves are based on certain assumptions regarding the uniaxial tensile strength and other parameters. The assumptions made in order to enable theoretical calculations are given in the figure-text. Fig 4.2 (17) indicates that eq (4.2:14) seems to predict the relative influence of the different variables in a good or reasonable manner. The ability of eq (4.2:14) to predict the f flexural

strength is illustrated by Fig 4.2 (16). Where Fig 4.2 (17) is concerned, it may be noted that better agreements between tests and theory are possible if other values of ℓ_{ch} and m are adopted. Thus, for instance, if a larger scatter in strength than 8.7 % (m=14) is relevant for the concrete used by Wright (Fig 4.2 (17) a), b), c), and d)) then eq (4.2:14) is in better agreement with the tests than as indicated by the figure.

Naturally, the test results shown in Fig 4.2 (17) do not represent all the tests reported in literature, but are believed to be typical. The only test results which clearly deviate from other test results are those in Fig 4.2 (17) f) obtained by Nielsen in 1953: at beam depths of 100, 150 and 200 mm, length and width kept constant, an almost constant flexural strength was obtained: 47.6, 47.0 and 47.3 kp/cm^2. (Current theoretical prediction: 50, 47 and 45 kp/cm^2). These uncommon test results may be incidental or have a simple explanation, which is unknown to the writer.

The influence of the length of the beam is not very clearly indicated by the test results in Fig 4.2 (17) and consequently some additional information may be appropriate: in 1928 Gonnerman and Shuman found that an increase in length from 350 mm to 1550 mm resulted in an approximate 10 % decrease in strength during three-point bending but no systematic change during four-point bending (theoretically at m=14: a 10 % decrease); in 1932 Kellerman found that an increase in length from 460 mm to 690 mm resulted, in mean, in a 5 % decrease in flexural strength both during three- and four-point bending (theoretical at m=14: a 3 % decrease); in 1953 Johnsson found thats an almost four fold increase in length resulted in a 6 % decrease in flexural stength (theoretically at m=14: a 9 % decrease).

Naturally, the theoretical model represented by eq (4.2:14) is an idealization and simplification of reality. On the other hand, the model is based on basic material properties, the model is simple and furthermore there is no other theoretical model known to the writer at present which seems to be able to predict flexural strength of unreinforced concrete and similar materials as qualitatively correct and numerically accurate. In spite of this, one may of course not expect the model to produce exact predictions of flexural strength. Where the different models in Fig 4.2 (15) are concerned the current study also suggests, not very surprisingly, that the model which is based on the most realistic basic assumption with regard to the stress vs. deformation properties of concrete in tension also gives the best r

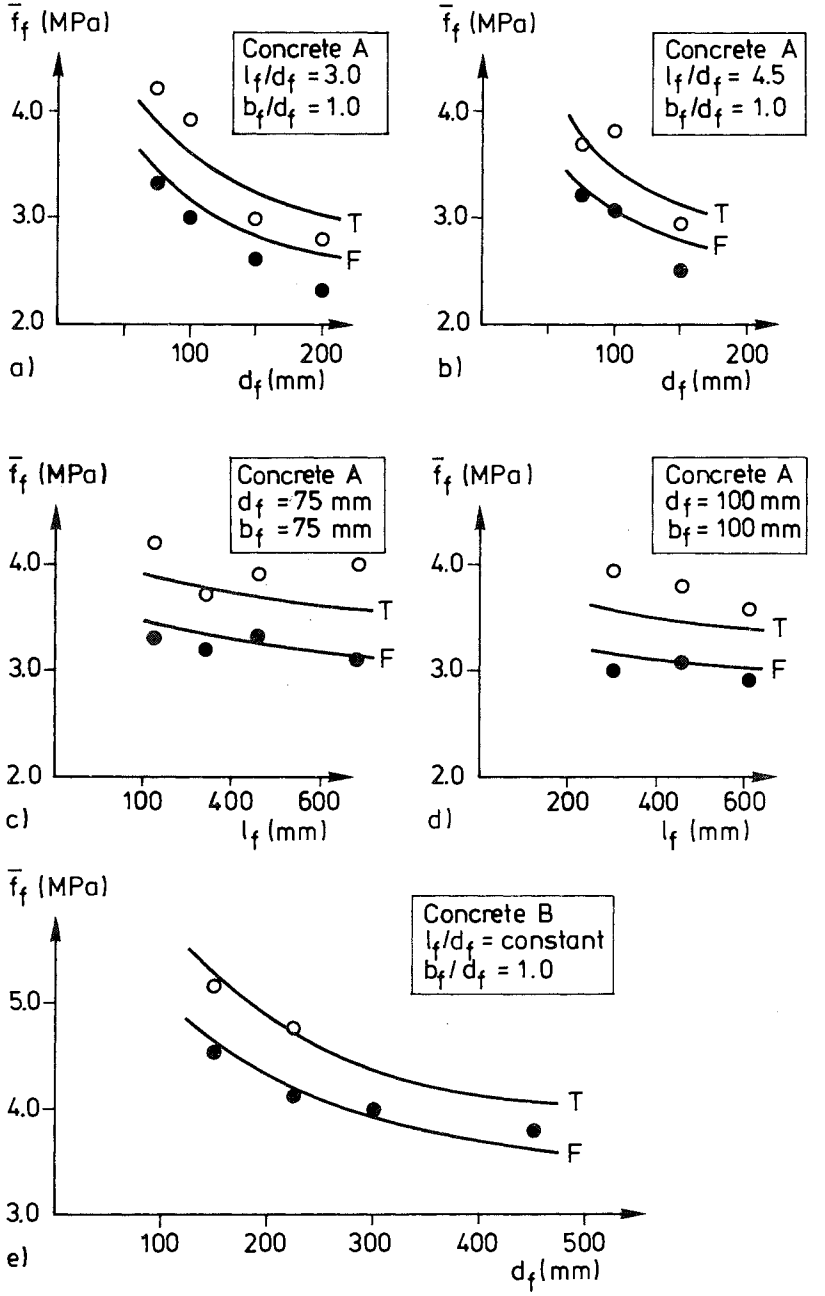
$\bar{f}_f$ (MPa)
Concrete A
l_f/d_f = 3.0
b_f/d_f = 1.0
4.0
3.0
2.0
T
F
100
200
a)
d_f (mm)
$\bar{f}_f$ (MPa)
Concrete A
l_f/d_f = 4.5
b_f/d_f = 1.0
4.0
3.0
2.0
T
F
100
200
b)
d_f (mm)
$\bar{f}_f$ (MPa)
Concrete A
d_f = 75 mm
b_f = 75 mm
4.0
3.0
2.0
T
F
100
400
600
c)
l_f (mm)
$\bar{f}_f$ (MPa)
Concrete A
d_f = 100 mm
b_f = 100 mm
4.0
3.0
2.0
T
F
200
400
600
d)
l_f (mm)
$\bar{f}_f$ (MPa)
Concrete B
l_f/d_f = constant
b_f/d_f = 1.0
5.0
4.0
3.0
T
F
100
200
300
400
500
e)
d_f (mm)

Fig 4.2 (17)

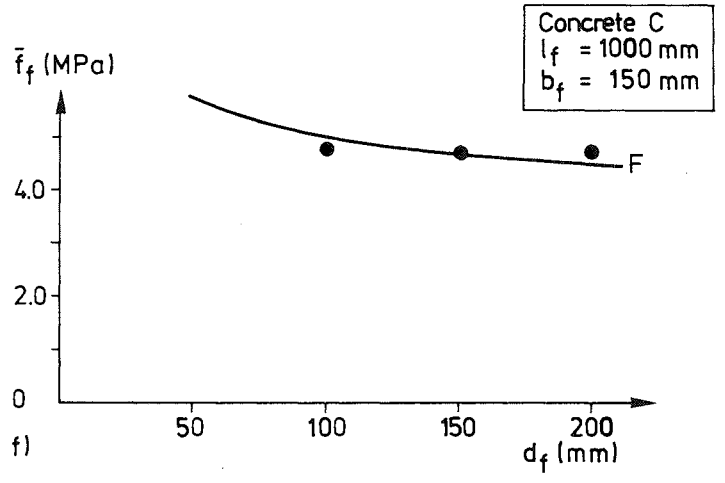

Fig 4.2 (17) a)-h) (Three pages). Flexural strength of concrete, mortar and plaster: Test results compared to theoretical results obtained by means of eq (4.2:14) and Fig 4.2 (3).

- o (test) and T (eq (4.2:14)) indicates three-point bending.
- • (test) and F (eq (4.2:14)) indicates four-point bending.

Figures a)-d): tests by Wright, 1952 (Bonzel, 1965); e) Linder and Sprague, 1955 (Ivanyi, 1976); f) Nielsen, 1953 (Bonzel, 1965); g) (Sabnis and Mirza, 1979); h) Berenbaum and Brodie, 1959 (Ivanyi, 1976). Assumptions regarding theoretical calculations: ℓ_{ch}=400 mm (concrete), 100 mm (mortar) and 50 mm (plaster); m=14 (concrete, mortar, plaster). (Chosen assumed values of f_t (with reference to ℓ_t=100 mm): figures a)-d) 2.09 MPa; e) 3.51 MPa (at ℓ_f/d_f=5); f) 3.57 MPa; g) 3.70 MPa; h) 3.13 MPa.

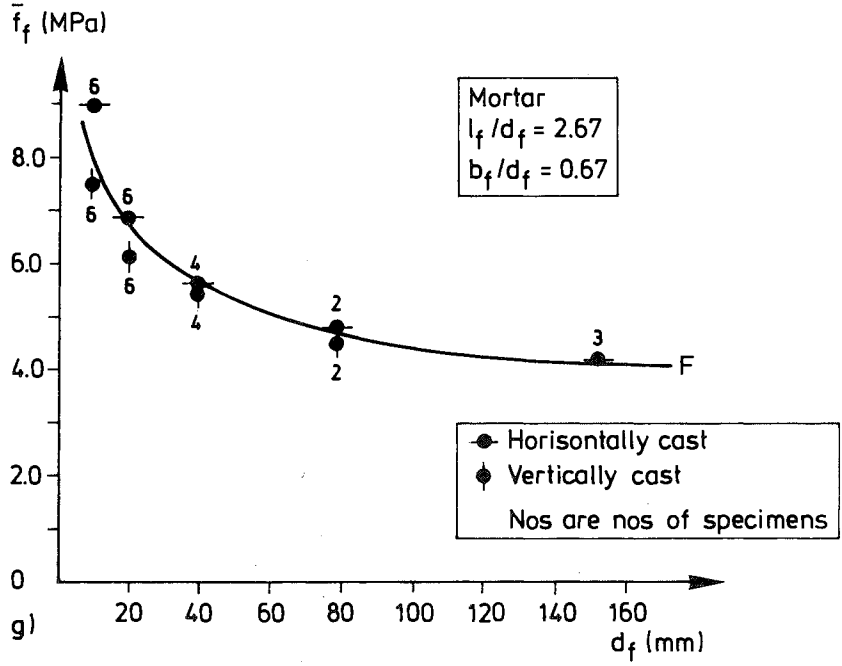
$\bar{f}_f$ (MPa)
Mortar
l_f/d_f = 2.67
b_f/d_f = 0.67
8.0
6.0
4.0
2.0
0
6
6
6
6
4
4
2
2
3
F
Horisontally cast
Vertically cast
Nos are nos of specimens
g)
20
40
60
80
100
120
140
160
d_f (mm)

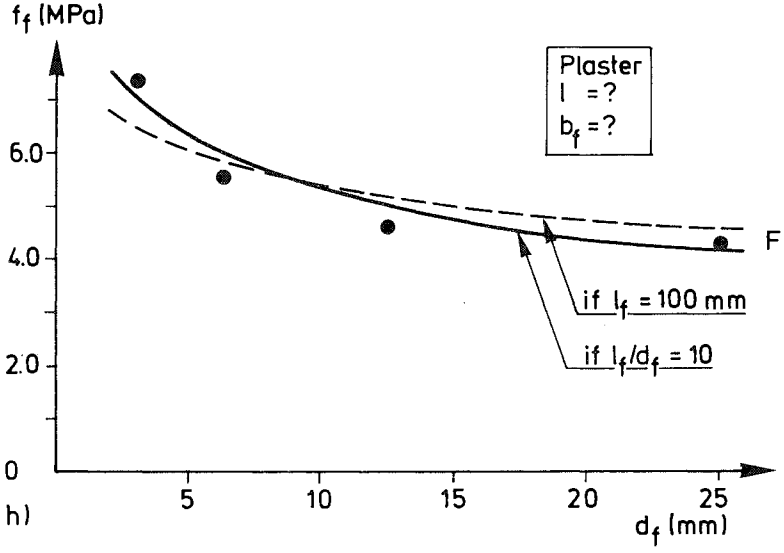
$\bar{f}_f$ (MPa)
Plaster
l = ?
b_f = ?
6.0
4.0
2.0
0
F
if l_f = 100 mm
if l_f/d_f = 10
h)
5
10
15
20
25
d_f (mm)

Fig 4.2 (17)

With regard to the study of the influence of initial stresses presented in Section 4.2.2, only a brief comment will be made in adition to those in Section 4.2.4. The computational results are valid for one certain assumption of the distribution and magnitude of initial stresses, while the real non-uniform distribution of shrinkage strains, assumed to cause the initial stresses, varies with time. Interaction with creep as well as increase in the true tensile strength during limited drying may even yield a higher flexural strength after drying than before the drying started. The assumed distribution and magnitude of the initial stresses are, however, not entirely unrealistic and initial stresses rather similar to those assumed are likely to occur at some instant during the course of drying. As to loading sustained during drying one may thus assume that the calculated values of flexural strength may in approximation form an upper limit of the load carrying capacity.

The bending moment vs. fracture hinge rotation relations in Section 4.2.3 enable at first hand fictitious crack analyses of statically indeterminate beams. An example of such an analysis is given in Section 4.6.5, see Fig 4.6 (10). This example is rather special as it concerns a curved beam when normal forces act across one of the fracture sections simultaneously to the bending moment. But in spite of this, the computational method described in Section 4.6.5 should be possible to apply also to the more simple case of a straight statically indeterminate beam in which the normal force is zero.

In general, numerical ultimate load analyses of statically indeterminate beams require information about the behaviour of the fracture hinge at unloading, i.e. at decreased rotation. In Section 4.2.3 only the behaviour at loading, i.e. at increased rotation, is dealt with. However, a simple assumption with regard to the unloading behaviour of fracture hinges and the corresponding unloading behaviour of fracture zones is dealt with in Section 4.6.5, see Fig 4.6 (12) and Fig 4.6 (13).

The M vs. curves in Section 4.2.3 describe the bending moment vs. additional deformation during the growth of one single crack, and in such a case it is natural to relate the moment to rotation, not to curvature. If the growth of several fracture zones is taken into account, the deformation should preferably be described by a bending moment vs. curvature diagram as long as the moment is increasing at increased deformation and when the moment

is decreasing during increased deformation. When the bending moment capacity in a section starts to decrease, the curvature becomes localized and it is hardly possible to describe a decreasing moment at increasing deformation as moment vs. curvature (unless the curvature softening is assumed to take place along some certain defined length of the beam). The "curvature localization" in ordinary plane-cross-sections-remain-plan beam analysis is analogous to the phenomenon of strain localization in a bar in tension. The analogous description of the strength and stiffness properties of a section of a beam is shown in Fig 4.2 (18).

Due to the method of analysis applied in Section 4.2.3, in which the growth of only one fracture zone was considered, both ascending and descending parts of the moment curves are included in Fig 4.2 (5) to 4.2 (10). In order to transform the ascending parts of these moment vs. rotation curves into moment verus curvature in a simple approximate manner, it is necessary to make an assumption regarding the distance between the fracture zones. This distance should preferably not be assumed to be a constant, but related to the depth of the fracture zones. A reasonable assumption with respect to this spacing between the cracks together with an assumption regarding the unloading properties of the fracture zones should enable the estimation of the moment verus curvature relations for the ascending parts of the moment curves. Such estimations, being left to the interested reader to carry out, may be of significant importance regarding predictions of deflection but probably of less importance where predictins of ultimate strength are concerned.

The ultimate load of statically indeterminate beams is governed by the strength of the fracture hinges and the ratios between the stiffness of the fracture hinges and the stiffness of the parts of the beam outside the fracture hinges. The dependence of stiffness properties makes it, in general, necessary to carry out a calculation of ultimate load in a numerical manner with the help of a computer program. It should, however, be possible to calculate upper and lower bounds of the ultimate load of statically indeterminate beams by more simple means. To illustrate this, the statically indeterminate beam shown in Fig 4.2 (19) is taken as an example, and it is assumed that the properties of the beam are described in the manner shown in Fig 4.2 (18). To simplify the calculations and facilitate the use of ordinary hand-books in structural mechanics, it is furthermore assumed that the moment vs. curvature relation may be

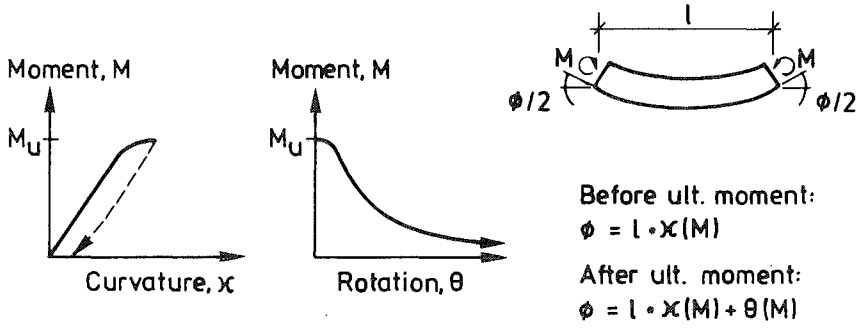

Fig 4.2 (18) Principle for description of strength and deformation properties of a section of a beam.

represented by a straight line. Simple considerations of equilibrium indicate that the load is proportional to a weighted sum of the absolute values of the bending moments in the fracture hinges: $P=3(|M_A|+3|M_B|)/(2\ell)$ for the beam in Fig 4.2 (19).

If the beam is very slender, the deformations of the fracture hinges (before their complete collapse) are very small in comparison to the deformations of the unfractured elastic parts of the beam. Thus there is no beneficial influence of the rotation capacity of the hinges. This means that the statically indeterminate very slender beam will behave in a brittle manner and that the bending moment distribution along the beam is the same as if the fracture hinges had zero rotation capacity. Accordingly, the ratio between the bending moments in the fracture hinges is constant during the course of loading and in accordance with the ordinary linear elastic bending moment distribution. For the studied beam: $|M_A| / |M_B| = 6/7$. Thus $P_u = 3 M_u (6/7+3)/(2\ell) = 81/14 (M_u/\ell)$. By knowing of f_t, d/ℓ_{ch} and the size of the cross section, M_u may be obtained with the help of Fig 4.2 (3). The limiting case of extreme slenderness, corresponding to a brittle global behaviour of the beam, forms a lower limit for the ultimate load of the statically indeterminate beam.

On the other hand, the parts of the beam between the fracture hinges may be considered as being indefinitely stiff. This means that the ratios between the rotations of the fracture hinges is constant during the entire course of loading and collapse. Accordingly, when the rotations in any one of the hinges h other hinges

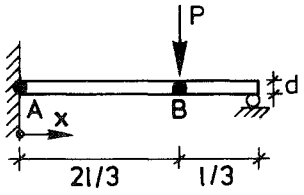

large ⟵ l/d ⟶ small

$$\frac{81}{14}\left(\frac{M_u}{l}\right) \leq P_u \leq \frac{84}{14}\left(\frac{M_u}{l}\right)$$

Fig 4.2 (19) An example and illustration of the calculation of upper and lower bounds of the ultimate load carrying capacity of statically indeterminate beams. M_u is the ultimate bending capacity of the fracture hinges A and B.

are also very small. Provided that the (descending) slope of the M vs. curve is finite, this means that the bending moment in the different fracture hinges reaches the maximum value, M_u, at the same time. This corresponds to an upper limit of the ultimate load of the statically indeterminate beam. For the beam in Fig 4.2 (19) one obtains: $P_u = 3M_u/(1+3)/(2\ell) = 84/14\ (M_u/\ell)$. Here P_u is the ultimate load in the theoretical limit of extreme stiffness of the beam, while M_u, i.e. the ultimate moment capacity of a section of the beam, has the same value as in the above discussion regarding the opposite limit of extreme slenderness of the beam.

Calculations of upper and lower bounds by means of the method exemplified above are simple to carry out and may be used for approximate estimations and during control of results obtained numerically with the help of a computer program with due consideration to the slenderness of the beam and to the bending moment vs. rotation curve. As compared to the general upper and lower bound hypotheses discussed in Section 3.5.2, the present upper and lower bounds give a more precise result but require knowledge of the actual ultimate load carrying capacity of the sections of the beam.

In the example in Fig 4.2 (19), the difference between the upper and lower bounds is small, and in such a casae a good estimation of the ultimate load may be obtained merely buy knowledge of M_u and without consideration of the M vs. θ curve of the fracture hinges. In other cases the difference is greater. Taking the beam in Fig 4.2 (19) as an example: a point load at $x=\ell/2$ gives $(16/3)(M_u/\ell) \leq P \leq (18/3)(M_u/\ell)$; a point load at $x=\ell/3$ gives $(54/10)(M_u/\ell) \leq P \leq (75/10)(M_u/\ell)$; and uniformly distributed load gives $8(M_u/\ell) \leq (q\ell)_u \leq (6+\sqrt{\ }$ rds a curved

beam, is dealt with in Section 4.6.5.

If the moment vs. rotation curve includes an ascending part, then one has to take into account the numerical values of the ratios beween the rotations of the hinges in order to accurately calculate the ultimate load corresponding to the theoretical limit of extreme stiffness of the unfractured parts of the beam. Additionally, if the M vs. θ curve includes an ascending part of extraordinary shape, it is possible to find types of beams for which the limit of extreme stiffness does not corrspond to an upper limit of the ultimate load.

It may also be noted that the locations of the fracture hinges is not always the same in two extreme limits. The case of a uniformly distributed load acting on the beam shown in Fig 4.2 (19) may serve as an example.

The influence of scatter in strength on the ultimate load of statically indeterminate beams may be a subject for future studies.

It has not been possible to carry out any direct comparison of the M vs. θ curves in Section 4.2.3 with experimental results. The lack of experimental results in available literature may be explained by difficulties in possible efforts to attain stable collapse of an unnotched unreinforced concrete beam. In addition, it is possible that fracture of unreinforced and un-notched concrete beams has not previously been described in terms of bending moment vs. rotation.

It has also proved somewhat difficult to carry out informative comparisons between the current M vs. θ curves and similar curves obtained by means of other theoretical models. The descending part of the M vs. θ curves is not possible to obtain during theoretical calculations based on a conventional linear or non-linar stress-strain descriptions of the material (unless the curvature localization is assumed to take place along some certain non-zero defined length). The ideal plastic models predict a trivial M vs. curve: a constant value of M independent of how much θ grows. Linear elastic fracture mechanics and other traditional fracture mechanics models are not directly applicable as there is not notch or initial crack in the studied type of beam.

In spite of this, if one assumes that an inital crack in the lower edge of the beam exists rves by means

of the linear elastic fracture mechanics. The results of such calculations are shown in Fig 4.2 (20) a) and b), where a comparison is also made with the result of the fictitious crack calculations. The fictitious crack results are according to Section 4.2.3 and have therefore been obtained without the assumption of the existence of an initial crack. a/d indicates the relative depth of the assumed pre-existing crack and it is quite obvious that the first part of the curves, as obtained by linear elastic fracture mechanics, is very dependent on the depth of the assumed pre-existing crack. If the depth is put equal to zero then M/M_o becomes infinitely large before fracture starts to develop. The linear elastic fracture mechanics result shown in Fig 4.2 (20) a) and b) have been obtained by means of finite element analysis of the beam shown in Fig 4.2 (1). Stress intensity factors (obtained from the rate of energy release) and deflections were determined by step-wise uncoupling of the nodes along the crack propagation path. In Fig 4.2 (20) a) and b), it might be of interest to note that the M/M_o vs. $\theta/(f_t/E)$ curves as obtained by the two theoretical models do not approach each other in a continious asymptotical manner, but crosses each other instead. This is to be expected as the area under the complete curves should become the same in fictitous crack analysis and in linear elastic fracture mechanics analysis (if the depth of the assumed crack is zero), compare Section 4.2.4 and eq (4.2:8).

It is possible to choose the depth of the assumed pre-existing crack in the linear elastic fracture mechanics analysis in such a way that the calculated ultimate bending moment coincides with the ultimate moment as obtained by fictitious crack analyses. In general, however, this proper choice is dependent on both the properties of the material and the depth of the beam, see Fig 4.2 (20) c). This figure has been obtained with the help of Fig 4.2 (2) and a polynomical series expression for the linear elastic stress intensity factor, K, which may be found in (Hayes, 1975). This expression was used instead of the values of K currently obtained by means of finite element analysis as the polynomical series is believed to be more accurate for small relative depths of the crack. For large values of d/ℓ_{ch}, $d/\ell_{ch} \gtrsim 3.2$, the figure indicates that the relevant choice of the depth of the pre-existing crack approaches a constant fraction of EG_c/f_t^2 and is thus dependent only on the properties of the material and independent of the size of the beam. The constant fraction of EG_c/f_t^2 obtained for large values of d/ℓ_{ch} is very close to 1/4 and is recognized as the parameter a_c, critical crack length, used in linear elastic fracture mecha[illegible]d according to

the linear elastic fracture mechanics at the crack length a_c is equal to the ultimate load according to the ordinary theory of linear elastic brittleness at crack length zero. According to Hayes (1975), the stress intensity factor for a surface crack in a half-space semi-infinite plate is $\sigma\sqrt{a}\ 1.12\sqrt{\pi}$, and thus $a_c=1/(1.12\sqrt{\pi})^2(K_c/f_t)^2 \approx 1/4(EG_c/f_t^2)=1/4(EG_F/f_t^2)=\ell_{ch}/4$, if $G_c=G_F$. The approximation $1/(1.12\sqrt{\pi})^2=1/4$ corresponds to 0.7 % deviation in ultimate load. The deviation between the current asymptotical value and the approximate theoretical value, 1/4, is very small and may be due to the approximations involved in the different numerical calculations. As to calculation of ultimate strength, the result shown in Figure c) means that linear elastic fracture mechanics may be used if $d/\ell_{ch} \gtrsim 3.2$ and the depth of the assumed crack is made to equal $\ell_{ch}/4$. If d/ℓ_{ch} is even greater, let us say if $d/\ell_{ch} > 20$ (compare also Fig 4.2 (2)), then $M_u/M_o \approx 1.00$ and for this case thus the ordinary linear elastic brittle theory may be used as an alternative if only the ultimate strength is to be calculated. As to the calculation of M vs. θ curves at $d/\ell_{ch} \gtrsim 3.2$, Fig 4.2 (20) suggests that approximately the same result will be obtained during fictitous crack analysis and linear elastic fracture mechanics analysis, provided that a pre-existing crack of depth $\ell_{ch}/4$ is assumed in the last type of analysis. This matter may be useful when analysing very large structures as fictitious crack analyses require a large number of finite elements in such cases. During increasing d/ℓ_{ch} the M vs. θ curves as obtained by the two methods of analyses should approach each other gradually. In "normal" or small values of d/ℓ_{ch} one may not expect the two methods of analyses to yield the same M vs. θ curves even if the depth of the assumed pre-existing crack is chosen in accordance with Fig 4.2 (20) c), see Fig a) and b).

Finally, in conjuction to the above discussion of the initial crack depths necessary to assume during linear elastic fracture mechanics analysis, computational results regarding the length of the fracture zone, s, are shown in Fig 4.2 (21). The fracture zone lengths were obtained during the fictitious crack analysis described in Sections 4.2.2 and 4.2.3. The two congruent full curves indicate the length (and the depth) of the fracture zone at the instant of ultimate load. The two dashed curves indicate the length of the fracture zone at the instant when the stress across the fracture zone in its lower edge is equal to $f_t/3$ (compare the actual bi-linear shape of the σ-w curve, Fig 3.2 (3) c)). The two point-dashed curves indicate int when the

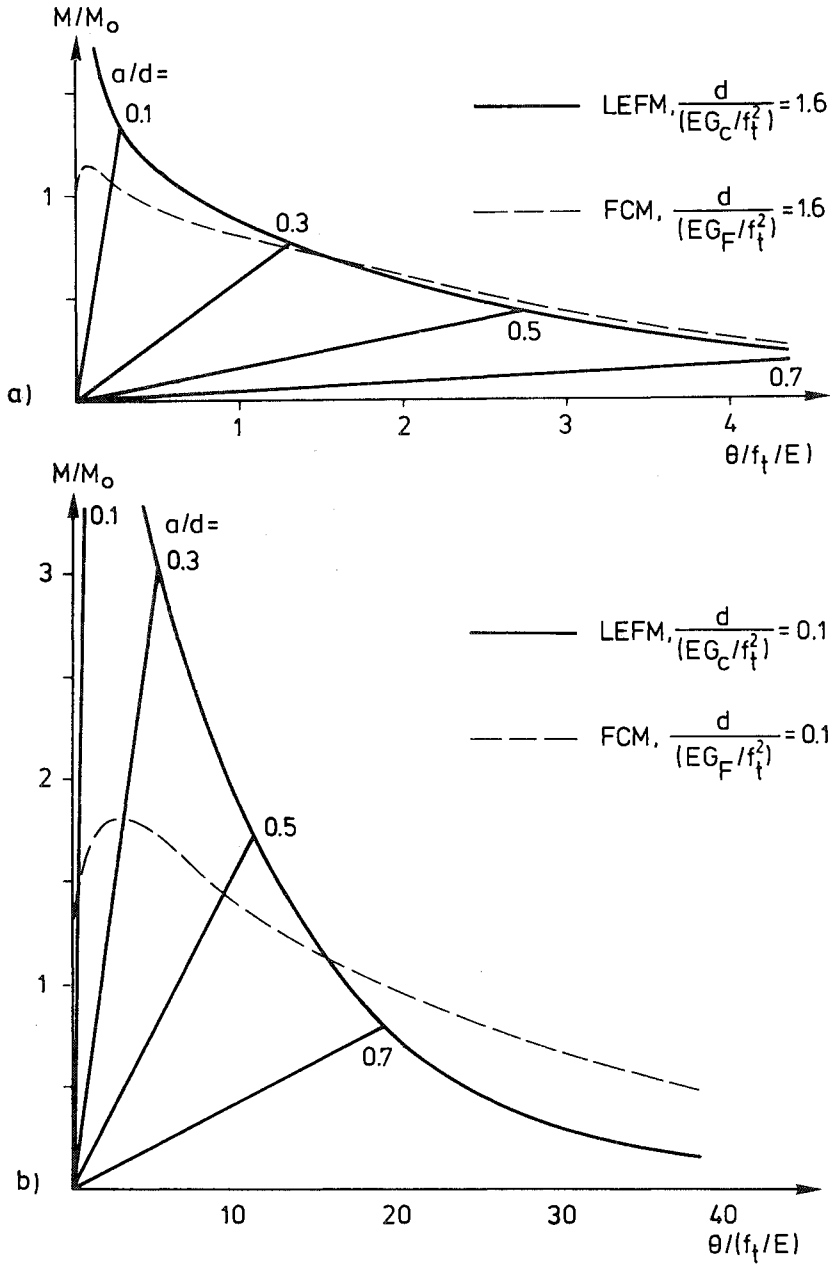
M/M$_o$
a/d=
0.1
0.3
0.5
0.7
1
2
3
4
a)
LEFM, $\frac{d}{(EG_c/f_t^2)}$ = 1.6
FCM, $\frac{d}{(EG_F/f_t^2)}$ = 1.6
θ/(f$_t$/E)
M/M$_o$
0.1
a/d=
0.3
0.5
0.7
1
2
3
b)
LEFM, $\frac{d}{(EG_c/f_t^2)}$ = 0.1
FCM, $\frac{d}{(EG_F/f_t^2)}$ = 0.1
10
20
30
40
θ/(f$_t$/E)

Fig 4.

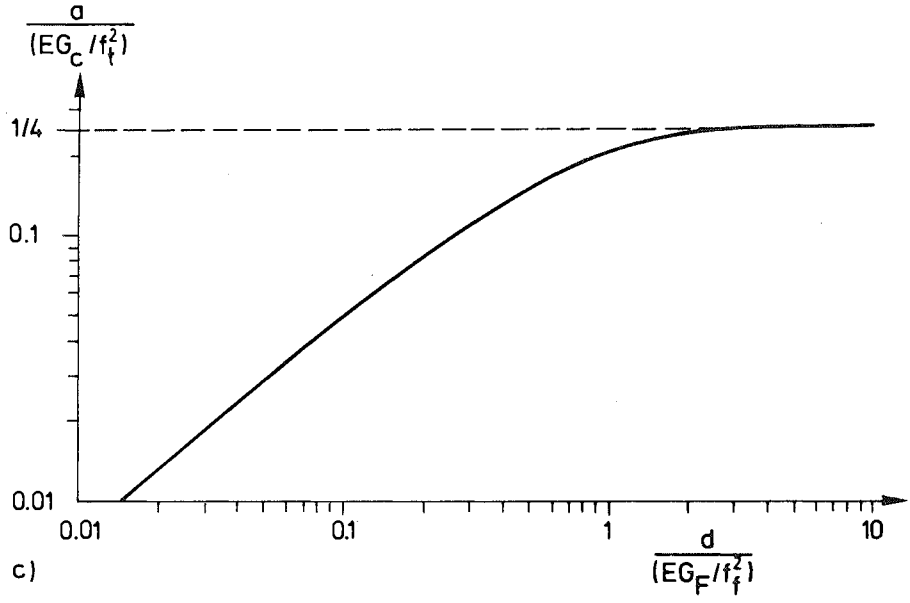

Fig 4.2 (20) Fracture hinge rotation of rectangular cross sections. Comparison between linear elastic fracture mechanics (LEFM) and fictitious crack model (FCM).

a) Bending moment, M/M_o, vs. fracture hinge rotation, $\theta/(f_t/E)$, according to LEFM at different depths, a, of assumed pre-existing crack and according to FCM at zero depth of initial crack. $d/\ell_{ch} = 1.6$

b) Same as a), but $d/\ell_{ch} = 0.1$

c) Depth, a, of pre-existing crack necessary to assume during LEFM-analysis in order to obtain the same ultimate flexural strength as in the FCM-analysis of the initially uncracked beam. It is assumed that $G_c = G_F$.

stress in the lower edge of the fracture zone has decreased to zero. It can be noticed that the length of the fracture zone at peak load seem to approach a constant value during increase in d/ℓ_{ch}. The asymptotical constant length happens to be almost exactly $\ell_{ch}/4$. However, the actual constant length is dependent of the shape of the σ-w curve and it is only an incidential occurance that this length happens to be equal to the relevant asymptotical depth of the initial crack, necessary to assume during linear elastic fracture mechanics analysis, Fig 4.2 (20) c). In Fig 4.2 (21) it can also be seen that only the first linear part of the actual bi-linear σ-w curve is activated at the instant of ultimate load. For the case of non-zero initial stress, the length of the fully developed fracture, if expressed as s/d, expose a drastic increase from $s/d \approx 0.3$ to $s/d \approx 0.8$ when d/ℓ_{ch} is decreased from about 0.8 to about 0.2. As a general result for concrete beams - concrete having values of ℓ_{ch} in the order of 400 mm - Fig 4.2 (21) suggests that the lengths of the fracture zone are significant: for small beams s/d is large, and for large beams s is large. As compared to specimens with a sharp initial crack, e.g. according to Sections 4.3 and 4.4, it is by principle interesting to notice that the length of the fracture zone at peak load does not approach the length of the fully developed fracture zone when d/ℓ_{ch} is increased towards very large values.

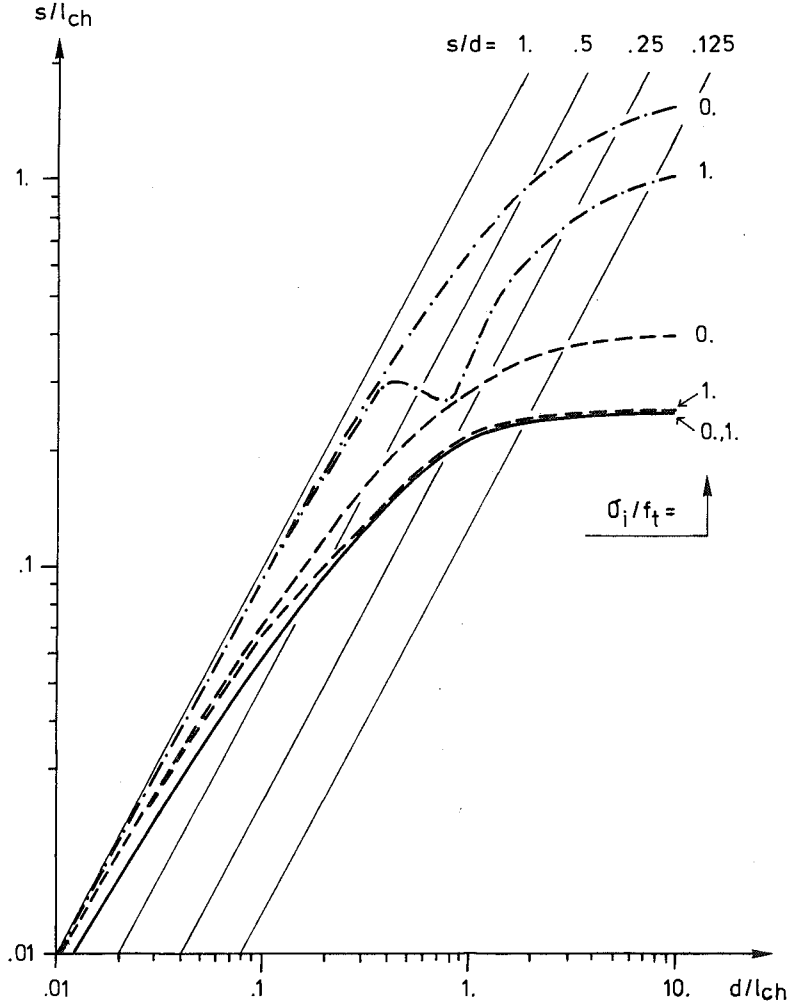

Fig 4.2 (21) Length (and depth), s/ℓ_{ch}, of fracture zone vs. d/ℓ_{ch}.
σ_i/f_t indicates magnitude of initial internal stress.
s/d indicates relative depth in beam.

———— Length at instant of ultimate load.

— — — — Length when stress=$f_t/3$ across lower edge of fracture zone.

—·——·— Length when stress=0 across lower edge

4.3 Wedge-force loaded cracked plate

4.3.1 Introduction. Geometry of specimen

About a decade ago Kesler, Naus and Lott (1971) and Naus (1971) presented an extensive experimental investigation concerning the applicability of linear elastic fracture mechanics to cement pastes, mortars and concretes. The test results, as presented in these references, very clearly suggest that linear elastic fracture mechanics is not applicable to the investigated types of materials. In particular it was found that K_c is very dependent on the depth of the crack and is therefore not a material property constant. The results and conclusions of Kesler, Naus and Lott have frequently been referred to in subsequent literature on fracture mechanics analyses of concrete and similar materials.

However, in 1980 Saouma, Ingraffea and Catalano (1980) presented a re-evaluation of the test results of Kesler et al. and reported that two serious errors had ben committed in the original calculation of K_c from the experimentally obtained values of ultimate load. The re-evaluation was carried out with the help of a finite element method, and at the re-evaluation it was found that K_c did not depend on the depth of the crack but had an almost constant value for each type of material, taking into account a normal and reasonable magnitude of scatter in test results. Saouma et al came to the conclusion that a K_c approach to cracking in concrete structures is valid and that the cause of the delay in integration of linear elastic fracture mechanics concepts into numerical codes for the study of concrete cracking has now been overcome.

The study presented in this Section has two purposes:

1. Verification of the linear elastic fracture mechanics analysis of Saouma et al.

2. By fictitious crack analysis and by comparisons between the fictitous crack analysis, the linear elastic fracture mechanics analyses and the test results, try to determine whether the tests of Kesler et al. may provide information or any conclusions regarding to the applicability of the two current theoretical models of fracture.

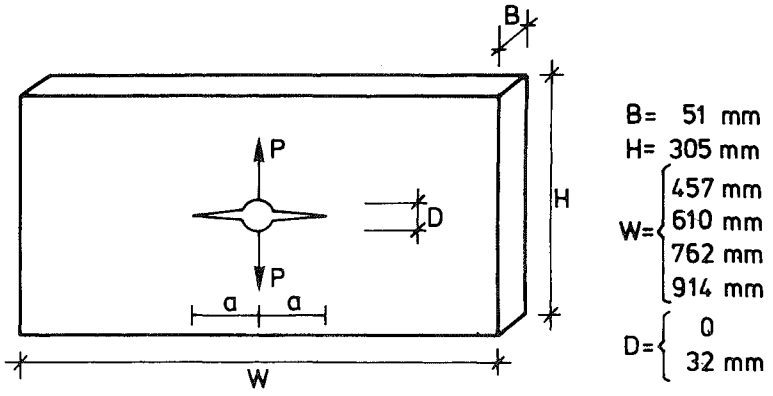

Fig 4.3 (1) Geometry of specimen. No tests for D=0. Present analyses only for H/W=0.5.

The type of specimen used by Kesler et al. was the rectangular plate specimen with a flaw (an initial crack) along its plane of symmetry and a loading hole located at the centre of the specimen, see Fig 4.4 (1). Plates of different geometrical shapes and different depths of the initial crack were used:

$H \approx$ const = 12 in (=305 mm);

$B \approx$ const = 2 in (= 51 mm);

$D \approx$ const = 1.25 in (= 32 mm);

W = 18, 24, 30 and 36 in (457, 610, 762 and 914 mm);

$0.1 < 2a/W < 0.6$.

A total of about 160 specimens were tested. The number of materials tested were eight: 2 pastes, 2 mortars and 4 concretes.

The present investigation only concerns one of the specimen shapes, that of W=24 in (610 mm). This size and shape were used during all the tests on one of the mortars. In order to enable verification of the results of the LEFM analysis, a specimen without the loading hole, i.e. D=0, is also studied.

The notation for specimen geometry adopted in this Section, 4.3, is partly in disagreement with the notations used in other parts of the report, but have been chosen instead in accordance with the main references of this Section. The fictitious crack analyses were first performed on the assumption of a single straight line relation between stress and widening w of th [illegible] analyses were

carried out on the assumption of the bi-linear shape of the σ-w relation. Saouma et al. have presented the computational results from their interesting re-evaluation also in (Saouma, Ingraffea and Catalano, 1982).*) Some of the results presented in Section 4.3.3 are also shown in (Hillerborg, 1982).

4.3.2 Determination of K

If D=0 and if H and W are very large, i.e. if $a/H \rightarrow 0$ and $a/W \rightarrow 0$, then according to Westergaard:

$$K = \frac{P}{B\sqrt{W}} \frac{\sqrt{2}}{\sqrt{\pi 2a/W}} \qquad (4.3:1)$$

With reference to studies by Westergaard, Irwin and Gallagher, Kesler et al used a modification of eq (4.3:1) which takes into account an influence of finite width, W, of the specimen:

$$K = \frac{P}{B\sqrt{W}} \frac{\sqrt{2}}{\sqrt{\sin(\pi 2a/W)}} \qquad (4.3:2)$$

It can be noticed that eq (4.3:1) and, for $2a/W<0.5$, also eq (4.3:2) predicts that K/P will decrease at increased length of the crack. $\partial(K/P)/\partial a<0$ means that a crack is predicted to grow in a stable manner and accordingly the ultimate failure load should not be corresponded to the initial length of the crack during the calculation of K_c. During the calculation of K_c, the ultimate failure load should correspond instead to the crack length where $\partial(K/P)/\partial a=0$. This was pointed out by Saouma et al. and was reported to be one of the errors committed in the original evaluation of K_c.

Eq (4.3:2) does not take into account the influence of finite height, H, and presence of the hole. In 1971 Newman published an analytical solution for K in which finite values of both W and H, but not the presence of any hole, are taken into account. He presented his results in tabular form, but the results of Newman used in the present subsequent comparisons are taken from a diagram shown by (Saouma, Ingraffea and Catalano, 1980). The solution of Newman was most probably not availabe to Kesler et al. in 1971.

*) Please also notice recent literature and additional analyses refered to in the er

In order to take both finite width, finite height and the hole into consideration (and also in order to demonstrate the usefulness of modern finite element methods) Saouma et al. calculated K by means of the finite element method. The difference between the results obtained during these calculations and the results of eq (4.3:2) is great, in particularly for the larger values of 2a/W, and this difference was reported to be the second error in the original evaluation of K_c.

In the finite element analysis of Saouma et al., the symmetrical quarter part of the specimen was divided into a mesh of 45 8-node square elements 54 6-node linear strain triangular elements, the triangular elements being located along the crack propagation path. The total number of degrees of freedom was about 600. In order to model the crack tip singularity, the four triangular elements around the crack tip were distorted by placing the side nodes of the elements on the quarter-points along the side. K was obtained by the displacements substitutation technique: calculated nodal displacements are substituted into an analytical expression for the displacements close to the tip of crack.

During the present finite element analysis, K is obtained by the energy release rate technique. Calculations are carried out with and without consideration to the centre hole of specimen, the purpose of the latter analysis being to control the results by comparison to the solution of Newman. Substructure technique makes it feasible to devide the quarter part of the specimen into a uniform and fine element mesh: in the case of no hole 18 x 36 = 648 4-node square elements of the type of Turner and Clough; in the case of consideration of the hole 18 x 36 - 4 = 644 square elements and, around the hole, 7 quadrilateral 4-node elements. The quadrilateral element is an assembly of four constant strain triangular elements. The total number of degrees of freedom is about 1400 before the static condensations and 148 after elimination of degrees of freedom outside the crack propagation path. No special crack tip element is used and consequently the same element mesh was used for all different lengths of the crack. The energy release rate is obtained by step-wise uncoupling of the nodes along the crack path, and it is assumed that the difference in strain energy at locations a respectively a + Δa of the crack tip equals the rate of the strain energy release at the location a + Δa/2 of crack tip. In this way K (= $\sqrt{EG}$ in the present case of plane stress) is obtained for 34 discrete values of 2a/W. A continuous numerical relation between K and 2a/W is then obtained by means of cubic spline interpolation.

In Fig 4.3 (2) the relations between K/(P/(B W)) and 2a/W as obtained by the different methods of analyses are shown. The solution of Newman and the present analysis, the centre hole not considered, agrees very well. Eq (4.2:2), used by Kesler et al., deviates considerably from the finite element solutions and also from the solution of Newman. Compared to the solution of Newman, the results of Saouma et al. suggest that the presence of a hole decrease K while the present results suggests that the presence of a hole increases K. At 2a/W=0.1 the results of Saouma et al. suggest a 16 % lower value of K than the present results, and at 2a/W=0.5 the results of Saouma et al. suggest a 7 % lower value than the present results. The deviation between the finite element solutions is, however, rather uniform and small in comparison to the deviation from eq (4.3:2).

It is interesting to note the present results reveal a maximum for K (at 2a/W=0.1045). K versus 2a/W has to have a maximum in the case of a centre hole because K=0 when 2a/W=D/W (=1.25/24=0.052083). It is also interesting that $0.1045 \approx 0.1042$, i.e. $(2a/W)_{max} \approx 2D/W$.

The good agreement between the solution of Newman and the present results, the centre hole not considered, suggests that the present results should be satisfactorily accurate also in the case of the presence of a hole. In comparison to the displacement substitution technique, the currently used energy release rate technique has both advantages and disadvantages. As to the present type of analysis, the energy release technique has been estimated to be more advantageous (Section 3.6.1).

By general estimations one may expect the presence of a hole to increase K, but as the results of Saouma et al. suggest the opposite, some additional calculations were carried out in order to check the present results. These additional analyses were carried out only for 2a/W=0.2 and 0.5, with aid of a standard plane stress finite element program and with coarser element meshes: 12 x 24 (mesh B) respectively 9 x 18 (mesh C) square elements of equal size and of the same type as used in the more accurate and complete analysis (mesh A, 18 x 36 elements). In meshes B and C the presence of the hole was modelled simply by omitting one corner element. For mesh C, this means that the size of the hole was substantially exaggerated. Values of K are directly obtained only for discrete values of 2a/W and for meshes B and C the values of K at 2a/W=0.2 and 0.5 were obtained by simple straight line interpolation. The computational ешes the

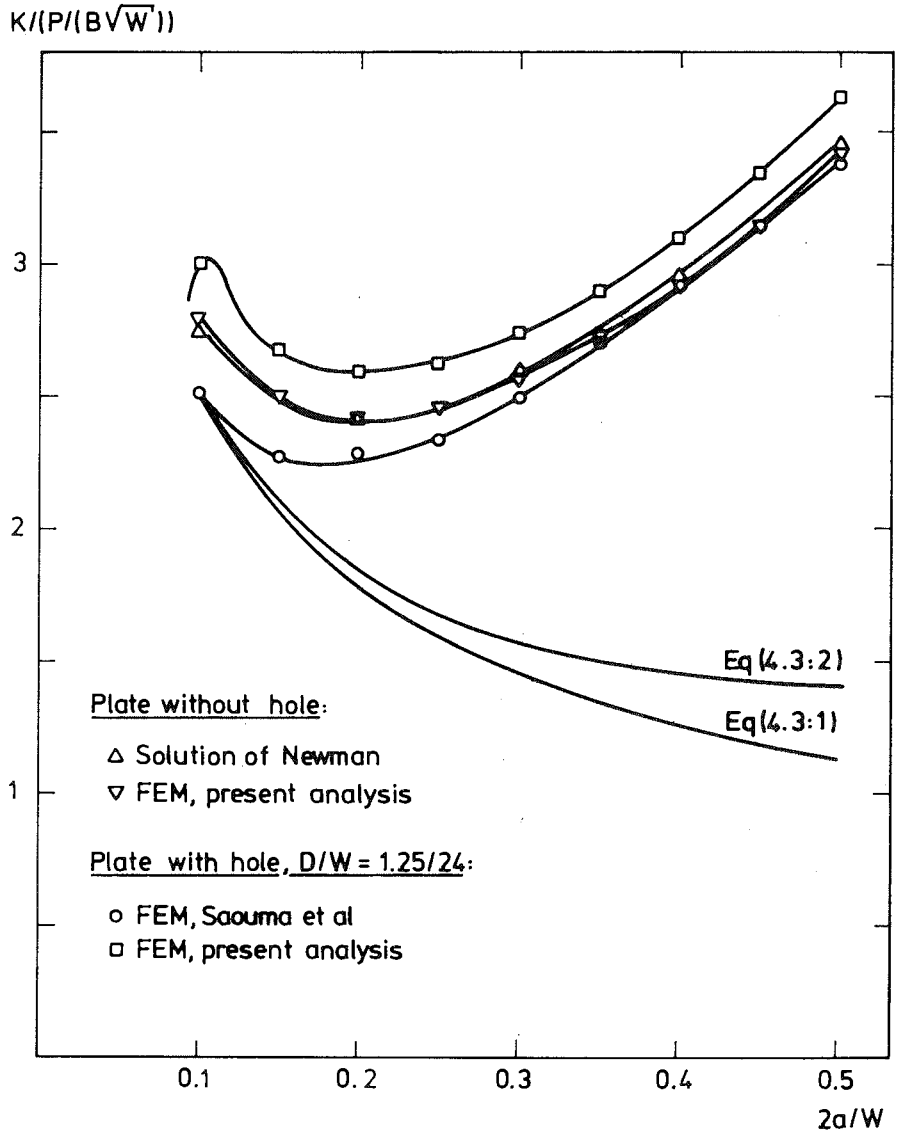

Fig 4.3 (2) Stress intensity factor, K, for the specimen shown in Fig 4.3 (1) according to different analyses. H/W=0.5.

	2a/W=0.20		2a/W=0.50	
	Specimen without hole	Specimen with hole	Specimen without hole	Specimen with hole
Eq (4.2:1)	1.78	-	1.13	-
Eq (4.2:2)	1.85	-	1.41	-
Newman	2.42	-	3.45	-
Saouma et al	-	2.29	-	3.39
Present, mesh C	2.44	2.62*	3.38	3.66*
Present, mesh B	2.43	2.55	3.40	3.57
Present, mesh A	2.42	2.59	3.41	3.63

*Size of hole exaggerated

Fig 4.3 (3) Dimensionless stress intensity factors, $K/(P/(B\sqrt{W}))$, for the specimen shown in Fig 4.2 (1). Underlined values are estimated to be the most accurate ones. H/W=0.5

presence of a hole increases K, and judging by Fig 4.3 (2) and Fig 4.3 (3) one might estimate the maximum error in K in the range $0.1<2a/W<0.5$, as obtained in the present mesh A analysis, to be of the magnitude 1 %. It is rather remarkable how well the energy release rate technique predicts K also in the case of the coarse meshes, taking in to account that the stress field around the crack tip is not modelled by som special type of element. For mesh C and 2a/W=0.2, the value of K is based on calculated potential energy when only one, two and three nodes are in between the crack tip and the load. In spite of this very coarse mesh, the computed value of K deviates, or happens to deviate, less than 1 % from the solution of Newman.

In order to facilitate numerical comparisons in possible future K-analyses of the current specimen, the present results (mesh A) have been tabulated in Fig 4.3 (4) for some different values of 2a/W in the range 0.05 to 0.99. The values of K for 2a/W 0.80, and in particular the value for 2a/W=0.99, are not believed to be very accurate. When plotting the values of Fig 4.3 (4) in a diagram, it is interesting to see that the values of K for the cases D/W=0 respectively D/W=1.25/24 do not approach each other in proportion to the distance between the hole and the tip of the crack. Instead the presence of a hole has an approximate constant magnitude of influence on K for a large range of variation in 2a/W. For the current type of specimen, this may be explained by [illegible] presence of a hole.

2a/W	K/(P/(B$\sqrt{W}$))		2a/W	K/(P/(B$\sqrt{W}$))	
	D/W=0	D/W=1.25/24		D/W=0	D/W=1.25/24
1) .05	3.744	-	.45	3.138	3.343
2) .0508	-	-0.0006	.50	3.411	3.632
.10	2.785	3.009	.55	3.735	3.975
3) .1045	-	3.026	.60	4.119	4.383
.15	2.496	2.675	.65	4.570	4.864
.20	2.419	2.588	.70	5.085	5.416
4) .2038	-	2.588	.75	5.645	6.016
5) .2051	2.419	-	.80	6.199	6.610
.25	2.457	2.625	.85	6.678	7.114
.30	2.563	2.736	.90	7.040	7.464
.35	2.716	2.896	.95	7.456	7.807
.40	2.908	3.099	.99	11.015	11.213

1) K not defined when D/W=1.25/24=.05083
2) K should theoretically equal zero when D/W=1.25/24
3) Maximum point when D/W=1.25/24
4) Minimum point when D/W=1.25/24
5) Minimum point when D/W=0

Fig 4.3 (4) Values of the stress intensity factor for the specimen shown in Fig 4.3 (1) as obtained in the present analysis. H/W=0.5

4.3.3 Fictitious crack analysis. Comparisons with tests. Conclusions

The finite element mesh used during the fictitious drack calculations is the same as used during the determination of K, see 4.3.2. The geometry of the specimen analysed is shown in fig 4.3 (1): H/W=0.5 and D/W=1.25/24. To obtain a general impression of the results of the FCM versus LEFM during analysis of the specimen of Kesler et al., some fictitious crack calculations were first carried out on the simple assumption of a single straight line relation between σ and w. The results of these calculations are shown in Fig 4.3 (5) a) to e).

A basic requirement for the applicability of linear elastic fracture mechanics is that the size of the fracture zone is small in comparison to the depth of the crack and to the size of the specimen. In Fig 4.3 (5) b)

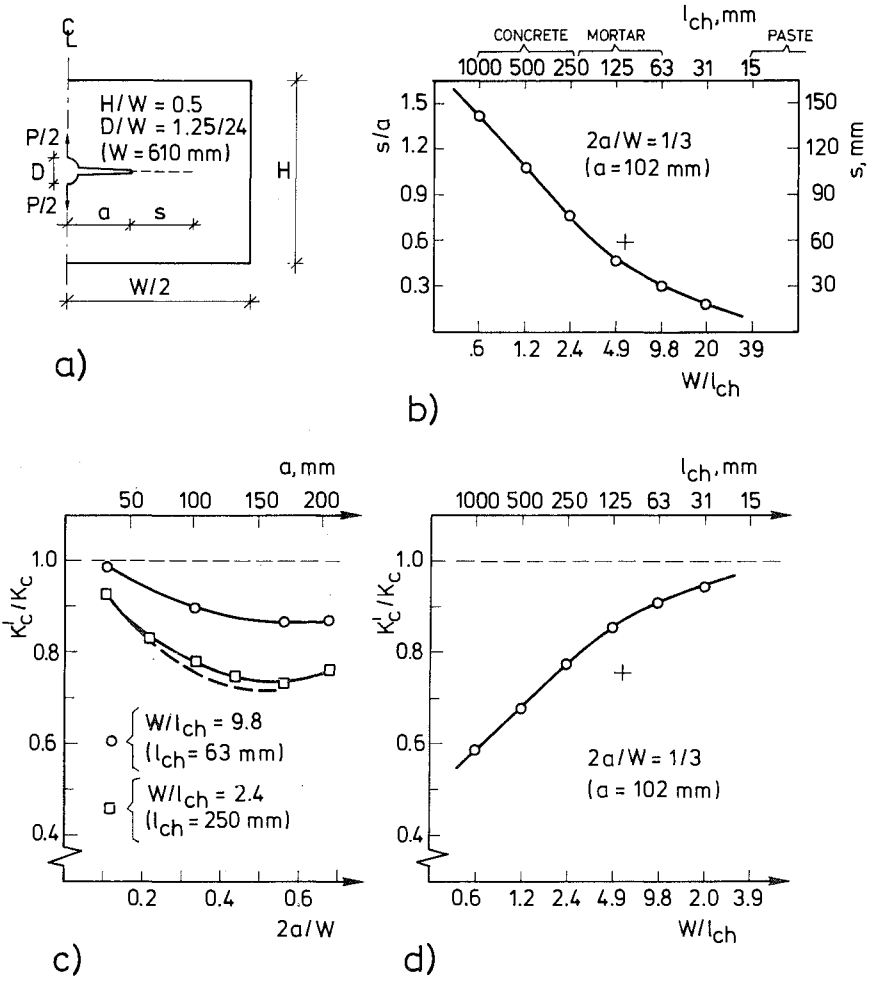

Fig 4.3 (5) Fictitious crack analysis of the specimen used by Kesler et al.

a) Geometry.

b) Length of fracture zone of failure.

c) K_c'/K_c versus notch depth.

d) K_c'/K_c versus W/ℓ_{ch}. Upper and right side axes and values in brackets correspond to the actual size of the specimen: W = 24 in = 610 mm. Full curves are valid for the straight line σ-w relation. Dashed curve (---) in Fig c) and mark "+" in Fig b), d) and e) are valid for

ℓ_{ch}=110 mm).

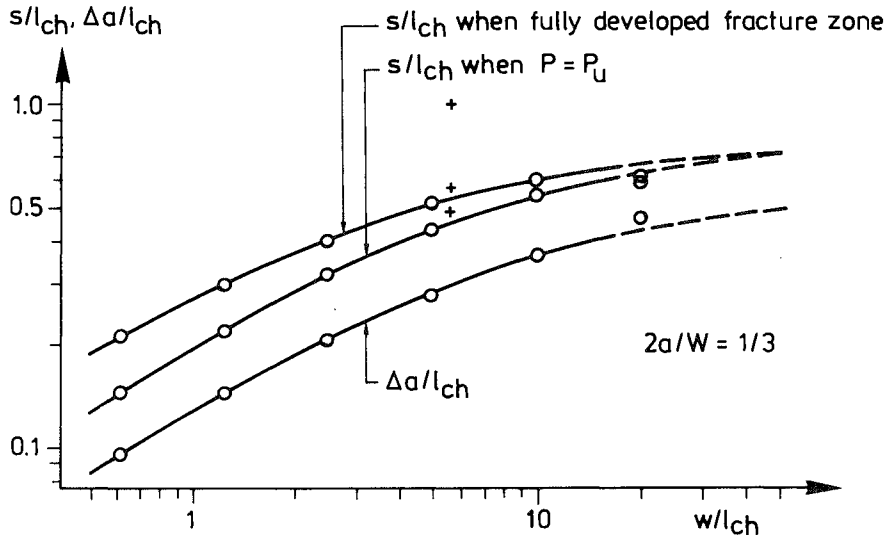

Fig 4.3 (5) e) Normalized length of fracture zone, s/ℓ_{ch}, at failure and when fully developed respectively, vs. W/ℓ_{ch}. "Effective" addition to crack length, $\Delta a/\ell_{ch}$, vs. W/ℓ_{ch}.

the normalized depth of the fracture zone, s/a, is shown versus W/ℓ_{ch}. The absolute values of s on the right hand side of the diagram and the absolute values of ℓ_{ch} on the upper axis of the diagram correspond to W= 24 in= 610 mm and a= 4 in= 102 mm. s is defined as the distance from the tip of the pre-fabricated notch to the point where $\sigma=f_t$. The results shown in Figure b) suggest that one may expect s to be 70-130 mm for concretes, 30-70 mm for mortars and about 5 mm or less for pastes. On some of the specimens, Kesler et al. measured the strains at different locations along the crack propagation path and one of the specimens made of mortar had the same dimensions as those for which Figure b) is valid, and the measured strains suggest that the depth of the fracture zone was about 2.5 in (about 60-65 mm) at 99 % of the ultimate load. For concretes and mortars Figure b) suggests such magnitudes of s that one may hardly expect linear elastic fracture mechanics to produce accurate results during analysis of the current specimen. On the other hand, where paste is concerned, ℓ_{ch} is of the order 10 mm and linear elastic fracture mechanics may therefore be successfully applied. If the tensile strength of the material is assumed to be indefinitely large (which means that $\ell_{ch}=0$) then

the assumptions and results of the fictitious crack model coincides with those of linear elastic fracture mechanics and accordingly the size of the fracture zone is found to approach zero when $\ell_{ch} \rightarrow 0$.

Figs 4.3 (5) c) and d) show a ratio K_c'/K_c versus 2a/W respectively W/ℓ_{ch}. The ratio K_c'/K_c indicates the ratio between the value of the critical stress intensity factor as evaluated by means of linear elastic fracture mechanics and the "true" value of the critical stress intensity factor. The "true" value is the value which, according to the fictitious crack model, would have been obtained by means of linear elastic fracture mechanics if the specimens were very large. This value of K_c is equal to $\sqrt{EG_F}$. The definitions of K_c' and K_c valid in Fig 4.3 (5) are thus:

$$K_c' = P_u(K/P) \qquad (4.3:3)\ (a)$$

$$K_c = \sqrt{EG_F} \qquad (4.3:3)\ (b)$$

K_c' may be called the apparent critical stress intensity factor. K/P is taken from the finite element results of the writer, Section 4.2.2, and P_u, the ultimate laod, was calculated by means of the fictitious crack model at different values of 2a/W and W/ℓ_{ch}. With a given specimen size and a given shape of the σ-w curve, the ratio K_c'/K_c is governed by a and ℓ_{ch}. Independent of 2a/W (D/W<2a/W<1.0), $K_c'/K_c \rightarrow 1.0$ if $W/\ell_{ch} \rightarrow \infty$ and $K_c'/K_c \rightarrow 0$ if $W/\ell_{ch} \rightarrow 0$. For the actual size of the specimen Figure d), being valid for 2a/W=1/3, it is suggested that K_c'/K_c is 0.6-0.8 for concretes, 0.8-0.9 for mortars and 0.98-1.00 for pastes. Figure c) shows how the initial depth of the crack, a, is predicted to influence K_c'/K_c.

Fig 4.3 (5) e) shows the ratio between the length of the fracture zone at ultimate load and ℓ_{ch} vs. W/ℓ_{ch}, and the corresponding ratio with regard to the length of the fracture zone at the instant when a non-force transferring crack starts to grow from the tip of the inital notch. The Figure also shows a ratio $\Delta a/\ell_{ch}$ vs. W/ℓ_{ch}. a+Δa is the so called "effective" length of the crack: Δ a has been determined in such a way that the ultimate load at crack length a+Δa as obtained during the linear elastic fracture mechanics analysis coincides with the ultimate load at initial notch depth a as obtained during the fictitious crack analysis. a+Δa may also ar elastic

brittle crack. For specimens with constant geometrical shape, constant relative depth of the initial crack and made of materials with equal shape of the σ-w curve, ratios s/ℓ_{ch} and $\Delta a/\ell_{ch}$ may be expected to approach a constant value at an increasing ratio between size of the specimen and ℓ_{ch}. The currently used finite element mesh is too coarse close to the tip of the crack to enable accurate calculations of s/ℓ_{ch} and $\Delta a/\ell_{ch}$ at large W/ℓ_{ch}, but the available results seem to suggest that $s/\ell_{ch} \approx 0.7$ and $\Delta a/\ell_{ch} \approx 0.5$ when $W/\ell_{ch} \gtrsim 50$ in the current geometry of the specimen and when the σ-w curve has the single straight line shape. At lower values of W/ℓ_{ch}, s/ℓ_{ch} and $\Delta a/\ell_{ch}$ are not constant. It is interesting that the shape of the σ-w curve seems to have a strong influence on s/ℓ_{ch} and $\Delta a/\ell_{ch}$. Computational results obtained by Petersson (1981) for a notched three-point bend beam and on the single straight line shape of the σ-w curve seem to suggest that the length of the fracture zone at ultimate load approaches 0.5-0.6 ℓ_{ch} when ratio absolute size to ℓ_{ch} increases. s and also Δa may be roughly estimated in different simple ways. A very simple method, see (Knott, 1973), gives $\Delta a = (K_c/f_t)^2/(2\pi) \approx 0.16\,\ell_{ch}$ and $s = (K_c/f_t)^2/\pi \approx 0.32\,\ell_{ch}$. According to Hillerborg (1983) these estimations must be regarded as lower limits. With the aid of the same type of estimations as discussed by Knott and by Hillerborg and with the aid of comparison to the Dugdale model, the rough estimations $s \approx 0.6\,\ell_{ch}$ and $\Delta a \approx 0.4\,\ell_{ch}$ may be obtained for specimens where size >> a >> ℓ_{ch} and for a straight line relation between σ and w. For large specimens without an initial crack, i.e. when size >> ℓ_{ch} > a=0, $\Delta a \approx 0.25\,\ell_{ch}$ independently of the shape of the σ-w curve: see Section 4.2.5 and Fig 4.2 (20) c). The concept of effective crack lengths may be useful for linear elastic fracture mechanics analysis of very large specimens, the exact choice of Δa being of much less importance in the case size >> a >> ℓ_{ch} (in which case $(a+\Delta a)/a \to 1.0$) than in the case size >> ℓ_{ch} > a=0 (in which case $(a+\Delta a)/a \to \infty$).

The complete curves shown in Fig 4.3 (5) are valid for the straight line relation between σ and w. Similar analyses were, for a much smaller range of variation in ℓ_{ch}, carried out on the assumption of the bi-linear concrete-imitating shape of the σ-w curve, shown in Fig 3.2 (3) c). The purpose of these analyses was primarily to enable evaluation of one of the specific test series of Kesler et al. The marked curve in Fig 4.3 (5) c) and the "+" in b) and d) and e) shows results from these analyses.

During evaluation of K ($= \sqrt{EG}$) by means of the fictitious crack model an

estimation of the tensile strength of the material has to be available. (During linear elastic fracture mechanics evaluations, the tensile strength is tacitly assumed to be infinitely large). The mortar in the test series M-0-AD-C, a series which is currently being studed, hade a splitting tensile strength of 441 psi (=3.04 MPa) and a modulus of rupture of 653 psi(=4.51 MPa). The modulus of rupture is known to be larger than the tensile strength, see Section 4.2, and in the present evaluation the uniaxial tensile strength is assumed to be equal to the splitting tensile strength. Accordingly it is assumed that f_t=3.04 MPa.

The notation "M-0-AD-C" means "mortar-0 in (size of coarse aggregate) - air dry (type of curing) - circular centre loading hole". By relative weights, the mortar mix was 1.0:0.6:3.0 (cement:water:river sand). The graduation of the sand was: 0 % sieve size # 4, 10.2 % # 8, 24.1 % #16, 42.9 % # 30, 83.7 % # 50, 98.4 % # 100. The specimens were covered by plastic sheeting one day and one night, and were then demoulded and placed in an air dry laboratory environment until they were tested at an age of 14 days. The rate of loading was 500 lb (2.2 KN) per minute.

In Fig 4.3 (6) the test results of Kesler et al. regarding ultimate load are shown together with values of the critical stress intensity factor as evaluated by different methods. It is clear that K_c as evaluated by eq (4.3:2), used by Kesler et al., showed a dependency of a. As pointed out by Saouma et al., this dependency may be explained by the inaccuracies of eq (4.7:2). The more accurate linear elastic fracture mechanics evaluations do not expose any influence of the geometrical variable a on the material property parameter K_c. From the current test results regarding the relative influence of a on the ultimate load, one should therefore not conclude that linear elastic fracture is not applicable. This does not exclude the possibility of applicability of the fictitious crack model - neither this model expose any influence of a on K_c. The scatter in K_c, if K_c is evaluated by linear elastic fracture mechanics or by the fictitous crack model, is small. This suggests that Kesler et al. carried out the tests in a careful manner.

If one makes the probable assumption that the fictitious crack evaluation, taking into account the bi-linear shape of the σ-w curve, represents the best of the present evaluations, then Fig 4.3 (6) indicates that the straight line σ-w assumption gives a 14 % under-estimation of K_c and that the linear el[illegible] on the writers

Test results 2a/W	P_u/B (MN/m)	K_c (MPa$\sqrt{m}$) acc. to diff. methods of evaluation. Lin. elast. fract. mech. ($f_t \to \infty$) 1)	2)	3)	Fict. crack, f_t=3.04 MPa 4)	5)
.209	.250	.58	.73	.83	.91	1.01
.249	.228	.49	.69	.77	.84	.96
.291	.227	.46	.72	.79	.88	1.03
.332	.199	.39	.67	.72	.81	.94
.374	.205	.39	.74	.78	.90	1.06
.417	.188	.35	.72	.77	.90	1.05
.459	.171	.31	.70	.74	.96	1.02
.500	.165	.30	.71	.77	.93	1.09
Mean value		.408	.708	.771	.882	1.018
Coeff. of var.		24 %	3 %	4 %	4 %	5 %

1) K acc to eq (4.3:2). $\partial(K/P)/\partial a<0$ ignored.

2) K acc to FEM-results of Saouma et al.

3) K acc to FEM-results of the writer.

4) Valid when the σ-w relation has the single straight line shape.

5) Valid when the σ-w relation has the bi-linear shape.

Fig 4.3 (6) Critical stress intensity factor, K_c, for mortar as evaluated from ultimate loads by means of different methods of evaluation. Test results from (Naus, 1971). Test series M-0-AD-C. Geometry acc. to Fig 4.3 (1): H/W=0.5. For 1), 2) and 3) $K_c=\sqrt{EG_c}$; for 4) and 5) K_c is an abbreviation of $\sqrt{EG_F}$.

determination of K) gives a 24 % under-estimation of K_c. In comparison to the linear elastic fracture mechanics evaluation of K_c of the writer, the evaluation of Saouma et al. gives a 8 % underestimation while eq (4.3:2) gives a 47 % underestimation. It may be concluded that Fig 4.3 (6) satisfactorily illustrates the importance of the two main aspects of theoretical strength analyses, namely the modelling of the behaviour of the material and the method of numerical calculations.

$K_c = (=\sqrt{EG_F}) = 1.018$ MPa$\sqrt{m}$ and f_t=3.04 MPa means that $\ell_{ch}=EG_F/f_t$=112 mm. Modeer (1979) determined, by direct experimental methods, G_F, E and f_t for mortar and found G_F=60 N/m, E=29000 MPa and f_t=3.5 MPa, which means that $K_c=(=\sqrt{EG_F}) = 1.3$ MPa$\sqrt{m}$ and that $\ell_{ch}=EG_F/f_t^2$ = 140 mm. The mix, age and curing of the mortar tested by Modeer was however not reported and

therefore this mortar might not be of the same quality as the mortar used by Kesler et al.

In Fig 4.3 (7) the test values of ultimate load are shown vs. a together with the theoretical results according to linear elastic fracture mechanics (K_c=0.77 MPa$\sqrt{m}$) and according to the fictitious crack model (f_t= 3.04 MPa and ℓ_{ch}=110 mm, bi-linear σ-w curve). The value of K_c and ℓ_{ch} respectively has been chosen by means of the method of the least squares to give the best fit to the experimental results of P_u. The least square fits P_u gives slightly, and almost negligible, different values of K_c respectively ℓ_{ch} than the corresponding values of these parameters as shown in Fig 4.3 (5) and obtained as mean values of K_c. Fig 4.3 (7) shows that the two models of fracture both predict the relative influence of a on P_u in a satisfactory manner. In Fig 4.3 (7) the writers determination of K_u has been used. The results of the fictitious crack model happens to produce an almost straight line in Fig 4.3 (7). This is coincidential and the almost straight line is a curve which is based on values of P_u/B for five different values of a in the range 60 mm - 150 mm.

In a total of 9 tests Kesler et al. meausured the strain across the crack at some different locations along the crack propagation path. 6 of these tests belonged to the test series M-0-AD-C, which is why the specimen with the specific geometrical shape H/W=0.5, and D/W=1.25/24 was chosen to be dealt with in the currently presented study. However the gauge length of the strain measurement devise is not known. This makes theoretical comparisons somewhat difficult. In spite of this, the measurements of strain are revealing and show, for loads close to the ultimate load, that the strain at the tip of the notch is very great and that the depth of the fracture zone, i.e. the depth of the zone where the strain is greater than any reasonable estimation of the limiting strain, is of the magnitude 2-3 in (50-75 mm). Due to strain localization, the measured post limit strains are probably very dependent on the length of the gauge, but in spite of this, it may be of some interest to notice that the reported values of the strain at the notch, at loads close to the ultimate load, is of the magnitude ten times any reasonable estimation of the limiting strain.

Kesler et al. estimated the limiting strain of the mortar tested to be 150 μ. If adopting this assumption, one may determine the length of the fracture zone with the aid of the meaured strains. The strains were not measured conti[illegible] '3) the length of

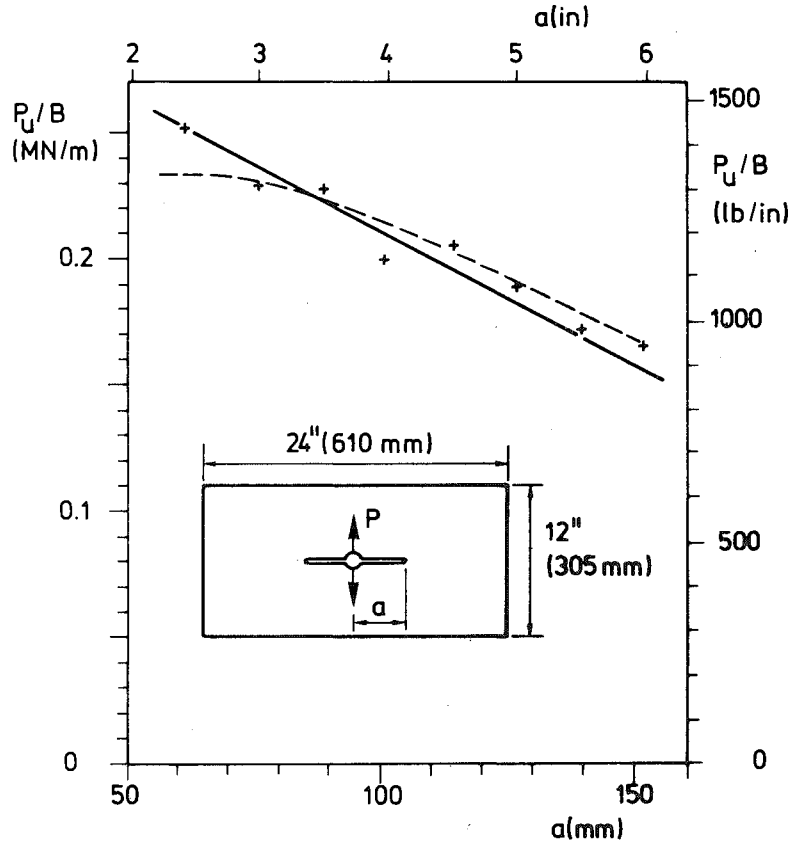

Fig 4.3 (7) Ultimate load versus depth of notch. Comparison between theoretical results and test results from (Naus, 1971), test series mortar M-0-AD-C.

——— Fictitous crack model, f_t=3.04 MPa, ℓ_{ch}=110 mm

— — — — Linear elastic mechanics, K_c=0.77 MPa$\sqrt{m}$

the fracture zone at 97-99 % of the ultimate load is shown versus the depth of the notch of each respectively specimen. This Figure also shows the corresponding theoretical prediction of the fictitious crack model (ℓ_{ch}=110 mm, f_t=3.04 MPa, bi-linear σ-w curve). The theoretical curve is valid for P=100 % of P_u. The values of f_t and ℓ_{ch} have not been chosen in order to fit the test results shown in Fig 4.3 (8), but have been determined in the manner previously described from reported splitting

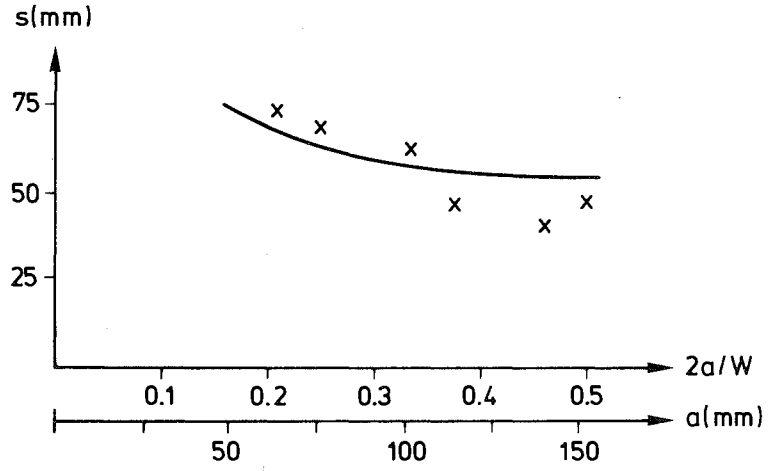

Fig 4.3 (8) Length of fracture zone, s, in mortar (tests series M-0-AD-C) at, or close to, ultimate load versus depth of notch.

x From test results of (Naus, 1971), $P=(97\%-99\%)P_u$.

——— Theoretical result, fictitious crack model, $f_t=3.04$ MPa, $\ell_{ch}=110$ mm, $P=P_u$.

tensile strength, and ultimate failure loads respectively. The theoretical predictions are in agreement with the test results both regarding absolute values of the length of the fracture zone and regarding influence of length of the notch on the length of the fracture zone. For a=64 mm, 114 mm and 152 mm Fig 4.3 (9) shows the location of the tip of the fracture zone, a+ a, during increase in load, P. The theoretical predictions also agree well with the test results in this case.

Any comparison, regarding the strains close to the tip of the crack, between the test results and the predictions of the linear elastic fracture mechanics model has not been found worthwhile carrying out. Linear elastic fracture mechanics predict the strains in the vicinity of the fracture zone to be proportional to K, but a non-zero K means that the stress approaches infinity in the actual vicinity of the tip of the crack. This is obviously unrealistic. In general, linear elastic fracture mechanics may be successfully applied during calculation of the ultimate load of large specimens with deep pre-existing cracks, but this theory is not suitable for any realistic studies [illegible] tip of a crack.

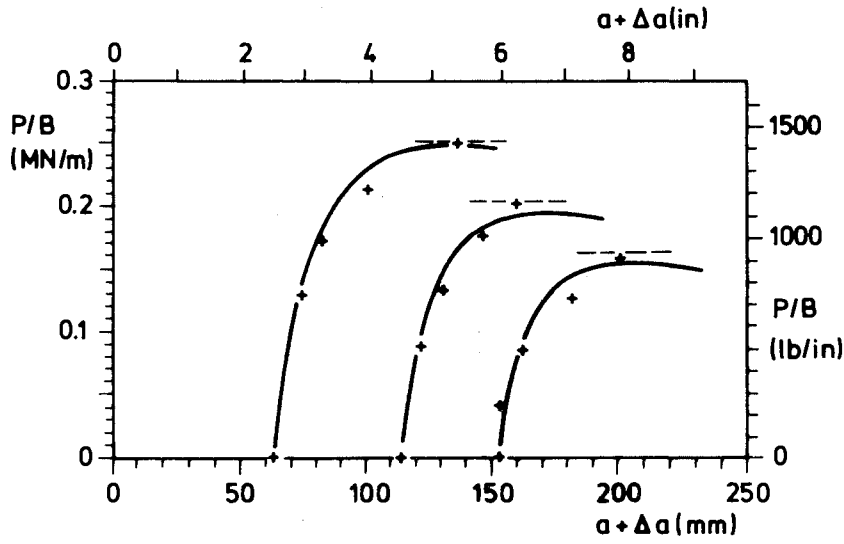

Fig 4.3 (9) Location of tip of fracture zone, a+s, vs. load, P/B, for three of the specimens in test series M-0-AD-AC, mortar.
+ From test results of (Naus, 1971).
— — — Ultimate loads in accordance with the tests.
——— Theoretical results, fictitious crack model, f_t=3.04 MPa, ℓ_{ch}=110 mm.

Finally some concluding remarks should be made with reference to the main purposes, see 4.3.1, of the study presented in Section 4.3:

1) The determination of the stress intensity factor, K, of Saouma et al. seem to under-estimate K by about 10 % as compared to the present determination. The underestimation is, however, not very large and approximately uniform in the present interesting range of 2a/W, from 0.2 to 0.5.

2) Both linear elastic fracture mechanics and the fictitious crack model predict approximately the same relative influence of the depth of the notch, a, on the ultimate load, P_u, as obtained during the tests (series M-0AD-C).

3) The fictitious crack evaluation (bi-linear -w curve) of the test results (mortar, M-0-AD-C) gave $K_c = (\sqrt{EG_F} =) 1.02$ MPa$\sqrt{m}$, while the linear elastic fracture mechanics evaluation (K according to the results of the writer) gave $K_c = 0.77$ MPa$\sqrt{m}$.

4) By the re-evaluation, carried out by Saouma et al., of the test results of Kesler et al. one may hardly conclude that linear elastic fracture mechanics is generally applicable to concrete. In particular, one may hardly expect this theory to produce accurate results during the analysis of the currently studied specimen when made of concrete or mortar, but probably if it is made of paste. To obtain accurate results for mortars and concretes, the specimens have to be very large and much larger than the present size (W=0.6 m): according to the present calculations, approximate requirements of minimum size appear to be W>3 m and W>10 m, respectively.

5) Experimental results regarding the absolute length of the fracture zone, its dependence on the depth of the notch and its dependence on the load agrees well, or at least reasonably well, with theoretical results obtained during the fictitious crack analysis.

6) The agreements with respect to influence of depth of notch on ultimate load and with respect to absolute length of fracture zone suggest that the fictitious crack model may be applied during studies of the fracture performance of the actual specimen.

Finally, the literature refered to in the introduction must be supplemented with more recent references. Ingraffea and Gerstle (1984) have extended the analysis of Saouma, Ingraffea and Catalano (1980 and 1982) and studied the actual specimen also by means of non-linear fracture mechanics (a fictitious crack model). Findings made by Ingraffea and Gerstle are consistent with the present study. Also Bazant and Oh (1983) have carried out a study of the actual specimen by means of a non-linear fracture mechanics model.

4.4 Prestressed DCB-specimen with a groove

4.4.1 Introduction. Geometry of specimen

The study presented in this Section is of a similar type to that presented in Section 4.3: It concerns LEFM and FCM analyses of a fracture mechanics test specimen with a pre-fabricated crack, and from the study it is indicated that the modelling of the fracture behaviour of the material is of significant importance and that the computational method of K-value determination is of great significance if LEFM is to be applied. The differences in principle between the currently studied specimen and that of Section 4.3 is that the current specimen is pre-stressed before external load is applied and that the specimen has a groove along the crack propagation path. The specimen, a large double cantilever beam, has been developed at the Laboratoire Central des Ponts et Chaussees, Paris, and has been used during tests on concrete: (Sok, 1978), (Sok, Baron and Francois, 1979) and (Sok, Benkirane, Baron and Francois, 1981). Subsequently, ("Test to ...", 1982), the specimen has been proposed as a RILEM recommendation for use during tests of K_c of concretes.

The geometry of the specimen considered in the present theoretical analyses is shown in Fig 4.4 (1). During some of the tests, specimens of greater length, 3.5 m, and other locations of the pre-stressed steel cables were used. The specimen is large, the weight of the specimen shown in fig 4.4 (1) is probably about 1500 kg and from the dimensions one might at first sight expect linear elastic fracture mechanics to be applicable.

The total prestressing force in the cables was assigned different values from 0 tons to 212 tons (2.08 MN). It can be noticed that the prestress is applied eccentrically. The centre of gravity of the symmetrical upper half of the cross section is located 244.2 mm from the upper edge, while the centre of gravity of the three steel cables is located 329.3 mm from the upper edge. Therefore the eccentricity is 85.1 mm. The intertia factor of the cross section of each of the two cantilevers is 0.00240 m^4, which is equal to $0.578\ b(d/2)^3/12$.

A specimen similar to that in Fig 4.4 (1) is shown in Fig 4.4 (2). This type of specimens has been used during fracture mechanics investigations of cement composites carried out at the University of Illinois in Chicaco Circle: (Visalvanic and Naaman. 1980). (Wechatarana and Shah, 1980),

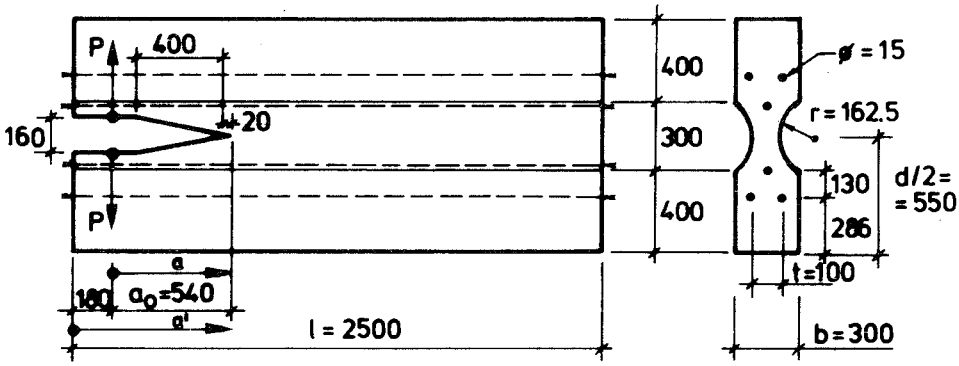

Fig 4.4 (1) Current studied prestressed DCB-specimen with a narrower central section. Geometry in accordanc with (Sok, Baron and Francois, 1979). Measures in mm.

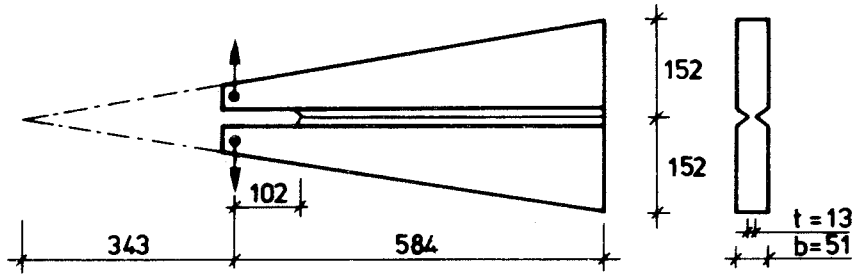

Fig 4.4 (2) DCB-specimen with contoured depth used in tests carried out at University of Illinois at Chicago Circle. Geometry according to (Visalvanich and Naaman, 1981). Measures in mm.

(Visalvanich and Naaman, 1981), (Wecharatana and Shah, 1982) and (Wecharatana and Shah, 1983). The specimen shown in Fig 4.4 (2) is not prestressed, but has a tapered shape instead and is much smaller than the specimens used at the Laboratoire Central. The purpose of the prestress and the contoured shape respectively, is most probably, to avoid bending fracture perpendicular to the desired crack propagation path (compare Section 3.2.4). The groove facilitates crack growth along the desired path, but is estimated to make the length of the fracture zone greater and thereby reduce the possibility for successful application of linear elastic fracture mechanics.

4.4.2 LEFM analysis

In a specimen with a groove along the crack propagation path, the state of strain and stress will be three dimensional. This matter has sometimes, or perhaps always, been tacitly ignored during LEFM analyses of specimens with grooves and thus the ordinary LEFM methods, strictly valid only for plane structues, have been utilized. This will be done also in the present study. It is thereby assumed that the out-of-plane shear strains, γ_{xz} and γ_{yz}, are zero. This assumption may be looked upon as a complete shear rigidity of the mateiral when exposed to out-of-plane shear stresses and means that such stresses are prohibited from contributing to the release in strain energy when the crack propagates. In the present finite element calculations, plane stress (ν=0.2) finite elements are used. In such elements $\sigma_z = \sigma_{xz} = \sigma_{yz} = \gamma_{xz} = \gamma_{yz} = 0$ and a difference in thickness between two elements is, with respect to the stiffness properties of the elements, equivalent to a difference in the modulus of elasticity.

When adopting the assumption of plane stress in the sense described above, the influence of a groove may conveniently be studied by means of the well-known relation:

$$K^2 = EG \qquad (4.4:1)$$

where

$$G = \frac{-1}{t}\frac{\partial U}{\partial a} \qquad (4.4:2)$$

U is the sum of the potential energy of the external loads and the strain energy within the specimen. Therefore, if the displacements of the

external loads are temporarily fixed, then $\partial U/\partial a$ is equal to the rate of strain energy release. In the case of a single temporarily constant external load, P, and zero intial stress:

$$\frac{\partial U}{\partial a} = \frac{-P^2}{2} \frac{\partial c(a)}{\partial a} \qquad (4.4:3)$$

where c(a) is the compliance of specimen. 1/c(a) is by definition equal to the stiffness of the specimen k(a).

Eq (4.4:1) may be derived, see for example (Owen and Fawkes, 1982), from the distribution of stresses and displacements in the actual vicinity of the tip of a crack and these stresses and displacements, being governed by K alone, are, for each constant K, not influenced by changes in the thickness of the specimen "far away" from the tip of the crack. Consequently, if the groove has a finite width, i.e. not an arbitrary small non-zero width, and if the state of plane stress in the sense described above is assumed, then eq (4.4:1) is also valid for specimens with a groove along the crack propagation path. If the finite width of the groove is very small (and if γ_{xz} and γ_{yz} are made equal to zero), then the influence of the groove on $\partial U/\partial a$ is negligible and accordingly $K \sim 1/\sqrt{t}$. Thus, for instance, at constant b, a reduction in t/b from unity to 1/4 will theoretically produce a reduction in the load carrying capacity of only 50 %. The width of the groove of the specimen shown in fig 4.4 (1) is not small, and therefore the groove also influences $\partial U/\partial a$ to some extent.

In literature eq (4.4:1) is often written as $K = \sqrt{EG}$. For the current study it is, however, of importance to note that eq (4.4:1) gives:

$$K = \pm\sqrt{EG} \qquad (4.4:4)$$

The proper sign of K is usually very simple to determine from the type of load acting on the structure. From the distribution of stresses and displacements close to the tip of a crack, it can be seen that G cannot attain a negative value (provided that E>0).

In the specimen studied, initial stresses are present. The stresses are caused by prestressing the steel cables. When calculating K vs. crack length, a, for arbitrary combinations of the magnitude of prestress and external load, it is convenient to separate the action of the prestress and the external load and to consider the prestress as an external load

acting on both the concrete and on the cables, but in opposite directions. Such separation, see Fig 4.4 (3), is possible because stress intensity factors may be added.

In Fig 4.4 (3) and also in other parts of this Section, the notation F is used for the prestressing force and the notation P is used for the external load. These notations are reversed in comparison to the valid ISO-standard, but are used in order to conform to the main references of this Section and to the corresponding proposal for a RILEM recommendation.

The separation of the stress intensity factors gives:

$$K = K_P + K_F \qquad (4.4:5)$$

K_P is the stress intensity factor at load P, at crack length a and at zero force in the cables when P=0. It is obvious that $K_P>0$ and eq:s (4.4:2), (4.4:3) and (4.4:4) give:

$$K_P = \frac{P}{\sqrt{2t}} \sqrt{\frac{\partial(E_c c_{PP})}{\partial a}} \qquad (4.4:6)$$

The modulus of elasticity, E, in eq (4.4:4) refers to the material in the actual vicinity of the tip of the crack. Thus E_c denotes the modulus of elasticity of the concrete. c_{PP} is equal to $1/k_{PP}$, k_{PP} being defined in Fig 4.4 (3). $\partial(E_c c_{PP})/\partial a$ is not only dependent on E_c, but is also dependent on E_s, the modulus of elasticity of the steel in the cables.

K_F is the stress intensity factor at the total force F in the cables, at crack length a and at zero external load. F, the total force in the cables when P=0, is dependent on a. Equilibrium and compatibility give:

$$F(a) = F_o\left(\frac{k_{FF}(a_o)+E_s A_s/\ell}{k_{FF}(a_o)}\right)\left(\frac{k_{FF}(a)}{k_{FF}(a)+E_s A_s/\ell}\right) \qquad (4.4:7)$$

where F_o is the total prestressing force, i.e. the total force when $a=a_o$ (=0.54 m) and P=0. $k_{FF}(a)$ is defined by Fig 4.4 (3) c). A_s is the total cross section area of the cables and ℓ is the length of the cables: see Fig 4.4 (1). It is informative to look upon F(a) as an external load that acts on the concrete: $k_{FF}(a)$ is the stiffness of the concrete specimen

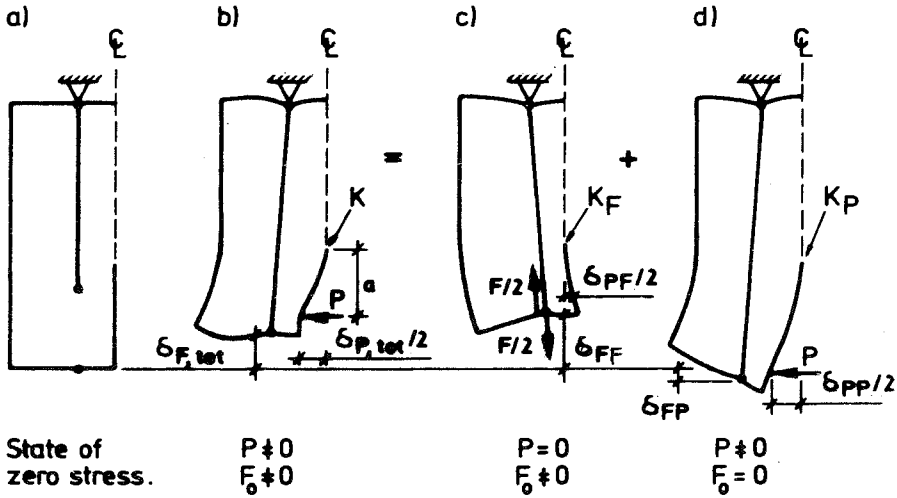

Fig 4.4 (3) Separation of action of pre-stress, F, and external load, P. F_o is the pre-stress when $a=a_o$ (=0.540 m). K, K_F and K_P are stress intensity factors. $F/\delta_{FF}=k_{FF}$ (=$1/c_{FF}$) and $P/\delta_{PP}=k_{PP}$ (=$1/c_{PP}$). The deformations shown are exaggerated and based only on general estimations.

(the stiffness of the steel cables not being taken into account) and when calculating $\partial U/\partial a$ by means of eq (4.4:3) F(a), not F_o, may be kept constant. It is obvious that $K_F<0$, and eq:s (4.4:2), (4.4:3), (4.4:4) and (4.4:7) give:

$$K_F = \frac{-F_o}{\sqrt{2t}} \left(\frac{k_{FF}(a_o) + E_s A_s/\ell}{k_{FF}(a_o)}\right)\left(\frac{k_{FF}(a)}{k_{FF}(a) + E_s A_s/\ell}\right) \frac{\partial(E_c c_{FF})}{\partial a} \qquad (4.4:8)$$

When calculating K_F and K it has tacitly been assumed that the crack surfaces are allowed to overlap each other without any resistance, see Fig 4.4 (3) c). In reality crack surfaces cannot overlap each other, but a compressiv force will develop across the crack instead. If theoretical results indicate K<0 it is obvious that such a compressive force will develop, but it is also theoretically possible that such a force will develop when K>0, although in this latter case such a force will not develop close to the tip of the crack. From the point of view of the laboratory tests, closing of the crack and active resistance to overlapping may influence the behaviour of the specimen at unloading, i.e.

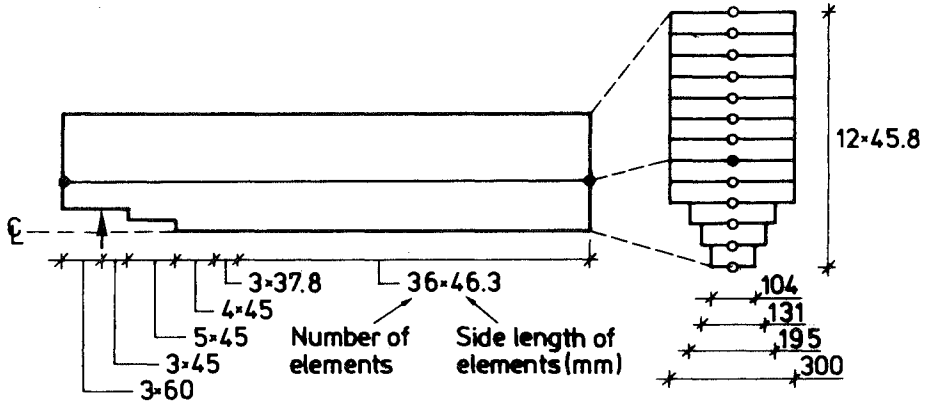

Fig 4.4 (4) Plan and cross section of finite element mesh.

when $\Delta\delta<0$. This is indicated in test results by (Chhuy, Benkirane, Baron and Francois, 1981) as a type of break-point in recorded unloading branches of the P vs. δ curve. In the present study the behaviour of the specimen at unloading, i.e. when $\Delta\delta<0$, will not be dealt with and the influence of resistance to possible overlapping will not be considered in the analysis. Theoretically, resistance to overlapping will also develop when the prestress, F_o, is applied at P=0 and a=a_o, but in practice it is quite possible that this resistance will not develop due to the short length (20 mm) and the non-zero width of the notch.

The finite element mesh used during the numerical calculations is illustrated in Fig 4.4 (4). The number of degrees of freedom left after statical condensation is 82, and the same type of rectangular plane stress 4-node element as used in Section 4.3 is utilized. The three steel cables within the symmetrical half of the specimen are modelled by one bar element placed close to the centre of gravity of the three cables. It would have been more accurate to place the bar exactly at the centre of gravity, and if this had been made then a somewhat greater influence of the prestress on the stress intensity factor would have been obtained. One may expect K_F to be approximately proportional to the distance between the centre of gravity of the three cables and the centre of gravity of the symmetrical half of the specimen, and accordingly one may estimate that the computational results will underestimate the influence of F_o on K, i.e. underestimate K_F, by approximately 8 %. Ratio E_s/E_c is made equal to 5.25. This assumption is based on the value of E_s reported by (Sok and

Baron, 1979):E_c =40.000 MPa. k(a) is calculated as $(k(a-\Delta a/2) + k(a+\Delta a/2))/2$ and $c(a)/\Delta a$ as $(-c(a-\Delta a/2) + c(a+\Delta a/2))/\Delta a$ where Δa is the distance between the nodes along the crack propagation path.

The computational results regarding K are shown in Fig 4.4 (6) as $K/(P-P_o)$ vs. a, where P_o is given in Fig 4.4 (7). P_o is a "zero-stress-intensity-load" which is defined by means of eq (4.4:5) as the external load, P, which gives a zero stress intensity factor. Thus

$$K = (P - F_o(\frac{P_o}{F_o})) \frac{K}{(P-P_o)} \qquad (4.4:9)$$

where by the definition of P_o:

$$\frac{K}{(P-P_o)} = \frac{K_p}{P} \quad \text{and} \quad \frac{P_o}{F_o} = \frac{-K_F/F_o}{K_p/P} \qquad (4.4:10)$$

$K/(P-P_o)$ and (P_o/F_o) are given in the figures, P is the external load and F_o is the total force in the cables when $a=a_o$=0.540 m and P=0.

In (Sok, 1978) and (Sok and Baron, 1979) the following relation was used:

$$K = P\sqrt{\frac{a^2}{tb(d/2)^3/12}}\ \sqrt{\xi} \qquad (4.4:11)$$

where $\xi = 1 + 1.32(\frac{d/2}{a}) + 0.532(\frac{d/2}{a})^2$

For the size of the specimen shown in fig 4.4 (1), eq (4.4:11) is shown in Fig 4.4 (6). According to (Visalvanich and Naaman, 1981), eq (4.4:11) was derived by Wiederhorn, Shorb and Moses in 1968. The equation does no take the influence of prestress into account and is, at zero prestress, only approximately valid for the current shape of the specimen. Originally eq (4.4:11) was most probably derived for specimens where $(\ell-a) \gg d/2$ and where the width of the groove is very small in comparison to d/2. At zero prestress and a<1.4 m eq (4.4.11) gives about 16-18 % lower values of K than the present finite element results. When $a \gtrsim 1.5$ m, i.e. when $(\ell-a) \lesssim 1.5(d/2)$, the increased flexibility due to proximity to the end of the specimen becomes of great importance. As indicated by the finite

element results, this increase in flexibility produces a drastic increase in the stress intensity.

The error in K_c when evaluated from ultimate load without considering the influence of prestress is dependent on the properties of the material, i.e. the true value of K_c, and the magnitude of the prestress, F_o. If linear elastic fracture mechanics are applicable and the true value of K_c is 2.0 MPa$\sqrt{m}$, then according to the present finite element results, an evaluation of K_c from ultimate load without considerating the influence of prestress would give a 60 % over-estimation at F_o=0.48 MN, 130 % over-estimation at F_o=1.06 MN and a 250 % overestimatsion at F_o=2.12 MN. The corresponding errors in evaluated values of G_c are of course greater. The magnitudes of deviation are such that they may hardly be considered acceptable. thus, - even if the fracture behaviour of concrete was in accordance with the concepts of linear elastic fracture mechanics -, values of K_c as evaluated from experimental results without consideration of the influence of prestress would hardly be considered accurate.

In (Chhuy, Benkirane, Baron and Francois, 1981) the following relation was used during the evaluation of G_c (and K_c):

$$G = \frac{1}{2t}(P-P_o)^2 \frac{\partial c_{pp}}{\partial a} \qquad (4.4:12)$$

This relation is in agreement with the current study, eq (4.4:9), provided, however, that P_o is obtained in accordance with the definition of P_o as given above. P_o is the external load that corresponds to zero stress intensity, and, in particular, it may be noted that δ=0, δ being defined by Fig 4.4 (3) and eq (4.4:19), does not mean that K=0. In the RILEM proposal 1982, it was proposed that the steel cables should be placed centric in order to avoid any influence of the prestress on K. This simplifies the evaluation of experimental results.

For the purpose of comparison, Fig:s 4.4 (6) and 4.4 (7) show $K/(P-P_o)$ and P_o/F_o for the limiting type of specimen shown in Fig 4.4 (5). In the case of plane stress in the sense described above, the stress intensity factor for this specimen is:

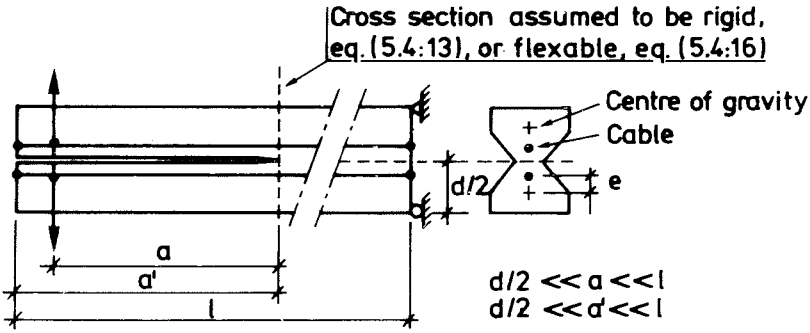

Fig 4.4 (5) Pre-stressed DCB-specimen for which the stress intensity factor may be obtained by means of the ordinary beam theory.

$$K = (P - F_o(\frac{P_o}{F_o}))\ \frac{K}{(P-P_o)} \qquad (4.4:13)$$

where $\frac{P_o}{F_o} = \frac{e}{2a}$

and $\frac{K}{(P-P_o)} = \frac{a}{\sqrt{tI}}$

Eq (4.4:13) is shown for e=0.0851 m, t=0.1 m and I=00240 m^4. The equation may be derived by means of eq:s (4.4:2)-(4.4:5) and the ordinary beam theory, taking into account only the curvature of the cantilevers and not their shear deformations. The omittance of shear deformations means that the equation does not predict any influence of the shear force on K. Thus K is predicted to equal zero when the bending moment at the tip of the crack is zero: $P_o a=(F_o/2)e$. Eq (4.4:13) is believed to approach an exact equality when the unequalities indicated in Fig 4.4 (5) are increased. $\ell >> a$ means that the force in the cables is constant during crack growth, i.e. $F(a)=F_o$, and that the cables do not give any significant contribution to the stiffness of the cantilevers. On the assumption that the inertia factor, I, is reasonable in comparison to $A_s(E_s/E_c)e^2$, let us say if $I > 50\ A_s(E_s/E_c)e^2$, eq (4.4:13) may be roughly estimated to be accurate within "engineering accuracy" when:

$$8(d/2) \lesssim a \lesssim \ell - 1.8(d/2) \qquad (4.4:14)$$

Eq (4.4:13) is not sufficiently accurate to enable verification of the finite element results and does not exclude the possibility of gross errors where the finite element results of P_o/F_o are concerned. However, simple and more accurate results than those of eq (4.4:13) may be obtained by means of the assumption:

$$c_{PP} = \frac{2}{3E_c I}(a + \frac{2}{3}(d/2))^3 \qquad (4.4:15)$$

This useful assumption is essentially based on finite element analyses of cantilever beams, not rigidly clamped to an ideally rigid half-space but clamped in the way the cantilevers of a DCB-specimen are clamped. The assumption does not represent an exact equality but is believed to represent a good combination of accuracy an simplicity. (a+2/3(d/2) may be looked upon as an equivalent length of the cantilever when loaded by the external force P: Comparison can be made to a study of a cantilever clamped to an elastic half-space included in (Petersson, H., 1974). By means of derivation, eq (4.4.15) may be compared to the ξ-factor of eq (4.4:11): $E_c I/2\, \partial c_{PP}/\partial a = (a+2/3(d/2))^2 = a^2(1+1.33(d/2)/a+0.44((d/2)/a)^2)$.

In eq (4.4:15), the cubic term, a^3, corresponds to the curvature of the cantilever; the quadratic term, a^2, corresponds to the rotation at the clamp due to its flexibility; the linear term, a, corresponds to the shear deformation along the cantilever; the constant term corresponds to the shear deformation at the clamp due to its flexibility and to the local deformations at the point where the load is applied. The identification of the different terms enables the calculation of c_{FF} and c_{PF}.

Eq (4.4:15) together with the identification of the different terms and together with eq:s (4.4:2)-4.4:5) gives:

$$K = (P - F_o(\frac{P_o}{F_o}))\frac{K}{(P-P_o)}$$

$$\text{where } \frac{P_o}{F_o} = \frac{e}{2(a+2/3(d/2))} \qquad (4.4:16)$$

$$\text{and } \frac{K}{P-P_o} = \frac{a+2/3(d/2)}{\sqrt{tI}}$$

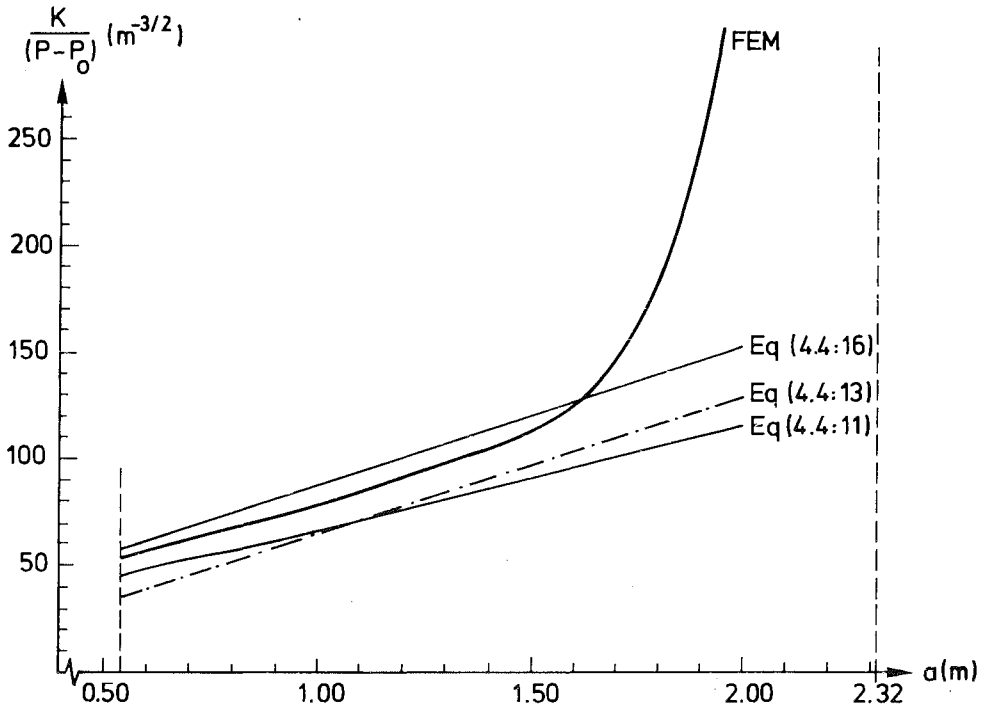

Fig 4.4 (6) Stress intensity factor, $K/(P-P_o)$, vs. crack length, a, for the specimen shown in Fig 4.4 (1).

Eq (4.4:16) is shown in Fig:s 4.4 (6) and 4.4 (7) for e=0.0851 m, t=0.1 m, d/2=0.55 m and $I=0.00240\ m^4$. The deviation between the finite element results and eq (4.4:16) may be explained by the approximation of eq (4.4:15), the general approximations involved in finite element analyses, the variation of I along the cantilever, the influence of the stiffness of the steel cables on the total stiffness and the simplified finite element modelling of the shape of cross section. For reasons previously described it is probable that the finite element results under-estimate P_o/F_o by about 8 %. By means of rough estimations, eq (4.4:16) is estimated to be accurate within "engineering accuracy" when:

$$0.8(d/2) \lesssim a \lesssim \ell - 1.8(d/2) \qquad (4.4:17)$$

The type of results shown in Fig:s 4.4 (6) and 4.4 (7) may be utilized when evaluating K_c from experimental results only if linear elastic fracture mechanics are applicable. Thus, for instance, eq:s (4.4:14) and

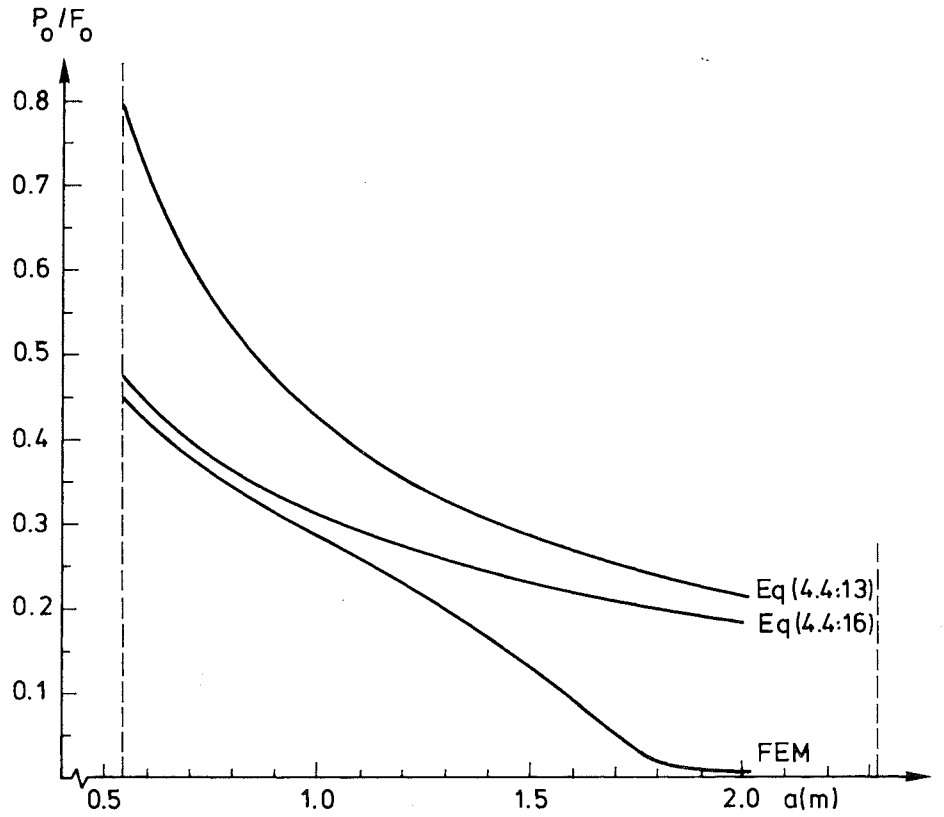

Fig 4.4 (7) Ratio P_o/F_o vs. crack length, a, for the specimen shown in Fig 4.4 (1). P_o is the external load that produces zero stress intensity at prestress F_o.

(4.4:17) are sufficient approximate requirements only if the material tested behaves in an ideal linear elastic brittle manner. To ensure applicability of LEFM when a material with some finite tensile strength is tested, the specimen should not be too small. For a specimen with a groove, the size requirement may be expressed by :

$$d/2 > A(b/t)(K_c/f_t)^2 \qquad (4.4:18)$$

Where A is a coefficient which depends on the length of the crack, the desired degree of accuracy, the actual geometrical shape of the DCB-specimen and the magnitude of the prestress. It is interesting to know that a groove along the crack propagation path has a strong and very

unfortunate influence on the required size. The proportionality between the size requirement and ratio (b/t) is a result of eq:s (4.4:1) and (4.4:2), and is theoretically strictly valid only if the width of the groove is small. In order to obtain very rough estimations of the required size one may make A equal to 3. This rough estimation may be assumed to be valid if $(d/2)<a<\ell-(d/2)$. The estimation is arrived at from experience of fictitious crack analyses and by means of the results presented in Section 4.4.3 and by means of comparison to ASTM standards. Fictitious crack analyses do however additionally suggest that the actual stress-elongation properties of the material at fracture, i.e. the shape of the σ-w curve, has a significant influence on the load carrying capacity. This means that it is difficult to define an exact size requirement, corresponding to some certain degree of accuracy, only in terms of the single material property parameter $(K_c/f_t)^2 (= \ell_{ch})$, while the actual shape of the stress-elongation curve should preferably be taken into account. Only if the specimen is extremely large, the shape of the σ-w curve is of no importance. $A \approx 3$ means that the large DCB specimen shown in Fig 4.4 (1) and used during the tests is much too small to ensure applicability of linear elastic fracture mechanics during tests of ordinary conrete qualities. For A=3, ℓ_{ch}=400 mm, b=0.3 m and t=0.1 m, the size requirement suggest d/2=3.6 m and ℓ=16.4 m. Such a specimen, with a concrete volume of about 30 m^3, is of course not very suitable for use during laboratory tests of materials properties. Eq (4.4:18) may be compared to the size requirement of the ASTM standards during testing of K_c of metals by means of compact tension specimen: $a>2.5 (K_c/f_t)^2$. The CT specimen of the ASTM standards has no groove along the crack propagation path, and may be described as a short DCB specimen where $a \approx d/2 \approx \ell/2$.

During the tests carried out at the Laboratoire Central, load, P, vs. displacement, δ, was recorded. The displacement δ is defined by means of Fig 4.4 (3):

$$\delta = \delta_{P,tot} - \delta_{PF}(a_o) = \delta_P + \delta_{PF} - \delta_{PF}(a_o) \qquad (4.4:19)$$

If adopting the same assumptions as required for validity of eq (4.4:16), it is possible to relate forces and displacements of the two loading systems acting on the specimen by means of an analytical compliance matrix:

$$\frac{1}{E_c I}\begin{bmatrix} \frac{2}{3}(a+\frac{2}{3}(d/2))^3 & \frac{-e}{2}(a^2+\frac{4a}{3}(d/2) \\ \frac{-e}{2}(a^2+\frac{4a}{3}(d/2)) & \frac{e^2}{2}(a'+\frac{2}{3}(d/2))+\frac{I\ell}{A_c} \end{bmatrix}\begin{bmatrix} P \\ F_o \end{bmatrix} = \begin{bmatrix} \delta_{P,tot} \\ \delta_{F,tot} \end{bmatrix} \qquad (4.4:20)$$

This matrix enables a linear elastic fracture mechanics prediction of load vs. displacement:

$$\begin{cases} P = \dfrac{K_c\sqrt{tI}+F_o/2\ e}{(a+2/3(d/2))} \\ \delta = \dfrac{1}{E_c I}\left\{\dfrac{2P}{3}(a+\frac{2}{3}(d/2))^3 - \dfrac{F_o e}{2}(a^2-a_o^2+\dfrac{4a}{3}(d/2) - \dfrac{4a_o}{3}(d/2))\right\} \end{cases} \qquad (4.4:21)$$

Eq (4.4:21) emanates from eq (4.4:15) and is therefore not an exact relation, but is believed to produce fairly accurate results for the range of crack depths, a, indicated by eq (4.4:17). For zero prestress, $F_o=0$, and e=0.0851 m, d/2=0.55 m, a_o=0.54 m, t=0.1 m and I=0.00240 m^4, eq (4.4:21) is shown in Fig 4.4 (8) as P/K_c vs. $\delta/(K_c/E_c)$. This Figure also shows load vs. displacement for the specimen in Fig 4.4 (1) as obtained by the finite element analysis. For $a \lesssim 1.4$ m the agreement between the two methods of analysis is fairly good.

During the finite element analysis only the two diagonal terms of the compliance matrix, neccessary when calculating K_p and K_F, were determined, while the off-diagonal term, c_{PF}, was not determined. However, if it is assumed that a finite element analysis would yield $c_{PF} = e/(2E_c I)(a^2+4a/3(d/2))$, then the finite element prediction of load vs. displacement would be:

$$\begin{cases} P = \dfrac{K_c}{K/(P-P_o)} + F_o(P_o/F_o) \\ \delta = P\,c_{pp}(a) - \dfrac{F_o\,e}{2E_c I}(a^2 - a_o^2 + \dfrac{4a}{3}(d/2) - \dfrac{4a_o}{3}(d/2)) \end{cases} \qquad (4.4:22)$$

where $K/(P-P_o)$ is given in Fig 4.4 (6), (P_o/F_o) is given in Fig 4.4 (7) and $c_{pp}(a)$ ($=\delta/P$ when $F_o=0$) may be obtained from Fig 4.4 (8). For F_o=0.48 MN, eq (4.4:22) is shown in Section 4.4.3, Fig 4.4 (10) b). Where the

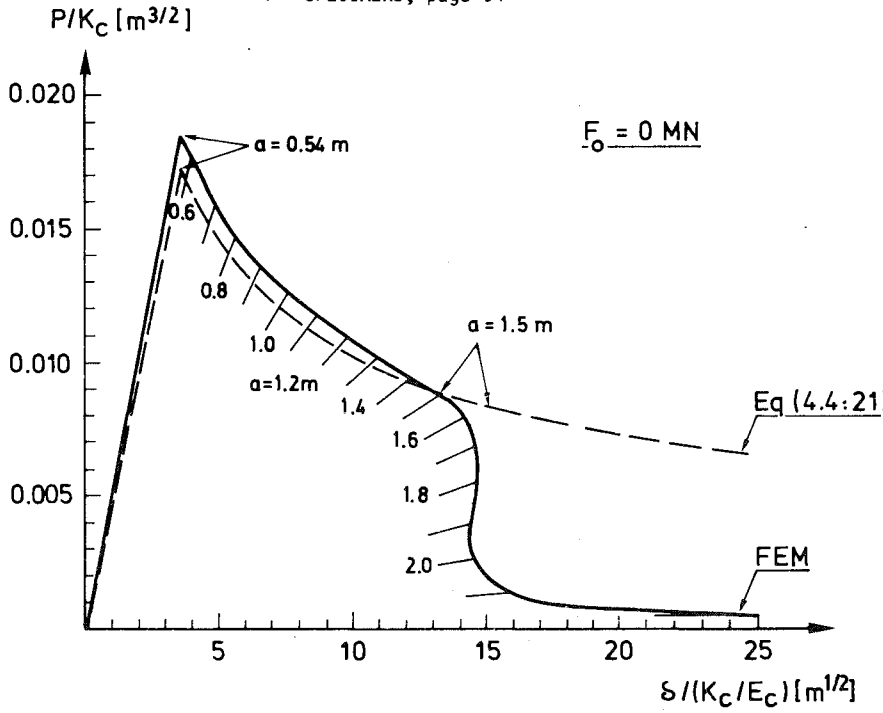

Fig 4.4 (8) Linear elastic fracture mechanics prediction of load vs. displacement of the specimen shown in Fig 4.4 (1).

specimen in Fig 4.4 (1) is concerned, eq (4.4:22) is believed to give fairly accurate results when $a \lesssim 1.3$ m, but poor results when $a \gtrsim 1.6$ m.

In Fig 4.4 (8) load vs. displacement as obtained during finite element analysis, is also shown beyond the point where $\partial\delta/\partial P=0$. This part of the curve is purely theoretical and, due to instability, can not be obtained during ordinary tests.

When $F_o=0$ one may expect G_c $(=K_c^2/E)$ times the total fracture area to equal the area under the complete P vs. δ curve. This seems to be in agreement with the finite element results shown in Fig 4.4 (8). When $F_o>0$ one may expect the area under the total P vs. δ curve to decrease in proportion to F_o, and is therefore not equal to G_c (or G_F) times the total fracture area. This is because the non-zero strain energy within the specimen at the instant when the external load, P, is applied does not equal the strain energy within the specimen after complete fracture: Comparison can be made to Section 4.2.4, where the influence of initial shrinkage stresses on the load displacemei

4.4.3 Fictitious crack analysis. Comparisons to tests. Conclusions

The finite element mesh used during the FCM analysis is the same as used during the LEFM analysis, see Fig 4.4 (4). Computational results are choosen to be presented for the prestress F_o=0.48 MN, while test results regarding load vs. displacement, load vs. crack length and experimental observations of the fracture zone are available for this particular magnitude of prestress.

Although the same finite element mesh (i.e. the same substructure element) apart from the modelling of the fracture zone, is utilized for the FCM calculations as for the LEFM calculations, the numerical methods of analysis are basically different. The FCM calculations are carried out in the tangential stiffness incremental manner and the prestress is taken into account as an initial stress field that acts within the specimen. The LEFM analysis, on the other hand, was carried out in a total (or direct) incremental manner and the prestress was treated as a separate external loading system acting on both the concrete and the steel cables, but in opposite directions. The latter type of approach provides more general results, and is possible because stress intensity factors may be added. Results obtained from FCM analyses are dependent on the loading history and are non-linear. By non-linear it is then meant that it is, in general, not possible to determine the behaviour when several loading systems acts simultaneously by means of a linear combination of the behaviour obtained during separate analyses of different loading systems.

The water-to-cement ratio of the concrete tested by (Sok, Baron and Francois, 1979) was 0.48 and the maximum particle size was 12 mm. The specimen may have been tested in a dry environment and the concrete may have been exposed to shrinkage and creep. In the theoretical analysis, possible influences of these possible phenomena are not taken into accounot. Theoretically, one may expect the crack to grow exactly along the line of symmetry of the specimen. In reality the crack does not grow along a straight line but also passes through parts of the specimen where the thickness is substantially more than 100 mm: See a figure shown by (Sok, 1978). The influence of this type of behaviour is difficult to model properly in theoretical analyses, but may be taken approximately into account by means of a somewhat increased value of the tensile strength, f_t, and a corresponding proportional increase of the fracture energy G_F.

FCM analyses

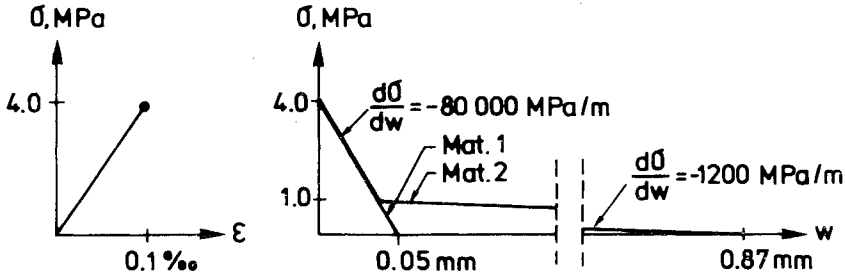

Material 1: $E = 4.0 \times 10^4$ MPa
$f_t = 4.0$ MPa
$G_F = 1.0 \times 10^{-4}$ MPa m
($\sqrt{EG_F} = 2.0$ MPa$\sqrt{m}$)

Material 2: $E = 4.0 \times 10^4$ MPa
$f_t = 4.0$ MPa
$G_F = 5.0 \times 10^{-4}$ MPa m
($\sqrt{EG_F} = 4.52$ MPa$\sqrt{m}$)

LEFM analyses

Material 1: $E = 4.0 \times 10^4$ MPa
$K_c = 2.0$ MPa$\sqrt{m}$

Material 2: $E = 40\,000$ MPa
$K_c = 4.52$ MPa$\sqrt{m}$

Fig 4.4 (9) Material property assumptions used during calculations. For the FCM analyses, "Material 1" corresponds to ℓ_{ch} = 0.25 m while "Material 2" corresponds to ℓ_{ch} = 1.275 m.

Computational results of the fictitious crack model are obtained from two assumptions of the proprties of the material, and the corresponding results of the linear elastic fracture mechanics obtained from the corresponding assumptions of the properties of the material are also shown. The assumed material properties are shown in Fig 4.4 (9). The difference between the two assumptions concerns the slope of the last parts of the σ-w curve: E, f_t and the slope of the first part of the σ-w curve are kept constant. The assumed material properties have not been chosen primarily to correspond exactly to the experimental results, but have been chosen instead to illustrate the possibilities of carrying out analyses by means of the FCM, to illustrate the influence of the slope of the last part of the σ-w curve and to illustrate the difference between the results of the FCM and the LEFM. When making a judgement of the concrete mix and taking into account that the crack in reality temporarily grows through parts of the specimen where the thickness is greater than 100

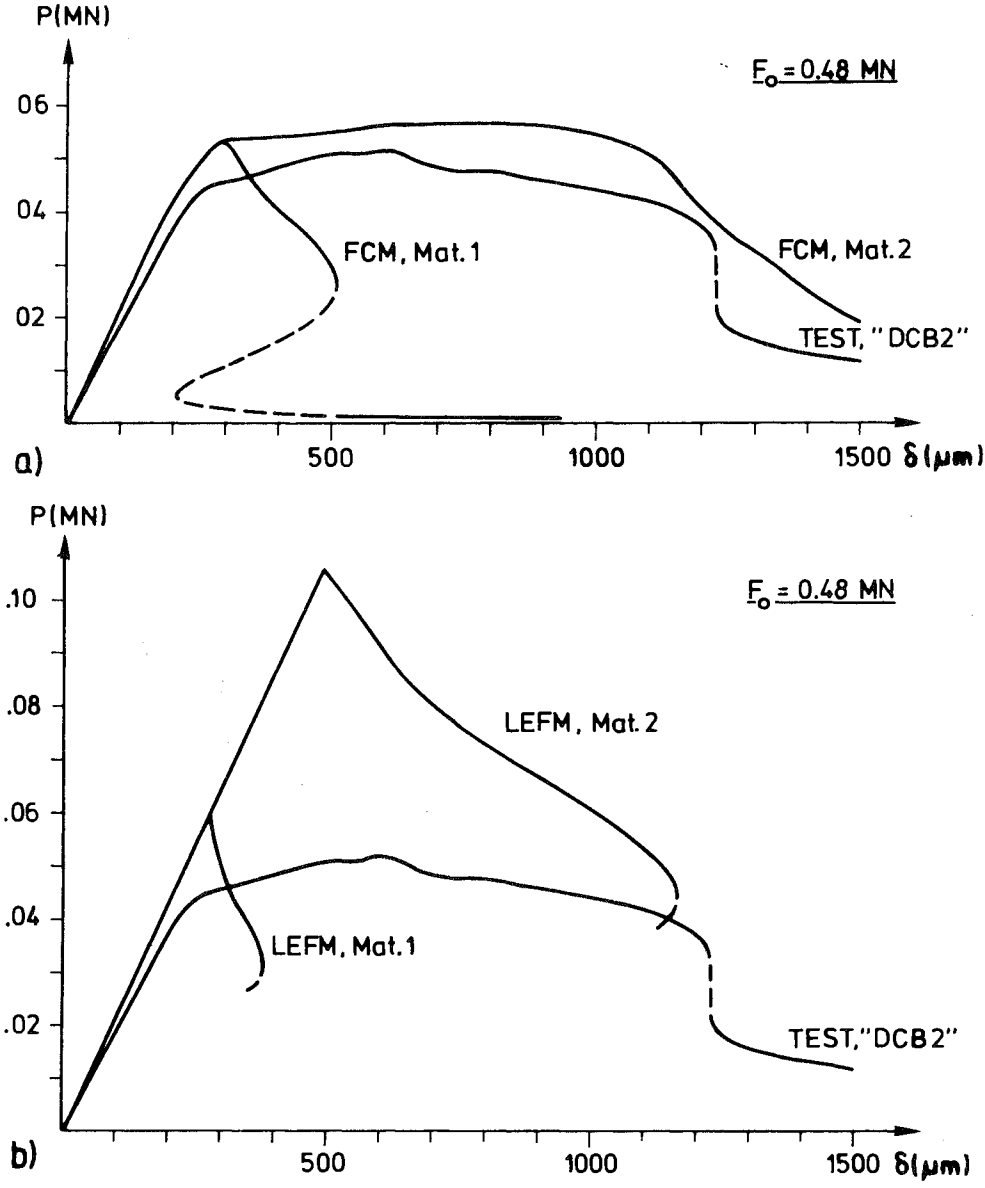

FIG 4.4 (10) Load vs. displacement. a) FCM results compared to test. b) LEFM results compared to test. The test results are from (Sok, Baron and Francois, 1979) and are shown in a simplified manner. The material property assumptions "Material 1" and "Material 2" are defined in Fig 4.4 (9).

mm, it seems reasonable to believe that the true properties of the material are somewhere in between the two assumptions adopted during the theoretical calculations.

Fig 4.4 (10) shows load vs. displacement as obtained during the theoretical calculations and as obtained in the test of (Sok, Baron and Francois, 1979). The test results are, however, only shown in a simplified manner: the unloading-loading cycles are omitted. The Figure suggests that it seems possible to obtain good correlation between the test and the FCM results if the properties of the material are chosen in a proper manner. It does not seem possible to attain such a correlation by means of LEFM. The Figure also suggests that the last part of σ-w curve has a great influence on the ductility of the specimen, but only a very slight influence on the ultimate load. This observation is valid for the actual size of the specimen, but is not of a general nature. If the specimen had been extremely large, then "Material 2" would have produced a much larger ultimate load than "Material 1".

In (Sok, 1978) test results are presented regarding load vs. crack length. These test results were obtained by means of the type of specimen shown in Fig 4.4 (1), but the total length of the specimen used during the tests was longer: not 2.5 m but 3.5 m. The length of the initial crack, a_o, was as shown in Fig 4.4 (1), i.e. 0.54 m. In spite of the difference in total length of the specimens, the test results are shown in Fig 4.4 (11) together with the present theoretical results, strictly valid for the total length 2.5 m of the specimen only. In the Figure, the crack length, a, is, where the LEFM results are concerned, defined as the distance from the point of load application to the tip of the crack. For the FCM results, the crack length is defined as the distance from the point of load application to the point where $\sigma=f_t$. During tests it is not very easy to accurately observe and clearly define the location of the tip of the crack. For the test results in Fig 4.4 (11), the crack length seems to have been determined as the distance from the point of load application to the tip of the crack as observed by using a magnifying glass.

Fig 4.4 (10) and Fig 4.4 (11) indicate that a proper modelling of the fracture behaviour of the material is important in theoretical analyses, or - vice versa - that the fracture mechanics properties of the material strongly influence the behaviour of the current specimen. These Figures

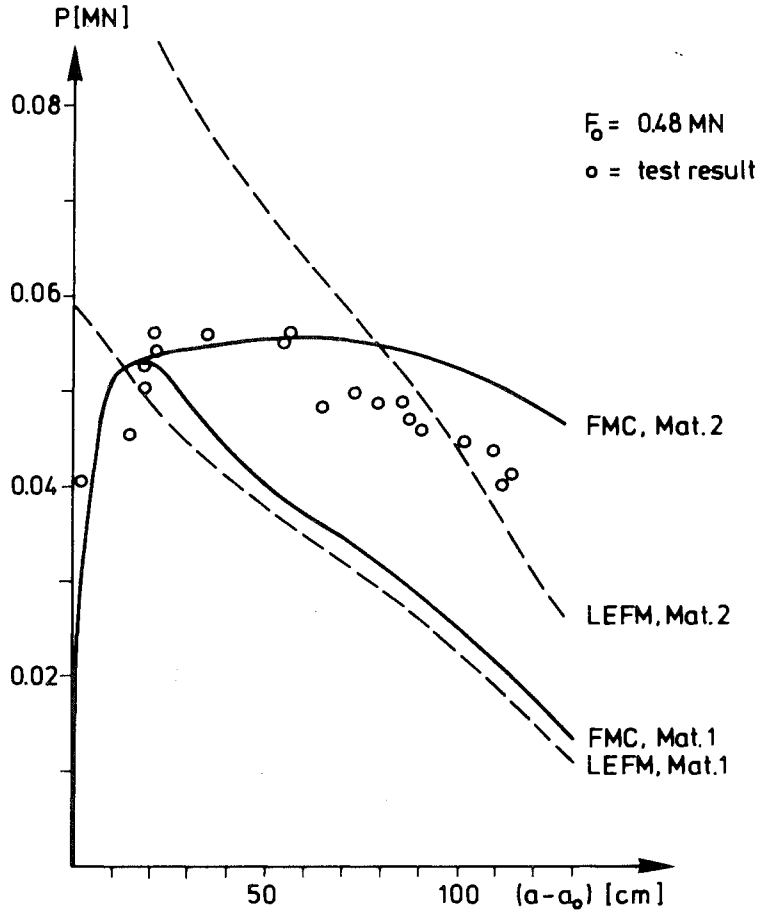

Fig 4.4 (11) Load vs. crack length. Test results according to (Sok, 1978). The material property assumptions "Material 1" and "Material 2" are defined in Fig 4.4 (9).

also suggest that it may be possible to analyse the behaviour of the specimen accurately by means of the FCM, but not by means of the LEFM.

For the straight line assumption of the σ-w curve, the FCM results shown in Fig 4.4 (11) happen to follow the LEFM results fairly well when $(a-a_o) >$ 25 cm. This is because the straight line σ-w curve predicts, during the currently studied conditions, an almost constant shape of the fracture zone once the zone is fully developed and starts to move along the crack

propagation path. For the straight line assumption of the σ-w curve, a non-stress transferring open crack starts to develop when $(a-a_o) \approx 20$ cm. For the present bi-linear shape of the σ-w curve, a non-stress transfering open crack starts to develop first when $(a-a_o) \approx 160$ cm. In the latter case, the fracture zone is fully developed at a very late stage of the collapse and, since the size of the fracture zone is large in comparison to the distance to the boundaries of the specimen, the shape of the fracture zone does not remain constant when it subsequently moves along the crack propagation path.

For the test specimen DCB2 (the load displacement response being shown in Fig 4.4 (10)), Sok, Baron and Francois (1979) have presented interesting experimental observations regarding the depth of the fracture zone and the acoustic emission during crack propagation. In Fig 4.4 (12) c) and d) these experimental observations are shown for $\delta = 560\ \mu m$. Corresponding theoretical result regarding stresses across the fracture zone is shown in Fig 4.4 (12) a), and in Fig 4.4 (12) b) corresponding theoretical results regarding width and length of the fracture zone are shown. The theoretical results are valid for the instant when the calculated displacemet is 560 μm and the assumed properties of the material are according to "Material 2", Fig 4.4 (9). When $\delta = 560\ \mu m$, the load is very close to the ultimate load, Fig 4.4 (10). The almost constant stress in the range 0-45 cm of $(a-a_o)$ is of course due to the assumed very small slope in the last part of the σ-w curve. An estimation of the fracture phenomena taking place along the fracture zone and causing softening of the material is shown in Fig 4.4 (12) e).

The real length and width of the fracture zone and the real stresses across the fracture zone may not be exactly as indicated in Fig 4.4 (12) a) and b). In spite of this, Fig 4.4 (12) is believed to give a rather accurate and interesting illustration of the characteristics of a fracture zone and its gradual development into an open crack.

One particular comment, which is believed to be of negligible practical importance, should be made with regard to Fig 4.4 (12) a) and b). The histogram of Fig a) shows stresses calculated as the force across the partly opened nodes divided by the sum of half the area of the neighbouring elements and the points in Fig b) show the crack opening displacement at the nodal points. A comparison to Fig 4.4 (4), where the element mesh is illustrated, shows that the location of the points in Fig b) do not

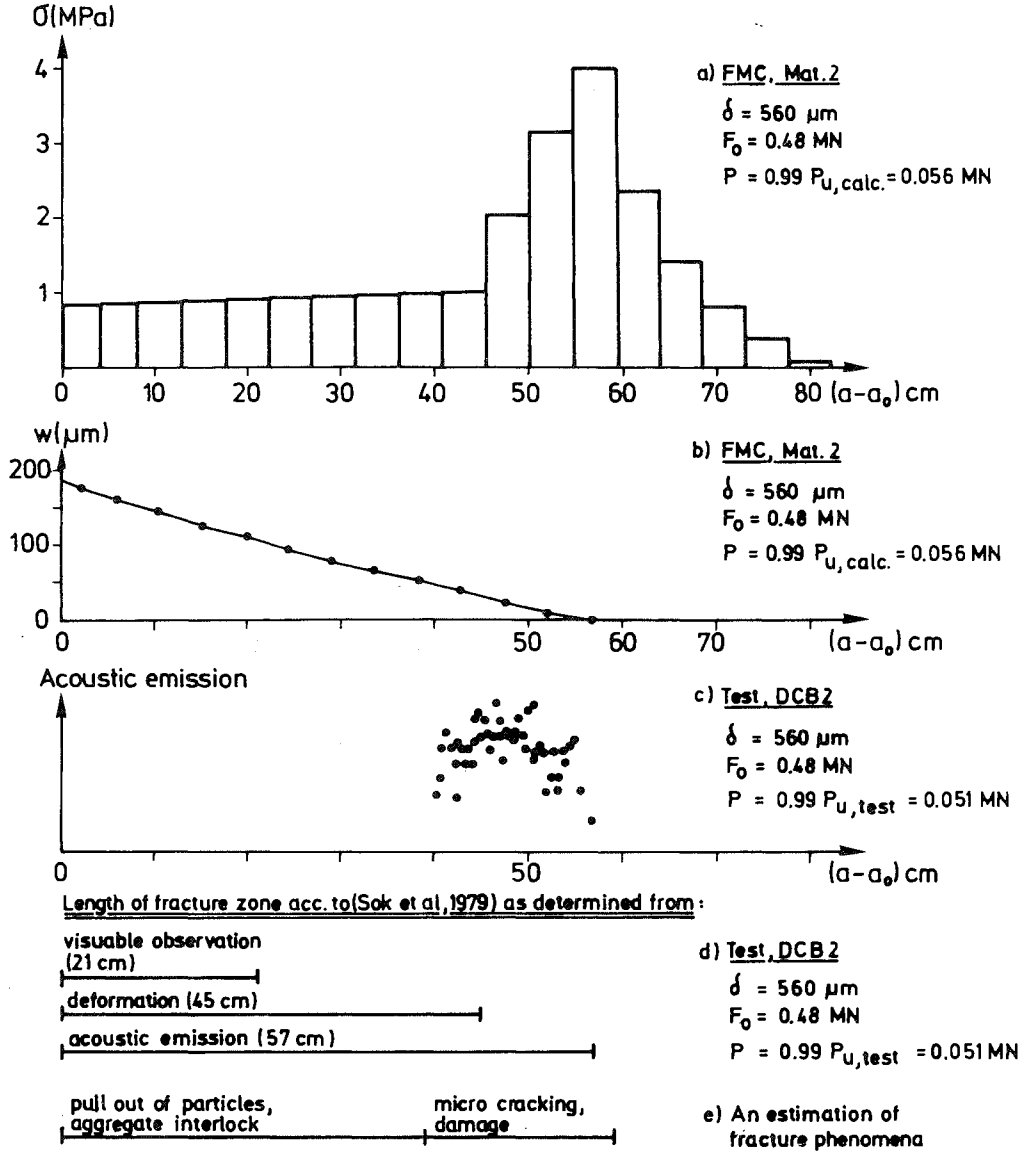

Fig 4.4 (12) Characteristics of fracture zone in specimen shown in Fig 4.4 (1) when δ = 560 μm and P = 0.99 P_u. Compare Fig 4.4 (10). Material property assumption "Material 2" is defined in Fig 4.4 (9). Test results are from (Sok, Baron and Francois, 1979).

coincide with the location of the nodes. This is because Fig 4.4 (12) is valid for δ = 560 μm while computational results, due to the incremental type of analysis, are not available for δ = 560 μm but for δ = 534 μm (P= 0.556 MN, $(a-a_o)$=54.9 cm) and δ = 574 μm (P=.0559 MN, $(a-a_o)$=58.5 cm). Fig 4.4 (12) a) and b), being valid for δ = 560 μm, show the distribution of stresses and width of the fracture zone as obtained when δ = 574 μm resectively, but the stresses and deformations have been moved along the crack propagation path in such a way that $(a-a_o)$=56.9 cm, corresponding to a linear interpolation between δ = 534 μm and δ = 574 μm. For $(a-a_o)$<0 the stress is of course zero and the load corresponding to δ = 560 μm is .0558 MN.

The type of specimen shown in Fig 4.4 (1), a large prestressed DCB specimen with a groove, has enabled interesting experimental observations of the type shown in Fig 4.4 (12) c) and d). But, in the opinion of the writer, the specimen is not suitable for tests of fracture mechanics parameters of concretes. Due to the prestress and the size of the specimen, the specimen is probably not very convenient to handle during manufacturing, curing, testing and disposal. In spite of the size, the specimen is too small to enable an reliable determination of LEFM material property parameters. When determining the FCM parameter G_F the specimen must behave in a stable manner from the start of loading until complete collapse. The specimen does not appear to meet this requirement for all types of concrete and in particular not if the prestress is greater than 0.48 MN. The excentric prestress influences the load carrying capacity and the total area under a stable load-displacement cuve, and therefore must be taken into account during evaluation of K_c or G_F. This complicates the evaluation of experimental results. The groove along the crack makes it more difficult to meet the size requirement of LEFM. On the other hand, a groove may make it easier to study the gradual development of a fracture zone. While the crack can hardly be expected to grow exactly along the theoretical crack propagation path, it will, due to the groove, grow through parts of the specimen where the thickness is more than 100 mm. To sum up, the writer has not found that the specimen shown in Fig 4.4 (1) is suitable for the determination of fracture mechanics parameters of concretes.

Finally the findings of Section 4.4 should be summarized as follows:

1) The LEFM analysis indicates that the prestress influences K and the influence is of such a magnitude that it should not be ignored.

2) A groove along the crack propagation path has a strong and unfortunate influence on the size requirement for the applicability of LEFM. This matter is of importance also for studies of the specimen shown in Fig 4.4 (2).

3) The finite element method enables more reliable and accurate calculations of K than other more or less approximate analytical methods.

4) The actual behaviour of the current concrete specimen does not seem possible to reproduce by means of LEFM analysis. By means of the FCM, it seems possible to analyse the global behaviour of the specimen as well as length, growth and properties of the fracture zone.

5) Where the FCM analyses of the current specimen are concerned, the slope of the first part of the σ-w curve is decisive to the ultimate load while the slope of the last part of the σ-w curve has a strong influence on the ductility of the specimen.

6) Tests on the specimen shown in Fig 4.4 (1) have provided interesting experimental observations, but the specimen is not, in the opinion of the writer, suitable for tests of fracture mechanics parameters of concretes.

4.5 Some analyses concerning determination of tensile fracture properties of concrete

4.5.1 Introduction

In Section 4.5 some theoretical studies concerning experimental determination of tensile fracture properties of concrete and similar materials have been collected. The studes are essentially based on the fictitous crack model. Sections 4.5.2 and 4.5.3 deal with the influence of internal initial stresses on the apparent material properties of a uniform prismatic tensile specimen: the influence on ultimate strength and the influence on apparent stress vs. strain behaviour respectively. Section 4.5.4 deals with the significance of the non-uniform tensile stresses within a specimen used by Petersson (1981) during a series of stable tensile tests, carried out in order to evaluate the shape of the σ-w curve of concrete. In Section 4.5.5 there is a discussion regarding possible methods by which the σ-w curve of materials may be evaluated from recorded load vs. displacement diagrams of specimens where the stress across the fracture section is non-uniform. Two numerical examples in the latter Section concerns the same specimen as dealt with in Section 4.5.4.

4.5.2 Prismatic specimen: influence of initial stress on tensile failure load

A uniform prismatic specimen, see Fig 4.5 (1), exposed to a tensile load is studed by means of the fictitious crack model. Initial internal stresses, which for instance, may be caused by drying shrinkage, are assumed to be present within the specimen. These initial streses have a two-dimensional distribution, and the distribution and magnitude are such that the stresses across the mid-section may be represented by a parabola where $\sigma=f_t$ at the edge, see Fig 4.5 (1). During the tensile loading, the fracture of the specimen is assumed to take place as a development and growth of a fracture zone across the mid-section of the specimen, while other parts of the specimen are assumed to behave in a linear elastic manner even if the tensile stress in some of these other parts of the specimen temporarily may exceed f_t. During the finite element analysis, the symmetrical quarter part of the specimen is divided into a mesh with 20 4-node plane stress (ν=0.2) elements along the depth, d/2, and 30

elements along the length, 2d.

The elements close to the fracture propagation path were assigned a quadratic shape, while the elements close to the end of the specimen were assigned a rectangular shape with the side length ratio 1:5. The ultimate tensile load of the specimen was calculated for the straight line and the bi-linear shape of the σ-w curve respectively, see Fig 3.2 (3), for some different values of d/ℓ_{ch}. The result is shown in Fig 4.5 (2).

The results of Fig 4.5 (2) show that the ultimate failure load gradually transforms at increased ratio size of the specimen to characteristic length of the material from the prediction of the theory of unlimited plasticity, i.e. no influence of the initial internal stress, to the precition of the theory of brittle fracture, i.e. zero load carrying capacity at the current magnitude of initial stress. This general feature of the computational results is believed to be obtained also if a non-linear stress strain relation is assumed. For a constant value of d/ℓ_{ch}, Fig 4.5 (2) also shown that the bi-linear shape of the σ-w curve suggests a somewhat stronger influence of the initial stress than the single straight line shape of the σ-w curve. When only the first part of the bi-linear σ-w curve has been activated at the instant of ultimate load, the prediction of P_u of the two shapes of the σ-w curve coincide if the slope of the first part of the curve is the same. This means that d/ℓ_{ch} of the bi-linear shape of σ-w curve corresponds to $5/3(d/\ell_{ch})$ of the single straight line shape of the σ-w curve. In a logaritmic diagram of the type of Fig 4.5 (2), this simply means a transfer of the curve along the x-axis. However, if the second part of the bi-linear curve is activated at the instant of ultimate load, which was the case for $d/\ell_{ch}=1.44$ and $d/\ell_{ch}=1.60$, such a transfer is not applicable.

The computational results suggests that one should use small specimens in order to reduce the influence of undesired initial stresses. If the initial stresses are caused by drying shrinkage or variations in temperature, a small specimen is also preferable due to the better possiblities of attaining uniform moisture and temperature conditions within the specimen. On the other hand, one may expect a greater scatter in experimental results if too small specimens are used and, furthermore, the mean behaviour of very small specimens, if for instance they are made of concrete with a coarse aggregate, may not be representative for the material. The computational results also suggest that the possible

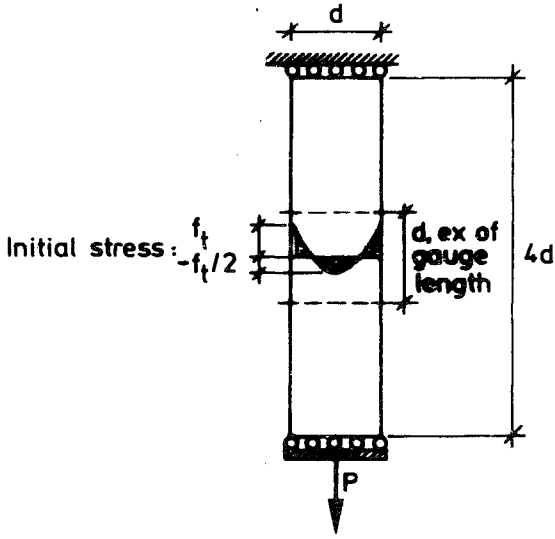

Fig 4.5 (1) Plane stress uniform prismatic tensile specimen.

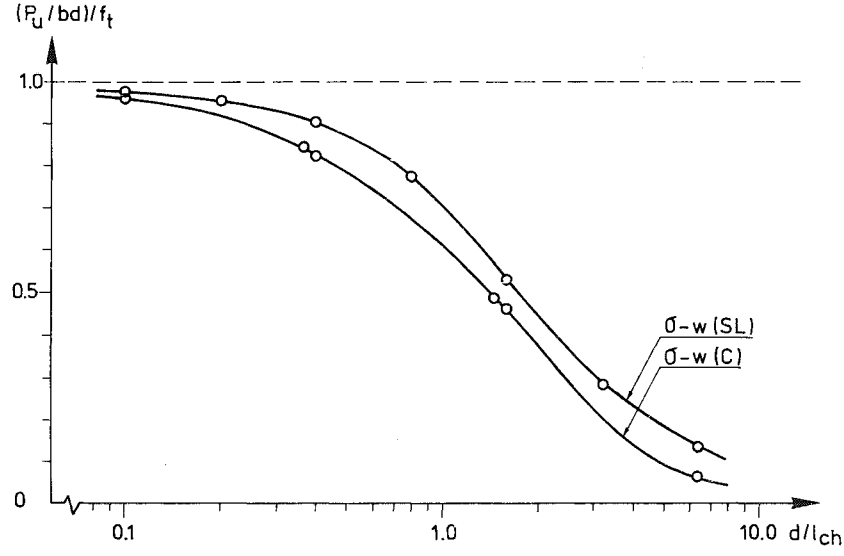

Fig 4.5 (2) Influence of initial stress on tensile strength: theoretical ratio between the apparent tensile strength, P_u/bd, and the true tensile strength, f_t, vs. ratio d/ℓ_{ch}. Geometry of specimen and initial stress acc. to Fig 4.5 (1).
(SL) = straight line, (C) = bi-linear (concrete).

influence of the size of the cross section on ultimate load must not necessarily be explained by scatter in strength, i.e. by means of the Weibull-theory or similar theories, but may be explained by undesired initial stresses (or undesired excentric loading). Fig 4.5 (2) may be used for approximate estimations of the influence of shrinkage also where other specimens than the current prismatic specimen is concerned: see for instance Section 4.6.6 where the bending failure of concrete pipes is discussed. For specimens made of cement paste, - cement paste having a ℓ_{ch} of about 10 mm -, it appears that experimental results may be very sensitive to shrinkage unless the thickness of the specimen is very small, about 1 mm or less.

4.5.3 Prismatic specimen: influence of initial internal stress on recorded stress-strain behaviour

During the calculations of ultimate load presented in 4.5.2, the load vs. the total elongation of the specimen was also obtained. At zero initial stress, the pre-ultimate load-displacement response is linear in direct accordance with the stress-strain porperties of the material. However, when initial stress are present, the load-displacement response, and thereby the apparent stress strain properties, become non-linear in spite of the actual linear stress-strain properties of the material. This is due to additional deformations during growth of the fracture zone before ultimate load. In the analysis only the growth of one fracture zone is taken into account and the computational results presented are valid on the assumption that the elongation, i.e. the apparent strain, is measured along the length d of the specimen: see Fig 4.5 (1). This assumption is approximately equivalent to the asumption that the distance between fracture zones is d. It should be noticed that the assumed gauge length, d, is made proportional to the size of the specimen. If the gauge length was kept constant with increased size of the specimen, then a greater influence of the size of the specimen on the non-linearity of the apparent stress-strain properties would have been obtained during the theoretical analysis.

The computational results are shown in Fig 4.5 (3) as the normalized stress, σ/σ_u, vs. the normalized strain, $\varepsilon/(\sigma_u/E)$ for d/ℓ_{ch}=0.1, 0.36 and 1.6. The stress, σ, is calculated as P/bd and the Figure shows that the apparent stress-strain properties become clearly non-linear if initial

stresses are present, in particular if ratio d/ℓ_{ch} is large. The real stress-strain behaviour of concrete and similar materials may not be linear all the way up to tensile failure, but the present results suggest that the recorded non-linearity of the material may be greatly exaggerated due to initial stresses whithin the specimen. Such initial stresses are in practice very difficult, and probably impossible, to avoid completely. It is somewhat unfortunate that the apparent non-linearity may be very smooth, see Fig 4.5 (3), and thus difficult to distinguish from a possible true non-linearity of the material. The present results are valid for a certain parabolic distribution of initial stresses, but it is believed that any types of initial stresses (or any type of undesired excentric loading) produce an apparent exaggeration of the non-linearity of the stress-strain properties of the material. Also initial stresses on the micro-level within the material are likely to produce an exaggeration of the non-linearity. Within concrete such micro-level initial stresses may occur due to chemical shrinkage of the paste when hardening and due to uniform drying whithin the specimen resulting in shrinkage of the paste, but not the aggregate. However, non-linearity due to initial stresses at the micro-level should not be considered as apparent when a specimen or a structural member is analysed at the macro-level. Fig 4.5 (3) suggests that tests of the stress-strain behaviour of concrete and similar materials should be carried out in a careful manner - in particular if the specimen is large and/or made of a brittle material, and that stress-strain curves of concrete in tension reported in literature are likely to - more or less - exaggerate the true non-linearity of the pre-failure stress-strain properties of the material.

From the results in this Section together with considerations of influence of scatter in strength, it seems to be probable that significantly different σ-ε curves of concrete in tension may be recorded for the same quality of concrete. If, 1), the test is carried out in careful manner where undesired initial stresses and undesired excentric load are avoided; 2), the cross section area of the prismatic specimen is small; 3), the length of the prismatic specimen is very great; and 4), the strain is measured along a short part of the specimen outside the part which subsequently proves to include the fracture section, then it is probable that an almost linear tensile stress vs. strain behaviour of the concrete can be recorded. If these conditions are reversed, then it is probable that a pronounced non-linear tensile stress vs. strain behaviour of the same quality of concrete can be recorded.

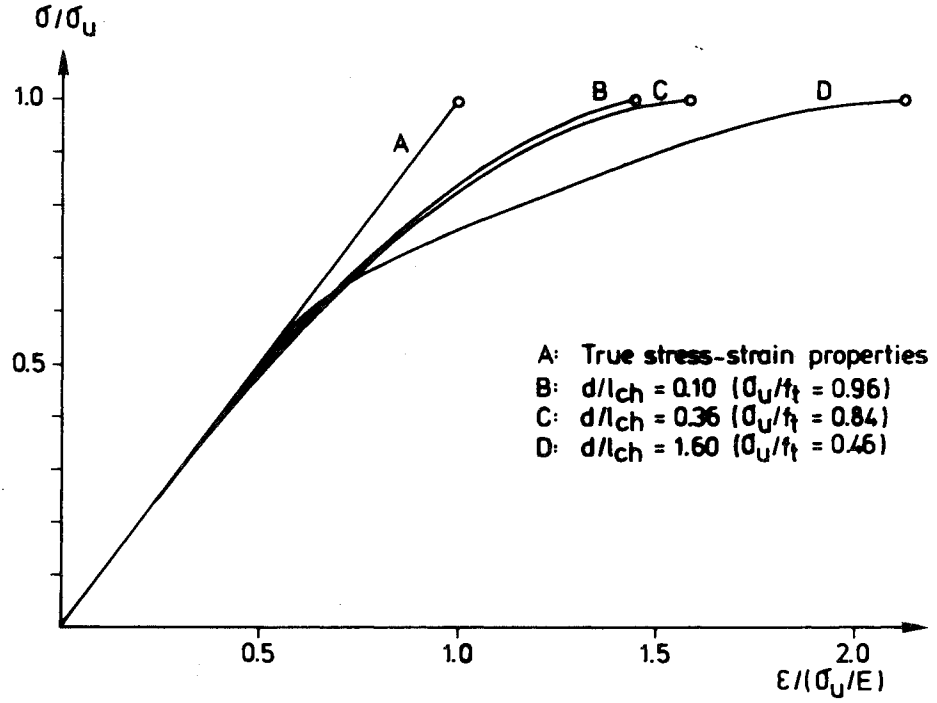

Fig 4.5 (3) Theoretical apparent stress-strain properties of a material with a linear stress-strain relation. Initial stress, gauge length and geometry of specimen acc. to Fig 4.5 (1). Bi-linear σ-w curve acc. to Fig 3.2 (3) c).

4.5.4 Influence of non-uniform stress during a stable tensile test of concrete

(Petersson, 1981) used the specimen shown in Fig 4.5 (4) during stable tensile tests of concrete carried out in order to determine the shape of the σ-w curve of concrete. The test results were evaluated on the assummption that the tensile stresses across the fracture section were uniform. However, (Petersson, H., 1982) pointed out that the stresses across the fracture section are not uniform, at least not in the pre-fracture elastic range, and suggested that this matter ought to be investigated with regard to the type and magnitude of the possible error in the σ-w curve when evaluated in the simplified manner without considerating the non-uniform tensile stresses. Such an investigation

seems justified and desirable because the results of stable tensile tests of concrete carried out by Petersson and others form a very essential part of the experimental "proof" for validity of the fictitious crack model and the existence of a descending branch in the tensile stress-deformation response of concrete.

In order to come to an understanding regarding the type and the magnitude of the possible error, a model-material is assigned certain known properties. For these properties the load-displacement behaviour of the specimen is obtained by means of the theoretical analysis, taking into account the actual shape of the non-uniform stresses. From the load-displacement behaviour obtained, a σ-w curve is then evaluated on the assumption of uniform stresses across the fracture section. The difference between the input and the output σ-w curves gives a measure of the error introduced by the simplified evaluation of the experimental results.

At this point it is necessary to give a more detailed description of the assumption of uniform stresses across the fracture section. In the present adopted sense, this assumption is equivalent to complete shear rigidity of the material in a very thin band along the section of symmetry and fracture. This is in turn equivalent to the assumption that the two cross sections on each side of the fracture section and indefinitely close to the fracture section remain plane during the entire course of loading and fracture. This means that the shape of the stress field in the unfractured parts of the specimen is forced to be constant and equal to the shape before start of fracture, whereas the stresses across the fracture section are forced to be uniform. The stiffness of the specimen before start of fracture is not affected.

The finite element model of the specimen is shown in fig 4.5 (5) a) together with the properties of the model material, Fig 4.5 (5) b). In order to model the boundary conditions at the ends of the specimen accurately, the influence and properties of the glue at the end of the steel plates is taken into account. The thickness and the properties of the glue are, however, only roughly estimated. The modulus of elasticity, E=30000 MPa, and the tensile strength, f_t=4.63 MPa, is taken from an experimental load vs. displacement curve as presented by Petersson. This experimental curve, also utilized in Section 4.5.5, represents a mean curve (three tests) for a concrete with a water-to-cement ratio of 0.5, a maximum aggregate particle size of 8 mm, an aggregate content of 1755

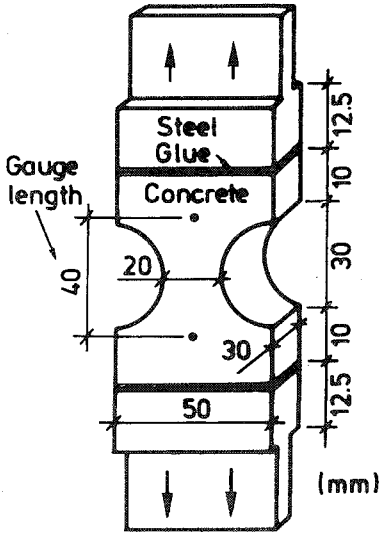

Fig 4.5 (4) Specimen used by Petersson (1981) during stable tensile tests of concrete.

kg/m^3 and tested at the age of 28 days. The constant slope of the σ-w curve, $d\sigma/dw$=-135400 MPa/m, corresponds to the steepest part of the σ-w curve as obtained in the test. The steepest part is chosen because the effect of the non-uniform stresses becomes greater at decreased ℓ_{ch}, i.e. when the slope of the σ-w curve is steep in comparison to the slope of the σ-ε curve. The properties of the model material correspond to ℓ_{ch}=0.111 m and G_F=79.2 N/m. The Poissons ratio is made equal to zero for the concrete, the glue and the steel.

The computational results, see Fig 4.5 (6) a), b), c) and d), show that the stresses across the fracture section are definitely non-uniform at the instant of start of fracture zone development and that the fracture zone starts to develop long before the ultimate load is reached. These findings are clearly in disagreement with the assummptions utilized by Petersson. However, once the front of the fracture zone has grown through the entire cross section, the stresses become almost entirely uniform. According to the computational results, this instant of complete development of the fracture zone coincides exactly with the instant of maximum load, but if a finer element mesh was used one should find that the fracture zone is completely developed, not exactly at, but immediately after, ultimate load.

The non-uniform stress field appears to have only a small influence on the load-displacement behaviour. This influence is noticeable only before

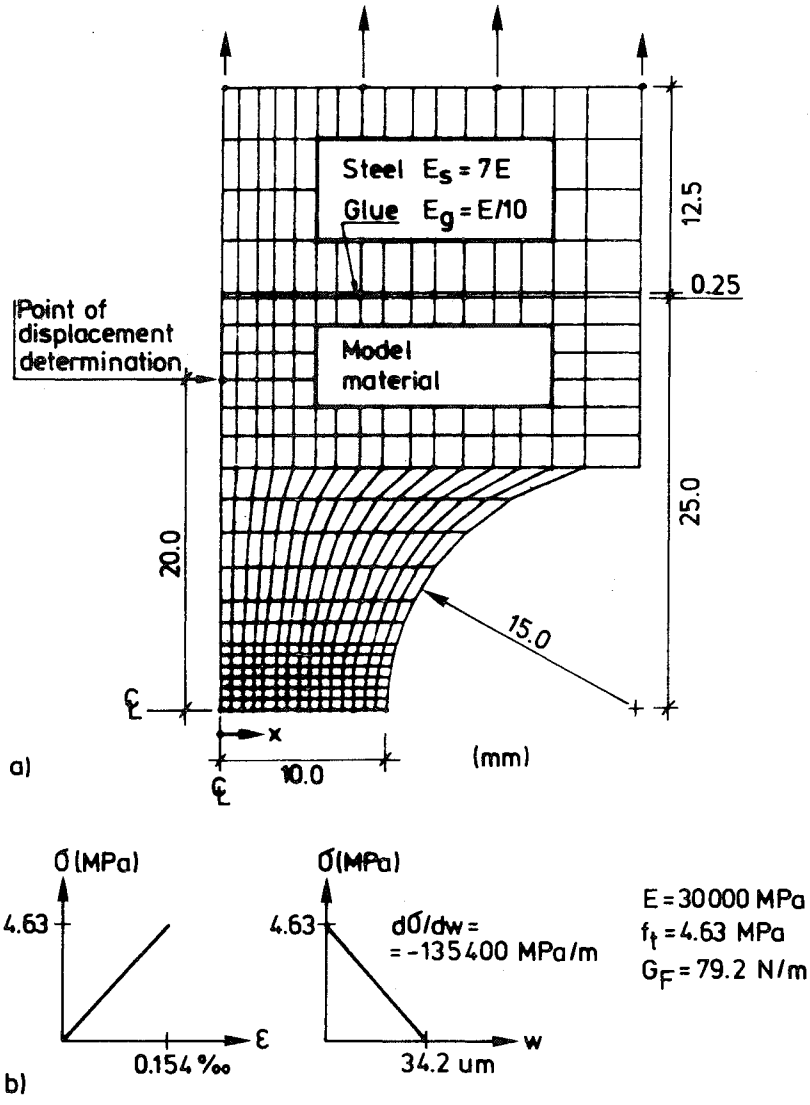

Fig 4.5 (5) a) Finite element model of specimen shown in Fig 4.5 (4).
b) Properties of a model material.

ultimate load and during the very last stage of the collapse when the load is extremely close to zero and an open crack, i.e. a not stress-transferring crack, starts to grow through the fracture section. Also the difference between the true σ-w curve of the current model-material and the σ-w curve as obtained during the simplified evauation is small. While the true tensile strength of the material is 4.63 MPa, the simplified evaluation of the simulated experimental result gives f_t=4.57 MPa and while the true fracture energy of the material is 79.2 N/m, the simplified evaluation of the simulated experimental result gives G_F=77.1 N/m. The present simplified evaluation of the σ-w curve and G_F is carried out in accordance with the method used by Petersson: the unloading behaviour of the unfractured material is represented by a straight line from the point of ultimate load and parallel to the initial slope of the load-displacement curve.

In connection with the computational results in Fig 4.5 (6) it is also interesting to note that the area under the complete load vs. displacement curve divided by the area of the fracture section is equal to 79.1 N/m and therefore not equal to the true fracture energy of the model material, 79.2 N/m. This is because the area under a load vs. displacement curve may be expected to equal the work carried out by the external loads only if the external loads acts on the points where the displacement is measured. The total work carried out by the external loads divided by the area of the fracture section is equal to 79.2 N/m. This work, carried out by the external loads, is obtained as the sum of the areas under the load vs. displacement curves of the different loads, the displacements being obtained at the respective point of loading. The difference between 79.1 and 79.2 N/m reflects the influence of the simplified experimental method of measurement of displacement. This influence seems to be of negligible magnitude.

In addition to the theoretical results valid for the theoretical model material of Fig 4.5 (5) b), Fig 4.5 (6) a) and b) show also the experimental load displacement curve for one of the concretes tested by (Petersson, 1981). This experimental curve was used during the choice (see above) of the properties of the model material, i.e. E, f_t and the constant $d\sigma/dw$ of the model material is taken from this experimental curve. However, it must be noticed that the differences between the experimental curve and the curves valid for the theoretical model material should not be utilized for estimations of the magnitude of the

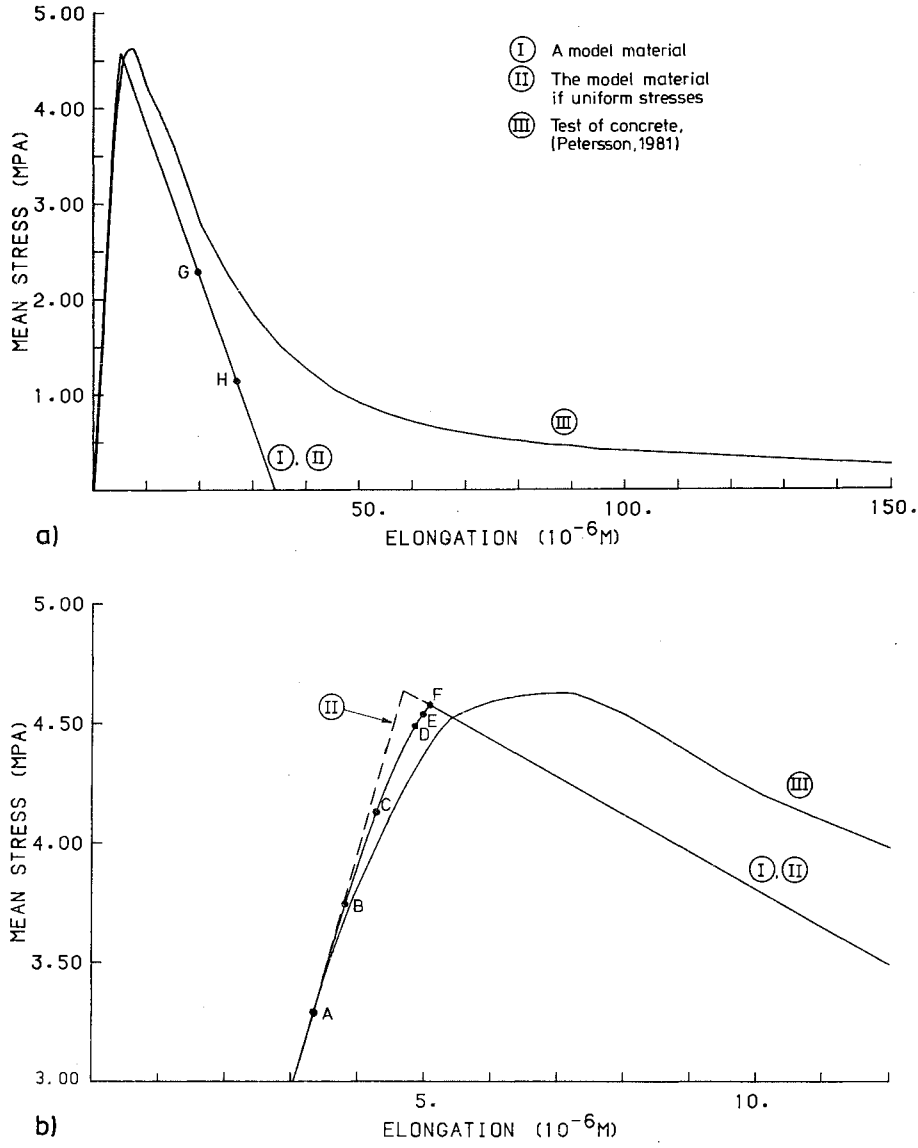

Fig 4.5 (6) a) Load-displacement behaviour of specimen shown in Fig 4.5 (4). Model material acc. to Fig 4.5 (5) b).
b) Enlarged detail of Fig a).
Notations A-H refer to fig c).

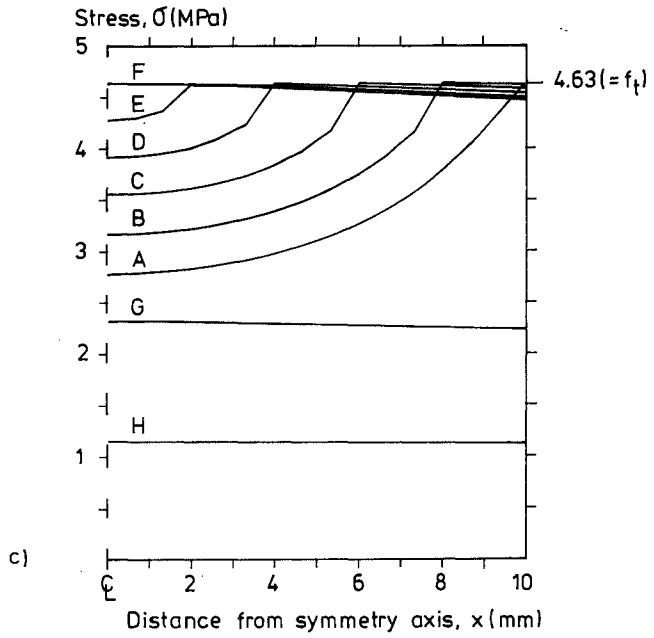

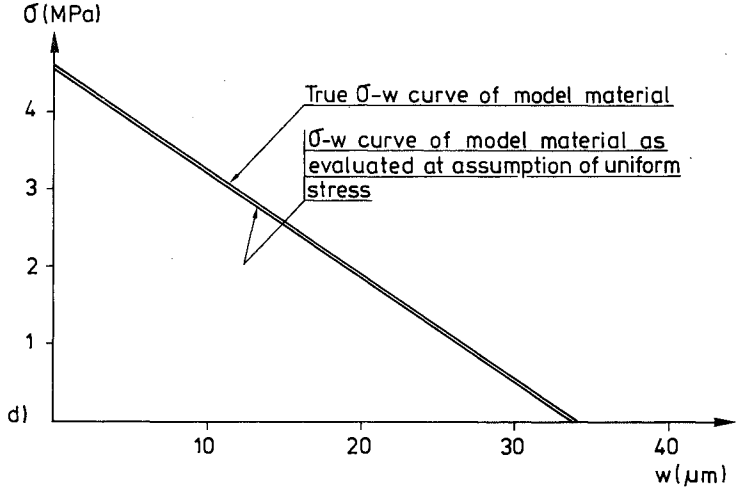

Fig 4.5 (6) c) Stress across fracture section during loading and collapse. Notations A-H refer to Fig a) and b).

d) Influence of assumption of uniform stress in the evaluation of the σ-w curve.

approximation involved in the simplified method of evaluation of the σ-w curve. The actual model material is assigned a constant $d\sigma/dw$ and a constant $d\sigma/d\varepsilon$, while the real concrete exhibits a non-linear performance.

Judging from the results of Fig 4.5 (6), it may be concluded that the assumption of uniform stress across the fracture section, tacitly adopted by Petersson in evaluation of σ-w curves and values of G_F and f_t, involves only a small approximation.

However, if the actual material has a steeper slope in the σ-w curve than the model material of Fig 4.5 (5) b), or in more general terms, if the value of $d(-d\sigma/dw)/E$ (where d is a measure of the size of the specimen) is high, then the conclusion above may not be valid. Thus, for instance, an extremely steep slope in the first part of the σ-w curve may give a significant under-estimation of the tensile strength of the material and the first steep part of the σ-w may therefore not be detected during the test. This is illustrated by the computational results shown in Fig 4.5 (7) b). These computational results are valid for a model material defined by Fig 4.5 (7) a). For this model material f_t=5.63 MPa and $d\sigma/dw$=-2710000 MPa/m in the range σ=5.63 MPa to σ=4.63 MPa, but for the rest is similar to the model material in Fig 4.5 (5) b) and Fig 4.6. While the true tensile strength of the model material in Fig 4.5 (7) is 5.63 MPa, the simplified evaluation of the simulated experimental results gives f_t=4.78 MPa and while the true value of G_F is 80.2 N/m, the simplified evaluation gives G_F=76.9 N/m. Consequently the influence on f_t is significant, while the influence on G_F is rather small.

If a specimen where the stresses across the fracture section may be non-uniform is used in the tensile strength test, knowledge about the stress-deformation properties of the material must be available otherwise the test may provide very little information about the tensile strength of the material tested. If only the recorded ultimate load is known, and nothing is known about the stress-deformation properties, only a lower limit value of the true tensile strength may be evaluated. This value may be evaluated by means of the theory of unlimited plasticity. If in addition the shape of the stress-strain behaviour is known, an upper limit value of the true tensile strength may also be evaluated. This value may be evaluated by means of the theory of ideal brittleness. On the assumption of a linear elastic stress-strain behaviour, this means, with reference to the specimen in Fig 4.5 (4), that the true value of f_t is between 1.00 $\sigma_{u,mean}$

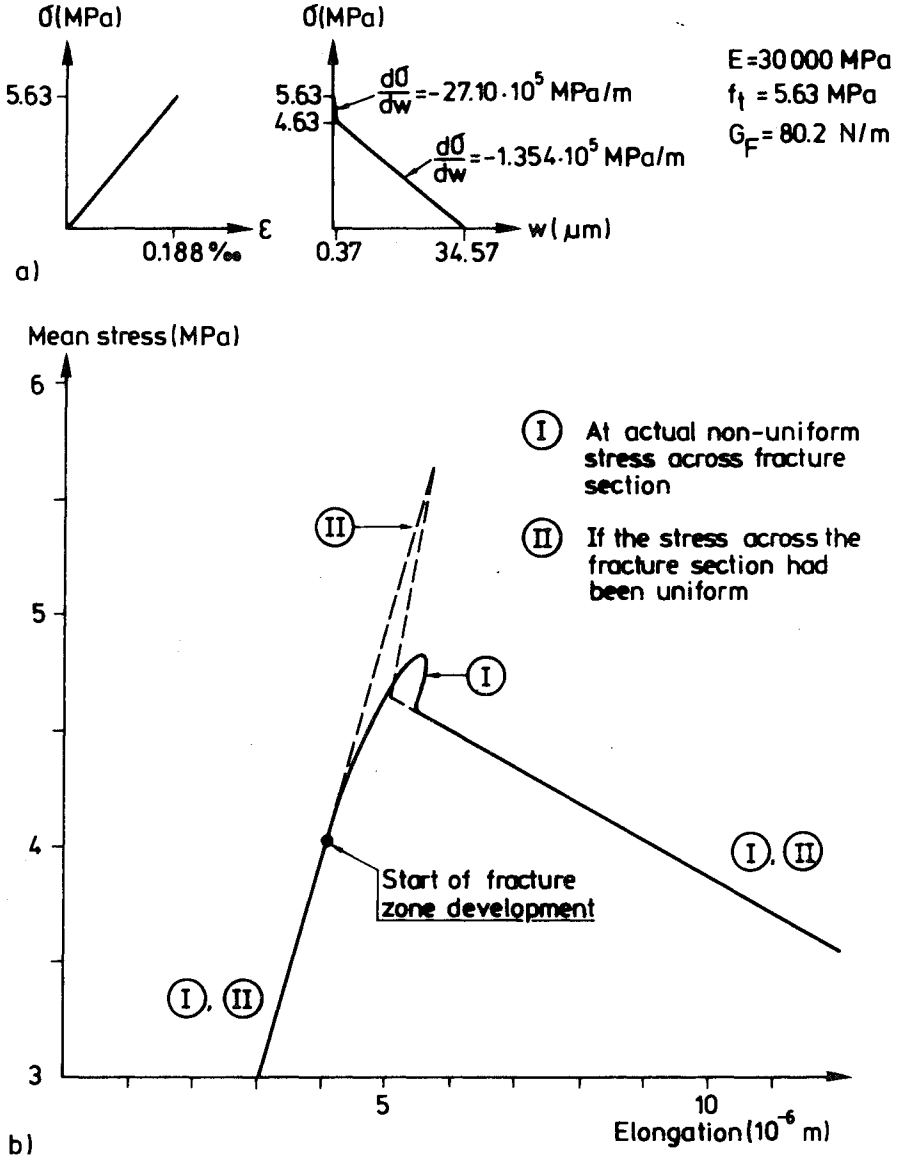

Fig 4.5 (7) a) Properties of a model material with a steep first part in the σ-w curve.

b) Load-displacement behaviour of specimen shown in Fig 4.5 (4) at material property acc. to fig a).

and 1.41 $\sigma_{u,mean}$, where $\sigma_{u,meam}$ is the recorded ultimate load divided by the area of the fracture section. The factor 1.41 is obtained from the finite element results in Fig 4.5 (6): In the linear elastic range, the ratio mean stress, to stress at the edge of the fracture section, to stress in the centre of the fracture section is 1.00:1.41:0.84. Consequently, if the σ-ε curve is known to be a straight line, and nothing is known about the σ-w curve, and if a test gives $\sigma_{u,mean}$=4.63 MPa then all that can be said about f_t is that it is in between 4.63 MPa and 6.51 MPa.

As the accuracy of the evaluation of stable tensile tests may thus be strongly dependent on the ratio $d(-d\sigma/dw)/E$ if the stresses across the fracture section are non-uniform (see also Fig 4.5 (2)) and as the value of $d\sigma/dw$ is obtained during the test, an undesirable uncertainty factor is involved. In order to avoid this one should try to strive for the use of specimens where the stresses are as uniform as possible. At completely uniform stress, the results of an evaluation should be independent of the ratio $d(-d\sigma/dw)/E$. This ratio is proportional to d/ℓ_{ch} and comparison can be made to hypotheses II and III in Section 3.5.2. In cases of non-uniform stresses, no matter whether these are caused by the geometry of the specimen, excentric loading or internal initial stresses, the dependence of the ratio $d(-d\sigma/dw)/E$ suggests that particular care should be taken if large specimens made of a brittle material are tested. While, from the beginning, large specimens made of brittle materials are difficult to test in a stable manner, it is unfortunate that increased uniformity of the stress across the fracture zone makes it more difficult to carry out a stable test. This is because the stability of a uniform specimen is governed by the steepest part of the σ-w curve, while in the case of non-uniform stresses several parts of the σ-w curve are active at the same time. Modern advanced types of fast and sensitive "closed loop" tensile testing equipment may, however, significantly reduce the difficulties in stable tensile testing. In Section 4.5.5 a few possibilities of evaluating the σ-w curve from tests on specimens where the stresses are non-uniform are discussed.

Recently, (Glemberg, 1984) presented research which included an interesting finite element study of the specimen shown in Fig 4.5 (4). The purpose of this study was to verify a finite element method and therefore not the same as purpose of the present study. Glemberg applied a certain smeared modelling of the tensile fracture and demonstrated that the finite

element method used by Glemberg is objective in the sense that the area under the calculated load vs. displacement curve divided by the area of the fracture section seems to approach the input value of G_F when the number of finite element is increased. From an exact theoretical point of view, one might, however, question whether it is desirable to approach such a limit value of the area under the calculated load vs. displacement curve. But this matter is not believed to be of any practical importance where the study and conclusion of Glemberg are concerned. For the model material in Fig 4.5 (5) b) it appears from the present computational results that the area under the load vs. displacement curve should approach a value about 0.2% below G_F times the area of the fracture section. The cause of the difference has been dealt with above. The presently utilized finite element method is such that G_F times the area of the fracture section may be expected to equal the work carried out by the external loads, regardless of the number of elements.

4.5.5 Discussion on indirect evaluation of the σ-w curve

From the results in Section 4.5.4, one rather obvious possibility of determining the σ-w curve is to choose the curve in such a way that the experimentally recorded load vs. displacement curve conincides with the theoretical load vs. displacement curve. By means of the finite element method, the theoretical load vs. displacement curve may be calculated even if the stress across the fracture zone is non-uniform. This opens up the possiblity of using the specimen in Fig 4.5 (4) even if the ratio $d(-d\sigma/dw)/E$ is large and may also enable the use of other types of specimens, for instance the notched three point bend beam, when determinating the σ-w curves. The σ-w curve which, in one sense or another, produces the best fit between the experimental load vs. displacement curve and the corresponding theoretical load vs. displacement curve may be found by means of "trial and error" or by means of some systematic method which may be coded into a computer.

Regardless of the numerical method of the curve-fitting, it is not believed to be possible to evaluate both an unique σ-ε curve, including an unique unloading brach, and an unique σ-w curve only from the recorded load vs. displacement curve of one type and size of a specimen. Thus the shape of the σ-ε curve must be determined in separate tests or by means of simultaneous measurements of load vs. deformation along at least two

different parts of the specimen. Theoretically it may be possible to determine both the σ-ε curve and the σ-w curve from one measurement if the unloading branch of the σ-ε curve is known. As to the present numerical examples, it is assumed that the shape of the σ-ε curve may be represented by a straight line both at loading and at unloading.

The present numerical examples concern the specimen shown in Fig 4.5 (4) and the experimental load vs. displacement curve shown in Fig 4.5 (6) a) and b) is used as a starting point. The finite element mesh in Fig 4.5 (5) a) is used when calculating the theoretical load vs. displacement curve.

When a specimen of the type showing Fig 4.5 (4) is used, there is a close connection between the load vs. displacement curve and the σ-w curve. This makes it easy to obtain a fair fit between the load vs. displacement curves by means of "trial and error": see Fig 4.5 (8). In one of the tables in Fig 4.5 (8) c), the σ-w curve obtained is described in a general form in terms of f_t and G_F. The adopted value of G_F, 189.0 N/m, is, however, uncertain as the last part of the experimental load vs. displacment curve is unknown. For the same reason, the shape of the σ-w curve for $w>150$ μm and $\sigma/f_t<0.054$ only represents a guess. The plateau in the first part of the σ-w curve is interesting, but the size of this plateau is of course dependent on the assumption regarding the shape of the σ-ε curve.

Close to ultimate load, the curve fitting would have been better if $d\sigma/dw$ were assigned a value greater than zero in a small first part of the σ-w curve. For a homogenous material the σ-w curve is, however, not activated before ultimate stress, i.e. strain localization does not occur before ultimate stress, and a $d\sigma/dw>0$ in the first part of the σ-w curve is in conflict with the basic fictitious crack model separation of the σ-ε curve and the σ-w curve. However, as mentioned in Section 3.2.2, when the actual scatter in strength of a material is not explicitly taken into account in an analysis, it might be that more realistic results can be obtained if $d\sigma/dw$ is assigned a value greater than zero in the very first part of the σ-w curve.

We turn to another and more well defined method of evaluation of E, f_t and the σ-w curve. It is assumed that the σ-ε curve is a straight line where E and f_t are unknown and it is further assumed that the σ-w curve consists of n linear pieces where the slope and the length of each piece are

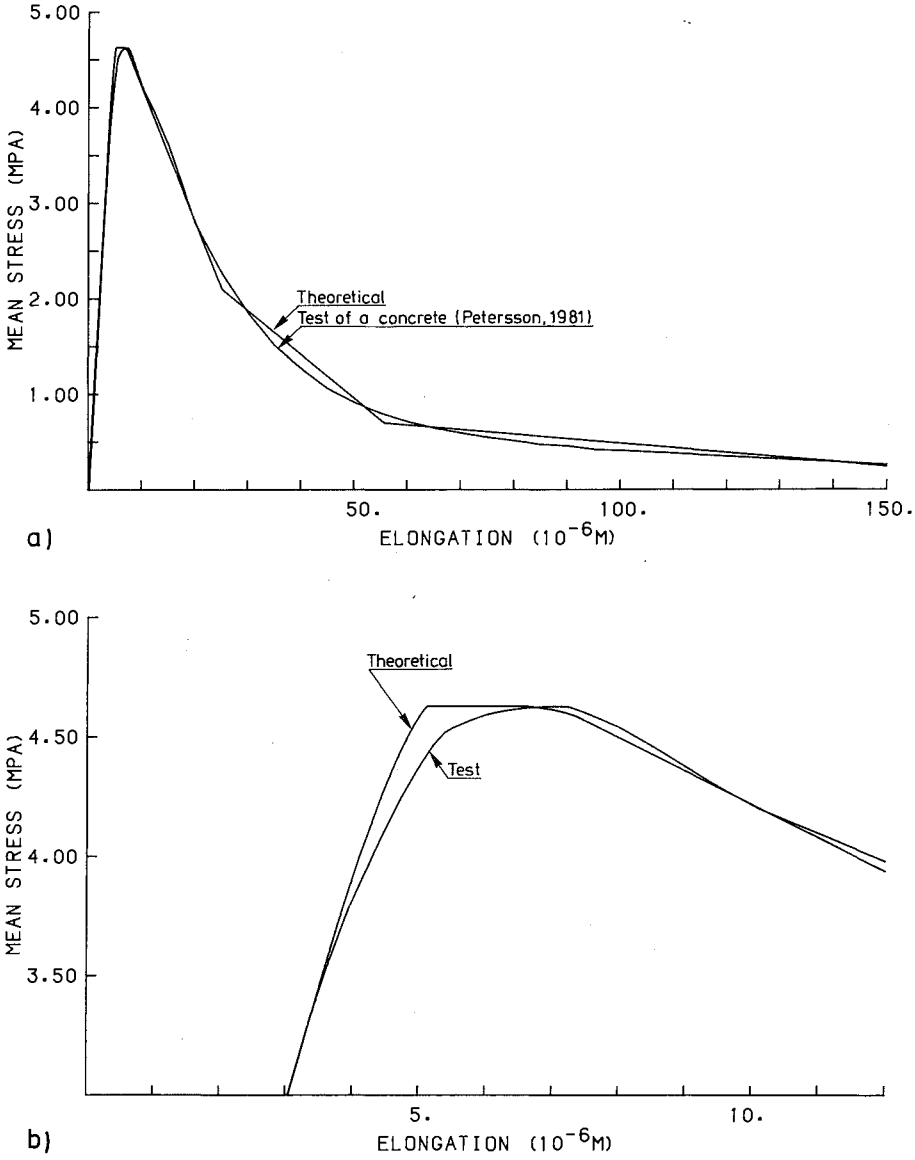

Fig 4.5 (8) a) Loads vs. displacement of specimen shown in Fig 4.5 (4). Test result compared to theoretical result valid for material properties found by "trial and error".
b) Enlarged detail of fig a).

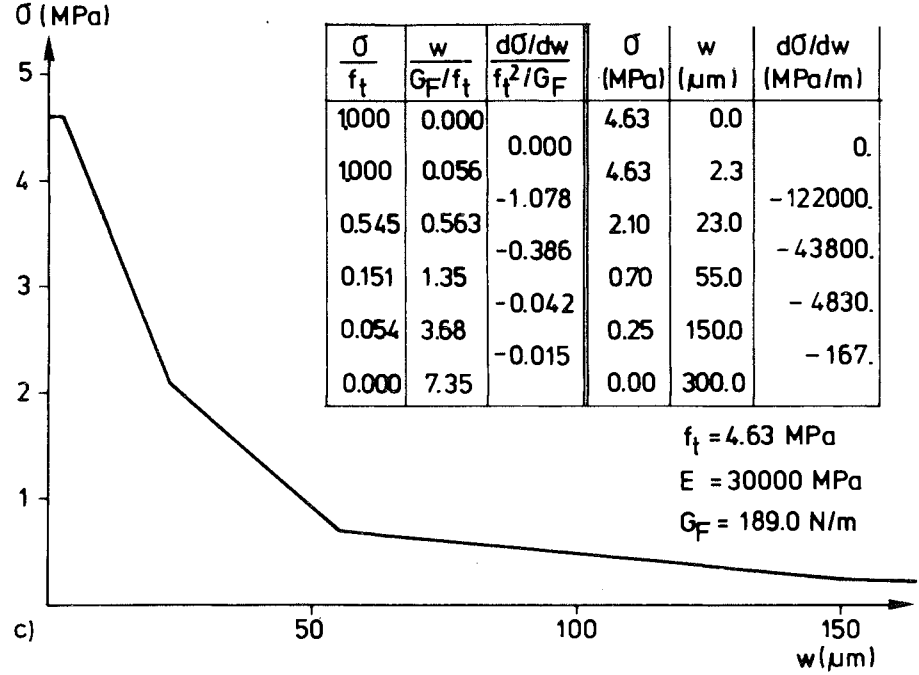

$\frac{\sigma}{f_t}$	$\frac{w}{G_F/f_t}$	$\frac{d\sigma/dw}{f_t^2/G_F}$	σ (MPa)	w (μm)	dσ/dw (MPa/m)
1.000	0.000		4.63	0.0	
		0.000			0.
1.000	0.056		4.63	2.3	
		-1.078			-122000.
0.545	0.563		2.10	23.0	
		-0.386			-43800.
0.151	1.35		0.70	55.0	
		-0.042			- 4830.
0.054	3.68		0.25	150.0	
		-0.015			- 167.
0.000	7.35		0.00	300.0	

Fig 4.5 (8) c) σ-w curve, E and f_t as obtained at a "trial and error" fitting of load vs. displacement.

unknown. n+2 points are taken from the experimental load vs. displacement curve. The n+2=7 points chosen for the present numerical example are given in the table included in Fig 4.5 (9) a). The first point is the origin of the load vs. displacement curve and the second point is the point were the load vs. displacement curve starts to deviate from a straight line. The last n points are chosen more or less at random along the rest of the curve. The two first points may be used for the evaluation of E. The second point is in addition used for determination of the stress at which a fracture zone starts to develop, i.e. f_t. This second point is very difficult to define accurately and it is accordingly difficult to obtain an accurate value of f_t by mean of this method. The n last points are used for step-wise evaluation of the slope and the length of the n linear pieces of the σ-w curve.

By means of a single linear elastic finite element analysis, E and f_t are evaluated first. In the present example E=30 000 MPa and f_t=4.77 MPa are obtained. By means of iterations the slope of the first linear part of the σ-w curve, $(d\sigma/dw)_1$, is the evaluated. These iterations are carried out in

such a way that the theoretical load displacement response will pass through, or very close to, the third point, 3, chosen from the experimental load vs. displacement curve. In more general terms, the purpose of the iterations is to find and to solve an equation with regard to $d\sigma/dw$:

$$P_{t,i+2}(d\sigma/dw) = P_{e,i+2} \qquad (4.5:1)$$

$P_{e,i+2}$ is the experimentally obtained load at displacement δ_{i+2}, where i+2 is the number of the point chosen from the load vs. displacement curve. On the left hand side of the equation the corresponding theoretical load is found. Eq (4.5.1) may be solved in different manners. Presently, a first value of $P_{t,i+2}$ is calculated for a more or less random value of $d\sigma/dw$. The result of the calculations indicates whether $d\sigma/dw$ should be increased or decreased. By means of a second value of $P_{t,i+2}$ and by means of linear interpolation, a third value of $d\sigma/dw$ is calculated. By means of a third value of $P_{t,i+2}$ and by means of parabolic interpolation a fourth value, and in the present analysis the final value, of $d\sigma/dw$ is calculated.

Knowing the $d\sigma/dw$ of the first part of the σ-w curve, a fourth calculation is carried out in order to determine the length of this first part. The length is given by the width of the fracture zone where w has its largest value at the displacement δ_{i+2}.

The first part of the σ-w may now be fixed as the P vs. δ curve always will pass through (P_3, δ_3), regardless of the shape of the rest of the σ-w curve. The same method as described above may then be used for evaluating the second, and the subsequent, linear parts of the σ-w curve.

If n+2 points chosen on the experiental P vs. δ curve altogether 4n+1 finite element calculations have to be carried out and a σ-w curve consisting of n linear pieces is obtained together with E and f_t. In spite of the number of calculations, it has been found that the evaluation is rather simple to carry out. If a number of evaluations are to be carried out, it should be possible, and may be convenient, to develop a computer program which automatically performs the evaluations.

The results obtained in the applied numerical example are shown in Fig 4.5 (9). In Fig 4.5 (9) a) the points chosen on the experimental P vs. δ curve are shown numerically together with the corresponding results obtained during the iterations. The example shows that the σ-w curve obtained is

such that the theoretical load vs. displacement curve passes very close to the given points. In between these points, however, the load vs. displacement curves deviates substantially and the first part of the σ-w has an undulating and not very realistic shape where the stress also temporarily exceeds f_t. A cause of the undulating shape close to peak stress may be the assumption of a linear σ-ε curve. For $\delta > 20\,\mu m$, Fig 4.5 (10) a) shows that the theoretical P vs. δ curve changes its direction very rapidly into a new direction once the curve has passed through a given point. By increasing the value of n the theoretical load vs. displacement curve may be forced to pass through an arbitrary large number of given points. In such a case, however, one may suspect that the σ-w curve may become of a similar undulating type as high degree polynomials which are forced to pass through a large number of given points.

The discussed step-wise method of calculation of the σ-w curve is general in the sense that it may be applied to the evaluation of other types of properties of materials. A convenient feature of the method is that the material property curve is evaluated and fixed step-wise. This enables the use of very simple numerical methods during the iterations. A disadvantage of the method is that only a very small part of the experimental information is utilized during the evaluation. Because of this disadvantage, it is probable that the same basic method of evaluation will turn out to be more sucessfull if each interval of the material property curve is determined in such a way that the deviaton between the response curves is minimized (for instance in the sense of least squares) along the entire corresponding interval of the response diagram.

In the method of evaluation dealt with above, the σ-w curve is evaluated and fixed in an incremental manner. An alternative method, the non-linear least square optimization of several parameters, is basically different: all parts of the material property curve are evaluated simultaneously and the parameters defining the material property curve are therefore not evaluated one at a time. In this alternativ method the σ-w curve is first described in terms of some function with m degrees of freedom, i.e. m parameters C_1, C_2 ... C_m. Putting $\bar{c} = \{E, f_t, C_1, C_2 \ldots C_m\}$, the optimum of $\bar{c}$ may be determined by means of minimizing a least square function $Q(\bar{c})$:

$$Q(\bar{c}) = \int_0^\infty \alpha(\delta)\,(P_t(\delta,\bar{c}) - P_e(\delta))^2\,d\delta \qquad (4.5:2)$$

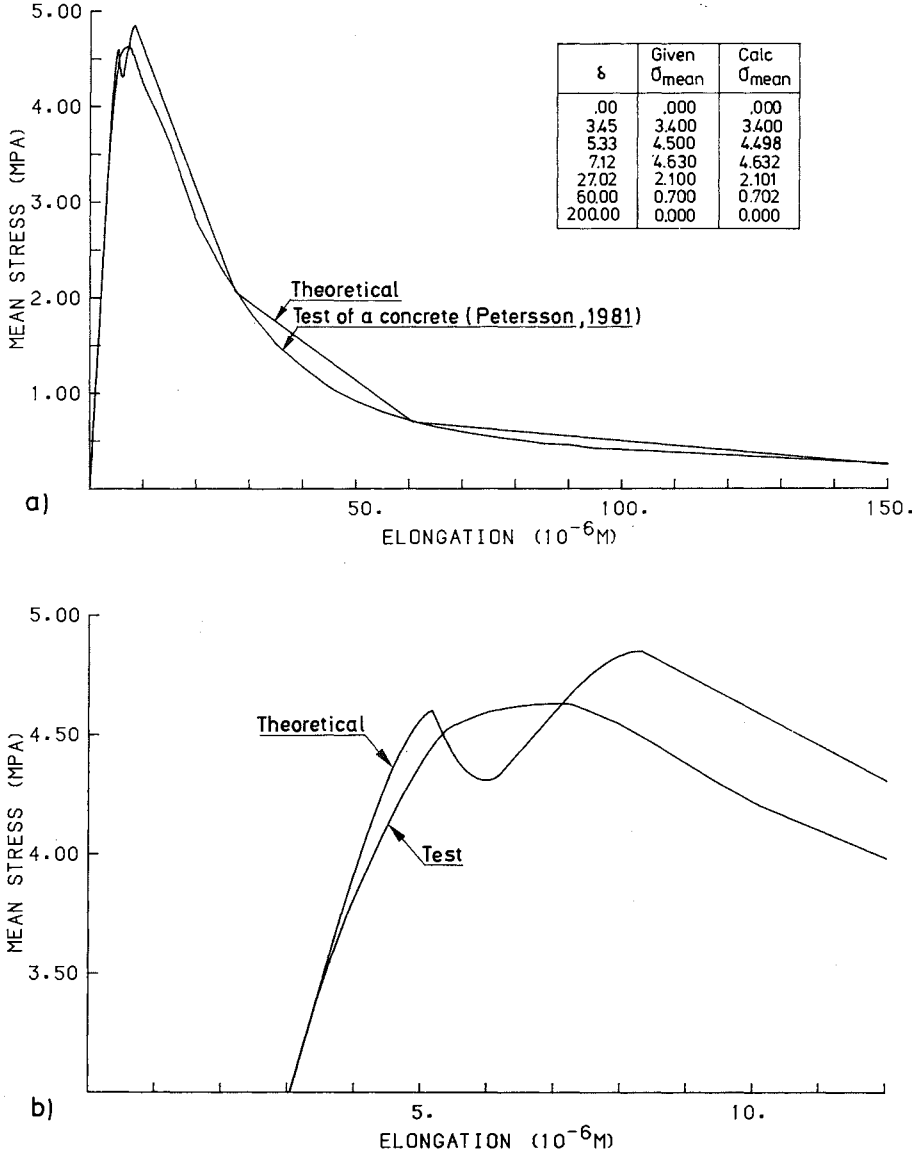

δ	Given σ_{mean}	Calc σ_{mean}
.00	.000	.000
3.45	3.400	3.400
5.33	4.500	4.498
7.12	4.630	4.632
27.02	2.100	2.101
60.00	0.700	0.702
200.00	0.000	0.000

Fig 4.5 (9) a) Load vs. displacement of specimen shown in Fig 4.5 (4). Test result compared to theoretical result valid for material properties found by step-wise iterations to given points.
b) Enlarged detail of fig a).

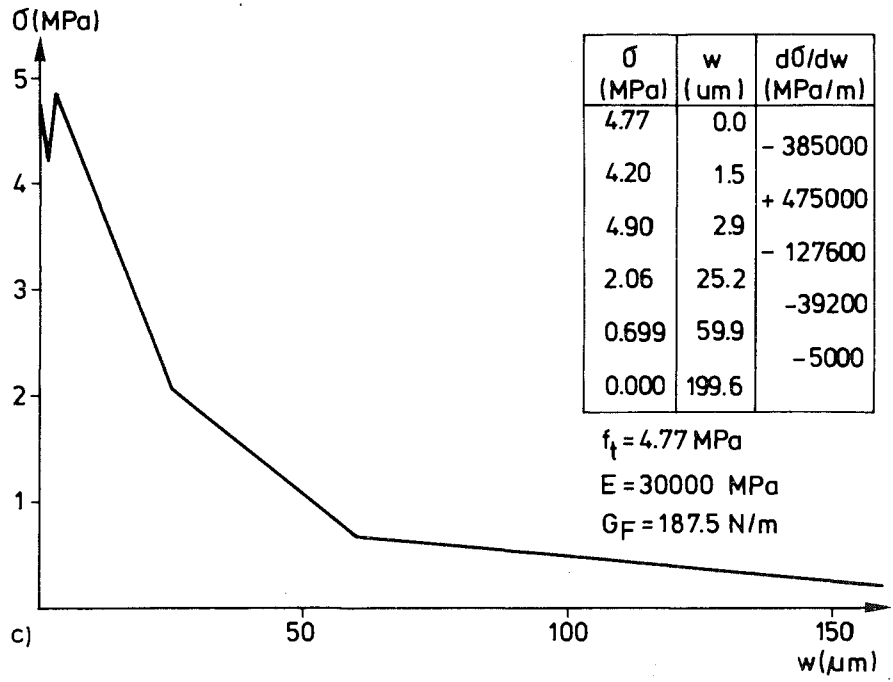

Fig 4.5 (9) c) σ-w curve, E and f_t as obtained by step-wise iterations to given points on the load vs. displacement curve.

$P_e(\delta)$ is the experimental load vs. displacement curve and $P_t(\delta,\bar{c})$ is the corresponding theoretical curve. $\alpha(\delta)$, or $\alpha(\delta, P)$, is a weight function which makes it possible to reduce the influence of experimental errors. In order to find the global minimum of Q and the corresponding optimum of $\bar{c}$ without having to try too many $\bar{c}$, an efficient and reliable numerical algorithm should be available. Such algorithms, or computer programs, are believed to be available in most large computers. (Lin and Sackman, 1975) and (Distefono, 1970), see also previous and later papers published by these authors, have applied least square optimization to the identification of linear and non-linear viscoelastic materials, thermorheological materials and subsurface hydrological systems. The type of evaluation represented by eq (4.5:2) has not been tested by any numerical example during evaluation of any σ-w curve. However, on a proposal of Wickström (1979), some test calculations have been carried out with regard to evaluation of non-linear thermal properties of concrete, and it was found that the method appears to be useful and meaningful for determination of material properties which are difficult to measure

directly. In general, however, it is necessary that a one-to-one relation exists between the unknown material property curve and the measured response curve, and it is desirable that the specimen is such that the recorded response is clearly sensitive to the properties of the material. If the actual method is applied to very complex material properties, described by a large number of curves and parameters, then possible small sensitivity to the material properties, possible great sensitivity to experimental errors and possible lack of a one-to-one relation may reduce the meaningfulness of the actual method where determination of materials properties are concerned. In such cases the parameter values obtained may not always give an accurate description of the real material properties, and might even become only mathematical best-fit values without any realistic physical correspondance. Consequently, as simple and downright experimental test methods as possible are believed to be preferable also when recorded test results are to be treated by means of a non-linear least square optimization method.

4.6 Strength analyses of concrete pipes

4.6.1 Introduction

This Section deals with analyses of bending strength and crushing strength of unreinforced concrete pipes. The methods of analyses and the computational results are, however, essentially theoretical and consequently not related to any specific material. Accordingly most of the theoretical results may, as a matter of principle and more or less successfully, be applied to strength analyses of pipes made of other materials than concrete. However, the present application concerns concrete.

Unreinforced concrete pipes are fabricated in series, the output production represents a visible part of the total consumption of concrete and the costs caused by pipe failures are probably not to be considered as negligible. (The cost of repairs to sewage and water supply pipelines in England and Wales was estimated by Brennan (1978) at about £ 40 m per annum at 1975 prices.) In spite of this, basic analyses of the fracture behaviour of unreinforced concrete pipes appear rather scarce and strength design seem to have been based essentially on previous practical experiences and experimental investigations. Theoretical stength analysis of unreinforced concrete pipes based on basic assumptions with respect to the behaviour of the material have with few, if any, exceptions been limited to analysis on the assumption that concrete is an homogenous linear elastic brittle material. This assumption is rather convenient as to numerical calculations and might seem natural as failure mostly takes place as tensile fracture of the material and as, by tradition, concrete in tension is assumed to behave in a linear elastic brittle manner. However, results of this conventional theory have proved to contradict experimental results. To these contradictions, a number of phenomenological explanations have been proposed: increase in strength due to use of powerful vibrating equipment, decrease in strength due to different kinds of parasitical stresses within the pipes, varying strength due to development of stable harmonic waves during the vibration, different strength in different directions due to orthotropic properties of the material, experimental errors, systematic variability in geometry of pipes and in properties of the material, etc. These different explanations probably have, - more or less -, relevance to the real strength and fracture behaviour of unreinforced concrete pipes. However, according to

results presented in this Section, it seems that the basic assumption of linear elastic brittle behaviour of the material should be questioned before great efforts are made to develop and examine the different rather special supplementary possible explantions to the different deviations between practical experiences and the conventional theory.

Experimental investigations as well as design regulations have previously been concentrated on "crushing" (or "ring") failures, Fig 4.6 (1) a). Crushing is, however, only one of the possible types of failure and Brennan (1978) found that "bending" failures, Fig 4.6 (1) b), are more common than crushing failure in pipes of diameter less or equal to 300 mm. Experience has also proved that the "bending strength" is considerably less than the "crushing strength". Furthermore, for practical reasons of construction, it is desirable to use longer pipes and to lessen the requirements of the underground preparation. Because of these reasons, the importance of considering bending action has been increasingly realized in recent years.

The present investigation deals with crushing failure and bending failure. Theoretical relationships between failure load and basic material property parameters are established by means of four basically different assumptions with regard to tensile fracture behaviour of concrete: linear elastic brittle (Section 4.6.2), ideal plastic (Section 4.6.3), stochastic linear elastic brittle (Weibull-model, Section 4.6.4) and linear elastic fracture softening (fictitious crack model, Section 4.6.5). Sections 4.6. 6, 4.6.7 and 4.6.8 deal with some special topics: influence of initial stresses, effect of limitation in concrete compressive strength, and the effect of non-zero breadth of line load of crushing-loading. Experimental comparisons and some concluding remarks are found in Section 4.6.9. Formulas similar to those in Section 4.6.2, regarding fracture load calculations by assuming the linear elastic brittle behaviour of the material, may be found elsewhere, i.a. in (Wästlund and Eggwertz, 1949) and (Pettersson and Plem, 1975), but are reproduced in order to facilitate comparisons.

The four different models of the behaviour of material are illustrated in Fig 4.6 (2). The models are similar with regard to pre-fracture behaviour and to criterion of fracture: before fracture the concrete is assumed to behave in a linear elastic manner and fracture (or yielding) is assumed to arise when the first principle stress reaches the uniaxial tensile

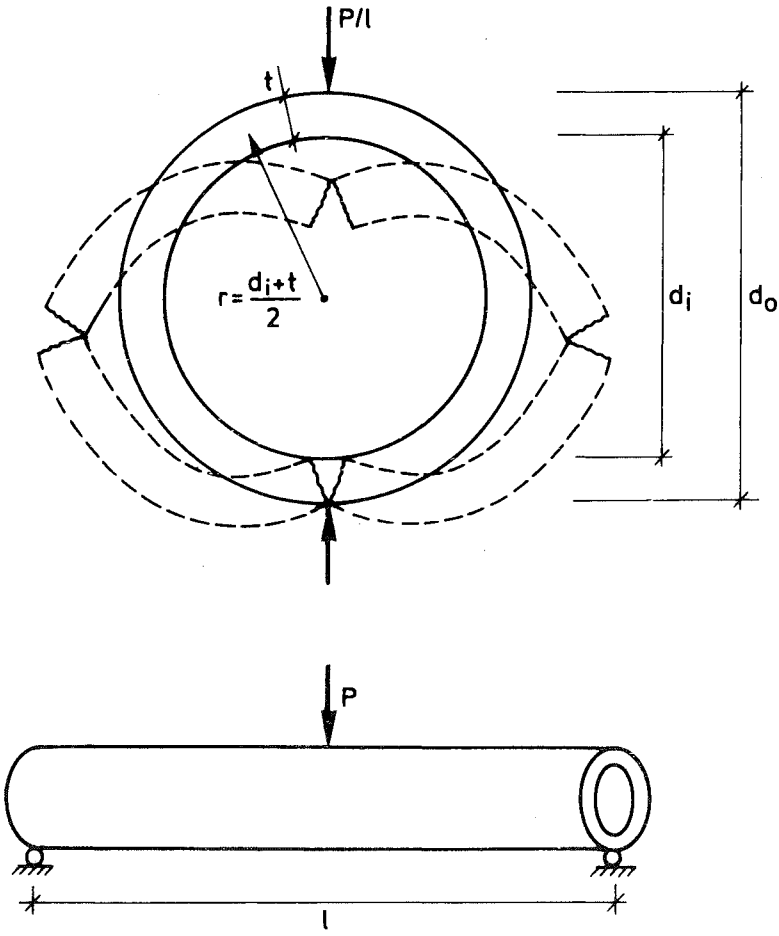

Fig 4.6 (1) a) Geometry of cross-section of pipe. Deflected form after crushing failure caused by line-load P/ℓ is indicated by the dotted figure.
b) Three point bending of a pipe.

strength of the concrete. Where the post-fracture behaviour of the material is concerned, the models are basically different, the behaviour being illustrated in Fig 4.6 (2) and briefly described in the introduction in the corresponding Sections. The models require knowledge of very few material property parameters in order to enable calculation of ultimate load: The first two models require knowledge of the uniaxial tensile

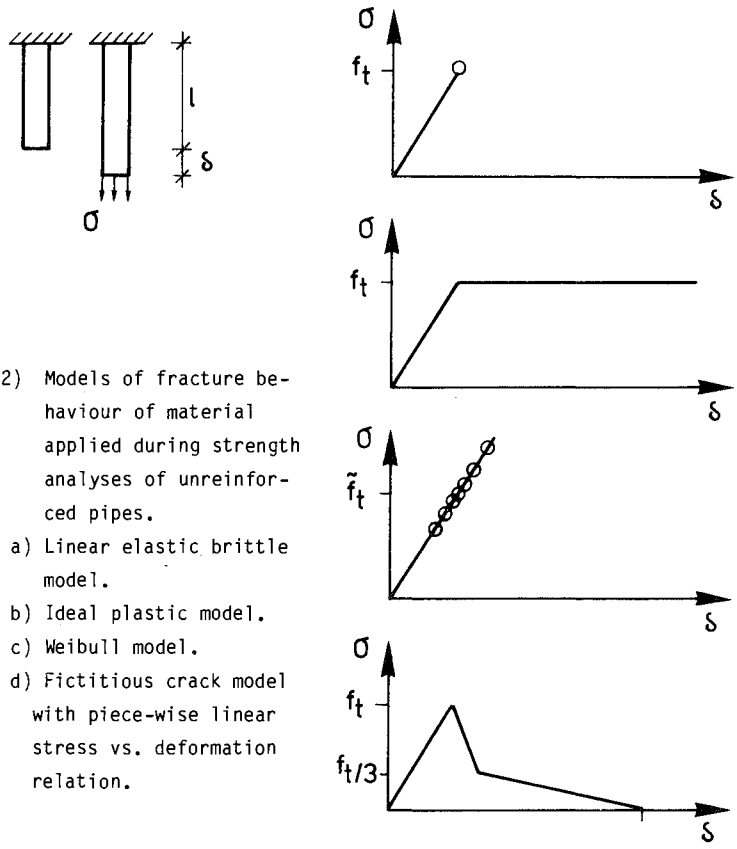

Fig 4.6 (2) Models of fracture behaviour of material applied during strength analyses of unreinforced pipes.
a) Linear elastic brittle model.
b) Ideal plastic model.
c) Weibull model.
d) Fictitious crack model with piece-wise linear stress vs. deformation relation.

strength, f_t. The Weibull-model requires knowledge of f_t and a measure of scatter in strength, m. The fictitious crack model requires knowledge of f_t and the characteristic length, ℓ_{ch}.

Geometrical parameters are defined in Fig 4.6 (1). The shape of cross sections of pipes is usually described by either of the following alternative ratios: t/d_i, d_i/d_o and r/t. Mapping between these ratios may be carried out by means of Fig 4.6 (3). During general discussions of concrete pipes ratio t/d_i is usually preferred, but this ratio has a tendency to yield lengthy analytical strength-formulas. In the present study ratio d_i/d_o is adopted during definition of the shape of a cross-section. Ratio r/t is sometimes more convenient to use during theoretical analyses of crushing.

		r/t	d_i/d_o	t/d_i
r/t	=	r/t	$\frac{1 + d_i/d_o}{2(1-d_i/d_o)}$	$\frac{1 + t/d_i}{2\ t/d_i}$
d_i/d_o	=	$\frac{2\ r/t - 1}{2\ r/t + 1}$	d_i/d_o	$\frac{1}{1 + 2\ t/d_i}$
t/d_i	=	$\frac{1}{2\ r/t - 1}$	$\frac{1 - d_i/d_o}{2\ d_i/d_o}$	t/d_i

Fig 4.6 (3) Transformations between different descriptions of shape of section of a pipe.

The terms "bending strength" and "crushing strength" (or "ring strength") are often used in descriptions and discussions about the strength of conrete pipes and before proceeding these terms ougth to be defined. Bending strength and crushing strength should not be considered material properties, but as an alternative descripton of the load carrying capacity of a pipe of a defined size and shape and at loading corresponding to bending failure and crushing failure, according to Fig 4.6 (1). In this case the notation f_f will be used for bending strength and the notation f_{cr} for crushing strength. f_f is defined by

$$f_f = \frac{M_u}{W} \quad , \qquad W = \frac{\pi}{32} d_o^3 (1 - (d_i/d_o)^4) \tag{4.6:1}$$

M_u is the bending moment at ultimate failure and W is the elastic flexural resistance of the cross section. (If the material behaves in a linear elastic brittle manner, then, according to the engineering beam theory, f_f coincides with the material property parameter f_t.) The crushing strength, f_{cr}, is defined by:

$$f_{cr} = \frac{6}{\pi} \frac{(P/\ell)_u}{d_o} \frac{(1 + d_i/d_o)}{(1 - d_i/d_o)^2} \tag{4.6:2}$$

$(P/\ell)_u$ is the line load at ultimate failure. (If the material behaves in a linear elastic brittle manner then, according to the beam theory of curved beams, f_{cr} coincides with f_t if the pipe is very thin-walled.)

The current study was initiated by a few fictitious crack analyses of the crushing failure, and has been encouraged by the building contractor

Skanska, as represented by civ. ing. Christer Isgren, who also proposed the analysis of bending failure and has contributed valuable information about design practice, manufacturing and practical experiences. The contents of Section 4.6 are fairly similar to those presented in Swedish in (Gustafsson, 1983). However, in this Section numerical results and methods of calculation are presented in a somewhat more detailed manner and the number of comparisons to experimental results reported in literature is significantly increased. Results from experimental tests carried out in cooperation with Skanska have been reported in short test-reports, put at the disposal of the actual building contractor. Of the experimental results obtained, those of interest for the current study are reproduced in Section 4.6.9. While only bending and crushing failures are being studied in this Section, it is appropiate to mention that other types of failures may sometimes become important, e.g. local punching failures at pipe connections, occurring as a result of heavy loads concentrated on a small region, and inclined tensile cracking through the cross-section, occuring as a result of combined action of shear force and bending moment. It is also appropiate to add that sufficient strength is only one of the requirements of a high quality sewage pipe. From the technical point of view, such a pipe should also be suitable for rational manufacturing and placing and fulfil demands made on tightness, stiffness and durability.

4.6.2 Linear elastic brittle model

The behaviour of concrete assumed in the linear elastic brittle model is illustrated in Fig 4.6 (2) a): before fracture a linear elastic behaviour is assumed, a fracture arises when the stress reaches f_t and takes place as a sudden drip in stress from f_t to zero. This fracture behaviour applies to each individual point of the material but, in currently investigated pipe geometries and types of loading, one may assume that fracture in one point, i.e. in the point exposed to the highest stress, immediately yields a fracture of the entire pipe. Thus the material strength concept of the linear elastic brittle model coincides with the structural stength concept of the same model. (This is not always the case: Where the crushing strength of certain pipes with a "foot" are concerned, Ingwersen (1982) has demonstrated that the structural strength concept predicts a lower ultimate load than the material strength concept. In general terms, the structural strength concept always predicts an ultimate failure load which is less or equal to the ultimate load as predicted by the material strength concept.)

According to the current model and assuming that the slenderness of the pipe is such that plane cross-sections remain plane during bending, the bending strength f_f, normalized with regard to the uniaxial tensile strength, f_t, becomes unity:

$$\frac{f_f}{f_t} = 1.0 \qquad (4.6:3)$$

The assumption of plane cross-section, i.e. the assumption of validity of the beam theory, is an approximation which simplifies numerical calculations very substantially. Isgren and Palmgren (1982) carried out 3D linear elastic finite element analyses of a concrete pipe with $d_i/\ell \approx 0.20$ and found that the distribution of bending stresses at mid-span of the pipe were almost linear through the depth of the pipe. (The pipe was uniformly loaded along its length and supported at its ends.)

As to crushing strength, formulas of the theory of curved beams, (Petersson and Plem, 1975), give:

$$\frac{f_{cr}}{f_t} = f(d_i/d_o) \qquad (4.6:4)$$

where $f(d_i/d_o) =$

$$= \frac{3d_i/d_o(1+d_i/d_o)}{(1-d_i/d_o)} \left\{ \frac{-(1+d_i/d_o)\ln(d_i/d_o)-2(1-d_i/d_o)}{(1-d_i/d_o)^2+d_i/d_o\{(1+d_i/d_o)\ln(d_i/d_o)+2(1-d_i/d_o)\}} \right\}$$

This expression is exact within the assumed theory, but is not very convenient to use. (Some numerical values of $f(d_i/d_o)$ can be found in Fig 4.6 (4).) An approximate simplification of (4.6:4) is found in (Wästlund and Eggwertz, 1949):

$$\frac{f_{cr}}{f_t} = \frac{3d_i/d_o}{1+2d_i/d_o} \qquad (4.6.5)$$

A further simplification often used is:

$$\frac{f_{cr}}{f_t} = 1.0 \qquad (4.6:6)$$

d_i/d_o	(4.6:4)	(4.6:5)	(4.6:6)
1.0	1.000	1.000	1.000
0.9	0.965	0.964	1.000
0.8	0.926	0.923	1.000
0.7	0.883	0.875	1.000
0.6	0.834	0.818	1.000
0.5	0.777	0.750	1.000

Fig 4.6 (4) Numerical values of f_{cr}/f_t according to the "exact" formula (4.6:4) and according to the approximate formulas (4.6:5) and (4.6:6).

(4.6:4), (4.6:5) and (4.6:6) are compared in Fig 4.6 (4). The comparison indicates that the deviation in (4.6:6) from the "exact" expression (4.6:4) is on the border of what could be called "engineering accuracy" for common values of d_i/d_o. Eq (4.6:4) is exact only in terms of the beam theory, while the true value of f_{cr}/f_t on the current assumption of fracture behaviour of the material and obtained by means of the plane stress theory instead of the beam theory, is probably somewhat higher than predicted by (4.6:4). In order to estimate a more accurate value than (4.6:4), comparison to the stresses in a short straight three point bend beam, (Timoshenko and Goodier, 1951), may be meaningful. A more accurate value may of course also be numerically obtained by means of plane stress or plane strain finite element analysis. The exact plane stress linear elastic brittle solution is believed to be nearest to eq (4.6:4) and in between eq (4.6:4) and eq (4.6:6). For common values of d_i/d_o the deviation between the beam theory and the plane stress theory is therefore estimated to be rather small, and subsequent comparisons to test results are carried out for both eq (4.6:4) and eq (4.6:6).

4.6.3 Ideal plastic model

The basic assumption of this model is that the stress, after the fracture criterion, $\sigma=f_t$, has been reached, is kept equal to f_t independent of how large the strain or deformations may become, Fig 4.6 (2) b). As to bending strength, equilibrium between external bending moment and internal bending stresses yield:

$$\frac{f_f}{f_t} = \frac{4(1-(d_i/d_o)^2)}{(1-(d_i/d_o)^4)} \qquad (4.6:7)$$

Where crushing strength is concerned, consideration of equilibrium between external load and internal stresses caused by bending moments and normal forces yield:

$$\frac{f_{cr}}{f_t} = \frac{6}{\pi} \frac{(1+d_i/d_o)}{d_i/d_o} \qquad (4.6:8)$$

The ideal plastic model predicts considerably higher failure loads than the linear elastic brittle model, especially at crushing. When $d_i/d_o=0.8$, for instance, the ideal plastic model predicts a 2.4 times higher bending strength and a 4.6 times higher crushing strength.

In the above application of the ideal plastic model no limitation is introduced to the compressive strength of the material. The effect of limited compressive strength may, however, be of importance as the compressive stress theoretically becomes infinitely high in the edges of the fracture surfaces. Therefore, influence of limited compressive strength will be dealt with in Section 4.6.7.

4.6.4 Stochastic linear elastic brittle model (Weibull-model)

The basic assumption of the Weibull-model is similar to at of the linear elastic brittle model, but the tensile strength is not assumed to be equal at all points of the material, Fig 4.6 (2) c). Instead the tensile strength at different points is described by means of a probabalistic density function, the density function of Weibull, and defined by the median of the tensile strength, $\tilde{f}_t$, and a measure of scatter, m. The density function of Weibull and the Weibull-method of stength analyses are dealt with in Section 3.4.4. In this Section formulas regarding bending and crushing strength of pipes obtained by means of the basic relations in 3.4.4 are presented. During the calculations, the stress distibutions within the pipes were obtained in accordance with the theory of straight and curved beams respectively.

A special feature of the current model, as compared to the other models,

is that the strength predictions do not yield a single deterministic value, but instead a probability density function. The coefficient of variation of this density function is directly defined by the parameter m, and used as input in the analyses. To further characterize the density function some kind of mean value should be defined, and one may use the median or the arithmetic mean as such a characterictis value. During Weibull-analyses the median is usually used as this value often enables analytical calculations. However, in the case of proportional loading (i.e. when the stress in different parts of the structure are proportional to each other all the time, which, at zero initial stress, is the case if the external loads are proportional to each other) one may alternatively use arithmetic means as the ratio between the mean and median has a certain value for each m independent of the type of (proportional) load and independent of the geometry of the structure, see Section 3.4.4. Presently the strenght will be characterized by arithmetic means, and with respect to ratios between strength in different types of (proportional) load and in different types of geometry of the structure it does not matter whether means or medians are used. Thus, for instance, $\bar{f}_f/\bar{f}_t = \tilde{f}_f/\tilde{f}_t$. Numerically obtained relations between m and coefficient of variation, between ratio mean/median and m respectively are shown in Fig 3.4 (5) and 3.4 (6).

The scatter in strength means that the strength of the pipes in bending is not only governed by the maximum bending moment along the pipe, but is dependent on the entire bending moment distribution. Accordingly the predicted bending strength depends on the type of loading: the predicted bending strength at three point bending should for instance be higher than at uniformly distributed load along the pipe. Denoting predicted mean value of bending strength by $\bar{f}_f$, the volume of concrete in the pipe by V_p, and the mean value of the tensile strength by $\bar{f}_t$, $\bar{f}_t$ having reference to tensile tests of specimens of volume V_o, then, by means of eq:s (3.4:9) and (3.4:10) the following result is obtained:

$$\frac{\bar{f}_f}{\bar{f}_t} = \left\{ \frac{V_o}{V_p} \right\}^{1/m} \left\{ h_1(d_i/d_o, m)\ h_2(m) \right\}^{1/m} \qquad (4.6:9)$$

where

$$h_1(d_i/d_o,m)=\begin{cases}\dfrac{(1-(d_i/d_o)^2)\ (m+2)\ 2^m\ (\frac{m}{2}\ !)^2}{(1-(d_i/d_o)^{m+2})\ (m\ !)} & \text{when } m = 2,4,6\ldots \\ \dfrac{(1-(d_i/d_o)^2)\ \pi\ (m+2)\ (m\ !)}{(1-(d_i/d_o)^{m+2})\ 2^m\ (\frac{m-1}{2}\ !)^2} & \text{when } m = 1,3,5\ldots\end{cases} \qquad (4.6{:}10)$$

and

$$h_2(m)=\begin{cases}1.0 & \text{at constant bending moment along pipe} \\ m+1 & \text{at three point bending, load at } \ell/2 \\ \dfrac{3(m+1)}{m+3} & \text{at four point bending, loads at } \ell/3 \\ \left[\dfrac{2^{2m+1}}{(2m+1)}\prod_{r=1}^{m}\left\{\dfrac{(m+1-r)}{(m+r)}\right\}-\dfrac{1}{(m+1)}\left\{1+\sum_{i=1}^{m}\left[\prod_{r=1}^{i}\left\{\dfrac{(m-r+1)}{(m+r+1)}\right\}\right]\right\}\right]^{-1} & \text{at uniformly distributed load along pipe:}\end{cases} \qquad (4.6{:}11)$$

The derivation on the formulas above is not presented in detail as the calculations are rather lenghty and do not comprise any fundamental difficulties. In the derivation one may utilize substitution of variables, Standard Mathematical Tables (Beyer, 1976) and, where the analysis of uniformly loaded pipes is concerned, repeated integration by parts. For convenience, some numerical values of $h_1^{1/m}$ and $h_2^{1/m}$ may be found in Fig 4.6 (5).

d_i/d_o	m=5	m=7	m=10	m=14	m=20	m=28
1.0	1.426	1.317	1.233	1.175	1.129	1.097
0.9	1.497	1.381	1.292	1.228	1.178	1.141
0.8	1.565	1.440	1.341	1.270	1.210	1.165
0.7	1.629	1.492	1.381	1.299	1.231	1.180
0.6	1.685	1.534	1.411	1.320	1.245	1.189
0.5	1.732	1.567	1.433	1.335	1.255	1.196

Type of load	m=5	m=7	m=10	m=14	m=20	m=28
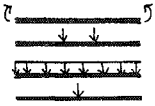	1.000	1.000	1.000	1.000	1.000	1.000
	1.176	1.133	1.098	1.072	1.052	1.038
	1.220	1.178	1.140	1.110	1.085	1.066
	1.431	1.346	1.271	1.213	1.164	1.128

Fig 4.6 (5) Some numerical values of $h_1^{1/m}$ (upper table) and $h_2^{1/m}$ (lower [illegible]) and eq (4.6:11).

Regarding crushing strength, it has not been thought possible to find any closed analytical expression. Firstly the stress field within the pipe is rather complex, secondly the volume of integration, i.e. the part of the pipe where the stress is greater than zero, has not an uncomplicated shape. Instead the crushing strength was obtained by means of numerical calculations:

$$\frac{\bar{f}_{cr}}{\bar{f}_t} = f(d_i/d_o) \left\{ \frac{V_o}{V_p} \right\}^{1/m} \gamma^{1/m} \qquad (4.6:12)$$

The function $f(d_i/d_o)$ is defined in eq (4.6:4) and some values of $\gamma^{1/m}$ at different m and d_i/d_o may be found in Fig 4.6 (6).

$\gamma^{1/m}$

d_i/d_o	m=5	m=7	m=10	m=14	m=20	m=28
1.0	2.767	2.298	1.934	1.687	1.501	1.377
0.9	2.801	2.327	1.954	1.701	1.511	1.384
0.8	2.840	2.362	1.978	1.718	1.522	1.392
0.7	2.888	2.404	2.009	1.738	1.537	1.402
0.6	2.948	2.458	2.047	1.764	1.555	1.416
0.5	3.030	2.530	2.097	1.798	1.578	1.433

Fig 4.6 (6) Numerically obtained values of the term $\gamma^{1/m}$ in eq (4.6.12) at different values of d_i/d_o and m.

The most essential difference between the Weibull-model predictions of strength as compared to prediction by the two previous models is naturally that the strength is predicted to depend on the size of the pipe, not only on its geometrical shape. From Figures 4.6 (5) and 4.6 (6) it is evident that $\bar{f}_f/\bar{f}_t$ and $\bar{f}_{cr}/\bar{f}_t$ increase at increased scatter in strength, i.e. at decreased m. Of course this does not mean that scatter is desirable, only that the ratio between median strength of pipes and median tensile strength at uniform tensile stress increases at increased scatter. Furthermore, a large scatter requires a larger safety-factor. From Figures 4.6 (5) and 4.6 (6) it is also evident that both $\bar{f}_f$ and $\bar{f}_{cr}$ increase at decreasing ratio d_i/d_o, that $\bar{f}_f$ and $\bar{f}_{cr}$ is of about the same magnitude and that $\bar{f}_f$ is predicted to be noticeably dependent on the type of load.

4.6.5 Linear elastic fracture softening model (fictitious crack model)

The fictitious crack model has been described in Section 3.2.2. In the current analyses of concrete pipes the bi-linear concrete-imitating shape, see Fig 3.2 (3) c), of the stress-elongation curve of the fracture zone is adopted. Furthermore, the stress vs. strain relation is assumed to be linear elastic. In contradiction to the calculations previously dealt with during the study of pipes, the calculations may now not be simplified by the aid of the conventional plane-cross-sections-remain-plane assumption, and thus the beam theory may not be used by itself. Instead the numerical calculations are simplified by the assumption of plane stress (ν=0.2) and carried out by means of the finite element method. In the case of crushing failure analysis, a combination of plane stress theory and beam theory is used in order to reduce the numerical work. Although there is more computational work in the fictitious crack analysis than in the other types of analysis, the results, once obtained, are no more complicated to use than those from the other models.

The bending failure analyses of pipes is carried out in a similar manner to the bending failure analyses of beams with rectangular cross-section, see 4.2. However, in the analyses of pipes the width is not assumed to be uniform along the depth of the pipes but is assigned variations in the manner exemplified in Fig 4.6 (7). The type of loading studied is shown in Fig 4.6 (1) b). Regarding short deep pipes, it is probably that the ultimate bending moment, as predicted during the current type of analysis, is to some extent dependent on the type of loading causing the bending of the pipe. But if the slenderness of the pipe is such that the risk of bending failure becomes of practical importance then presumably, the influence of the type of load on the ultimate bending moment is predicted to be of minor importance. In the current analyses pipes of the slenderness ratio ℓ/d_o = 4.0 is assumed, d_i/d_o is varied from 0.400 to 0.909 and the size of the pipes, as normalized with respect to the characteristic length of the material, varies from d_i/ℓ_{ch} = 0.0625 to 0.8. The symmetrical half of the pipe is devided into 40 finite elements along its depth and 30 elements along its length, the element mesh along the length of the pipe being finer close to the fracture zone propagation path than close to the supports of the pipe. The type of element used is the rectangular 4-node non-conformal plate element of Turner and Clough.

The ultimate b[illegible] moments as obtained in the incremental finite element

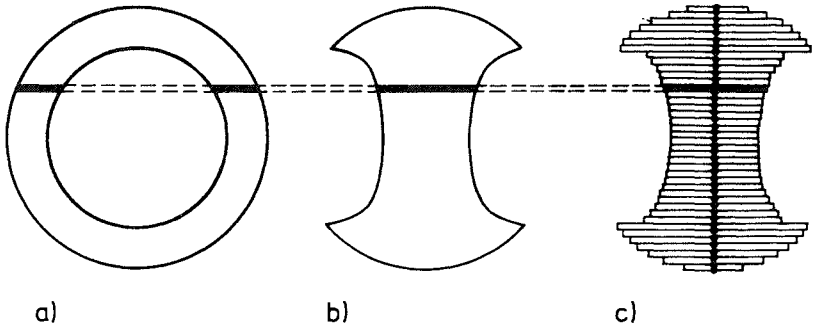

Fig 4.6 (7) a) Cross-section of pipe. b) "Equivalent" cross-section of beam. c) Cross-section of finite element mesh. Width of element are such that shaded areas are of equal size. The size of fracture elements corresponding to the nodal points were made equal to mean of the cross-section areas of the adjoining plate elements.

analyses are presented numerically in Fig 4.6 (8). The value of f_f/f_t at the limit $d_i/\ell_{ch} \to 0$ is obtained by means of eq (4.6:7). The value of f_f/f_t at the limit $d_i/\ell_{ch} \to \infty$ is obtained from the pre-fracture stress in the lower edge of the pipe as calculated in the current finite element analyses. If incremental finite element analyses were carried out at the limit $d_i/\ell_{ch} \to 0$ the same results as those in (4.6:7) should be obtained. In the limit $d_i/\ell_{ch} \to \infty$, (4.6.3) predicts $f_f/f_t = 1.00$ and the deviation as compared to the results of Fig 4.6 (8) is a result of limited slenderness of the pipe and the deviation is obtained due to different types of simplifications utilized during the numerical calculations: beam theory and plane stress analysis by means of finite elements respectively. The latter is probably more accurate than the beam theory. The values of f_f/f_t at $d_i/\ell_{ch} = 8.0$ are not believed to be very accurate due to the present choice of finite element mesh.

The results in Fig 4.6 (8) are in agreement with the general hypotheses in Section 3.5.3: The currently predicted ultimate strengths are in between those of the linear elastic brittle model, eq (4.6:3), and those of the ideal plastic model, eq (4.6:7), and the strength is predicted to decrease with increasing size of the pipes, the decrease not being faster than as stated by hypothesis IV. The decrease in strength during increase in size is somewhat suprisingly uniform, taking the rather large variations in the

d_i/ℓ_{ch}	d_i/d_o= 0.9091	0.8333	0.6667	0.5556	0.4000
→ 0	2.190	2.361	2.769	3.057	3.448
0.0625	1.604	1.657	1.773	1.840	1.894
0.125	1.479	1.525	1.622	1.675	1.703
0.250	1.358	1.399	1.482	1.520	1.520
0.50	1.254	1.292	1.359	1.378	1.342
1.00	1.179	1.211	1.252	1.243	1.205
2.00	1.131	1.150	1.156	1.138	1.114
4.00	1.093	1.102	1.085	1.070	1.062
8.00	1.063	1.053	1.036	1.041	1.053
→ ∞	1.033	1.023	1.019	1.024	1.035

Fig 4.6 (8) Bending strength, f_f/f_t, of concrete pipes of different shape, d_i/d_o and size, d_i/ℓ_{ch}, as calculated by means of the fictitious crack model.

width of the cross section along the depth of the pipes into account and bearing in mind that the depth of the fracture zone at ultimate load is dependent on the size of the pipe.

Practical utilization of Fig 4.6 (8) may perhaps not be very convenient as it is usually necessary to carry out interpolations with regard to both d_i/ℓ_{ch} and d_i/d_o. During designing d_i is normally chosen in advance and the wall-thickness, t, has to be calculated. In Fig 4.6 (9) f_f/f_t vs. t for some different common values of d_i is shown. The absolute values of t and d_i in this Figure are valid when ℓ_{ch}=380 mm, where the value of ℓ_{ch} may be considered to be typical of a normal concrete used in pipe manufacturing. Fig 4.6 (9) may of course also be used for other values of ℓ_{ch} than 380 mm provided that the values of t and d_i are altered in such a manner that the ratios t/ℓ_{ch} and d_i/ℓ_{ch} are kept constant. Numerical interpolation in Fig 4.6 (8) may be carried out by using differnt methods. The curves in Fig 4.6 (9) were obtained from Fig 4.6 (8) in the following manner: First cubic spline functions without end restrictions were developed for the discrete values of d_i/ℓ_{ch} with d_i/d_o as variable, then linear interpolations were carried out with $\ell n(d_i/\ell_{ch})$ as the variable.

We now turn to the analyses of the crushing strength. If a high degree of accuracy is required even when d_i/d_o is small, i.e. when the pipe is thick-walled, the cross section of the pipe should be modelled as a plate, Fig 4.6 (10) a). However, while the growth of two fracture zones has to be considered and ent values of

shapes and sizes of the pipes, this type of modelling would lead to a substantial amount of numerical work. As an alternative approach, a quarter of the cross-section was modelled by one curved beam element and two moment springs, Fig 4.6 (10) b). This approach drastically reduces the number of degrees of freedom involved in the analyses and is made possible by the fracture hinge moment rotation relations from Section 4.2.3.

General expressions of the linear elastic stiffness properties of curved beams are provided by Martin (1966). Where the curved beam element in Fig 4.6 (10) b) is concerned, numerical evaluation of these analytical expressions yields:

$$\begin{bmatrix} P_1 \\ Q_1 \\ M_1 \\ P_2 \\ Q_2 \\ M_2 \end{bmatrix} = \frac{E\ell}{12}\left\{\frac{2(1-d_i/d_o)}{(1+d_i/d_o)}\right\}^3 \underline{k} \begin{bmatrix} u_1 \\ v_1 \\ \Theta_1 \\ u_2 \\ v_2 \\ \Theta_2 \end{bmatrix} \qquad (4.6:13)$$

where $\underline{k} = \underline{k}^t$ and

$k_{11} = k_{22} = k_{44} = k_{55} = k_{15} = -k_{24} = 42.875\ 030\ 900\ 349$

$k_{12} = k_{25} = -k_{14} = -k_{45} = 39.371\ 154\ 112\ 581$

$k_{13} = k_{35} = k_{46} = -k_{26} = 9.484\ 516\ 680\ 684\ (d_i+t)/2$

$k_{23} = -k_{16} = -k_{34} = -k_{56} = 12.988\ 393\ 468\ 453\ (d_i+t)/2$

$k_{33} = k_{66} = 5.458\ 802\ 035\ 264\ ((d_i+t)/2)^2$

$-k_{36} = 1.954\ 925\ 247\ 496\ ((d_i+t)/2)^2$

A similar numerical stiffness matrix as that in eq (4.6:13) is provided by Martin, but was not found to be sufficiently accurate. Naturally, the high degree of accuracy does not correspond to the accuracy to which properties of materials is known, but is desirable within the numerical calculations since the global incremental stiffness shows very large variations during fracture (i.e. variations from positive to negative values) and since a high accuracy makes it meaningful to check the equilibrium after each increment in external load. The boundary conditions, i.e. the conditions of symmetry, are introduced by omitting the rows and columns corresponding to u_1 and u_2 and accordingly the 6 by 6 matrix is reduced to a 4 by 4 matrix.

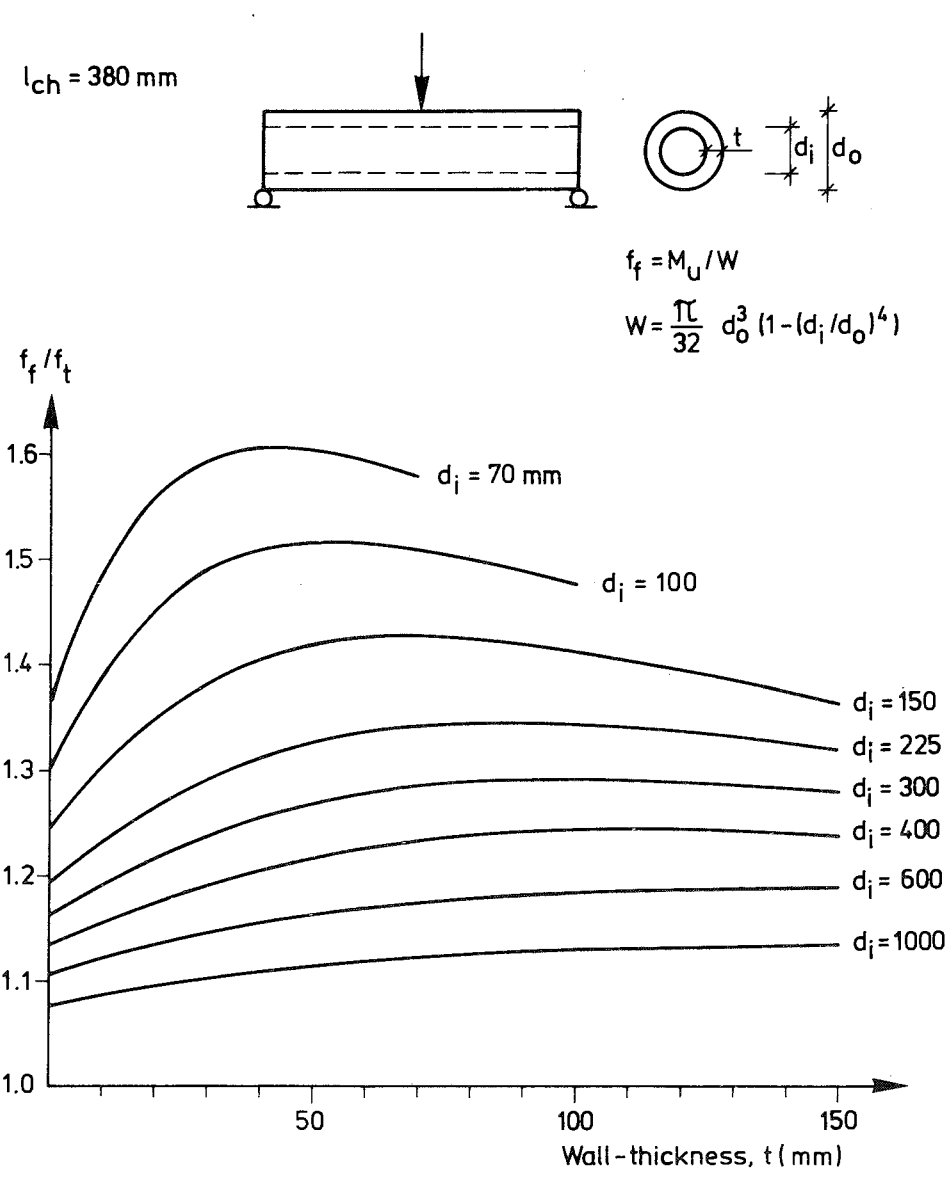

Fig 4.6 (9) Bending strength, f_f/f_t, of concrete pipes vs. wall-thickness, t, for different inner diameters, d_i, as obtained by the fictitious crack analysis. The diagram is valid for ℓ_{ch}=380 mm.

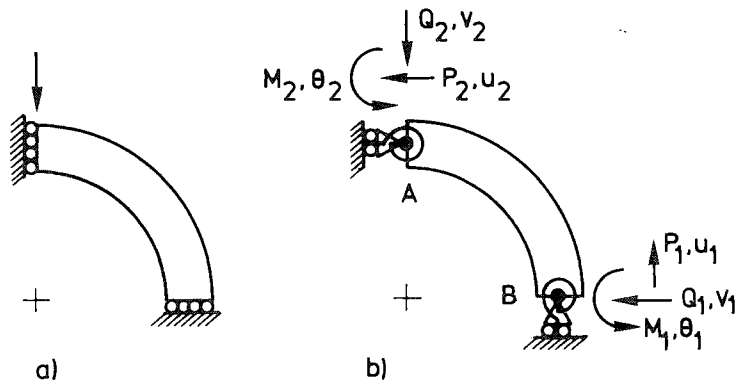

Fig 4.6 (10) Symmetrical quarter of cross-section of a pipe modelled as a plate, a), as a curved beam, b), respectively.

The hinge moment-rotation relations in Section 4.2.3 are valid for straight beams and at zero net compressive force across the section of fracture zone growth. Regarding the analyses of crushing strength this means that these moment-rotation relations apply strictly only in the limit $d_i/d_o \to 1.0$, while when $d_i/d_o < 1.0$ curvature of the beam has an influence on the stress distribution in the fracture sections and, furthermore, non-zero net compressive forces arise in two of the four fracture zones. In order to compensate ultimate crushing strengths calculated at $d_i/d_o < 1.0$ for these two approximations, knowledge of the fictitous crack predictions of f_{cr}/f_t at the limits $t/\ell_{ch} \to \infty$ and $t/\ell_{ch} \to 0$ both at analysis with and without considerating the curvature of the beam is utilized. Curvature of the beam taken into account, f_{cr}/f_t is provided by (4.6:4) respectively (4.6:8) at the limits $t/\ell_{ch} \to \infty$ respectively $\to 0$. Curvature of the beam not taken into account, i.e. the two approximations not compensated for, i.e. for $d_i/d_o = 1.0$, (4.6:4) gives $f_{cr}/f_t = 1.0$ for the limit $t/\ell_{ch} \to \infty$ and (4.6:8) gives $f_{cr}/f_t = 12/\pi$ for the limit $t/\ell_{ch} \to 0$. Knowing the influence of curvature in the limits of t/ℓ_{ch} the approximations during calculation of f_{cr}/f_t are compensated for by interpolation in such a manner, that A/B=C/D: see Fig 4.6 (11). To exemplify the magnitude of this compensation: at $t/\ell_{ch} = 0.40$ f_{cr}/f_t is increased by 0 %, 2 % and 7 % at $d_i/d_o = 1.0$, 0.8 and 0.6, and at $t/\ell_{ch} = 0.10$ by 0 %, 6 % and 20 % at the same values of d_i/d_o.

As discussed above, the special cases $t/\ell_{ch} \to \infty$ and $t/\ell_{ch} \to 0$ should not require incremental numerical calculations in order to determine the fictitious crac which does not

require numerical calculations is that of an arbitrary fixed non-zero value of t/ℓ_{ch} and $d_i/d_o \to 1.0$. In this case the stiffness of the curved beam element approaches zero and accordingly the magnitude of rotation of the moment-springs is negligible in comparison to the magnitude of deformation of ~~the bending moment distribution along~~ the curved beam element ~~independent of the (small) rotations of the moment springs~~ and accordingly the ratio M_2/M_1 is bound to be constant during the entire course of fracture. Ratio M_2/M_1 is governed by the linear elastic properties of the curved beam element and is equal to $2/(\pi-2)$. Knowing M_2/M_1, an equation of equilibrium yields:

$$\frac{f_{cr}}{f_t} = \frac{M_u}{M_o} \qquad \text{when} \quad d_i/d_o \to 1.00 \tag{4.6:14}$$

M_u is the ultimate bending capacity and M_o is the bending moment at the start of fracture zone development. The ratio M_u/M_o depends on t/ℓ_{ch} and may be obtained from Section 4.2.2 or 4.2.3.

The limit $d_i/d_o \to 1.0$ is a geometrical limit, but may alternatively be looked upon as a lower limit of the stiffness of the beam element. The opposite limit, that of an infinitely stiff beam element, corresponds to the geometrically completely absurd case $d_i/d_o \to -1.0$. This case is of course impossible in reality, but is of interest as a theoretical limit. If the beam is infinitely stiff then $\theta_1 = \theta_2$ and accordingly $M_2/M_1 = 1.0$, which yields:

$$\frac{f_{cr}}{f_t} = \frac{4}{\pi}\frac{M_u}{M_o} \qquad \text{when} \quad d_i/d_o \to -1.00 \tag{4.6:15}$$

In (4.6:15) the influence of normal force across the fracture hinges is not taken into account nor is the influence of deviation between the stress distribution of a straight and a curved beam taken into account. However, if these two approximations, previously dealt with, are adopted, then, for any non-zero constant value of t/ℓ_{ch}, (4.6:14) forms a lower limit of f_{cr}/f_t while (4.6:15) forms an upper limit of f_{cr}/f_t. An example of f_{cr}/f_t vs. d_i/d_o at a constant value of t/ℓ_{ch} and before and after compensation for the two approximations may be found in Fig 4.6 (11). The limits of f_{cr}/f_t given by eq (4.6:14) and eq (4.6:15) may be useful when checking numerical calculations and making approximate estimations. As a matter of principle it may be noted that the distribution of bending moments within the structure is independent of the properties of [illegible] structures is

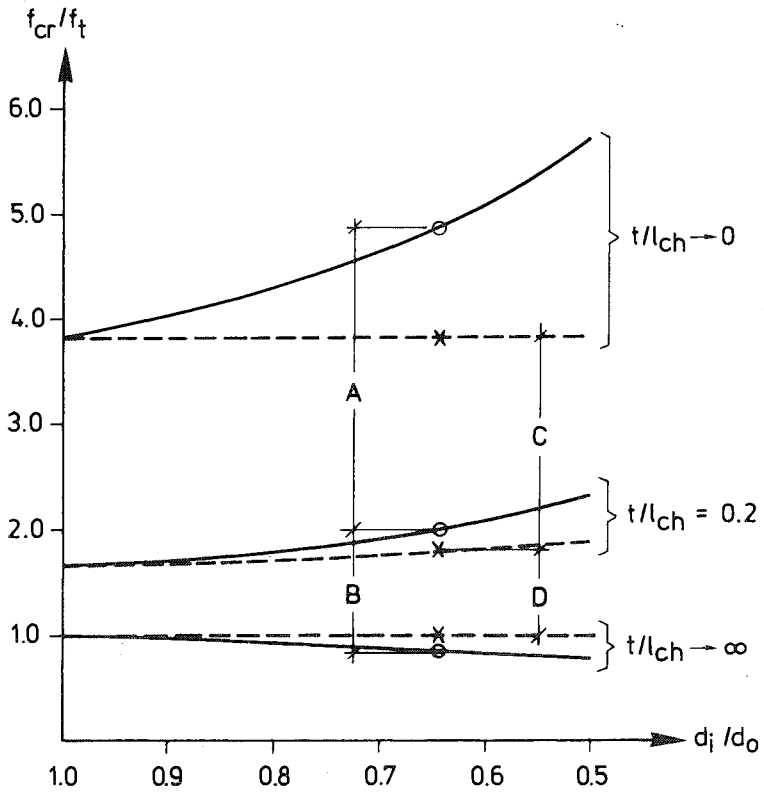

Fig 4.6 (11) Example (d_i/d_o=0.647, t/ℓ_{ch}=0.2), which illustrates method used to compensate for approximations during calculation of f_{cr}/f_t. x = value when influence of curvature of beams is not considered, o = value when curvature is taken into account. A/B=C/D.

very small (progressive collapse), while the distribution of the displacements of the structure (the kinematical fracture behaviour) is independent of the properties of the fracture hinges when the stiffness of the structure is very great. The matter of upper and lower boundaries of strength during fictitious crack analyses of statically indeterminate beams is also dealt with in Section 4.2.5.

Before proceeding to the numerical results of f_{cr}/f_t at different intermediate values of t/ℓ_{ch} and d_i/d_o, i.e. at values in between the

extreme limits dealt with above, a few things concerning the computational method should be discussed. The fracture hinge moment-rotation springs are on the whole non-linear, but as a result of the method used during determination of their properties, Section 4.2.3, defined by a large number of piece by piece linear relations and accordingly in the incremental sense are exactly linear. In order to carry out the numerical calculations a small special-purpose finite element program was developed. The incrementally linear type of stiffness properties facilitates the development of such a program, the size of each increment in external load and deflection being defined by the incremental global stiffness and by the limits of the linear pieces of the moment-rotation relations. In this type of direct incremental analysis equilibrium is always maintained exactly (within the limits of the numerical precision, i.e. the number of digits, chosen to be used for the calculations), while other types of non-linear analysis may yield numerical errors due to too large increments or due to too few iterations.

The adopted method of numerical calculation is thus comparatively simple and reliable, but three interesting difficulties did, however, arise during the calculations. Two of these have been briefly discussed in Section 4.3 and have to do with the determination of the correct sign of the external deflection increment and with possible numerical errors in the size of the increment when the incremental stiffness of the structure is close to zero. The third difficulty is due to structural interaction between the two fracture softening hinges. This interaction seems to be rather complicated and may cause sudden and temporary negative rotations (unloading) in any of the fracture hinges during the course of structural breakdown. The possibility of the occurrence of this type of behaviour may be exemplified in a simple manner by considerating the limiting case $d_i/d_o \rightarrow 1.0$. In this case M_2/M_1 is constant during the course of collapse and accordingly θ_1 has to start to decrease (unloading) when θ_2 increases beyond the point of ultimate bending capacity (softening).

In the currently presented analyses the moment vs. rotation behaviour at unloading was assumed in accordance with Fig 4.6 (12), which also shows the corresponding assumption regarding the unloading behaviour of the fracture zone and the elastic surroundings of the fracture zone. Fig 4.6 (12) apparently illustrates different stiffness in an infinitely small negative increment during rotation and in an infinitely small positive increment during rotation respectively. The fundamental difficulty of such

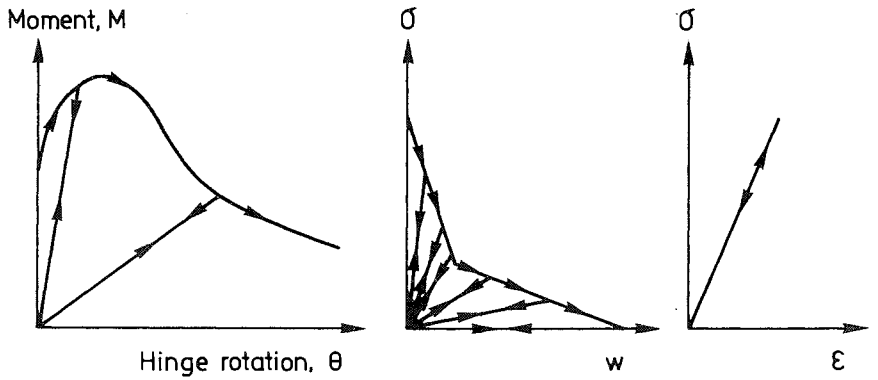

Fig 4.5 (12) Assumed behaviour of fracture hinges at unloading, i.e. decreasing θ, (two examples), and the corresponding behaviour within the fracture zone (σ-w diagram) an in the surroundings of the fracture zone (σ-ε diagram).

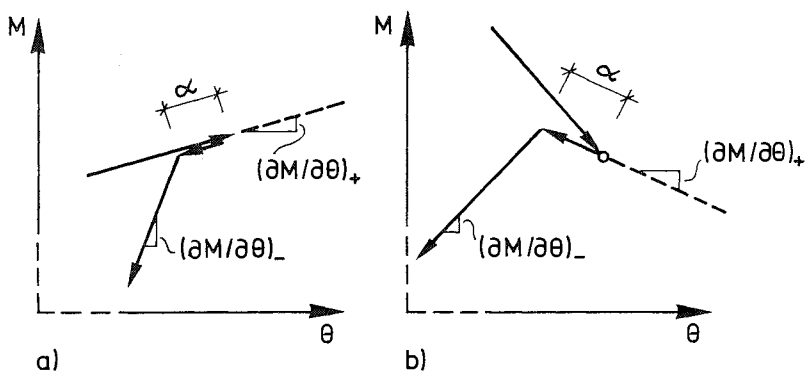

Fig 4.6 (13) Greatly enlarged details of Fig 4.6 (12) illustrating assumed behaviour of material of transition from loading to unloading. α is very small but greater than zero.
a) Transition at the ascending branch of the M-θ curve.
b) Transition at the descending branch of the M-θ curve and immediately after an incremental change in stiffness.

an assumption is, however, that the derivate $\partial M/\partial\theta$ would not exist. Fig 4.6 (13) a) shows an enlargement of Fig 4.6 (12) and illustrates more closely the assumed behaviour of transition from loading to unloading:

derivate $\partial M/\partial\theta$ is assumed to be equal at an infinitely small positive respectively negative increment, but the derivates $(\partial M/\partial\theta)_+$ and $(\partial M/\partial\theta)_-$, which indicate the slope of the M-θ curve after a very "small" positive respectively negative incremental rotation, are not equal. In applied numerical calculations the "small" increment is set equal to zero and the assumption in Fig 4.6 (13) may thus perhaps be considered as a theoretical subtlety, but is of practical importance as it makes calculations possible and as futhermore it means that $(\partial M/\partial\theta)_+$, and not $(\partial M/\partial\theta)_-$ nor any other value, is decisive with respect to occurance of start of unloading. The principle in Fig 4.6 (13) a) is adopted consistently and Fig 4.6 (13) b) shows an additonal example with respect to the assumed behaviour of the material during transition from loading to unloading: in this example transition from loading to unloading occurs at the descending branch of the M-θ curve and immediately after (and as a result of) an incremental change in stiffness of the same hinge that subsequently exhibits unloading. Regarding return from the unloading branch to the loading branch, no special assumption has to be made as this transition does not involve any change in sign of rotation.

During the applied calculations, possible transition from loading to unloading was dealt with in the following manner: if at any instant an incremental rotation turns negative (this can only happen immediately after an incremental change in stiffness of either of the two fracture hinges) then the absolute size of the increment in external displacement is set equal to a "small" value and then a new increment is made with the stiffness of the spring that exhibit unloading set equal to $(\partial M/\partial\theta)_-$. The "small" increment is in reality set equal to zero, simply by not adding the increment in load and deflection etc. to the previously accumulated values. Although the size of the increment in practice may be set equal to zero, the corresponding calculation has to be carried through as information concerning the incremental global stiffness is required in order to determine the sign of subsequent increments (eq (3.6:1)) and as, of course, the transition from loading to unloading may not be precasted but is detected first when the current incremental calculation is carried out. The present computational approach has not yet been found to fail to work in a satisfactory manner during any applied calculation. A basic requirement of the approach to work is that if θ starts to decrease when the stiffness of the corresponding fracture hinge is $(\partial M/\partial\theta)_+$ then θ must also decrease when the stiffness is $(\partial M/\partial\theta)_-$, all other properties of the structure are kept constant. A hypothesis emanating from consideration of

this basic requirement but not proved to be true, is that the current computational approach will always work if $(\partial M/\partial\theta)_+ \leq (\partial M/\partial\theta)_-$. In the opposite case, $(\partial M/\partial\theta)_+ > (\partial M/\partial\theta)_-$, which seems unrealistic for concrete and most other engineering materials, situations may occur during which the computational increments may turn out to become an infinite series of altering positive and negative "small" increments. Such oscillatory behaviour may thus occur if, for instance, the apparently simple assumption of equal M-θ curve at loading and unloading is adopted, as in the last part of the M-θ curve, normally $(\partial M/\partial\theta)_+ > (\partial M/\partial\theta)_-$ (both derivates being less than zero).

The interation between the two fracture hinges is illustrated in Fig 4.6 (14), which shows an example of the global load vs. deflection response and the moment-rotation responses at some different corresponding points of "time" during the course of crushing fracture of a concrete pipe as obtained in a computational analysis. The example is valid when $t/\ell_{ch}=0.025$ and $d_i/d_o=0.980$. These values are unrealistic for normal concrete pipes, but are chosen in order to provide an illustrated example. The non-linear scale of the rotation axes in the Figure should be observed.

In addition to interaction between the two fracture hinges, Fig 4.6 (14) also illustrates that an almost linear load vs. deflection response up to ultimate load does not prove that the material may approximately be regarded to behave in a linear elastic brittle manner. If the material actually did behave in a linear elastic brittle manner then the ultimate load, σ_u/f_t, would be 1.0, i.e. less than half of the current ultimate load, 2.15. In more general terms this exemplifies that the local behaviour of the material within a small part of a structure may have great influence on the ultimate load carrying capacity of the entire structure, even if the local behaviour has very little influence on the global stiffness.

Regarding the calculation of crushing strength of concrete pipes, the modelling and the consideration of the unloading behaviour of the fracture hinges proved to be of minor practical importance as the fracture hinges in concrete pipes of normal geometry proved not to unload (but soften) before $\partial Q_2/\partial v_2=0$ and as this first maximum point also proved to represent the global maximum point of the load vs. deflection response of concrete pipes of normal geometry. In spite of this, the study of the unloading-

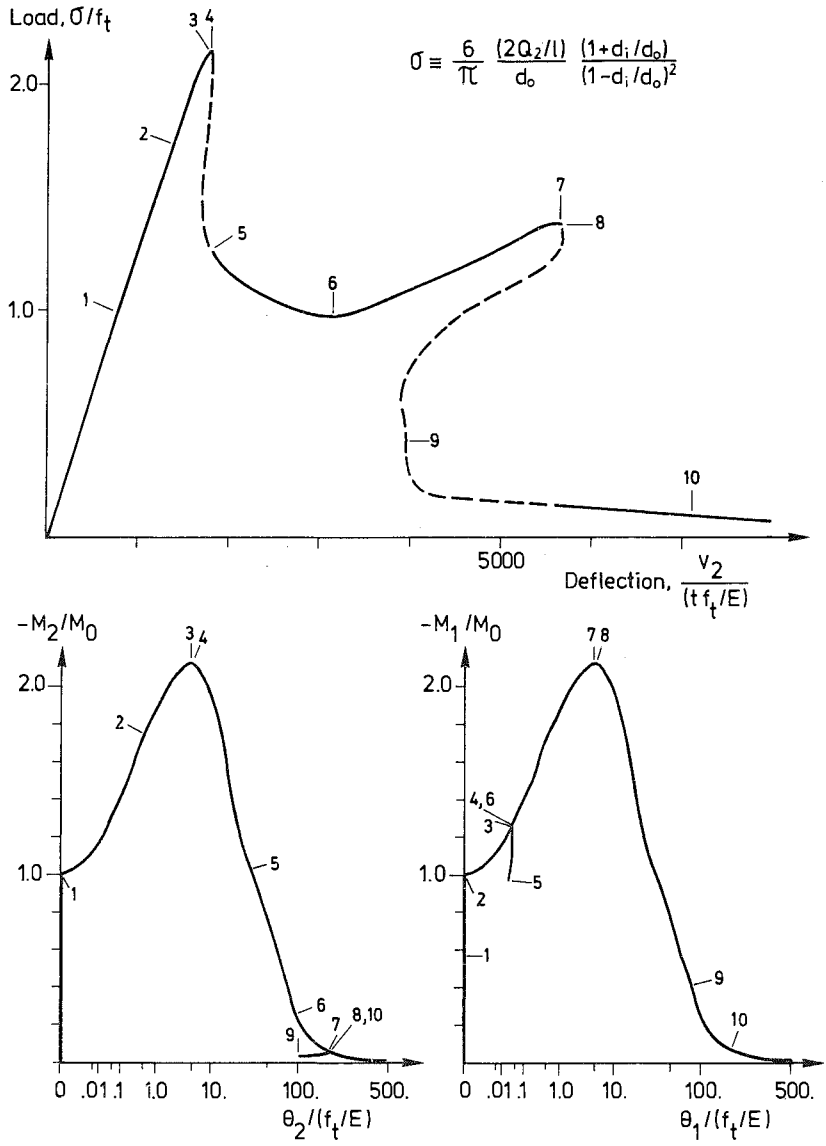

Fig 4.6 (14) Example (t/ℓ_{ch} =0.025, d_i/d_o =0.980) of computational results regarding crushing collapse behaviour of a pipe: load vs. deflection and bending moment in fracture hinges vs. rotation. Numbers 1-10 indicate simultaneous events. Notations acc. to Fig 4.6 (10). Non-linear scale of the rotation-axes ($\sim\theta^{0.2}$).

softening iteraction between the fracture hinges has been estimated to be of some interest, partly because it might be of some interest to be able to study not only the ultimate load but also the post ultimate behaviour of the structure, and partly because the method of analysis might be of some interest where other types of structures are concerned, for instance different types of statically non-determinate beams with or without reinforcement.

t/ℓ_{ch}	d_i/d_o = →1.0	0.9990	0.8947	0.7778	0.6471	0.5000
→ 0	Not def.	3.822	4.044	4.365	4.862	5.730
0.025	2.115	2.252	2.548	3.006	3.425	4.012
0.050	1.944	2.070	2.250	2.562	2.995	3.549
0.100	1.759	1.873	1.979	2.159	2.477	2.989
0.200	1.570	1.672	1.727	1.821	1.992	2.342
0.800	1.239	1.318	1.315	1.318	1.333	1.382
1.600	1.126	1.198	1.181	1.163	1.145	1.137
3.200	1.058	1.126	1.101	1.071	1.037	0.999
→ ∞	1.000	1.000	0.963	0.917	0.858	0.777

Fig 4.6 (15) Crushing strength, f_{cr}/f_t, of concrete pipes at different t/ℓ_{ch} (size) and d_i/d_o (shape) as calculated by means of the fictitious crack model.

The crushing strength, f_{cr}/f_t, of unreinforced concrete pipes at different values of t/ℓ_{ch} and d_i/d_o as obtained by means of the fictitious crack description of the behaviour of the material is presented in Fig 4.6 (15). f_{cr}/f_t at intermediate values of t/ℓ_{ch} and d_i/d_o have been obtained by means of the incremental calculations, while f_{cr}/f_t at the extreme limits has been obtained in accordance with (4.5:4), (4.6:8) and (4.6:14). Compensation (illustrated in Fig 4.6 (11)), for the approximations during the calculations are included in Fig 4.6 (15). f_{cr}/f_t in the limit point $t/\ell_{ch} \to 0$, $d_i/d_o \to 1.0$ is not defined while $f_{cr}=3.82$ when $t/\ell_{ch} \to 0$ and d_i/d_o is fixed to some constant value very close to 1.0 and while $f_{cr}/f_t=3.0$ when $d_i/d_o \to 1.0$ and t/ℓ_{ch} is fixed to some constant value very close to zero.

Fig 4.6 (15) indicates that the crushing strength decreases at increased size of the pipe, and that, for normal values of t/ℓ_{ch}, the crushing strength increases at decreasing d_i/d_o (which result contradicts the conventional theory). The computational results suggest also that the crushing strengt tensile strength

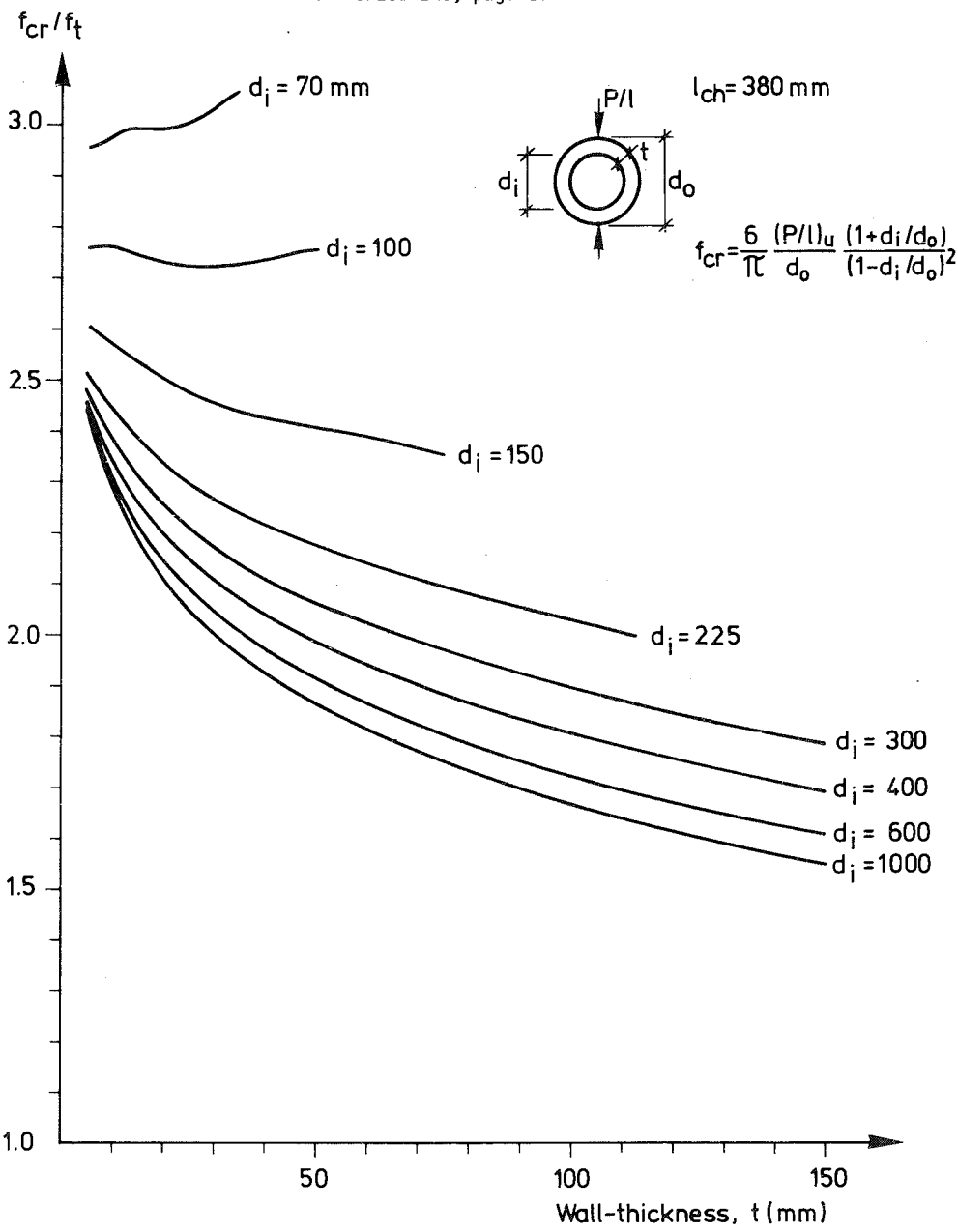

Fig 4.6 (16) Crushing strength, f_{cr}/f_t, vs. wall-thickness, t, for concrete pipes of different inner diameter, d_i, as obtained by [illegible] lid for l_{ch}=380 mm.

and also considerably higher than the bending strength, Figs 4.6 (8) and 4.6 (9).

With regard to influence of material properties, f_{cr} is predicted to increase about 50 % if the tensile strength is doubled at constant E and G_F. f_{cr} is predicted to increase about 15 % if the modulus of elasticity or the fracture energy is doubled at constant f_t. These values only being examples of typical approximate values with practically common values of t/ℓ_{ch} and d_i/d_o.

In Fig 4.6 (16) the results from Fig 4.6 (15) are presented as f_{cr}/f_t vs. t for some different values of d_i. Fig 4.6 (16) is valid for ℓ_{ch}=380 mm, but may also be used for other values of ℓ_{ch} if the absolute values of t and d_i are altered so that t/ℓ_{ch} and d_i/ℓ_{ch} are kept constant. The results from Fig 4.6 (15) were transformed to Fig 4.6 (16) by means of the same method of interpolation as that used in connection with the bending strength analysis, Figs 4.6 (8) and 4.6 (9). The values of f_{cr}/f_t at $d_i/d_o \rightarrow 1.0$ were, however, not utilized when the spline-functions were established as the change in crushing strength is very rapid when d_i/d_o is very close to 1.0. When interpreting Fig 4.6 (16) it may be noticed that a variation of t at a constant value of d_i means that both the size and shape of the pipe are varied.

4.6.6 Influence of initial internal stress

In this case initial streses mean macroscopical non-uniform stresses within a structure at zero external load. Such initial, or internal, stresses are very likely to develop in concrete pipes, and these stresses are also very likely, more or less, to influence the bending strength and the crushing strength. But it is a difficult task to investigate initial stresses within concrete pipes, and accordingly little is known about the magnitude and the distribution of the initial stresses as well as little is known about their influence on load carrying capacity. Specifically where concrete pipes are concerned, it may be that initial internal stresses are of importance before the pipes are placed in the ground, i.e. during handling and storing due to possible significant variations in

moisture conditions and temperature, while the magnitude of the initial stresses may be less after some time in the ground.

The present study regarding the influence of initial stresses is based on a single assumption regarding magnitude and distribution of the stresses, while no special investigation has been made regarding why and how the initial stresses may develop. The current assumption is shown in Fig 4.6 (17): the distribution through the thickness of the wall of the pipe is parabolic and the sign and magnitude are such that the stresses at the surfaces of the pipe equal the uniaxial tensile strength of the concrete. Although this assumption only represents an example of possible initial stresses, the assumption should not be entirely unrealistic and should accordingly and in a reasonable manner form a base for illustration and discussion of the influence of initial stress on strength, as predicted by the different theoretical models of the fracture properties of concrete.

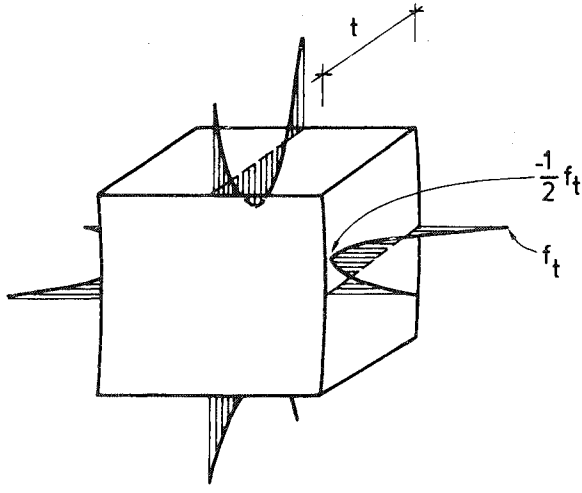

Fig 4.6 (17) Assumed distribution and magnitude of initial stresses within a pipe.

Starting with the linear elastic brittle model, this model predicts that the bending strength as well as the crushing strength is zero at the current magnitude of initial stress.

Regarding the ideal plastic model, one of the theorems of the theory of ideal plastic materials states that initial stresses or strains have no influence on ul ıgly eq (4.6:7)

and (4.6:8) are predicted to be valid independent of the magnitude and distribution of possible initial stresses.

Numerical predictions of the influence of initial stress according to the Weibull-model have not been obtained as such predictions requires rather extensive numerical work. The principles of a method of analysis is, however, described in Section 3.4.4, eq (3.4:12). The rather extensive numerical work required for Weibull-model analysis, taking into account initial stress, is not primarely due to the more complex stress-field but instead due to the simultaneous action of two non-proportional loads. Generally speaking this makes it necessary to apply incremental methods of calculation when median or mean values of strength are to be determined. Although no applied numerical analysis has been caried out, it is supposed that the Weibull-model would yield a prediction of the influence of initial stress which does not deviate very much from the prediction of the linear elastic brittle model. But the accuracy of such an assumption is of course dependent on the value of m. If the scatter is zero then $m \to \infty$, and in this limiting case the models coincide.

We now turn to the influence of initial stress when estimated by means of the fictitious crack model. Calculations of crushing strengths, taking into account initial stress, were carried out in the same manner as for zero initial stress, see Section 4.6.5, but the fracture hinge moment-rotation relations used were naturally not the same. The moment-rotation relations currently used were those presented in Section 4.2.3 and obtained during consideration of initial stress. The results of the calculations are shown in Fig 4.6 (18) as f_{cr}/f_t for different values of t/ℓ_{ch} and d_i/d_o.

In the previously presented values of f_{cr}/f_t at zero initial stress, compensation for certain approximations were included, and in the currently presented values of crushing strength the same relative amount of compensation is included for each individual combination of t/ℓ_{ch} and d_i/d_o. If, for instanace, a value of f_{cr}/f_t was increased by 3 % at zero initial stress then the corresponding value obtained during consideration of inital stress was also increasesd by 3 %. The currently adopted method of percentage compensation simplifies the calculations and facilitates comparisons, but it may of course be questioned whether or not the amount of compensation should be determined by means of interpolation between the extreme limits $t/\ell_{ch} \to \infty$ and $t/\ell_{ch} \to 0$, i.e. by means of the same principle as used in Secti[illegible] the reader to

t/ℓ_{ch}	d_i/d_o → 1.0	0.9990	0.8947	0.7778	0.6471	0.5000
→ 0	Not def.	3.822	4.044	4.365	4.862	5.730
0.025	2.047	2.181	2.490	2.922	3.320	3.885
0.050	1.822	1.940	2.140	2.446	2.832	3.339
0.100	1.555	1.655	1.777	1.964	2.252	2.683
0.200	1.246	1.327	1.393	1.496	1.701	1.987
0.400	0.917	0.976	1.023	1.115	1.248	1.385
0.800	0.653	0.639	0.644	0.654	0.674	0.730
1.600	0.401	0.427	0.444	0.467	0.481	0.492
3.200	0.178	0.204	0.243	0.239	0.236	0.229
→ ∞	0.000	0.000	0.000	0.000	0.000	0.000

Fig 4.6 (18) Crushing strength, f_{cr}/f_t, of concrete pipes of different t/ℓ_{ch} (size) and d_i/d_o (shape) as calculated by means of the fictitious crack model, taking into account initial stresses within the pipe in accordance with Fig 4.6 (17).

apply the method used in Section 4.6.5.

The results in Fig 4.6 (18) obtained by the method of interpolation used in Section 4.6.5 were transformed into crushing strength, f_{cr}/f_t, vs. wall-thickness, t, at ℓ_{ch}=380 mm and at different values of d_i. The the relative influence of the initial stress was obtained by comparison to the results shown in Fig 4.6 (16). These calculations, see Fig 4.6 (19), turned out to indicate that the fictitious crack model does not predict any drastic decrease in crushing strength due to presently assumed initial stress in pipes of common size and shape. Fig 4.6 (19) also indicates that the relative decrease in crushing strength due to initial stresses clearly increases at increasing wall-thickness, t. The relative influence of initial stresses do not vary very much at variations of the inner diameter of the pipes. It appears, however, that thick-walled pipes are in particular sensitive to initial stress if the inner diameter is more than 400 mm.

The fictitious crack prediction of the influence of initial stress on the bending strength may be approximately estimated by means of the results in Section 4.5.2. More accurate estimations might be obtained by 3D finite element analysis or by means of some type of modified 2D analysis. To obtain an estim ıy means of the

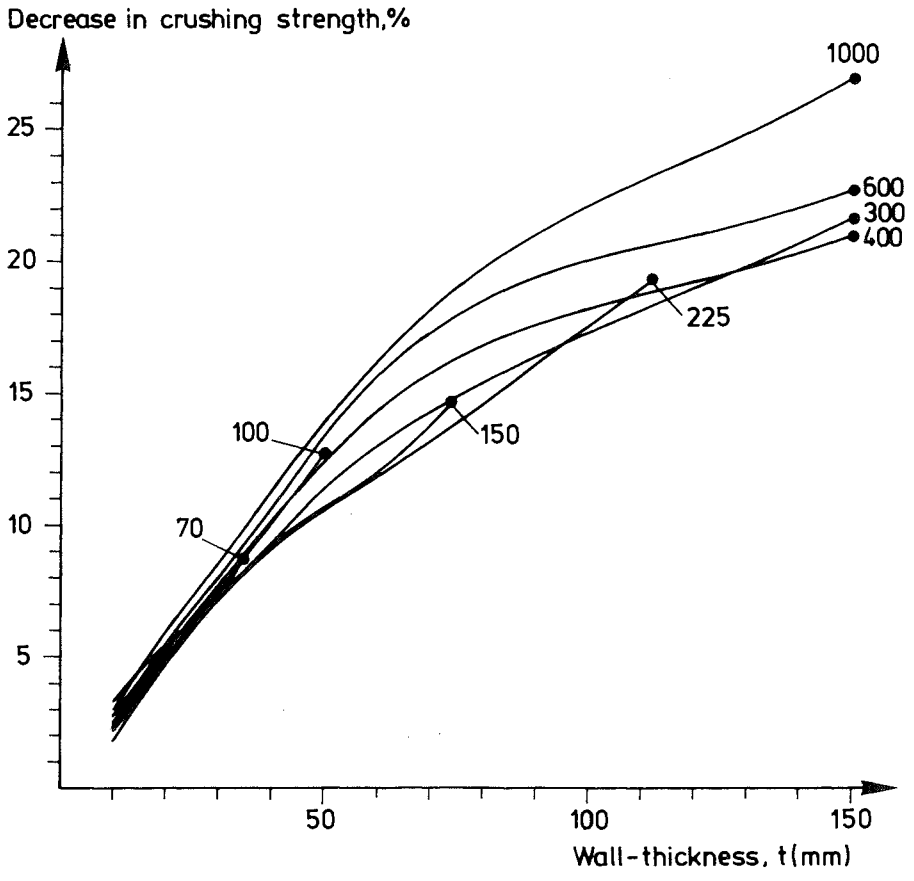

Fig 4.6 (19) Fictitious crack model prediction of the decrease in crushing strength of concrete pipes due to initial stresses in accordance with Fig 4.6 (17). The number at the end of each respective curve denotes the inner diameter of the pipe, d_i, (mm). The current values of t and d_i are valid for ℓ_{ch}=380 mm.

results in Section 4.5.2 (Figs 4.5 (1) and 4.5 (2)), one can imagine that the pipe is divided into a large number of strips along its length, the thickness of each strip being equal to the wall-thickness of the pipe. If the ratio d_i/d_o of the pipe is not very much less than 1.0, then the strips are near)ad carrying

capacity of each of the strips is reduced due to the initial stress in accordance with Fig 5.5 (2). An approximate estimation is then that the bending capacity of the concrete pipe is reduced to the same extent. During such an estimation, the thickness of the pipe, t, is made equal to the thickness, d, of the prismatic specimen. This type of estimation, see Fig 4.6 (20), indicates that the fictitious crack model predicts a rather limited influence of the currently assumed initial stresses on the ultimate bending capacity of pipes with a common wall-thickness. Furthermore the estimation suggests that the relative decrease in bending capacity due to initial stress is independent of the diameter of the pipe, and that the relative decrease increases with increased wall-thickness. A comparison between Figs 4.6 (20) and 4.6 (19) indicates that the initial stresses are predicted to have less influence on the bending strength than on the crushing strength. The current estimation is approximate not only by geometrical reasons, but also because the initial stresses do not only reduce the ultimate load carrying capacity of the prismatic specimen in Fig 4.5 (1) but they have also influence on the apparent σ-ε curve, Fig 4. 5 (3), and on an apparent σ-w curve.

To sum up, in the studied magnitude and distribution of initial stresses the linear elastic brittle model predicts a 100 % decrease in both bending strength and crushing strength. The ideal plastic model predicts a 0 % decrease in both bending strength and crushing strength. The fictitious crack model predicts a 3-25 % decrease in bending strength and crushing strength for common shapes and sizes of concrete pipes, the decrease being greater for thick-walled pipes than for thin-walled pipes and somewhat greater with respect to crushing than with respect to bending. Any numerical estimation using the Weibull-model has not been obtained, but it may be guessed that a Weibull-model prediction would not deviate very much from the prediction of the linear elastic brittle model and accordingly predict a very great influence of initial stress on strength.

4.6.7 Influence of limited compressive strength

The compressive strength of concrete is to the order ten times the tensile strength, and it is not probable that the limited compressive strength in reality has any major influence on the load carrying capacity of unreinforced concrete pipes when exposed to the currently studied types of loading. Regar it is possible

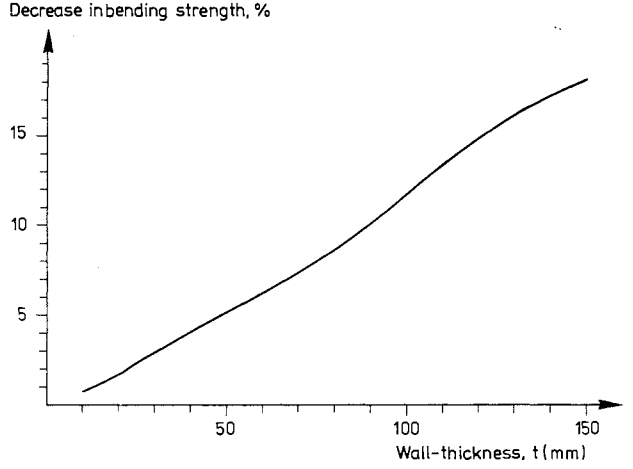

Fig 4.6 (20) Approximate estimation of fictitious crack model prediction of decrease in bending strength of concrete pipe due to initial stresses in accordance with Fig 4.6 (17). The current values of t are valid when ℓ_{ch} = 380 mm.

that the ideal plastic model model predicts substantially lower ultimate loads if a reasonable limitation of the compressive strength is taken into account. When predicting the ultimate load by means of the other three models being studied at present, the influence of a reasonable limitation in compressive strength is probably slight and substantially less than the influence according to the ideal plastic model. Consequently it seems fair to limit a study regarding the influence of limited compressive strenght to analysis by means of the ideal plastic model.

When the ideal plastic model is adopted, the equations of equilibrium provide sufficient information to enable prediction of bending strength and crushing strength. But, due to the extensive analytical expressions required for definition of area and centre of gravity of a segment of a circle with a centre hole, it has not been thought possible to obtain any explicit analytical expression for the bending strength, f_f/f_t, vs. the ratio between compressive strength and tensile strength, f_c/f_t, for different shapes of the cross section of the pipe, d_i/d_o. Instead the bending strength may be obtained by means of numerical integration. Such numerical calculations gave the following result:

$$\frac{f_f}{f_t} = \frac{4(1-(d_i/d_o)^2)}{(1-(d_i/d_o)^4)} \quad r_f(f_c/f_t,\ d_i/d_o) \qquad (4.6:18)$$

where values of the function $r_f(f_c/f_t,\ d_i/d_o)$ may be found in Fig 4.6 (21). When $f_c/f_t \to \infty$ then $r_f \to 1.0$, and accordingly r_f may be interpretated as a reduction-factor (compare eq (4.6:7)) which quantifies the influence of limited compressive strength on the bending strength. Regarding common values of d_i/d_o, Fig 4.6 (21) indicates that the ideal plastic model predicts about 10 % lower bending strength when a reasonable limitation of the compressive strength is taken into account.

d_i/d_o	f_c/f_t = 8	10	12	14	16
→ 1.0	0.980	0.987	0.990	0.993	0.994
0.9	0.939	0.948	0.955	0.961	0.965
0.8	0.902	0.915	0.925	0.932	0.938
0.7	0.875	0.891	0.903	0.912	0.920
0.6	0.853	0.872	0.885	0.896	0.904
0.5	0.836	0.857	0.873	0.885	0.894

Fig 4.6 (21) Numerical values of the function $r_f(f_c/f_t,\ d_i/d_o)$ in eq (4.6:18), i.e. the influence of limitation in compressive strength on bending strength.

With respect to the prediction of crushing strength by means of the ideal plastic model, taking into account limited compressive strength, an explicit analytical expression may be obtained by means of the equations of equilibrium:

$$\frac{f_{cr}}{f_t} = \frac{6}{\pi} \frac{(1+d_i/d_o)}{d_i/d_o} \quad r_{cr}(f_c/f_t, d_i/d_o) \qquad (4.6:19)$$

The function $r_{cr}(f_c/f_t,\ d_i/d_o)$ represents the reduction (compare eq (4.6:8)) in crushing strength due to limited compressive strength.

$$r_{cr} = \frac{d_i/d_o}{(1-d_i/d_o)} \left(\sqrt{A^2+2f_c/f_t} - A\right) \qquad (4.6:20)$$

where $A = 1 + \frac{d_i/d_o}{(1-d_i/d_o)} (1+f_c/f_t)$

The reduction in predicted crushing strength is of the same magnitude as the reduction in predicted bending strength. When $f_c/f_t=12$, for instance, r_{cr} is equal to 0.923, 0.904 and 0.866 for d_i/d_o equal to 1.0, 0.8 and 0.6 respectively. Eq (4.6:20) is not very convenient to use when $A^2>>2f_c/f_t$, but in such cases the approximate relation $r_{cr} \approx ((d_i/d_o)/(1-d_i/d_o))((f_c/f_t)/A)$ may be used. This approximate relation is obtained by means of a Taylor-series expansion and is accurate to within 0.1 % when $A^2/(f_c/f_t)>500$. $r_{cr} \rightarrow (f_c/f_t)/(1+(f_c/f_t))$ when $d_i/d_o \rightarrow 1.0$.

Eq (4.6:18) and eq (4.6:19) represent the bending and crushing strength when the material behaves in an ideal plastic manner both in tension and in compression (and consequently not the strength if the material behaves in a plastic manner on the tensile side and a linear elastic brittle manner on the compressive side.)

4.6.8 Influence of non-zero breadth of line load

The crushing strength, f_{cr}, of a concrete pipe is defined by eq (4.6:2). In this eq, $(P/\ell)_u$ is the ultimate line load along the pipe. In the crushing strength predictions dealt with in previous Sections, the load (P/ℓ) has been assumed to be a true line load, according to Fig 4.6 (1) a) and according to the adopted definition of crushing strength. In practice, the so-called "line loads" always have some non-zero breadth both when testing and, of course even more so, when the pipe has been placed in the ground.

The influence of this non-zero breadth is sometimes disregarded during the evaluation of experimental results but may be of significant importance and should, in general, always be taken into account although only some rather approximate considerations may be required if the breadth of the "line-load" is small in comparison to the size of the pipe. In this case formulas which enable consideration of non-zero breadth are provided only with regard to the two "extreme" models of fracture, i.e. the model of ideal plasticity and the model of linear elastic brittleness, respectively. But, as is evident from the formulas below, these two "extreme" models predict almost the same, and rather small, influence of non-zero breadth if the pipe has a normal shape and if the breadth of the "line-load" is reasonable. It may therefore be fair to use any of these models, or some [illegible] the influence of

non-zero breadth also when the fictitious crack model is used during interpretation of experimental results. During the evaluation of test results in Section 4.6.9, this approach is adopted also where the Weibull model is concerned.

On the other hand, during design calculations the breadth of load (P/ℓ) is often assumed to be large and corresponding to $\alpha=60^{o}$ or $\alpha=45^{o}$, see Fig 5.6 (22). In such cases it may be questioned whether the plastic or brittle models yield sufficient accuracy with regard to the influence of non-zero breadth of the load if design calculations are intended to be carried out by means of, e.g., the fictitious crack model. The accuracy, is, however, believed to be substantially improved if the principle of interpolation illustrated in fig 4.6 (11) is used. If, in order to simplify such interpolations, the arithmetric mean between the influence according to the brittle and plastic model is used throughout, then, according to upper and lower bound estimations, it is probable that the accuracy will be within about ± 5 % for $\alpha=45^{o}$ and if the pipe has a normal size and shape.

The linear elastic formulas provided by Wästlund and Eggwertz (1949) yield the following relation between the ultimate line load $(P/\ell)_u$ and the ultimate load, $(P/\ell)_{u,b\neq 0}$, at non-zero breadth, b, of the load:

$$(P/\ell)_u = (P/\ell)_{u,b\neq 0} \frac{(\pi-2\alpha+3\sin(2\alpha)-4\alpha\cos^2\alpha)}{8\cos\alpha} \qquad (4.6:23)$$

where $\alpha = \arccos(\frac{b/2}{r}) = \arccos(\frac{b}{d_i} \frac{2d_i/d_o}{(1+d_i/d_o)})$

This relation is valid for a linear elastic brittle material and is grafically illustrated by the full curves in Fig 4.6 (22).

Analysis by means of the ideal plastic model yields:

$$(P/\ell)_u = (P/\ell)_{u,b\neq 0} \left(1 - \frac{b/2}{d_i}\right) \qquad (4.6:24)$$

The ideal plastic model therefore predicts a very simple relation between $(P/\ell)_u$ and $(P/\ell)_{u,b\neq 0}$: the relation is linear with respect to the normalized breadth of the load, b/d_i, and independent of the shape of the pipe, d_i/d_o. However, if the breadth, b, is normalized with respect to r, and thus not wi on becomes more

complicated while the linear elastic relation becomes more simple. (4.6:24) is grafically illustrated by the dashed straight line in Fig 4.6 (21). In neither of the two formulas above is any limitation in compressive strength taken into account.

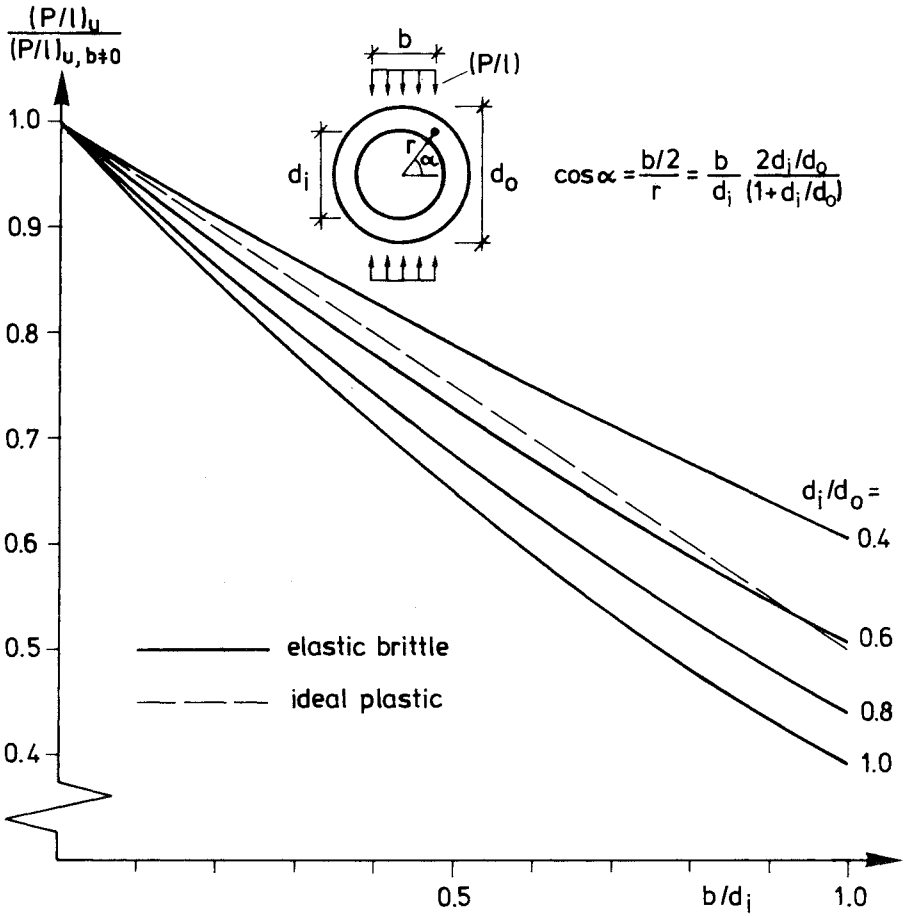

Fig 4.6 (22) Ratio between ultimate line load, $(P/\ell)_u$, and ultimate "line load", $(P/\ell)_{u,b\neq 0}$, of non-zero breadth, b, vs. b/d_i according to eq (4.6:23) (elastic brittle model, full lines) respectively eq (4.6:24) (ideal plastic model, dashed line).

4.6.9 Comparisons and remarks

In this Section the different fracture models shall be compared. First some general comparisons are made with respect to predicted influence of different variables on bending and crushing strength. The precision of the models is then compared by means of experimental results. The comparisons are accompanied with a few remarks.

Four basically different models have been dealt with in Sections 4.6.2-4.6.5. Two of these basically different fracture models may each be divided into two models. During engineering applications of the linear elastic brittle model, the influence of the value of the ratio d_i/d_o is often ignored when calculating the crushing strength, i.e. eq (4.6:6) is used instead of eq (4.6:4). In this case use of eq (4.6:6) shall be called the engineering linear elastic brittle method, while eq (4.6:4) is simply referred to as the linear elastic brittle model. Within the concept of beam-theory, the latter model may be considered exact if the material behaves in a linear elastic brittle manner. In predictions of bending strength the same equation, eq (4.6:3), is used in both models. The ideal plastic model may also be divided into two models: in Section 4.6.3 the compressive strength of the material is assumed to be unlimited and in Section 4.6.7 limitation in compressive strength is taken into account. Consequently altogether six different models are available and these models are collected in Fig 4.6 (23).

Name of model	Notation	Material property parameters	Strength prediction	
			Bending, f_t	Crushing, f_{cr}
Linear elastic brittle	1	f_t	4.6:3	4.6:4
Engineering linear elastic brittle	2	f_t	4.6:3	4.6:6
Ideal plastic	3	f_t	4.6:7	4.6:8
Ideal plastic, f_c limited	4	f_t, f_c/f_t (=12)	4.6:18	4.6:21
Weibull	5	$\bar{f}_t$, m (=14)	4.6:9	4.6:12
Fictitious crack	6	f_t, ℓ_{ch} (=380 mm)	4.6 (9)	4.6 (16)

Fig 4.6 (23) Summing up of fracture models. The numerical values of material property parameters in brackets are used in the current

None of the models is empirical, they all predict ultimate load carrying capacities from basic material property parameters, and the number of material property parameters involved in each model is very limited. The material property parameters are listed in Fig 4.6 (23), and it is interesting to note that all the models predict both the bending strength and crushing strength to be directly proportional to the uniaxial tensile strength of the concrete, if the "secondary" material property parameters (f_c/f_t, m and ℓ_{ch} ($=EG_F/f_t^2$)) are constant. This direct proportionality does not only mean that the tensile strength of the concrete is of major importance, but it also somewhat paradoxically suggests a conclusion of practical importance: The ratio between the crushing and/or bending strength of any two pipes of equal and/or different size and geometrical shape is predicted to be independent of the tensile strength of the concrete, provided, of course, that the pipes are made of the same concrete. (For different qualities of concrete, the "secondary" material property parameters may have different values.) This feature of the material property parameter f_t does not apply to either f_c/f_t, m or ℓ_{ch}. Accordingly, one has, for instance, to estimate the value of ℓ_{ch}, but not the value of f_t, in order to obtain a fictitious crack prediction of the ratio between the crushing strength and bending strength of a pipe.

The material property parameters of the Weibull-model indicated in Fig 4.6 (23) require a special comment: the Weibull-model does not state that $\bar{f}_t$ is a true material property parameter, but one also has to consider V_o, the volume of the uniaxial tensile test specimen coresponding to the current value of $\bar{f}_t$. In spite of this, since $\bar{f}_t$, V_o and m are not independent of each other, only two material property parameters are required. Accordingly, maybe it would be more correct to define the material parameters of the Weibull-model by $\bar{f}_t V_o^{1/m}$ and m instead of by $\bar{f}_t$ and m. Within the Weibull-model, $\bar{f}_t V_o^{1/m}$ may be considered to be a true material property parameter, but this parameter has a strange dimension which is why $\bar{f}_t$ is chosen for use instead of $\bar{f}_t V_o^{1/m}$. But then, of course, one has to remember that $\bar{f}_t$ must always be related to some specified value of V_o.

When comparing the different models there are four different groups of "degrees of freedom" which may be studied with regard to predicted influence on the strength of the pipes, namely the type of loading (bending or crushing), geometrical shape of the pipe (ratios t/d_i and d_i/ℓ), size of the pipe and finally the "secondary" material property

parameters (f_c/f_t, m and ℓ_{ch}). It is of course not possible to carry out any complete comparisons with regard to all the variables involved and presently only a few illustrative examples will be dealt with. In order to simplify, first the "secondary" material property parameters f_c/f_t, m (and V_o) and ℓ_{ch} are assigned certain constant values, used throughout this Section: f_c/f_t=12.0, m=14.0, V_o=0.05*.05*.08 m^3 and ℓ_{ch}=380 mm. The reasons for these specific choices are stated below.

Although certain constant values are currently assigned to f_c/f_t, m (and V_o) and ℓ_{ch}, it is of course desirable to estimate these parameters as accurately as possible during practical utilization of the corresponding models of strength prediction. So for instance, the predicted ratio between the bending strength and the crushing strength, f_f/f_{cr}, of common types of pipes decreases slightly at increased f_c/f_t, increases at increased m and decreases at increased ℓ_{ch}. Specifically with respect to the fictitious crack model, the influence of ℓ_{ch} on ratio f_f/f_{cr} means that one may expect a decrease in the bending strength, if the crushing strength is kept constant but the maximum aggregate particle size of the concrete is increased. The infuence of maximum particle size on ratio f_f/f_{cr} is probably not of an entirely negligible magnitude: The tests of Petersson (1981), regarding ℓ_{ch} for different qualities of concrete, together with Fig 4.6 (9) and Fig 4.6 (16) suggest that a change in maximum particle size from 8 mm to 16 mm means a decrease in f_f/f_{cr} of about 10 %.

The ratio f_c/f_t was made to equal 12.0 so that this value can be considered typical for a normal quality of concrete. The choice of m, m=14, corresponds to an 8.7 % coefficient of variation of the ultimate load of different pipes of equal geometry and of equal quality of the material. This value, s=8.7 %, may be compared to the result of a maximum-likelihood estimation of s with the help of 137 test results subsequently dealt with. This estimation gave s=10.8 %, corresponding to m=11.2. But this value does not only include scatter in strength of the pipes due to scatter in strength within the material in a pipe, but also the scatter in the recorded strengths due to unavoidable variation in support and loading arrangements, errors in measuring of load and geometry and possible differences in manufacturing and curing of the different but nominally equal pipes. The current choice of ℓ_{ch}, ℓ_{ch}=380 mm, is believed to be typical for most pipe-concretes and was, with the aid of experimental results reported by Petersson (1981), derived from the mix of the concrete

used during manufacturing of pipes used in experimental tests carried out in Staffanstorp by Isgren and the writer. The water-cement-ratio of this concrete mix was 0.39-0.41, the maximum particle size was 12 mm, the cement content was 325-375 kg/m^3, and ℓ_{ch} was estimated for a 28 days old concrete. The experimental results reported by Petersson also suggest that the uniaxial tensile strength of such a concrete is about 4.1-4.5 MPa in wet conditions and probably somewhat higher at moisture equilibrium with a normal indoor climate. The uniaxial tensile test of Petersson was carried out on prismatic specimens with an effective test-volume of about .05*.05*.08 m^3, which is why this specific volume is used as a reference-volume for mean tensile strength in calculations using the Weibull-model. As the difference between ℓ_{ch}=380 mm and ℓ_{ch}=400 mm is neglible where calculated strengths are concerned, maybe it would have been more appropiate to adopt the round value ℓ_{ch}=400 mm.

Fig 4.6 (24) illustrates how the different models predict the strength to be influenced by the absolute size of the pipes, and this Figure also illustrates the difference between predicted bending strength and crushing strength respectively. Models 1-4 do not predict any variation in strength in variation of the absolute size, while the Weibull-model and the fictitious crack model both predict the strength to decrease at increased size. The Weibull-model predicts the same influence of size on both bending strength and crushing strength, while the fictitious crack model predicts a stronger influence of the size on the crushing strength than on the bending strength. Another difference between models 5 and 6, not clearly indicated in Fig 4.6 (24), is that the Weibull-model predicts an unlimited increase in strength when the size is decreased towards zero and zero strength when the size is increased towards infinity, while the fictitious crack model predicts a limited variation in strength: a variation bounded by the strength predictions of models 1 and 3.

Regarding the comparison between bending strength and crushing strength, Fig 4.6 (24) indicates that the three elastic brittle models, i.e. the two deterministic linear elastic brittle models, 1 and 2, and the stochastic model of Weibull, 5, all predict the same or almost the same strength at bending and crushing respectively. The two ideal plastic models and the fictitious crack model predict substantially lower bending strength than crushing strength.

Practical experi [illegible] reinforced

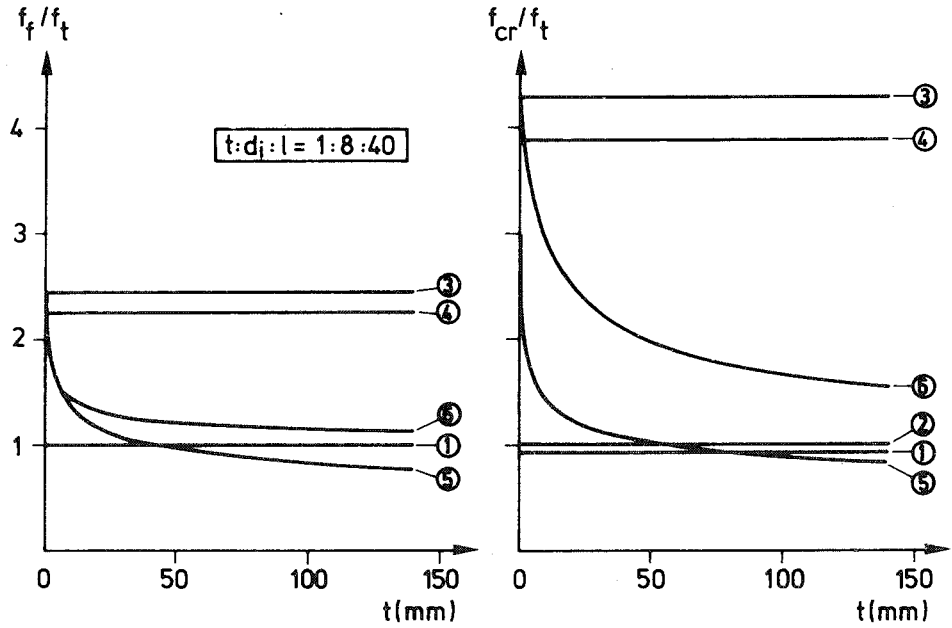

Fig 4.6 (24) Influence of absolute size on bending strength, f_f/f_t, and crushing strength, f_{cr}/f_t, of pipes as predicted by models. See Fig 4.6 (23).

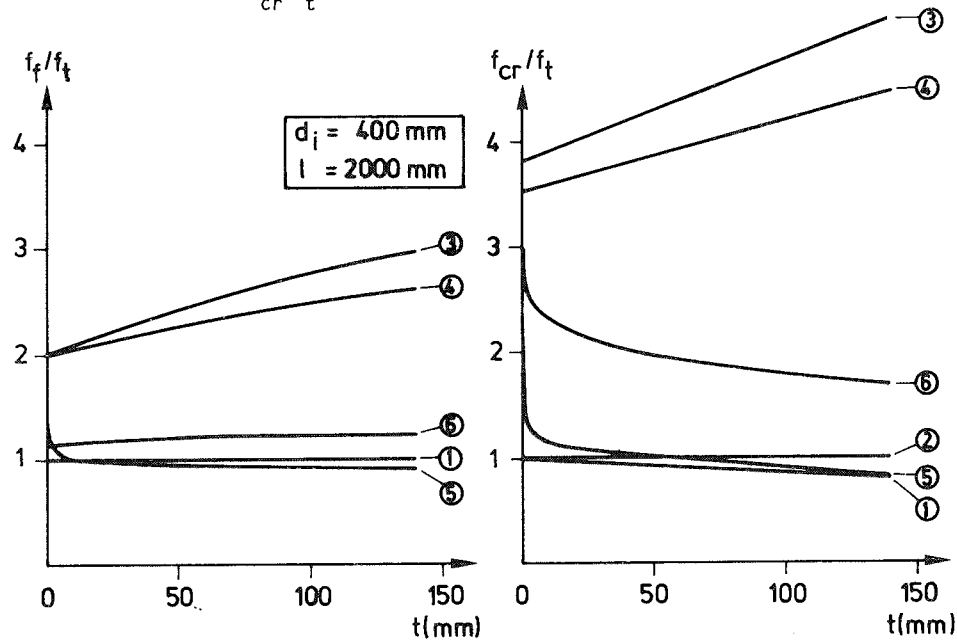

Fig 4.6 (25) Ini ength, f_f/f_t, and crushing strengt See Fig 4.6 (23).

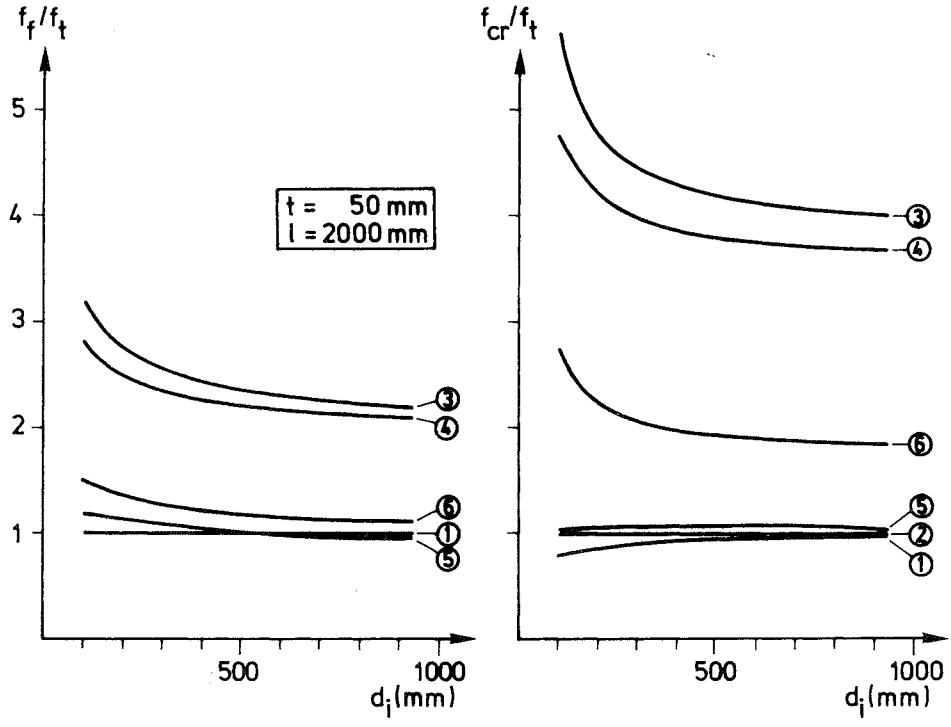

Fig 4.6 (26) Influence of inner diameter, d_i, on bending strength, f_f/f_t, and crushing strength, f_{cr}/f_t, of pipes as predicted by models. See Fig 4.6 (23).

concrete pipes decreases at increased size and that the bending strength is substantially less than the crushing strength. These two features are both in accordance with the fictitious crack predictions. The ideal plastic models and the Weibull-model respectively predict one of these features each. The conventional linear elastic brittle models, 1 and 2, do not predict any of these features.

It may also be of interest to consider how the different models predict that the strength varies at variations of the shape of the cross-section of the pipes, and an example of these variations can be found in Fig 4.6 (25). The Figure shows how the bending and crushing strengths are predicted to vary at increased wall-thickness of the pipe, when the inner diameter and the length of the pipe are kept constant. The two deterministic linear elastic brittle models, 1 and 2, predict a minor, or zero, influence of the wall-thickness. Regarding any normal variations of the wall-thickness the Weibull-model also predicts a minor variation in

strength. The ideal plastic models, 3 and 4, both predict a substantial increanse in both bending and crushing strength at increased wall-thickness. The fictitious crack model predicts a slight increase in bending strength and a substantial decrease in crushing strength at increased wall-thickness. It can be noticed that the latter model is the only one that predicts a qualitatively different influence of wall-thickness on the bending and crushing strength respectively. No experimental results or practical experiences regardning variations of strength at a varying wall-thickness and at a constant inner diameter is known to the writer.

An additional illustration concerning the influence of varying shape of the cross-section can be found in Fig 4.6 (26): in this Figure the inner diameter, d_i, is varied while the wall-thickness, t, is kept constant at 50 mm.

Regarding variation in length of the pipe with constant size and shape of the cross-section, all models, except the Weibull-model, predict constant strength. The Weibull-model predicts that both the bending strength and the crushing strength decrease 4.8 % at every doubling of the length (at m=14), other variables kept constant. Where the actual strength of pipes is concerned, it is very probable that the bending strength decreases somewhat with increased length: Compare Section 4.2.5 and eq (4.2:14). But whether the crushing strength is influenced by the length of the pipe to the same (minor or possibly significant) extent is questionable.

The predictions of the different models with regard to the influence of length on bending strength are valid only for pipes of such length to depth ratio that the stress distribution in the fracture-section is not significantly influenced by the finite length of the pipe. Regarding short pipes, let us say if $d_o/\ell > 1/4$, it is probable that not only the Weibull-model but also the linear elastic brittle description of the behaviour of the material, as well as the fictitious crack model, would predict increased bending strength at decreased length.

In Figs 4.6 (24) to 4.6 (26) f_f and f_{cr} are normalized with regard to the uniaxial tensile strength, f_t, of the concrete. It is indicated that models 1 and 2 predict f_f and f_{cr} to be almost equal to, or equal to, f_t. The plastic model of unlimited compressive strength, 3, predicts f_f and f_{cr} to be very much higher than f_t - about 2.5 and 4.5 times higher than

f_t respectively. Consideration of limited compressive strength, model 4, yields somewhat decreased values of ratios f_f/f_t and f_{cr}/f_t. The Weibull-model predicts, - at the present choice of reference volume -, f_f and f_{cr} to be of the same magnitude as f_t. The fictitious crack model predicts that, for a normal size and shape of the unreinforced concrete pipe, f_f will be in magnitude 20 % higher than f_t and f_{cr} will be in magnitude 100 % higher than f_t. Experimental experiences suggest that the real crushing strength is much higher, and the real bending strength somewhat higher, than the uniaxial tensile strength of the concrete, the uniaxial tensile strength then being estimated from knowledge of the concrete mix. Unfortunately it is difficult to obtain any reliable experimental values of the uniaxial tensile strength of the concrete in pipes. During attempts to drill and saw test specimens from pipes, it was found that the specimens became exposed to significant damage. Where manufacturing of special uniaxial test specimens is concerned, it has been said that it is very difficult to reproduce the same type of vigorous vibration of the fresh concrete as attained in the special equipment used during pipe manufacturing. Concrete used for pipe manufacturing is usually very dry and it has sometimes been argued that the vigorous vibration is a prime cause of the high strength of concrete pipes, i.e. the high crushing strength of concrete pipes.

For practical design applications, a value of the uniaxial tensile strength is normally obtained in an indirect manner by means of experimental results regarding the ultimate load of pipes in one, or possibly several, combinations of size, shape and type of loading, and then this (apparent) value is utilized for predicting the ultimate load in other considered combinations of size, shape and type of loading. This approach in principle requires that the quality of the concrete is kept constant. Relative changes in the apparent tensile strength due to considered changes in the quality of concrete, i.e. alternations in water-to-cement ratio etc, may be estimated by experience or by means of information provided by literature.

It is more convenient, and from the designers point of view also more reliable, to obtain a value of the tensile strength by means of testing pipes than by testing special uniaxial test specimens. Accordingly the ability of the different models to correctly reproduce the influence of size, shape and type of loading is of prime practical importance, while their ability t uniaxial

tensile strength is of smaller practical importance. Naturally, however, the ability to correctly reproduce the true tensile strength is of interest during general comparisons between theoretical models with regard to their general ability to realistically reproduce the real fracture behaviour of a material.

In Fig 4.6 (27) test results have been collected in order to facilitate comparisons with respect to the applicability of the different fracture models. The Figure includes all tests, known to the writer at present, where both crushing and bending tests have been made on pipes made from the same quality of concrete. An estimation of the true uniaxial tensile strength of the concrete is available only for the concrete used during the test-series denoted "Staffanstorp". As previously mentioned the true tensile strength of this concrete was estimated to be 4.1-4.5 MPa in wet conditions, and probably somewhat higher at moisture equilibrium in a normal indoor climate. The lack of knowledge of the true tensile strength of the other concretes is unimportant where the subsequent comparison of precision is concerned.

The experimental tests on which Fig 4.6 (27) is based will be briefly commented on before proceeding. The effective length of the pipes used in the Staffanstorp tests was 1 m and three point bending was applied during the bend tests. During the crushing tests true line loads were not applied, but a standard loading arrangement, used by Skanska, was used instead. The width of the "line loads" was 50 mm. The age of the pipes was not equal, but all pipes were at least 4 weeks old. In spite of different age, the strength of the concrete was assumed to be constant. The pipes were tested in an in-door climate (in a concrete factory) and they were stored in the actual climate for 8 or 9 days before testing. The type of pipes tested had a somewhat varying wall-thickness along the length of the pipe, and the wall-thickness used when calculating the strength was the mean value of measured wall-thicknesses of the fracture surfaces. The pipes were all made of the same quality of concrete (the concrete mix may be found above) and manufactured at the same factory.

The test results of Nygårds and Lärkfeldt (1954) are different from the other test results in the sense that they comprise a number of different qualities of concrete. However, for each quality of concrete the same number of tests were carried out for each of the two pipe geometries investigated. As the quality of the concrete varied, it is not meaningful

Series no.	Type of failure	Number of tests	Wall-thickness t (mm)	Inner diam. d_i (mm)	Mean strength f_{cr} resp. f_f (MPa)	Coeff. of var.
Staffanstorp, 17 tests						
1	Bend	4	34.6	100	7.38	6.4 %
2	Bend	4	31.3	150	6.75	11.2 %
3	Bend	1	33.8	225	6.56	- %
4	Crush	4	35.0	225	11.00	3.1 %
5	Crush	4	55.2	400	9.62	2.3 %
Nygårds and Lärkfeldt (1954), 72 tests						
1	Crush	36	33	300	7.4	-
2	Crush	36	22	150	8.3	-
Brennan (1978) make "A", 16 tests						
1	Bend	4	30.0	225	5.33	24.8 %
2	Bend	4	42.2	300	5.44	5.5 %
3	Crush	4	30.0	225	9.18	12.9 %
4	Crush	4	42.2	300	8.16	8.3 %
Brennan (1978) make "B", 4 tests						
1	Bend	2	50.6	300	4.07	8.4 %
2	Crush	2	50.6	300	5.62	7.1 %
Brennan (1978) make "C", 14 tests						
1	Bend	7	50.5	300	5.99	12.9 %
2	Crush	7	50.5	300	9.74	5.0 %
Brennan (1978) make "D", 4 tests						
1	Bend	2	33.8	300	7.44	14.5 %
2	Crush	2	33.8	300	11.93	3.0 %
Brennan (1978) make "E", 4 tests						
1	Bend	2	36.6	225	6.55	6.8 %
2	Crush	2	36.6	225	11.98	0.2 %
Brennan (1978) make "F", 2 tests						
1	Bend	1	36.9	225	4.42	-
2	Crush	1	36.9	225	10.70	-
Brennan (1978) make "G", 4 tests						
1	Bend	2	55.8	375	5.77	14.7 %
2	Crush	2	55.8	375	9.10	14.6 %

Fig 4.6 (27) Experimental results regarding strength of unreinforced concrete pipes.

to calculate any coefficient of variation, and consequently only the relative difference between the two mean values of strength is of interest. The length of the pipes is unknown, but is assumed to have been 0.5 m. The assumed length of the pipes is of significance only for the Weibull-model calculations.

Brennan (1978) tested 7 different makes of concrete pipes, i.e. pipes made of different qualities of concrete and/or manufactured at different factories. Four-point-bending was used to determine the bending strength, and the distances between the points of load application were about equal to the effective test length of the pipes divided by three. The effective test lengths at bending were 1.6 m (make A, d_i=255 mm), 2.2 m (A, d_i=300 mm), 2.2 m (B), 1.5 m (C and D), 1.4 m (E), 1.1 m (F) and 1.6 m (G). The crushing tests were carried out on the same pipes as those previously tested and broken in bending, which means that the length at crushing were about half of the values above. In (Brennan, 1978) the crushing strengths were calculated without consideration to the width of the "line-loads", and during the calculations the fact that two closely located "line-loads" were applied at the bottom side of the pipe (and consequently not a single "line-load") was not considered. Unfortunately, the writer has not been able to obtain information about the width of the "line loads" and about the distance between the two closely located bottom-side loads. In order to and in spite of this, attain some correction, the crushing strengths reported by Brennan have been recalculated taking into account an assumed width of 50 mm of the "line loads". This assumption is intended to cover both the influence of width the "line loads" and the influence of the distance between the two bottom-side "line loads". The choice of 50 mm was made simply because this is believed to be a probable and reasonable value and because this specific width of the loads was used during the tests carried out in Staffanstorp. The wall-thickness of the pipes tested by Brennan were not reported in an explicit manner, but have now been calculated with the aid of the reported relation between ultimate load and ultimate strength and the reported values of ultimate load and ultimate strength. The length to depth ratio of the single pipe of the make "F" is probably somewhat too small to yield any reliable value of the bending strength when determined by means of four-point-bending. It may be noted that the number of tests in some of the series is very limited: series number 3 from the Staffanstorp tests and the series corresponding to makes B, D, E, F and G of the Brennan tests.

To sum up the comments of the tests, it may be said that they all have their drawbacks. The drawback of the tests made by Nygårds and Lärkfeldt is essentiallly that they do not comprise any tests of bending strength. In spite of the drawbacks, it is believed that the test results collected may provide some information regarding the acccuracy of the different fracture models. However, it is not believed to be advisable to apply any advanced statistical methods in order to investigate the test results of Fig 4.6 (27), as in such analysis one may easily forget the drawbacks of the different individual test series. It may also be noticed that the test results in Fig 4.6 (27) do not comprise results from very large pipes, while in practise unreinforced concrete pipes with an inner diameter of 1000 mm or more are manufactured (abroad). The bending strength of such large pipes is, however, normally not very interesting and the crushing strength in large variations in wall-thickness will be dealt with later on in this Section by means of additional test results recently presented in literature.

The mean strengths in Fig 4.6 (27) have been calculated as the mean of the strengths of the individual pipes, and consequently not from mean values of ultimate load and wall-thickness. The coefficients of variation in Fig 4.6 (27) represents the scatter in strength within each series and are therefore essentially independent of the computational method used during the transformation of ultimate load to ultimate strength. Accordingly these coefficients are essentially dependent on the true scatter of strength of the material, the ability of the factory to keep a constant quality of their pipes and the precision at the testing of the pipes respectively. If the coefficients in Fig 4.6 (27) are put together by means of maximum likelihood estimation, taking into account the different number of tests in each series, one obtains s=10.8 %. (s=6.7 % for the pipes manufactured in Staffanstorp and s=12.0 % for the pipes tested by Brennan.)

The experimentally obtained strengths in Fig 4.6 (27) may be transformed into corresponding values of the uniaxial tensile strength of the concrete, Fig 4.6 (28). The transformations are carried out by means of the different fracture models. From a designers point of view, a good model should primarily yield a approximately constant value of tensile strengths within each group. From a more general point of view, a good model should also yield tensile strengths which do not deviate from some reasonable estimation of the true uniaxial tensile strength. The

Series No.	Tensile strength, f_t (MPa), according to different models of fracture: Elastic brittle	Engineering elastic brittle	Ideal plastic (f_c unlimited)	Ideal plastic (f_c/f_t=12)	Weibull (m=14)	Fict. crack (ℓ_{ch}=380mm)
Staffanstorp, 17 tests						
1	7.38	7.38	2.49	2.82	6.25	4.92
2	6.75	6.75	2.53	2.80	5.91	4.87
3	6.56	6.56	2.61	2.84	6.00	5.05
4	12.06	11.00	2.49	2.77	9.97	4.92
5	10.45	9.62	2.21	2.45	9.31	4.91
Nygårds and Lärkfeldt (1954), 72 tests						
1	7.94	7.40	1.75	1.93	6.35	3.44
2	9.05	8.30	1.90	2.11	6.70	3.33
Brennan (1978), make "A", 16 tests						
1	5.33	5.33	2.16	2.34	5.69	4.12
2	5.44	5.44	2.19	2.38	6.20	4.32
3	9.96	9.18	2.10	2.33	7.36	4.06
4	8.89	8.16	1.87	2.07	7.03	3.89
Brennan (1978), make "B", 4 tests						
1	4.07	4.07	1.59	1.74	4.67	3.21
2	6.22	5.62	1.26	1.41	4.90	2.74
Brennan (1978), make "C", 14 tests						
1	5.99	5.99	2.34	2.56	6.68	4.72
2	10.78	9.74	2.18	2.44	7.07	4.73
Brennan (1978), make "D", 4 tests						
1	7.44	7.44	3.10	3.33	8.18	5.98
2	12.80	11.93	2.81	3.10	9.86	5.56
Brennan (1978), make "E", 4 tests						
1	6.55	6.55	2.57	2.81	6.97	5.03
2	13.22	11.98	2.70	3.01	9.67	5.36
Brennan (1978), make "F", 2 tests						
1	4.42	4.42	1.73	1.89	4.63	3.39
2	11.81	10.70	2.41	2.69	8.64	4.76
Brennan (1978), make "G", 4 tests						
1	5.77	5.77	2.30	2.50	6.66	4.67
2	9.96	9.10	2.07	2.30	7.95	4.62

Fig 4.6 (28) Apparent tensile strengths as obtained by means of different models of fracture from the experimentally determined mean bending and crushing strengths Fig 4.6 (27).

Staffanstorp tests and make A of the Brennan tests provide the best general outline, and the tensile strengths obtained from these tests are graphically shown in Fig 4.6 (29).

Fig 4.6 (30) shows the deviations in tensile strength between the different series with in each group by the corresponding coefficent of variation. Accordingly this Figure gives a illustration of the ability of the different fracture models to correctly predict variations in ultimate load capacity for variations in size, shape and type of loading.

For interpretation of Fig 4.6 (30) it is appropriate to include a remark regarding influence of scatter. The coefficients of variation in Fig 4.6 (30) apply to deviation in apparent mean tensile strength between different test series within a group, and therefore do not apply to deviation in strength between different individual pipes. If systematic experimental errors are avoided and if the number of tests within each series were infinite, then these coefficients of variation would depend only on the precision of the fracture model used, and an ideal exact model would yield a zero coefficient of variation. For a limited number, n, of tests within each series even a ideal exact model may be expected to yield a non-zero value of the coefficient of variation, and the mean value for such an ideal exact model would be $s/\sqrt{n}$, where s represents an estimation of the coefficient of variation for the strength of the individual pipes within each serie.

When interpreting Fig 4.6 (30), it is also of importance to notice that the use of a computational model which accurately predicts the mean influence of size and shape of the pipes, type of loading and properties of the material does not decrease the scatter in strength between individual nominally equal pipes. Naturally, this basic type of scatter in strength is independent of the fracture model used and is only dependent on the homogenity of the material and the ability to keep a constant quality of the pipes during manufacturing. During determination of appropriate safety factors one has to consider both the basic type of scatter and the additional artificial scatter produced at the writing-table and caused by the, more or less, poor reliability and precision of the computational method used when predicting strength.

The Staffanstorp test and the make A test, Fig 4.6 (29), are in an almost detailed manner in accordance with each other with regard to suggested

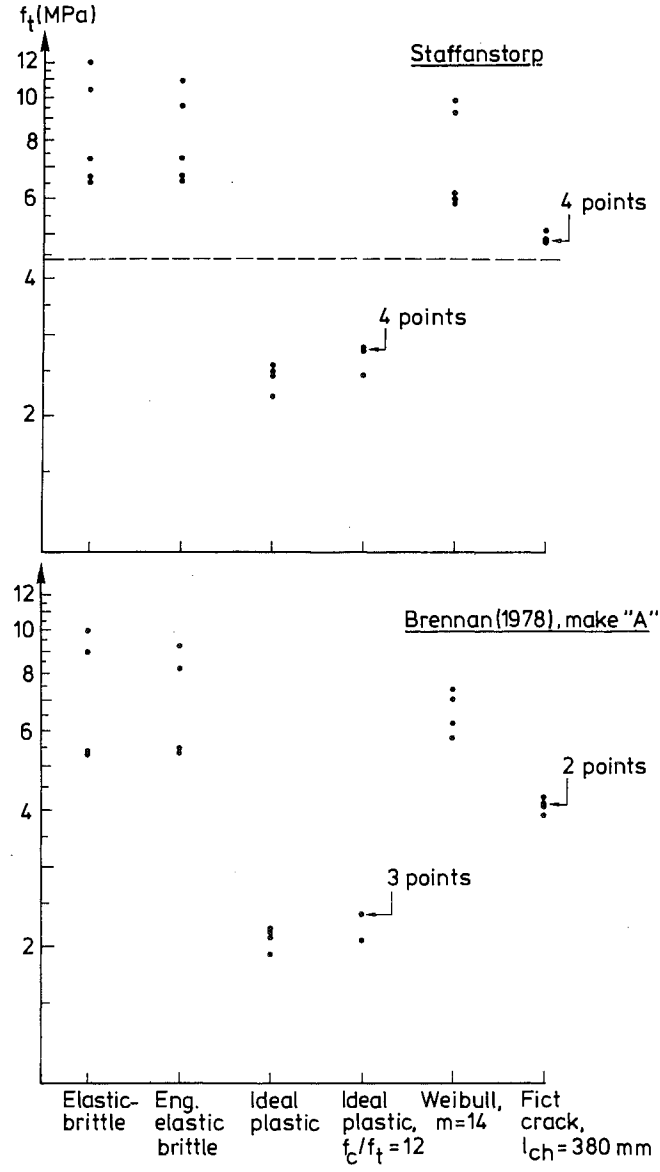

Fig 4.6 (29) Apparent tensile strength of the concrete in group Staffanstorp (5 series) and in group Brennan (1978), make "A" (4 series) according to different fracture models. The dashed line represents an estimation of the true uniaxial tensile strength.

features of the different fracture models. The only essential difference is that the Weibull-model appears somewhat better when evaluating the make A tests. The better Weibull-model result of the make A tests are most probably only apparent and due to the different volume of concrete in the pipes at bending and crushing of the make A pipes, respectively. In both test groups, both the ideal plastic model, taking into account limited compressive strength, and the fictitious crack model yield very small deviations in tensile strength between the different series. Furthermore it is of interest to notice that the ideal plastic model yields a somewhat lower value of f_t for one of the series in each of the two groups than for the other series. These two series correspond to crushing of comparatively large pipes, and the deviation in tensile strength is due to the inability of the ideal plastic models to predict any influence of size, see Fig 4.6 (24) and (25). The fictitious crack the model, on the other hand, seems to predict also this feature correctly. The approximate estimation, obtained from knowledge of the concrete mix, of the true uniaxial tensile strength of the concrete used during manufacturing of the Staffanstorp pipes, Fig 4.6 (29), indicates that the fictitious crack model is the only model that yields a reasonable agreement between true tensile strength and the strength of the pipes. The fictitious crack model seems to overestimate the estimated true tensile strength by about 10 %. The two deterministic linear elastic brittle models do not predict any constant value of the tensile strength and the predictions are roughly about twice the estimated true value. The two plastic models predict roughly about half the value of the true value. The Weibull-model does not predict any constant value, but the predictions on an average overestimate the approximate true value by about 70 %.

While results of the Staffanstorp test and the make A test are discussed above, the large number of tests in the Nygårds-Lärkfeldts group provide additional information concerning the ability of the different models to predict crushing strength with variation in geometry of the pipes. The rather large number of tests in the make C group provide additional information concerning the ability of the models to predict bending strength from crushing strength and vice versa. The numbers of tests in the other test groups are small, but the results of these other groups seem to be in general agreement with the results of the more comprehensive test groups.

Group	Number of tests within serie	Number of series	Range of t (mm)	Range of d_i (mm)	Range of type of loads	Mean apparent tensile strength, f_t (MPa)						Rel. dev. (%) in tensile strength between series					
						1	2	3	4	5	6	1	2	3	4	5	6
taff.	4	5	35-55	100-400	b.-cr.	9.0	8.6	2.4	2.7	7.8	4.9	29	24	6	6	24	1
lygår.	36	2	22-33	150-300	cr.	8.5	7.9	1.8	2.0	6.5	3.4	9	8	6	6	4	2
r. A.	4	4	30-42	225-300	b.-cr.	7.4	7.0	2.1	2.3	6.6	4.1	32	28	7	6	12	4
r. B	2	2	51	300	b.-cr.	5.2	4.9	1.4	1.6	4.8	3.0	30	23	16	15	3	11
r. C	7	2	51	300	b.-cr.	8.4	7.9	2.3	2.5	6.9	4.7	40	34	5	3	4	0
r. D	2	2	34	300	b.-cr.	10.1	9.7	3.0	3.2	9.0	5.8	28	33	7	5	13	5
r. E	2	2	37	225	b.-cr.	9.9	9.3	2.6	2.9	8.3	5.2	48	41	3	3	23	4
r. F	1	2	37	225	b.-cr.	8.1	7.6	2.1	2.3	6.6	4.1	46	42	23	17	43	24
r. G	2	2	56	375	b.-cr.	7.9	7.4	2.2	2.4	7.3	4.7	38	32	7	4	13	1

ig 4.6 (30) Mean apparent tensile strength of the concrete in each test-group and relative deviation (coefficient of variation) between the apparent tensile strengths of the different series within each group. Notations 1-6 according to Fig 4.6 (23).

Recently an interesting thesis, (Fuchs,1982), on the crushing strength of unreinforced concrete pipes became available. Fuchs carried out an extensive statistical survey and indicated that the crushing strength decreases at increased wall-thickness. The survey includes 2366 crushing tests, collected in Germany. In the survey, the pipes were divided into 14 groups of different ranges of wall-thickness, from 30-39 mm to 160-169 mm, see Fig 4.6 (31). According to private communication, the pipes were manufactured in different factories and the quality of the concrete in the different pipes may not quite equal. The diameters of the pipes is not known, but as a rough approximation one might assume that the inner diameter of the pipes is about proportional to the wall-thickness, and in Fig 4.6 (31) theoretical results of the fictious crack analysis are shown for $t/d_i=1/7$, $\ell_{ch}=380$ mm and $f_t=4.5$ MPa. The absolute value of f_t is chosen by means of the method of least squares, applied in the range t=50-169 mm. The choice of f_t is of no importance with regard to the relative influence of wall-thickness (and inner diameter). The absolute values of ℓ_{ch} and t/d_i are of some, but rather little, importance. The important assumptions for validity of the comparison in Fig 4.6 (31) is that f_t = const., ℓ_{ch}=const. and t/d_i=const.

The theoretical curve in Fig 4.6 (31) agrees very well with the test results in the range t=50-169 mm. In the range t=30-49 mm the theoretical curve overestimates the crushing strength by about 10%. This overestimation may have a number of different explanations. One possible explanation is systematic difference in the concrete mixes: it is, for instance, possible that the maximum aggregate particle size used during manufacturing of pipes with a wall-thickness less than 50 mm is smaller than when manufacturing pipes with wall-thicknesses greater than 50 mm. Another possible explanation is that the smaller pipes might have been manufactured and tested somewhere else than the larger pipes. A third possible explanation is that manufacturers are perhaps more careful and use higher qualities of concrete when manufacturing large thick-walled pipes than when manufacturing the small thin-walled pipes. Due to the uncertainties involved, one should not make any far-reaching conclusions with the aid of the comparison in Fig 4.6 (31). However, the actual survey of test results do not seem to contradict the theoretical fictitious crack analysis. The absolute value of the uniaxial tensile strength that coincides best with the test results is of a probable and reasonable magnitude, and the actual survey indicates a decrease in crushing strength at increased wall-thickness, the rate of decrease also being of about the

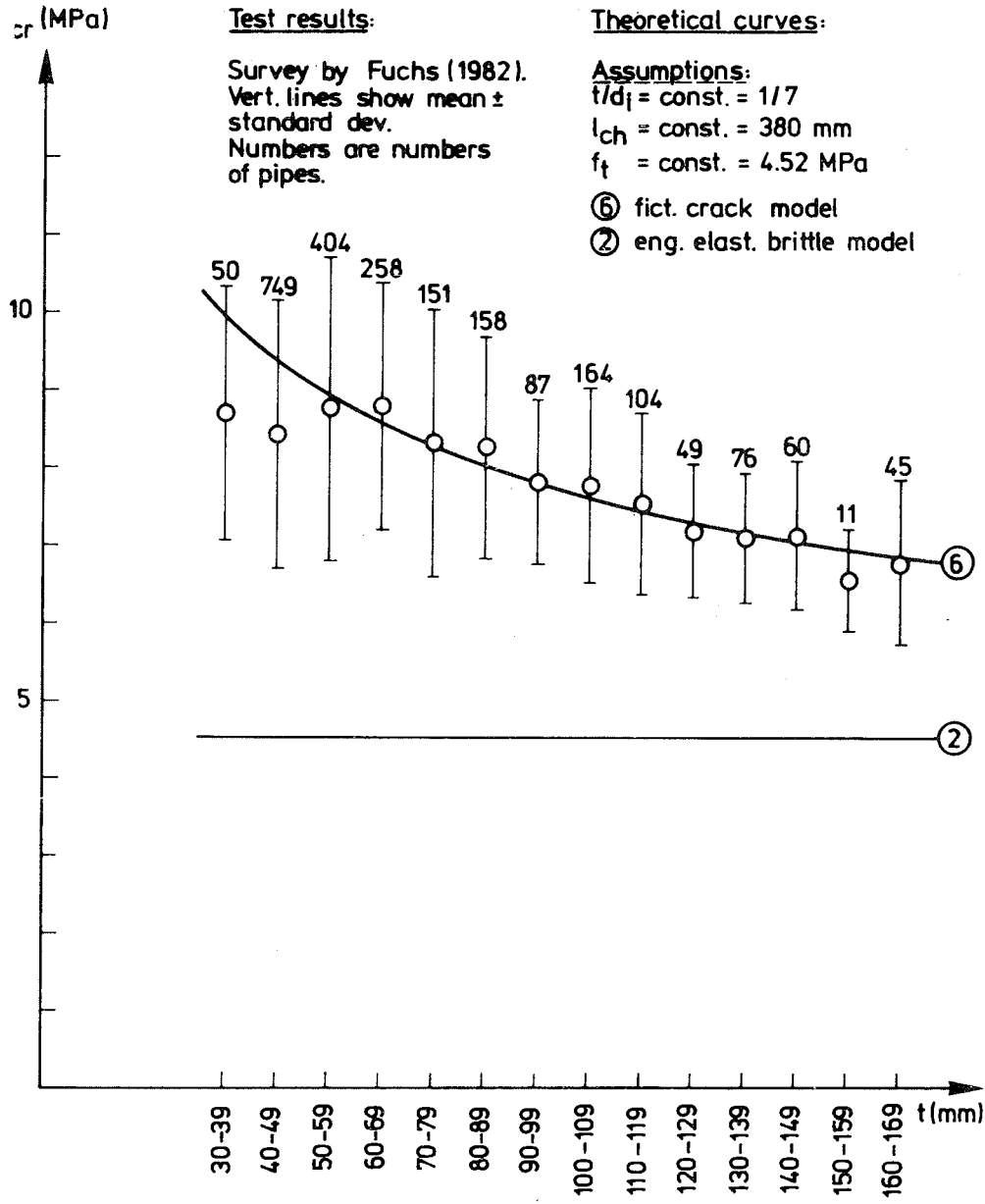

Fig 4.6 (31) Crushing strength of concrete pipes vs. wall-thickness.

same magnitude as predicted by the fictious crack analysis.

In conjuction with Fig 4.6 (31) and the prediction of crushing strength, it may be mentioned that a new standard is being developed in Denmark (1985: has been developed) for the crushing strength of unreinforced concrete pipes. The new standard may be described as being based on test results (i.a. obtained in Denmark and not published), but may, according to Ingwersen (1983)*), alternatively be described as being based on the theoretical results shown in Fig 4.6 (15) (ℓ_{ch}=380 mm).

Fig 4.6 (28) to Fig 4.6 (31), not forgetting the assumed numerical values of the material property parameters indicated in Fig 4.6 (23), may be discussed and interpreted from a number of different points of view. In this case, however, such discussions will not be continued. Instead some general conclusions as suggested by the current study and regarding the different fracture models and their applicability during the strength analysis of unreinforced pipes will be summarized.

During the present comparisons to test results, the two deterministic linear elastic brittle models have in a consistent manner exposed the worst characteristics of the different fracture models studied. Therefore it may be concluded that the two conventional models, both the "exact" model and the engineering model, do not seem suitable where predictions of crushing strength and bending strength of unreinforced concrete pipes are concerned. From the practical point of view, it is of special importance to notice that these models should not be used during prediction of bending strength from experimentally known values of crushing strength. When designing one may possibly treat crushing and bending separately, using different apparent values of the tensile strength of the material. This approach yields a substantial improvement in accuracy, but requires experimental information from both crushing tests and bending tests, and it seems that even if this approach is adopted, the elastic brittle models still yield poor strength predictions as compared to other fracture models. Although the linear elastic brittle models do not seem to be appropiate for prediction of ultimate strength, the linear elastic theory may be useful for estimation of deformation and distribution of stresses within the pipe at normal service magnitudes of load, provided that these loads are substantially less than the ultimate load.

*) See also Ingwersen (1984).

The Weibull-model, just like the deterministic linear elastic brittle models, is not capable of predicting the difference between strength during bending and during crushing respectively. The essential nice features of the Weibull-model are that it takes influence of scatter of strength into account in a simple manner and that it predicts an influence of absolute size. However, the general accuracy and precision of the Weibull-model do not appear to be very good.

The ideal plastic models expose a surprisingly good precision, especially when taking the unrealistic basic assumption with respect to the fracture behaviour of the unreinforced concrete into consideration. Consideration of limitation in compressive strength yields a somewhat improved precision and, of course, a somewhat more realistic correlation to the absolute magnitude of the true uniaxial tensile strength. The considerable deviation between true and apparent tensile strength suggests that the real distribution of stresses within a concrete pipe is not in accordance with the model. Another drawback of the plastic models is that they are not able to predict any influence of size. A nice feature, besides the surprisingly good precision, is that the plastic models enable comparatively simple derivations of ultimate strength. This simplicity might become handy if one also wants to derive the theoretical ultimate load for more complicated failure modes than bending and crushing. The simplest, but not necessarily simple, way to treat more complicated failure modes is probably by the utilization of the kinematical theorem of plasticity. Starting from a known value of tensile strength, this theorem yields an upper boundary of the ultimate load both in comparison to an exact plastic calculation and in comparison to a calculation based on a more realistic basic assumption with regard to the fracture behaviour of concrete.

The calculations based on the fictitious crack model expose a very good precision and appear to be more reliable than any of the other computational models currently dealt with. The very good precision and the comparatively very good agreement between the estimatemd true tensile strength and the apparent tensile strength suggests that this theoretical model of fracture reproduces the true fracture behaviour in a more realistic manner than any of the other models. It is not possible to exactly predict failure loads, but when designing one has to use some computational model and at a choice, at the current stage of knowledge, between the six models currently dealt with it appears quite clear that

one ought to choose the fictitious crack calculations when predicting the bendning strength and crushing strength of unreinforced concrete pipes. However, it may be recalled that the available test results used in the present comparisons all have their different draw-backs and that the available bend tests cover only a rather limited range of variation in size and shape of the pipes. Naturally, it is therefore very possible that future studies may indicate that the present analysis ought to be refined or made more realistic in other ways.

The present theoretical results obtained by means of fracture mechanics are believed to be practically useful and it may be of some interest to reflect on the efforts required if a corresponding study were to be carried out by mere experimental and statistical means. During experimental tests, experimental errors are added to the basic scatter, and this rather substantial total scatter in experimental results suggests that a large number of tests is required. Thus, for instance, if one (only) wants to determine the mean value of the ratio f_f/f_{cr} for a specific geometry and size of a pipe made of a specific quality of concrete, one has to carry out about $13(s/\alpha)^2$ bend tests and the same number of crushing tests in order to estimate the true mean ratio with an accuracy of $\pm 100\alpha$ % at a reliability of 99 %. This number of tests corresponds to a 100s % coefficient of variation in the experimental results and may be obtained from the Gauss approximation formulas for several (in this case two) independent stochastic variables, see for instance (Blom, 1970). (It is assumed that bending strength and crushing strength are independent stochastic variables. This assumption should be fair if the tests are carried out on different nominally equal pipes.) If s=10.8 %, accordingly 15+15 tests only yield an accuracy of about ±10 % for an estimation of the mean value of ratio f_f/f_{cr} for the specific type of pipe investigated. Consequently, if general, accurate and reliable strength relations are to be obtained only by experimental means without reflecting on the fracture behaviour of the material, then an enormous number of tests are required. Taking the very high price of the moulds used in concrete pipe manufacturing into account, it seems to be hardly possible to develop general relations merely by experimental and statistical means. This suggests a conclusion of the present study: It is meaningful to apply fracture mechanics during strength analysis of concrete, also from practical points of view.

In Section 4.2.5 a combination of the fictitious crack model and the

Weibull model is applied to the flexural strength of statically determinate beams with rectangular cross section. Any such combination has not been applied during the present study of pipes, but it may be appropiate to include a few remarks. Where design is concerned the study of Section 4.2.5 suggests that one may reflect on multiplying the bending strength predictions of the fictitious crack calculations by the factor $(1/\beta)^{1/m}$ at an increase in length of the pipes by the factor β,. Thus, for instance, when m=14 an increase in length from 1.5 m to 3.0 m would be predicted to yield a 5 % reduction in the bending strength. Similarly, see eq (4.2:14), one may reflect on possible scatter induced influence of type of load on the ultimate bending capacity. When m=14 the ratios between ultimate bending capacity at three-point bending, four-point third point bending, uniformly distributed load along the pipe, and constant bending moment along the pipe would be predicted to be 1.000:0.884:0.915:0.824.

A similar type of reasoning might apply to the crushing strength in variation of the diameter of the pipes and in variation of the width of the "line"-loads at crushing. But for small or normal diameters, the lengths, as calculated by the assumption of a homogeneous medium of the regions exposed to high stresses are small, and the regions where the stress (or bending moment) raised to m is great are even smaller and of the same magnitude of size as the local heterogeneities of the concrete. For such small sizes of the highly stressed regions, calculation of the size of these regions by assuming ideal homogeneous material are not valid and it is not very probable that a further theoretical decrease in the size of the highly stressed regions by a decrease in the diameter of the pipe would yield an increase in ultimate global strength. In order to take this feature into account when predicting the influence of scatter on mean ultimate strength, the integration with regard to possible failure mechanisms might preferably be carred out by assuming a finite thickness of the volume of material corresponding to each possible failure mechanism, i.e. each possible location of the fracture surfaces. Another essential difference when considerating the influence of scatter on the fictitious crack predictions of crushing strength, as compared to prediction of bending strength, is that the crushing failure corresponds to a statically indeterminate system, whereas the bending failure does not. This means that the concept of the "weakest link" (the "weakest fracture surface") does not apply in the case of crushing. If, in spite of this, the actual type of combination between the fictitious crack model and the Weibull model were to be applied during interpretation of crushing

strength test results, it should be noticed that the width of the "line loads" is normally not changed during testing of pipes with different diameter.

From the point of view of design of an entire pipe-line, the scatter-in-strength induced decrease in the mean bending strength of a pipe at increased length of the pipe, may not be of great importance: The probability of failure somewhere along a pipe-line is governed by the sum of the lengths of the pipes, i.e. by the length of the entire pipe-line, and not by the length of the individual pipes.

This Section, Section 4.6, has dealt with theoretical strength analyses of pipes by means of models of the fracture behaviour of materials, and then the theoretical results were applied to the analyses of pipes made of unreinforced concrete. The models of fracture and the computational results are, however, not related to any specific material and may, - more or less successfully -, be applied to strength analyses of pipes made of any material. Some examples of such possible additional applications may finally be listed:

1) The fictitious crack analysis and/or the Weibull analysis may perhaps be meaningful for application in the analysis of pipes made of cast iron.

2) Reinforced concrete pipes are often reinforced only in the tangential direction and it therefore appears fair to believe that the fictitious crack analysis may be meaningful for application in the analyses of bending strength of such reinforced concrete pipes.

3) Due to the requirement of tightness (in order to avoid leakage of subsoil water into the pipes) of sewage pipes, the cracking load is of interest for the reinforced pipes, and this load might be studied by means of the fictious crack analysis.

4) Plastic analysis, taking into account limited compressive strength, may perhaps be applied in short time load analysis of pipes made of plastics.

5) Features of the fictious crack analysis might be of interest for long time load analysis of pipes made of plastics.

6) Pipes made of clay seem to exhibit similar features with regard to to strength relations as pipes made of unreinforced concrete (See (Brennan, 1978)), and it is therefore probable that the fictitious crack analysis is meaningful for application in strength analysis of pipes made of clay.

As a postscript to this Section it may be added that theoretical fracture mechanics analysis of concrete pipes has proved to be practically useful. With the assistance of the fracture mechanics results Isgren, working at a design-office, has designed new concrete pipes, developed a new loading arrangement for factory-testing of pipes (bending instead of crushing) and calculated economical optimum for the length of concrete pipes. As previously mentioned, the theoretical results in Fig 4.6 (15) has been utilized during the development of a crushing-strength design formula, included in a new Danish design standard for concrete pipes. According to private communication, during a present development of a new Swedish design standard, it has been found that the fracture mechanics results are applicable also to calculation of the cracking load of reinforced concrete pipes. Bazant and Cao (1985) has utilized above calculated tensile strengths during an evaluation by means of the size effect law of Bazant (Section 3.5.3) of the strengths of the pipes in the corresponding tests groups. During this application of the actual size effect law, an additional empirical parameter, not discussed in Section 3.5.3, was introduced so that both bending and crushing could be treated.

4.7 Strength of wood beams jagged at support

4.7.1 Introduction

The fictitious crack model was originally developed for the analysis of cement based materials, and the results in the previous parts of this Chapter suggest that the model can be useful during analysis of such materials. The purpose of the study in this Section is primarly to obtain an understanding of the possibility for application of this model also during the analysis of an other type of material. Primarily at this purpose, the strength of wood beams, jagged at support according to Fig 4. 7 (1) is studied. In contrast to the analyses in the other parts of Chapter 4., the present strength analysis concerns an orthotropic material, crack growth from a corner and the development of a fracture zone in which the stress is not perpendicular to the crack growth direction. The study should not merely be of theoretical interest as the current type of detailing is not unusual at wood construction.

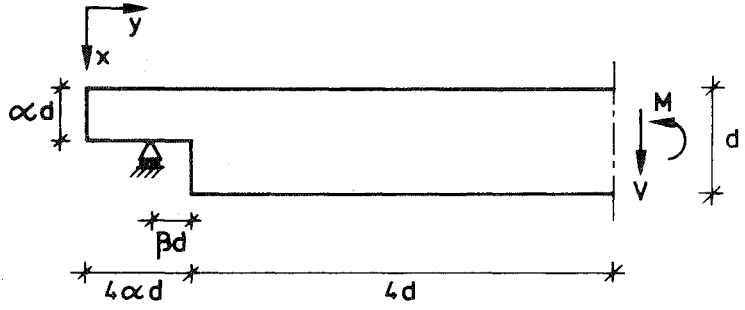

Fig 4.7 (1) Wood beam with a jag at support.

From the point of view of fictitious crack analyses, a study of the strength of a corner in an orthotropic material should not involve any difficulties in principle. From the point of view of conventional methods of strength analyses, a study of the strength on an internal corner involves basic difficulties. The strain in the tip of the jag is infinite and, if a conventional method of theoretical analysis is to be applied during a strength analysis, it seems that restriction must be made to the theory of unlimited plasticity. However, because of the brittle properties of wood during fracture perpendicular to the grain, (See Fig 3.2 (4).), one may hardly expect the theory of unlimited plasticity to give any reasonable results. and if the contrary is true then this should be

suggested by results obtained during fictitous crack analysis. The conventional linear elastic fracture mechanics can not be used as the singularity in the tip of a corner is weaker than the singularity in the tip of a sharp crack (Fig 3.4 (9), isotropic material). By the definition of the conventional stress intensity factor ($K \sim \sigma(r)\sqrt{r}$, $r \to 0$), the conventional linear elastic fracture mechanics simply predicts that internal corners cannot fracture (if $K_c > 0$). Again due to the singularity, the conventional Weibull theory (in which the property of a linear elastic material is defined with reference to an infinitesimal volume) can not be used unless an artificial assumption, governed by the geometry of the corner and not by the actual properties of the material, is made with respect to the stochastic properties of the material.

The method of analysis of corners in brittle specimens discussed in Section 3.4.5 makes it possible to analyse the relative influences of size and material properties on strength at different opening angles of a corner. But, even if the specimen is very brittle, it is not believed to be possible to calculate any absolute value of the strength (i.e. the value of the constant C in eq (3.4:17)) without account taken to the fracture properties of the material (i.e. the shape of the σ-w curve) and to the development of a fracture zone of non-zero size.

Any theoretical study of the current structural detail was not found in the small amount of literature searched through. On the other hand, a formula for the strength of the current structural detail, most probably developed by means of experimental results, may be found in building codes and elsewhere, see Section 4.7.4. The somewhat related problem of the strength of tapered wood beams, i.e. wood beams with a gradually decreased depth from midspan to support, has been treated in a theoretical manner by means of the Weibull theory by Liu (1981). (See also discussion by Guthowski (1982)).

Section 4.7.2 deals with calculation of the load of start of unstable crack growth along the beam. Section 4.7.3 deals with mechanics at ultimate failure of the jagged wood beams, and in Section 4.7.4 is found a comparison to experimental results together with some concluding remarks.

4.7.2 Fictitious crack analysis of crack stability

Wood may ideally be assumed to be an orthotropic material with three principal material axes in each point: parallel to grain, tangential to the annual rings and perpendicular to the annual rings. The properties parallell to the grain are very much different from the properties in the other two directions, while differences between the tangential and radial axes are less and further on very unpractical to take into account both in design, construction and theoretical strength analyses. At theoretical analyses the associated difficulties have mainly to do with the out-of-plane variations of the tangential and radial directions. In the current plane stress analysis the material is accordingly assumed to be orthotropic with one principal axis parallel to the grain and equal properties in all directions perpendicular to the grain.

In an experimental investigation (Valentin and Morlier, 1982)) of the critical value of the J-integral, J_c, of wood (northern pine, Pinus silvestris L) fracture along the grain perpendicular to the tangential axis respectively perpendicular to the radial axis was considered exclusively and it was concluded that the difference between these two fracture directions was negligable. The at present only available values of G_F of wood (tall; "ordinary Swedish pine"; Pinus silvestris) were obtained by Helmersson (1978) and in his investigation differences between the two perpendicular-to-grain directions were not studied. Bodig and Jayne (1982) have presented a literature-survey of fracture toughness values, K_c, of some different kinds of wood. These values relate to linear elastic fracture mechanics and it may be noted that K_c, refering to mode 1 fracture along a principle direction of an orthotropic material, is not only dependent on the perpendicular to crack-plane direction but also on the crack growth direction, while G_F and J_c theoretically only depends on the perpendicular-to-crack-plane direction.

According to Zienkiewics (1977), the stress vs. strain relation of the assumed linear elastic ortotropic material in plane stress is:

$$\begin{bmatrix} \sigma_x \\ \sigma_y \\ \tau_{xy} \end{bmatrix} = \frac{1}{1-\nu_x\nu_y} \begin{bmatrix} E_x & \nu_y E_x & 0 \\ \nu_x E_y & E_y & 0 \\ 0 & 0 & G \end{bmatrix} \begin{bmatrix} \varepsilon_x \\ \varepsilon_y \\ \gamma_{xy} \end{bmatrix} \qquad (4.7:1)$$

In this relation four parameters are independent: E_x, E_y, G and ν_y. The fifth parameter, ν_x, is equal to $\nu_y E_x/E_y$ due to symmetri in the stress vs. strain relation, which in turn is a consequence of invariant energy irrespective of the path taken to reach a given strain state.

The fracture currently studied is assumed to take place as a fracture zone and crack growth in the y-direction along the grain of the beam, starting from the corner of the jag. The fracture might perhaps essentially be looked upon as a perpendicular-to-grain tensile fracture, but the forces transferred across the fracture plane are not, due to the orthotropic kind of material, perpendicular to the fracture plane. Thus a shear stress component has to be taken into account in addition to the pure tension stress. In order to achieve this with respect to criterion of start of fracture zone development, a two-parameter criterion according to Fig 4.7 (2) was adopted. The two parameters corresponds to the tensile strength, f_t, perpendicular to the grain respectively shear strength, f_s, parallel to the grain. Once the currently assumed fracture criterion is reached in some point along the fracture plane, a fracture zone is introduced in this point. In lack of experimental investigations of the fracture softening properties of wood, the fracture zone is assumed to be sufficiently described by simple straight line relations between force transferred across the fracture zone, $\sqrt{\sigma^2 + \tau^2}$, and the deformation of the fracture zone, $\sqrt{w_\perp^2 + w_{//}^2}$, Fig 4.7 (3). At zero deformation, the force transferred is determined by the fracture criterion, and the slope of the relations between $\sqrt{\sigma^2 + \tau^2}$ and $\sqrt{w_\perp^2 + w_{//}^2}$ is choosen to be independent of the value of $\sqrt{\sigma^2 + \tau^2}$ at start of fracture and further on choosen in such a way that the area below the stress vs. deformation curve at zero shear is equal to the fracture energy at pure perpendicular-to-grain tensile fracture, here denoted G_F.

The numerical values of the strength and deformation ratios used in the analysis aimed to approximately reflect the properties of Pinus silvestris, free of defects, with a moisture content of 12 % by weight (roughly corresponding to about 60 % relative humidity in the air) and tested at room-temperature (about 20°C) at short time loading: E_x=460 MPa, E_y=12000 MPa and ν_y=0.4 (Bergström et al., 1970), f_t=3.7 MPa and G_F= 360 N/m (Helmersson, 1978), $G=0.35\sqrt{E_x E_y}$=822 MPa and $f_s=\sqrt{10}/2\, f_t$=5.85 MPa. The expression of moduli of rigidity, G, ought to be a reasonable engineering approximation which, at the choosen value of E_x, also may be expressed as G , 1967) and

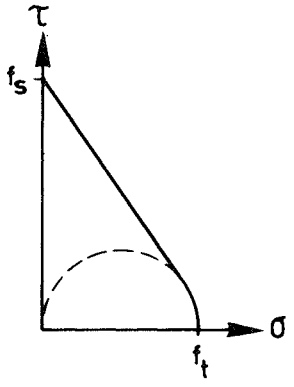

Fig 4.7 (2) Fracture criterion. σ=tensile stress perpendidular to grain. τ=shear stress along grain.

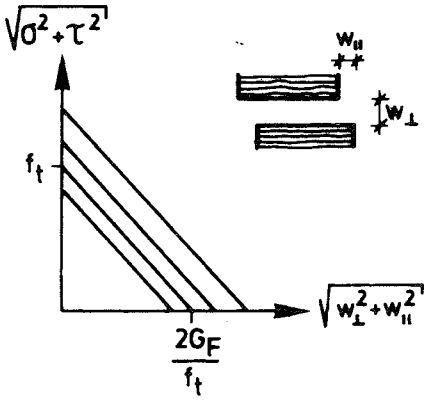

Fig 4.7 (3) Softening properties of fracture zone perpendicular to grain.

G/E_y=0.050 (SBN-80, 1980). The value of f_s is probably too low with respect to Pinus silvestris at current conditons, but was used in order to facilitate utilization of a computer program orginally developed in order to analyse concrete. For the characteristic length of the material perpendicular to the grain, the values above give $E_x G_F/f_t^2$=12.1 mm.

During the numerical calculations it is not necessary to specify the absolute values of the material property parameters, only dimensionless ratios. This makes the results more general. In accordance with the examples of absolute values given above, the following values of the ratios required during the strength analysis were used. E_y/E_x=26.1, G/E_x = 1.79, ν_y=0.40 and f_s/f_t=1.58, while ratio $d/(E_x G_F/f_t^2)$ was assigned different values which are given below. (During deflection analysis also ratio f_t/E_x must be specified.)

The value of G_F, 360 N/m, reported by Helmersson and obtained as the total work of fracture at three point bending is in fair agreement with the values of J_c obtained by Valentin and Morlier. These later investigators used DCB-specimens and obtained mean values of J_c from 285 (300) N/m to 348 (377) N/m dependent on the method used to evalute the experimental results. The figures in brackets corresponds to fracture perpendicular to the tangential direction of the annual rings and outside brackets

fracture perpendicular to the radial direction. Regarding coefficient of variation at constant experimental conditions and constant method of evaluation, the exerimental results suggests approximately 20 % for J_c and approximately 10 % for G_F.

The present numerical calculations regarding the fracture zone development in wood were carried out with the help of the finite element method and in essentially the same manner as the similar analyses of concrete. The beam was divided into a mesh of rectangular 40-node plane stress elements, each such element basically being an assembly of 4 triangular constant strain elements. The number of 4-node elements along the depth of the beam was 16. The distance between the nodes along the fracture zone propagation path was d/13.5 in the analysis of beams with α=0.25 and d/6.75 in the analysis of beams with α=0.50. Prior to the incremental analysis of the fracture zone development, all degrees of freedom except those along the fracture zone path and those at the point of load application were eliminated by means of condensation. The force transfer across the fracture zone was, as in previous analyses of concrete, modelled by use of single discrete springs between corresponding nodal points at opposite sides of the fracture zone. The springs were placed, and kept, in the direction of the force across the fracture zone at the instant at which the fracture criterion is reached. Perpendicular to this direction of the force across the fracture zone, the resistance to deformation of the fracture zone was put equal to zero.

Altogether 16 beams were analysed. The geometry shape parameters and were assigned the following values: (α,β) = (.25, .25), (.25, .50), (.50, .50) and (.50, 1.00). For each geometrical shape of the beam, ratio $d/(E_x G_F/f_t^2)$ are assigned four different values: 1.31, 2.61, 5.22 and 10.4 during the analysis of beams with α=0.5 and 2.61, 5.22, 10.4 and 20.9 during the analysis of beams with α=0.25.

The calculations primarily aimed to determine the load at which the fracture zone development becomes unstable during a monotonic increase in the external load. However, before going on to those results, it may be of interest to study results regarding load vs. depth of fracture zone. In Fig 4.7 (4) a) load vs. depth of the fracture zone is shown for α= β=0.5 and the different values of $d/(E_x G_F/f_t^2)$. The corresponding results obtained for the other combinations of α and β are similar. The distance a indicated in the figure is the distance between the tip of the corner and

the nodal point where the fracture criterium is reached. V is the shear force. The figure shows that the load carrying capacity is predicted to decrease almost drastically during increase in $d/(E_x G_F/f_t^2)$. The figure also shows that the element mesh is coarse: For the higher values of $d/(E_x G_F/f_t^2)$, the distance between the nodal points is large in comparison to the depth of fracture zone, the fracture zone at peak load being modelled by only one element for largest $d/(E_x G_F/f_t^2)$. This suggests that a large number of elements may have to be used during finite element analysis of wood beams with normal or large size. On the other hand, it may not be necessary to carry out finite element calculations in order to obtain the load carrying capacity for beams with a high value of the ratio $d/(E_x G_F/f_t^2)$: See below and Section 3.5.3.

One interesting result indicated by Fig 4.7 (4) a) is that the depth of the fracture zone at the instant of instability is constant, with the exception only for the smallest $d/(E_x G_F/f_t^2)$. Of course, the result that this depth is exactly constant for $d/(E_x G_F/f_t^2)>2.61$, is partly a result of the coarse finite element mesh. In spite of this, with $E_x G_F/f_t^2=12.1$ mm, the computational results suggest that the depth of the fracture zone of instability is approximately constant and about 20 mm for beams with d greater than 50 mm. The same approximate value, 20 mm, was obtained for all studied combinations of α and β, but for $\beta=0.25$ it seems that the beam must be somewhat larger before the constant value of the critical fracture zone depth is reached with the same accuracy. For other shapes of the σ-w curve than the presently assumed, one may expect to obtain other critical lengths of the fracture zone, even if $d/(E_x G_F/f_t^2)$ is put equal to 12.1 mm.

We now turn to the load at instability, V_f. As the characteristic length of wood perpendicular to the grain, $E_x G_F/f_t^2$, is small, the matters dealt with in Section 3.4.5 may arouse the suspicion that the following relation, valid for a very brittle isotropic beam with a 90-degree jag, might be applicable also to the similar beam made of an ortotropic material.

$$\frac{V_f}{f_t b \alpha d} \sim \left\{ \frac{d}{E_x G_F/f_t^2} \right\}^{-0.4555} \qquad (4.7:2)$$

However, this relation requires that the size of the fracture zone is very small in comparison to the size of the beam. In the present case, the size of the fracture zone is not very small in comparison to the size of normal beams. But the size of the fracture zone at the instant of peak load seems

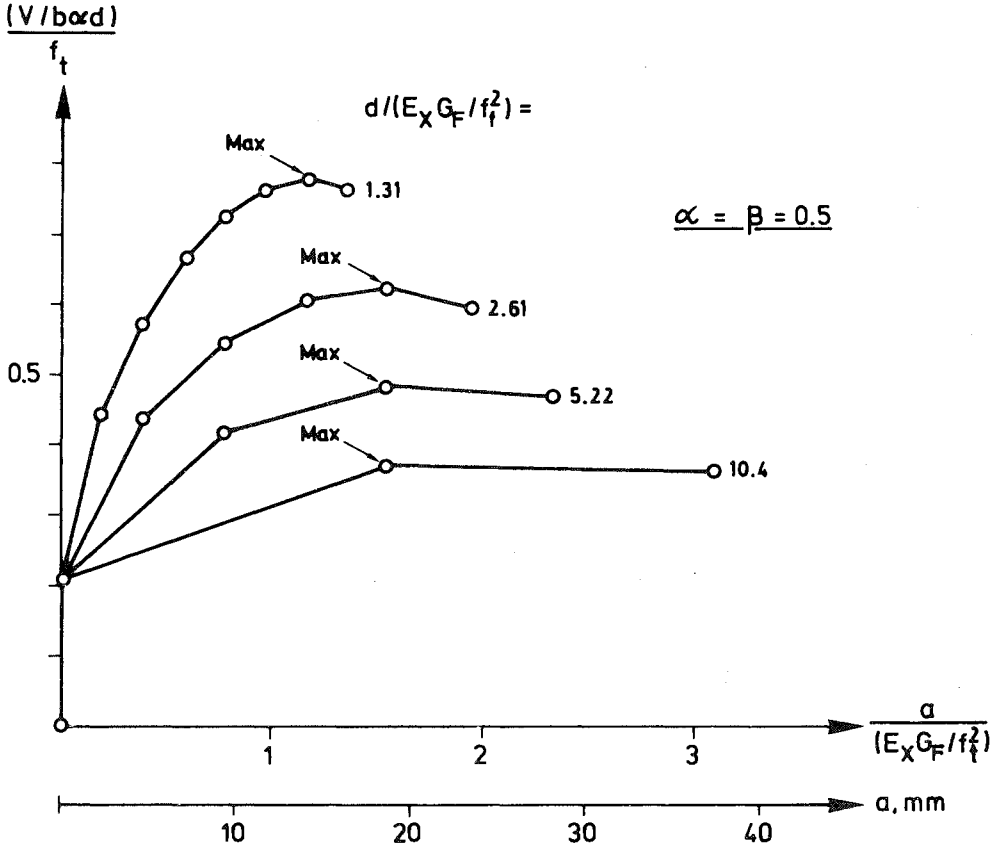

Fig 4.7 (4) a) Load, V, vs. depth of fracture zone, a, at different $d/(E_x G_F/f_t^2)$. Geometry acc. to Fig 4.7 (1) with $\alpha = \beta = 0.5$. Lower axis of abscissa valid when $E_x G_F/f_t^2 = 12.1$ mm.

to be approximately constant. This suggests (Section 3.5.3) that the following relation might be a good approximation for beams of normal and large sizes:

$$\frac{V_f}{f_t b \alpha d} \sim \left\{ \text{const.} + \frac{d}{E_x G_F / f_t^2} \right\}^{-0.4555} \qquad (4.7:3)$$

Introducing the constants C and e, this relation can be written:

$$\frac{V_f}{f_t b \alpha d} = C \left\{ \quad + \quad \frac{d}{} \right\}^{-0.4555} \qquad (4.7:4)$$

				$V_f/(f_t b\alpha d)$ acc. to FEM-calc. / $V_f/(f_t b\alpha d)$ acc. to eq (4.7:4)				
				$d/(E_x G_F/f_t^2)$ =				
α	β	C	e	1.31	2.61	5.22	10.4	20.9
0.25	0.25	1.263	1.16	-	.690 / .690	.543 / .543	.427 / .414	.327 / .309
0.25	0.50	0.963	0.87	-	.546 / .546	.423 / .423	.319 / .319	.239 / .237
0.50	0.50	1.109	0.92	.777 / .770	.624 / .624	.485 / .485	.373 / .367	-
0.50	1.00	0.785	0.42	.605 / .612	.474 / .474	.357 / .357	.274 / .265	-

Fig 4.7 (4) b) Load at instability, V_f, acc. to FEM-calculations and acc. to eq (4.7:4). Constants e and C in eq (4.7:4) determined from the FEM-results for $d/(E_x G_F/f_t^2)$=2.61 and 5.22.

As compared to eq (3.5:6), other notations of the two constants are used in this Section, so that it is made clear that eq (3.5:6) is intended for isotropic materials while it is not known whether the relation is valid for the present orthotropic material. The dimensionless constants C and e depends on the geometrical shape of the beam. C may be looked upon as a measure of the strength of very large beams and is dependent of the absolute size of the fracture zone. The constant e may be interpreted as a measure of the influence of the finite relative size of the fracture zone. The numerical values of C and e can be determined by means of fictitious crack analyses carried out with the help of the finite element method for two different values of $d/(E_x G_F/f_t^2)$.

Presently the values of C and e are determined from the calculated values of $V_f/(f_t b\alpha d)$ for $d/(E_x G_F/f_t^2)$=2.61 and 5.22. From the point of view that eq (4.7:4) should be more accurate the greater $d/(E_x G_F/f_t^2)$ is, large values of this ratio should be used when C and e are determined. On the other hand, the values of $V_f/(f_t b\alpha d)$ presently obtained for the larger values of ratio $d/(E_x G_F/f_t^2)$ may not be very accurate due to the coarse finite element m[illegible]mediate

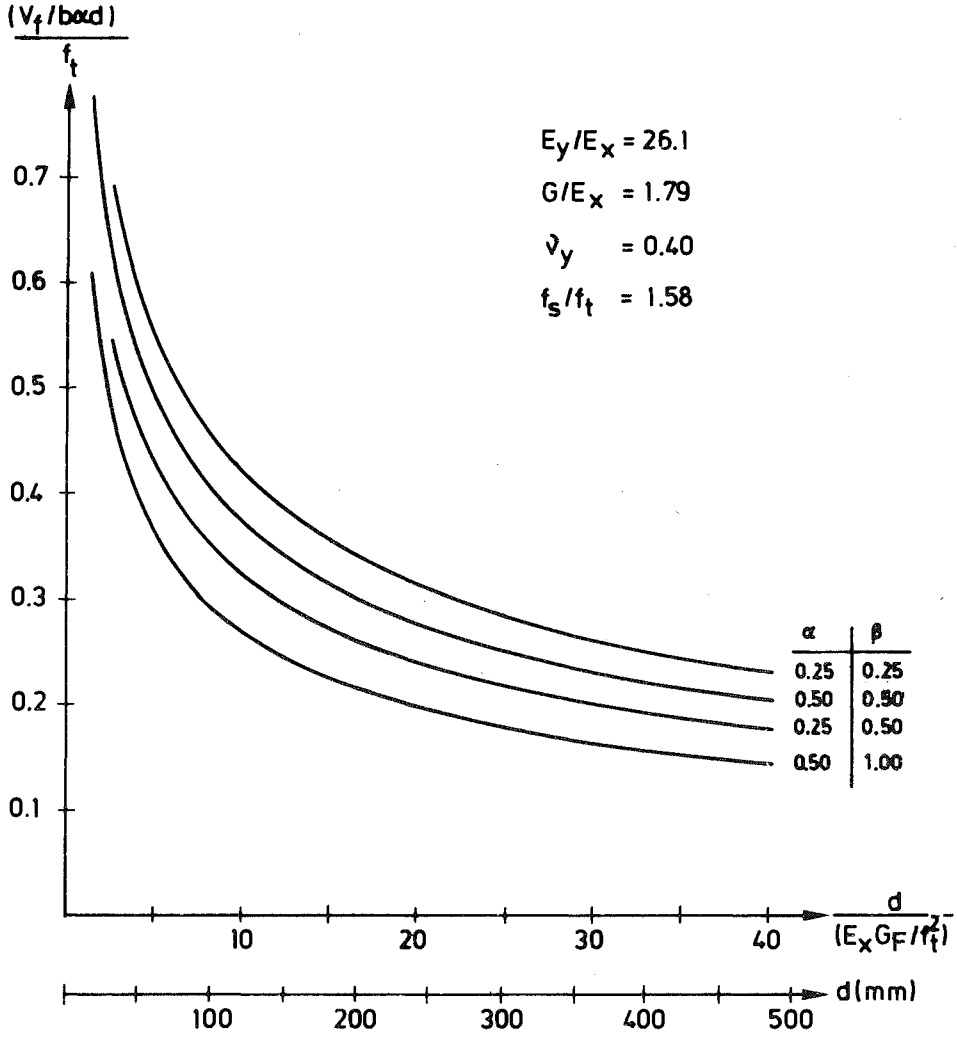

Fig 4.7 (4) c) Theoretical prediction of the shear force, V_f, in jagged wood beams at start of unstable fracture zone propagation. Geometry acc. to Fig 4.7 (1). Lower axis of abscissa valid when $E_x G_F/f_t^2 = 12.1$ mm.

$d/(E_x G_F/f_t^2)$ have presently been utilized. In Fig 4.7 (4) b) is found $V_f/(f_t b\alpha d)$ as obtained during the finite element calculations and also as obtained by means of eq (4.7:4). The values of constants C and e can also be found in this figure.

Due to the coarse finite element meshes for largest $d/(E_x G_F/f_t^2)$ and the adopted method for calculation of the stress in the tip of the fracture zone (Section 3.6), one may expect the finite element results to give somewhat higher values of V_f for the largest $d/(E_x G_F/f_t^2)$ than eq (4.7:4). Such somewhat higher values are also suggested by the numerical results.

Here it may also be of interest to make an estimation regarding the accuracy of eq (4.7:2). Taking the case $\alpha=\beta=0.5$ (which gave e =0.92) as an example and assuming that eq (4.7:3) is accurate, then eq (4.7:2) with $E_x G_F/f_t^2$=12.1 mm gives a 10 % overestimation of V_f for d=50 mm, a 5 % overestimation for d=100 mm and a 3 % overestimation for d=200 mm.

As can be seen in Fig 4.7 (4) b), the values of the dimensionless constant e decrease with increasing β, i.e. with increasing distance from the fracture region to the point of load application. Keeping d constant, this suggests that e is governed by the distance from the fracture zone to the major disturbances in its vicinity. By disturbance is then meant loads and boundaries that disappear from any finite vicinity of the fracture region, or changes its shape within the vicinity, if the size of the specimen is increased towards infinity. Naturally, the numerical value of e is dependent of how the absolute size of the specimen is measured. Here the absolute sizes of the specimens are compared by the depth of the beams. This is convenient, but it may be that it would be more informative to compare the absolute size of specimens with different shape by the distance from the fracture region to the closest major disturbance. If knowing the value of e, a generalized measure of the absolute size of specimens with different shape would be d/e. This measure is independent of how d is defined. The corresponding dimensionless generalized measure of size would be $(d/e)/(E_x G_F/f_t^2)$.

The results regarding $V_f/(f_t b\alpha d)$ vs. $d/(E_x G_F/f_t^2)$ are also shown in the diagram of Fig 4.7 (4) c). The extrapolation in this figure into large values of $d/(E_x G_F/f_t^2)$ has been carried out by means of eq (4.7:4). The figure shows that a decrease in α or an increase in β gives a decrease in V_f. The influence of α on V_f seems, however, rather small and appears, in

particular, not to be linear. It is interesting that E_x, G_F and d has influence on V_f, that this influence is greater than the influence of f_t and that f_t appears to have only a small influence on V_f. A doubling of E_x or G_F or a halving of d increases V_f with about 30 %, while a doubling f_t increases V_f with only about 10 %. A further discussion of these results can be found in subsequent Sections together with a comparison to a few experimental results.

4.7.3 Mechanisms at ultimate failure

V_f, the shear force at start of unstable crack growth along the grain, does not necessarily coincide with the ultimate shear force, V_u of the beam. Firstly, a crack along the beam does not change the geometry of the beam into a geometrically non-determinate system, which means that V_u may be larger than V_f. Secondly, only one crack path, failure mode or failure mechanism, is considered at determination of V_f while other failure modes may be more dangerous, which means that V_u may be less than V_f. It appears thus appropriate to make some simple considerations of the mechanisms at ultimate failure of jagged beams in order to determine when V_f coincides with V_u. Apart from V_f, quantifying of loads corresponding to the different possible failure mechanisms is carried out by means of engineering beam theory and by means of the strength concept of linear elastic brittle materials. These assumptions are convenient, commonly used at design of wooden structures and, as to the assumed behaviour of the material, theoretically on the safe side. However, it should be emphasized that the assumptions may yield very approximate theoretical relationships, only forming a basis for discussions of experimental results and more refined types of theoretical analyses.

Possible failure mechanisms are choosen to be discussed with reference to a symmetrical beam carrying a point load at mid-section. If the beam is very slender, Fig 4.7 (5) a), it will of course fail in bending and not due to shear, and in this case $V_u/bd=1/3(d/\ell)f_f$, f_f being the flexural strength. If the beam is made somewhat less slender, Fig 4.7 (5) b), then $1/3(d/\ell)f_f$ becomes greater than $\alpha(V_f/(b\alpha d))$ and a crack will thus propagate in an unstable manner along the grain of the beam before the entire cross section fails in bending. The unstable fracture zone propagation ideally leaves a net cross section of size $b\alpha d$ and of bending capacity $b\alpha^2 d^2 f_f/6$ to carry the be ed because:

1) The fracture zone is not an entirely open crack when its unstable growth reaches the mid-section of the beam and thus the net cross section, $b\alpha d$, has support in bending capacity from the lower part of the cross section, $b(1-\alpha)d$.

2) Possible inclination or curvature of the grain may cause the net cross section at mid span to become more or less than $b\alpha d$.

3) The flexural strength of wood beams increase slightly at decreased depth of the beam acc. to (Both and Reece, 1967) and (Kollmann, 1951).

However, if assuming "ideal" behaviour, which assumption in a mean sense ought to be on the safe side, then the bending capacity of the beam, after unstable fracture zone propagation, corresponds to the shear force $1/3\,\alpha^2(d/\ell)f_f$. At the intermediate slenderness, Fig 4.7 (5) b), this shear force is less than the shear force at start of unstable fracture zone propagation and accordingly $V_u/bd=\alpha(V_f/(b\alpha d))$. Finally, if the beam is rather short and deep, Fig 4.7 (5) c), then $1/3\,\alpha^2(d/\ell)f_f$ is greater than $\alpha(V_f/(b\alpha d))$ and thus $V_u/bd=1/3\,\alpha^2(d/\ell)f_f$. Putting $A\equiv(f_f/3)/(V_f/(b\alpha d))$, a summing up yields:

$$\frac{V_u}{bd} = \begin{cases} \dfrac{1}{3(\ell/d)}\, f_f & \text{if } \dfrac{1}{\alpha} \le \dfrac{(\ell/d)}{A} \\ \alpha\,(V_f/b\alpha d) & \text{if } \alpha \le \dfrac{(\ell/d)}{A} \le \dfrac{1}{\alpha} \\ \dfrac{\alpha^2}{3(\ell/d)}\, f_f & \text{if } \dfrac{(\ell/d)}{A} \le \alpha \end{cases} \qquad (4.7{:}5)$$

The reasoning above has reference to beams with significant jagging. In the case of no or minor jagging, short deep beams should also be checked regarding "ordinary" shear failure. This failure does not develop from the jag but develops close to the horisontal centerline of the net beam, d, according to either of the two types of fracture configurations at ultimate load shown in Fig 4.7 (5) d). Using ordinary engineering beam formulas, this requirement implies $V_u/bd \le 2/3\,\alpha f_s$. This simple inequality is approximate and is probably conservative at low ratios of slenderness due to support in shear capacity from the end of the beam outside the support and due to compressive stress across the shear fracture plane. If an "ordinary" shear fracture has developed then the beam is theoretically

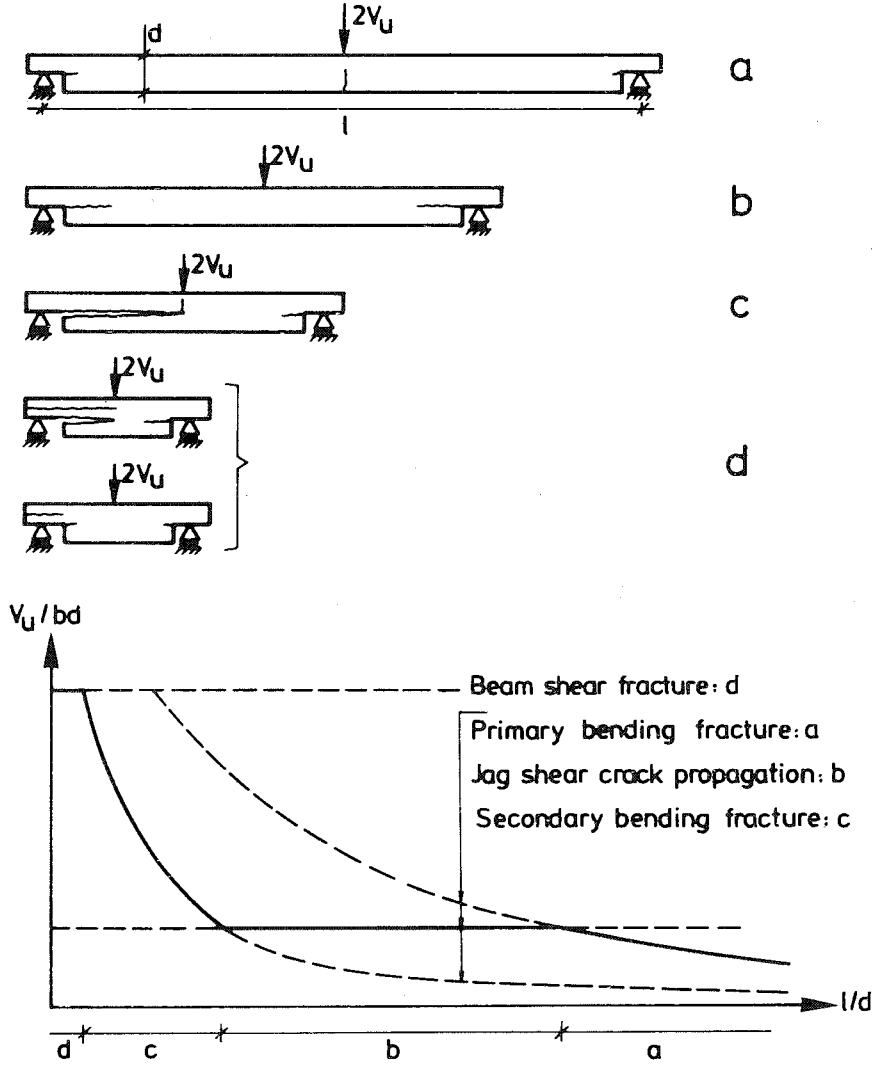

Fig 4.7 (5) Fracture zone configurations at ultimate load and illustration on principle of relationship between ultimate load and slenderness.

not able to carry any higher load and thus if either of the if-statements of (4.7:6) are true then (4.7:6) will override (4.7:5):

$$V_u/bd = \frac{2\alpha}{3} f_s \quad \text{if} \quad \frac{(\ell/d)}{(f_f/3)/f_s} \leq \frac{3\alpha}{2} \qquad (4.7:6)$$

$$\text{or if} \quad \frac{V_f/b\alpha d}{f_s} \leq \frac{2}{3}$$

According to the above, a short deep beam should behave with respect to ultimate load as a beam without a jag and of depth αd. If this is the case, i.e. if the simple engineering formulas apply do bending capacity and "ordinary" shear capacity, it does not appear very meaningful to use a jagged beam at construction if the beam has a low slenderness ratio: in the case of a three point bend beam if $\ell/d \leq \alpha A$ (assuming $V_f/(b\alpha d) \leq 2/3\ f_s$). The convenient concept to regard jagged beams of slenderness ratio less than αA as beams without jag and of depth αd may be useful at design as it ought to be an approximamtion on the safe side.

It should be added that if unstable crack propagation from the jag is prevented by a bolt through the depth of the beam or by some other arrangement, or if the distance from jag to support is considerable, then, in addition to the failure mechanisms of Fig 4.7 (5), consideration should also be taken to possible bending failure at the corner of the jag.

In Fig 4.7 (6) is shown a numerical example of V_u/bd vs. ℓ/d, obtained by means of Fig 4.7 (4) c) and (4.7:5) and (4.7:6). The example shown, being related to Section 4.7.4, is valid for α=0.5, β=0.5 and some different values of the beam size, d. The numerical values of the material property parameters required in order to quantify ($V_f/(b\alpha d)$) are assumed in accordance with 4.7.2 (f_t=3.7 MPa and $E_X G_F/f_t^2$=12.1 mm), and, in order to exemplify bending capacity, the flexural strength, f_f, has been assumed to be a constant and equal to 70 MPa. (According to Bergström et al.: f_f=2/3 100 MPa at "normal" sizes of pieces of Pinus Silvestris). The "ordinary" shear failure, (4.7:6), is incorporated in the figure by means of the previously adopted (conservative) assumption f_s=5.85 MPa.

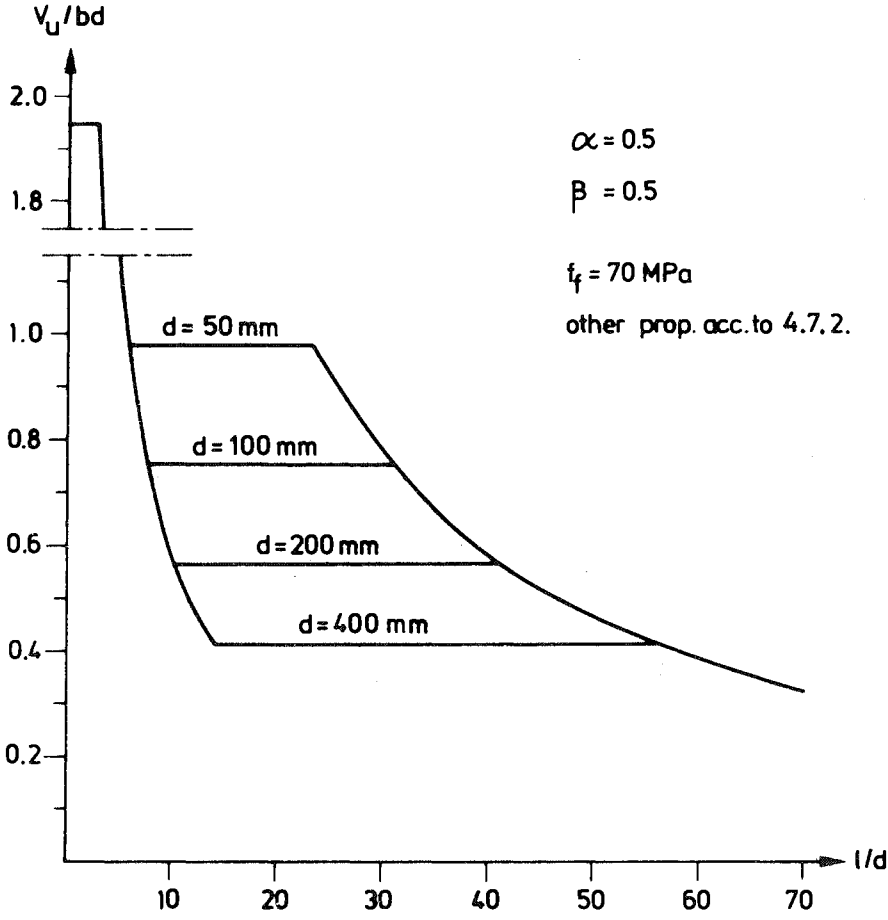

Fig 4.7 (6) A numerical example of theoretical ultimate loads, V_u/bd, vs. slenderness, ℓ/d, at different beam depths, d. The flexural strength, f_f, is assumed to be constant.

4.7.4 Comparisons. Concluding remarks

The study of Section 4.7.2 was carried out some years ago and the results have been used during teaching in building materials in order to provide an example of possible influence of absolute size on strength. In order to study whether these purely theoretical results had some relevance to the behaviour of r[illegible]ing (1983)

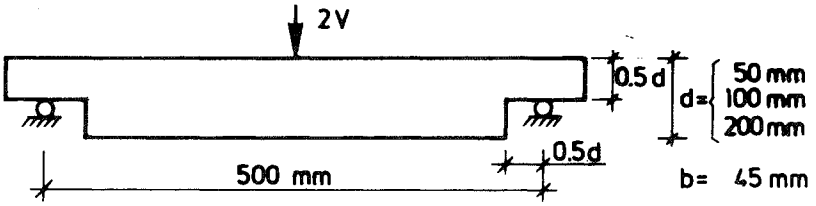

Fig 4.7 (7) Geometries of beams used in an experimental study carried out by Carlsson, Shahabi and Sunding (1983).

Geometry		Unstable crack propagation		Ultimate failure	
		$\alpha(V_f/b\alpha d)$ (MPa)		V_u/bd	f_f
d (mm)	ℓ/d	Theoretical prediction	Experimental results	(MPa)	(MPa)
50	10	0.98	0.89	0.98	118
			1.11	1.49	179
			(1.00)	(1.24)	(149)
100	5	0.75	0.67	2.33	140
			0.78	2.33	140
			(0.73)	(2.33)	(140)
200	2.5	0.56	0.56	3.28	98
			0.61	3.41	102
			(0.59)	(3.35)	(100)

Fig 4.7 (8) Strength of specimen shown in Fig 4.6 (7): Load at start of unstable crack propagation, $\alpha(V/b\alpha d)$, (theoretical prediction and experimental results) and at ultimate failure (experimental results and corresponding apparent flexural strength). Experimental res. acc. to (Carlsson, Shahabi and Sunding, 1983). Values in brackets are mean values.

carried out a limited experimental investigation as a seminar in a course of building materials. Their investigation primarely conserned the influence of beam depth, d, on $(V_f/b\alpha d)$. Specimens of Pinus silvestris with the geometries shown in Fig 4.7 (7) were used, and altogether 6 beams were tested. The shear forces at unstable crack growth, V_f, and at ultimate failure, V_u, were recorded.

The beams all exhibited the failure mode shown in Fig 4.7 (5) c). Thus the ultimate shear force, V_u, was greater than the shear force at the instant of unstable crack growth from the jag, V_f. The experimentally recorded values of V_f and V_u are indicated in Fig 4.7 (8), and this figure also indicates the theoretical preditions of V_f. These shear forces are given by the absolute values of the formal mean shear stress. The absolute values of the material property parameters required to obtain the theoretical predictions of strength expressed in absolute values of V_f were chosen in accordance with Section 4.7.2 and before the experimental tests were carried out: $E_x G/f_t^2 = 12.1$ mm and $f_t = 3.7$ MPa. Fig 4.7 (8) also indicates the formal flexural strength, f_f, as evaluated from the experimentally recorded ultimate loads by menas of the expression $V_u/bd = \alpha^2 (d/\ell) f_f/3$, eq (4.7:5).

As to $(V_f/b\alpha d)$, the agreement between the theoretical predictions and the experimental results is remarkably very good both with respect to absolute values and relative influence of beam depth. The agreement may of course be coinsidential and, especially regarding the absolute values of $(V_f/b\alpha d)$, one may hardly expect the same very good agreement in prospective future experimental investigations. However, the relative influence of beam depth seems significant and apparently not of minor practical importance: an increase in depth from 50 mm to 200 mm almost halves $(V_f/b\alpha d)$. As to V_u/bd, the experimental results yields high values of the coresponding formal flexural strength, f_f, and f_f is, as might be expected, greater for the small beams than for large beams. The strong influence of slenderness, ℓ/d, on $V_u bd$ may be of interest to observe.

In the Swedish building Code (SBN-80, 1980), in British Standard Code of Practice CP 112 (Booth and Reece, 1967) and in the timber construction manual of the American Institute of Timber Construction (AITC, 1966) are jags in wood beams of the type shown in Fig 4.7 (1) taken into account by means of a shear reduction factor, α^2:

$$V_u/bd = \frac{2}{3} f_s \alpha^2 \qquad (4.7:7)$$

The same formula is adopted also in (Larsen, 1967), (Kollmann 1951) and (ASCE, 1975). In eq (4.7:7), f_s is normally reduced by some general safety factor but is for the rest a material property parameter. Where the geometry of the beam, d,

distance from jag to support, β, nor slenderness, ℓ/d, is taken into account. At variations of the depth of the jag, i.e. at variations of α, other variables held constant, (4.7:7) corresponds to eq 4.7 (5) c). This relation is valid for short deep beams which fail in the manner illustrated in Fig 4.7 (5) c).

If the ultimate failure of jagged beams is pre-supposed to be governed by shear force one might perhaps be declined to carry out experimental investigations with respect to influence of jagging by use of short deep beams, i.e. beams with low slenderness ratio. Thus the widely adopted design formula (4.7:7) perhaps might be explained by experimental studies in which short deept beams were used and only the depth of the jag varied. According to the present hypothesis of failure mechanisms, it is however not the shear force but the bending moment which is decisive to the ultimate failure of short deep jagged beams, while the shear force governs the ultimate failure of jagged beams of intermediate slenderness. (It is here assumed that the beams are significantly jagged so that "ordinary" shear failure, eq (4.7:6), does not become the determining factor.)

If the results of the present study are correct, then it may be concluded that the widely adopted design formula (4.7:7)) does not seem to be very good. It may be questioned whether not the influence of d, β and the different types of failure mechanicms, and accordingly ratio ℓ/d, should be taken into account as these parameters seem to be of significant importance. With respect to variations of α at intermediate slenderness, the present theoretical values of $V_u/(b\alpha d)$ exhibit some dependency, but not as strong as predicted by eq (4.7:7). If the material property parameters $\sqrt{E_x G_F}$, f_t, f_s and f_f are proportional to each other, then the results of the present study coincide with the design formula where the relative influence of the quality of the wood is concerned. If these material property parameters are not proportional, then the design formula may be questioned also with respect to the predicted relative influence of the quality of the wood, i.e. with respect to the relative influence of f_s.

The only experimental results concerning jagged beams found in the literature searched through were published by Kollmann (1951) and obtained by Longland in the 1930s. These results are reproduced in in Fig 4.7 (9), are valid for Red tulip oak and were presented as relative influence of α o [illegible] intervall

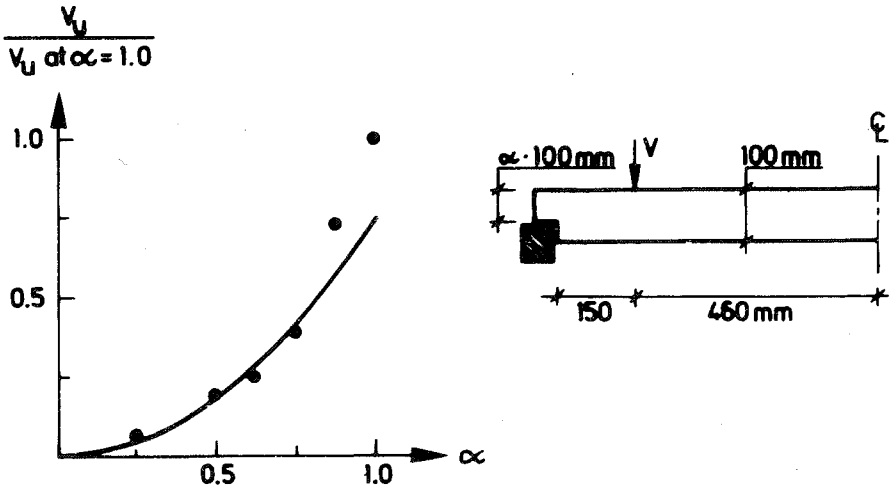

Fig 4.7 (9) Experimental results published in (Kollmann, 1951) with a comparison to a α^2-curve.

$0.25 < \alpha < 0.75$, V_u is approximately proportional to α^2, which might be expected having in mind the low slenderness ratio, $\ell/d \approx 3$, implying that the ultimate failure might have been bending failures. At $\alpha = 1.0$, no jag, and at $\alpha = 0.875$, minor jagging, V_u is greater than expected by the α^2-relation. This is not in accordance with the engineering formulas for bending failure and ordinary shear failure dealt with in Section 4.7.3.

Before ariving to the final conlusion, it is appropiate to include a few remarks with regard to application of linear elastic fracture mechanics to wood. As wood is a brittle material during fracture along the grain and as, accordingly, the absolute size of the process region (the length of the fracture zone) is small, it might be argued that linear elastic fracture mechanics is applicable and that fracture mechanics analysis with account taken to the non-zero size of the fracture zone and to the fracture properties of the material (the shape of the σ-w curve) is not meaningful. However, the basic requirement for successful aplication of linear elastic is not that the absolute length of a fracture zone is small, but that the length of the fracture zone is small in comparison to the length of a pre-existing sharp crack. With the exception from test-specimens, this means that the practical applicability of linear elastic fracture mechanics may not be very great where wood is concerned. During analysis of the development of a crack (e.g. a crack developing from a nail or a shrin[illegible]ch does not

develop from a crack (e.g. fracture developing from a corner, a hole or a notch with a smooth tip or shear fracture developing from the interior of a beam) and during analysis of short pre-existing cracks, one may expect fracture mechanics of the type represented by the fictitious crack model to be more successful than the linear elastic fracture mechanics. On the other hand, the brittleness of the actual material is believed to facilitate generalization of numerical results obtained during fracture analyses with account taken to the development of a fracture zone of non-zero size. An example may be found above in this Section.

A convenient feature of fracture analysis of wood, as compared to isotropic materials such as concrete, is that the path of fracture zone development is often known in advance. However, where wood is concerned, it is more seldom sufficient to know only the fracture properties in pure tension but knowlegde may more often be required also with regard to the properties in combined tension (or compression) and shear in the fracture zone.

Where the presently studied beam is concerned, Fig 4.7 (1), prospective future extended analysis of $(V_f/(b\alpha d))$ maybe ought to be carried out in a more modulated manner than as in Section 4.7.2 both with respect to relations of material behaviour and with respect to the numerical calculations. On the other hand, it is believed that also more crude facture mechanics considerations would be valuable during design and during interpretation of experimental results. Finally it may be concluded that it appears possible and, making a judgement from a limited experimental comparison, meaningful to utilize the fictitious crack model in strength analyses of wood.

---

5. SHEAR STRENGTH ANALYSIS OF LONGITUDINALLY REINFORCED CONCRETE BEAMS

5.1 Introduction

In this introduction, first a few general introductory remarks are made, then distinctions are made between shear strength, shear in fracture zones and shear fracture zones, and finally the subsequent sections in this chapter are surveyed. In this conjuction a few remarks are made with regard to existence of shear fracture zones and with regard to dowel action analysis.

The shear strength of concrete beams and slabs has been the subject of comprehensive research during at least 80 years. It attracted attention among reseachers as early as in the first decade of this century and at least 40 reports were published. Since then, thousands of tests have been carried out and several hundred articles that present new experimental and/or theoretical results have been published. This comprehensive research has produced the empirical experience on which the current building codes are based, but has not resulted in any generally accepted approach on shear strength analysis.

The reasons for the great interest in shear strength analysis are probably several: lack of knowledge; fear for the typically sudden and "brittle" shear failure; the extensive number of structural members that in practice are exposed to shear forces; and, if a general approach is developed by means of which shear failures can be analysed in a very general and very modulated manner, then it is probable that almost any type of failure in reinforced concrete can be analysed. The uncertainty and the risk for sudden and "brittle" failure seems to be in particular great where the diagonal tension failure in the longitudinally reinforced beam, or slab, is concerned. This may be due to lack of confidence in the tensile strength and the tensile fracture properties of concrete.

It is probable that an understanding of failure mechanisms and a development of a general theoretical approach must be based on a description of stress vs. deformation properties of the material. Furthermore, according to the recent decade of finite element and computer aided research, it seems that approaches based on descriptions of the properties of t[illegible] modulated

manners. From a general point of view, a purpose of the present study is to give a contribution to research towards the development of such a general approach. In more detail, the purpose of the present study is primarily to study whether it may be fruitful to take into account the tensile fracture properties of the concrete, i.e. the descending branch of the tensile stress vs. deformation curve, i.e. fracture mechanics, during analysis of the diagonal tensile failure of longitudinally reinforced beams. Accordingly, the analysis primarily concerns the sensitivity of shear strength to the tensile fracture mechanics properties of concrete and to the absolute size of the beam. The shear failure in longitudinally reinforced beams is much more complicated than the failures studied in Chapter 4 and it has been necessary to make rather crude simplifying assumptions during the analysis.

Perhaps due to tradition, shear strength analysis and shear failure in beams and slabs is very often associated with shear stress. Therefore it must be made clear that the magnitude of shear stress is totally dependent on the choice of orientation of the coordinate system in which the components of stress are defined. Where diagonal tension shear failure is concerned, the tensile principal stresses should be of prime interest, not the shear stresses. The insignificance of shear stresses is made clear in a somewhat drastic statement made by Leonhardt (1978): "Shear stresses do not exist in structures, they are only a mental aid. ..... A shear stress means nothing else but that the principal stresses are not parallel to the x- and y-axes". For isotropic homogeneous materials, shear stress has no physical meaning. A physical orientation of the coordinate system within a material can be defined only when the material has different properties in different directions. When referring to the shear strength, normally the ability of a beam or slab to carry a shear force is intended. This global shear strength is not a material property but is much dependent on the geometry of the beam and the magnitude of bending moment and axial force.

When a tensile fracture zone develops within a material, its properties become different in different directions. Consequently, in this case a physical orientation of the coordinate system can be defined. If shear deformations subsequently develop in this local coordinate system, physical shear stresses are very likely to develop in the fracture zone. These "secondary" shear stresses may develop due to aggregate interlocking and are often assumed to carry a great part of the global shear force. In the present app[illegible]e, the

influence of this shear in the fracture zones is not taken into account. Instead, the influence of the tensile fracture properties of the material is emphasized.

A distinction must also be made between shear in fracture zones and shear fracture zones. By a shear fracture zone is meant a fracture zone which does not develop perpendicular to the first principal stress. It is rather obvious that such fracture zones can develop during shear failure in beams made of an orthotropic material, e.g. wood (Section 4.7). The question whether shear fracture zones exist or not for materials which are isotropic has been debated in the recent years. In the present analysis of the diagonal tension failure it is basically assumed that shear fracture zones do not develop in concrete (although, however, along reinforcement bars). In spite of this basic assumption, due to the presently used method of numerical calculations in which the fracture path is assumed in advance, it has been possible to let the fracture zone grow only approximately according to the direction of the first principal stress. For this numerical reason, a simple model for the development of shear fracture zones is utilized during the calculations.

It may be appropiate to make a few remarks with regard to the debate on the existence of shear fracture zones. If the material is isotropic at the instant when the fracture criterion is reached, according to the fictitious crack model, the fracture plane will orientate it self perpendicular to the first principal stress and, consequently, a shear fracture zone cannot develop. However, it is likely that fictitious crack analysis of certain specimens would indicate development of a string of short and closely located fracture zones, which are inclined as compared to the direction of the string. In such cases, it might be suitable to treat the string of inclined fracture zones as if being one fracture zone. This means that the structure is analysed at a higher scale of size and that the "macroscopical", or "global", fracture zone is a shear fracture zone. In two cases it might be suitable to analyse the string of inclined fracture zones as if being one shear fracture zone: (1) if the distance between the individual inclined fracture zones is of the same order of magnitude as the size of the heterogenities of the material, then it is not suitable to assume homogenity of the material (See Fig 3.4 (2)) and then, if not a model of the type indicated to the far right in Fig 3.4 (2) is developed, it might be necessary to assume existence of shear fracture zones; (2) even if the distance between the individual inclined zones is

great as compared to the size of the heterogenities of the material, then, if the string consists of a large number of inclined zones, it might be beneficial to assume the existence of shear fracture zones in order to reduce the required number of elements during finite element calculations. If it is assumed that a shear fracture zone can develop in an isotropic material, then it is an open question whether the properties of such a zone may be regarded as being true material properties or if the properties of the shear fracture zone is dependent on the geoemetry of the specimen, the loading and the boundary conditions. Examples of concrete beams in which shear fracture zones (i.e. fracture zones identyfied by the development of a string of inclined zones during detailed analysis on the assumption of homogenity of the material) may develop are: (1) hollow core beams with a very thin and narrow web (and, more generally, beams with I-shaped cross-sections with a thin and narrow web); (2) beams, with or without a notch, exposed to such a loading system that the shear span becomes very short and concentrated (cutting).

In Section 5.2 general literature references may be found and different types of approaches to shear strength analyses are briefly surveyed. Section 5.3 concerns the present fracture mechanics shear strength analysis: assumptions, method of calculation and computational results. In Section 5.4, a few remarks are made and the calculated shear strengths are compared to experimental results, other theoretical results, empirical formulas and design expressions.

Shear force carried by dowel action has not been taken into account during the present shear strength calculations. However, in conjuction to the present shear strength study, a small study of dowel action was also carried out. In order to reduce the size of this report, it has been decided not to present the actual small study of dowel action. Instead only a few experiences shall be referred to in this introduction. In general, dowel analysis has to be carried out in 3D. However, a simplified alternative is to first analyse the fracture zone development in between reinforcement bars in a section of the beam and then utilize the load-displacement response obtained during this first analysis during a subsequent 2D analysis of the development of fracture along the bars. This later analysis may be compared to analysis of a beam lying (or hanging) on a bed of springs, where the stiffness of the springs is non-linear (including softening) in accordance with the first analysis of a section of the beam. By ıfluence of the

thickness of the concrete cower, the distance in between the bars, the diameter of the bars and the strength and fracture properties of the concrete may be studied. By means of comparison to a beam lying on a bed of springs, numerical results may be generalized. According to a few preliminary results, it seems that the theoretical dowel strength and (total) dowel force-displacement response as obtained by means of fracture mechanics are consistent with experimental results reported in literature. If interaction between dowel action and slip between reinforcement and concrete is to be analysed, then, particularly if the reinforcement consists of deformed bars, the fracture analysis is likely to become much more complicated than if only the pure dowel action is considered. From the actual small study of the pure dowel action it may be concluded that it seems possible and meaningful to utilize finite elements and the fictious crack model during dowel action analysis. Due to the large stress gradients during the development of dowel fracture, it is probably necessary to take into account the fracture softening of concrete during theoretical analyses of dowel action or else the theoretical analysis may not be very meaningful.

5.2 General literature references. Approaches for shear failure analysis

Shear strength analyses by means of fracture mechanics seem to be few and rather recent. Hillerborg, Modeer and Petersson (1976) suggested that it might be meaningful to analyse shear failure by means of fracture mechanics (the fictitious crack model) and finite elements. Subsequently, calculation tests were carried out by Modeer (1979). To a large extent the present shear strength analysis may be considered only as an amplification of the test calculation carried out by Modeer. An independent early application of fracture mechanics in shear strength analysis was presented by Hawkins, Wyss and Mattock (1977). These authors studied the influence of a potential crack in a spherical stress relaxation zone, developed approximate analytical relations based on the Griffith energy release criterium and concluded that it should be possible to use the fracture mechanics approach outlined in the actual paper to predict the strength of a variety of concrete members behaving in a brittle manner.

Another indepen[illegible] g shear

strength analysis was presented by Reinhardt (1981 a,b). The analysis presented in these papers was less complicated and attention was attracted to agreement between the size effect law of the linear elastic fracture mechanics and experimental results regarding the relative influence of the absolute size of a beam. A much more detailed linear elastic fracture mechanics analysis of a beam failing in shear was presented by Saouma and Ingraffea (1981). In this paper the load vs. deflection response and the crack pattern in a beam, tested by Bresler and Scordelis about 25 years ago, were studied by means of a sofisticated finite element program, specially developed for linear elastic fracture mechanics analyses of concrete members.

The studies referred to above may be considered as pioneering where the application of fracture mechanics during shear strength analysis is concerned. According to the subsequent trends within research, it seems that the linear elastic fracture mechanics has attracted less interest for further developments of the fracture mechanics shear strength analyses than the non-linear fracture mechanics of the type represented by, e.g., the ficitious crack model.

In connection to the pioneering studies referred to above, it is appropriate also to mention a thesis presented by Loov (1972). In the last namned thesis, a finite element method for analysis of discrete cracking in concrete members was developed and this method may be considered as a kind of fracture mechanics approach. Naturally, it is possible that consepts of fracture mechanics may have been applied also during other comparatively early studies of shear strength.

Shear failure analyses by means of fracture mechanics only represent a very small part of the huge number of shear failure studies carried out in this century. In Section 2.3, the methods of failure load prediction were divided into three large groups: the direct experimental method, the statistical method by means of more or less arbitrary interpolation formulas, and the methods based on a description of the mechanical properties of the material. Where the diagonal tension failure in longitudinally reinforced beams is concerned, it seems that current building codes are essentially based on the statistical method with the more arbitrary interpolation formulas. By arbitrary interpolation formulas is then meant formulas which do not emanate in consideration to failure

mechanisms, but instead are chosen only in such a way that they fit to test results. Within the statistical methods with less arbitrary interpolation formulas, efforts are made to develop rational strength formulas based on clever observations and assumptions regarding the shear force carrying mechanism. The methods based on a description of the mechanical properties of the material can be divided into at least two sub-groups: according to one "school" very drastic simplifications are made at the description of the properties of the material, but then the shear strength analysis is carried out in a theoretically consistent and exact manner without any additional approximations; according to the other "school" the description of the properties of the material is made in a more realistic manner, but then it is necessary to make additional approximations during the applied shear strength calculations. The latter type of approach has gained from the development of computers and the development of the finite element method, but can still not be regarded as a general method due to the limitations of available finite element methods and due to limited knowledge of the mechanical properties of concrete. The only available theoretically consistent and "exact" method of shear strength analysis seems to be the analysis based on the theory of ideal plasticity. However, the unfortunate feature of this theory is that the assumed mechanical properties of concrete are unrealistic to such an extent that the theoretical results can hardly be regarded as reliable unless they are carefully compared to, and adjusted to, test results. Where the methods based on more realistic descriptions of the properties of the material are concerned, it is evident that research and development is far from completed. An indication of this is that the majority of finite element analyses of shear failure seem, in fact, not to be devoted to studies of shear failure and shear strength, but instead devoted to verification of the actual finite element approach. Such verification analyses seem usually to indicate good agreement between the theoretical results and the results obtained during an experimental test of a beam, but the conclusions regarding shear strength obtained by means of finite element analyses seem still to be few. One of the reasons for this may be that it would probably still be expensive and time-consuming to carry out a number of systematic detailed finite element analysis of shear failure.

Due to the huge literature on shear failure analyses, it is neither possible nor meaningful to attempt to list all the articles, papers and reports that deal with the actual subject. However, it may be appropriate

to list a few general references in which a great number of references to additional literature may be found. Hognestad et al. (1962) have put together a bibliography which includes a general review and short summaries of 466 selected articles published from 1897 through 1960. In the 1000-page publication (ACI, 1974) 40 papers covering different aspects of shear strength analysis may be found, and in the 100-page paper (ASCE-ACI, 1973), in which 200 reports and articles are referred to, research results and design proposals are reviewed in order to establish the state-of-the-art. One of the most well-known researchers within the field of shear strength analysis was professor Kani. Significant parts of his research have been put together in a book: (Kani, Huggins and Wittkopp, 1979). A report that summarizes great parts of usage of the theory of plasticity in shear strength analysis has been put together by Nielsen, Braestrup, Jensen and Bach (1978). Findings regarding the application of the theory of plasticity may also be found in (Thurlimann, 1979). CEB/FIP has prepared a Model Code for concrete structures and, for the shear and torsion, the explanatory and viewpoint papers on the Model Code may be found in (Regan and Taylor, 1978). Subsequently a comission of CEB has published (Grasser, 1982).

According to the recent years of finite element aided research it seems that the shear problem is, in most cases, not treated as a special problem, but more as a possible application of more general finite element aided approaches for the analysis of reinforced concrete. Bergan and Holand (1979) have presented a survey of finite element analyses of concrete structures and given an outline of a number of proposed mathematical models for the behaviour of concrete, and in (Grootenboer, 1979) the facilities of 15 finite element models are summarized. In (Thurlimann, 1981) a number of papers concerned with finite element aided advanced analyses of reinforced concrete may be found. A comprehensive state-of-the-art report on finite element analysis of reinforced concrete has been prepared by Nilson et al. (1982). In an appendix in the last namned report, a collection of information on 25 generally available programs for non-linear finite element analysis of reinforced concrete structures is presented. As an example of a recent study in which references to other recent studies may be found, the report by Rots, Nauta, Kusters and Blaauwendraad (1985) may be mentioned.

5.3 Present fracture mechanics shear strength analysis

5.3.1 Introduction

The shear force carrying mechanisms taken into account in the present study of diagonal tension strength in the longitudinally reinforced beams are illustrated in Fig 5.3 (1). This figure shows the forces acting on the conrete blocks ot the left and to the right of a potential inclined fracture section. The resulting axial force that acts across the actual section is zero, even if the reinforcement is pre-stressed. The figure illustrates that dowel action and aggregate interlocking are not considered during the calculations.

The general approach used in the present analysis is to calculate the load carrying capacity during the development and growth of a diagonal fracture zone, taking into account the slip between reinforcement steel and concrete, the tensile softening of the concrete along the fracture path, different possible locations of the fracture path, and the ability of the ligament above the fracture zone to carry the forces transferred by this ligament. The concrete blocks at each side of the potential inclined fracture section, and also the reinforcement bars, are assumed to be linear elastic.

As compared to most previous fracture mechanics analyses of shear strength, the aim of the present analysis is to calculate the load carrying capacity at the ultimate collapse of the beam and consequently not only the load at start of unstable growth of a diagonal crack. As compared to most previous finite element analyses of shear failure, the present calculations are not modulated or detailed. Thus, for instance, the development of only one diagonal crack is considered in each calculation. On the other hand, the present purpose is not to analyse the failure of a specific experimental test beam in a detailed manner, but instead to calculate ultimate shear strength and, in particular, its sensitivity to the tensile fracture energy of concrete and consequently also its sensitivity to the absolute size of the beam.

5.3.2 Assumptions at load vs. crack depth calculation

During the discussion in this section, Section 5.3.2, it is assumed that the diagonal tension fracture is bound to take place along a certain path, or section. This fr[illegible] according to Fig 5.3 (1).

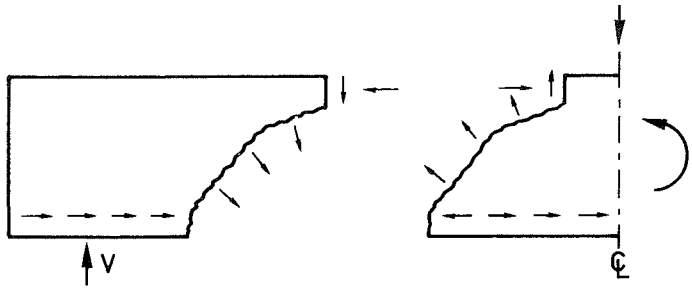

Fig 5.3 (1) Forces acting on the blocks of concrete to the left and to the right of a potential diagonal tension fracture section.

Knowing the fracture path, the diagonal tension failure may develop in the following manner: First a tensile fracture zone starts to develop in a slow and stable manner, then, as the external load increases, the growth of the fracture zone (the crack) may become unstable during simultaneous sliding between the reinforcement and the concrete. This unstable crack growth may then, depending on the location the crack, either lead to an immediate collapse of the beam or it may be stopped when the crack grows into the upper edge of the beam. If the unstable crack growth is stopped, then the question is whether the remaining ligament (which becomes smaller and smaller during the subsequent stable crack growth) is large enough to carry the compressive force in the upper edge of the beam. Accordingly, there are two reasons for calculating the load vs. crack depth: the load at start of unstable crack growth must be determined and the size of the remaining ligament must be calculated in order to make it possible to determine when, and at which external load, the ligament will fail.

The description of the assumptions used during the calculation of load vs. crack depth is divided into two parts. First, the finite element model is described, then the assumed properties of the materials.

The finite element model is illustrated in Fig 5.3 (2). The concrete blocks at each side of the tensile fracture path are modelled by two linear elastic substructure elements. These two elements are built up of quadrilateral elements of the type described in Section 3.6.2. (The quadrilateral element consists of four constant strain elements.) The substructure elements have 25 nodes along the fracture path, and 12 + 12 nodes along the e beams with

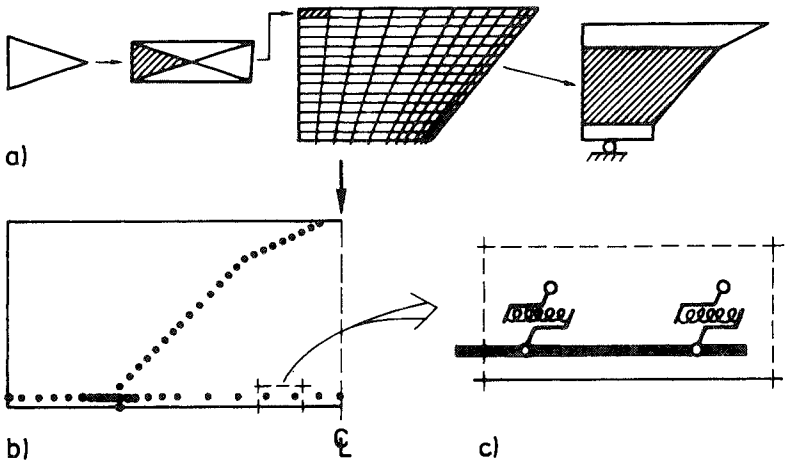

Fig 5.3 (2) a) Building up of a typical concrete block from constant strain elements.
b) Nodes in assembled concrete blocks before start of node opening.
c) Linkage of reinforcement bar elements to concrete by bond stress-slip elements.

the span to depth ratio of 3. For the beams with span to depth ratios 6 and 9, the number of nodes along the reinforcement is greater: 22 + 12. The reinforcement is modelled by truss elements, which are connected to the nodes of the concrete blocks through springs. These springs model the sliding between the reinforcement and the concrete. The development and the properties of the fracture zone in between the concrete blocks is modelled by means of node opening and internodal springs. The geometrical shapes of the beams studied are indicated in Section 5.3.5, as well as the the studied crack paths.

The concrete blocks are assumed to be in the state of plane stress (ν=0.2) and are assumed to behave in a linear elastic manner, defined by the modulus of elasticity denoted E_c. The reinforcement steel is also assumed to behave in a linear elastic manner, defined by the modulus of elasticity denoted E_s.

The interaction between reinforcement and concrete is described by means of bond stress-slip relations. Such relations are often used during finite element analyses of reinforced concrete and should give a more modulated description of reality than the sometimes used assumption of completely rigid interaction and than the sometimes used assumption of coupling between the reinforcement and the concrete only at the ends of the beam, i.e. at the ends of the reinforcement bars. In spite of the widespread use of bond stress-slip relations, some theoretical and experimental objections can be put forward to the use of such relations: the theorem of conjugate shear stresses may be violated at the free surfaces of concrete which are crossed by a reinforcement bar (e.g. a fracture surface); lateral stress is known to have influence on the bond (which means that splitting of the concrete along deformed bars, the thickness of the concrete cover, the spacing of the bars and the large lateral stresses at the supports of the beam are of importance); it may be discussed whether the deformation term in the bond stress-slip relation always should be described in terms of absolute deformation and not in terms of strain. In most of the present calculations the linear elastic perfectly plastic bond stress-slip relation shown in Fig 5.3 (3) and indicated by the letter A has been used. This assumed shape of the relation may be compared to the experimental results presented by Nilson (1971). During a few of the calculations the other bond stress slip relation shown in Fig 5.3 (3) has been used in order to determine the sensitivity to the shape of the bond stress-slip relation. A number of papers and also references to additional literature on steel-concrete interaction may be found in the 1979 January, February and March issues of the Journal of the American Concrete Institute.

The criterion for development and growth of the tensile fracture zone in between the two concrete blocks is illustrated in Fig 4.7 (2) and the softening properties of the fracture zone is illustrated in Fig 4.7 (3). These figures may be found in Section 4.7 because the actual criterion and the actual properties, originally used during the present analysis of concrete, were subsequently used in the analysis of the shear failure of wooden beams. Where the analysis of wood is concerned, the direction of the local coordinate system is fixed by the direction of the grain. Where the present analysis of concrete is concerned, the direction of the local coordinate system is fixed by the assumption with respect to direction of the crack propagation path. This path is assumed in accordance with general approximate estimations of the directions of the first principal

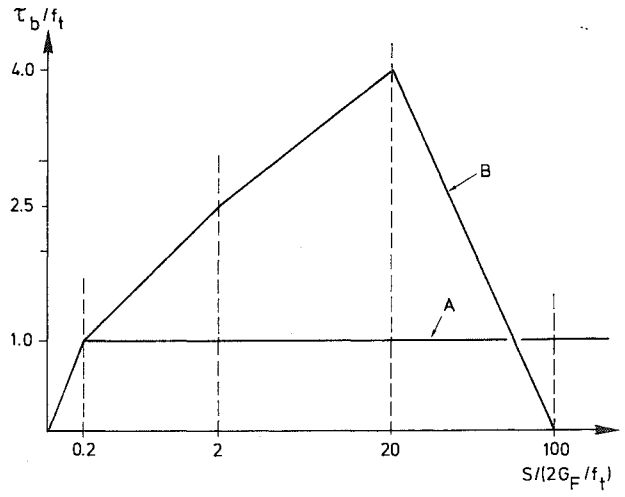

Fig 5.3 (3) Bond stress-slip relations.

stresses within the beam. The actual criterion is such (See Section 5.3.3) that ratio f_s/f_t is equal to $\sqrt{f_c/f_t}/2$, where f_c is the unaxial compressive strength and where ratio f_c/f_t is put equal to 10 during the calculations.

The stresses (or tractions) acting across the fracture path are calculated from the nodal forces acting between the two blocks of concrete. Accordingly, these stresses do not represent the state of stress in the points along the fracture path, but instead they represent the tractions acting across the path. The internodal fracture zone modelling springs are one dimensional and are inserted and kept in the same direction as the direction of the nodal force at the instant when the criterion for start of fracture zone development is reached in the actual node. In the direction perpendicular to the one dimensional spring, no force (or traction) is acting across the fracture zone. The adopted fracture criterion, Fig 4.7 (2), is also dealt with in Section 5.3.3. The most essential reason for the actual choice of properties of the fracture zone is that it is the simplest choice.

By means of the above assumptions it is possible to calculate the development of the load carrying capacity during initiation and growth of the fracture zone, but the possibility of final collapse of the beam due to large compressive stresses in the upper edge has so far not been dealt with. This matter will be dealt with in the next section.

5.3.3 Assumptions for checking failure of ligament

See Fig 5.3 (4) a). At the stage shown in this figure, the fracture zone has grown close to the upper edge of the beam, leaving only a small ligament, t, to carry the axial force, N_o, and the shear force, T_o, acting across the unfractured ligament. t, N_o and T_o vary during the growth of the tensile fracture zone and are calculated according to Section 5.3.2. To check whether the ligament is able to carry the forces T_o and N_o, a failure criterion for the entire ligament is used. This failure criterion is accordingly not a failure criterion for the local points of material within the ligament, but a global failure criterion for the entire ligament.

If the normal force and the shear force acting across a potential fracture surface are denoted N_α and T_α according to Fig 5.3 (4) b), then equilibrium gives:

$$\begin{cases} \sigma_\alpha = \sigma_o c^2 + \tau_o sc \\ \tau_\alpha = -\sigma_o sc + \tau_o c^2 \end{cases} \qquad (5.3:1)$$

where

$c \equiv \cos\alpha$ $\qquad$ $s \equiv \sin\alpha$

$\sigma_o = N_o/(tb)$ $\qquad$ $\tau_o = T_o/(tb)$

$\sigma_\alpha = N_\alpha/(tb/c)$ $\qquad$ $\tau_\alpha = T_\alpha/(tb/c)$

As $c^2 + s^2 = 1$, the mean stresses σ_α and τ_α may be represented by a circle in a σ-τ diagram. This circle has the radius $\sqrt{\sigma_o^2 + \tau_o^2}/2$ and its centre is located in the point $(\sigma_o, \tau_o)/2$, Fig 5.3 (5) a). Accordingly, for $T_o \neq 0$ the circle is excentrically located with respect to the σ-axis. This is because σ_α and τ_α do not represent the stresses in a point but mean stresses across a section of finite size. Accordingly, as nothing is stated about the location of resultants to σ_α and τ_α, the excentric location of the stress-circle does not mean that moment equilibrium of the triangle in Fig 5.3 (4) b) is violated nor does does it mean that the theorem of conjugate shear stress is violated. The stresses σ_α and τ_α may be obtained graphically in the manner illustrated in Fig 5.3 (5) a).

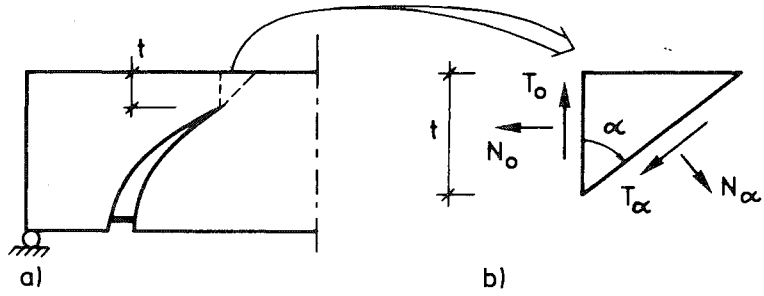

Fig 5.3 (4) Forces acting on the ligament.

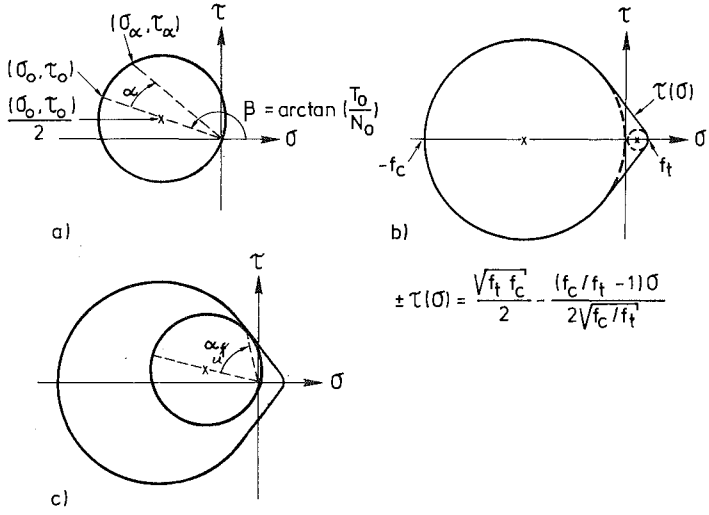

Fig 5.3 (5) a) Grafical representation of mean stresses acting on the ligament.
b) Failure criterion
c) Conditions at the instant of failure of the ligament.

To see whether the ligament is capable of carrying the actual forces, it is checked whether the corresponding stresses σ_α and τ_α for some α has reached the failure criterion shown in Fig 5.3 (5) b). This linear Coulomb-Mohr criterion with tension cut-off is well-known and is probably the simplest criterion if the concrete is to be assumed to have a non-zero tensile strength. As soon as the stress circle touches the failure criterion, Fig [illegible] ire beam, is

assumed to collapse. The angle and the stresses that correspond to failure are denoted α_u, σ_{ou}, τ_{ou}, $\sigma_{\alpha u}$ and $\tau_{\alpha u}$. For $T_o \neq 0$, α_u may be obtained from

$$\alpha_u = \frac{1}{2}\left\{ \arctan\left(\frac{1-f_t/f_c}{2\sqrt{f_t/f_c}}\right) + \arctan\left(\frac{T_o}{N_o}\right) - \pi/2 \right\} \qquad (5.3:2)$$

For $T_o = 0$, the stress circle touches the failure criterion in several points at the same time and the angle α_u can consequently not be calculated. Knowing T_o, N_o and t, the instant of failure of the ligament and the magnitude of the forces carried by the ligament at this instant can be obtained from:

$$\frac{\tau_o}{f_t} < h(f_t/f_c,\ N_o/T_o) \qquad \text{before failure}$$
$$\text{-"-} \quad = \quad \text{- " -} \qquad \text{at failure} \qquad (5.3:3)$$

where the function $h(f_t/f_c, N_o/T_o)$ is

$$h = \frac{1}{2\sqrt{f_t/f_c}\,((-N_o/T_o)sc + c^2) + (1-f_t/f_c)((N_o/T_o)c^2 + sc)} \qquad (5.3:4)$$

In eq (5.3:4) $s \equiv \sin\alpha_u$ and $c \equiv \cos\alpha_u$, where α_u may be obtained from eq (5.3:2). In Fig 5.3 (6) a) the force carrying capacity of the ligament, as calculated by means of eq (5.3:4), is shown for $f_c/f_t = 10$ and $N_o/T_o \lesssim -1.0$. The angle β is defined in Fig 5.3 (5) a). Calculation of the corresponding $\sigma_{\alpha u}$ shows that $\sigma_{\alpha u} > 0$ when $N_o/T_o \gtrsim -1.4$, while $\sigma_{\alpha u}$ is a compressive stress when $N_o/T_o \lesssim -1.4$. As N_o/T_o may be expected to be roughly proportional to the span to depth ratio of the beam, one may consequently expect that the final collapse of beams of normal or great span to depth ratios will involve a compressive failure in the upper edge of the beam, while very short beams might fail due to the development of a fracture zone with a tensile normal stress all the way through the beam, also through the very upper edge of the beam. However, in such very short beams there may not be space enough to make it possible to let the inclined tensile fracture zone grow all the way through the beam. The final collapse of all the beams presently studied (Section 5.3.5) has involved a compressive failure of the ligament. While Fig 5.3 (6) a) shows the force carrying capacity of the ligament vs. ratio N_o/T_o at a constant f_c/f_t, Fig 5.3 (6) b) shows the sensitivity to changes in f_c/f_t. The sensitivity is indicated by C and, as an example, at o 10.1 gives a

0.57 % increase in τ_{ou}/f_t. The sensitivity is fairly constant during normal variations in f_c/f_t, and accordingly approximate values of τ_{ou}/f_t for other values of f_c/f_t than 10 may be obtained by means of an exponential relation. This relation may be found in the actual figure. As an example, at $-N_o/T_o=2$ an increase in f_c/f_t from 10 to 15 gives approximately 26 % increase in τ_{ou}/f_t. (The exact increase according to eq:s (5.3:2) and (5.3:4) is 25 %.) It must be noticed that the actual

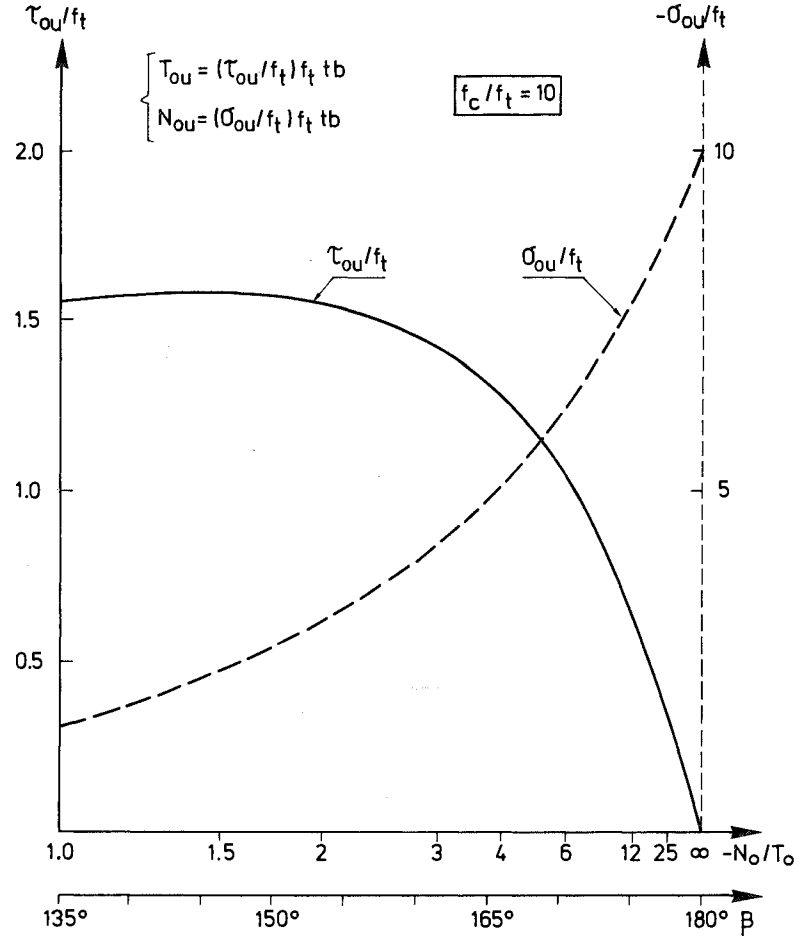

Fig 5.3 (6) a) [illegible] ratio N_o/T_o.

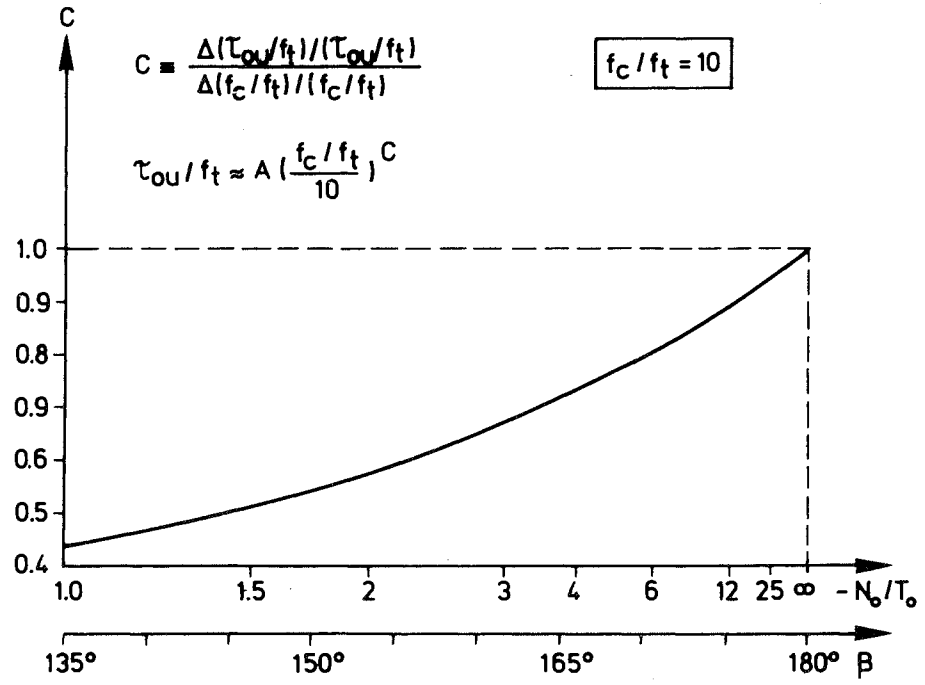

Fig 5.3 (6) b) Sensitivity of force carrying capacity of a ligament to changes in ratio f_c/f_t. "A" is the value of τ_{ou}/f_t when $f_c/f_t = 10.0$ (See Fig 5.3 (6) a).), and the approximate expression for τ_{ou}/f_t is reasonably accurate in the region $8 < f_c/f_t < 16$.

sensitivities are valid for the force carrying capacity of the ligament, not the ultimate load carrying capacity of the beam, i.e. the shear strength. The sensitivity in shear strength of the beam, f_v/f_t, to variations in f_c/f_t is probably ~~to be~~ smaller because ratio f_c/f_t should also have influence on the location of the critical crack path and accordingly also on the size, t, of the ligament at the final collapse of the beam. The estimation of a smaller influence on the shear strength may also be supported by Fig 5.3 (7) and Fig 5.3 (14).

Above, the failure criterion, Fig 5:3 (5) b), for check of the ability of the ligament to carry the actual forces has been treated as a global failure criterion for the entire ligament. As an alternativ, this criterion may be looked upon as a yield criterion for the local points of material. In th a work

equation, the actual method for calculating the mean shear stress in the ligament at failure, eq (5.3:3), may be looked upon as an upper bound solution of the theory of plasticity. It is not a lower bound solution because it is not checked whether a statically admissable stress distribution can be found, such that constant yield stresses $\sigma_{\alpha u}$ and $\tau_{\alpha u}$ along the α-surface does not violate the yield criterion in a point outside the α-surface. During application of the theory of plasticity in concrete analysis, the tensile strength of the concrete is often assumed to be zero. This would correspond to $f_t/f_c=0$ in the above relations. It may be noticed that the assumption of zero tensile strength of the concrete, i.e. $f_t=0$, means that the load carrying capacity of the ligament would be predicted to be zero for all $T_o \neq 0$. During the present calculations the ratio f_t/f_c has been put equal to 1/10.

In Fig 5.3 (5) b) the actual failure criterion is shown as a failure envelope in the τ-σ space. If the actual criterion is looked upon as failure criterion for the local points of material, then it may be transformed into a principal stress diagram, σ_1-σ_2. In this diagram the actual criterion consists of three straight lines in between the four points $(\sigma_1, \sigma_2) = (-f_c, -f_c)$, $(0, -f_c)$, $(f_t, 0)$ and (f_t, f_t). This Coulomb criterion with tension cut-off is fairly well-known. Experimental results with respect to the failure criterion in the σ_1-σ_2 space are often shown and referred to in literature, see e.g. (Nilson, 1982). With exception from the tension-tension region in the σ_1-σ_2 space, comparisons between the actual criterion and experimental results seem to indicate that the criterion is somewhat conservative, i.e. the actual criterion seems commonly to give a underestimation of the load carrying capacity.

5.3.4 Assumptions for calculation of ultimate load

If only one crack path is considered during the analysis of the reinforced concrete beam, its ultimate load carrying capacity can be calculated by means of the assumptions of the preceeding sections. This ultimate load carrying capacity is either equal to the load at start of unstable crack growth (Section 5.3.2) or equal to the load at failure of the ligament (Section 5.3.3). These loads are in turn dependent on the assumed location of the crack path. In this section the used method for determination of the most dangerous, or the critical, location of the crack shall be described.

See Fig 5.3 (7) a). This figure shows, in a schematical manner, the load vs. crack depth response of one typical vertical "bend crack" and of one typical diagonal "shear crack". The bend crack nucleates close to the mid-section of the beam at a low load and this crack also becomes unstable at a low load. The unstable growth of the bend crack is, however, soon stopped and a significant increase in the load is then required before the beam finally fails due to crushing of the ligament (or due to anchourage failure or yielding of the reinforcement). The typical diagonal "shear crack" nucleates and becomes unstable at higher loads, but then the unstable growth of the diagonal crack continues very deep into the beam. During this unstable crack growth the size of the ligament decreases and the load corresponding to compression failure of the ligament becomes less than the load at the start of the unstable growth of the diagonal crack. This means that the start of unstable growth of the diagonal crack is immediately followed by a collapse of the beam. In Fig 5.3 (7) a) the unstable crack growth is indicated by dashed lines and the stable crack growth is indicated by full lines.

Naturally, the properties of the reinforcement bars and the properties of the bond stress-slip relation influence both the load at the start of the unstable crack growth and the load at the fracture of the ligament. These influences are entered into the computational results through the assumptions of Sections 5.3.2 and 5.3.3.

For beams sensitive to shear failure, the most dangerous crack is somewhere in between the two "extreme" types of cracks illustrated in Fig 5.7 (7) a). To find the location of the most dangerous crack, different crack paths must be studied. These paths may be characterized by their position in the lower edge of the beam and in Fig 5.3 (7) b) examples of such paths are shown together with a schematical diagram for the corresponding loads at start of unstable crack growth (indicated by circles) and the corresponding loads at failure of the ligament (indicated by crosses). For the typical shear sensitive beam, at increased distance from the mid-section of the beam, the load that corresponds to start of unstable crack growth increases and the load that corresponds to failure of the ligament decreases. The most dangerous location of the crack and the corresponding ultimate load carrying capacity of the beam is obtained from the point where the two curves intersect. At this point the load carrying capacity of the beam vs. the location of the crack, i.e. the dashed curve in slender beams

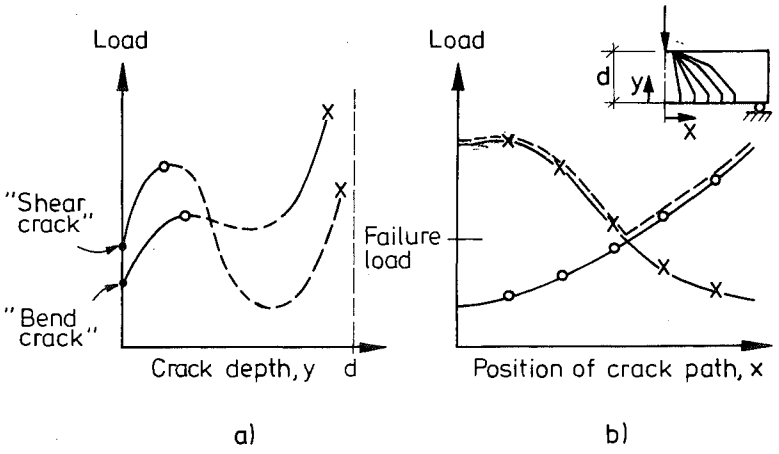

Fig 5.3 (7) Determination of failure load
a) Load vs. crack depth
b) Load at start of unstable crack growth indicated by "o") and load at final collapse of the ligament (indicated by "x") vs. position of crack path.

and/or very lightly reinforced beams, one may expect the "load capacity valley" to have its minimum at the centre of the beam and accordingly the failure of such beams may be expected to be a pure bending failure. For less slender beams the minimum of the load capacity valley is located away from the centre of the beam and accordingly a diagonal failure, i.e. a "shear failure", will develop.

5.3.5 Shear strength: computational results

Where the main series of calculations is concerned, the geometrical shapes of the studied beams are indicated in fig 5.3 (8) and the dimensionless ratios that define the properties of the material are indicated in Fig 5.3 (9). In the main series of calculations 15 beams with different combinations of ratios d/ℓ_{ch}, ℓ/d and ρ (percentage of reinforcement) are dealt with. In addition to those beams, four beams are studied in order to obtain some knowledge regarding the sensitivity to the bond stress-slip relation and the existence of pre-existing cracks. The crack paths considered durir .3 (10). Not

all crack paths are considered for each beam, but at least one path immediately to the left and one path immediately to the right of the intersection point of Fig 5.3 (7) b).

The 19 beams referred to above have values of ratio d/ℓ_{ch} in the range 0.3-4.8. However, for the purpose of comparison limit values for the shear strength corresponding to $d/\ell_{ch}=0$ and $d/\ell_{ch}\rightarrow\infty$ are also given. For the purpose of comparison calculated load carrying capacities of corresponding beams without reinforcement are also given.

In the end of this section a few analyses regarding influence of prestress in the reinforcement bars are dealt with. Those analyses are treated separately because only one possible crack path is considered during those calculations.

In order to facilitate the interpretation and in order to make the calculations more general, dimensionless ratios are used in the definition of the input variables to the calculations. The corresponding dimensionless shear strength is f_v/f_t, where f_v is defined by:

$$f_v = \frac{V_u}{bd} \qquad (5.3:5)$$

V_u is the shear force, i.e. the support reaction, at the ultimate failure of the beam. Please note that d is the total depth of the beam and accordingly not the total depth minus the depth of the concrete cover and half the thickness of the reinforcement. The total depth, d, is used in

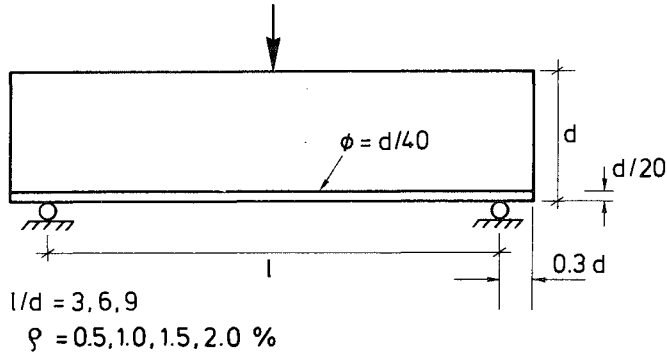

Fig 5.3 (8) Geometrical shapes of beams. ϱ =percentage of re-

Ratio	Assumed value	
f_c / f_t	10.0	
ν	0.2	
E_s / E_c	7.0	
f_{bo} / f_t	1.0	A
$S_o / (2G_F / f_t)$	0.2	A
d / l_{ch}	0.3 - 4.8	

Fig 5.3 (9) Material parameter ratios. "A" refers to the bond stress-slip relation shown in Fig 5.3 (3).

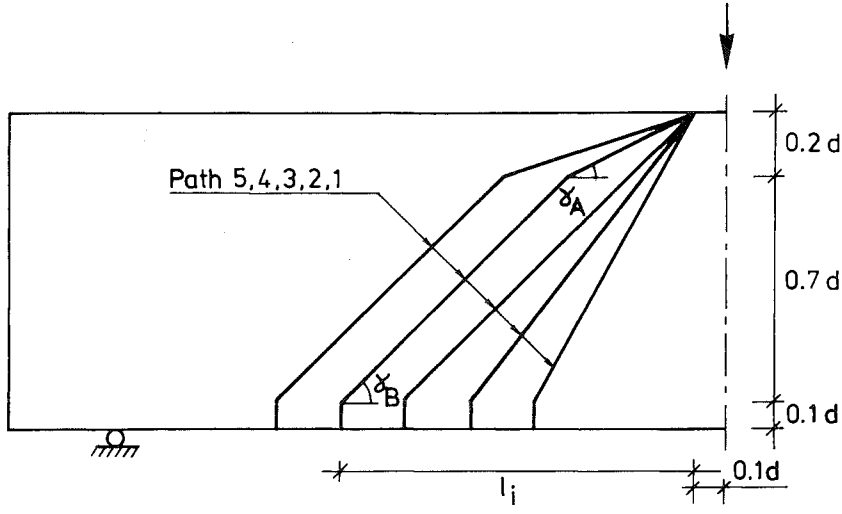

Path	γ_A	γ_B	l_i / d	$\gamma = \arctan(d/l_i)$
1	61°	61°	0.5	63°
2	52°	52°	0.7	55°
3	45°	45°	0.9	48°
4	27°	45°	1.1	42°
5	18°	45°	1.3	38°

Fig 5.3 (10) Lc

the definition of f_v in order to avoid confusion between depth and height of beams. While (5.3:5) defines shear strength, the load acting on the beams is indicated by τ_v/f_t, where τ_v is indential to V/(bd) (=P/(2bd)). At the instant of ultimate failure $\tau_v/f_t = f_v/f_t$.

Before going on to the calculated shear strengths, examples of more detailed results shall be shown. These examples concern the six beams with $(d/\ell_{ch}, \rho, \ell/d)$ = (0.6, 1 %, 3), (2.4, 1 %, 3), (0.6, 1 %, 6), (2,4, 1 %, 6), (0,6, 2 %, 3) and (2.4, 2 %, 3).

Fig 5.3 (11) (six diagrams) shows the theoretical load vs. deflection responses at the current quasi-static condition. For each beam the response at two different crack paths, indicated by the angle γ (See Fig 5.3 (10)), is shown. The actual crack paths are to the left and to the right of the bottom of the load carrying capacity valley, indicated in Fig 5.3 (7) b). The load vs. deflection curves consist of a number of straight lines which are drawn between the points of load and deflection that correspond to the opening of a node. The instant of final collapse of the ligament is indicated by a cross. Each diagram in Fig 5.3 (11) gives an illustration to the influence of ratio d/ℓ_{ch} on the load vs. deflection response and on the loads at instability and collapse of the ligament. It is evident that the size of the beam and the brittleness of the concrete are of importance.

In Fig 5.3 (12) an enlargement of a part of one of the curves in Fig 5.3 (11) is shown. In this enlargement not only the load and deflection at instants of opening of nodes is shown, but the load and deflection at each instant and accordingly also at those instants which correspond to changes in the stiffness of the bond stress-slip relation and to complete separation of the nodes between the two concrete blocks. The curve in Fig 5.3 (12) consists of 46 straight lines.

Since only one crack is considered during each calculation, the theoretical deflections become small. The current analysis concerns strength, but if the magnitude of deflection at shear failure was to be analysed in a realistic manner it would have been quite necessary to take into account the fact that several cracks are present in the beam at the same time.

Fig 5.3 (13) (6 ure zone, a/d,

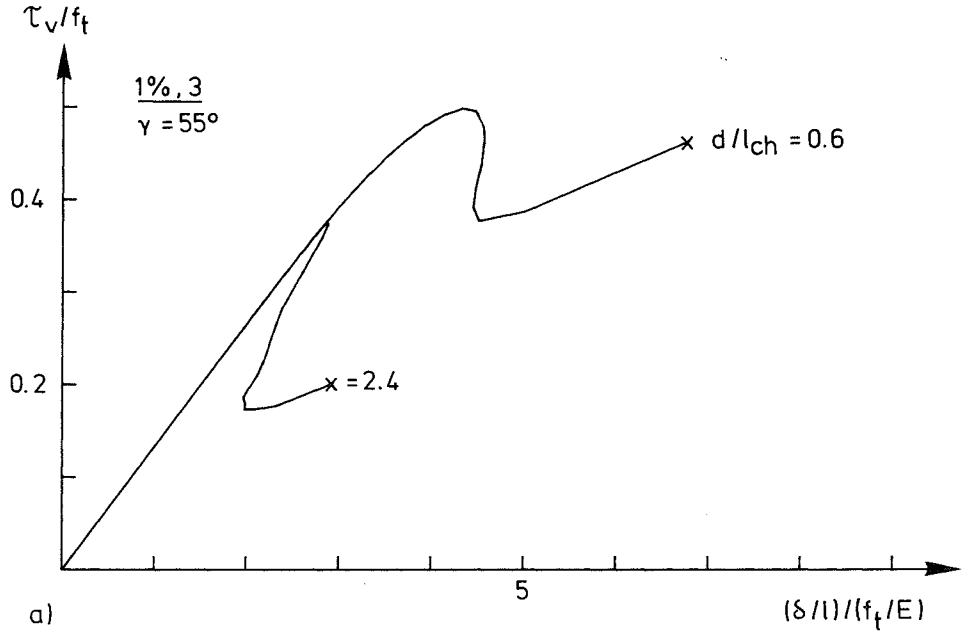
τ_v/f_t
1%, 3
$\gamma = 55°$
$d/l_{ch} = 0.6$
0.4
0.2
$x = 2.4$
5
a)
$(\delta/l)/(f_t/E)$

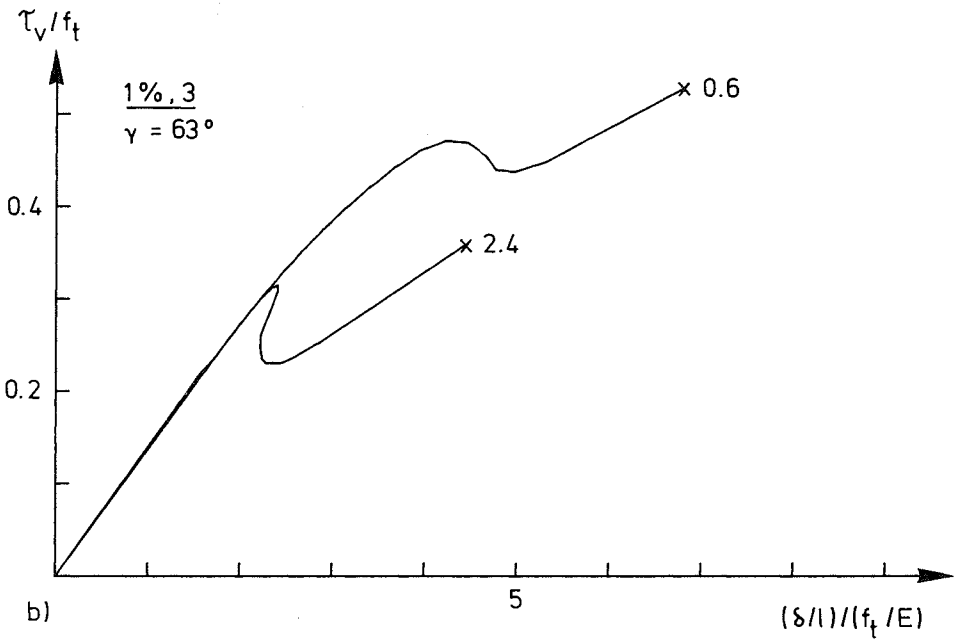
τ_v/f_t
1%, 3
$\gamma = 63°$
0.6
0.4
2.4
0.2
5
b)
$(\delta/l)/(f_t/E)$

Fig. 5.3 (11)

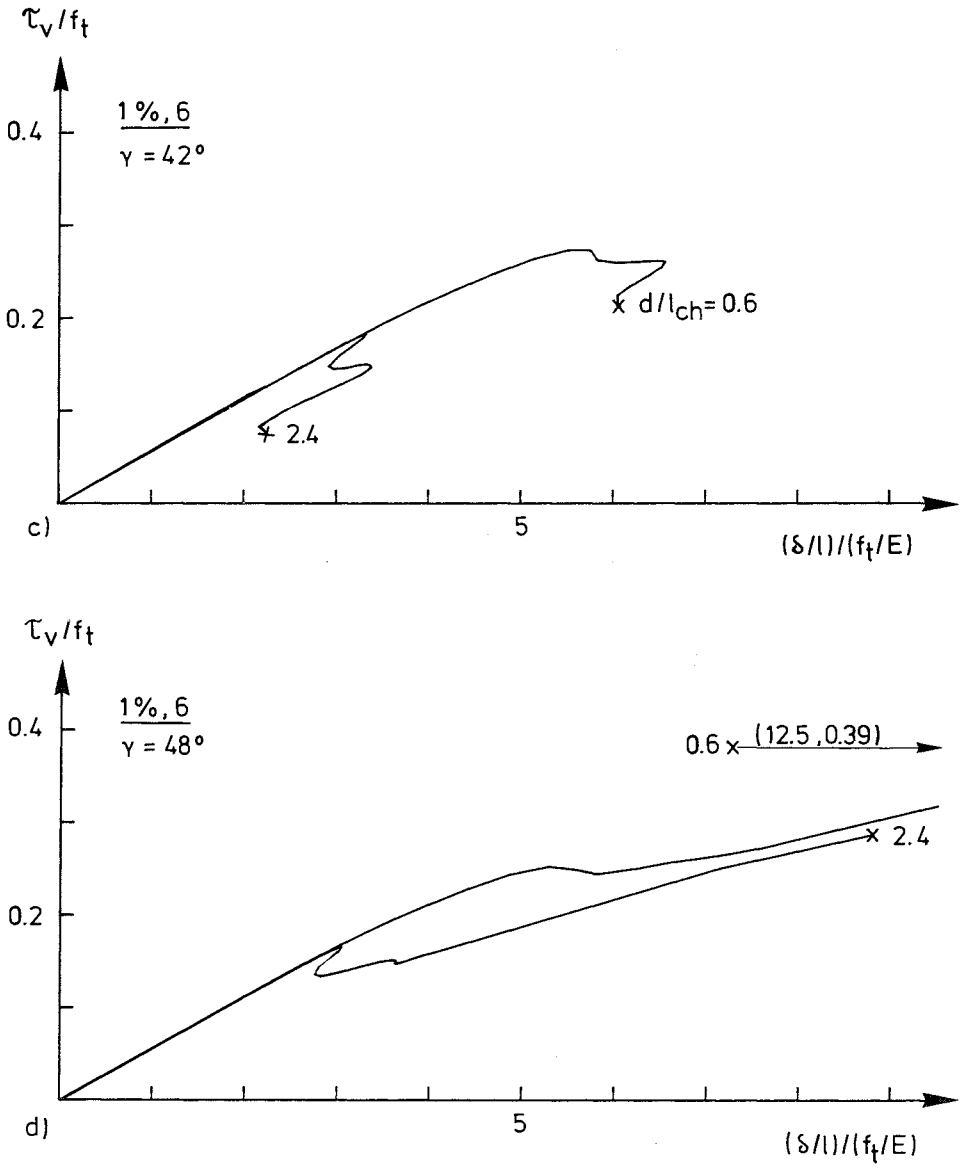

Fig 5.3 (11) (Three pages) Theoretical shear load-deflection response for different beams at different crack paths, γ. Underlined numbers indicate ρ and ℓ/d.

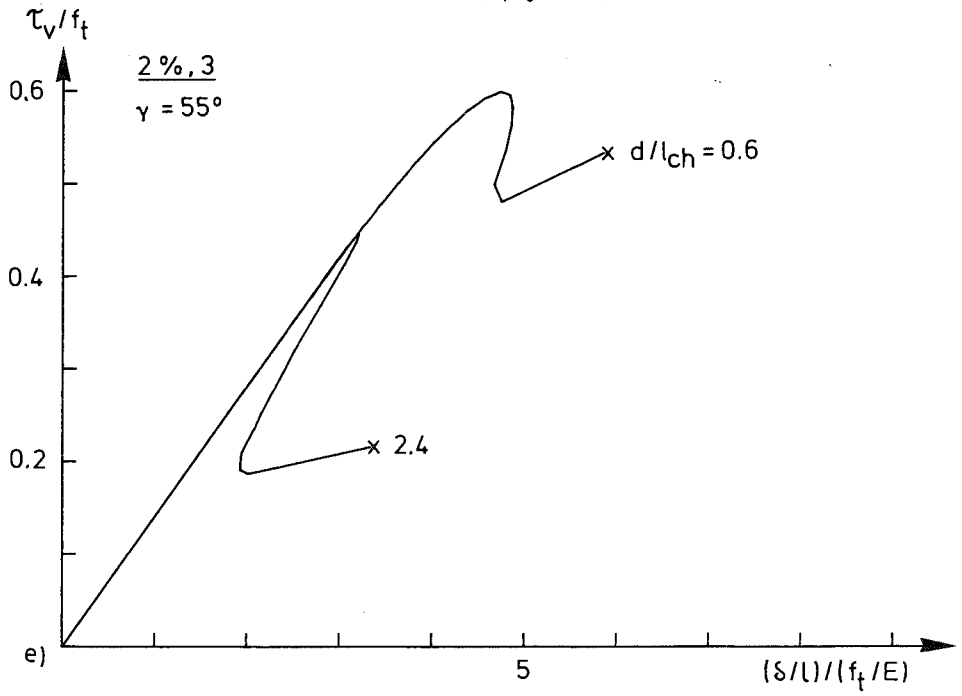
τv/ft
2 %, 3
γ = 55°
0.6
0.4
0.2
d/lch = 0.6
2.4
e)
5
(δ/l)/(ft/E)

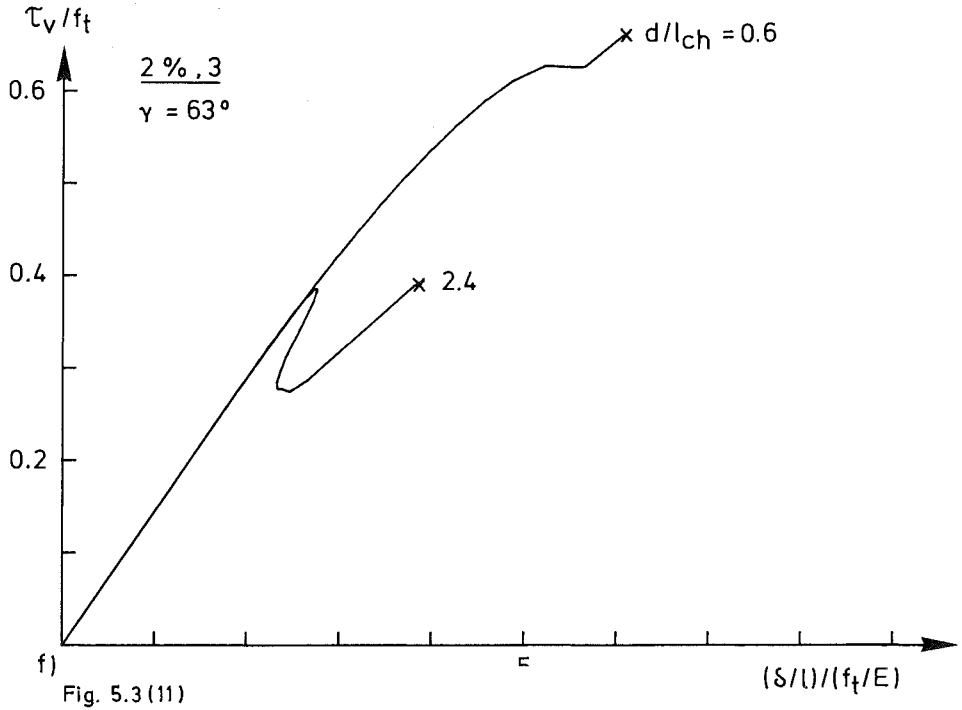
τv/ft
2 %, 3
γ = 63°
0.6
0.4
0.2
d/lch = 0.6
2.4
f)
(δ/l)/(ft/E)

Fig. 5.3 (11)

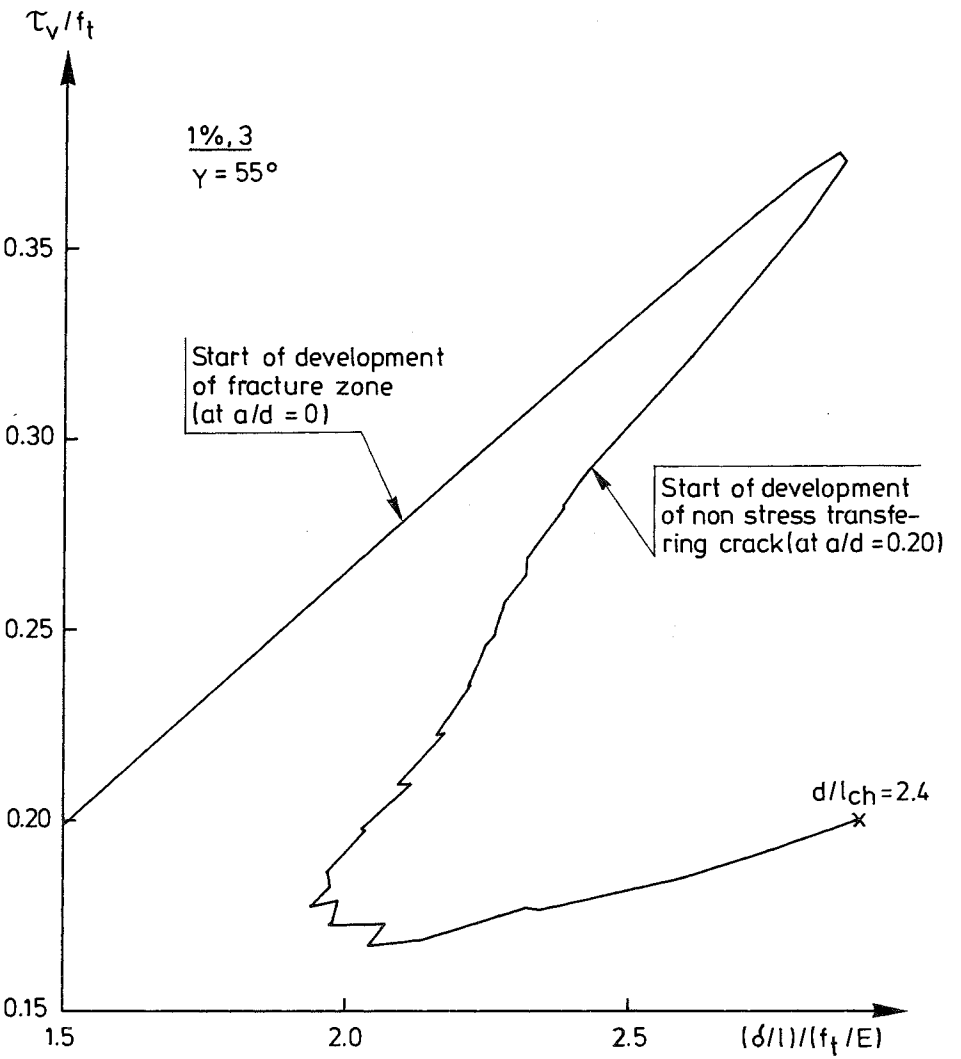

Fig 5.3 (12) Enlarged detail of a load-deflection response shown in Fig 5.3 (11). a = vertical distance from the lower edge of beam.

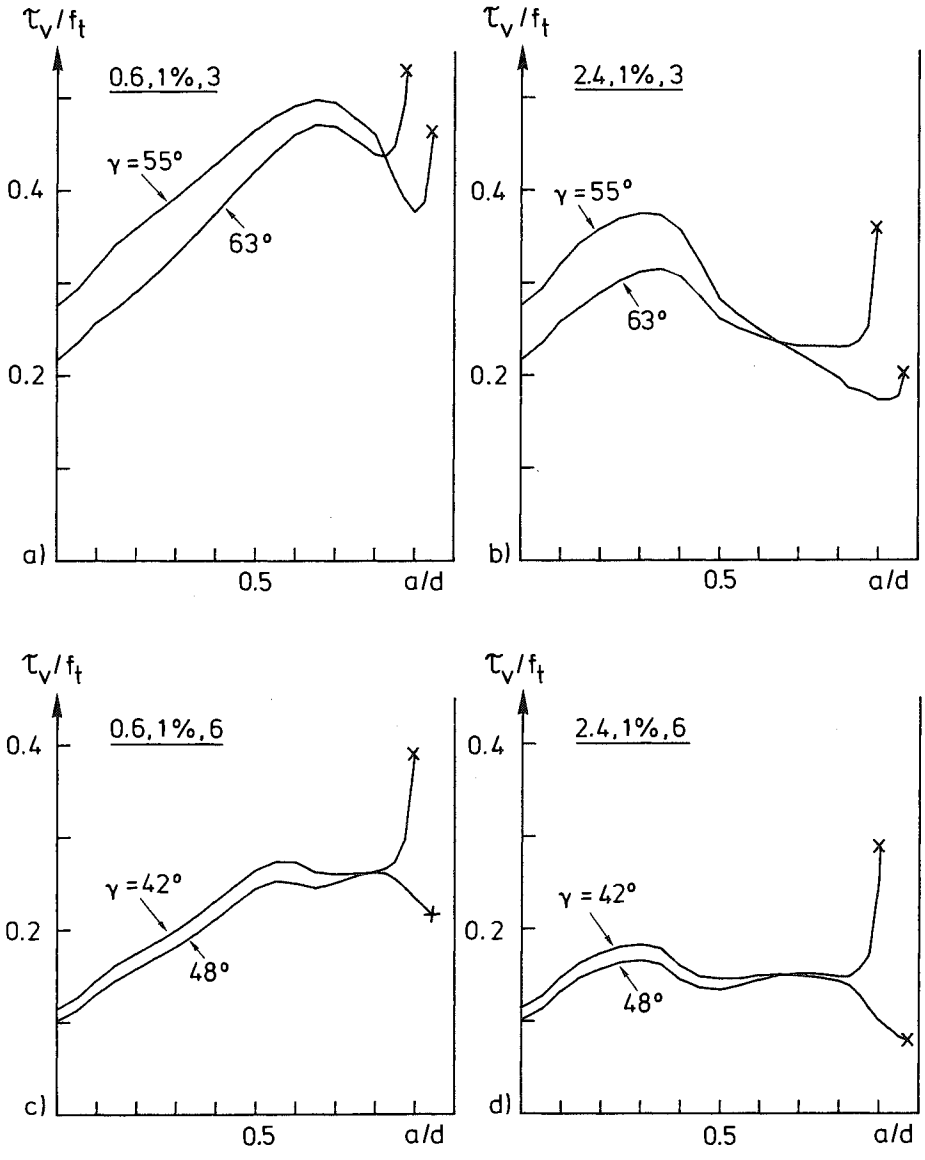
τ_v / f_t
0.6,1%,3
γ = 55°
63°
0.4
0.2
a)
0.5
a/d
τ_v / f_t
2.4,1%,3
γ = 55°
63°
0.4
0.2
b)
0.5
a/d
τ_v / f_t
0.6,1%,6
γ = 42°
48°
0.4
0.2
c)
0.5
a/d
τ_v / f_t
2.4,1%,6
γ = 42°
48°
0.4
0.2
d)
0.5
a/d

Fig 5.3 (13)

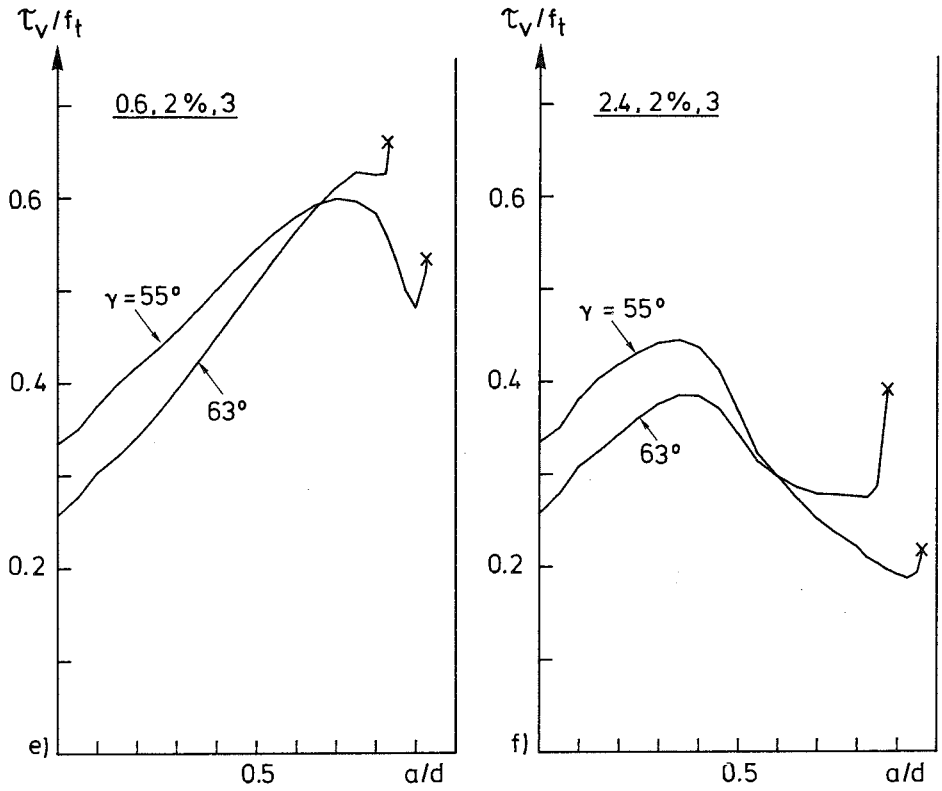

Fig 5.3 (13) (Two pages) Shear force versus depth of fracture zone for different beams of different crack paths. Underlined numbers indicate d/ℓ_{ch}, ρ and ℓ/d.

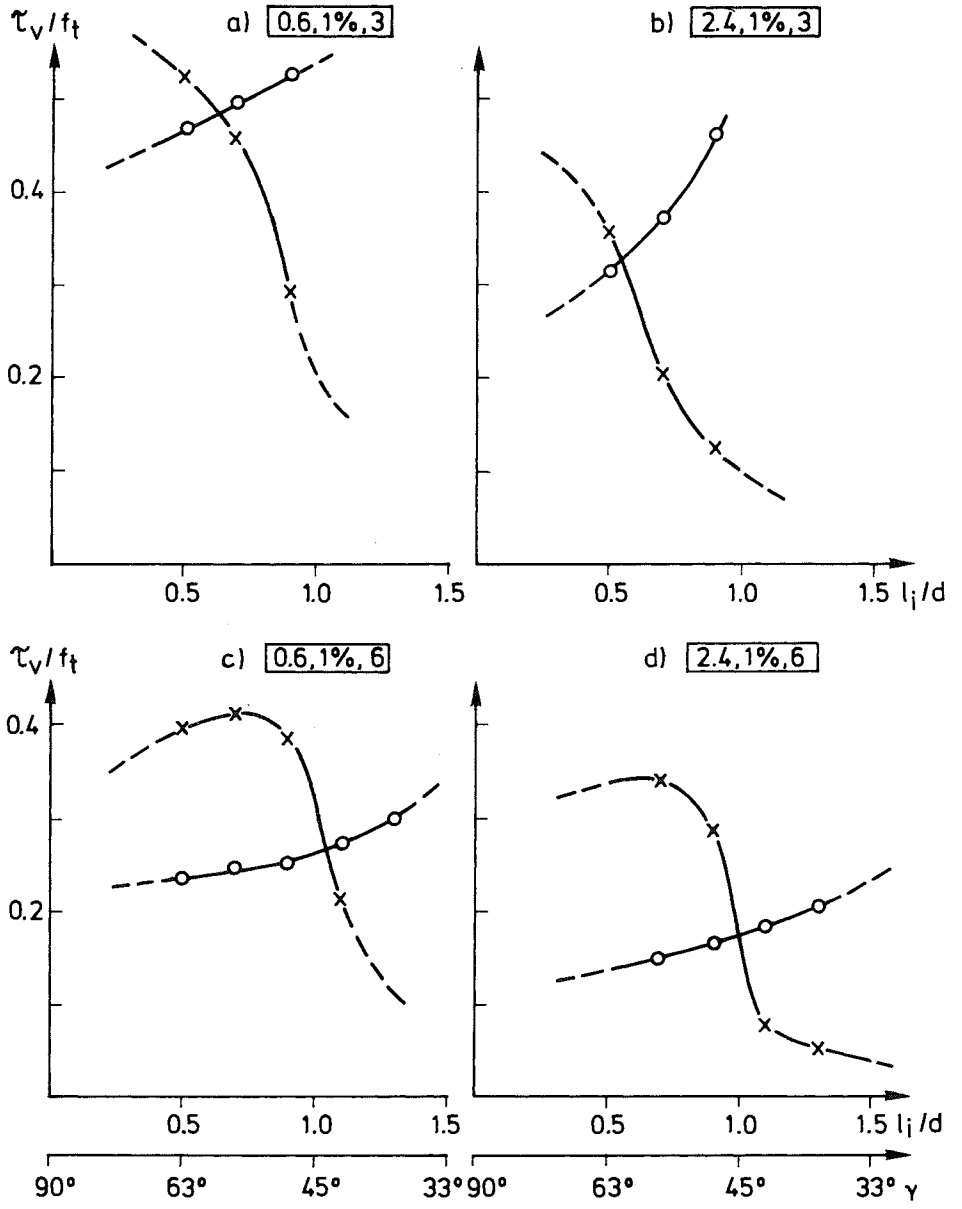
τv / ft
a) 0.6,1%,3
b) 2.4,1%,3
0.4
0.2
0.5
1.0
1.5
0.5
1.0
1.5 li/d
τv / ft
c) 0.6,1%,6
d) 2.4,1%,6
0.4
0.2
0.5
1.0
1.5
0.5
1.0
1.5 li/d
90°
63°
45°
33°
90°
63°
45°
33°
γ

Fig 5.3(14)

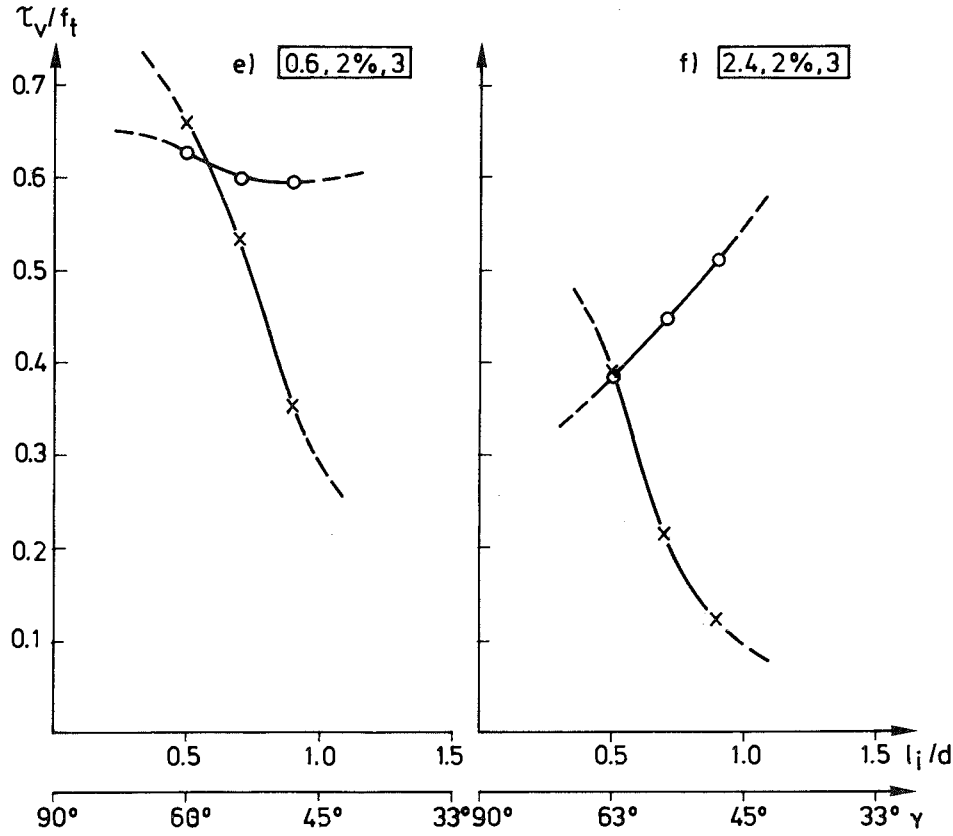

Fig 5.3 (14) a)-f) (Two pages) Load at start of unstable crack growth (indicated by circles: O) and at the collapse of the ligament (indicated by crosses: x) versus position of the crack path. The numbers in frame indicate: d/ℓ_{ch}, ρ, ℓ/d.

for the same beams and crack paths as in Fig 5.3 (11). The depth of the fracture zone, a, is the vertical distance from the lower edge of the beam to the node where the fracture criterion just has been reached. In Fig 5.3 (13) each diagram illustrates how the inclination, γ, of the fracture path influences the load vs. fracture zone depth response. Comparisons between the diagrams sh... ...l response.

While the loads at instability and final collapse of the ligament can be found only for two cracks paths in Fig 5.3 (13), Fig 5.3 (14) (six diagrams) shows these loads for several paths. Ratio ℓ_i/d and the angle γ are defined in Fig 5.3 (10), circles indicate the load at instability and crosses the load at collapse of the ligament. The diagrams of Figs 5.3 (12) and 5.3 (13) are numerical correspondances to the schematical and theoretical diagrams shown in Fig 5.3 (7).

By means of the type of diagrams shown in Fig 5.3 (14) the shear strength, f_v/f_t, and the corresponding fracture path, γ_{pes}, can be obtained (pes= pessimum). These quantities and also the depth of the fracture zone at instability, a_{inst}/d, and the size of the ligament at its final collapse, t_f/d, are indicated in Fig 5.3 (15). The results for $d/\ell_{ch}=0$ and $d/\ell_{ch} \to \infty$ given in this table have not been obtained by means of incremental finite element calculations, but by other methods which will be described later on in this section.

However, it may be appropriate to first explain some numerical details on how the results for $0.3 \leq d/\ell_{ch} \leq 4.8$ have been obtained from the results of the finite element calculations. The values of f_v/f_t and γ_{pes} have been obtained by means of linear interpolation between the known points in the type of diagrams shown in Fig 5.3 (14). During the finite element calculations, the size of the ligament, t, has been defined as the vertical distance from the node where the fracture criterion just has been reached, to the upper edge of the beam minus half the vertical distance between two nodes along the path. During extension of the fracture zone, the size of the ligament decreases in a step-wise manner and commonly, for each individual crack path studied during the finite element analyses, the instant of failure of the ligament corresponds to a location of the tip of the fracture zone in between two nodes. In these common cases the load at the failure of the ligament and the size of the ligament at its collapse have, for each individual crack path, been obtained by means of linear interpolations in diagrams that show the actual external load and the proportional external load corresponding to failure of the ligament vs. size of the ligament. The loads indicated by crosses in Fig 5.3 (14) are obtained in this manner. Knowing γ_{pes} and knowing the size of the ligament at its failure for the paths studied in the finite element analyses, the size t_u/d corresponding to γ_{pes} is obtained by means of linear interpolation.

The results for $d/\ell_{ch}=0$ have been obtained by means of the upper bound theorem of the theory of plasticity. Thus, according to hypothesis II in Section 3.5.2, the actual shear strength values are upper bounds to the shear strength at $d/\ell_{ch}=0$. According to hypothesis I the values are then also upper bounds to the shear strength at any d/ℓ_{ch}.

The actual plasticity results for $d/\ell_{ch}=0$ have been calculated with the help of basic relations given by (Nielsen, Braestrup, Jensen and Bach 1978). The criterion shown in Fig 5.3 (5) b) is used as yield criterion for the concrete, plane stress is assumed and the reinforcement is assumed not to yield. The displacement field for calculation of the internal and external work is chosen in accordance with Nielsen et al. This displacement field consists of two inclined straight yield lines (one at each symmetrical half of the beam) from the lower edge of the beam to its upper edge. The inclination of the straight yield lines is denoted γ (Compare Fig 5.3 (10)) and the value of γ which minimizes f_v/f_t is denoted γ_{pes}. The central rigid part of the beam is assigned a vertical rigid body motion, u, and the rigid end parts of the beam are not moved. For the actual yield criterion and the actual displacement field, the work equation becomes:

$$V_u u = \frac{ubd}{\sin\gamma}\left\{\frac{f_c}{2}\left(1-\sin(\pi/2-\gamma)\right)+f_t\frac{(\sin(\pi/2-\gamma)-\sin\varphi)}{(1-\sin\varphi)}\right\}$$

when $\pi/2-\varphi \geq \gamma \geq 0$, and

$$V_u u = \frac{ubd}{\sin\gamma}\left\{\frac{f_c}{2}\left(1-\sin(\pi/2-\gamma)\right)\right\}$$

when $\pi \geq \gamma \geq \pi/2-\varphi$, where

$$\varphi = \arctan\left(\frac{f_c/f_t-1}{2\sqrt{f_c/f_t}}\right)$$

.....(5.3:6)

The geometrical subsidiary condition is $\tan\gamma \geq d/(\ell/2)$ and for the current beams minimizing gives $\gamma_{pes}=\pi/2-\varphi=35^o$. At this angle the state of stress in the yield line is indeterminable and may be anything along the line from $(f_t, 0)$ to $(0, -f_c)$ in the 2D representation of the yield criterion. The constant value of γ_{pes} means that f_v/f_t is predicted to have the same value for all current beams without any initial crack. For

the beam with an initial crack, f_v/f_t is reduced in proportion to the reduction in the depth of the beam. The plasticity prediction of a constant f_v/f_t does not seem very realistic. However, at their applied theoretical shear strength analyses, Nielsen et al. assume that the tensile strength of concrete is zero, i.e. $f_t/f_c=0$. If adopting this assumption, the theory of plasticity gives more realistic results, at least with respect to the influence of ratio ℓ/d. On the other hand, during the adjustment between theoretical results and test results, Nielsen et al. found that the shear strength is approximately proportional to $\sqrt{f_c'}$, i.e. approximately proportional to the tensile strength of the concrete. In the present calculations the yield criterion of Fig 5.3 (5) b), which includes a non-zero tensile strength, is used in order to make the calculations consistent with the finite element analyses for non-zero d/ℓ_{ch}. Furthermore, the prime purposes of the present calculations for $d/\ell_{ch}=0$ are only to make clear that f_v/f_t does not approach infinity when d/ℓ_{ch} is decreased towards zero and to exemplify that f_v/f_t for any non-zero d/ℓ_{ch} must be smaller than, or equal to the f_v/f_t given by any upper bound solution for $d/\ell_{ch}=0$.

The results for $d/\ell_{ch}\rightarrow\infty$ have been obtained by means of linear elastic finite element analyses of the current beams, i.e. from the results from the first incremental step in the non-linear finite element calculations. For each of the studied crack paths, the load that gives start of development of a fracture zone is obtained from the finite element results. By means of interpolation, the load that gives start of development of fracture zone at crack path γ_{pes} as obtained for the largest d/ℓ_{ch} analysed (i.e. 2.4 or 4.8) is then calculated. In that way the lower bounds indicated in Fig 5.3 (15) have been determined. Accordingly, these lower bounds are lower bounds in its strict sense only if the critical fracture path at $d/\ell_{ch}\rightarrow\infty$ is same as for the largest d/ℓ_{ch} (i.e. 2.4 or 4.8) numerically analysed. In this case the indicated strengths represent the strength according to the structural strength concept of brittle structures/materials. The structural strength concept predicts a lower, or equal, strength than the material strength concept. Thus, according to hypothesis III in Section 3.5.2, the actual strength values are lower bounds to the strength when $d/\ell_{ch}\rightarrow\infty$. According to hypothesis I, the actual strengths are then also lower bounds to the shear strength at any d/ℓ_{ch}. For the beam with an initial crack of a depth proportional to d, the actual lower bound is zero. In spite of this, the strength of thi $/\ell_{ch}$ is

increased. For the beams without the initial crack it can be noticed that the strengths when $d/\ell_{ch} \to \infty$ are not much smaller than when d/ℓ_{ch}=2.4. For all these beams an increase in d/ℓ_{ch} from 2.4 to infinity gives a reduction in shear strength which is less than 50 %. This means that the sensitivity in shear strength to changes in d/ℓ_{ch} is small for extremely large beams and/or extremely brittle concretes. However, this conclusion is uncertain as the actual lower bound, i.e. the presently indicated and discussed strength when $d/\ell_{ch} \to \infty$, is not a lower bound in its strict sense (See above.).

For $0.3 \leq d/\ell_{ch} \leq 4.8$ and $\rho \geq 0.5$ %, the calculated shear strengths of Fig 5. 3 (15) are shown graphically in Fig 5.3 (16) as f_v/f_t vs. d/ℓ_{ch}. In this diagram the circles show the computational results while the lines in between and beyond the circles only represent estimations. Please note that the scales on the axes of the diagram of Fig 5.3 (16) are logarithmic. This means that a constant sensitivity in f_v/f_t to changes in d/ℓ_{ch} corresponds to a straight line.

For studies and evaluation of the kind of results regarding strength presented in Fig 5.3 (15) it is helpful to calculate the sensitivity to the different variables involved. The result of such sensitivity calculations may be found in Fig 5.3(17).

The results of Fig:s 5.3 (11)-5.3 (17) offer the possibility for a number of conclusions or observations. In Section 5.4 some such discussions and remarks may be found together with comparisons to experimental results. In this section, a few particular remarks will be made. While the present remarks and discussions will concentrate on the results regarding ultimate strength, the actual figures give also the possibility to make observations regarding critical location of crack path, depth of fracture zone at instability, size of ligament at its collaps, load vs. deflection response, load vs. fracture zone depth and load vs. location of fracture path.

Firstly, it should be emphasized that the results shown in the actual figures are nothing more, and nothing less, than the results of theoretical calculations. Accordingly, of course, the results should not be looked upon as if they represent the strength and the behaviour of real beams or real slabs. Conversely, during comparisons to other analyses and during comparisons to test results it should be noticed that no adjustment or fitting paramet ;. At the time

	d/ℓ_{ch}	ρ(%)	ℓ/d	f_v/f_t	γ_{pes}(°)	a_{inst}/d	t_u/d
	.0	.0	3	$\leq$ .303	90	1.00	-
1)	.6	.0	3	.168	90	.40	-
	2.4	.0	3	.137	90	.15	-
	∞	.0	3	.118	90	.00	-
	.0	.5	3	$\leq$1.581	35	1.00	-
	.6	.5	3	.367	60	.50	.05
	2.4	.5	3	.267	63	.30	.05
	∞	.5	3	$\geq$ .200	63	.00	-
	.0	1.0	3	$\leq$1.581	35	1.00	-
	.3	1.0	3	.602	56	.85	.07
	.6	1.0	3	.488	58	.65	.07
	1.2	1.0	3	.394	61	.50	.08
	2.4	1.0	3	.327	62	.35	.08
	4.8	1.0	3	.287	62	.20	.08
	∞	1.0	3	$\geq$ .221	62	.00	-
	.0	1.5	3	$\leq$1.581	35	1.00	-
	.6	1.5	3	.564	60	.75	.10
	2.4	1.5	3	.358	63	.35	.10
	∞	1.5	3	$\geq$ .242	63	.00	-
	.0	2.0	3	$\leq$1.581	35	1.00	-
	.6	2.0	3	.618	61	.75	.12
	2.4	2.0	3	.385	63	.40	.11
	∞	2.0	3	$\geq$ .263	63	.00	-
	.0	1.0	6	$\leq$1.581	35	1.00	-
	.6	1.0	6	.267	44	.55	.05
	2.4	1.0	6	.176	45	.30	.05
	∞	1.0	6	$\geq$ .113	45	.00	-
	.0	1.0	9	$\leq$1.581	35	1.00	-
	.6	1.0	9	.192	39	.55	.06
	2.4	1.0	9	.123	42	.30	.03
	∞	1.0	9	$\geq$ .069	42	.00	-
	.0	1.0	3	$\leq$1.423	35	1.00	-
2)	.6	1.0	3	.461	60	.68	.09
	2.4	1.0	3	.307	61	.35	.06
	∞	1.0	3	$\geq$ .000	61	.10	-
	.0	1.0	3	$\leq$1.581	35	1.00	-
3)	.6	1.0	3	.490	58	.65	.07
	2.4	1.0	3	.328	62	.35	.09
	∞	1.0	3	$\geq$ .221	62	.00	-

1) Bending failure of unreinforced concrete beams (straight line σ-w curve)
2) Initial open crack of depth 0.1 d in lower edge of beam.
3) Bond stress-slip relation "B", shown in Fig 5.3 (3).

Fig 5.3 (15) Theoretically calculated shear strength, f_v/f_t, decisive fracture pa... ...ity, a_{inst}/d, and si... ...fferent beams.

when the calculations were carried out, the writer had little knowledge about test results regarding shear strength of concrete beams.

An evident result of the calculations is that the shear strength decreases at increased size of the beam and at increased brittleness of the concrete. For the common intermediate range of d/ℓ_{ch} an approximate easy-to-remember thumb rule is that halving two times of ratio d/ℓ_{ch} gives a 50 % increase in f_v/f_t. According to conventional strength theories the increase would be zero %, and according to the linear elastic fracture mechanics, the increase would be 100 %. A comparison to the results in Section 4.2 shows that ratio d/ℓ_{ch} has a greater influence on the shear strength than on the flexural strength of (proportionally loaded) unreinforced concrete beams.

The computational results regarding shear strength are all in agreement with the four general hypotheses in Section 3.5.2. In this regard also two details of the results can be noticed in Fig 5.3 (17): during variation in d/ℓ_{ch}, the (absolute value of the) sensitivity in f_v/f_t to changes in d/ℓ_{ch} expose a maximum (in the region $0.6 \leq d/\ell_{ch} \leq 1.2$) and, secondly, the corresponding maximum sensitivity is less than 0.5. Even if the actual hypotheses are true, it is not self-evident that the finite element calculations would not produce contradictions. Thus, since only a few possible crack paths are considered it is theoretically possible that the calculations could turn out to produce a shear strength greater than that produced by the upper bound theorem of plasticity.

Where the results of Fig 5.3 (15) are concerned it may, in particular, be noticed that the depths of the fracture zone at instability, a_{inst}, are great. For the small beams a_{inst}/d is great and for the large beams a_{inst}/ℓ_{ch} is great. Furthermore, a_{inst}/ℓ_{ch} is not constant and, for all of the current beams, at the instant of instability no part of the fracture zone had developed into an open crack. These matters suggest that the basic assumptions of the linear elastic fracture mechanics are not fulfilled. These matters also contradict basic conditions which most probably are required for validity of the size effect law of Bazant (1984). The actual two theories have previously been applied during studies of the relative influence of absolute size on shear strength, and a comparison to the present results may be found in Section 5.4.

The sensitivity ensitivity to

reinforcement is greater for small beams than for large beams. The reason for this may be that the co-operation between stress transfer in the reinforcement and in the fracture zone is better in small beams. Fig 5.3 (17) also suggests that the sensitivity to ratio d/ℓ_{ch} is greater in the heavily reinforced beams than in the lightly reinforced beams.

Commonly the empirical and semi-empirical formulas for the shear strength consists of a function of only ρ times a function of only ℓ/d times a function of only f_t (or f_c) times a function of only d (while the influence of d were not taken into account in older formulas, it seems that the influence of d is taken into account in most recent formulas). According to above, the present computational results suggest that the influence of the different variables is coupled and accordingly that it is not suitable to express shear strength as the product of functions of the individual variables.

The sensitivity to ratio ℓ/d is close to unity. This means that the shear strength is strongly dependent on the bending moment. Conversely, this also means that the load carrying capacities of the current beams, if expressed in terms of their formal flexural strength, are close to being independent of the shear force in the beams. In spite of this, it is good to distinguish between flexural strength and shear strength as the failure modes are different, i.e. $\gamma_{pes}=90^o$ and less than 90^o respectively.

On the whole, the computational results summarized in Fig 5.3 (15) seem to be consistent with each other. However, one of the results is in conflict with ones intuition: one would expect that a change in the bond stress-slip relation from curve A to curve B, shown in Fig 5.3 (3), would produce a greater change in the calculated shear strength. The basic explanation to the actual smallness of the influence might be that the phenomenon of aggregate interlocking has not been considered in the present calculations.

As evident from Fig 5.3 (15), t_u/d has not been calculated for the beams without reinforcement. These beams fail in bending and γ_{pes} is known in advance to be 90^o. In general, if the decisive fracture path, γ_{pes}, is known in advance, it is not necessary to calculate t_u/d and the load at the final collapse of the ligament, in order to calculate the ultimate strength of beams with a brittle type of failure.

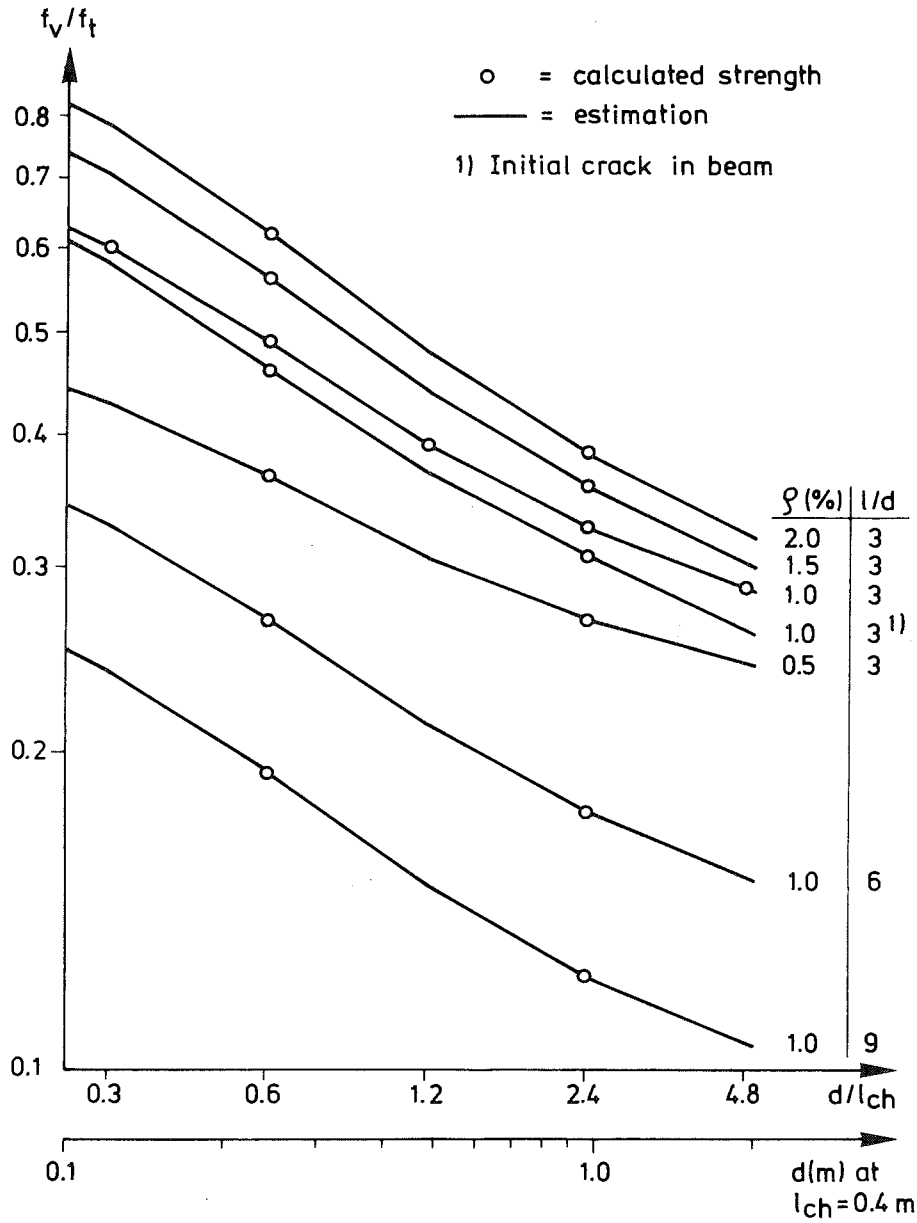

Fig 5.3 (16) Shear strength vs. ratio d/ℓ

a)

d/ℓ_{ch}	$\rho(\%)$	ℓ/d	C_m	Sensitivity -m (% / %)
1) .6-2.4	0.0	3	.156	.15
.6-2.4	0.5	3	.326	.23
.6-2.4	1.0	3	.421	.29
.6-2.4	1.5	3	.477	.33
.6-2.4	2.0	3	.519	.34
.6-2.4	1.0	3	.421	.29
.6-2.4	1.0	6	.229	.30
.6-2.4	1.0	9	.163	.32
.3-.6	1.0	3	.420	.30
.6-1.2	1.0	3	.417	.31
1.2-2.4	1.0	3	.414	.27
2.4-4.8	1.0	3	.386	.19

1) Bending failure; single straight line σ-w curve.

b)

d/ℓ_{ch}	$\rho(\%)$	ℓ/d	C_n	Sensitivity -n (% / %)
.6	1.0	3-6	1.269	.87
.6	1.0	6-9	1.139	.81
2.4	1.0	3-6	.868	.89
2.4	1.0	6-9	.851	.88

c)

d/ℓ_{ch}	$\rho(\%)$	ℓ/d	C_p	Sensitivity p (% / %)
.6	0.5-1.0	3	.488	.41
.6	1.0-1.5	3	.488	.36
.6	1.5-2.0	3	.495	.32
2.4	0.5-1.0	3	.327	.29
2.4	1.0-1.5	3	.327	.22
2.4	1.5-2.0	3	.323	.25

Fig 5.3 (17) Sensitivity in shear strength to changes in:
a) d/ℓ_{ch}: $f_v/f_t = C_m\,(d/\ell_{ch})^m$

Let us now turn to the results regarding influence of prestressing of the reinforcement bars. Prestressing can be carried out in different manners: before or after hardening of the concrete; with end anchorage of reinforcement or with bonded reinforcement; and with direct contact steel-concrete or with reinforcement placing in pipes. The current calculations concern the case of prestressing before hardening of the concrete, bonded reinforcement without end anchorage and with direct contact steel-concrete. This is a common method for the prestressing of factory-made beams or slabs. The current calculations concern only the load at instability and only crack path number 1, shown in Fig 5.3 (10). While the prestress in the reinforcement bars, f_p, is varied, the other variables are held constant according to Fig 5.3 (18). The bond stress-slip curve "A", shown in Fig 5.3 (3), is adopted and no initial cracks are assumed to be present on the beams.

According to the finite element calculations the mechanical events within the beams are as follows: first, before the external load is applied, a slip develops between the steel and the concrete at the ends of the beam. This slip is of course the result of release of the external force applied during stressing of the steel. Next, when a certain external load has been applied, a fracture zone starts to develop in the concrete. This stable development starts from a point at approximately half the depth of the beam. Later on, the maximum load carrying capacity (the instability load) is reached and, if the external load is constant, the subsequent events become rapid and unstable. These events may start with a further development of the fracture zone and a subsequent slip between the steel and the concrete all the way between the end of the beam and the location of the crack path. This slip may give a great opening of the crack and a great increase in the deflection of the beam at a fairly constant load carrying capacity. During this opening of the crack, the size of the ligament decreases and one may expect that finite element analyses of the subsequent performance would indicate extremely large stresses in the upper edge of beam, resulting in a failure of the ligament.

Fig 5.3 (18) shows the calculated load at instability. Here, these instability loads will be assumed to represent the ultimate shear strength. Evidently, the calculations suggest a significant benificial effect of prestressing on shear strength. However, at prestress, f_p/f_t, greater than about 200, the shear strength becomes approximately constant and even exposes a slight decrease. The reason for this plateau is that

plastic slip (i.e. slip at constant bond stress) between the steel and the concrete develops all the way from the end of the beam to the location of the subsequent crack path already before the external load is applied, i. e. when the prestressing force is released. The development of such a slip means that the effective prestress across the subsequent fracture path cannot be increased above a certain value. An equilibrium calculation by hand shows that the actual slip develops if the initial prestressing, f_p/f_t, is greater than 192. Of course this break-point value is different for other bond strengths, other locations of the crack path and other diameters of the reinforcement bars.

The results for $d/\ell_{ch} \to \infty$ indicated in Fig 5.3 (18) represent the load at start of development of the fracture zone. The upper bound for the shear strength at $d/\ell_{ch}=0$, $f_v/f_t=1.58$, above calculated for beams without prestressing, is valid also for the prestressed beams. Naturally, the exact shear strength at $d/\ell_{ch}=0$ may be smaller.

Fig 5.3 (18) suggests that the relative benificial effect of prestressing is greater for the extremely large beams than for the beams with $d/\ell_{ch}=0.6$. The increase in the instability load due to prestressing, f_p/f_t, equal to 100, 200 and 300 is 85 %, 170 % and 160 % when $d/\ell_{ch} \to \infty$ and 52 %, 85 % and 78 % when $d/\ell_{ch}=0.6$. As a result of a theorem of the theory of plasticity and hypothesis II in section 3.5.2, one may expect prestressing to give a zero % increase in the shear strength when $d/\ell_{ch}=0$. The actual results also suggest that the sensitivity to changes in d/ℓ_{ch} is smaller for prestressed beams than for beams without prestressing. In the current case, the increase in the instability load due change in d/ℓ_{ch} from infinity to 0.6 is 52 % when $f_p/f_t=0$, 25 % when $f_p/f_t=100$, 4 % when $f_p/f_t=200$ and 5 % when $f_p/f_t=300$.

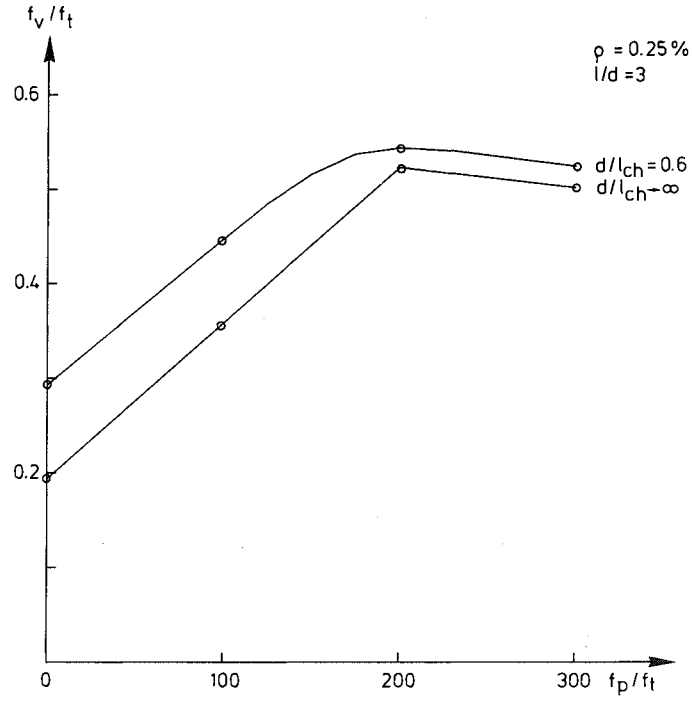

Fig 5.3 (18) Shear strength vs. prestress. Only one crack path considered and only the load at start of unstable crack growth analysed.

5.4 Comparisons and remarks

In this section first comparisons between the calculated shear strength and empirical formulas will be made with respect to the relative influence of different variables. Then a comparison with respect to absolute values of shear strength will be made. Subsequently the influence of prestressing is dealt with. A few remarks, in addition to those in Section 5.3.5, may also be found.

The comparisons with respect to the relative influence of different parameters are made by means of the results of three surveys of very large numbers of test [illegible] cording to

Hedman and Losberg (1978), the second is according to Leonhardt (1978) and the third is according to Nielsen, Braestrup, Jensen and Bach (1978). The formula of Leonhardt is analogous to a formula presented by Rafla (1971).

A great number of empirical formulas for the shear strength may be found in literature. For instance, Elzanaty (1985), in a recent study of shear strength, references to more than ten formulas may be found. The three surveys used in the present comparisons are adopted because they have been proposed by well-known researchers in the field of shear strength, because the surveys include consideration to the influence of absolute size of beams and because the empirical formulas corresponding to these surveys are believed to be rather typical.

In the actual three surveys, shear strength is expressed as a function of the compressive strength of concrete ,f_c, times a function of ℓ/d times a function of ρ (=cross-section area of reinforcement/bd) times a function of d. In all three cases the function of the compressive strength is stated to be $\sqrt{f_c}$. For the mathematical description of the other functions, the reader is referred to the actual references.

Where the definition of d is concerned, the following should be noticed: during the present calculations and in the third survey, d is defined as the total depth of the beam. In the first and second survey, d is defined as the effective depth of the beam. During the present comparisons d is throughout treated as if it represents the total depth of the beam. As the present comparisons concern the relative influence of variables it seems fair to believe that the difference in definition of d is of small importance. The second empirical result is valid for the 5 % fractile of shear strength while the other empirical results presently used are valid for the mean strength. This difference should also be of small importance.

Fig 5.4 (1) shows the influence of the absolute size of beams on their strength. In this figure the strengths are normalized with respect to the strength at d=0.12 m. The theoretical result is shown for ℓ_{ch}=400 mm. This is a typical value of ℓ_{ch} for normal concrete. If the theoretical result is plotted for other reasonable values of ℓ_{ch}, it is found that the exact choice of ℓ_{ch} is not of great importance where the actual relative influence is concerned.

Fig 5.4 (2) shows the influence of ratio ℓ/d. In this figure the strengths are normalized with respect to the strength at $\ell/d=3$.

Fig 5.4 (3) shows the influence of ρ when $\rho \geq 0.5$ %. In this figure strength is normalized with respect to the strength at $\rho=0.5$ %. Fig 5.4 (4) shows the influence of ρ when $\rho \leq 0.5$ %. The theoretical curves in this latter figure are uncertain as they are based only on a smooth extension of the curves for $\rho \geq 0.5$ % and on the calculated flexural strength of concrete beams without any reinforcement at all, i.e. with $\rho = 0.0$ %.

With the exception of the influence of ℓ/d, the theoretical results seem to be in good agreement with the empirical results: the deviation is not greater than between the results of the surveys of experimental tests. Where the influence of ratio ℓ/d is concerned, the empirical results suggest a greater influence in the region $3<\ell/d<6$ and a smaller influence in the region $6<\ell/d<9$.

The difference between the size effect relations shown in Fig 5.4 (1) shall be more clearly illustrated and also compared to the size effect of linear elastic fracture mechanics and to a size effect law of Bazant (1984). The actual illustration may be found in Fig 5.4 (5) and shows the sensitivity in shear strength to changes in absolute size, i.e. $(\Delta f_v/f_v)/(\Delta d/d)$, vs. the absolute size of the beam, d. The trivial result of the conventional strength theories is not shown. According to those theories the sensitivity in strength to changes in size is zero.

During analyses of the size effect in shear strength, Reinhardt (1981, a and b) has applied the size effect of linear elastic fracture mechanics and Bazant and Kim (1984)* have applied the size effect law of Bazant. According to the size effect law of Bazant $f_v \sim 1/\sqrt{1+d/(\lambda d_a)}$, where λ is an adjustment parameter and d_a the maximum particle size of the aggregate. By means of adjustment to test results, Bazant and Kim found that $\lambda=25$ seems to be suitable for the shear strength of concrete beams. The size effect law of Bazant and the linear elastic fracture mechanics both predict a decrease in strength at increased size. On the other hand, according to Section 5.3.5 and Section 3.5.3, for the case of shear strength analysis, basic assumptions behind the actual two size effect theories do not seem to be fulfilled.

Fig 5.4 (5) ind … between the

*) See also dis …

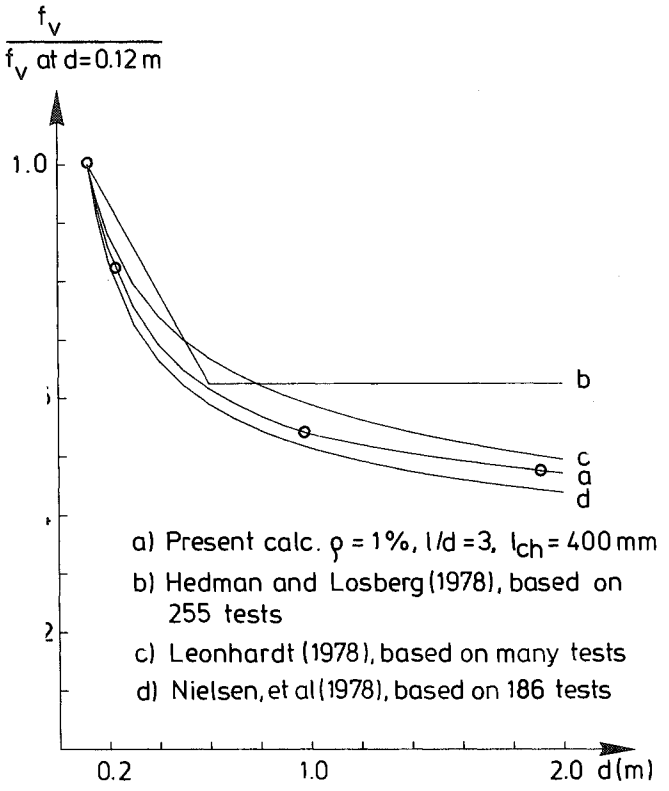

Fig 5.4 (1) Influence of size on shear strength.

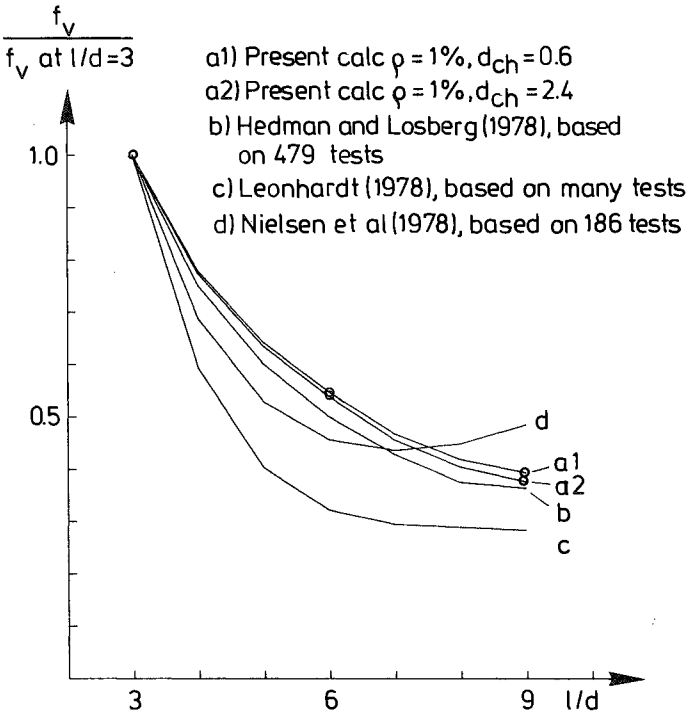

Fig 5.4 (2) Influence of ratio ℓ/d on shear strength.

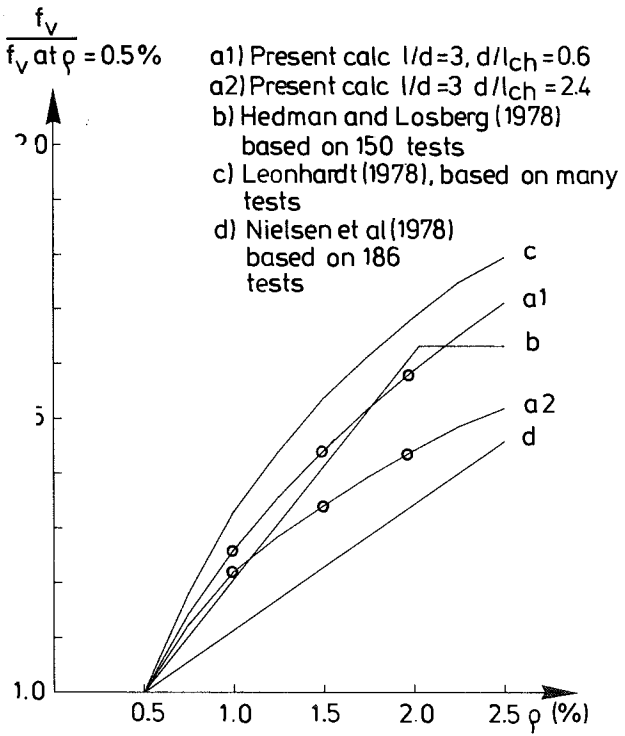

Fig 5.4 (3) Influence of ρ on shear strength. $\rho \geq 0.5$ %.

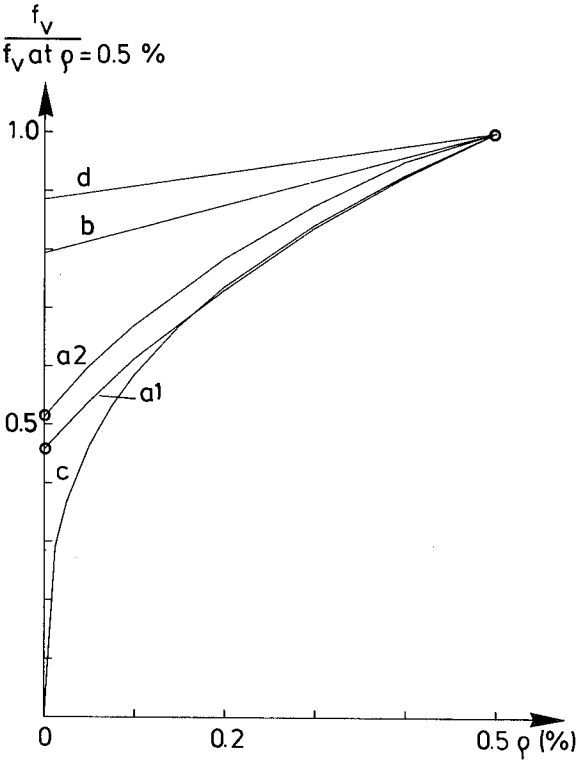

Fig 5.4 (4) Influence of ρ on shear strength. $\rho \leq 0.5$ %.

size effect relations. The three empirical relations and the semi-empirical relation of Bazant and Kim all suggest approximately the same mean sensitivity in the region 0.2 m < d < 1.0 m. This suggests that these relations have been developed by fitting to test results valid for normal qualities of concrete in this normal region of d. The empirical mean sensitivity seems to be about (-0.25)-(-0.30) in the actual normal region. The present theoretical results suggest approximately the same mean sensitivity in the corresponding region of ratio d/ℓ_{ch}.

Although the four empirical relations crosses each other in the region 0.2 m < d < 1.0 m, the relations are of quite different types: while one relation suggest a continuous decrease in sensitivity, another suggests a constant sensitivity, a third suggests a continuous increase in sensitivity and a fourth suggests a maximum in the sensitivity at d=0.6 m. This suggests that it is difficult to develop consistent strength formulas from test results even if the results from a large number of tests are available.

Even if the empirical relations represent different types of sensitivity curves, they all happen to be such that they violate the general hypotheses in Section 3.5.2. Besides, the semi-empirical relation of Bazant and Kim, as well as the linear elastic fracture mechanics violate the hypotheses. In order not to contradict the hypotheses, the sensitivity curve should be of the type suggested by the result of finite element analyses: the sensitivity should be in between -0.5 and zero and should approach zero both when d approaches zero and when d approaches infinity. However, the empirical relations are most probably not intended to be used outside some normal region of d and perhaps not either intended to be used for concrete with an unusually small or large characteristic length, ℓ_{ch}.

In the new Swedish concrete building code, the influence of size on shear strength is taken into account. The relation used in the code is a modification of the original proposal of Hedman and Losberg, and is a piece-wise linear relation: $f_v \sim$ constant=1.4 when $d \leq 0.2$ m; $f_v \sim 1.6-d$ when $0.2\ \text{m} \leq d \leq 0.5$ m; $f_v \sim 1.3-0.4d$ when $0.5\ \text{m} \leq d \leq 1.0$ m; $f_v \sim$ constant=0.9 when $d \geq 1.0$ m. The modification is such that the hypotheses of section 3.5.2 are no contradicted as far as the properties of the sensitivity curve are concerned. The reason for the modification in the region d<0.2 m (f_v = constant) is not known, while the reason for the modifications in the region d>0.2 m [illegible] description of test

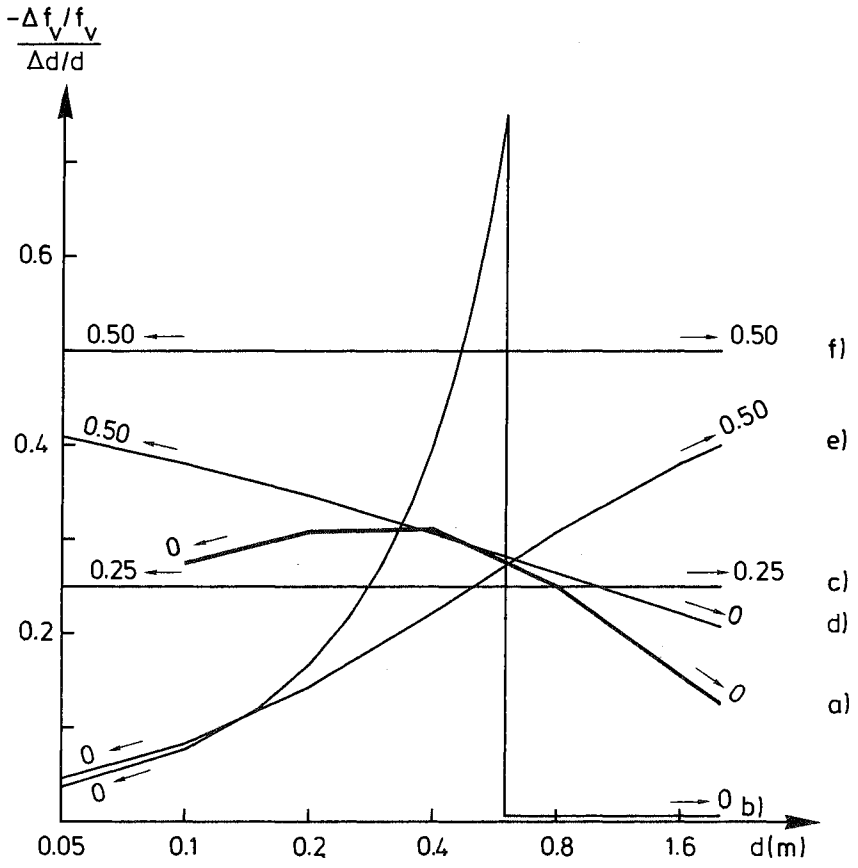

Fig 5.4 (5) Sensitivity in shear strength to changes in beam size vs. beam size.

a) Present theoretical result obtained for ρ =1 %, ℓ/d=3 and ℓ_{ch} =400mm

b) Empirical, Hedman and Losberg (1978), $f_v \sim 1.75\text{-}1.25\ d \geq 1.0$

c) Empirical, Leonhardt (1978), $f_v \sim d^{-0.25}$ (Also Weibull-model)

d) Empirical, Nielsen et al. (1978), $f_v \sim 1+d^{-0.5}$ $(.08 \leq d \leq .7)$

e) Semi-empirical, Bazant and Kim (1984), $f_v \sim (1+d/25d_a)^{-0.5}$, max particle size, d_a, =.02 m

f) Theoretical, Reinhardt (1981 a, b), $f_v \sim d^{-0.5}$ (Linear elastic fracture mechanics).

The dimension of d in the above relations is metre.

results. If a judgement is made from the present theoretical results or from test results, the size effect at small size ($d<0.2$ m) seems to be significant enough to be exploited in the design of shallow beams and slabs.

During a change-over period both the new Swedish concrete building code and the older Swedish code has been allowed to be used. According to the design rules of the older code, the absolute size has no influence on the shear strength. In the model code of Comite Euro-International du Beton, the influence of size is considered. According to design expressions shown by Elzanaty (1985), the influence of size is not considered in the American Concrete Institute Code.

In Fig 5.4 (5), the curve showing the result of the present calculations is drawn for ℓ_{ch} =400 mm. For concrete qualities with a larger characteristic length, the curve will be moved to the right and for more brittle qualities of concrete, the curve will be moved to the left. It may be noticed that the theoretical results predict the characteristic length of the concrete to be of equally great importance as the absolute size of the beam. The present discussion and comparisons have mainly concerned the influence of the absolute size while a comparison with respect to the influence of ℓ_{ch} has not been made. The only reason for this is that influence of absolute size has been detected previously and a number of experimental results are available while no experimental results regarding the influence of the characteristic length of the concrete are available.

It may also be noticed that the theoretical curve is valid if all geometrical dimensions of the beams, including the diameter of the bars, are changed proportionally at a constant quality of the concrete, i.a. at a constant absolute size of the aggregate. If the diameter of the bars is kept constant during increase in the absolute size of the beam, one may expect a smaller influence of the absolute size than predicted by the present calculations. This smaller influence may be expected due to the relative increase in stiffness and strength in the bond between the bars and the concrete. According to experimental results shown by Leonhardt (1978), shear strength decreases about 20 % if the bar diameter is increased from 10 mm to 20 mm at constant percentage of reinforcement (1.88 %). Thus the influence of the bar diameter does not seem to be of negligible importance. Where the size of the aggregate is concerned, one may expect a smaller influence of the absolute size of the beam than

predicted by the present calculations, if the absolute size of the aggregate is not constant but is larger for the larger beams.

According to experimental results of Petersson (1981), ℓ_{ch} increases at increased maximum particle size of the aggregate, but the increase is not proportional: for a concrete with the maximum particle size 8 mm ℓ_{ch}=280 mm is reported, while ℓ_{ch}=400 mm is reported for a corresponding concrete with the maximum particle size 16 mm. Taylor (1972) tested beams of different absolute size both with a constant maximum particle size and with maximum particle sizes scaled in proportion to the size of the beam. As may be expected from present calculations together with the ℓ_{ch} values reported by Petersson, Taylor found that both approaches gave a decrease in strength at increased size of the beam and that this decrease is smaller if the maximum particle size is scaled in proportion to the size of the beam. An increase in d from 250 mm to 1000 mm gave a 16 % decrease in shear strength for the constant maximum particle size (19 mm) and a 10 % decrease when the maximum particle sizes were scaled (9 mm and 38 mm, respectively). The actual magnitude of the influence of size recorded by Taylor seems to be unusually small: this is shown by Taylor in a comparison to previous test data and the same thing is found if comparisons are made to subsequent test data.

At this point, it may be suitable to include a few remarks with respect to model-concretes and model-testing of shear failure. According to the conventional theories for description of the properties of materials, i.e. the methods based on a description of stress vs. strain response of the material, at certain conditions (negligible influence of dead-weight, proper scaling of loads and no change in the properties of the material) the quasi-static behaviour of a full size structure is quite similar to the corresponding behaviour of a small scale model. This convenient general result of the conventional theories form the base for the model-testing of structures made of concrete or other materials. However, according to the concepts of fracture mechanics one may expect the scale model to behave differently than the full-size structure. This is in agreement with experiences reported in literature and it seems to be a well-known experimental fact that one may not expect the scale-model of a concrete structure to behave in the same manner as the full-size structure. Therefore, model-concretes are used during model-testing. However, the difficulty is to choose suitable properties of model-concrete. No generally accepted rule seems to be available. Often

concretes with a small maximum particles size (mortar) is used and the particle size is then scaled in proportion to the scaling of the structure. The present study and the test results of Taylor (see above) and, more clearly, the test results of Chana (see below) suggest that suitable model-concretes are not achieved in this manner. According to the fictitious crack model, similitude in behaviour can be achieved if the shapes of the σ-ε curves, the σ-w curves and, in the case of multidimensional states of stress, the failure envelopes are equal for the concrete and the model-concrete and if the ratio between the slope of the σ-ε curve and the σ-w curve is made proportional to the size of the structure. The last requirement corresponds to a constant d/ℓ_{ch} and means that brittle materials should be used during model-testing. Of course, practical difficulties are involved in the development of a model material with the required properties. However, while the shapes of the material property characteristic curves should be equal for the concrete and the model-concrete, it is not required that the absolute values of the corresponding material property parameters, i.e. E, G_F and f_t, must be equal. Where the value of ratio d/ℓ_{ch} is concerned, it is possible to choose the size of the model-structure according to the characteristic length of the model-concrete instead of doing the reverse.

Chana (1981) tested beams which were exact geometrical scale models of each other: (total depth: breadth: bar diameter: concrete cover: shear span = 1.0:0.5:0.05:0.1:3.0 and with 1.5 % reinforcement). The prototype beams' size was d=406 mm and the three series of model beams had the sizes d=202 mm, 121 mm and 47 mm. The maximum aggregate sizes of the concretes were scaled almost proportionally: d_a=20 mm, 10 mm, 5 mm and 2.4 mm. The mean cube strength of the concretes were 47 MPa, 37 MPa, 42 MPa and 46 MPa. These strengths of the concretes were determined from 150 mm, 100 mm, 70 mm and 25 mm cubes. This should neutralize or reduce possible size effects of the Weibull type. By the assumption $f_v \sim \sqrt{f_c}$, recorded shear strengths were normalized to the shear strength at f_c=40 MPa. It was found that the normalized shear strengths were 1.09 MPa, 1.41 MPa, 1.59 MPa and 2.17 Mpa corresponding to 30 %, 47 % and 100% greater strength in the model-beams. Thus the influence of size is clear, and greater than found by Taylor. As the characteristic lengths of the actual concretes is unknown, it is difficult to make a comparison to the present theoretical result. However, Modeer (1979) tested a concrete (aggregate size unknown) and a mortar (aggregate size unknown) and found ℓ_{ch}=260 mm and 140 mm, respectively. At the crude assumption that these values are representative

for the prototype concrete (aggregate size 20 mm) and the "smaller" model-concrete (aggregate size 2.4 mm), the theoretical results predict that the smallest model beam should be about 60 % stronger than the prototype beam. Thus, while the results of Taylor indicate a smaller size effect than the theoretical, the results of Chana indicate a greater size effect than the theoretical. According to the size effect law of Bazant, model-beams with scaled aggregate size should have the same strength as the prototype beam. The evident, possible explanation for the experimentally found size effect is that ℓ_{ch} is not proportional to the aggregate size. If the ℓ_{ch}-values of Modeer are representative for the concrete qualities used by Chana, the present method of analysis predicts that the model-beam with aggregate size 2.4 mm should have the size d=220 mm instead of d=47 mm in order to achieve the same strength and behaviour as the prototype beam with aggregate size 20 mm and size d=406 mm.

A matter which sometimes is of great importance in the interpretation of model-testing data and size effect tests is the influence of dead weight. If dead weight is not considered during the evaluation of experimental results, one will obtain an apparent decrease in strength at increased size. Where the shear strength of concrete beams in three point bending is concerned, according to Fig 5.4 (2), it seems reasonable to assume that the equivalent contribution to the external load from the dead weight is approximately equal to an external load that produces the same bending moment in the mid-section of the beam as produced by the dead weight, i.e. as a reasonable approximation, half the dead-weight of the beam may be added to the external load. Although not clearly stated, it seems that Taylor added the total dead weight of the beam while Chana may have disregarded dead weight. This may explain a part of the difference between the results of Taylor and the results of Chana.

With regard to the significance of the characteristic length of the concrete it is also of interest to refer to the properties of high strength concretes. High strength concretes are often reported to performe in a brittle manner, which suggests that the characteristic length of such concretes is small. This has been explained by the tendency of the crack to pass through the aggregate particles instead of around the particles. This gives a smooth fracture surface, and one may expect a low fracture energy of the concrete, and one may also expect that the aggregate size is of smaller importance than in ordinary concrete. Where shear failure is concerned, the actual type of crack growth in high strength concretes has

recently been reported by Elzanaty (1985). Elzanaty also found that the crack surfaces were smoother as the concrete strength increased. As a rather pessimistic assumption with regard to the properties of high strength concretes vs. the properties of normal concretes, one may assume that the modulus of elasticity times the fracture energy, $E_c G_F$, is constant during the increase in the tensile strength, f_t. If adopting this assumption, according to the computational results of Fig 5.3 (16), a 100 % increase in the tensile strength, f_t, gives approximately only a 35 % increase in the shear strength, f_v. For the normal qualities of concrete it is commonly assumed that f_v is proportional to f_t. However, Elzanaty refers to a recent study presented by Mphonde and Frantz in 1984: these researchers tested the shear strength of beams made of both normal and high strength concretes (20 MPa $\leq f_c \leq$ 100 MPa) and proposed that $f_v \sim f_c^{1/3} + 1.34$ (f_c measured in MPa). This proposal suggests that an increase in f_c from 25 MPa to 100 MPa gives only a 40 % increase in the shear strength. At the assumption $f_t \sim \sqrt{f_c}$, the examplified increase in f_c corresponds to a 100 % increase in the tensile strength. Consequently the actual 40 % increase may be compared to the above rather pessimistically estimated theoretical 35 % increase. (According to the researchers referred to, shear failure also becomes more sudden and explosive as the concrete strength increases.)

The present analysis indicates proportionality between f_v and f_t only if ℓ_{ch} is constant. In accordance with the above mentioned, it seems fair to believe that an increase in f_t is in general accompanied with a small or great decrease in ℓ_{ch}. With regard to this matter and the consequential small influence of concrete strength on shear strength it may also be referred to the extensive research on the "so-called shear failure" carried out by G. Kani and summarized by M. Kani, Huggins and Wittkopp (1979). After testing 133 beams (f_c from 17 MPa to 34 MPa, ρ from 0.5 % to 2.8 %, rectangular cross section, no shear reinforcement) Kani concluded that shear strength of concrete beams does not depend on concrete strength. However, this conclusion may have been made somewhat drastic for the purpose of making experimental findings clear and easy to remember: according to a more modulated interpretation of the actual test results, it seems that f_v in general shows a slight increase during increase in f_c. The increase can be roughly estimated to be about 10 % when f_c is increased from 17 MPa to 34 MPa. The corresponding increase suggested by the above relation of Mphonde and Frantz is 17 % and the corresponding increase suggested by the above type of a rather pessimistic theoretical

estimation from the present computational results is 16 %. The conventional assumption $f_v \sim \sqrt{f_c}$ predicts a 41 % increase and the assumption $f_v \sim f_c^{2/3}$ (See below) predicts a 59 % increase. During applications of the theory of plasticity at shear strength analysis it is commonly assumed that $f_t/f_c=0$ and if some effectiveness parameter is not used, i.e. if fitting to test results is not carried out, this theory predicts a 100 % increase in f_v during the actual increase in f_c from 17 MPa to 34 MPa. Consequently, the different proposals cover the region 0-100 % for the increase in shear strength at the doubling of the concrete compressive strength.

While it is commonly assumed that f_v is proportional to f_t, in practice the direct tensile strength of the concrete is usually not tested but it is instead commonly assumed that $f_t \sim \sqrt{f_c}$ and consequently that $f_v \sim \sqrt{f_c}$. An exception from this proportionality may be found in the new Swedish concrete building code and also in the Model Code of Comite Euro-International Du Beton. According to the design tables in these codes f_v is approximately proportional to $f_c^{2/3}$. This means that the increase in f_c from 25 MPa to 100 MPa is predicted to give a 150 % increase in f_v. As compared to the above crude theoretical estimation and as compared to the above expression of Mphonde and Frantz, there is a difference in f_v corresponding to the approximate factor 1.8. This is not a small difference. The reason for the choice $f_v \sim f_c^{2/3}$ in the actual codes is not known. In the explanatory and viewpoint papers on the Model Code of CEB, Regan (1978) briefly states that the actual relation probably over-estimates the influence of concrete strength but the errors involved are relatively insignificant and are almost lost in the general scatter of test results. Here it must be mentioned that the design table of the Model Code only includes concretes with characteristic compressive strengths from 12 MPa to 50 MPa, and that the Swedish code only includes concretes with chracteristic compressive strengths from 12 MPa to 57 MPa (light-weight concretes not being included). On the other hand, the mean compressive strengths are greater than the corresponding characteristic compressive strengths referred to in the codes.

In order to develop a rational shear design expression for the many different qualities of concrete available today, it may prove necessary to consider not only the tensile strength of the concrete but also its brittleness. This may reduce the apparently large scatter in shear strength and may be achieved simply by replacing the measure of absolute

size in shear design expressions, d, with ratio d/ℓ_{ch}. As d/ℓ_{ch} is a dimensionless ratio this would also produce a pedagogical improvement of shear design expressions. The current use of d instead of d/ℓ_{ch} can be looked upon as being equivalent to the tacit assumption of equal brittleness of all qualities of concrete.

Let us now turn to a comparison with respect to the absolute values of shear strength. Two related recent Swedish test series will be utilized for this comparison. The tests were carried out by Liaretidis and Zamani (1980) and by Aronsson and Eskilsson (1981) and have been summarized by Petersson, T (1983). The total of 15 beams were shear strength tested in three point bending. The concretes may be described as low or normal strength concretes (intended concrete quality: K20) with cube compressive strengths of about 30 MPa, with rather high water-cement ratios, with a normal content of aggregate and with 18 mm maximum aggregate size. For much more detailed information about the concrete mixes and the tests, the reader is referred to the above references.

For each beam, the cube compressive strength of the concrete was tested. Other mechanical properties of the concretes are unknown. In the present comparison it is assumed that the mechanical properties of the actual concretes are in accordance with the assumptions adopted during the calculations presented in Section 5.3. Consequently, the tensile strengths of the concretes are simply assumed to be one tenth of the recorded compressive strengths. ℓ_{ch}=400 mm has previously been used as an example of a typical value for the characteristic length of a normal concrete, and this value of ℓ_{ch} is also adopted during the present comparison. Of course, the assumptions with respect to f_t and ℓ_{ch} are decisive for the theoretical calculation of the absolute values of shear strength. This reflects a common difficulty during utilization of test results reported in literature: often the reported experimental data do not include all the particular data required during a theoretical study.

In Fig 5.4 (6) the experimental and theoretical shear strengths are indicated. Ratios d/ℓ_{ch} (with ℓ_{ch} =400 mm), b/d, and ℓ/d and percentage of reinforcement are also indicated. During the evaluation of experimental shear strengths, account is taken to dead weight according to above: the ultimate shear force is taken as the ultimate external load divided by two plus the shear force at support due to dead weight divided by two. According to above f_t is taken as the recorded cube compressive strength

divided by ten and f_v is defined according to eq (5.3:5) where d is the total depth of the beam.

Where the theoretical shear strengths are concerned, since the actual values of d/ℓ_{ch}, ϱ and ℓ/d do not happen to coincide with the particular values studied in the finite element calculations, it has been necessary to carry out interpolations and extrapolations. Naturally, the method of interpolation has some influence on the theoretical results but is estimated to have no importance where the major conclusion of the actual comparison is concerned.

Fig 5.4 (6) indicates that the theoretical results underestimate the shear strength with about 30 %. Underestimation of the absolute values of the shear strength has also been found during comparison to other test results and is consequently not unique for the comparison shown in Fig 5.4 (6). A number of possible reasons for the underestimation may be proposed. Here, only two possible reasons shall be mentioned: the presently used model for the stress transfer in the fracture zone is crude (in particular, the possible beneficial effect of aggregate interlocking across open cracks is disregarded) and, secondly, the effect of dowel action has not been considered during the calculations. Underestimation is of course not satisfactory, but it would had been more remarkable if underestimation was not found. The comparison in Fig 5.4 (6) suggests that theoretical shear strength analysis should be carried out in a more realistic and modulated manner than the present analysis.

Fig 5.4 (6) also indicates a 6 % standard deviation in the deviation between the test results and the theoretical results. This is a small deviation. If all the theoretical strengths are increased with the mean deviation, then the standard deviation between the experimental results and the theoretical results will be 6 %/(1-30 %)=9 %. This is not greater than a reasonable (See below) experimental scatter. Consequently, if taking into account such a reasonable scatter, the shear strength of the different beams is equally underestimated. However, it must be remarked that the actual 9 %-value is sensitive to the metod of interpolation at the evaluation of the theoretical strengths. This means that the actual value is only an approximate estimation.

If making a judgement from a survey of different test results where experimental shear strengths are compared to each other by means of some

simplifying and inappropriate statistical or empirical expression, one may arrive at the conclusion that the scatter in the shear strength of concrete beams must be great. On the other hand, if the present theoretical calculations correctly reproduce the relative influence of the variables in the test series of Fig 5.4 (6), then the experimental shear strength scatter is only about 9 % and accordingly not greater then what may be considered as normal for the strength of concrete and concrete structures. To gain knowledge on this matter the test results of Taylor and Chana, referred to above, are utilized. The tests of these researchers include tests of nominally identical beams made of nominally identical concretes. Chana applied excentric three point bending, which made it possible to test the strength of both the left side of the beam and the right side of the beam. As there appears to be a correlation (although only slight) between the strength of the left side and the right side of the nominally identical beams, the scatter in the strengths of the two sides are calculated individually. In the below presentation of the scatter, the following notation is used: (number of tests, side of beam, depth of beam, maximum aggregate size): coefficient of variation in failure load. The tests of Chana give: (3, left, 406 mm, 20 mm): 7 %, (3, right, 406 mm, 20 mm): 1 %, (3, left, 202 mm, 10 mm): 6 %, (3, right, 202 mm, 10 mm): 5 %, (4, left, 121 mm, 5 mm): 12 %, (4, right, 121 mm, 5 mm): 15 % and (9, -, 47 mm, 2.4 mm): 11 %. Only one side of the smallest beams was tested. The nominally identical beams tested by Taylor in centric three point bending give: (4, -, 250 mm, 9 mm): 9 % and (4, -, 150 mm, 2.4 mm): 6 %. The arithmetic mean of these coefficients of variation in the shear failure load is 8 %. Accordingly, the true experimental scatter in the shear strength of concrete beams does not seem to be very large.

The test results of Chana give also the possibility to test the argument that the scatter in the shear strength produces a considerably smaller shear strength in beams with two shear spans, e.g. beams in centric three point bending, than in beams with one shear span, e.g. cantilever beams. According to the actual test results, the weakest side of the beams is in mean 6 % weaker than the strongest side. This means that the mean shear strength of beams in centric three point bending is about 3 % less than the mean shear strength of cantilever beams. Thus, the effect of scatter in strength does not seem to be very great.

As indicated in Fig 5.4 (6), one of the variables studied in the experimental in ... presented by T. Petersson was the breadth, b,

Beam	1), 5) d/ℓ_{ch}	ℓ/d	4) b/d	$\rho(\%)$	2), 3) $(f_v/f_t)_{exp}$	$(f_v/f_t)_{theor}$	Deviation
A1	0.58	6.09	0.77	0.55	0.31	0.21	-32 %
A2	0.57	6.11	1.56	0.55	0.29	0.21	-28 %
A3	0.58	6.04	2.34	0.55	0.28	0.21	-25 %
B1	0.98	6.56	0.46	0.58	0.27	0.17	-37 %
B2	0.98	6.46	0.92	0.57	0.29	0.17	-41 %
B3	0.98	6.45	1.38	0.57	0.25	0.17	-32 %
B4	0.97	5.77	0.46	0.58	0.26	0.19	-27 %
B5	0.97	5.88	0.46	0.33	0.28	0.16	-44 %
C1	1.86	6.60	0.24	0.60	0.21	0.15	-29 %
C2	1.85	6.71	0.49	0.60	0.21	0.15	-29 %
C3	1.86	6.72	0.72	0.60	0.20	0.15	-24 %
D1	2.77	6.22	0.16	0.60	0.18	0.14	-20 %
D2	2.77	6.24	0.16	0.34	0.18	0.12	-33 %
E1	3.66	6.27	0.12	0.60	0.20	0.14	-30 %
E2	3.65	6.26	0.12	0.35	0.16	0.12	-26 %
					Mean deviation		-30 %
Standard deviation in deviation from mean deviation							6 %

1) ℓ_{ch} assumed to be 400 mm
2) f_t assumed to be one tenth of the cube compressive strength
3) Ultimate shear force is calculated as (ultimate load)/2 + (dead-weight)/4
4) b indicates breadth of beam
5) Depth of beam, d, is throughout defined as the total depth

Fig 5.4 (6) Comparison between experimental results presented by Petersson, T. (1983) and theoretical calculations.

of the beam. Possible influence of the breadth will be discussed below in conjuction to a few remarks on application of the Weibull theory.

Let us now turn to the influence of prestressing: see Fig 5.4 (7). In this figure shear strengths are normalized to the shear strength at zero prestress. The figure shows the present computational results, an empirical relation proposed by Nielsen et al. (1978) and the result of a computational method proposed by Hedman and Losberg (1978).

The present use of the empirical relation proposed by Nielsen at al. must be explained. According to this relation $f_v \sim 1+0.81\, f_p/\sigma_{0.2}$, where $\sigma_{0.2}$ is the 0.2-stress of the prestressing bars. In the present calculations no limitation was introduced with respect to the strength or yielding stress of the prestressing bars. Instead $\sigma_{0.2}$ has been interpreted as the prestress that produces plastic sliding between the steel and the concrete all the way from the end of the beam to the location of the crack. In the present case this limit stress corresponds to $f_p/f_t=192$.

The present interpretation of the computational method of Hedman and Losberg must also be explained. According to this method the increase in load carrying capacity due to prestressing is equal to the load that produces zero strain in the lower edge of the mid-section of the beam in centric three point bending. This gives an absolute value of the increase in shear strength. In Fig 5.4 (7) this increase has been normalized to the strength at $f_p/f_t=0$ as obtained during the present finite element calculations.

The computational results shown in the actual figure are valid for $d/\ell_{ch}=0.6$. For $d\rightarrow\infty$, the computational results suggest a much greater relative influence of prestressing. For $d\rightarrow\infty$, also the computational method of Hedman and Losberg also suggests a much greater relative influence of prestressing.

Fig 5.4 (7) shows that the theoretical results seem to be in agreement with empirical experiences where the influence of prestressing is concerned.

The shear strength of factory-made prestressed beams without stirrups is of special interest since it involves practical difficulties to place stirrups in such beams, at least in the prestressed hollow core slabs. However, one may ask if it is necessary to use stirrups in order to increase shear strength. The shear failure is associated with inclined cracking and the inclination is roughly around 45^o. The most effective inclination of shear reinforcement is probably perpendicular to this diagonal tension crack, but for practical reasons the shear reinforcement in ordinary beams is commonly placed vertically, i.e. at about 45^o inclination to the crack. From a theoretical point of view one may ask whether not a placing of the shear reinforcement at the inclination minus 45^o to the crac[illegible] equally effective. This means that the

shear reinforcement is a longitudinal reinforcement placed at about half the depth of the beam. Such a placing might also be of some interest to study where the ordinary beams without prestress are concerned.

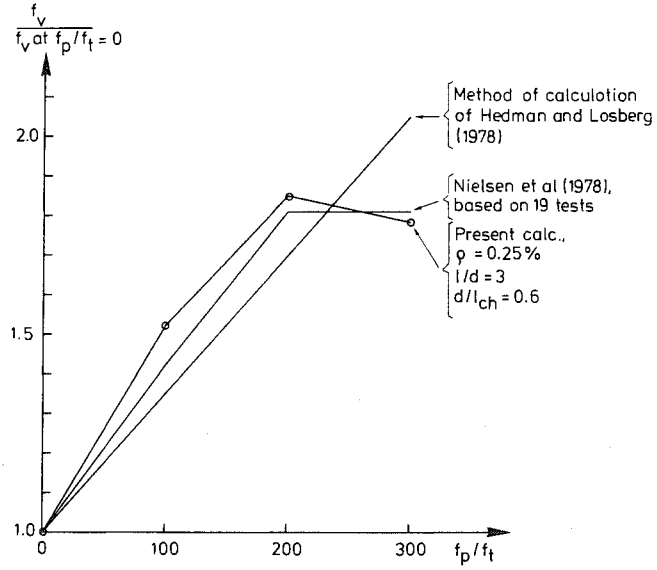

Fig 5.4 (7) Influence of prestress on shear strength.

In this discussion of shear strength, it may be appropriate to include also a few remarks with respect to reasons for size effect in shear strength and with respect to modes of shear failure.

The direct reason for the size effect obtained during the present calculations is, of course, that stiffness relations used as input are given in terms of stress versus absolute deformation. Absolute deformations are used in the description of the fracture softening of concrete and in the description of the bond between concrete and steel. A fundamental theoretical justification to description of bond slip in terms of absolute deformation is not known. In spite of this, there seems to be a long tradition and a general agreement with respect to the use of absolute deformation at the description of the bond. This might have been justified by experimental observations which indicate that the deformations around a reinforcement bar takes place in local layer of zero or constant thic[illegible]s a shear

fracture zone, discussed in Section 5.1. It is not known whether theoretical size effect in shear strength due to description of bond in terms of absolute deformation has been analysed or noticed in studies of shear failure. The description of the fracture softening of the concrete in terms of absolute deformation is justified by the occurance of strain instability and strain localizaion at start of fracture. Strain instability and localization represent concepts of fracture mechanics.

Apart from explanations based on fracture mechanics, a theoretical explanation to the size effect in shear strength is not known by the writer to have been proposed (for proposed phenomenological explanations, see below). In particular, it might be somewhat remarkable that the Weibull theory does not seem to have been applied during analyses of size effect in shear strength. In some ways, the Weibull theory and the linear elastic fracture mechanics are analogous: both theories give simple, general numerical expressions for the relative influence of size. Furthermore, the orders of magnitude of the predicted influence of size are the same as known from test results. If the coefficient of variation in strength is assumed to be 10 %, then the Weibull parameter is 12 (See Fig 3.4 (5)) and accordingly the sensitivity to changes in absolute size at constant geometrical shape is -3/12=-0.25 (the factor 3 is because volume is proportional to length raised to the third power.). This result of the Weibull theory happens to be identical with the empirical expression for size effect proposed by Leonhardt, Fig 5.4 (5). The Weibull theory and the linear elastic fracture mechanics are also analogous in an other respect: both theories are estimated to be unrealistic where shear strength analysis is concerned because fundamental assumptions behind the actual two size effect laws are not fulfilled where the shear strength analysis is concerned.

With respect to the prediction of shear strength produced by the Weibull theory and linear elastic fracture mechanics, a difference on principle concerns the influence of the breadth of the beam. The latter theory, and the present method of analysis as well, predict zero influence of the breadth. The Weibull theory predicts a decrease in strength at increased breadth. According to the experimental results shown in Fig 5.4 (6), increased breadth seems to give a slight decrease in strength. These experimental results are fairly consistent with experimental results presented in (Kani, Huggins and Witthopp, 1979). Three pairs of beams with a four times di[illegible] nominally

indentical, were tested by Kani: the beams were cast with f_c about 28 MPa, ϱ about 2.8 %, d about 0.3 m and ℓ/d about 6, 8 and 12. The ratios (ultimate shear force at b=0.6 m divided by four)/(ultimate shear force at b=0.15 m) became 0.96, 0.93 and 1.07. The mean 1 % decrease in strength at the four times increase in the breadth is quite insignificant. This may be compared to the approximate mean decrease 30 % in shear strength obtained by Kani at a four times increase in the depth from d=0.3 m to d=1.2 m (and at a proportional increase in the length) at constant breadth, 0.15 m. Kani proposed that an increase in breadth might produce an increase in strength due to lateral restraint in the compressive zone. This proposal is the opposite to the prediction produced by the Weibull theory. According to test results, it seems that increase in breadth does not produce a very great increase nor a very great decrease in the shear strength of concrete beams without stirrups.

If defining phenomenological explanations to size effect as being qualitative and not quantitative, the common or traditional phenomenological explanation emanates from consideration of possible influence of aggregate interlocking: in larger beams the crack widths are greater and the grip between the aggregate particles at the sides of the crack becomes consequently less firm. This is an apparently reasonable explantion. However, on the basis of experimental observations, the actual explanation has repreatedly been refuted or questioned (See below). Instead, it has been proposed that the size effect is due to the great strain gradients in small beams, i.e. the size effect is attributed to the same kind of phenomenon as often referred to during discussions of the size effect in the flexural strength of concrete beams. During the present calculations, the shear stress transfer across cracks of great widths (associated with aggregate interlocking) has not been considered. Accordingly, to the extent the present calculations and the corresponding computational results can be considered as being realistic, the present theoretical results suggest that aggregate interlocking is not decisive for the size effect. Instead, the present calculations give some support to the strain gradient explanation: the strain gradient concept may be looked upon as a kind of pheomenological correspondence to the effect of fracture softening in localised tensile fracture zones. The beneficial effect of the non-brittle fracture softening is greater in structures where the formal linear elastic strain gradients are great. The definitions of the strain gradient effect and the aggregate interlock effect available are not very strict, but to some extent these two

phenomena might be distinguished from each other and related to the present study by means of Fig 5.3 (7) b): while the strain gradient effect is of significance for the load at start of unstable crack growth (curve indicated by circles), the aggregate interlock effect may be of significance for the load at final collapse of the ligament and the entire beam (curve indicated by crosses). However, as in the present calculations, even though the aggregate interlock in its common sense is disregarded, the load at the final collapse of the ligament and the entire beam (at each certain assumpmtion with respect to crack path) is found to be significantly affected by the size of the beam: see Fig 5.3 (14) a)-f).

The prime experimental justification for refuting the aggregate interlock explanation is that a size effect is also found if the aggregate size is scaled in proportion to the size of the beam. Swamy and Qureshi (1971), Taylor (1972) and Chana (1981) report such experimental results and mention the strain gradient effect as a possible reason for the size effect in shear strength. Chana argues against the aggregate interlock explanation also on the basis of comparisons between the shear stress at first cracking and ultimate load, and he discusses the size effect in shear strength by means of direct reference to the strain gradient effect in unreinforced concrete beams in bending. Walrawen (1978) tested beams made of gravel concrete and lightweight concrete. From his test results, Walrawen inferred that it was highly unlikely for the enhanced shear strenghts of shallow beams to be due to high interlock strengths and he concluded that an explanation to the size effect can be found in the different tensile strain gradients in beams of different size. (The size effect for beams made of lightweight concrete appears to be equally great as for beams made of gravel concrete). Although aggregate interlocking may not be the (only) reason for the size effect in shear strength, it is possible that aggregate interlock may carry a significant part of the shear force. As previously mentioned, this may be a reason to why the present theoretical results underestimate the absolute values of shear strength.

The absolute shear deformations during slide between the reinforcement and the concrete does not seem to have attracted attention during studies and discussions of possible phenomenological explanations to the size effect. A possibility to study the significance of this slide for the size effect would be to compare the size effect for beams with only end anchorage of the reinforceme[illegible] effect for beams with the normal direct

anchorage of the reinforcement all along the reinforcement bars. In the case of end anchorage, possible size effect cannot be attributed to bond stress slip. Relevent experimental results are not known. However, during a theoretical fracture mechanics calculation, carried out in a manner rather similar to the present calculations, Modeer (1979) assumed end anchorage of the reinforcement. The sensitivity to changes in absolute size suggested by the calculation of Modeer is approximately the same as the sensitivity obtained during the present analysis of a comparable beam. Accordingly, by judging from this comparison, the bond stress slip is not of great significance for the size effect in shear strength. However, due to differences between the calculation of Modeer and the present calculations, the actual comparison might not be relevant and accordingly the above conclusion is uncertain. In addition, application of other bond stress-slip relations than those presently adopted may give other results. The loads at instability indicated by Modeer give the sensitivity m=-0.26 (Compare Fig 5.3 (17)) in the region $0.48 \leq d/\ell_{ch} \leq 2.4$ for a cantilever beam with 0.5 % reinforcement and with a length to depth ratio corresponding to $\ell/d=3.5$ for a beam in three point bending.

Shear failure is often discussed in terms of different modes and it may be appropriate to relate the commonly discussed modes to the present study of shear strength. Firstly, the actual modes are divided into modes of cracking and modes of ultimate failure. The two modes of cracking are the flexural shear cracking (start of cracking in the lower edge of the beam) and the web shear cracking (start of cracking in the web). Since cracks in concrete close smoothly and may be narrow without limit during their first development, no generally accepted definition of cracks and cracking is available and thus the definitions of cracking modes are not quite clear. If "cracking" is defined by the development of a fracture zone (not visible by the naked eye) then the present analysis indicates flexural shear cracking in the cases of non-prestressed beams and web shear cracking in the case of prestressed beams. If "cracking" is defined by the extension of the open crack, i.e. a non stress transferring crack, after arrest of its unstable growth (visible by the naked eye) then the analysis indicates flexural shear cracking in the cases of non-prestressed beams, while information is not available for the prestressed beams. If "cracking" is defined by the location of the first open crack (hardly visible because the crack is narrow and because its development and subsequent growth is unstable and accordingly very rapid) then the analysis indicat d web shear

cracking in some cases: in general the analysis indicates the development of an open crack in the lower parts of the beams at almost the same "time". The modes of ultimate failure are often separated into the diagonal tension failure (extension of a discrete crack all the way through the depth of the beam), bond failure, shear compression failure (compressive failure and crushing of the concrete in the upper edge of the beam) and web compression failure (compressive failure in an inclined concrete truss in the web of the beam). For the sake of simplicity, the type of failure presently analysed has been called diagonal tension failure, but it might be more appropriate to refer to it as a combination of the three first mentioned modes of ultimate failure: according to the present method of analysis both the development of a diagonal crack, failure in the upper edge of the beam and the bond strength influence the shear strength of the beam, and it is not possible to separate the three modes of ultimate failure as they are linked to each other. The web crushing failure has not been considered in the present analysis. This mode of failure may be decisive for the strength of beams reinforced with stirrups and may also be decisive for the strength of longitudinally reinforced beams with T or I shaped cross sections.

The shear strength of longitudinally reinforced concrete beams is estimated to represent the most purely empirical part of current concrete building codes. The present study, and also other studies, suggest that fracture mechanics and finite elements may be helpful at establishment of rational theoretical bases for shear strength design and at interpretation of shear strength test data. The most essential conclusions of the present study may be that the previously experimentally found size effect in shear strength can be explained by development of localized deformations in concrete during fracture softening and that the characteristic length, ℓ_{ch}, of concrete is theoretically identified as a material property parameter which may be of great significance for the shear strength of concrete beams. A pedagogical improvement of shear strength expressions would be achieved if the measure of absolute size, d, is replaced by the dimensionless ratio d/ℓ_{ch}.

6. REFERENCES

ACI (1974). Shear in reinforced concrete. Publication SP-42, ACI.

AITC (American Inst of Timber Construction) (1966). Timber construction manual. John Wiley and Sons, Inc, N.Y., London, Sidney.

Akin, J. E. (1980). Computational methods for local singularities. Computational methods in nonlinear mechanics. Ed Oden, J. T., North Holland Publishing Company, pp 1-12.

ASCE-ACI (1973). The shear strength of reinforced concrete members. J of the Structural Div, ASCE, Vol 99, pp 1091-1187.

Alford, N. M., Groves, G. W. and Double, D. D. (1982). Physical properties of high strength cement pastes. Cem and Concr Res, Vol 12, pp 349-358.

Andersson, H. and Bergkvist, M. (1970). Analysis of a non-linear crack model. J Mech Phys Solids, Vol 18, pp 1-28.

Argyris, J. H., Faust, G., and Willam, K. I. (1979). Finite element analysis of concrete cracking. ISD-Report No 254, Univ of Stuttgart, BRD.

Aronsson, C.-G. (1984), Tensile fracture of laminates with cracks. Report (in preparation). Dept of Aeronautical Struct and Materials, The Royal Inst of Techn, Stockholm, Sweden.

Aronsson, R. and Eskilsson, J. (1981). Brottskjuvspänningens dimensionsberoende vid armerade betongbalkar utan byglar. (The size effect in the shear strength of reinforced concrete beams without stirrups.) Examensarbete 194, Inst f Brobyggnad, Royal Inst of Techn, Stockholm.

ASCE (1975) Wood structures. Compiled by Task Committee on Status-of-the-Art: Wood. Committee on Wood, ASCE, Struct Division. ASCE, New York.

Barenblatt, G. I. (1962). The mathematical theory of equilibrium cracks in brittle fracture. Advances in applied mechanics, Vol 7, pp 55-129.

Barr, D. I. H. (1984). Consolidation of Basics of Dimensional Analysis. J of Eng Mech, Vol. 110, ASCE, pp 1357-1376.

Bäcklund, J. (1977). Brottmekanik (Fracture mechanics), IKP-S-073, Tekniska Högskolan i Linköping, Sweden.

Bazant, Z. P. and Oh, B. H. (1981). Concrete fracture via stress-strain relations Report No 81-10/665 c, Techn Inst, Northwestern Univ, Evanstone, Illinois.

Bazant, Z. P. and Oh, B. H. (1983). Crack band theory for fracture of concrete. RILEM, Materiaux et Constructions, Vol 16, No 93, pp 155-177.

Bazant, Z. P. (1984). Size effect in blunt fracture: Concrete, rock, metal. J of Struct Eng, ASCE, Vol 110, pp 518-535.

Bazant, Z. P. and Kim J.-K. (1984). Size effect in Shear failure of longitudinally reinforced beams. ACI Journal, Sept-Oct 1984, pp 456-468.

Bazant, Z. P. and Cao, Z. (1985). Size effect in brittle failure of unreinforced pipes. Report No. 85-2/679s, Center for Concrete and Geomaterials, Nor

Bazant, Z. P. (1985). Fracture mechanics and strain softening of concrete. Seminar on Finite Element Analysis of Reinforced Concrete Structures, Tokyo, May 21-24, 1985, Vol. 1, pp 47-67, Japan Soc. for the Promotion of Science.

Bellander, U., Petersons, N. and Samuelsson, P. (1980). Hållfasthet (Strength). Chapter in Betonghandbok. Material. Svensk Byggtjänst, Stockholm.

Bergan, P. G. and Holand, I. (1979). Nonlinear finite element analysis of concrete structures. Computer Methods in Applied Mechanics and Engineering, Vol 17/18, pp 443-467.

Bergström, S. G., Nielsen, A., Ahlgren, L. and Fagerlund, G. (1970). Byggnadsmateriallära, del III (Science of build mat, part III), Div of Build Mat, Univ of Lund, Sweden.

Blom, G. (1970). Sannolikhetsteori med tillämpningar. (A och B). (Theory of probability with applications (A and B)). Studentlitteratur, Lund, Sweden.

Bodig, J. and Jayne, B. A. (1982) Mechanics of wood and wood composites. Evan Nostrand Reinhold Comp Inc.

Bonzel, J. (1965). Biegezug- und Spaltzugfestigkeit des Betons. Beton-Verlag GmbH, Dusseldorf, BRD.

Booth, L. G. and Reece, P. O. (1967). The structural use of timber. A commentary on the Brittish Standard Code of Practice CP 112. E. & F. N. Spon Ltd, London.

Brennan, G. (1978). A test to determine the bending moment resistance of rigid pipes. Supplementary report 348, Earthworks and Underground Pipes Division, Transport and Road Research Laboratory Crowthorne, Berkshire, UK.

Broberg, K. B. (1982). The Foundations of Fracture Mechanics. Engineering Fracture Mechanics, Vol 16, No 4, pp 497-515.

Burt, N. J. and Dougill, J. W. (1977). Progressive Failure in a Model Heterogeneous Medium. J of the Eng Mech Div, EM3, pp 365-376.

Carino, N. J., Nilson, A. H., Slate, F. O. (1974). The Behaviour of a Model of Plain Concrete Subjected to Compression-Tension and Tension-Tension Biaxial Stresses. Report 357, Dep of Struct Eng, Cornell Univ, Ithaca, N.Y.

Carlson, T. Shahabi, A. and Sunding, L. (1983). Träs brottbeteende. (Fracture behaviour of wood) Seminar essay, Div of Build Mat, Univ of Lund, Sweden.

Carpenter, W. C. (1984). A collocation procedure for determining fracture mechanics parameters at a corner. Int J of Fracture, Vol 24, pp 255-266.

Catalano, D. and Ingraffea, E. R. (1982). Conrete fracture: A linear elastic fracture mechanics approach. Report 82-1, Dept of Struct Eng, Cornell Univ, Ithaca.

Chana, P. S. (1981). Some aspects of modelling the behaviour of reinforced concrete under shear loading. Technical Report 543, Cement and Concrete Association, Wexham Springs, UK.

Chen, W. F. and Saleeb, A. F. (1982). Constitutive Equations for Engineering Materials. John Wiley & Sons, N.Y.

Chiu, K.D. (1985). Discussion of "Size effect in shear failure of longitudinally reinforced beams." ACI Journal, July-Aug 1985, pp 579-583.

Cook, R. D. (1973). Concepts and applications of finite element analysis. John Wiley & Sons, Inc.

Dahlblom, O. and Peterson A. (1982). CAMFEM-Computer Aided Modelling based on the Finite Element Method. Report TVSM-3001, Div of Struct Mech, Lund Inst of Techn, Sweden.

Distefano, N. (1970). On the indentification problem in linear viscoelasticity. ZAMM 50, pp 683-690.

Dyrbye, C., Gravesen, S., Krenk, S., Lund, N. C. and Madsen, H. O. (1979). Konstruktioners sikkerhed. (Safety of constructions). Den private Ingeniörsfond ved Danmarks Tekniske Höjskole, Copenhagen.

Elzanaty, A. H. (1985). Shear-critical high strength concrete beams. Report 85-1, Dep of Struct Eng, Cornell University, Ithaca, New York.

Evans, R. H. and Marathe, M. S. (1968). Microcracking and stress-strain curves for concrete in tension. RILEM, Materiaux et Constructions, No 1.

Fuchs, W. P. (1982). Zuverlässigkeitsanalyse von Rohrleitungen aus unbewahrtem Beton. Thesis, Institut fur Bauingenieurwesen III, Lehrstuhl fur Massivbau, Technische Universität Munchen, BRD.

Glemberg, R. (1984). Dynamic analysis of concrete structures. Publication 84:1, Dep of Struct Mech, Chalmers Univ of Techn, Sweden.

Gopalaratnam, V. S. and Shah, S. P. (1984). Softening responce of plain concrete in direct tension. Report, The Tech Inst, Northwestern Univ, Evanstone, Illinois. (Accepted for publicatiom, ACI Journal (MS 5256)).

Grasser, E. (Editor) (1982). Bulletin d´information No 146, Shear, Torsion and Punching, Progress report, CEB, Paris.

Grootenboer, H. J. (1979). Finite element analysis of two-dimensional reinforced concrete structues, taking account of non-linear physical behaviour and the development of discrete cracks. Thesis, Univ of Delft, Holland.

Gustafsson, P. J. (1977). Brottmekaniska studier; lättbetong och fiberarmerad betong (Fracture mechanics studies; lightweight concrete and fibre-reinforced concrete). Report TVBM-5001, Div of Build Mat, Univ of Lund, Sweden.

Gustafsson, P. J. (1983). Oarmerade betongrörs böjbrottlast och ringbrottlast. Teoretiska beräkningsmetoder. (Bending strength and crushing strength of unreinforced concrete pipes. Theoretical methods of calculation.) Report TVBM-3012, Div of Build Mat, Univ of Lund, Sweden.

Gutkowski, R. M. (1982). Shear strength of tapered wood beams. J of the Structural Div, ASCE, Vol 108, pp 698-700.

Gylltoft, K. (1983). Fracture mechanics models for fatigue in concrete structures. Report 1983:25D, thesis, Div of Struct Eng, Luleå Univ of Techn, Sweden.

Hawkins, N. M., Wyss, A. N. and Mattock, A. H. (1977). Fracture analysis of cracking in concrete beams. J of the Structural Div, Vol 103, pp 1015-1030.

Hayes, D. J. (1975). Origins of the stress intensity factor approach to fracture. The Journal of Strain Analysis, Vol 10, no 4, pp 198-100.

Hedman, O. and Losberg, A. (1978). Design of concrete structures with regard to shear forces. Bulletin d´information No 126, Shear and Torsion, CEB, Paris, pp 184-209d.

Hedner, G. et al (1976). Formelsamling i hållfasthetslära. (Handbook in mechanics of materials). Publ nr 106, Inst f Hållfasthetslära, KTH, Stockholm.

Hellan, K. (1979). Bruddmekanik (Fracture mechanics). A-L Tapir, Trondheiim, Norway.

Hernelind, J. and Pärletun, L. G. (1976). EUFEMI - a finite element computer program for solid mechanics and heat conduction. Report TMHL-3006, Div of Solid Mech, Univ of Lund, Sweden.

Hult, J. (1966). Hållfasthetslära (Mechanics of materials). Almqvist & Wiksell/Gebers Förlag AB, Stockholm.

Heilmann, H. G., Hilsdorf H. H. and Finsterwalder, K. (1969). Festigkeit und Verformung von Beton unter Zugspannungen. Deutscher Ausshuss fur Stahlbeton, Helft 203, W Ernst & Sohn, Berlin.

Helmersson, H. (1978). Materialbrott för olika byggnadsmaterial (Fracture of different building materials). Examination work, Div of Build Mat, Univ of Lund, Sweden.

Hillerborg, A. (1973). Brottförlopp (Fracture). Chapter in Byggnadsmateriallära FK 1. (A students compendium in build mat), Div of Build Mat, Lund Inst of Techn, Sweden, 1974.

Hillerborg, A., Modeer, M. and Petersson P. E. (1976). Analysis of crack formation and crack growth in concrete by means of fracture mechanics and finite elements. Cement and Concrete Research. Vol 6, pp 773-782.

Hillerborg, A. (1978). A model for fracture analysis. Report TVBM-3005. Div of Build Mat, Lund Inst of Techn, Sweden.

Hillerborg, A. (1980). Materialbrott (Fracture of materials). Chapter in Byggnadsmateriallära FK 1, 1981. Div. of Building Materials, Univ of Lund, Sweden.

Hillerborg, A. (1980). Brott (Fracture). Chapter in Byggnadsmateriallära FK 1, 1984. Div of Build Mat, Lund Inst of Techn, Sweden.

Hillerborg, A. (1982). Numerical methods to simulate softening and fracture of concrete. To appear in "Application of fracture mechanics to concrete structures", Vol 2, Eds: Carpinteri, DiTommaso, Ingraffea and Sih. Martin Nijhoff Publishers, 1984-1985.

Hillerborg, A. (1983). Analysis of one single crack. Fracture mechanics of concrete. Ed F. H. Wittmann, Elsevier Science Publishers, Amsterdam, pp 223-249.

Hillerborg, A. (1983). Theoretical analysis of the double torsion test. Cement and Concrete Research, Vol 13, pp 69-80.

Hillerborg, A. (1983). Concrete fracture energy tests performed by 9 laboratories according to a draft RILEM recommendation. Report TVBM-3015, Div of Build Mat, Lund Inst of Techn, Sweden.

Hognestad, E. et al (1962). Shear, diagonal tension and torsion in structural concrete. ACI Bibliography No 4, ACI.

Hughes, B. P. and Chapman, G. P. (1966). The complete stress-strain for concrete in direct tension. Bulletin RILEM, No 30, pp 95-97.

Ingraffea, A. R., Gerstle, W. H., Gergely, P. and Saoma, V. (1983). Fracture Mechanics of bond in Reinforced Concrete. Cornell Univ, 1983. Report submitted to ASCE for publication in a Journal.

Ingraffea, A. R. and Gerstle, W. H. (1984). Non-linear fracture models for discrete crack propagation. Application of Fracture Mechanics to Cementitious Composites, Preprints of the proceedings, NATO-ARW, Sept-1984, Editor S. P. Shah, Northwestern Univ, USA.

Ingraffea, A. R. Gerstle, W., Gergely. P., and Saouma, V. (1984). Fracture Mechanics of Bond in Reinforced Concrete. J of the Structural Div, ASCE, Vol 110, pp 871-890.

Ingwersen, J. B. (1982). Statitische Berechnung von unbewahrsten Betonrohren mit Fuss auf Grund einer neuen Bruchtheorie. Betonwerk + Fertigteil-technik, Heft 4/82.

Ingwersen, J. B. (1983). Private communication.

Ingwersen, J.B. (1984). Beregning af betonrør efter brudmekanisk model. (Analysis of concrete pipes according to a fracture mecanics model.) Dansk Beton, Nr 1, pp 45-49.

Isgren, C. and Palmgren, H. (1982). Private communication.

Ivanyi, G. (1976). Zugfestigkeit von Beton in örtlich veränderlichen Beanspruchungszuständen - Gradientenwirkung. Institut fur Baustoffkunde und Stahlbetonbau, Der Technischen Universität Braunschweig, BRD.

Jiang, J.J. (1983). Finite element techniques for statical analysis of structures in reinforced concrete. Publication 83:2, thesis, Dep of Struct Mech, Chalmers Univ of Techn, Sweden.

Kani, M. W., Huggins, M. W. and Wittkopp, R. R. (1979). Kani on shear in reinforced concrete. Dep of Civ Eng, Univ of Toronto.

Kaplan, M. F. (1961). Crack propagation and the fracture of concrete. J of the American Concr Inst, Vol 58, 591-610.

Kesler. C. E. Naus, D. J. and Lott, J. L. (1971). Fracture mechanics - its application to concrete. Proceedings of the 1971 Int Conf on Mech Behaviour of Materials, Vol IV, Japan 1972, pp 113-124.

Knott, I. F. (1973). Fundamentals of fracture mechanics. Buttorworths, London.

Kollmann, F. (1951). Technologie des Holzes und der Holzwerkstoffe. (Erster band), Springer-Verlag, BRD.

Krech, W. W. and Chamberlain, P. G. (1974). New techniques for measuring rock fracture energy. Society of Petroleum Engineering Journal, June, pp 237-242.

König, G. and Jahn, M. (1983). Uber die verschiedenen Erscheinungsformen der Betonfestigkeit und ihre Bedeutung fur das Tragverhalten von Massivbauten. Beton- und Stahlbetonbau, Heft 9, pp 243-247, and Heft 10, pp 281-286.

Larsen, H. J. (1967). Beregning af traekonstruktioner. (Analysis of wood structures.) Teknisk Forlag, Köpenhavn, Denmark

Lehman, R. S. (1959). Development at an analytic corner of solutions of elliptic partial differential equation, J Math Mech 8, pp 727-760.

Leonhardt, F. (1978). Shear in concrete structures. Bulletin d'information No 126, Shear and Torsion, CEB, Paris, pp 67-124.

Liaretidis, J. and Zamani, M.-E. (1980). Brottskjuvspänningens dimensionsberoende vid armerade betongbalkar utan byglar. (The size effet in the shear strength of reinforced concrete beams without stirrups.) Examensarbete 190, Inst f Brobyggnad, Royal Inst of Techn, Stockholm.

Lin, E. I-Ho and Sackman, J. L. (1975). Indentification of the dynamic properties of nonlinear viscoelastic materials and the associated wave propagation problem. Int J Solids and Struct, Vol 11, pp 1145-1159.

Liu, I. Y. (1981). Shear strength of tapered wood beams. J of the Struct Div, ASCE, Vol 107, pp 719-731.

Loov, R. E. (1972). Finite element analysis of concrete members considering the effects of cracking and the inclusion of reinforcement. Thesis, Univ of Cambridge.

Lusche, M. (1972). Beitrag zum Bruchmechanismus von auf Druch beanspruchten Normal- und Leichbetong mit geschlossenem Gefuge. Schriftenreihe der Zementindustrie, Heft 39/1972, Beton-Verlag GmbH, Dusseldorf, BRD.

Martin, H. C. (1966). Introduction to matrix methods of structural analysis. Mc Graw-Hill Inc, N.Y.

Mendelson, A. (1968). Plasticity: theory and application. The MacMillan Company, New York.

Mindess, S. (1983). The application of fracture mechanics to cement and conrete: a historical review. (pp 539-561), chapters in Fracture mechanics of concrete, Ed H. Wittmann, Elsivier Science Publichers, Amsterdam.

Modéer, M. (1979). A fracture mechanics approach to failure analyses of concrete materials. Report TVBM-1001, thesis, Div of Build Mat, Univ of Lund, Sweden.

Naus, D. J. (1971). Applicability of linear-elastic fracture mechanics to portland cement concretes. Thesis, Theoretical and Applied Mechanics, Univ of Illinois at Urbana-Champaign, Urbana, USA.

Nemat-Nasser, S. (1980). On stability of the growth of interacting cracks, and crack kinking and curving in brittle solids. Numerical methods in fracture mechanics, Eds Owen, D. R. J. and Luxmoore, A. R., Pineridge Press, Swansea, U.K.

Neville, A. M. (1981).Properties of Concrete. Third Edition, The Pitman Press. Bath, Great Britain.

Ngo, D. and Scordelis, A. C. (1967). Finite element analysis of reinforced concrete beams. American Concrete Institute Journal, Vol 64, No 3, pp 152-163.

Nielsen, M. P., Braestrup, M. W., Jensen, B. C. and Bach, F. (1978). Concrete plasticity, beam shear - shear in joints - punching shear. Specialpublikation, Danish Society for Structural Science and Engineering.

Nilson, A. H. (1971). Bond stress-slip relations in reinforced concrete. Report No 345, Dep of Struct Eng, Cornell Univ, Ithaca, New York.

Nilson, L. (1979). Impact Loading on Concrete Structures. Thesis, Publication 79:1, Dep of Struct Mech, Chalmers Univ of Technolgy, Sweden.

Nilson, A. H. et al (1982). Finite Element Analyses of Reinforced Concrete. State-of-the-Art Report, ASCE, N.Y.

Nilsson, L. and Oldenburg, M. (1982). Nonlinear wave propagation in plastic fracturing materials - A constitutive modelling and finite element analysis. Paper presented at the IUTAM Symposium "Nonlinear Deformation Waves", Tallin, Aug 22-28.

Nygårds, J. and Lärkfeldt, O. (1954). Redogörelse för undersökning av betongrör. (Report on investigation of concrete pipes), Skanska, Stockholm.

Ouchterlony, F. (1981). Extension of the compliance and stress intensity formulas for the single edge crack round bar in bending. Fracture Mechanics Methods for Ceramics, Rocks and Concrete, ASTM STP 745, Freiman and Fuller, Eds, American Society for Testing and Materials, pp 237-256.

Owen, D. R. I. and Fawkes, A. I. (1982). Engineering fracture mechanics: numerical methods and applications. Pineridge Press Ltd, Swansea, U.K.

Peterson, A. and Petersson, H. (1981). CALFEM (Computer Aided Learning of the Finite Element Method), Avd f Byggnadsmekanik, Tekniska Högskolan i Lund, Sweden.

Petersson, H. (1974). Analysis of loadbearing walls in multistorey buildings. Stresses and displacements calculated by a continuum method. Thesis, Chalmers Univ of Techn, Sweden.

Petersson, H. and Bäcklund, J. (1979). SERFEM. Report 1973:8, Byggnadskonstruktion, Chalmers Tekniska Högskola, Sweden.

Petersson, H. and Thelandersson, S. (1982). Byggnadsmekaniska grunder. (Bases of structural mechanics.) Report TVBM-7003, Div of Struct Mech, Lund Inst of Techn, Sweden

Petersson, H. (1982). Private communication. Prof Div of Struct Mech, Lund Inst of Techn, Sweden.

Petersson, P.-E. and Gustafsson, P. J. (1980). A model for calculation of crack growth in concrete-like materials. Numerical Methods in Fracture Mechanics, Proc of the Sec Int. Conference, pp 707-719. Ed:s Owen and Luxmoore. Pineridge Press, Swansea, UK.

Petersson, P.-E. (1981). Crack growth and development of fracture zones in plain concrete and similar materials. Report TVBM-1006, thesis, Div of Build Mat, Univ of Lund, Sweden.

Petersson, P.-E. (1982). Brottmekaniska egenskaper hos en kvalitet av MDF-pasta. (Fracture mechanics properties of a quality of macro-defect-free cement paste.) Internal Report. Cementa AB and Div of Build Mat, Lund Inst of Tech, Sweden.

Petersson, P.-E. (1982). Comments on the method of determining the fracture energy of concrete by means of three-point bend tests on notched beams. Report TVBM-3011, Div of Build Mat, Univ of Lund, Sweden.

Petersson, T. (1983). Balkhöjdens inverkan på betongbalkars skjuvhållfasthet. (The influence of the beam depth on the shear strength of concrete beams). Meddelande 2/83, Inst f Brobyggnad, Royal Inst. of Techn, Stockholm.

Petterson, O. and Plem, E. (1975). Byggnadsmekanik, FK 1 - del 1 (Compendium in Struct Mech, FK 1 - part 1) Inst f Byggnadsstatik, Univ of Lund, Sweden.

Pietruszczak, S. and Mroz, Z. (1981). Finite Element Analysis of Deformation of Strain-Softening Materials. Int J for Num Meth in Eng. Vol 17, pp 327-334.

Rafla, K. (1971). Empirische Formeln zur berechnung der Schubträgfähigkeit von Stahlbetonbalken. Strasse, Brucke, Tunnel, Vol 23, No 12, pp 311-320.

Reinhardt, H. W. (1981,a). Masstabseinfluss bei Schubversuchen im Licht der Bruchmechanik. Beton & Stahlbetonbau, Vol 76, No 1, pp 19-21.

Reinhardt, H. W. (1981,b). Similitude of brittle fracture of structural concrete. Advanced mechanics of reinforced concete, Final Report, IABSE Colloquium Delft 1981, pp 175-184.

Reinhardt, H. W. (1984). Fracture mechanics of an elastic softening material like concrete HERON, Vol 29, No 2, pp 3-42.

Rots, J. G., Nauta, P., Kusters, G. M. A., and Blaauwendraad, J. (1985). Smeared crack approach and fracture localization in concrete. HERON, Vol 30, No 1, Delft Univ of Techn and Inst. TNO for Build Mat and Build Struct, The Netherlands.

Sabnis, G. M. and Mirza, S. M. (1979) Size effects in model Concretes? J of the Struct Div, ASCE, Vol 105, pp 1007-1020.

Saouma, V. E., Ingraffea, A. R. and Catalano, D. M. (1980). Fracture tougness of concrete - K_{1c} revisited. Report 80-9, Cornell Univ, Ithaca, N. Y.

Saouma, V. E. and Ingraffea, A. R. (1981). Fracture mechanics analysis if discrete cracking. Advanced mechanics of reinforced concrete, Final Report, IABSE Colloquium. Delft 1981, pp 413-436.

Saouma, V. E., Ingraffea, A. R. and Catalano, D. M. (1982). Fracture tougness of concrete: K_{1c} revisited. J of the Eng Mech Div, vol 108, No EM6, pp 1152-1166.

SBN-80 (1980). Svensk Byggnorm (Swedish Building Code). Statens planverks författningssamling 1980:1, Liber förlag, Stockholm.

Sok, C., (1978). Etude de la propagation d´une fissure dans un beton non arme. Bull Liason Labo. P et Ch., Vol 98, pp 73-84.

Scordelius, A. C., Nilson, A. H. and Gerstle, K. (1982). Introduction. Chapter in inite element analysis of reinforced concrete, ASCE, pp 1-33

Shareef, S. D. and Buyukozturk, O. (1983). Constitutive Modelling of Concrete in Finite Element Analysis. Research Report R83-16. Dept of Civ Eng, Mass Inst of Techn, Cambridge, Massachusetts.

Sok, C., Baron, J. and Francois, D. (1979). Cement and Concrete Research, Vol 9, pp 641-648.

Sok, C., Benkirane, M. E., Baron, J. and Francois, D. (1981). Crack propagation in prestressed concrete. Interaction with reinforcement. Advances in Fracture Research: Preprints of the 5th Int Conf on Fracture, Cannes, France. Ed D Francois, Vol 4, pp 1507-1514.

Ståhle, P. (1983). On the small crack fracture mechanics. Int J of Fracture, Vol 22, pp 203-216.

Swamy, R. N. and Qureshi, S. A. (1971). Strength, cracking and deformation similitude in reinforced T-beams under bending and shear. J of the ACI, March 1971, pp 187-195.

Taylor, H. P. J. (1972). Shear strength of large beams. J of the Struct Div, ASCE, Vol 98, pp 2473-2490.

Test to determine the critical stress intensity factor K_{1c} of concrete. (1982). Proposed RILEM recommendation.

Timoshenko, S. and Goodier, J. N. (1951). Theory of elasticity. McGraw-Hill Book company Inc, New York.

Thurlimann, B. (Editor) (1979). Plasticity in Reinforced Concrete. Final Report, IABSE Colloquium Copenhagen 1979.

Thurlimann, B. (Editor) (1981). Advanced Mechanics of Reinforced Concrete. Final Report, IABSE Colloquium, Delft 1981.

Valentin, G. and Morlier, P. (1982). A criterion of crack propagation in timber. Bulletin RILEM, No 88, pp 291-298.

Visalvanich, K. and Naaman, A. E. (1980). Evaluation of Fracture Techniques in Cementious Composites. Fracture in Concrete: Proceedings of the ASCE National Convention in Hollywood, Florida, pp 65-81. Ed:s Chen and Ting.

Visalvanich, K. and Naaman A. E. (1981). Fracture methods in cement composites. J of the Eng Mech Div, ASCE, Vol 107, pp 1155-1171.

Walraven, J. C. (1978). The influence of depth on the shear strength of lightweight concrete beams without shear reinforcement. Report 5-78-4, Stevin Laboratory, Univ of Delft, The Netherlands.

Walraven, J. C. (1985). Discussion of "Size effect in shear failure of longitudinally reinforced beams." ACI Journal, July-Aug 1985, pp 579-583.

Wästlund, G. and Eggwertz, S. (1949). Dimensionering av betongrör. (Design of concrete pipes), Svenska Kommunal-Tekniska Föreningens Handlingar N:r 6. Nytryck: Svenska Vatten- och avloppsverksföreningen, VAV, Stockholm 1973.

Wecharatana, M. and Shah, S. (1980). Resistance to crack growth cement composites. Fracture in Concrete: Proceedings of the ASCE National Convention in Hollywood, Florida, pp 82-105. Ed:s Chen and Ting.

Wecharatana, M. and Shah, P. (1982). Slow crack growth in cement composites. J. of the Struct Div, ASCE, Vol 108, pp 1400-1413.

Wecharatana, M. and Shah, S. (1983). Predictions of nonlinear fracture process zone in concrete. J of Eng Mech, ASCE, Vol 109, pp 1231-1246.

Weibull, W. (1939). A statistical theory of the strength of materials. Proceedings no 151, Ingeniörsvetenskapsakademien, Sweden.

Weibull, W. (1939). The phenomenon of rupture in solids. Proceedings no 153, Ingeniörsvetenskapsakademien, Sweden.

Wennerström, H. Glemberg, R. and Petersson, H. (1979). GENFEM-3, a computer program for general finite element analysis. User´s manual. Publication 79:4, Dep of Struct Mech, Chalmers Univ of Techn, Sweden.

Wickström, U. (1979). TASEF - 2, a computer program for temperature analysis of structures exposed to fire. Report 79-2, Dep of Struct Mech, Lund Inst of Techn, Sweden.

Zienkiewics, O. C. (1977). The Finite Element Method. Third Edition, McGraw-Hill Book Company Ltd, UK.
